

Computational Pathology and Deciphering the Complexity of HER2 Expression in Breast Cancer

Nehal Mohammed Nabil Gaber Atallah

MB.BCH, MSc

Thesis submitted to the University of Nottingham for the Degree of Doctorate of Philosophy.

Department of Pathology, School of Medicine, University of Nottingham, UK

October 2024

ACKNOWLEDGEMENTS

First of all, I would like to thank ***ALLAH the Almighty***, for giving me the strength to finish this project and gain this achievement.

First, I would like to express my gratitude to Professor Emad Rakha for his wise supervision, advice, and guidance from the very early stage of this research and for giving me his time and experience throughout the work. Above all, and most importantly, he provided me with resolute encouragement and support in diverse ways. I am indebted to him more than he knows.

I gratefully acknowledge prof Nigel Mongan for his advice, supervision, and crucial contribution. His true scientific intuition has made him a constant supporter with limitless ideas and passion; I am grateful in every possible way and hope to keep up our collaboration in the near future.

Special thanks go to Professor Cinzia Allegrucci for her tremendous advice, encouragement, and helpful feedback, which assisted me throughout this project and the writing of this thesis. I am much indebted to her.

I am grateful to Dr Catrin Rutland for her help, guidance and continuous support. She did not save effort guiding me whenever I needed her.

Many thanks are due to Dr Michael Salah, Dr Islam Abdelaziz, Mrs Jennifer Baldwin, Mr Chris Nolan, Miss Holly Brown and Mr Alexander Dean for their invaluable assistance and to all members of the Breast Team, Pathology Department, Nottingham City Hospital for their kind help and advice.

I would like to thank everybody who participated in the successful realisation of this thesis and express my apology for not being able to mention everyone who has been a part of the journey here.

This study was completed with the financial support of the Ministry of Higher Education, Egypt, to whom I am indebted. I also want to thank my colleagues in the Pathology Department, Faculty of Medicine, Menoufia University, Egypt, for their spiritual support.

DEDICATION

My special gratitude is to my father, Mr Mohammed Atallah; my mother, Mrs Wafaa Qassem; my sister Associate Prof. Marwa Atallah; and my brother, Mr Mohammed Atallah Junior, who has always been caring and praying for me. I appreciate their limitless encouragement and support from the bottom of my heart.

Words fail me in expressing my appreciation to my husband, Mr Mohamed Hashhash, whose dedication, love and persistent confidence in me has taken the load off my shoulders.

To my loving children, Lara and Ali, your encouragement and willingness to stand by me when times get rough are much appreciated and duly noted. I would not be this strong without you as my inspiration. You are why I keep pushing; I keep facing all the struggles, pains and hardships. I love you all so much!

DECLARATION

I declare that this thesis is the result of my own work and has not, in this, or any other form, been presented to this or any other University in support of an application for any degree other than for which I am now a candidate.

Nehal Atallah

October 2024

This work attained ethics approval under the title.: Refining the prognosis of breast cancer and breast cancer precursor lesions for personalised therapy, IRAS ID 266925 under reference number REC 19/YH/0293. Favourable Opinion granted 23/08/2019.

LIST OF ABBREVIATIONS

ADC	Antibody Drug Conjugate
ADH	Atypical Ductal Hyperplasia
AI	Artificial Intelligence
AKT	Protein Kinase B
ALH	Atypical Lobular Hyperplasia
ANN	Artificial Neural Network
ATM	Ataxia Telangiectasia Mutated
AUC	Area Under the Curve
B2M	Beta 2 Microglobulin
BC	Breast Cancer
BCAA	Branched chain amino acid
BCAT1	Branched-Chain Amino Acid Transaminase 1
BCSS	Breast Cancer-Specific Survival
BL	Basal-like
CDK	Cyclin Dependent Kinase
CEP17	Centromeric Probe for Chromosome 17
CISH	Chromogenic In Situ Hybridisation
CL	Claudin low
CM	Correlation Matrix
CPATH	Computational Pathology
CSC	Cancer Stem Cell
CT	Cycle Threshold
DCIS	Ductal Carcinoma In Situ
DGE	Differential Gene Expression
DL	Deep learning
DMFS	Distant Metastasis Free Survival
DP	Digital Pathology
ECL	Enhanced Chemiluminescence
EGF	Epidermal Growth Factor
EGFR	Epidermal Growth Factor Receptor
EMT	Epithelial-Mesenchymal Transition
ER	Oestrogen Receptor
ERBB2	Erb B2 Receptor Tyrosine Kinase 2 (HER2)
ERK	Extracellular Signal-Regulated Kinase
FDA	Food and Drug Administration
FDR	False Discovery Rate
FFPE	Formalin Fixed Paraffin Embedded
FHIT	Fragile Histidine Triad
FISH	Fluorescence In Situ Hybridisation
FOXO3a	Forkhead Box O3
GEO	Gene Expression Omnibus
HER2	Human Epidermal Growth Factor Receptor 2
HER2-E	HER2 Enriched
HGF	Hepatocyte Growth Factor
HRT	Hormone Replacement Therapy
ICC	Intraclass Correlation Coefficient

IDC	Invasive Ductal Carcinoma
IGF-1R	Insulin-like Growth Factor 1 Receptor
IHC	Immunohistochemistry
ILC	Invasive Lobular Carcinoma
IM	Immunemodulatoru
ISH	In Situ Hybridisation
KEGG	Kyoto Encyclopedia of Genes and Genomes
LCIS	Lobular Carcinoma In Situ
LN	Lymph Node
LVI	Lymphovascular Invasion
M	Mesenchymal
MSL	Mesenchymal stem like
mAB	Monoclonal Antibody
MASCS	Mesenchymal Stem Like Cancer Stem Cells
Maspin	Mammary Serine Protease Inhibitor
mBC	Metastatic Breast Cancer
ML	Machine Learning
mTOR	Mammalian Target of Rapamycin
MUC4	Mucin 4
NACT	Neoadjuvant Chemotherapy
NCBI	National Centre for Biotechnology Information
NK	Natural Killer
NmU	Neuromedin U
NPI	Nottingham Prognostic Index
NRF-1	Nuclear Respiratory Factor 1
Nrf2	Nuclear Factor Erythroid 2-Related Factor 2
NRG1	Neuregulin 1
NST	Non Special type (related to invasive ductal carcinoma)
NUH	Nottingham University Hospitals
OD	Optical Density
OR	Odds Ratio
ORR	Objective Response Rate
PCR	Polymerase Chain Reaction
pCR	Pathologic Complete Response
PGC-1α	Peroxisome Proliferator-Activated Receptor Gamma Co-activator 1-Alpha
PI3K	Phosphoinositide 3-Kinase
PIK3CA	Phosphatidylinositol-4,5-Bisphosphate 3-Kinase Catalytic Subunit Alpha
PPI	Protein-Protein Interaction
PR	Progesterone Receptor
PTEN	Phosphatase and Tensin Homolog
PVDF	Polyvinylidene Fluoride
QC	Quality Control
RAS	Rat Sarcoma Virus (oncogene family)
RB1	Retinoblastoma 1
RICTOR	Rapamycin-Insensitive Companion of mTOR
ROC	Receiver Operating Characteristic
RTKI	Receptor Tyrosine Kinase Inhibitor

RT-qPCR	Real Time Quantitative Polymerase Chain Reaction
SD	Standard deviation
STR	Strom to tumour ratio
SPSS	Statistical Package for the Social Sciences
SRA	Sequence Read Archive
SRC	Sarcoma gene
TAF10	TATA-box Binding Protein Associated Factor 10
TAS	Tumour Associated Stroma
TBP	TATA Box Binding Protein
TDLU	Terminal duct lobular unit
T-DM1	Trastuzumab Emtansine
TFIID	Transcription factor IID
TFAM	Mitochondrial Transcription Factor A
TILs	Tumour Infiltrating Lymphocytes
TMA	Tissue Microarray
TNBC	Triple Negative Breast Cancer
TP53	Tumour Protein p53
TSR	Tumour to stroma ratio
VEGFR	Vascular Endothelial Growth Factor Receptor
WB	Western Blot
WSI	Whole Slide Imaging
β-F1-ATPase	Beta Subunit of F1-ATPase (part of the ATP synthase complex)

ABSTRACT

Background

Breast cancer (BC) is the most common cancer and second leading cancer-related death in women. Despite significant advancement in the detection, prognostic and predictive classification of BC, there remains a proportion of patients who recur and die of their disease. Further research on BC diagnosis and classification is needed. Digital pathology (DP) and molecular assays, including whole slide imaging (WSI), digital image analysis (DIA) and artificial intelligence (AI), are revolutionising BC diagnosis and treatment, enabling detailed cyto-morphometric assessments that enhance diagnostic accuracy, personalise treatment, and improve outcomes. Although the therapeutic roles of HER2 protein in BC have been defined for more than two decades, the spectrum of HER2 expression in BC is evolving, and therapeutic modalities are expanding. HER2-positive cases are candidates for targeted anti-HER2 therapy, but patient response varies, with recurrence rates ranging from 20-40%. The introduction of HER2-Low BC and antibody-drug conjugates (ADCs) has transformed the management of HER2-negative BC but added complexity to HER2 assessment, particularly regarding the lower limits of ADC therapy eligibility.

This thesis evaluates the integration of computational pathology and advanced molecular approaches in identifying novel BC prognostic parameters and deciphering the complexity of HER2 expression, including its biological and clinical characterisation. It highlights differential responses to targeted anti-HER2 therapies among HER2-positive classes, the role of hormone receptor (HR) expression, and refines the definition of HER2-Low BC.

Methods and Results

A large cohort of 40,160 breast WSIs was analysed to assess the accuracy and utility of WSI compared to traditional microscopy. The assessment focused on the presence, frequency, location, and tissue type of missing tissue and its clinical implications. Additionally, scanning time, specimen type, time to implement WSIs and quality control measures were evaluated. The results indicated

that while missing tissue's frequency, area, and location varied, all cases involved fat tissue, and none affected final diagnoses. Quality control measures significantly improved image quality and reduced WSI failure rates by sevenfold.

We also used AI to identify novel prognostic parameters in breast cancer. All slide images were analysed using AI-based DP tools to extract stromal and tumour features, focusing on the tumour-stroma ratio and spatial distribution of stromal cells. Deep learning algorithms were employed for feature extraction and spatial analysis, following extensive annotation at the cellular and region levels. The tumour-stroma ratio was found to be a significant prognostic factor, with higher ratios associated with worse outcomes. AI-based spatial analysis revealed patterns of stromal cell distribution that correlated with tumour aggressiveness and patient survival. This demonstrated the utility of AI in enhancing understanding of the tumour microenvironment and its impact on BC prognosis.

A substantial BC cohort with clinical, transcriptional, and survival data was utilised to develop a HER2-driven morphometric signature reflecting HER2-positive tumours with active oncogenic signalling and better response to targeted anti-HER2 therapy. WSIs of invasive BC cases with HER2-positive and HER2-negative controls were analysed. Image acquisition, segmentation, and spatial distribution analyses were performed using DIA algorithms. Statistical correlations between HER2-driven morphometric features and patient outcomes were analysed. A total of 57 morphometric features were evaluated, with 22 significantly associated with HER2 positivity. HER2 IHC score 3+/oestrogen receptor (ER) negative tumours were significantly associated with HER2-related morphometric features and showed the least intra-tumour morphological heterogeneity. The HER2-driven morphometric signature was validated on PAM50 HER2-Enriched molecular subtype (HER2-E) cases, correlating with prolonged distant metastasis-free survival (DMFS) post-adjuvant anti-HER2 therapy.

For deciphering the response of HER2-positive BC to targeted anti-HER2 therapy, we first compared both HER2-positive classes regarding clinicopathological features, pathological complete response (pCR), patient survival, and the role of ER status on therapy response. Differentially expressed genes and molecular pathways within both classes were identified, with TAF10 and BCAT1 selected for further validation through transcriptomic and proteomic analyses. Tissue microarray blocks were constructed, and IHC staining, scoring, and analysis were performed. The value of concomitant use of multigene assays that assess *ERBB2, ESR1, PGR*, and *MKI67* (MammaTyper® assay) with HER2 IHC for predictive stratification of HER2-positive BC patients to anti-HER2 therapy was investigated. RNA was extracted from formalin-fixed paraffin-embedded (FFPE) tissue, quantified using RT-qPCR, and discordant HER2 status cases were validated through staining on excision specimens and patient record reviews.

Our results revealed that compared to HER2 IHC 3+ tumours, patients with IHC 2+/Amplified BC had a significantly lower pCR rate (22% versus 57%, $p<0.001$) and shorter survival regardless of HER2 gene copy number level. ER positivity was significantly associated with decreased response to anti-HER2 therapy in IHC 2+/Amplified but not in HER2 IHC 3+ BC patients. Compared to IHC 3+, HER2 IHC 2+/Amplified tumours were less frequently classified as HER2-E molecular subtype (16% versus 49%, $p<0.001$), with downregulation of HER2 oncogenic pathway genes, upregulation of trastuzumab resistance genes, and enrichment in ER signalling pathway genes.

TAF10 mRNA expression was significantly associated with HR-positive and HER2-positive tumours, particularly the HER2-E molecular subtype ($p<0.001$). High *TAF10* mRNA expression correlated with prolonged breast cancer-specific survival (BCSS) in both the TCGA and METABRIC cohorts ($p<0.008$ and $p<0.001$, respectively). Multivariate Cox regression confirmed *TAF10* mRNA as an independent predictor of better survival, which was also validated at the protein level. High TAF10 protein expression levels predicted a better response to trastuzumab-based chemotherapy, whereas in chemotherapy-only treated HER2-positive patients, high TAF10 expression had no predictive role. *TAF10* mRNA significantly correlated with low *PIK3CA, mTOR, RICTOR and MIB1*

mRNA expression, known resistance genes to trastuzumab therapy. At the same time, *BCAT1* showed a poor prognostic and predictive role in HER2-positive BC cases with high expression associated with short BCSS and DMFS in trastuzumab-treated patients.

Regarding the role of multigene assays in predicting response to anti-HER2 therapy, *ERBB2* mRNA identified 251/287 (87.5%) cases as HER2-positive, 10.8% (31/287) as HER2-Low, and 1.7% (5/287) as HER2-negative. According to the MammaTyper® assay, *ERBB2*-positive patients treated with anti-HER2 therapy had significantly prolonged 5-year disease free survival (DFS) and DMFS (HR=0.56, p=0.003 and HR=0.62, p=0.023, respectively). MammaTyper®-defined HER2-E subtype showed a better response to anti-HER2 therapy compared to IHC-defined subtypes, with significant prolongation in both 5-year DFS and BCSS. For *ERBB2*-negative patients, there were no significant differences in survival rates between those treated with trastuzumab and those who received only chemotherapy ($p > 0.05$). Validation analysis revealed that 11/36 *ERBB2*-negative cases were IHC 2+/ISH positive with very low gene amplification levels.

For HER2-Low tumours, we refined this category by integrating IHC scoring with mRNA levels and artificial neural network (ANN) models to achieve a refined scoring algorithm with high concordance. HER2 staining intensity, pattern, and subcellular localisation were assessed in detail, and inter-observer concordance in scoring HER2-Low class according to current guidelines was evaluated. ANN analysis successfully distinguished HER2 score 0 from 1+ with high sensitivity and specificity, improving the consistency of HER2 scoring and pathologist concordance. The study provided a clearer definition of HER2-Low BC, facilitating better patient stratification for ADC therapy. Most HER2-Low tumours were HR-positive, enriched with luminal intrinsic molecular subtype, lacking significant HER2 oncogenic signalling gene expression, and exhibiting favourable clinical behaviour compared to HER2-negative BC. In HR-positive BC, no significant prognostic differences were detected between HER2-Low and HER2-negative tumours. However, in HR-negative BC, HER2-Low tumours were less aggressive, with longer patient survival. Transcriptomic data

showed that most HR-negative/HER2-Low tumours were luminal androgen receptor (LAR) intrinsic subtypes, enriched with T-helper lymphocytes, activated dendritic cells, and tumour-associated neutrophils, while most HR-negative/HER2-negative tumours were basal-like, enriched with tumour-associated macrophages.

Conclusion

The research demonstrated the efficacy of integrating DP, including WSI and AI, in enhancing diagnostic accuracy and identifying novel BC prognostic parameters. HER2 protein overexpression is the primary oncogenic driver and the main predictor of response to anti-HER2 therapy in HER2-positive BC. ER signalling pathways are more dominant in BC with equivocal HER2 expression compared to HER2 3+ tumours. The differential response to anti-HER2 therapy based on IHC classes should inform treatment decisions for HER2-positive BC patients. The concomitant use of multigene assays with IHC could improve the prediction of therapeutic response to anti-HER2 therapies. A more precise definition of HER2-Low BC was established, integrating protein expression levels and mRNA data. This refined definition aids in identifying patients who may benefit from novel therapies, such as ADCs. Integrating computational pathology and molecular approaches offers a pathway to more precise and effective clinical management of HER2-positive and HER2-Low BC patients.

PUBLICATIONS

A: Thesis-related Peer-Reviewed Publications

1. Potential quality pitfalls of digitalized whole slide image of breast pathology in routine practice**.**
   Atallah NM, Toss MS, Verrill C, Salto-Tellez M, Snead D, Rakha EA.. Modern Pathology. 2022;35(7):903-10.

2. Differential response of HER2-positive breast cancer to anti-HER2 therapy based on HER2 protein expression level.
   Atallah N, Alsaleem M, Toss M, Mongan N, Rakha E. Differential response of HER2-positive breast cancer to anti-HER2 therapy based on HER2 protein expression level. British Journal of Cancer. 2023;129(10):1692-705.

3. Characterisation of luminal and triple-negative breast cancer with HER2 Low protein expression.
   Nehal M Atallah, Maria Haque, Cecily Quinn, Michael S Toss, Shorouk Makhlouf, Asmaa Ibrahim, Andrew R Green, Mansour Alsaleem, Catrin S Rutland, Cinzia Allegrucci, Nigel P Mongan, Emad Rakha. European Journal of Cancer. 2023;195:113371.

4. Refining the definition of HER2-low class in invasive breast cancer.
   Atallah NM, Toss MS, Green AR, Mongan NP, Ball G, Rakha EA. Histopathology. 2022;81(6):770-85.

5. Prediction of HER2 positive breast cancer patients' response to anti-HER2 therapy using mRNA level**.**
   Atallah NM, Makhlouf S, Li X, Zhangy Y, Rakha E. European Journal of Cancer. 2024;200.

6. Deciphering the morphology of tumor-stromal features in invasive breast cancer using artificial intelligence**.**
   Nehal M Atallah, Noorul Wahab, Michael S Toss, Shorouk Makhlouf, Asmaa Y Ibrahim, Ayat G Lashen, Suzan Ghannam, Nigel P Mongan, Mostafa Jahanifar, Simon Graham, Mohsin Bilal, Abhir Bhalerao, Shan E Ahmed Raza, David Snead, Fayyaz Minhas, Nasir Rajpoot, Emad Rakha. Modern Pathology. 2023;36(10):100254.

7. Artificial intelligence-based mitosis scoring in breast cancer: Clinical application
   Asmaa Ibrahim, Mostafa Jahanifar, Noorul Wahab, Michael S Toss, Shorouk Makhlouf, **Nehal Atallah**, Ayat G Lashen, Ayaka Katayama, Simon Graham, Mohsin Bilal, Abhir Bhalerao, Shan E Ahmed Raza, David Snead, Fayyaz Minhas, Nasir Rajpoot, Emad Rakha Modern Pathology. 2024;37(3):100416.

8. AI-based intra-tumor heterogeneity score of Ki67 expression as a prognostic marker for early-stage ER-positive /HER2− breast cancer**.**
Wenqi Lu, Ayat G Lashen, Noorul Wahab, Islam M Miligy, Mostafa Jahanifar, Michael Toss, Simon Graham, Mohsin Bilal, Abhir Bhalerao, **Nehal M Atallah**, Shorouk Makhlouf, Asmaa Y Ibrahim, David Snead, Fayyaz Minhas, Shan E Ahmed Raza, Emad Rakha, Nasir Rajpoot. The Journal of Pathology: Clinical Research. 2024;10(1):e346.

9. Evaluation of tumour infiltrating lymphocytes in luminal breast cancer using artificial intelligence**.**
Shorouk Makhlouf, Noorul Wahab, Michael Toss, Asmaa Ibrahim, Ayat G Lashen, **Nehal M Atallah**, Suzan Ghannam, Mostafa Jahanifar, Wenqi Lu, Simon Graham, Nigel P Mongan, Mohsin Bilal, Abhir Bhalerao, David Snead, Fayyaz Minhas, Shan E Ahmed Raza, Nasir Rajpoot, Emad Rakha. British Journal of Cancer. 2023;129(11):1747-58.

10. AI-enabled routine H&E image based prognostic marker for early-stage luminal breast cancer**.**
Noorul Wahab, Michael Toss, Islam M Miligy, Mostafa Jahanifar, **Nehal M Atallah**, Wenqi Lu, Simon Graham, Mohsin Bilal, Abhir Bhalerao, Ayat G Lashen, Shorouk Makhlouf, Asmaa Y Ibrahim, David Snead, Fayyaz Minhas, Shan E Ahmed Raza, Emad Rakha, Nasir Rajpoot. npj Precision Oncology. 2023;7(1):122.

B: Other publications

11. Concordance ofHER2-low scoring in breast carcinoma among expert pathologists in the United Kingdom and the republic of Ireland–on behalf of the UK national coordinating committee for breast pathology**.**
Mohamed Zaakouk, Cecily Quinn, Elena Provenzano, Clinton Boyd, Grace Callagy, Soha Elsheikh, Joe Flint, Rebecca Millican-Slater, Anu Gunavardhan, Yasmeen Mir, Purnima Makhija, Silvana Di Palma, Susan Pritchard, Bruce Tanchel, Emad Rakha, **Nehal M Atallah**, Andrew HS Lee, Sarah Pinder, Abeer M Shaaban. The Breast. 2023;70:82-91.

12. Novel 2 Gene Signatures Associated With Breast Cancer Proliferation: Insights From Predictive Differential Gene Expression Analysis**.**
Ibrahim A, Toss MS, Alsaleem M, Makhlouf S, **Atallah NM**, Green AR, Rakha EA. Modern Pathology. 2024;37(2):100403.

13. Combined proliferation and apoptosis index provides better risk stratification in breast cancer**.**
Ibrahim A, Toss MS, **Atallah NM**, Al Saleem M, Green AR, Rakha EA.. Histopathology. 2023;82(7):1029-47.

14. Deciphering the Clinical Behaviour of Invasive Lobular Carcinoma of the Breast Defines an Aggressive Subtype.
Makhlouf S, **Atallah NM**, Polotto S, Lee AH, Green AR, Rakha EA.. Cancers. 2024;16(10):1893.

15. Quantitative expression of oestrogen receptor in breast cancer: Clinical and molecular significance.
Makhlouf S, Quinn C, Toss M, Alsaleem M, **Atallah NM**, Ibrahim A, Rutland CS, Mongan NP, Rakha EA.. European Journal of Cancer. 2024;197:113473.

C: Presentations and Conference Communications

Oral presentations:

1. Role of digital pathology in breast cancer
Oral presentation, Early career researcher showcase, Nagoya University visit, University of Nottingham, April 2023.

2. Deciphering the Clinicopathological, Immunological and Molecular Profile of HER2 Low Breast Cancer within Luminal and Triple-negative Breast Cancer
Oral presentation, Pathological Society summer meeting, June 2023.

3. Characterisation of luminal and triple negative breast cancer with low HER2 expression**.**
Oral presentations, Research impact forum, University of Nottingham, September 2023.
4. Deciphering the differential response of HER2 positive breast cancer to therapy
Oral presentation, Sue-Watson event, University of Nottingham, February 2023.

5. HER2-driven morphometric signature in breast cancer and risk of recurrence
Oral presentation, 1St Prize for best presentation, NBCRC Research Day, May 2024.

6. Characterisation of HER2-Enriched signature in breast cancer and prediction of the risk of recurrence using fine morphometric features.
Plenary oral presentation, Pathological Society winter meeting, January 2024.

7. A Morphometric Signature for HER2 Activity Predicts Recurrence Risk in Breast Cancer

Oral presentation, 8th World Congress on Controversies in Breast Cancer (CoBrCa), September 2024.

Poster presentations as presenting author

- Potential pitfalls of whole slide image in histopathology: frequency and clinical implications of missing tissues on the digitalised images" in EBCSS January 2021 and Pathological society summer meeting 2021.
- Refining the definition of HER2 low class in invasive breast cancer" in Pathological society winter meeting February 2023.
- Differential response of HER2 positive breast cancer based on HER2 protein expression level" in Pathological Society winter meeting February 2022.
- The prognostic significance of tumour to stroma ratio in risk stratification of the luminal breast cancer patient: An artificial intelligence study" in Pathological society winter meeting February 2022.
- Deciphering the clinicopathological, immunological and molecular profile of HER2 low breast cancer within luminal and triple-negative breast cancer" in Edinburgh breast cancer special symposium, February 2022.
- Is it important to characterise HER2-low in breast cancer?" Cancer Research Nottingham, February 2024.
- Can tumour-associated stroma impact breast cancer patient's outcome? An artificial intelligence study" Cancer research Nottingham, February 2024.
- Prediction of HER2-positive breast cancer recurrence using mRNA level" in the European Breast Cancer Conference March 2024.
- TAF10 and trastuzumab response in HER2-positive breast cancer" in the 8th World Congress on Controversies in Breast Cancer (CoBrCa), September 2024.
- Predicting HER2-positive risk of recurrence using multigene assay" in the 8th World Congress on Controversies in Breast Cancer (CoBrCa), September 2024.

Conferences:

- Edinburgh breast cancer special symposium, February 2021.
- Pathological Society summer meeting, Manchester, June 2021
- Nottingham Breast Pathology Masterclass, June 2022.
- Association of Breast Pathology fifth annual meeting, September 2022.
- Birmingham Breast Pathology Masterclass, November 2022.
- Pathological Society winter meeting, London, January 2023.
- Attendance of Edinburgh breast cancer special symposium, February 2023.
- Sue-Watson event, University of Nottingham, February 2023.
- Attendance of Path Lake showcase meeting, March 2023.
- Early career researcher showcase, Nagoya University visit, University of Nottingham, April 2023.
- Drug development and prostate cancer workshop and symposium, University of Nottingham, May 2023.
- Research impact forum, University of Nottingham, June 2023.
- Pathological Society summer meeting, Liverpool June 2023.
- Research impact forum, University of Nottingham, September 2023.
- Nottingham breast pathology masterclass, July 2023.
- Birmingham Breast Pathology Update Course, November 2023.
- Pathological Society, winter meeting, London, January 2024.
- Pathological Society, summer meeting, Sheffield, June 2024.
- Cancer research Nottingham, February 2024.
- Singapore & Nottingham Breast Pathology Online Masterclass, April 2024, as attendance and a moderator for Q&A session.
- 8th World Congress on Controversies in Breast Cancer (CoBrCa), September 2024.

Chapter 1. General Introduction.....1

1.1 Breast cancer mortality and incidence..... 2

1.2 Risk factors of BC 2

1.2.1 Aging..... 2

1.2.2 Family History 2

1.2.3 Reproductive factors 3

1.2.4 Oestrogen exposure..... 3

1.2.5 Lifestyle..... 4

1.2.6 Genetic Inheritance 4

1.2.7 Other breast lesions 5

1.3 Pathogenesis of BC..... 6

1.4 Molecular Classification 10

1.4.1 Luminal A -like Breast cancer..... 11

1.4.2 Luminal B -like BC..... 11

1.4.3 HER2-Enriched 12

1.4.4 Triple negative breast Cancer (TNBC) 12

1.5 Prognostic and predictive factors in BC 15

1.5.1 Prognostic variables..... 15

1.5.2 Predictive (biomarkers) factors..... 20

1.6 Human Epidermal growth factor receptor 2..... 24

1.6.1 History of HER2 receptor 24

1.6.2 Biology of HER2 receptor..... 24

1.6.3 Detection of HER2 25

1.6.4 History of HER2 Scoring 30

1.6.5 Spectrum of HER2 expression in breast cancer 34

1.6.6 HER2-Low and ADC 35

1.6.7 Intra-tumour HER2 Heterogeneity..... 39

1.6.8 Management of HER2-positive BC 41

1.6.9 Treatment modalities in early stage HER2-positive BC..... 47

1.6.10 Management of metastatic HER2-positive BC 50

1.6.11 The Resistance to Anti-HER2 Treatments 55
1.6.12 Role of ER in response to anti-HER2 therapy (triple positive BC) 60

1.7 Digital Pathology and Artificial intelligence 61
1.7.1 Digital Pathology and WSI Applications 61
1.7.2 Digital Image Analysis 62
1.7.3 Artificial intelligence applications 63
1.7.4 Artificial intelligence and assessment of HRE2 status 67
1.7.5 Challenges to AI application in breast pathology 69

1.8 Hypothesis and Aim of the Work. 71
1.8.1 Hypothesis 71
1.8.2 Aims 71

Chapter 2. Patients And Methods 73

2.1 Patient cohorts 74
2.1.1 Nottingham BC cohort 74
2.1.2 Transcriptomic cohort 80

2.2 Construction of tissue microarray (TMA) 84
2.2.1 Collection of the study cohort, preparation of the donor blocks and their corresponding slides 85
2.2.2 Preparation of the recipient array blocks 87
2.2.3 Construction of the individual array blocks 87
2.2.4 Designing the Array Grids 87
2.2.5 Preparation of the array block for sectioning 88

2.3 Biomarkers data 89
2.3.1 BC molecular subtypes in Nottingham cohort 90
2.3.2 Selection of biomarkers for this research 90

2.4 Validation of antibody Specificity 91
2.4.1 Western blotting (WB) 91
2.4.2 Peptide Blocking 95

2.5 Immunohistochemistry 96
2.5.1 Optimisation of primary antibody 96

2.5.2 Slide heating, Deparaffinisation and Rehydration 97
2.5.3 Antigen retrieval 97
2.5.4 Applying Leica Max Polymer Detection Kit 98
2.5.5 Dehydration and mounting 99
2.5.6 Positive and negative controls 101
2.5.7 Assessment of IHC staining 101
2.5.8 Setting up cut-off points 102

2.6 RNA extraction and reverse transcriptase quantitative polymerase chain reaction (RT-qPCR) 103

2.6.1 Formalin fixed paraffin embedded block retrieval and sample preparation 103
2.6.2 RNA extraction. 103
2.6.3 Assessment of RNA concentration 108
2.6.4 mRNA quantification with RT-qPCR 110

2.7 Chromogenic in situ hybridisation (CISH) 113

2.7.1 Interpretation of CISH 115

2.8 Whole slide image quality control (QC) 116

2.8.1 Comparison of the missing tissue between glass slide and WSIs 118

2.9 Annotation and development of machine learning algorithm. 119

2.9.1 Digital scanning of slides: 119
2.9.2 Whole slide annotations 119
2.9.3 Deep learning-based feature computing 123
2.9.4 Nuclei segmentation/classification and nuclear features 124
2.9.5 Region segmentation and region features. 124
2.9.6 Defining the morphological features 125
2.9.7 AI-based STR quantification and spatial distribution. 126

2.10 Digital Image Analysis (DIA) 129

2.10.1 Image acquisition and scanning 129
2.10.2 Image preprocessing 130
2.10.3 Cellular and Nuclei segmentation and classification 130
2.10.4 Spatial distribution and arrangement of tumour cell 131

2.11 Bioinformatics 133
2.11.1 Gene Expression Omnibus dataset..... 133
2.11.2 Identification of valid DEGs and their functional analysis 134
2.11.3 Functional and pathway enrichment analyses of DEGs. 135
2.11.4 Construction of the protein-protein interaction (PPI) network and identification of hub genes 135
2.12 Statistical analysis 136
2.12.1 Conventional Statistical Approach..... 136
2.12.2 Other analysis 137
2.12.3 Ethical approval..... 141
Chapter 3. The Performance of Digital Pathology in Clinical Practice 144
3.1 BACKGROUND 145
3.2 INTRODUCTION 145
3.3 HYPOTHESIS 147
3.4 AIMS OF THE STUDY 147
3.5 MATERIAL AND METHODS 148
3.5.1 Missing tissue in WSIs compared to glass slides 150
3.5.2 WSI Quality Control..... 150
3.5.3 Statistical Analysis 151
3.6 RESULTS..... 151
3.6.1 Missing Tissue Characteristics..... 151
3.6.2 Quality Control Data..... 156
3.6.3 Missing tissue and confounders..... 159
3.7 DISCUSSION 160
Chapter 4. Assessment of BC stroma features using AI 167
4.1 BACKGROUND 168
4.2 INTRODUCTION 169

4.3 HYPOTHESIS 171

4.4 AIMS OF THE STUDY 172

4.5 MATERIALS AND METHODS 172

4.5.1 Cohort characteristics and image acquisition 173

4.5.2 Tissue and Cellular Annotation 173

4.5.3 Deep learning-based feature computing 173

4.5.4 Nuclei segmentation/classification and nuclear features 174

4.5.5 Region segmentation and region features. 174

4.5.6 Stroma tumour ratio quantification and spatial distribution 174

4.5.7 Visual assessment of STR 175

4.5.8 Assessment of tumour burden 176

4.5.9 Statistical Analysis 176

4.6 RESULTS 177

4.6.1 Cell density, STR and spatial distribution 183

4.6.2 Association between STR ratios and tumour behaviour 184

4.6.3 Impact of tumour burden on tumour behaviour 184

4.6.4 Impact of STR, tumour burden and spatial distribution related features on patient outcome 193

4.7 DISCUSSION 204

Chapter 5. Morphometric Signature for HER2 Activity and response to therapy 210

5.1 BACKGROUND 211

5.2 INTRODUCTION 211

5.3 HYPOTHESIS 212

5.4 AIMS OF THE STUDY 212

5.5 MATERIALS AND METHODS 213

5.5.1 Study cohorts 213

5.5.2 Image acquisition and morphometric digital image analysis . 215

5.5.3 Visual-based assessment 216

5.5.4 Identification of HER2 driven morphometric features 218

5.5.5 Development of a single HER2-driven morphometric signature. 219
5.5.6 Differential gene expression and pathway enrichment analysis 220
5.5.7 HER2 risk of recurrence prognostic index 220
5.5.8 Webtool application 221
5.5.9 Statistical analysis 221

5.6 RESULTS 224

5.6.1 Basic Cohort Description 224
5.6.2 Characterisation of HER2 driven morphometric features 226
5.6.3 HER2-driven morphometric signature and response to anti-HER2 therapy. 242
5.6.4 HER2-positive BC patient risk of recurrence prognostic index 245

5.7 DISCUSSION 247

Chapter 6. Biological and clinical characterisation of HER2-positive breast cancer 253

6.1 INTRODUCTION 254

6.2 HYPOTHESIS 256

6.3 Aims of the Study 257

6.3.1 Evaluate the impact of HER2 protein expression levels on treatment response and outcomes 257
6.3.2 Investigate the role of *HER2* gene amplification levels: 257
6.3.3 Examine the interaction between ER status and HER2 signalling:..... 257
6.3.4 Decipher clinical, biological, and molecular signatures: 257
6.3.5 Enhance personalised treatment strategies: 258

6.4 MATERIALS AND METHODS 258

6.4.1 Study Cohort 258
6.4.2 CISH 259
6.4.3 HER2 and HR IHC staining 260

6.4.4 Assessment of pathological response to neoadjuvant therapy 261
6.4.5 HER2-positive BC patients' outcome in the adjuvant settings 261
6.4.6 Differential Gene Expression Analysis 262
6.4.7 Gene Expression Omnibus dataset..... 262
6.4.8 Statistical Analysis 264

6.5 RESULTS..... 265

6.5.1 Differential response of HER2-positive classes to therapy in the neoadjuvant setting 268
6.5.2 HER2-positive groups and patients' survival. 275
6.5.3 Molecular profile of HER2-positive classes and its impact on response to therapy..... 277
6.5.4 Differential expression of genes responsible for HER2 oncogenic signalling 278

6.6 DISCUSSION..... 289

Chapter 7. Modulators of response in HER2-positive BC 297

7.1 INTRODUCTION..... 298

7.2 HYPOTHESIS..... 301

7.3 AIMS OF THE STUDY..... 302

7.4 MATERIALS AND METHODS..... 302

7.4.1 Discover cohort..... 303
7.4.2 Transcriptomic Validation Cohorts 304
7.4.3 Proteomic Validation Cohort 306
7.4.4 Western blotting, peptide blocking and IHC 306
7.4.5 Statistical Analysis 307

7.5 RESULTS..... 308

7.5.1 Validation of TAF10 and BCAT1antibodies specificity 309
7.5.2 *TAF10* and *BCAT1* mRNA expression in BC 309
7.5.3 Association of *TAF10* and *BCAT1* mRNA expression with clinicopathological parameters 311

7.5.4 *TAF10* and *BCAT1* mRNA expression in molecular BC subtypes 314
7.5.5 *TAF10 and BCAT1* mRNA Expression and patients' Outcome 322
7.5.6 TAF10 and BCAT1 protein expression 330
7.5.7 Association of TAF10 and BCAT1 protein expression with tumour clinicopathological parameters 331
7.5.8 Association of TAF10 and BCAT 1 protein expression with patient outcome 331
7.5.9 Prediction of response to anti-HER2 therapy 340
7.5.10 TAF10 cytoplasmic protein expression 341
7.5.11 Correlation between *TAF10* mRNA and PI3K/AKT/mTOR signalling genes. 341

7.6 DISCUSSION 345

Chapter 8. Prediction of response to targeted anti-HER2 therapy using multigene assay 350

8.1 BACKGROUND 351

8.2 INTRODUCTION 353

8.3 HYPOTHESIS 354

8.4 AIMS OF THE STUDY 354

8.5 MATERIALS AND METHODS 355

8.5.1 Cohort selection and characterisation 355
8.5.2 Biomarker evaluation 356
8.5.3 Sample preparation and RNA extraction. 356
8.5.4 Assessment of RNA concentration 357
8.5.5 mRNA quantification with RT-qPCR 358
8.5.6 Validation of discordant results 358
8.5.7 Statistical analysis 359

8.6 RESULTS 359

8.6.1 Basic clinicopathological parameters of the study cohort 359
8.6.2 Quality of RNA among two extraction assays 360

8.6.3 *ERBB2* mRNA, *HER2* gene copy number and HER2 IHC score 360
8.6.4 MammaTyper® defined HER2 status 361
8.6.5 MammaTyper® assay based molecular subtyping. 364
8.6.6 Validation of discordant cases 368
8.6.7 Prediction of HER2-positive BC patients' response to anti-HER2 therapy according to *ERBB2*/HER2 status 371
8.6.8 Response to therapy according to MammaTyper® Molecular classification 372
8.6.9 Correlation between mRNA and IHC results 376

8.7 DISCUSSION 378

Chapter 9. Refining the definition of HER2-Low class in invasive breast cancer 383

9.1 INTRODUCTION 384

9.2 HYPOTHESIS 386

9.3 AIMS OF THE STUDY 386

9.4 MATERIALS AND METHODS 391
9.4.1 Study cohorts 391
9.4.2 HER2 IHC staining 392
9.4.3 Detailed re-assessment of HER2 IHC protein expression 393
9.4.4 HER2 IHC score interobserver concordance 394
9.4.5 Validation of HER2 status on resection specimen 394
9.4.6 Defining cut-off for HER2 score 1+ versus score 0 394
9.4.7 Reliability and reproducibility of the refined HER2 IHC score 398
9.4.8 Correlation between refined HER2 score with the clinicopathological variables 398
9.4.9 Statistical Analysis 398

9.5 RESULTS 399
9.5.1 Cohort characterisation 399
9.5.2 Concordance in HER2 scoring in the discovery cohort. 399
9.5.3 Patterns of HER2 protein expression 403

9.5.4 Correlation between HER2 IHC score and mRNA level 404
9.5.5 Clustering of *HER2* mRNA 405
9.5.6 ANN model sensitivity 405
9.5.7 Reproducibility of the refined HER2 IHC score 411
9.5.8 The association between various clinicopathological parameters and the refined HER2 score in comparison with the original score 412

9.6 DISCUSSION 417

Chapter 10. Molecular Characterisation of HER2-Low in breast cancer 424

10.1 INTRODUCTION 425

10.2 HYPOTHESIS 427

10.3 AIMS OF THE STUDY 427

10.4 MATERIALS AND METHODS 428

10.4.1 Study cohorts and data acquisition: 428
10.4.2 CISH 429
10.4.3 Assessment of stromal TILs 429
10.4.4 Differential gene expression analysis and pathway enrichment analysis 431
10.4.5 Validation of the results of in-house cohort 432
10.4.6 HER2-Low tumours: Molecular Signature and subtyping 432
10.4.7 Immunologic profile and immunophenotyping of HER2-Low tumours 433
10.4.8 KEGG and Gene Ontology enrichment analyses of DEGs ... 434
10.4.9 Protein-protein interaction network construction and hub genes selection 434
10.4.10 Validation of hub genes 434
10.4.11 Statistical analysis 435

10.5 RESULTS 436

10.5.1 Patients and tumour characterisation 436
10.5.2 Clinicopathologic characteristics of HER2-Low BC in cohort A1 439

10.5.3 Difference in patient outcome between HER2-Low and HER2-negative tumours according to HR status 443
10.5.4 HER2-Low molecular signature 447
10.5.5 CIBERSORT Immunophenotyping analysis 455
10.5.6 Gene Set Enrichment Analysis and Gene ontology 456
10.5.7 PPI network and hub genes 457
10.5.8 Immunohistochemical expression of AR 457
10.6 DISCUSSION 467
Chapter 11. General Discussion 475
11.1 General Background 476
11.2 Hypothesis and Aims of the Thesis 478
11.3 Cardinal Findings from Each Chapter 479
11.3.1 Computational Pathology in Clinical Practice 479
11.3.2 Morphometric Signature for HER2 Activity and Response to Therapy 481
11.3.3 Characterisation of HER2-Positive BC 482
11.3.4 Modulators of Response to Targeted Anti-HER2 Therapy 483
11.3.5 Characterisation of HER2-Low tumours 484
11.4 Conclusion 485
11.5 Clinical Application of Our Findings 486
11.6 Strengths of the study 487
11.7 Limitations and Weaknesses of the Study 490
11.8 Suggestions and Future Investigations 490
11.9 Ongoing work 491
Chapter 12. REFERENCES 492

List of Tables

Table 1.1: Additional genes associated with breast cancer [31] 6

Table 1.2: Classification of molecular subtypes of BC and therapies [63].... 14

Table 1.3: HER2 testing and scoring ASCO/CAP guidelines [141] 32

Table 1.4: HER2-targeted agents used in the current treatment of breast cancer [229] 42

Table 1.5: Summary of previous studies on the differential pathological response between HER2 IHC 3+ and HER2 IHC 2+/ISH positive [224] 43

Table 1.6: Efficacy of HER2-positive Drugs in Prospective Clinical Trials in mBC and Brain Metastases [277]. 53

Table 1.7: Mechanisms of resistance to anti-HER2 agents [284]..... 59

Table 2.1: Frequency of clinicopathological parameters of Nottingham BC series. 76

Table 2.2: Frequency of clinicopathological parameters of the METABRIC and TCGA cohorts. 84

Table 2.3: Validation of biomarkers used in the current research 99

Table 2.4. Details of the antibodies used in this research. 100

Table 3.1: Characteristics of the whole slide images (WSI) scanned in the routine diagnostic practice and showed missing tissues (number=4268) .. 152

Table 3.2: Detailed analysis of the proportion of missing tissue in all cases within cohort 1, scanned during routine diagnostic practice 153

Table 3.3: Relation between missing tissue and both the scanning time and average image file size with their impact on the clinical final diagnosis 159

Table 4.1: Summary of tumour associated stroma (TAS) extracted features with their descriptions. 178

Table 4.2: Patients and tumour characteristics 181

Table 4.3: Correlation between stroma-tumour ratio and clinicopathologic parameters..... 187

Table 4.4: Correlation between stroma-tumour ratio and clinicopathologic parameters in the endocrine treated only patients. 188

Table 4.5: Correlation between tumour burden and tumour density with clinicopathologic parameters 190

Table 4.6: Correlation between tumour burden and clinicopathologic parameters in the endocrine-treated patients 192

Table 5.1: Baseline patients and tumour characteristics..... 224

Table 5.2: Summary of the extracted morphometric features using digital image analysis software..... 226

Table 5.3: Correlation between different HER2 immunohistochemical scores and cyto-morphometric features in the discovery cohort..... 229

Table 5.4: Description of the biologically relevant morphometric features in TCGA cohort. 231

Table 5.5: Pathway enrichment analysis of HER2-morphometric signature positive vs HER2-morphometric signature negative cases 245

Table 6.1: Summary of GEO datasets used in this study..... 264

Table 6.2: Descriptions of the basic clinicopathologic parameters in our cohort..... 266

Table 6.3: Correlation between clinicopathologic parameters and HER2 IHC scores 270

Table 6.4: Comparison between pathologic complete response-related factors within each HER2-positive category..... 274

Table 6.5: Mean value of normalised reads of HER2 oncogenic pathway genes among HER2 IHC 3+ and IHC 2+ breast cancer cases 282

Table 6.6: Differential expression of HER2 oncogenic signalling pathway genes in HER2 3+ and 2+/ISH amplified. 283

Table 6.7: Genes for resistance to therapy in HER2 2+/Amplified 284

Table 6.8: Expression of ER signalling pathway genes in HER2-positive categories 286

Table 7.1: List of top upregulated genes in trastuzumab resistant and sensitive cell lines 308

Table 7.2: The association between *TAF10* mRNA expression and clinicopathological parameters in the METABRIC and TCGA breast cancer series. 315

Table 7.3: The association between *BCAT1* mRNA expression and clinicopathological parameters in the METABRIC and TCGA breast cancer series. 316

Table 7.4: Correlation between TAF10 protein expression and clinicopathological parameters in Nottingham cohort 335

Table 7.5: Correlation between BCAT1 protein expression and clinic-pathological parameters in Nottingham cohort 336

Table 8.1: Basic clinicopathological characteristics in both cohorts 363

Table 8.2: Comparison between the distribution of biomarker status in IHC and mRNA 365

Table 8.3: Correlation between *ERBB2* mRNA status and tumour clinicopathological characteristics 366

Table 8.4: Distribution of HER2 IHC expression of the discordant cases between core biopsy and resection specimen 371

Table 8.5: Comparison between patients' recurrence post adjuvant anti-HER2 therapy according to *ERBB2*/HER2 status 372

Table 8.6: Concordance between immunohistochemistry and mRNA assays in detection of biomarkers status 378

Table 8.7: Accuracy of mRNA in assessment of biomarker status..... 378

Table 9.1: Overview of the clinical trials on ADC in HER2-Low breast cancer* 388

Table 9.2: Summary of the ongoing clinical trials for management of HER2 expressing BC* 390

Table 9.3: Clinicopathologic characteristics of the study cohort..... 400

Table 9.4: Table summarising Inter-observer concordance for HER2 status in the discovery cohort..... 402

Table 9.5: Inter-observer concordance for HER2 status dichotomised in 3 tier system in the discovery cohort..... 402

Table 9.6: Inter-observer concordance for HER2 IHC score in the discovery cohort..... 402

Table 9.7: Description of HER2 expression patterns in the experimental cohort..... 403

Table 9.8: Comparison between HER2 score 1+ definition based on the existing guidelines against the refined criteria 406

Table 9.9: Concordance rates of the refined HER2 score..... 411

Table 9.10: Associations between clinicopathologic parameters and HER2 scores (using the refined and the original clinical score)..... 413

Table 9.11: Clinicopathologic parameters and *ERBB2* clusters..... 415

Table 10.1: Descriptions of the basic clinicopathologic parameters in Nottingham cohort..... 437

Table 10.2: Correlation between clinicopathologic parameters and HER2 IHC scores 440

Table 10.3: Difference in patients' outcome between HER2-Low and HER2-negative hormone receptor negative breast cancer 446

Table 10.4: Factors affecting pathologic complete response among HER2-Low and HER2-negative BC patients..... 447

Table 10.5: Differential expression of PAM50 molecular subtypes genes between HER2-Low and HER2-negative BC in TCGA sample..... 452

Table 10.6: Differential expression of TNBC molecular subtypes genes between HER2-Low and HER2-negative in TCGA cohort 453

Table 10.7: Differential expression of TNBC molecular subtypes genes between HER2-Low and HER2-negative in the overlapping genes between TCGA and NGS cohort (A3) 455

Table 10.8: Basic patient and tumour characteristics of Nottingham cases used to assess Androgen receptor immunohistochemical expression..... 466

List of Figures

Figure 1.1: The hallmarks of cancer, which represent alterations that take place in cell physiology during the malignant transformation. Created with BioRender.com 8

Figure 1.2:Two hypothetical theories of breast cancer initiation and progression. (A) All subtypes of tumours are derived from the same stem cell or progenitor cells. Different tumour phenotypes are then determined by subtype-specific transforming events. (B) Each tumour subtype is initiated from a single cell type (stem cell, progenitor cell, or differentiated cell). Random mutations can gradually accumulate in any breast cells, leading to their transformation into tumour cells when an adequate number of mutations have accumulated Created by Biorender.com. 9

Figure 1.3: HER2 receptor tyrosine kinase signalling pathway, Created with BioRender.com 26

Figure 1.4: A schematic overview of HER2 scoring in breast cancer. Breast cancers are considered HER2-negative if the IHC score is 0. An IHC score of 1 + or 2 + without HER2 amplification is categorised as HER2-Low. Breast cancers with an IHC score of 2 + with amplification or 3 + are HER2-positive (40× magnification). Created by Biorender.com. 27

Figure 1.5: Diagram shows the history of HER2 testing and cut-off Controversy. Created by Biorender.com 31

Figure 1.6: Spectrum of HER2 scoring using immunohistochemistry (IHC). [141] 31

Figure 1.7: Mode of action of HER2-directed ADCs in HER2-Low tumours. Classical mode of action of ADCs with cleavable linkers: (A) Targeted drug delivery in which monoclonal anti-HER antibody component binds to HER2 expressed on the cell surface of tumour cells, this leads to the ADC-HER2 complex internalisation by endocytosis. After linker cleavage by lysosomal proteases, the drug payload is released and induces the cytotoxic effect,

leading to tumour cell death. B, C, D: The monoclonal anti-HER antibody component of ADCs may retain its activity profile and engage in Fc-mediated interactions with immune cell players; complement, macrophages and natural killer (NK) cells), triggering antitumour immunity via complement-dependent cytotoxicity (CDC), antibody dependent cellular phagocytosis (ADCP) and antibody-dependent cellular cytotoxicity, respectively (ADCC). F: Bystander killing effect: Using cleavable linkers, ADCs can be designed to promote cytotoxic drug release from the target cell to the extracellular space to the surrounding and bystander cells, which may or may not express the ADC target antigen, Created with BioRender.com 38

Figure 1.8: Mechanism of action of anti-HER2 therapy. 1: Monoclonal antibody; 2: Receptor tyrosine kinase; 3: Antibody drug conjugate. Created with BioRender.com 45

Figure 1.9: Chronological outline of FDA approvals of ADCs for the treatment of breast cancer. ADC: antibody drug conjugate; FDA: Food and Drug Administration; HR: Hormone receptor; HER2: human epidermal growth factor receptor 2; mBC: metastatic breast cancer; pts, patients; ChT: chemotherapy; T-DM1, trastuzumab emtansine; T-DXd, trastuzumab deruxtecan; eBC, early breast cancer. 46

Figure 1.10: Schematic illustration for the management of early-stage breast cancer [229]. AC-TH, doxorubicin and cyclophosphamide followed by paclitaxel and trastuzumab; ER+, oestrogen-receptor positive; ET, endocrine therapy; pCR, pathologic complete response; TCH, docetaxel, carboplatin and trastuzumab; TH, paclitaxel and trastuzumab; pN0, no regional lymph node metastases; pN1, metastases to movable ipsilateral level I, II axillary lymph node(s); pT, pathologic primary tumour TNM stage. 49

Figure 1.11: Treatment algorithm for the treatment of HER2-positive metastasis breast cancer. ADC, antibody-drug conjugate; ChT, chemotherapy; CT, clinical trial; H, trastuzumab; HER2, human epidermal growth factor receptor 2; mBC, metastatic breast cancer; P, pertuzumab; T,

taxane; T-DM1, trastuzumab emtansine; T-DXd, trastuzumab deruxtecan [276]. 51

Figure 1.12: Mechanism of resistance to anti-HER2 targeted therapy. (1) Resistance to monoclonal antibodies (right, red box). Low HER2 expression, changes in the extracellular binding domain, and constitutive activation of the PI3K pathway can lead to resistance. Overexpression of receptor tyrosine kinase (RTKs) can promote the formation of HER2–EGFR and HER2–HER3 heterodimers, activating the pathway. Resistance to antibody-drug conjugates (ADCs) is also common, with drug efflux pumps reducing the intracellular cytotoxic action of ADCs. Resistance to TKIs is also common, with low HER-2 expression, activation of CD1 and CDK4-6, increased ER, constitutive activation of the PI3K pathway, and overexpression of NRG1. (2) Resistance to ADCs (centre, green box), and TKIs is shared among other drug classes, with some unique escapes. ADCs' cytotoxic action can be reduced by drug efflux pumps on cell walls. TKIs' binding site binding site mutations, such as L755S and T798I, confer specific resistance, preventing them from blocking HER2 function. Abbreviations: ADCs: antibody-drug conjugates; EGFR: epidermal growth factor receptor; HER2: human epidermal growth factor receptor 2; ER: oestrogen receptor; NRG1: neuroregulin 1; CDK: cyclin dependent kinase [285]. 55

Figure 1.13: Diagram illustrating the main applications of digital pathology and AI in pathology. AI, artificial intelligence; NGS, next-generation sequencing..... 68

Figure 2.1: Marking of invasive breast cancer using 0.6mm circle diameter using slide viewer software. 87

Figure 2.2: H&E sections of HER2-positive TMA. The grid represents an overview of 0.6mm needle core diameter TMA. A and B represent orientation cores from normal kidney and liver, respectively, included outside of the geometric margin of the array on the top and bottom left-hand side. C: core from invasive breast cancer. 89

Figure 2.3: Layout of the 96 well plate. Each colour columns represent triplicates of one master mix; yellow is master mix 1 for assessment of *ERBB2* and *ESR1*, blue is master mix 2 for assessment of *MKI67* and *B2M* reference gene and red is master mix 3 for assessment of *PGR* and *CALM2*, the other reference gene. Each sample "P" and distributed in the wells from 1 to 9, so each gene is assessed in triplicates. PC: is positive control included in the kit. NC is the negative control which is RNASE free water. Eight patients' samples can be assessed per kit..... 112

Figure 2.4: Figure showing RT-qPCR run temperature setting (left side) and the amplification curves after 40 cycles of gene amplification (right side).. 113

Figure 2.5: Different HER2 IHC scores and their corresponding CISH results. A) HER2 IHC 3+ with CISH amplification (1); B) HER2 IHC2+ with CISH amplified (2); C) HER2 1+ non amplified CISH (3), D), HER2 IHC0 with no CISH amplification (4)..... 115

Figure 2.6: H&E-stained BC sections showing regional and cell-level annotations. The regional annotations encompass different areas within the tissue, including invasive and in situ tumour regions, tumour-associated stroma (TAS), and normal breast tissue, level annotations highlight specific cellular components including tumour cells with degrees of pleomorphism, mitotic figures, stromal cells such as fibroblasts or myofibroblasts, normal epithelial cells, and TILs..... 121

Figure 2.7: Cellular annotations of Ki 67 and PR were performed separately, where positive and negative tumour cells were annotated as well as positive and negative non-tumour cells: Ki 67 stained BC sections showing cell level annotation, where specific cells within the tissue are labelled using coloured dots. The red dots represent positively stained tumour cells, the green dots denote negatively stained tumour cells, the yellow dots are used to label positively stained non-tumour cells and the blue dots are used to label negatively stained non-tumour cells..... 122

Figure 2.8 : Bar chart showing the total number of annotated morphological features used for the training of machine learning algorithms, both on regional and cellular levels..... 123

Figure 2.9: Graph illustrating deep learning (DL) based feature computing. A: DL pipeline for feature generation. Ductal carcinoma in situ (DCIS) is filtered out by CNNDCIS before CNNNuc performs nuclei segmentation and classification and CNNReg performs region segmentation for extracting different features. B Nuclei map generation for quantifying nuclei cooccurrences. Each detected nuclei type is mapped at its centroid in five times down sampled whole slide image. C: Tumour and tumour associate stroma (TAS) regions segmentation. The resulting regions are then used to calculate STR. D: Heatmap for stromal cell to tumour cell ratio measured in 256 × 256 pixels patches. E: Visual subjective assessment of STR into low (left), medium (Middle) and high (right). STR: Stroma to tumour ratio. 127

Figure 2.10: Number of times predicted tumour nuclei (T) neighbour with stroma nuclei (S) at a distance of one cell hop on any of the 8-direction shown (A). S occurring to the right (i.e., at angle 0) of T is 1 and is shown by an ellipse in B (and circled in D). Similarly, S occurring above (i.e., at angle 90) T is 2 and is shown by an ellipse in C (and circled in F). Such occurrences can be calculated at 8 different angles (0, 45, 90, 135, 180, 225, 270, and 315 shown in D, E, F, G, H, I, J and K, respectively) and then summed to get total occurrences (L). Note: to get the sum of occurrences of the same entity for example T with T, the total occurrences are divided by 2. The resulting values are then normalised (i.e., each value in the table is divided by the total sum of the values) and the resulting table – termed Co-occurrence Matrix (CM) (M) is then used to calculate different features such as contrast and heterogeneity..... 128

Figure 2.11: Schematic illustration summarising the digital image analysis workflow. ROIs: regions of interests..... 132

Figure 2.12: XGBoost architecture: It’s an ensemble of classifiers where each classifier is focused on the mistakes made with the previous classifier. 138

Figure 3.1: Schematic illustration of the study cohorts. WSI: whole slide image; IHC: immunohistochemical..... 149

Figure 3.2: Examples of missed tissue in WSI (left) compared with the corresponding glass slides (right). 154

Figure 3.3: Example of WSI missing normal breast duct at the periphery of the slides. A): overview image of a slide that was fully scanned, B): High power of the normal breast terminal lobular duct unit on a glass slide (x40 light microscope) present at the periphery of the slide and was missed upon scanning (C). The terminal lobular duct measured 1.5mm at its largest diameter..... 155

Figure 3.4: Examples of different quality control categories on failed WSIs. 157

Figure 3.5: Role of quality control in improving digitalised image quality; Failed images before (A, B) and after quality control (C, D). A: shows longitudinal scores, B: is out of focus..... 158

Figure 3.6: A flowchart demonstrates the WSI failure rate before and after the application of quality control measures for the three studied scanners..... 158

Figure 3.7: Example of an image scanned by the same scanner but at two different settings: A) High specimen threshold scanning with missing most of the fatty tissue on WSI, while B) the image was scanned at low specimen threshold scanning and no missing tissue was detected. 160

Figure 4.1: Roles of Carcinoma Associated Fibroblasts (CAFs) in Tumorigenesis. Tumour cells and the surrounding CAFs, interact to create a microenvironment that can either promote or suppress tumorigenesis. Tumours can stimulate normal fibroblasts to transform into CAFs, yet the biological mechanisms that dictate whether these fibroblasts adopt tumour-promoting or tumour-suppressing roles are still unclear. Tumour-promoting CAFs enhance tumour growth, survival, and metastasis both directly and indirectly by influencing other tumour-associated stromal cells. Conversely,

both normal fibroblasts and CAFs have been observed to inhibit or slow down tumorigenesis. [486]. 171

Figure 4.2: Graphical illustration of tumour associated stroma (TAS) features extraction using deep learning model. A: represent TAS annotation, followed by multiple convolutional neural network development. 175

Figure 4.3: Summary of distribution of assessed tumour and stroma features. A: Bar Chart displays the mean values ± standard deviation (SD) for tumour cell count, stromal cell count, stromal immune cells (sTILS), and the spatial co-occurrences of stromal cells. B: Scatter Plot shows a significant correlation between tumour cell counts and stromal cell counts ($p<0.001$). C: Bar Chart summarises the mean values ± SD of stroma-to-tumour ratio (STR) related features, highlighting a significant difference between the percentage of patches with high stroma and those with low stroma. D: 3D Scatter Plot reveals a significant correlation between tumour size, tumour cell density, and tumour burden ($p<0.001$). H-H: High to high co-occurrence, H-L: High to low co-occurrence score. 186

Figure 4.4: Box plot chart demonstrating the correlation between continuous values of stroma to tumour surface area ratio (STR) (A), Tumour cell count (B), tumour burden (C) and stroma to tumour cells count ratio (D). 189

Figure 4.5: Kaplan Meier curves showing significant correlation between high stroma to tumour surface area ratio (STR) with better patients' survival in the discovery cohort; both in breast cancer specific survival (A), and distant metastasis free survival (B) and in subgroup of patients with aggressive tumour behaviour as premenopausal (C,D); high tumour grade (E,F); lymph node metastasis (G,H) and poor Nottingham prognostic index (I,J). 196

Figure 4.6:Kaplan Meier curves showing significant correlation between high stroma to tumour surface area ratio (STR) with better patients' survival in the test cohort; both in breast cancer specific survival (A), and distant metastasis free survival (B). and the significant association between high tumour burden and wore patient's outcome (C, D). 196

Figure 4.7: Kaplan Meier curves showing significant correlation between larger tumour burden with worse patients' survival in the discovery cohort; both in breast cancer specific survival (A), and distant metastasis free survival (B) and in subgroup of patients with less aggressive tumour behaviour as postmenopausal (C,D); low tumour grade (E,F); negative lymph node metastasis (G,H) and good Nottingham prognostic index (I,J). 198

Figure 4.8: Kaplan Meier curves demonstrating effect of stroma to tumour ratio (STR) spatial intratumor contrast (A1,2), heterogeneity (B1,2) and spatial cooccurrence (C1, C2) on breast cancer specific survival and distant metastasis free survival in the discovery cohort. TTDM: time to distant metastasis..... 198

Figure 4.9: Illustrated diagram showing the difference between Stroma tumour ratio and spatial distribution as well as the value of tumour burden. 199

Figure 4.10: Kaplan Meier curves demonstrating the effect of stroma to tumour ratio (STR) spatial intratumor contrast (A1,2), heterogeneity (B1,2) and spatial cooccurrence (C1, C2) on breast cancer specific survival and distant metastasis-free survival in the test cohort. TTDM: time to distant metastasis..... 200

Figure 4.11: Forest plot illustrating the multivariate Cox regression model for stroma to tumour ratio (STR) adjusted for the clinicopathologic parameters showing that STR is an independent predictor of patient outcome. 201

Figure 4.12: Forest plot illustrating the multivariate Cox regression model for tumour burden adjusted for the clinicopathologic parameters showing that tumour burden is an independent predictor of patient outcome. 202

Figure 4.13: Forest plot illustrating the multivariate Cox regression model including both tumour burden and STR and showing that tumour burden is an independent predictor of patients' outcome and STR is not. 203

Figure 5.1: Schematic illustration summarising the characteristics of the study cohort. 214

Figure 5.2: A graph that summarises the process used in image processing to extract morphometric features and evaluate intra-tumour heterogeneity. Step 1 involved colour normalisation of the entire slide image and tumour cell detection. Step 2 involved creating a density map to identify the regions with the highest tumour density. Density maps were used to select the region of interest (ROI), and three annotation areas of 2000 by 2000 pixels each were made. Step 3: After nuclear annotations and object classifier training, segmented nuclei were divided into nuclei related to tumours and immune cells. Step 4: The Delaunay 2D spatial function was used to calculate the internuclear distance. Step 5: The nuclear/cell ratio was calculated, and cells were detected using the Cellpose plugin. The variance of morphometric characteristics inside each annotated ROI within the same tumour was used to measure intra-tumour heterogeneity. 215

Figure 5.3: A graph summarising different visually assessed features of tumour cell patterns (left panel) and architecture (right panel) 218

Figure 5.4: Screenshots from HER2-morphometric signature web tool 223

Figure 5.5: Box plot chart summarising the correlation between the significant morphometric features in the discovery cohort and different HER2 classes 234

Figure 5.6:Box plot showing the correlation between the preidentified morphometric features and PAM50 HER2-enriched molecular subtype in the test cohort 236

Figure 5.7: A heatmap showing how cases in the discovery and test cohorts were grouped hierarchically based on HER2-driven morphometric characteristics. A: The morphometric features allowed for a distinct separation of HER2 positive and negative. B: The panel shows the same cohort split up by ER status and HER2 IHC score. When compared to other classes, HER2 IHC3+/ER-negative tumours had a much higher enrichment of morphometric characteristics. C: Shows how the instances are grouped according to the morphometric feature's summed means for each class. Similar to HER2 oncogenic signalling genes (E), HER2-driven morphometric

characteristics in the test cohort effectively segregated the PAM50 molecular subtype into HER2-E and non-HER2-E (D). 237

Figure 5.8: A correlation matrix demonstrates the correlation between the significant HER2 morphometric features and tumour clinicopathological parameters (A) and both *ERBB2* mRNA and *ESR1* mRNA expression levels in HER2-positive tumours (B). * Represents significant p value<0.05, ** when p value <0.01. 239

Figure 5.9: Pie chart summarising the distribution of the visually assessed features between HER2 + and HER2-negative tumours. HER2-positive tumours are significantly associated with nested tumour architecture (A), hepatoid like cellular pattern (B) with pale eosinophilic cytoplasm (C) and distinct cell membrane (D). Within HER2-positive tumours, a significant difference was also seen in the visually assessed features between ER- and ER+ cases. HER2+: HER2-positive; HER2-: HER2-negative, ER-:ER-negative; ER+: ER-positive 240

Figure 5.10: Box blot chart demonstrating intratumor heterogeneity represented by feature variance among annotated areas in HER2+ cases adjusted for ER status. HER2+: HER2-positive; ER-positive: Oestrogen receptor-positive; ER-: ER-negative..... 242

Figure 5.11: HER2 morphometric signature component and its performance. The receiver operator characteristics curves (ROC) highlight the signature accuracy in the cross validation and external test cohort. AUC: Area under the curve. 243

Figure 5.12: A graph demonstrating the performance and clinical significance of HER2 morphometric signature. A: Receiver-operator characteristics curve comparing between HER2 morphometric signature and *ERBB2* mRNA in the prediction of HER2-E subtype. B, D: Kaplan Meier curve showing better response of HER2 morphometric signature positive patients to anati-HER2 therapy with prolonged distant metastasis-free survival in discovery and test cohorts, respectively. While in non-treated HER2 morphometric signature-positive tumours had a higher frequency of distant metastasis (C)..... 244

Figure 5.13: HER2 risk of recurrence prognostic index. A: A bar chart demonstrating the average accuracy of each prognostic index in the test cohort. B: A time-dependent ROC curve highlighting the AUC of each index at a given time point. Both charts show that “morphometric features +ER &PR status “is the most accurate index. 246

Figure 5.14: Graphical illustration summarising our study 252

Figure 6.1: Schematic illustration of different cohorts used for this study. Cases with HER2 status only (positive/negative) and without HER2 IHC score and/or *HER2* gene amplification status were excluded from the study. 260

Figure 6.2: Graphical chart illustrating the distribution of PAM50 intrinsic molecular subtypes among HER2 IHC scores (A). Correlation between HER2-E molecular subtype in PAM 50 molecular subtype among HER2-positive classes and HER2/CEP17 ratio (B), HER2 gene copy number (C) and HER2 protein expression level (D). U: value of Mann Whitney test. ... 272

Figure 6.3: Bar chart describing the difference in pCR between HER2 IHC 3+ and 2+/Amplified based on different levels of HER2 gene amplification. ... 273

Figure 6.4: Bar chart describing the difference in pCR between HER2 IHC 3+ and 2+/Amplified based on ER status and type of therapy. 273

Figure 6.5: Forest plot of multivariate regression model demonstrating independent predictors of pathologic complete response between HER2 IHC 3+ and IHC 2+/Amplified. Significance value $p<0.05$. 275

Figure 6.6: Kaplan-Meier curves showing differences in breast cancer-specific survival in HER2-positive BC patients upon administration of adjuvant anti-HER2 therapy. HER2 IHC 3+ patients who did not receive adjuvant anti-HER2 therapy have significantly worse survival compared to patients with HER2 IHC 2+/Amplified tumours (left side). No such difference between both HER2 + positive classes was detected upon treatment with anti-HER2 therapy (right side)..... 276

Figure 6.7: Survival curves showing differences in breast cancer and distant metastasis free survivals in HER2-positive BC patients upon administration of adjuvant anti-HER2 therapy. I: Kaplan-Meier curves showing the effect of addition of anti-HER2 to chemotherapy in adjuvant settings among HER2 IHC3+ patients and IHC 2+/Amplified (II). The impact of ER status on response to adjuvant anti-HER2 therapy within each group is also illustrated. 280

Figure 6.8: An illustrated diagram summarising the workflow that was carried out to identify the differential expression of HER2 oncogenic signalling pathway genes between HER2-positive IHC classes. A: The row data was extracted from GEO dataset and the bioinformatics analysis was carried out to identify genes responsible for HER2 oncogenic pathway and response to therapy. B: The mean values of the normalised reads of HER2 signalling genes were significantly enriched in HER2 IHC 3+ tumours compared to HER2 IHC 2+ tumours regardless of the amplification status. C, D: Unsupervised clustering analysis and heatmap illustrating the expression of HER2 oncogenic pathway genes among HER2-positive classes. 281

Figure 6.9: Venn diagram illustrating the intersection between trastuzumab-resistance genes in their differential expression in HER2-positive subclasses in both TCGA and METABRIC cohorts. 284

Figure 6.10: Genes identified as predictive of poor response to anti-HER2 therapy in HER2 IHC2+/Amplified breast cancer. 285

Figure 6.11: An illustrated diagram features two parts. A: presents a heatmap displaying the clustering and distribution of ER signalling genes among HER2-positive IHC 3+ and 2+/Amplified classes, with notable expression in the IHC 2+/Amplified group (p=0.008). B: demonstrates the role of ER positivity in these classes: HER2 IHC 3+ cases primarily rely on HER2-driven oncogenic signalling, where the response to therapy depends on HER2 pathway inhibition. In contrast, ER-positive/HER2 IHC 2+/Amplified cases involve ER pathways, influencing therapy response. 288

Figure 7.1: Illustration of the transcription association complex. The complex is made up of a number of components, including the enzyme RNA polymerase II (Pol II), TATA Box binding protein (TBP), transcription factor II A (TFIIA), transcription factor II B (TFIIB), transcription factor II D (TFIID), and other general transcription factors (TFIIF, TFIIE, TFIIH). Created by Biorender.com..... 299

Figure 7.2: Summary of mechanism of action of BCAT1 in breast cancer. BCAT inhibits the phosphorylation of ERK and upregulates the levels of transcription factors FOXO3a and Nrf2 during the development of BC. BCAT1 also activates the PI3K/AKT axis by stimulating the IGF-1R signalling pathway, while downregulating the RAS/ERK pathway. In addition, BCAT1 also activates mTOR signalling and the expression of PGC-1α, NRF-1, TFAM and β-F1-ATPase, all of which can promote the proliferation, migration and invasion of BC cells. “+” means promotion, “-” means inhibition. [594] 301

Figure 7.3: Graph showing validation of antibody specificity. A: IHC staining of TAF10 on TMA section. B: IHC staining of TAF10 after incubation with TAF 10 antigen (peptide blocking) of the same TMA section revealed no staining of the antibody. C: WB showing protein expression of BCAT1 antibody at the expected molecular weight (~43kDa) (right) and B-actin was used as a positive control (left). 310

Figure 7.4: Boxplot charts illustrating *TAF10* mRNA expression in normal breast versus cancer tissue (A) and its association with tumour clinicopathologic parameters in the combined multicentric cohort. 312

Figure 7.5: Boxplot charts illustrating *BCAT1* mRNA expression illustrating *TAF10* mRNA expression in normal breast versus cancer tissue (A) and its association with tumour clinicopathologic parameters in the combined multicentric cohort..... 313

Figure 7.6: Boxplot illustrating the correlation between *TAF10* mRNA and breast cancer hormonal receptor and HER2 status from the combined multicentric transcriptomic cohorts..... 317

Figure 7.7: Box plot illustrating TAF10 mRNA expression among molecular integrative clusters in METABRIC cohort. Cluster 5, which represents the HER2-positive cluster, shows a significantly high *TAF10* mRNA expression compared with other clusters. IntClustMemb: integrative cluster membership. 318

Figure 7.8: Box plot illustrating the association between *TAF10* mRNA and BC molecular subtypes from the combined multicentric cohorts. The graph shows different molecular subtyping platforms, including both DNA microarray (left) and RNA-seq (right) data. 320

Figure 7.9: Boxplot illustrating the correlation between *BCAT1* mRNA and breast cancer hormonal receptor and HER2 status from the combined multicentric cohorts. 320

Figure 7.10: Box plot illustrating the association between *BCAT1* mRNA and BC molecular subtypes from the combined multicentric cohorts. A significant association is found in HER2-E and basal-like subtypes compared to other luminal and normal-like subtypes. 322

Figure 7.11: Kaplan Meier curves showing the prognostic significance of high *TAF10* mRNA level in patient outcomes in the METABEIC cohort, TCGA cohort and multicentric combined cohort. OS: overall survival 323

Figure 7.12: Kaplan Meier curves showing the prognostic significance of *TAF10* mRNA level in different molecular subtypes in the METABRIC cohort. 324

Figure 7.13: Kaplan Meier curves showing the prognostic significance of *TAF10* mRNA level in different molecular subtypes in the TCGA cohort. .. 325

Figure 7.14: Kaplan Meier curves showing the prognostic significance of *TAF10* mRNA level in different molecular subtypes in the combined multicentric cohort. OS: overall survival. HER2-E: HER2 enriched 326

Figure 7.15: Forest plot demonstrating multivariate Cox regression analysis of factors affecting BCSS. *TAF10* mRNA was an independent predictor of

better patients survival when adjusted for other tumour clinicopathologic parameters both in METABRIC and TCGA cohort..... 327

Figure 7.16: Kaplan Meier curves showing the prognostic significance of high *BCAT1* mRNA level in patient outcomes in the METABEIC cohort, TCGA cohort and multicentric combined cohort. OS: overall survival..... 328

Figure 7.17: Kaplan Meier curves showing the prognostic significance of *BCAT1* mRNA level in different molecular subtypes in the METABRIC cohort. 329

Figure 7.18: Kaplan Meier curves showing the prognostic significance of *BCAT1* mRNA level in different molecular subtypes in the combined multicentric cohort..... 330

Figure 7.19: Immunohistochemical expression of TAF10 protein in breast cancer TMA sections. Nuclear intensity varied from mild (A) to moderate (B) and strong (C). High power scale bar=50 um. TAF10 also showed cytoplasmic expression. 333

Figure 7.20: Immunohistochemical expression of BCAT1 protein in breast cancer TMA sections. Cytoplasmic intensity varied from mild (A) to moderate (B) and strong (C). The scale bar for the TMA image is 100um, and 50 um.for the high power image..... 334

Figure 7.21: Kaplan Meier curve showing the association between TAF10 protein expression and patient outcomes in the Nottingham cohort..... 337

Figure 7.22: Forest plot demonstrating multivariate Cox regression analysis of TAF10 protein expression in predicting patients' survival when adjusted for other tumour clinicopathologic parameters in the Nottingham cohort. 338

Figure 7.23: Kaplan Meier curve showing the association between BCAT1 protein expression and patient outcomes in the Nottingham cohort. Dichotomising the cohort by ER status revealed better stratification of patients outcomes..... 339

Figure 7.24: Charts showing the predictive role of TAF10 in HER2-positive breast cancer. A, B: Boxplot charts showing the association between *TAF10* mRNA level and relapse-free survival in HER2-positive patients with and without anti-HER2 therapy. C-F: Kaplan Meier curves illustrating the correlation between TAF10 nuclear expression and response to treatment. In chemotherapy only treated cohort, high TAF10 protein levels had no predictive role (C, E). While in patients who received anti-HER2-therapy high TAF 10 nuclear expression is associated with better DMFS and BCSS (D, F). 342

Figure 7.25: Forest plot demonstrating multivariate Cox regression analysis of factors predicting response in patients treated with anti-HER2 therapy. TAF10 protein expression was an independent predictor of prolonged DMFS when adjusted for other tumour clinicopathologic parameters in the Nottingham cohort..... 343

Figure 7.26: Kaplan Meier curves demonstrating the role of BACT1 expression in response to anti-HER2 therapy..... 343

Figure 7.27: Forest plot demonstrating multivariate Cox regression analysis of factors predicting response in patients treated with anti-HER2 therapy. BCAT1 protein expression was an independent predictor of short DMFS when adjusted for other tumour clinicopathologic parameters in the Nottingham cohort..... 344

Figure 7.28: A correlation matrix displaying the relationships between the *BCAT1* and *TAF10* genes with other genes in the PI3K/AKT/mTOR pathway and the HER2 amplicon from TCGA cohort. Significant negative correlations are indicated in red, while significant positive correlations are shown in blue. The size of each circle represents the Spearman correlation coefficient (r), with larger circles indicating stronger correlations. Genes without significant correlations are not represented by circles. 345

Figure 8.1: Flow chart of the cohort used in the study. RT-qPCR: reverse transcriptase quantitative polymerase chain reaction 362

Figure 8.2: Graph describing the correlation between each *ERBB2* mRNA and HER2 gene amplification with HER2 IHC score and molecular class. CISH: Chromogenic in situ hybridisation, HER2-E: HER2 enriched, HER2+: HER2-positive 364

Figure 8.3: Alluvial plot demonstrating the difference in the distribution of molecular subtypes between IHC-based and MammaTyper®-based molecular subtyping. HER2-E: HER2 enriched, TNBC: triple negative breast cancer 368

Figure 8.4: Alluvial plot of HER2 IHC and *ERBB2* mRNA categories. Alluvial plot showing re-categorisation of HER2 IHC scores by MammaTyper® assay. IHC; Immunohistochemistry, ISH; insitu hybridisation. IHC: Immunohistochemistry; ISH: In situ hybridisation..... 370

Figure 8.5: Kaplan Meier curves showing the difference between MammaTyper®- defined *ERBB2*-positivity and IHC-defined HER2 positivity in predicting patients' response to therapy. BCSS: Breast cancer specific survival, TTDM: time to distant metastasis, IHC: immunohistochemistry ... 373

Figure 8.6: Kaplan Meier curves showing the absence of significant difference in the survival outcomes of MammaTyper®-defined *ERBB2*-negative patients upon the addition of anti-HER2 therapy to chemotherapy. 374

Figure 8.7: Kaplan Meier curves demonstrating response to trastuzumab based therapy in *ERBB2*-positive tumours according to oestrogen receptor status. 374

Figure 8.8: Kaplan Meier curves showing the difference in response of HER2-Enriched subtype between MammaTyper® and IHC-based molecular classification..... 375

Figure 8.9: Forest plot demonstrating the difference between MammaTyper® / IHC-based definition of HER2 positivity and response to trastuzumab-based represented in 5 years disease-free survival (DFS) and breast cancer-

specific survival (BCSS). LVI: lymphovascular invasion; LN: lymph node status; ER: oestrogen receptor 376

Figure 8.10: Correlation between biomarker protein expression and mRNA level. The top panel represents the correlation coefficient between *ESR1* mRNA and ER IHC percentage (A) and H score (B). C: is a violin plot representing the correlation between *ESR1* mRNA and ER status. The lower panel is the same for *PGR* mRNA and PR IHC protein expression. 377

Figure 9.1: Flowchart summarising cohort selection and different steps carried out 397

Figure 9.2: Box blot showing different patterns of HER2 expression in HER2-Low category with their median, minimum and maximum values. 404

Figure 9.3: A: Box plot demonstrating distribution of HER2 mRNA among HER2 IHC scores. B: Distribution of HER2 IHC scores in the original clinical sore and our score according to refined criteria. 405

Figure 9.4: Graph showing artificial neural network model prediction of HER2 IHC1+ cut off points. A: Sensitivity analysis curves showing the contribution of each factor to the model and its relation to HER2 1+ cluster. B: Faint complete staining of ≥20% of tumour cells; C: Faint incomplete staining of ≥20%; D: Weak complete staining in ≤10%; E: Weak incomplete staining in >10%, F: Moderate incomplete in ≤10% of tumour cells 407

Figure 9.5: Schematic illustration of different scenarios of HER2 expression in breast cancer and the corresponding score from different existing guidelines. 408

Figure 9.6: Recommended HER2 scoring algorithm based on immunohistochemistry-stained slides 408

Figure 9.7: An illustrated diagram and photomicrographs showing different HER2 membranous staining patterns and intensities; Faint complete (1, A), Faint incomplete (2, B), Weak complete (3, C), Weak incomplete (4, D), Moderate complete (5, E), Moderate incomplete (6, F)..... 409

Figure 9.8: Graphical description highlighting degree of Intratumoral heterogeneity within HER2-Low category. A: HER2 IHC stained slide showing different staining intensities within the same tumour; B: Pie chart showing that 60% of HER2 1+ cases were scored based on heterogenous mixed expression patterns, while only 40% were scored based on single homogenous staining. Moderate staining was present in addition to other staining patterns and not alone in HER2 1+ category. Sparklines show multiple combinations of heterogenous patterns in example of HER2 score 1+ (C) and another example of HER2 score 2+ (D). 410

Figure 9.9: Chart illustrating which HER2 score is more accurate in predicting score 1+ based on the true positive and false positive rates obtained from receiver operator characteristics(ROC)- area under the curve (AUC)..... 411

Figure 9.10: Graphs showing relation between *ERBB2* RNA level, HER2 protein level in the form of IHC expression and HER2 gene copy number. A: *ERBB2* RNA level significantly correlates with HER2 IHC scores (0-3+) and HER2-Low cases, B. Positive linear correlation between *ERBB2* RNA level and HER2 gene copy number in all HER2 scores and in HER2-Low cases as shown in C and D, respectively..... 416

Figure 9.11: Box plot chart showing the significant correlation between HER2 RNA level and HER2 IHC score in TCGA cohort. A: ALL HER2 IHC scores from (0-3+), while B shows HER2-Low cases only 416

Figure 10.1: Flowchart summarising cohorts enrolled in the study 431

Figure 10.2: A graph illustrating the relation between *ERBB2*, *ESR1* and oestrogen receptor expression in HER2-Low tumours. A: A scatterplot matrix demonstrating the significant positive correlation between *ERBB2* and *ESR1* mRNA levels, The bottom left corner shows the pairwise combination for *ERBB2* and *ESR1* levels in the analysed dataset. B: Box plot showing the correlation between ER H score and HER2 classes. The highest ER H score is in HER2-Low tumours. 443

Figure 10.3: Kaplan Meier's curve showing differences in breast cancer specific survival (BCSS) and distant metastasis-free survival (DMFS) between HER2-Low and HER2-negative generally (A&B) and stratified by hormone receptor (HR) status. C&D: No significant difference in patients survival between HER2 Low and HER2-negative in HR positive tumours: E&F: HER2-Low patients had significant improved outcome than HER2-negative in HR negative tumours. 445

Figure 10.4: Illustrated graph showing differential expression of HER2 oncogenic signalling pathway genes between HER2 -, HER2-Low and HER2-positive breast cancer. A, B: Unsupervised clustering for the normalised values of HER2 oncogenic signalling pathway genes among the 3 HER2 categories. It reveals that no significant difference in the expression of HER2 signalling genes (arrow) between HER2-negative and HER2-Low and both classes are considered as one cluster in the principal component analysis (PCA) (B). C: Heatmap showing the expression of the mean values of HER2 oncogenic signalling pathway genes which is highly enriched in HER2-positive, while no difference between HER2-negative and HER2-Low. D: Violin plot illustrating the non-significant difference between HER2 oncogenic signalling pathway genes between HER2-negative and HER2-Low 449

Figure 10.5: Distribution of PAM50 molecular subtypes and triple-negative breast cancer molecular subtypes between HER2 categories stratified by hormonal receptor status. A: Differences between HER2 categories regarding PAM50 intrinsic molecular subtype. B, C: Heatmaps illustrating the clustering of PAM50 gene expression among HER2 categories stratified by hormone receptor (HR) status. D: A correlogram summarising the distribution of TNBC molecular subtypes between HER2-Low (left) and HER2-negative (right). The luminal Androgen subtype (LAR) is more predominant in HER2-Low cases compared to HER2-negative, where other triple-negative breast cancer (TNBC) subtypes are most dominant. E: Volcano plot showing differentially expressed genes between HR-/HER2-Low versus HR-/HER2-negative BC. Blue dots stand for significantly upregulated genes in HR-/HER2-Low tumours, while orange dots stand for significantly downregulated

genes. Luminal Androgen-like genes are highlighted. BL1: Basal-like 1, BL2: Basal-like 2, IM: Immunomodulatory, M, MSL: Mesenchymal, Mesenchymal stem-like 451

Figure 10.6: Kaplan Meier curve illustrating Tumours infiltrating lymphocytes (TILs) score and patients outcome in (A) HER2-negative and B (HER2-Low) reveals that high TILs score is associated with improved patients DMFS in HER2-negative tumours compared to others of HER2 Low breast cancer. 456

Figure 10.7: Immunophenotyping of HR-/ HER2-Low (A) and HR-/HER2-negative breast cancer (B) using CIBERSORT analysis. C: Unsupervised clustering between HER2-Low and HER2-negative immunophenotypes. D: Volcano plot showing the distribution of significant immunophenotypes within each HER2 class. Red dots refer to immunophenotypes significantly enriched in HER2 Low BC, while blue dots refer to immunophenotypes significantly enriched in HER2-negative BC. Black dots refer to non-significant immunophenotypes..... 459

Figure 10.8: Bioinformatics analysis carried out in HR-/HER2 Low BC cases. A: Venn diagram of genes overlapping upregulated genes between TCGA and Nottingham cohort A3. B: KEGG pathways enriched in HR-/HER2-negative BC against HR-/HER2-Low, significant upregulated pathways in HR-/HER2-Low are presented in deep orange with FDR <0.05. C: Diagram illustrating gene ontology (Molecular function (MF), Cellular component (CC) and biological processes (BP)) of the upregulated genes in HR-/HER2-Low BC. D: Protein-protein interaction HUB genes of upregulated genes in HR-/HER2-Low with their rank, log2 fold changes and adj p value. Red colour means high rank with most significant adj p value. FDR: The False Discovery Rate, GO: Gene-ontology 461

Figure 10.9: Diagram illustration bioinformatics analysis carried out between HR-positive/HER2-Low and HR-positive/HER2-negative BC cases. A: Volcano plot showing differentially expressed genes between HR-positive/HER2-Low versus HR-positive/HER2-negative BC. Blue dots represent significantly upregulated genes in HR-positive/HER2-Low tumours,

while orange dots represent significantly downregulated genes. B: Bar chart showing KEGG pathways enriched in HR-positive/HER2-Low BC, no significant pathways were identified (FDR >0.05). C: Diagram illustrating gene ontology (Molecular function (MF), Cellular component (CC) and biological processes (BP)) of the upregulated genes in HR-positive/HER2-Low BC. D: Graph illustrating protein-protein interaction HUB genes of upregulated genes in HR-positive/HER2-Low; red genes have the highest rank, while blue ones have the lowest rank. 463

Figure 10.10: Androgen receptor immunohistochemical expression in HER2-Low tumours A&B while C&D are its expression in and HER2-negative BC. 464

Figure 10.11: Boxplot summarising the expression of AR among HER2 classes with the highest expression in HER2-Low category (A). B: Difference in AR expression between HER2-negative and HER2-Low in ER-positive and ER-negative (C) tumours 465

Figure 10.12: Chart summarising the workflow of this study..... 474

Chapter 1. General Introduction

1.1 Breast cancer mortality and incidence

Breast cancer (BC) is a significant global health concern, and its incidence has surged in recent years [1]. It is the most prevalent cancer in women and the fifth leading cause of cancer mortality worldwide [2]. BC is the most frequently diagnosed cancer in women worldwide, with 2.26 million new cases in 2020 and a second leading cause of cancer death in women worldwide, responsible for 684,996 deaths [2, 3]. In the UK, BC remains a prevalent health concern, with approximately 55,900 newly diagnosed cases reported annually, according to Cancer Research UK.

1.2 Risk factors of BC

1.2.1 Aging

Besides sex, ageing is one of the most important risk factors of BC because the incidence of BC is highly related to increasing age. In 2016, approximately 99.3% and 71.2% of all BC-associated deaths in America were reported in women over the age of 40 and 60, respectively [4]. Therefore, it is necessary to have a mammography screening ahead of time in women aged 40 or older.

1.2.2 Family History

Nearly a quarter of all BC cases are related to family history [5]. Women whose mother or sister has a BC are prone to this disease. A cohort study of over 113,000 women in the UK demonstrated that women with one first-degree relative with BC have a 1.75-fold higher risk of developing this disease than women without any affected relatives. Moreover, the risk becomes 2.5-fold or

higher in women with two or more first-degree relatives with BC [5]. The inherited susceptibility to BC is partially attributed to the mutations of BC-related genes such as BRCA1 and BRCA2.

1.2.3 Reproductive factors

Reproductive factors such as early menarche, late menopause, late age at first pregnancy and low parity can increase the BC risk. Each 1-year delay in menopause increases the risk of BC by 3%. Each 1-year delay in menarche or each additional birth decreases the risk of BC by 5% or 10%, respectively [6-8]. Reproductive factors are strongly associated with the oestrogen receptor (ER) status, with differences in the odds ratios (OR) between ER-positive and ER-negative BC for parity (OR: 0.7 vs 0.9 for ≥ three births vs nulliparae) and age at the first birth (OR: 1.6 vs 1.2 for age ≥30 vs <25 years) [9].

1.2.4 Oestrogen exposure

Both endogenous and exogenous oestrogens are associated with the risk of BC. The endogenous oestrogen is usually produced by the ovary in premenopausal women, and ovariectomy can reduce the risk of BC [10]. The main sources of exogenous oestrogen are oral contraceptives and hormone replacement therapy (HRT). Oral contraceptives have been widely used since the 1960s, and the formulations have been upgraded to reduce side effects. However, the OR is still higher than 1.5 for African American women and Iranian populations [11, 12]. Nevertheless, oral contraceptives do not increase the risk of BC in women who stop to use them for more than ten years [6].

1.2.5 Lifestyle

Alcohol consumption has been associated with an elevated risk of developing BC. According to the International Agency for Research on Cancer (IARC), the risk of developing BC can increase by up to 10% in women who have a daily intake of 10g of alcohol [13]. In addition, there is an association between excessive alcohol intake and increased breast density in mammogram images [14]. Cigarette smoking is another risk associated with BC. Long-term active smokers are more likely to develop cancer than women who are exposed to passive smoking. However, those who have never smoked or been exposed to passive smoking have a lower risk of developing BC [15]. A higher incidence of developing BC is also correlated with being overweight, particularly in postmenopausal women. Those with a Body Mass Index (BMI) >25 who are overweight or obese are 1.3 times more likely to develop cancer than women in the normal weight range [16]. In addition to the status of insulin resistance and hyperinsulinemia, which is an independent risk of BC in postmenopausal women, the association between obesity and BC can be attributed to the aromatase-driven oestrogen synthesis in adipose tissue [17, 18]. Contrarily, regular physical exercise is a factor that can greatly lower the risk of BC development [19].

1.2.6 Genetic Inheritance

Five to ten per cent of cancers are thought to be caused by gene mutations, with *BRCA1* or *BRCA2* DNA repair genes accounting for two-thirds of hereditary cancer cases [20]. Compared to the general population, those who carry these mutations are at increased risk of developing BC, with a lifetime risk of

the illness estimated to be greater than 80% [21]. Early onset BC caused by mutated BRCA1 and BRCA2 BCs usually affects both breasts [22]. Other gene mutations, though less frequent, are also linked to a higher risk of developing BC. These include mutated versions of *TP53*, *ATM*, *PTEN*, *CHEK2*, *CDH1*, *STK11*, and *BALB2*. People with these gene alterations are also more prone to other hereditary illnesses and malignancies [23] (**Table 1.1**).

1.2.7 Other breast lesions

Women with dense breasts on mammograms have a 1.5 times higher risk of developing BC than women with less dense breasts [24, 25]. There may be a slight correlation between the presence of non-proliferative lesions, including simple cysts, fibrosis, moderate hyperplasia, and adenosis with the development of BC [26, 27]. Some proliferative lesions without atypia, such as fibroadenoma, papillomatosis, and sclerosing adenosis, are also associated with a minor increase in the incidence of BC. However, the risk is five times higher in women with atypical proliferative lesions, such as atypical ductal hyperplasia (ADH) and atypical lobular hyperplasia (ALH) [28, 29]. Women who have unilateral BC also have a higher risk of developing the disease in the contralateral breast or another area of the affected breast [30].

Table 1.1: Additional genes associated with breast cancer [31]

Gene	Location	Function	Abnormality in Breast cancer
TP53	17p13.1	Tumour suppressor gene	Mutations in 30% of BCs
NME1	17q21.3	Metastatic suppressor gene	SNP of NME1 gene associated with higher BC-specific mortality (HR=1.4) and patients with an early-stage cancer (HR=1.7)
RB1	13q14.2	Tumour suppressor gene	Rb1 inactivation in 20-35% of BCs
PTEN	10q23.3	Tumour suppressor gene	Loss of PTEN protein expression in up to 33%of BCs
ATM	11q22-q23	Tumour suppressor gene	Mutation of ATM increases the risk of 2-to 3-fold in general, and 5-to 9- fold in women under 50 years of age
CDH1 **(E-Cadherin)**	16q22.1	Tumour suppressor gene	Inactivation of CDH1 in 85% of lobular breast carcinomas
FHIT	3p14.2	Putative tumour suppressor gene	The rate of FHIT hypermethylation in BC was 8.4-fold higher than that in normal breast tissues
Maspin	18q21.33	Tumour suppressor gene	Expression of Maspin in 20-80% invasive BC
PIK3CA	3q26.3	Oncogene	Mutations in 37% of the HR+/HER2−metastatic and 40% of early BC
CCND**1 (Cyclin D1)**	11q13	Oncogene	Overexpression in 50% of breast tumours

TP53: Tumour Protein p53**, NME1:** NME/NM23 Nucleoside Diphosphate Kinase 1**, RB1:** Retinoblastoma 1**, PTEN:** Phosphatase and Tensin Homolog**, ATM:** Ataxia Telangiectasia Mutated**, FHIT:** Fragile Histidine Triad**, Maspin:** Mammary Serine Protease Inhibitor**, PIK3CA:** Phosphatidylinositol-4,5-Bisphosphate 3-Kinase Catalytic Subunit Alpha**, SNP**: Single Nucleotide Polymorphism; **HR**: Hazard Ratio; **HR+**: hormone receptor-positive; **HER2**: human epidermal growth factor receptor 2

1.3 Pathogenesis of BC

Breast tissue has the potential to give rise to a wide variety of diseases, both benign and malignant. The ducts are where these lesions are found in the majority of cases (70–80%), however they can also appear in the lobules. (10-15%) or in the tissue in between [32]. Abnormal cell division or hyperplasia can lead to the development of either ductal or lobular hyperplasia, both of which

have the chance of progressing to pre-invasive lesions known as ductal carcinoma in situ (DCIS) or lobular carcinoma in situ (LCIS) [33, 34]. There is a high probability that in situ lesions may invade the myoepithelial layer as well as the basement membrane, which will ultimately result in the development of invasive BC. Malignant transformation is, mediated by extremely complex systems. These mechanisms cause severe cytological or architectural dysplastic changes and encourage cells to evade the mechanisms that control their viability, proliferation, and migration. These potentially malignant alterations are accompanied by a group of multistage processes that are referred to as the hallmarks of cancer (**Figure 1.1)**. Among these are the maintenance of proliferative signalling, the avoidance of growth suppressors, the prevention of cell death, the promotion of replicative immortality, the induction of angiogenesis, and the activation of invasion and metastasis [35]. Cancer cells possess a fundamental characteristic of sustained proliferation, which distinguishes them from normal cells. Unlike normal tissues that carefully regulate the production and release of growth-promoting signals to maintain a balance in cell growth and division, cancer cells have this regulation disrupted. This deregulation is often driven by the aberrant activity of growth factors that bind to specific receptors on the cell surface, typically with intracellular tyrosine kinase domains. These receptors initiate signalling pathways within the cell that regulate cell cycle progression, cell growth, and other cellular processes such as survival and energy metabolism. By subverting these signalling pathways, cancer cells gain the ability to grow and divide uncontrollably, leading to the development and progression of cancer [36]. Inactivation of tumour suppressor genes

and/or activation of oncogenes are also major contributors to the malignant transformation of nor mal cells.

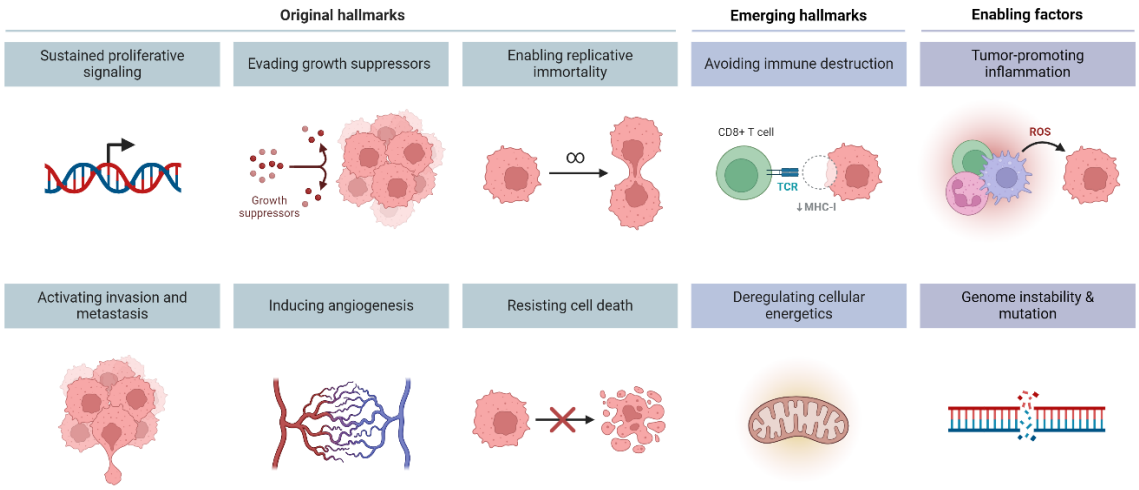


Figure 1.1: The hallmarks of cancer, which represent alterations that take place in cell physiology during the malignant transformation. Created with BioRender.com

Cancer stem cells (CSCs) are assumed to be responsible for the genesis and development of tumours, including BC. Two different explanations have been proposed to explain where these cells came from. The first hypothesis postulates that CSCs originate from the regular mammary cell hierarchy, whereas the second hypothesis postulates that these cells originate from the normal mammary stem cells (MaSCs) [37]. Two hypothetical theories for BC initiation and progression have been settled so far: the cancer stem cell theory and the stochastic theory [33, 38]. The cancer stem cell theory proposes that all tumour subtypes are derived from the same stem cells or transit-amplifying cells (progenitor cells). Acquired genetic and epigenetic mutations in stem cells or progenitor cells will lead to different tumour phenotypes **(Figure 1.2A).** While the stochastic theory suggests that each tumour subtype is initiated from a single

cell type (stem cell, progenitor cell, or differentiated cell) **(Figure 1.2B*).*** Random mutations can gradually accumulate in any breast cells, leading to their transformation into tumour cells when adequate mutations have accumulated. Although both theories are supported by plenty of data, neither can fully explain the origin of human BC [31].

It is important to emphasise the fact that these processes will give rise to a disease that can be classified into several distinct subtypes and that each subtype will exhibit clinical and genotypic characteristics that are quite dissimilar. It is of the utmost significance to differentiate between these subtypes since they each have distinct consequences with regard to prognosis and therapy [39].

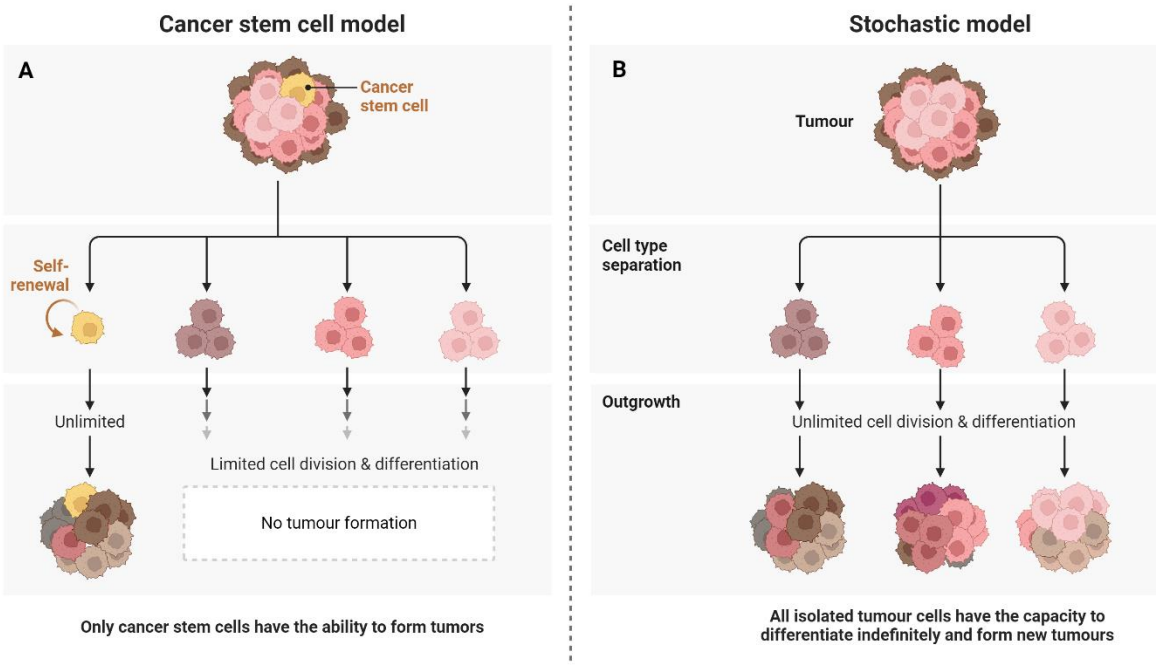


Figure 1.2:Two hypothetical theories of breast cancer initiation and progression. (A) All subtypes of tumours are derived from the same stem cell or progenitor cells. Different tumour phenotypes are then determined by subtype-specific transforming events. (B) Each tumour subtype is initiated from a single cell type (stem cell, progenitor cell, or differentiated cell). Random mutations can gradually accumulate in any breast cells, leading to their transformation into

tumour cells when an adequate number of mutations have accumulated Created by Biorender.com.

1.4 Molecular Classification

BC is recognised as a heterogenous family of diseases with variable presentation, morphology, molecular features, behaviour and response to therapy. With increasing treatment options in the era of precision medicine, the traditional morphological classification (nuclear grade, tubular grade, mitotic index, histological grade, and architectural characteristics), clinicopathological prognostic variables (tumour size, lymph node (LN) involvement, metastasis), and the few well-established molecular predictive markers seem insufficient to reflect such degree of heterogeneity [40].

Thus, many studies focused on analysing the molecular patterns of BC in order to group these tumours into classes or entities to assist in clinical management. Perou, Sorlie and colleagues classified BC molecularly into distinct subgroups based on similarities in gene expression profiles using the cDNA microarray technique [41-43]. The groups of genes responsible mainly for the segregation of the molecular subtypes of BC are genes related to the expression of ER, progesterone receptors (PR), Human epidermal growth factor receptor 2 (HER2), and cell proliferation regulator (Ki-67). The Immunohistochemical (IHC) panel with these four biomarkers (ER/PR/HER2/Ki-67) has been considered efficient and significant in the stratification of these molecular entities [44] **(Table 1.2).** Thus, based on these pioneering studies, BC can be stratified into subtypes with differences in gene expression patterns, reflecting the individual phenotype, disease prognosis and systemic treatment planning [45]. Four clinically relevant molecular subtypes were revealed through comprehensive gene

expression profile studies: Luminal A, Luminal B, HER2-enriched (HER2-E), and Triple Negative (TN) [45].

1.4.1 Luminal A -like Breast cancer

This molecular subtype is the most common and comprises approximately half of newly diagnosed BC cases. According to the last update of St. Gallen in 2016, the immunohistochemical profile of this subtype was defined as ER-positive, with high expression of PR, HER2-negative and low levels of Ki-67 [46]. In addition, these tumours have characteristics of luminal epithelial cells of the breast, such as the high expression of cytokeratin's 7/8/18/19 [47]. They include a wide range of low histological grade variants, such as invasive duct carcinoma-non-special type (IDC-NST), tubular, cribriform, mucinous, and classic invasive lobular carcinoma (ILC) [44, 47]. This subtype has been associated with a highly favourable prognosis, with a more indolent clinical course, and generally shows less LN involvement [48]. Nonetheless, due to the positive status of hormone receptors (HR), patients benefit from endocrine therapies, either with selective ER modulators (tamoxifen) or with aromatase inhibitors (anastrozole) **(Table 1.2)** [49].

1.4.2 Luminal B -like BC

Responsible for approximately 20% to 30% of invasive BC cases [48, 49]. This subtype can be categorised immunophenotypically into luminal B/HER2-negative: ER-positive, PR-negative, HER2-negative and high levels of Ki-67 (≥ 20%); or luminal B/HER2-positive: ER-positive, HER2-positive and any level of PR and Ki-67 [50, 51]. This molecular entity generally presents a moderate histological grade, including most of the IDC-NST and is associated with an

intermediate prognosis, with a greater likelihood of locoregional recurrence when compared to Luminal A [48, 52]. luminal B subtype is understood as the most aggressive form of hormone-dependent BC cases due to increased expression of genes related to cell proliferation, such as Nuclease sensitive element binding protein 1 (*NSEP1*) and *cyclin E1 (CCNE1*), in addition to the activation of certain alternative pathways of growth factors, such as Phosphatidyl inositol 3-Kinase (PI3K) and Proto-oncogene sarcoma (*SRC*) [53].

1.4.3 HER2-Enriched

It represents 15% to 20% of newly diagnosed BC cases [54, 55]. This subtype is characterised by a high expression of HER2, negativity for ER and PR and high expression of Ki-67 (> 20%) [51]. In addition to the immunophenotypic characterisation routinely used to assess the status of HER2 in BC, the Fluorescence in *situ* hybridisation (FISH) technique has also been employed to assess gene amplification [56]. HER2 overexpression has been related to tumours of greater histological grade, high proliferative index and propensities to metastasis, leading to short disease-free survival (DFS) and worse prognosis [32]. However, these tumours may respond well to drugs that block HER2 activity, especially humanised monoclonal antibodies (mAB) and molecular receptor tyrosine kinase inhibitors [45, 57].

1.4.4 Triple negative breast Cancer (TNBC)

This class of tumours constitutes 10% to 20% of all BC cases [58]. This subtype is characterised by the lack of expression of the HRs, and the oncoprotein HER2; moreover, they are highly proliferative tumours, according to the Ki-67 index (> 30%) [51]. Most TN tumours manifest as the IDC-NST histological

type. However, they also include variants of medullary, metaplastic and apocrine carcinomas [32]. These tumours are generally more prevalent in patients with *BRCA1* mutations and young women, with a higher histological grade, risk of loco-regional recurrence, contralateral disease and systemic relapse [59]. Many gene expression profile studies have been carried out to better understand the heterogeneity of this particularly aggressive form of BC. Thus, TN tumours can be further divided into seven other distinct entities, including two basal-like (BL) types (BL1 and BL2), with a basal pattern of gene expression, but showing differences in the immune response; one of the luminal androgen receptor type (LAR), which presents a differential expression of genes involved in androgen metabolism; one of the immunomodulatory type (IM), which presents important changes in the expression of genes involved in immunological signalling pathways; one of the claudin-low types (CL), characterised by the low expression of cellular junction proteins (claudins 3, 4 and 7, in addition to E-cadherin); and two of the mesenchymal type, namely, mesenchymal itself (M) and mesenchymal stem-like (MSL), both with positive regulation of the signalling pathways involved in epithelial mesenchymal transition (EMT), but differing in the signalling of genes associated to stem cells and angiogenic factors [60-62]

Table 1.2: Classification of molecular subtypes of BC and therapies [63]

Molecular Subtype	Luminal A	Luminal B		HER2-Enriched	Triple negative
		HER2-negative	HER2-positive		
Biomarkers	ER-positive PR-positive HER2-negative Ki67 low	ER-positive PR-negative HER2-negative Ki67 high	ER-positive PR-neg/pos HER2-positive Ki67 low/high	ER-negative PR-negative HER2-positive Ki67 high	ER-negative PR-negative HER2-negative Ki67 high
Frequency of cases	40-50%	20-30%		15-20%	10-20%
Histological Grade	Well Differenti-ated (Grade I)	Moderately Differentiated (Grade II)		Less Differentiated (Grade III)	Less Differentiated (Grade III)
Prognosis	Good	Intermediate		Poor	Poor
Response to Thera-pies	Endocrine	Endocrine Chemotherapy	Target therapy Endocrine Chemotherapy	Target therapy Chemotherapy	Chemotherapy PARP inhibitors

1.5 Prognostic and predictive factors in BC

In general, prognostic factors are characteristics of the tumour that can predict a patient's clinical outcome; they assess the risk of mortality, the development of distant metastases, or the recurrence of the disease at the time of the initial diagnosis, while predictive factors include variables that can reveal information about the degree of response to particular treatments. For the purpose of making treatment decisions and enhancing BC patient outcomes, precise prognostic and predictive parameters are essential. The following subsections contain a list of the most common prognostic and predictive variables that are regularly evaluated in pathologic reports of BC.

1.5.1 Prognostic variables

1.5.1.1 Histopathological types

There are several histological subtypes of BC, each with a unique clinical course and outcome. The most prevalent type is IDC, which constitutes a diverse collection of tumours with various morphologies. Approximately 75 per cent of IDC cases are classified as IDC-NST. Additionally, some IDC cases display unique cytoarchitectural characteristics and are categorised as special subtypes, such as tubular, invasive cribriform, mucinous, and medullary-like carcinomas [64]. The second most frequent type is ILC, accounting for 5–15% of all BC cases. ILC also exhibits a variety of histological variants [65]. The prognosis for other types, such as mucinous, tubular, and invasive cribriform carcinomas, is excellent, with survival rates of more than 80% at 10 years. In contrast, solid lobular, IDC-NST, and mixed ductal and lobular carcinomas have lower survival rates, with less than 50% at 10 years [66].

1.5.1.2 Tumour grade

The Nottingham grading system is widely accepted as a standard prognostic system for BC reporting [67, 68]. It assesses the similarity of the tumour to normal breast cells and serves as a predictor of prognosis, reflecting the biological aggressiveness of the tumour [69].

The BC grading system comprises three unique categories, each with three possible scores. The first category is tubule formation, with score 1 indicating the majority of the tumour (greater than 75%), score 2 indicating a moderate degree (between 10% and 75%), and score 3 indicating little or no tubule development (less than 10%). The second factor is nuclear pleomorphism, with score 1 indicating small, regular uniform cells, score 2 indicating a moderate increase in size and variability, and score 3 indicating marked variation. The last factor is mitotic count, with score 1 representing 1-9 mitoses, score 2 representing 10-19 mitoses, and score 3 representing 20 or more mitoses. Evaluating mitotic count is typically done using light microscopy with a field diameter of 0.58 mm, assessing ten high-power fields (HPFs). Mitotic count remains one of the key factors for prognosis in BC patients [70].

The tumour grade is determined by summing the scores of each component. Grade 1 tumours, with a total score of 3-5, are well-differentiated and have the most favourable prognosis. Grade 2 tumours, with a total score of 6 or 7, are moderately differentiated and have an intermediate prognosis. Grade 3 tumours, with a total score of 8 or 9, are poorly differentiated and associated with the poorest prognosis [71].

1.5.1.3 Size of the tumour

Another significant prognostic factor that predicts BC behaviour and patient outcome is tumour size. Invasive BC patients have a higher mortality rate in direct proportion to the size of their tumours, and patients with smaller tumours fare better than those with larger tumours [72].

1.5.1.4 Nodal stage

The presence or absence of axillary LN involvement is the most important prognostic factor for individuals with early-stage BC. Regarding DFS and BC-specific survival (BCSS), the degree of nodal involvement is significantly linked with patient outcomes [73, 74]. LN stage and patient survival are directly correlated, with lower LN stage being associated with longer survival. Additionally, an association between the number of affected axillary nodes and the likelihood of developing distant metastases was established [75]. The pathological staging system is categorised into three groups. 1) LN stage 1, in the absence of any LN involvement; 2) LN stage 2, in the presence of one, two, or three LNs; and 3) LN stage 3, in the presence of three or more LNs [76, 77]. The 5-year survival for patients with LN stage 1 is 83% compared with 73% for patients with LN stage 2 and 46% for patients with LN stage 3, from which the percentage declines to around 28% for patients with ≥13 positive LNs [73]. Nodal metastasis is seen in 30% of patients with tumour sizes less than 2 cm, while it is seen in 70% of patients with breast tumours larger than 5 cm, despite the fact that tumour size and LN stage are independent prognostic variables [78].

1.5.1.5 Nottingham Prognostic Index

The Nottingham Prognosis Index (NPI) is one of the most significant formulas that can improve the prognostic power for BC patients. It was developed on the principle that using a combination of prognostic indicators is more accurate than using a single one [79]. Tumour grade, tumour size, and LN stage are the three most potent prognostic factors used to formulate the NPI. The NPI is categorised into three prognostic groups: good, moderate, and poor. It is calculated using the following formula: NPI = [0.2 × tumour size (in centimetres)] + LN stage (1 to 3) + tumour grade (1 to 3). According to the original NPI grouping, patients are classified as having an excellent NPI if their NPI is less than 3.4, whereas those with NPI values of 3.4-5.4 and >5.4 are categorised as moderate and poor prognostic groups, respectively [79, 80]. An upgrade to the NPI grouping system has been suggested, broadening the prognostic groups from three to six, and they are as follows: excellent prognostic group (EPG) if NPI is 2.08-2.4; good prognostic group (GPG) if NPI is 2.41-3.40; moderate prognostic group 1 (MPG1) if NPI is 3.41-4.40; and moderate prognostic group 2 (MPG2) if NPI is 4.41-5 [80].

1.5.1.6 Lymphovascular invasion

Tumour emboli that are present in the lymphatic spaces and/or blood vessels in the breast tissue around the invasive carcinoma are known as lymphovascular invasion (LVI). LVI can help identify patients who are more likely to develop node-positive disease and experience metastatic events [81, 82]. Additionally, LVI exhibits a direct correlation with BC-related deaths and the emer-

gence of local recurrence [83]. While LVI is considered a standalone prognostic factor in LN-negative patients, its prognostic usefulness in LN-positive patients is still a subject of debate [84].

1.5.1.7 Tumour-infiltrating lymphocytes

Tumour-infiltrating lymphocytes (TILs) assessment is attracting attention as a prognostic marker. High numbers of TILs are associated with better outcome, better response to neoadjuvant therapy in triple-negative and HER2-positive breast carcinomas [85]. TILs counting and scoring is feasible on haematoxylin & eosin (H&E) stained tissue sections during the diagnostic procedure and follows international recommendations. The development of computational pathology methods is likely to make automated counting an option within the next few years [86].

1.5.1.8 Tumour associated stroma (TAS)

Tumour stroma, as an important component of tumour microenvironment (TME), promotes tumour progression through production of various nutrition, growth factors, chemokines, and cytokines [87-89]. Different studies have revealed that the stromal compartment of breast tumours contains more prognostic information than the epithelial component [90]. As a result, the tumour-stromal ratio (TSR), a new parameter that represents the proportion of tumour-associated stroma, was introduced to the field of cancer research [91]. Previous studies have demonstrated that the TSR is a new prognostic factor in different solid tumours [92-95] including BC [96]. Studies have repeatedly shown that the TSR is correlated to clinicopathological parameters and that tumours with a high amount of stroma are associated with a worse prognosis compared

to stroma-low tumours [97]. This resulted in the TSR being identified as a potentially new parameter for routine histological evaluation for patient prognosis.

1.5.2 Predictive (biomarkers) factors

The factors that can be used to predict a patient's response to a particular treatment are known as predictive factors or biomarkers. These are useful in stratifying patients with BC, in order to provide access to optimal management and to avoid the adverse effects associated with over- or under-treatment [98].

1.5.2.1 Hormone receptors

In all cases of BC IHC on paraffin sections is used to routinely evaluate the ER and the PR expression [99]. The American Society of Clinical Oncology/College of American Pathologists (ASCO/CAP) recommendations state that 1% of nuclear staining of any intensity should be used to determine ER and PR positivity in invasive BC [100]. The most accurate predictor for hormone therapy following surgery is the ER status [101]. However, there is ongoing discussion about whether ER-positive patients should receive endocrine therapy for a prolonged period of time [102]. For younger, pre-menopausal individuals, who are typically impacted by aggressive BC phenotypes, ER status provides minimal prognostic information [103]. When ER and PR are co-expressed, the predictive accuracy of the response to adjuvant hormonal therapy increases from 50% in ER-positive/PR-negative patients to 80% in ER-positive/PR-positive patients [104]. Furthermore, negative PR expression in ER-positive tumours may be a surrogate marker of abnormal growth factor signalling that may contribute to endocrine therapy resistance [105].

1.5.2.2 Ki67

Ki67 is a non-histone nuclear cortical protein, present in all active stages of the cell cycle except the G0 phase. This protein molecule is associated with cell growth. Ki67 antigen was first diagnosed in 1983 by Gerdes et al. in the Hodgkin's lymphoma cell line [106]. Ki67 expression varies throughout the cell cycle and peaks during mitosis. While the function of Ki67 is not fully understood, there is evidence of its role in cell division and ribosomal RNA synthesis.

Ki67, along with cell cycle progression and short half-life, is an important and effective biomarker for assessing tumour cell growth. Ki-67 is one of the useful IHC proliferation antigens and has been validated as an independent predictor and prognosis factor in BC [107]. Ki-67 is one of 21 particular genes used in the Oncotype DX assay to predict the risk of recurrence and the advantages of chemotherapy in women with ER-positive, node-negative BC. It is also an important parameter in luminal tumour sub-classification with a good prognosis in luminal A and a worse prognosis in luminal B [108].

Correlations between Ki67 expression, breast density and precancerous lesions have been described [109, 110]. Ki67 has been widely studied as a prognostic biomarker in the BC, proving that Ki-67 overexpression is connected with larger tumour size, higher histological grade, lymphatic involvement, shorter overall survival (OS), and DFS in the BC [111]

1.5.2.3 Circulating Tumour cells

The rapid progress of sequencing technologies has led to new analyses of blood in solid tumours based on circulating tumour cells (CTC) and circulating

tumour DNA (ctDNA). CTCs are rare cancer cells; these cells appear to be involved in tumour progression and are found in the peripheral blood. Many studies have identified CTCs as valuable biomarkers in the prognosis of BC [109]. An increase in the number of CTCs indicates a low probability of survival, and their persistence during treatment is associated with a poor response to treatment. Recent studies on the molecular properties of CTC have provided early evidence that CTC can operate as a genetic substitute for metastatic disease. These findings are important because CTC-based fluid sampling has a unique advantage over solid tumour sampling due to the relative ease of blood sampling and the possibility of serial sampling during the treatment period [112]. A prospective multicentre study (SWOG S0500) [113] has confirmed the superior capability of CTC measurements to predict the survival of patients with metastatic BC (mBC). The utilisation of CTC-based biomarkers to guide treatment is not included in practice due to the need for further technical and clinical validation. Methods for evaluating important biomarkers (e.g., ER and HER2) are not standardized in the CTC.

1.5.2.4 CEA and CA

Serum tumour markers play a significant role in screening, early detection of recurrence, and treatment of many malignancies. Quantitative alterations in serum tumour markers have been expanded as non-invasive instrumentation to assess the effectiveness of treatment in human malignancies [114]. In the BC, three serum tumour marker, CEA, CA-15–3, and CA125, are the most widely used serum tumour markers in the clinical field [115]. CEA is the first tumour antigen studied to be a glycoprotein molecule associated with cell ad-

hesion [116]. Serum CEA levels increase during inflammation or cancer of endodermal tissues, such as the breast, gastrointestinal, and pancreas [117]. CA-15–3 is a glycoprotein from the MUC-1 family whose glycosylation changes have made it a useful tumour marker [118]. Like CA-15–3, CA125 is a product of the MUC1 gene, which is the main regulator of multicellular survival pathways in ovarian and BC cells [119].

Various studies in recent years have shown that preoperative CEA levels along with CA-15–3 levels may supply helpful information for the recognition and treatment of BC [115]. Based on its studies and results, the European Group on Tumour Markers recommended the use of CEA and CA-15–3 levels for prognosis assessment, early detection of disease progression, and monitoring of treatment in patients with BC [120]. However, the prognostic importance of preoperative CA-15–3 and CEA levels in the BC stays controversial and the ASCO not recommend the use of CEA and CA-15–3 in the screening, diagnosis, staging, and monitoring of BC [119].

CEA, CA-15–3, and CA125 are straightly related to aggressive clinicopathological specifications and enhanced preoperative CA-15–3 and CEA negatively influence BC survival and progression among luminal A and basal-like subtypes. Hence, CA-15–3 and CEA may be combined with prognostic variables known for clinical practice in evaluating patient outcomes and directing therapies to pursue a better prognosis and determine individual therapies for patients with different molecular types [119].

1.6 Human Epidermal growth factor receptor 2

1.6.1 History of HER2 receptor

In 1962, Stanley Cohen's discovery of epidermal growth factor (EGF) marked the inception of HER2-targeted therapy, later acknowledged with a Nobel Prize in Physiology or Medicine shared with Rita Levi-Montalcini for their work on growth factors. The mid-1970s saw Harold Varmus and Michael Bishop pioneering the study of oncogenes, establishing a connection between oncogenes and growth factor receptors. In 1983, v-erb-b2 avian erythroblastic leukaemia viral oncogene homolog 2 (v-erbB2), closely related to EGFR, was identified as transforming, leading to the recognition of HER2 as a distinct tyrosine kinase receptor. Subsequent studies unveiled HER2's homology with neu and its association with chromosome 17 [121-126]. Overexpression of HER2 was found to occur in human breast tumours, and HER2 signalling and transforming functions leading to growth were associated with a poor prognosis [127, 128]. This work led the way to the development of a monoclonal antibody to target the HER2 receptor in human BC a humanised mAb to HER2, humAb4D5-8, eventually named trastuzumab or Herceptin [129, 130].

1.6.2 Biology of HER2 receptor

HER2 is an orphan receptor tyrosine kinase and has no ligand. Normal tissues have a low complement of HER2 membrane protein. BCs can have up to 25–50 copies of the HER2 gene, and up to 40–100 fold increase in HER2 protein resulting in 2 million receptors expressed at the tumour cell surface [131]. The differential in HER2 expression between normal tissues and tumours helps to define HER2 as an ideal treatment target.

Overexpression of HER2 protein in BC leads to its heterodimerisation with another family member like HER3 and HER4 or homodimerisation with itself. This activates downstream signalling pathways of EGFR including PI3K, Ras-Raf-MAPK and JNK, to promote cell proliferation, cell invasion, and angiogenesis and to protect cells against apoptosis [53, 132, 133] **(Figure 1.3)**. HER2 has the strongest catalytic kinase activity, and HER2-containing heterodimers have the strongest signalling activity [134-137].

HER2 can also be activated by complexing with other membrane receptors such as insulin-like growth factor receptor I [138]. An aberrant form of HER2 missing the extracellular domain, so-called p95, is found in some BCs [139, 140]. p95 is constitutively active since the external domain of these receptors acts as an inhibitor until it is bound by a ligand. p95 can cause resistance to trastuzumab, an antibody that works by binding to a domain in the external domain of HER2. This domain is missing in p95. p95 is not detected by antibodies that target the external domain of HER2 for the same reason [139, 140].

1.6.3 Detection of HER2

In diagnostic pathology, the HER2 status is routinely assessed by using a combination of IHC to evaluate HER2 protein expression levels and in situ hybridisation (ISH), to assess HER2 gene status, the only two techniques with acknowledged clinical validation [141, 142]. According to new experimental and clinical data, the recommendations for HER2 scoring have changed over the years.

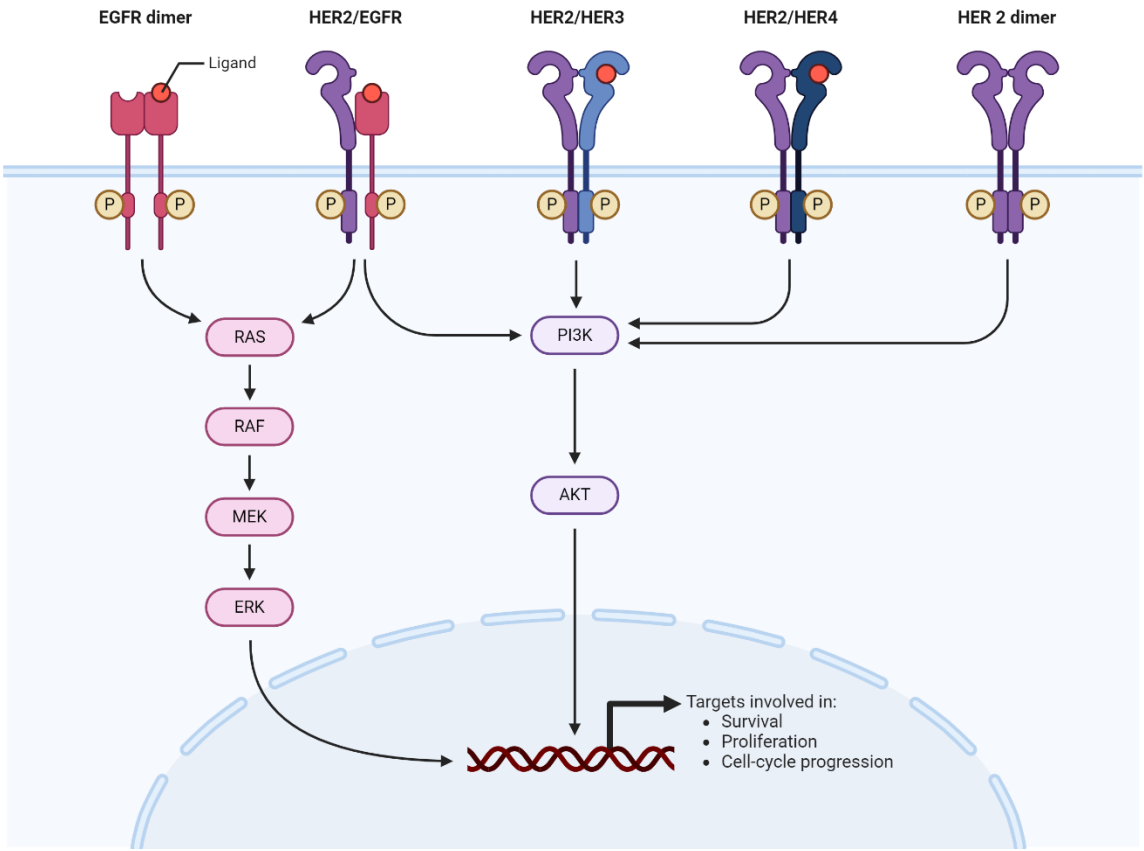


Figure 1.3: HER2 receptor tyrosine kinase signalling pathway, Created with BioRender.com

1.6.3.1 HER2 Immunohistochemistry

Immunohistochemistry detects HER2 protein overexpression using monoclonal or polyclonal antibodies that bind to the protein. Currently in the United States, there are two Food and Drug Administration (FDA) approved methods for HER2 assessment: HerceptTest™ (DAKO, Glostrup Denmark) and HER2/neu (4B5) rabbit monoclonal primary antibody (Ventana, Tucson, Arizona). Accurate HER2 evaluation is determined not only by choice of antibody but also by other determinants such as tissue fixation, fixation time, and determination of thresholds for reporting positive results.

According to ASCO/CAP guidelines, the optimal tissue handling requirements include: the time from tissue acquisition to fixation should be as short as possible; the formalin fixation in buffered formalin should range from 6–48 hours; and the time to fixation and duration of fixation should be recorded for each sample [143]. Additional IHC internal validation and quality assurance procedures, as well as external proficiency assessment, are recommended.

Only membranous staining of the invasive tumour should be considered when scoring HER2. Cytoplasmic staining and staining of in situ disease should not be scored, and normal epithelium should be negative. The HER2 IHC scoring method is a semiquantitative system based on the intensity of reaction product and percentage of membrane-positive cells, giving a score range of 0–3+ **(Figure 1.4)**. Cases scoring 3+ are regarded as unequivocally positive, and those scoring 0/1+ as negative. Borderline scores (2+) are regarded as equivocal and mandate further assessment using ISH. Each of these results triggers different patient management [143].

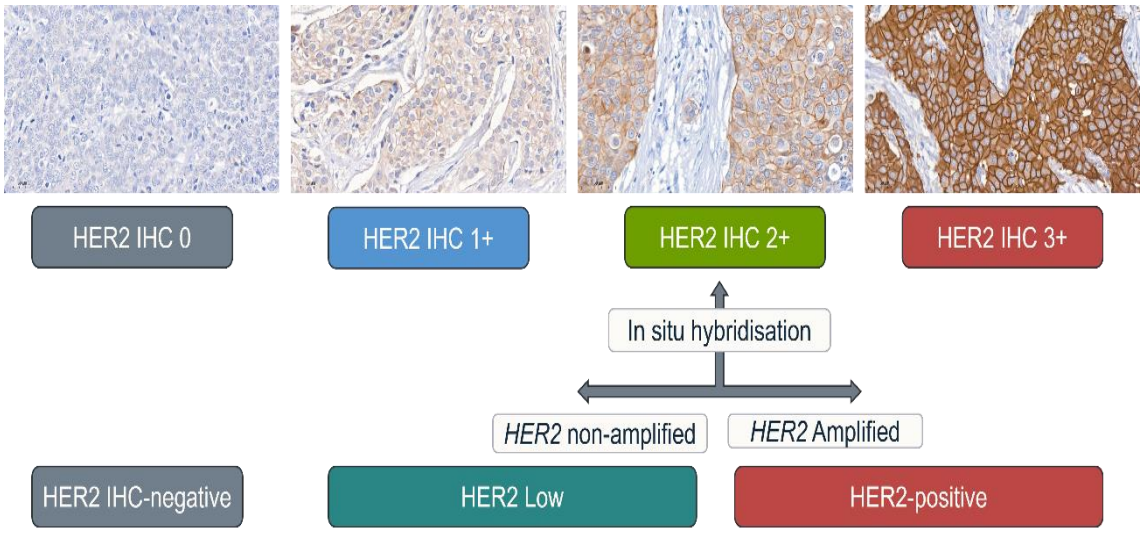


Figure 1.4: A schematic overview of HER2 scoring in breast cancer. Breast cancers are considered HER2-negative if the IHC score is 0. An IHC score of 1 + or

2 + without HER2 amplification is categorised as HER2-Low. Breast cancers with an IHC score of 2 + with amplification or 3 + are HER2-positive (40× magnification). Created by Biorender.com.

1.6.3.2 In situ Hybridisation

Chromogenic ISH (CISH) or FISH for *HER2* gene amplification has become an integral part of the diagnostic workup for patients with BC. The principles of ISH are simple: DNA probes complementary to genomic sequences of interest are generated, labelled and then hybridised to the target tissue [144, 145]FISH/CISH methods can be applied to a wide range of samples: cell lines, frozen tissue, paraffin-embedded tissue, and micro-tissue arrays. FISH utilizes fluorescence microscopy, while CISH employs light microscopy.

HER2 FISH positive is defined as an average of ≥ 6 *HER2* gene copies/nucleus for test systems without an internal control probe or HER2/ centromeric probe for chromosome 17(CEP 17) ratio ≥ 2 [141], where CEP17 is a centromeric probe for chromosome 17 on which the HER2 gene resides.

1.6.3.3 Other assays

1.6.3.3.1 Protein Assay (HERmark™)

HERmark™ allows for the accurate detection of HER2 expression in formalin-fixed paraffin-embedded (FFPE) tissue samples, covering the majority of the dynamic range from 0 to 3+ [146]. It was found to be highly concordant with conventional HER2 assays (IHC and ISH), with high sensitivity and specificity [147-149]. Nonetheless, the core technical requirements have restricted its application to the central lab, limiting its use in a broader range of clinical settings.

1.6.3.3.2 mRNA expression

A high correlation between HER2 gene status and *HER2* mRNA levels is well known, as documented by several studies [150-152]. This has allowed to consider RNA evaluation as a possible option for HER2 assessment. The question is whether RNA-based testing could be able to complement IHC and DNA FISH analysis, allowing a full resolution of the HER2 status. Several techniques have been applied for *HER2* mRNA analyses, including quantitative procedures like real-time quantitative PCR (RT-qPCR), Droplet digital PCR (ddPCR), and in situ detection methods such as RNASCOPE, however, they are not widely used in clinical practice even though the determination of biomarkers by RNA evaluation is becoming more feasible.

The possibility to perform *HER2* mRNA testing by RT-qPCR has been extensively evaluated [152-154]. The opportunity to use qPCR to assess in a single reaction HER2 DNA amplification and mRNA expression in microdissected BC has been investigated [152]. Despite the inherent challenges posed by the degradation of nucleic acids in FFPE tissue samples, successful detection of *HER2* mRNA was achieved in 94% of cases [152]. Given that qPCR provides a quantitative and objective measurement, as opposed to the semi-quantitative and observer-dependent nature of IHC, it has been suggested as a viable alternative for HER2 assessment.

Unfortunately, false-negative PCR results are often found, heterogeneity of HER2 expression/amplification is likely key in this respect. Furthermore, the mixing of non-invasive cancer components in the process of DNA/RNA extraction and the destruction of mRNA integrity in FFPE samples [150, 155, 156].

This is why mRNA-based techniques are not recognised as alternative methods to assess HER2 status in diagnostic practice, as stated also by the ASCO/CAP guidelines [157].

1.6.4 History of HER2 Scoring

HER2 positivity was defined as protein overexpression that qualified an IHC score of 3+, or equivocal protein that is assigned a score of 2 + with evidence of *HER2* gene amplification as confirmed by ISH reflex testing [141]. This scoring system was originally developed to predict the response to early anti-HER2 therapies such as trastuzumab[158] that showed efficacy limited to HER2-positive BC.

The initial clinical trials for trastuzumab used an IHC score 3+ or a score 2+ with a positive FISH test (defined by HER2/CEP17 ratio ≥2 in >50 % neoplastic cells) as eligibility criteria. In these trials, an IHC score 3+ was defined as intense/strong complete circumferential membrane staining in >10 % cells of neoplastic cells and 2+ was defined as weak to moderate complete circumferential membrane staining in >10 % cells of neoplastic cells [159]. In the 2007 ASCO/CAP guidelines the threshold for positivity was elevated to >30 % of neoplastic cells in IHC and to HER2/CEP17 ratio ≥2.2 by FISH in order to lower the number of false positive results, decreasing the administration of ineffective anti-HER2 therapy [143] **(Figure 1.5**). The 2013 ASCO/CAP guidelines reverted the positivity threshold to the original >10 % cells of neoplastic cells in IHC and HER2/CEP17 ratio ≥2 in FISH in order to avoid false negative results. In 2018 the ASCO/CAP provided an update of these guidelines did not

change the cut point for positivity, however it provided a detailed recommendations in cases with borderline HER2 protein expression [141] **(Figure 1.6 and Table 1.3) .**

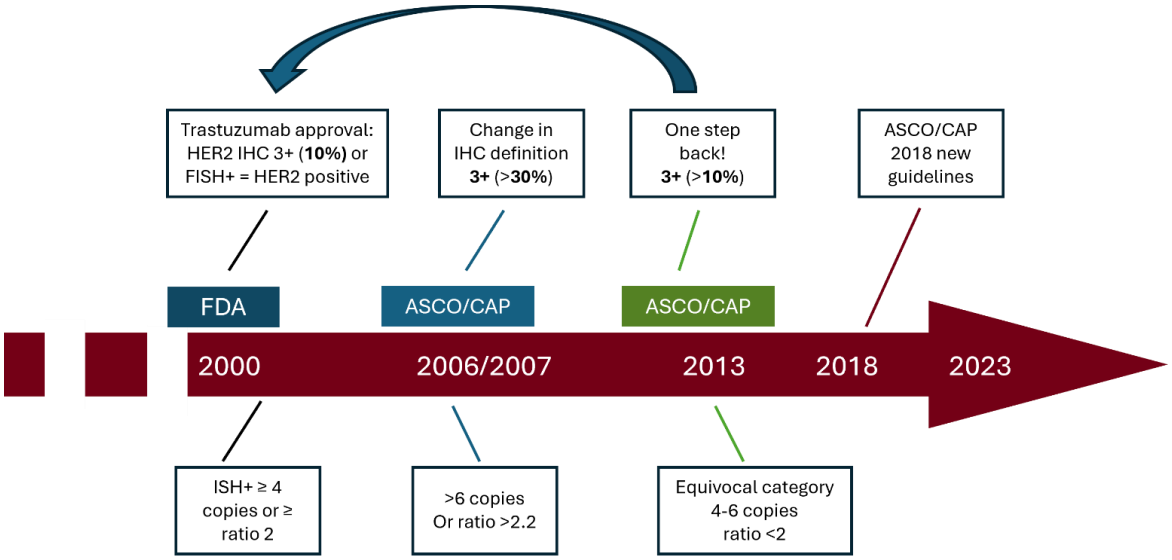


Figure 1.5: Diagram shows the history of HER2 testing and cut-off Controversy. Created by Biorender.com

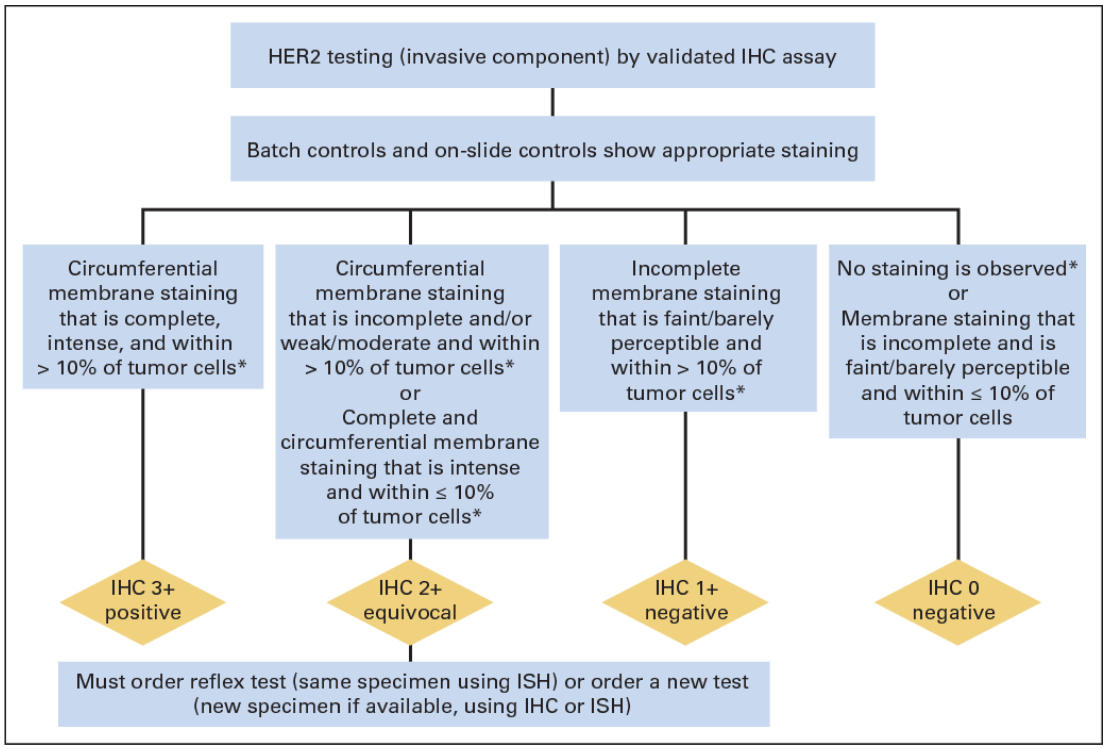


Figure 1.6: Spectrum of HER2 scoring using immunohistochemistry (IHC). [141]

Table 1.3: HER2 testing and scoring ASCO/CAP guidelines [141]

Assay	Method	Result	Additional work-up	Final HER2 assignment
Dual probe ISH	**ISH algorithm**	**Group 1** HER2/CEP17 ratio ≥2.0 and average HER2 copy number ≥4.0 signals/cell	/	**AMP/Positive**
		Group 2 HER2/CEP17 ratio ≥2.0 and average HER2 copy number <4.0 signals/cell	Concurrent IHC score 0/1+	NOT AMP/Negative with Comment
			Concurrent IHC score 2+, recount ISH: preliminary result confirmed	NOT AMP/Negative with Comment
			Concurrent IHC score 2+, recount ISH: other ISH result	Result should be adjudicated per internal procedures
			Concurrent IHC score 3+	**AMP/Positive**
		Group 3 HER2/CEP17 ratio <2.0 and average HER2 copy number ≥6.0 signals/cell	Concurrent IHC score 0/1+	NOT AMP/Negative with Comment
			Concurrent IHC score 2+, recount ISH: preliminary result confirmed	**AMP/Positive**
			Concurrent IHC score 2+, recount ISH: other ISH result	Result should be adjudicated per internal procedures
			Concurrent IHC score 3+	AMP/Positive
		Group 4 HER2/CEP17 ratio <2.0 and average HER2 copy number ≥4.0 and <6.0 signals/cell	Concurrent IHC score 0/1+	NOT AMP/Negative with Comment
			Concurrent IHC score 2+ (HER2 double-equivocal), recount ISH: preliminary result confirmed	NOT AMP/Negative with Comment

Table 1.3 continued

			Concurrent IHC score 2+ (HER2 double-equivocal), recount ISH: other ISH result	Result should be adjudicated per internal procedures
			Concurrent IHC score 3+	AMP/Positive
		Group 5 HER2/CEP17 ratio <2.0 and average HER2 copy number <4.0 signals/cell	/	NOT AMP/Negative
Single probe ISH	***HER2* copy number**	Average HER2 copy number <4.0 signals/cell	/	NOT AMP/Negative
		Average HER2 copy number ≥4.0 and <6.0 signals/cell	Concurrent IHC score 0/1+ and/or concurrent dual-probe ISH Group 5	NOT AMP/Negative
			Concurrent IHC score 2+	Perform dual-probe ISH for final result
			Concurrent IHC score 3+ and/or concurrent dual-probe ISH Group 1	**AMP/Positive**
		Average HER2 copy number ≥6.0 signals/cell	/	**AMP/Positive**

AMP: Amplified; **CEP**: centromeric enumeration probe; **ISH:** insitu hybridisation; **HER2**: human epidermal growth factor receptor**; IHC**: immunohistochemical

1.6.5 Spectrum of HER2 expression in breast cancer

The incidence of HER2-positive BC has emerged and refined with the successive publication of the updated recommendations and the refined guidelines for sample processing including preanalytical and analytical variables for HER2 testing [141, 160, 161]. Initial studies, which involved relatively small sample sizes, suggested that up to 30% of BC cases exhibited HER2 overexpression, with reported false positive rates reaching as high as 19% and false negative rates ranging from 5% to 10% [143, 148, 162]. With the implementation of standardised quality assurance measures, recent data indicates a lower frequency of HER2 positivity, ranging between 15% - 20% [143, 148, 163-165]. This class of BC comprised 15-20% of cases, while the remaining BC cases were considered HER2-negative. The latter comprised not only cases that lack HER2 expression or have undetectable levels of HER2 protein expression using IHC and are classified as score 0 but also BC with score 2+ without evidence of *HER2* gene amplification and cases that showed weaker expression than that of a score 2+ and are classified using IHC as score 1+ and don't require ISH reflex testing. The later 2 groups comprise approximately 60% of HR-positive and 40% of HR-negative BC cases [166]. Until recently, effective HER2-targeted therapies for these tumours were lacking [167]. However, the advent of novel antibody-drug conjugates (ADCs), such as trastuzumab deruxtecan (T-DXd), which deliver cytotoxic agents to cells with low HER2 levels, has opened a new therapeutic option for this substantial BC patient population and the introduction of concept of HER2-Low class of BC [167-169].

Since the results of the Destiny-breast-04 and Destiny-breast-06 trials [170, 171], HER-Low BC class has attracted considerable attention in the BC community as a novel therapeutic group of BC, Furthermore, the response of BC with such low levels of HER2 protein to T-DXd has led some to expand the definition of BC expressing very low levels of HER2 (> score 0 and <score 1+) which was termed HER2-Ultralow [172].

1.6.6 HER2-Low and ADC

The updated ASCO/CAP guidelines in 2018 have reinforced a dichotomous diagnostic approach, supported by robust clinical evidence indicating that only tumours with *HER2* gene amplification benefit from the addition of trastuzumab to chemotherapy [173, 174]. Consequently, oncologists have adopted a binary treatment decision-making process for HER2, focusing on HER2-positive patients defined by HER2 overexpression and amplification, who are deemed suitable candidates for anti-HER2 therapies.

In recent years, ADCs have been developed aiming to selectively target and deliver chemotherapy within cancer cells, thereby minimising systemic exposure to cytotoxic agents **(Figure 1.7).** ADCs consist of a humanised mAB bound to a cytotoxic agent called the payload via a molecular linker. Canonically, the antibody component, through the fragment antigen-binding (Fab) portion, recognizes and binds its target antigen on the cell surface, inducing internalization of the entire ADC complex via endocytosis and delivering chemotherapy inside cancer cells, thus reducing systemic exposure to the cytotoxic agent. Other actions include strong Fc-mediated immune functions, including antibody-dependent cell-mediated cytotoxicity (ADCC), antibody-dependent

cellular phagocytosis, and complement-dependent cytotoxicity [175]. Bystander killing is also another weapon of ADCs, in which the payload released into the extracellular space can be taken up also by neighbouring HER2-negative cells causing their death [176]. This approach overcame the need for HER2 overexpression and oncogenic activity to treat HER2-expressing BC, and cases with a low level of HER2 expression can now act as a carrier protein for internalising the payload into the cell.

HER2-Low BC accounts for 40–50% of all BCs [169] and appears to be a heterogeneous disease [176, 177]. Despite not being a novel or distinct BC subtype, has been extensively studied in recent literature, consistently revealing its heterogeneity across clinical, morphological, immunohistochemical, and molecular characteristics [178-182]. Studies aimed at deciphering the biological and clinical significance of HER2-Low BC were carried out [176, 179, 183-187], however, the debate over whether HER2-Low status constitutes a distinct biological entity within BC, carrying significant prognostic implications, and whether these variations are influenced by HR status remains unsettled [188-190]. It is now well established that HER2-Low disease is more frequently seen in HR-positive than in HR-negative BC [182, 186, 191]. Some studies have reported that HER2-Low tumours are associated with a low proliferation index, negative LN status and better patients' outcome [186, 187]. While other reports claimed that HER2-Low tumours are associated with higher tumour histologic grade, higher proliferation rate and increased regional LN metastases compared to HER2-negative tumours [176, 179, 183-185]. We believe that this controversy is due to the heterogeneity of the disease itself, which comprises multiple molecular subtypes.

HER2 scoring guidelines, whether from the UK or ASCO/CAP [141, 161], have predominantly focused on defining HER2 positivity, often side-lining cases with HER2 IHC scores of 0 and 1+, and this resulted in the low concordance among pathologists in separating those two categories [192, 193]. The emergence of the HER2-Low definition has flagged the necessity for detailed guidelines refining the definition of the lower end of HER2 expression spectrum (0 and 1+) with proper training of the pathologists to identify this category to enhance the reproducibility among pathologists and to solve the dilemma of HER2-Low, ultra-low and HER2 IHC 0[170].

Various new quantitative assays, such as the HERmark BC assay[146, 149], immunofluorescence-based automated quantitative analysis methods [194, 195], quantitative IHC method[196], and assessment of HER2 mRNA expression levels [197], are under investigation, the prevailing consensus is that any forthcoming assay or kit designed for the detection of HER2-Low tumours must undergo rigorous validation through clinical trials before being integrated into clinical practice. Moreover, it is essential that these assays demonstrate superiority over existing methods to be deemed clinically relevant.

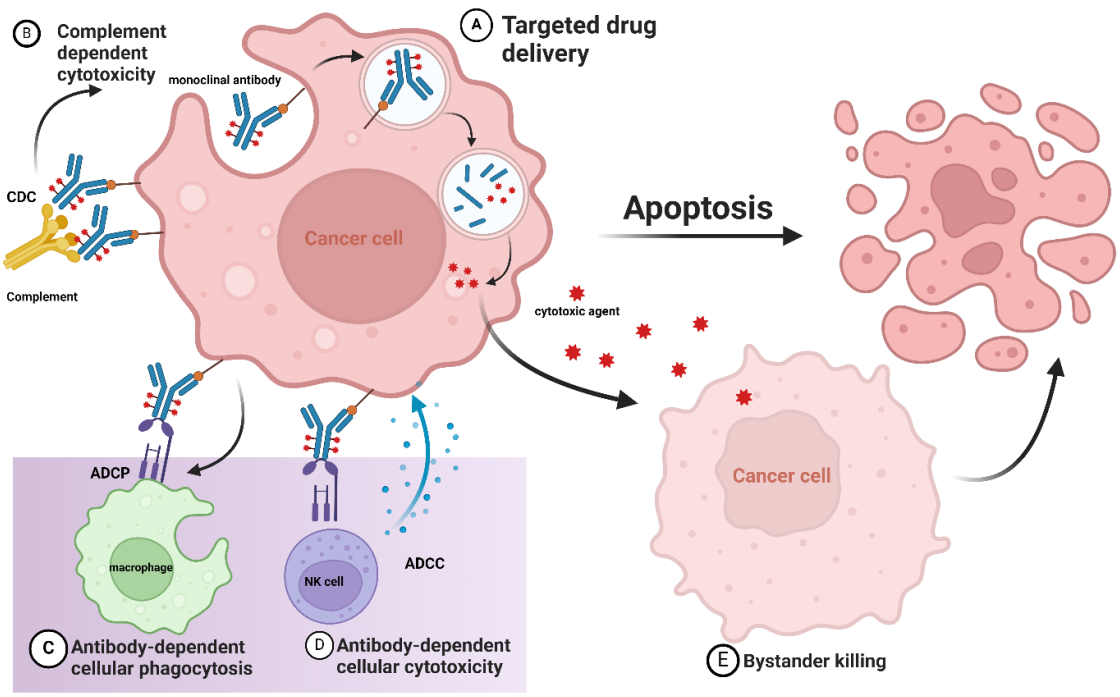


Figure 1.7: Mode of action of HER2-directed ADCs in HER2-Low tumours. Classical mode of action of ADCs with cleavable linkers: (A) Targeted drug delivery in which monoclonal anti-HER antibody component binds to HER2 expressed on the cell surface of tumour cells, this leads to the ADC-HER2 complex internalisation by endocytosis. After linker cleavage by lysosomal proteases, the drug payload is released and induces the cytotoxic effect, leading to tumour cell death. B, C, D: The monoclonal anti-HER antibody component of ADCs may retain its activity profile and engage in Fc-mediated interactions with immune cell players; complement, macrophages and natural killer (NK) cells), triggering antitumour immunity via complement-dependent cytotoxicity (CDC), antibody dependent cellular phagocytosis (ADCP) and antibody-dependent cellular cytotoxicity, respectively (ADCC). F: Bystander killing effect: Using cleavable linkers, ADCs can be designed to promote cytotoxic drug release from the target cell to the extracellular space to the surrounding and bystander cells, which may or may not express the ADC target antigen, Created with BioRender.com

1.6.7 Intra-tumour HER2 Heterogeneity

Intra-tumour genetic heterogeneity has been well-documented in various types of human cancer, including BC [198]. It is well known to pathologists routinely assessing HER2 in diagnostic practice that HER2 overexpression and amplification can present a heterogeneous pattern. Three distinct types of distribution of cells with heterogeneous HER2 status have been described [199]: “clustered” type, featuring the presence of two topographically distinct tumour clones of tumour cells, one harbouring HER2 amplification and the other with normal HER2 status; “mosaic” type, displaying either diffuse intermingling of cells with different HER2 statuses; “scattered type”, with isolated HER2-amplified cells in a HER2-negative tumour cell population. Several studies have demonstrated the presence of HER2 genetic heterogeneity at variable frequencies (1–34 %) in BC [199-205], being significantly more common in cases with HER2 equivocal status by ISH and/or IHC [204, 206-208]. For instance, Allison et al. [206] and Chang et al. [201] found that >90 % of FISH HER2 equivocal cases presented HER2 heterogeneity; Bukley et al. observed that the highest levels of heterogeneity were detected in HER2 border line cases as well as in HER2-negative cases with highest HER2/CEP17 ratios [177]. Some have suggested that HER2 heterogeneity is an important cause of equivocal HER2 results in BC by FISH and IHC. These cases typically feature low levels of HER2 amplification [38], as observed also by others [201, 205, 209]. Some studies have also associated increased frequency of chromosome 17 polysomy with HER2 heterogeneity. As already mentioned, chromosome 17 polysomy is a rare event in BC, which features more frequently gain or amplification of the CEP17 [210-213].

In terms of impact on patient outcome, Shafi et al. [208] found that HER2 FISH non-amplified tumours with genetic heterogeneity were associated with larger size, higher histologic grade and frequency of LN metastasis, which are important negative prognostic factors in BC. Several studies indicate that the presence of HER2 heterogeneity is associated with worse patient outcomes, in terms of shorter DFS and OS [200, 207, 214]. When analysing the response to treatment, patients with HER2 heterogeneity seem to be less responsive to anti-HER2 targeted therapy [215-217], as also demonstrated by lower achievement of pathologic complete response (pCR) following neoadjuvant treatment with trastuzumab-containing chemotherapy [202, 210]. These results have been recently confirmed in an elegant study presented at ASCO 2019 by Metzger Filho and co-workers[218], who designed a Phase II study in which evaluation of the response of stage II and stage III centrally confirmed HER2-positive breast carcinomas to neoadjuvant trastuzumab emtansine (T-DM1) and pertuzumab was performed. HER2 heterogeneity in diagnostic core needle biopsy samples was defined either as i) HER2 positivity by FISH in >5% and <50 % of tumour cells [219]; ii) an area of the tumour that was tested negative. HER2 heterogeneity was found in 10 % of cases (n = 16/157). pCR was not achieved in any of the heterogeneous cases compared to 55 % of HER2-positive carcinomas without evidence of HER2 heterogeneity. The association between HER2 heterogeneity and pCR remained significant when adjusted by ER status. These data suggest that HER2 heterogeneous breast carcinomas may represent a distinct subset of HER2-positive tumours for which different therapeutic approaches may be considered [218].

1.6.8 Management of HER2-positive BC

Treatment of HER2-positive BC has evolved rapidly over the past several years. The addition of HER2 targeting therapies to standard treatment has dramatically improved the prognosis for patients with HER2-positive BC in both the early and metastatic settings (**Table 1.4)** [220-223].

To date, BCs with HER2 protein overexpression or borderline protein level with evidence of HER2 gene amplification are equally considered candidates for anti-HER2 therapy [141]. However, the response rate in HER2-positive BC patients is not uniform (**Table 1.5).** The magnitude of response, measured by the rate of pCR of HER2 IHC score 3+ cases range from 55 to 70% compared to 17–20% in HER2-positive tumours with borderline HER2 protein expression [224-228]. This variability raises a concern about whether HER2 protein overexpression or HER2 gene amplification is the key driver of response.

Table 1.4: HER2-targeted agents used in the current treatment of breast cancer [229]

Drug	Mechanism of action	Indication
Monoclonal Antibodies		
Trastuzumab	Binds to HER2 juxtamembrane domain IV	In combination with chemotherapy for neoadjuvant and adjuvant early-stage disease [222, 230] Alone or in combination with chemotherapy for advanced disease [159]
Pertuzumab	Binds to HER2 heterodimerisation domain II	In combination with trastuzumab and chemotherapy in neoadjuvant/adjuvant treatment of early-stage disease [231, 232] In combination with trastuzumab and chemotherapy in advanced disease[233]
Margetuximab	Binds to HER2 heterodimerisation domain II	In combination with trastuzumab and chemotherapy for pretreated advanced disease (NCT02492711)
Tyrosine kinase inhibitors		
Neratinib	Pan-HER inhibitor	Extended adjuvant treatment of early triple-positive disease after trastuzumab-based therapy [234]. In combination with capecitabine for pretreated advanced disease[235]
Lapatinib	HER1 and HER2 inhibitor	In combination with capecitabine for pretreated advanced disease [236]
Tucatinib	Selective HER2 inhibitor	In combination with capecitabine and trastuzumab for pretreated advanced disease [237]
Pyrotinib	HER1 and HER2 inhibitor	In combination with capecitabine in pretreated advanced disease [238]

Table 1.4 continued

Drug	Mechanism	Indication
Antibody-drug conjugates		
Trastuzumab emtansine	Trastuzumab covalently linked to DM1	Treatment of pretreated advanced disease [239]. Adjuvant treatment of residual disease after neoadjuvant treatment with trastuzumab and chemotherapy [240]
Trastuzumab deruxtecan	Humanised HER2 antibody and topoisomerase I inhibitor	Treatment of pretreated advanced disease [241]

Table 1.5: Summary of previous studies on the differential pathological response between HER2 IHC 3+ and HER2 IHC 2+/ISH positive [224]

Neoadjuvant Setting	Study Title	Rate of pCR			*P* value
		Overall	IHC 3+	IHC 2+/Amplified	
Yan, Xiao [242]	Association Between the HER2 Protein Expression Level and the Efficacy of Neoadjuvant Chemotherapy in HER2-Positive BC	37.2% (110/296)	41.4% (99/139)	19.3% (11/75)	0.003
Krystel-Whittemore, Xu [228]	Pathologic complete response rate according to HER2 detection methods in HER2-positive BC treated with neoadjuvant systemic therapy	59% (330/560)	67% (303/455)	17% (12/76)	<0.001
Rakha, Miligy [243]	Retrospective observational study of HER2 IHC in borderline BC patients undergoing neoadjuvant therapy, with an emphasis on Group 2 (HER2 / CEP17 ratio≥ 2.0, HER2 copy number< 4.0 signals/cell) cases	25% (184/749)	54% (79/146)	19% (35/180)	<0.001

Table 1.5 continued

Neoadjuvant Setting	Study Title	Rate of pCR			*P* value
		Overall	IHC 3+	IHC 2+/Amplified	
Xu, Shen [244]	HER2 protein expression level is positively associated with the efficacy of neoadjuvant systemic therapy in HER2-positive BC	43.7% (73/167)	47.9 % (67/140)	22.2% (6/27)	0.014
Zhao, Krishnamurti [245]	HER2 IHC staining positivity is strongly predictive of tumour response to neoadjuvant chemotherapy in HER2-positive BC	64.5% (49/76)	80% (40/49)	34% (9/40)	<0.001
Chen, Chen [246]	Pathologic complete response to neoadjuvant anti-HER2 therapy is associated with HER2 IHC score in HER2-positive early BC	74/181 (40.9%)	46%	25%	0.016
Atallah, Alsaleem [224]	Differential response of HER2-positive BC to anti-HER2 therapy based on HER2 protein expression level	26% (194/751)	57% (88/155)	22% (35/162)	0.001
Chen, Li [225]	Differences between the efficacy of HER2(2+) /FISH-positive and HER2 (3+) in BC during dual-target neoadjuvant therapy	59.8%	63.3 %	41.7%	<0.05
Jiao, Li [226]	Comparison of the Response to Neoadjuvant Therapy Between Immunohistochemistry HER2 (3+) and HER2 (2+)/ISH+ Early-Stage BC: A Retrospective Multicenter Cohort Study	35.5%	40%	18%	<0.001

pCR: pathologic complete response**; IHC**: Immunohistochemistry; **HER2**: Human epidermal growth factor receptor 2; **CEP**: centromeric enumeration probe, **ISH:** in situ hybridisation

1.6.8.1 Monoclonal antibodies

Trastuzumab and pertuzumab are monoclonal antibodies which bind to the HER2 juxta membrane domain IV and heterodimerization domain II, respectively. They inhibit ligand-independent HER2 signalling, downregulate HER2 expression and trigger antibody-dependent cellular cytotoxicity (ADCC) [247-249] **(Figure 1.8)**.

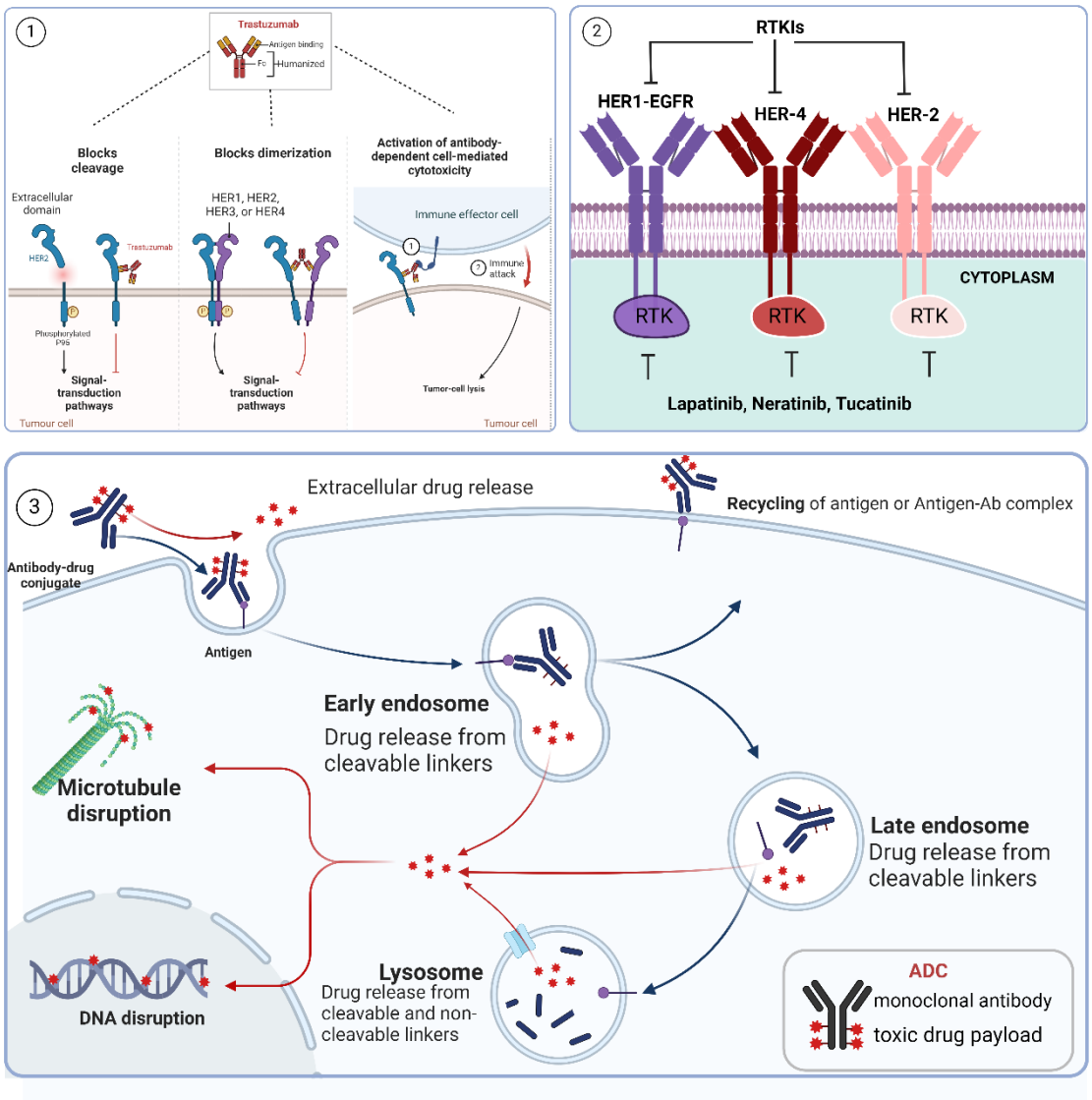


Figure 1.8: Mechanism of action of anti-HER2 therapy. 1: Monoclonal antibody; 2: Receptor tyrosine kinase; 3: Antibody drug conjugate. Created with BioRender.com

1.6.8.2 Receptor tyrosine kinase inhibitors (RTKI)

Lapatinib which is a reversible RTKI on the EGFR and HER2 domains, neratinib is an irreversible RTKI targeting the HER1, HER2, and HER4 pathways [250, 251]. RTKIs bind to the intracellular tyrosine kinase domain of HER2 and other HER members to suppress downstream signalling involving the MAPK/ERK1/2 and PI3K/AKT pathways [252, 253].

1.6.8.3 Antibody drug conjugates (ADCs)

T-DM1 and T-DXd are ADCs in which a cytotoxic agent is linked with an anti-HER2 antibody. After binding to HER2, the conjugate is internalised and the cytotoxic agent is released within the cell, resulting in cell death and toxic effects on surrounding cells [241, 254].

Figure 1.9 summarises the chronological outline of FDA approvals of ADCs for the treatment of BC.

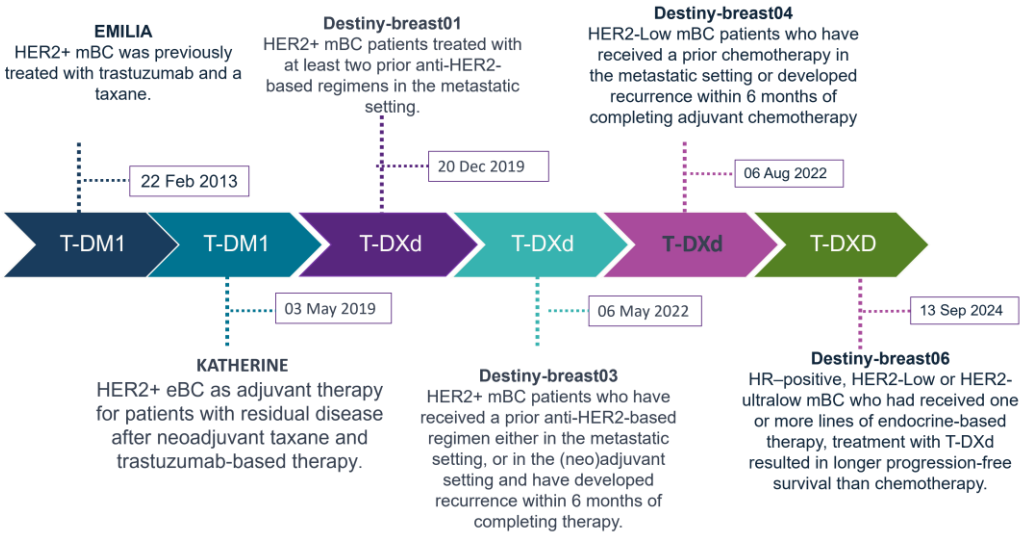


Figure 1.9: Chronological outline of FDA approvals of ADCs for the treatment of breast cancer. ADC: antibody drug conjugate; FDA: Food and Drug Admin-

istration; HR: Hormone receptor; HER2: human epidermal growth factor receptor 2; mBC: metastatic breast cancer; pts, patients; ChT: chemotherapy; T-DM1, trastuzumab emtansine; T-DXd, trastuzumab deruxtecan; eBC, early breast cancer.

1.6.9 Treatment modalities in early stage HER2-positive BC

1.6.9.1 Neoadjuvant therapy

Neoadjuvant systemic therapy for HER2-positive BC patients is now a well-established approach for the treatment of early BC with ≥ stage T2 or node-positive HER2-positive breast tumours [255, 256]. Pathological response at surgery correlates with patient outcomes and importantly, it can guide subsequent systemic adjuvant therapy [256]. Multiple randomised trials have shown significantly higher rates of pCR when trastuzumab is added to primary chemotherapy in the neoadjuvant treatment of HER2-positive early-stage BC [257-260]. The attainment of a pCR represents a surrogate marker of improved long-term outcomes in HER2-positive disease [261, 262].

Several trials have assessed the efficacy of neoadjuvant lapatinib, as a single anti-HER2 agent in combination with chemotherapy, and in combination with trastuzumab [263-265]. Overall, these trials demonstrated that lapatinib as a single HER2-directed therapy was not only inferior to trastuzumab in terms of pCR rates but also associated with significantly more toxicity. Dual blockade in combination with trastuzumab produced a significant improvement in pCR rates compared to trastuzumab alone. However, no improvement in DFS was noted. Hence lapatinib is not routinely used in the neoadjuvant treatment of HER2-positive early BC.

Neoadjuvant dual HER2 blockade with pertuzumab and trastuzumab was evaluated in the NeoSphere trial and several other phase 2 trials [232, 266]. The NeoSphere trial reported a significantly higher pCR rate with dual HER2 blockade plus docetaxel compared with the trastuzumab plus docetaxel (45.8% vs. 29%, p = 0.01). There is currently no data to support the use of neoadjuvant dual HER2 therapy for clinical T1N0 disease [256].

1.6.9.2 Adjuvant therapy

One year of adjuvant trastuzumab in combination with 3–6 months of chemotherapy remains the current standard of care for adjuvant systemic therapy. Adjuvant trastuzumab in combination with chemotherapy was shown to reduce the relative risk of recurrence by up to 40% and the relative risk of death by up to 30% in the pivotal HERA, BCIRG-006, NSABP B-31 and NCCTG N9831 trials [221, 222, 230, 267, 268]. The benefit of trastuzumab was across all subgroups and independent of patient and tumour characteristics [220, 221]. Several trials have evaluated the efficacy of reduced duration of adjuvant anti-HER2 treatment. The PERSEPHONE trial was the only trial which suggested that 6 months was non-inferior to 12 for DFS and that shorter duration therapy was associated with less cardiac toxicity [269].

1.6.9.3 Adjuvant therapy for patients who do not achieve a pathological complete response to neoadjuvant systemic therapies.

With the increasing use of neoadjuvant systemic therapy for patients with HER2-positive BC, there has been a significant change to the treatment algorithms for subsequent adjuvant therapies. Patients who do not obtain a pCR with neoadjuvant therapy have significant higher rates of recurrence, and the

functional assessment of treatment response with neoadjuvant therapy provides us with an opportunity to escalate treatment in these patients. T-DM1 was evaluated as an adjuvant therapy in patients who had residual disease after neoadjuvant treatment with trastuzumab and taxane-based chemotherapy in the KATHERINE trial [270] **(Figure 1.10).** The benefit of T-DM1 was observed irrespective of clinicopathological features and type of neoadjuvant treatment received. The results of this trial established a new standard of care for patients who do not achieve pCR after neoadjuvant therapy.

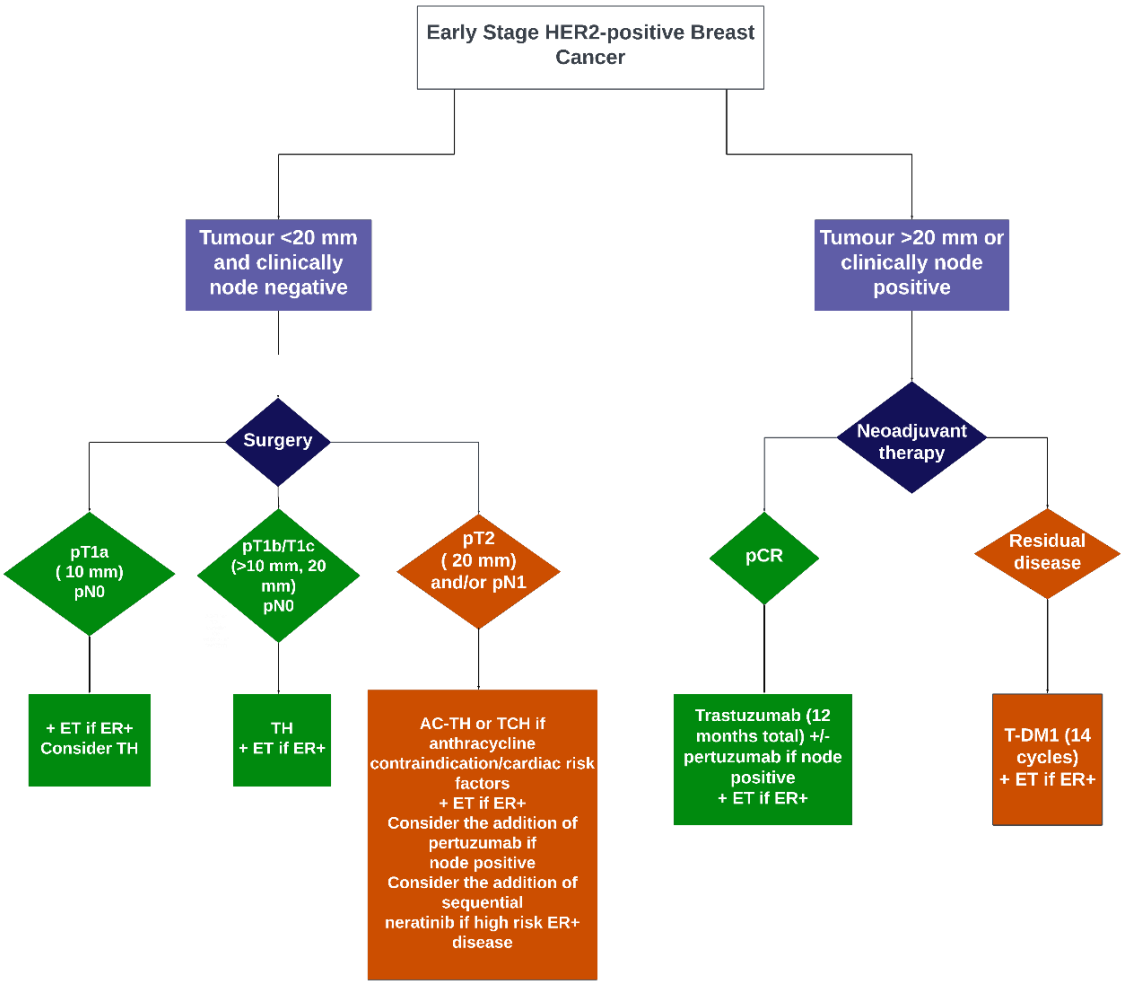


Figure 1.10: Schematic illustration for the management of early-stage breast cancer [229]. AC-TH, doxorubicin and cyclophosphamide followed by paclitaxel and trastuzumab; ER+, oestrogen-receptor positive; ET, endocrine therapy; pCR, pathologic complete response; TCH, docetaxel, carboplatin and

trastuzumab; TH, paclitaxel and trastuzumab; pN0, no regional lymph node metastases; pN1, metastases to movable ipsilateral level I, II axillary lymph node(s); pT, pathologic primary tumour TNM stage.

1.6.10 Management of metastatic HER2-positive BC

1.6.10.1 First-line therapy

The triplet of pertuzumab, trastuzumab, and chemotherapy (usually a taxane) is the standard first-line treatment for most patients with HER2-positive mBC, based on the results of the CLEOPATRA trial [233]. This phase III trial compared trastuzumab and docetaxel with pertuzumab or placebo as first-line treatment in HER2-positive ABC (**Figure 1.11**).

1.6.10.2 Second Line T-DXd

T-DXd is a stable ADC in plasma, linking an HER2-targeting antibody to a topoisomerase I inhibitor, deruxtecan, through a cleavable tetrapeptide-based linker. This yields a high drug: antibody ratio of 8. The payload can cross the cell membrane and diffuse to neighbouring cancer cells, intensifying its cytotoxic impact through the bystander effect [271]. Initially tested in heavily pretreated HER2-positive mBC patients, the single-arm phase II study DESTINY-Breast01 led to worldwide regulatory approvals [272]. In phase III DESTINY-Breast02, T-DXd notably enhanced progression-free survival (PFS) as a third-line therapy post T-DM1 progression compared to capecitabine + lapatinib or capecitabine + trastuzumab in HER2-positive ABC [273]. After highlighting third-line benefits, DESTINYBreast03 compared T-DXd to T-DM1 in the second line after first-line trastuzumab, pertuzumab, and taxane-based chemotherapy (62% were previously treated with pertuzumab), achieving substantial improvements in PFS, objective response rates (ORR), and OS in the second

interim analysis [274, 275]. It is worth mentioning that twenty-five patients (13.6%) experienced T-DXd-associated interstitial lung disease (ILD) [274, 275].

1.6.10.3 Later Lines in mBC

Figure 1.11 and Table 1.6 summarise other lines used for >3rd line for treatment of HER2-positive mBC**.**

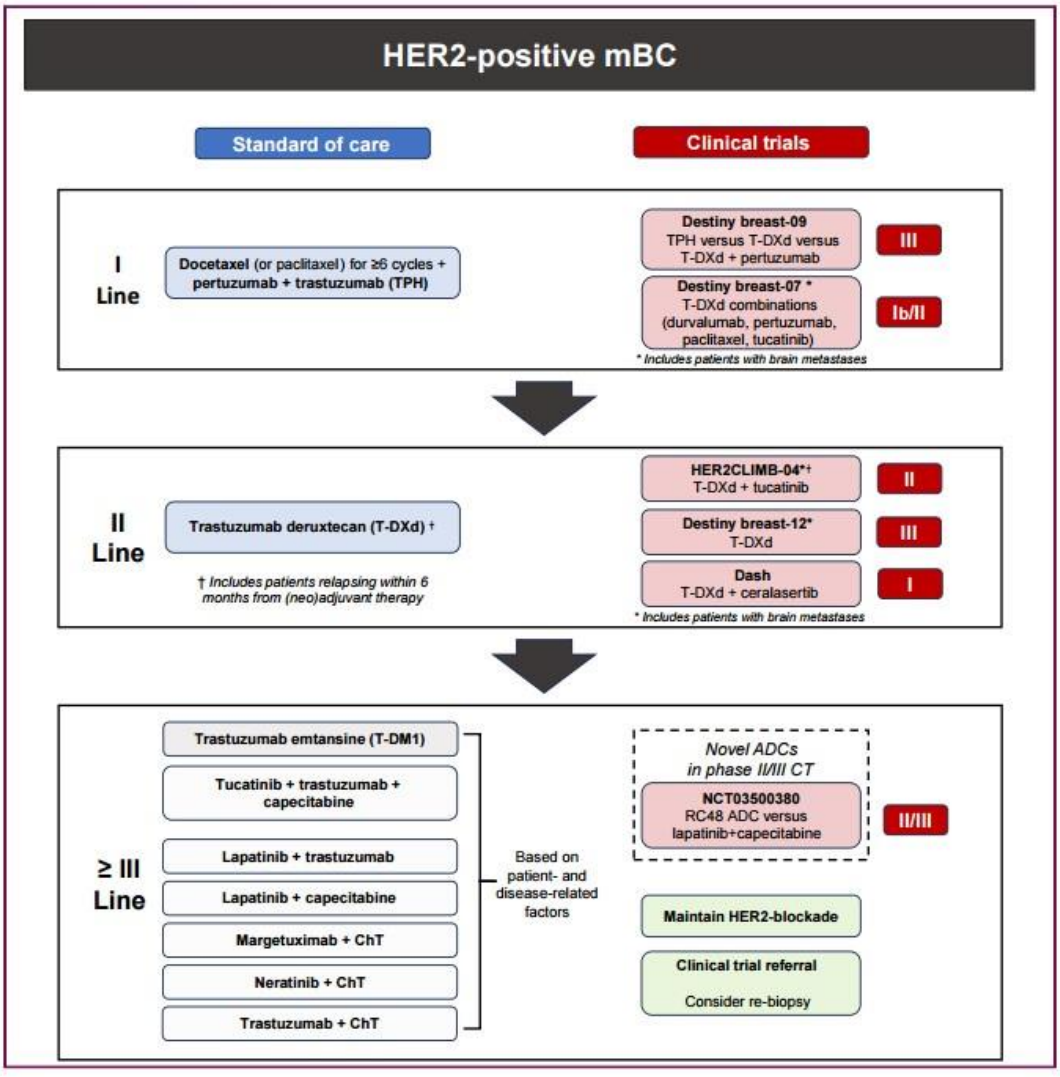


Figure 1.11: Treatment algorithm for the treatment of HER2-positive metastasis breast cancer. ADC, antibody-drug conjugate; ChT, chemotherapy; CT, clinical trial; H, trastuzumab; HER2, human epidermal growth factor receptor 2; mBC,

metastatic breast cancer; P, pertuzumab; T, taxane; T-DM1, trastuzumab emtansine; T-DXd, trastuzumab deruxtecan [276].

Table 1.6: Efficacy of HER2-positive Drugs in Prospective Clinical Trials in mBC and Brain Metastases [277].

Trial	Phase	Drug	Line	Treatment	N	Brain Metastases	ORR	mPFS	mOS
CLEOPATRA [233]	III	P	First line metastatic	Docetaxel + T + P vs docetaxel + T	808	Not included	80%	18.5 vs. 12.4 months (HR 0.62; **P < .001**)	57.1 vs. 40.8 months (HR 0.69; **P <.0001**).
PERUSE [278]	IIIb	P	First line metastatic	Taxane A: docetaxel, B: paclitaxel, or C: nab-paclitaxel) + T + P	1436	Treated	79%	19.4 23,2 and 19.2 months, respectively	66.5 64 70.9 months, respectively
PERTAIN [279]	II	P	First line metastatic	Taxane + T + P- > AI vs taxane+ T- > AI	129	Treated	63.3%	20.6 vs.15.8 months (HR 0.67, **P = 0.006)**.	60.2 vs. 57.2 months (HR 1.05; P = 0.78).
MARIANNE [215]	III	T-DM1	First line metastatic	Taxane + T vs. T-DM1 vs. T-DM1 + P	1095	Not included	82.6% for T-DM1	13.7, 14.1, and 15.2 months for the T + taxane, T-DM1 P = 0.31), and T-DM1 + P groups, **P = 0.14**).	50.9, 53.7, and 51.8 months for the T + taxane, T-DM1 and T-DM1 + P groups
EMILIA [280]	III	T-DM1	Second line metastatic	T-DM1 vs. L + C	991	95 (45 T-M1 / 50 L+C)	43.6%	9.6 vs. 6.4 months (HR 0.65; **P < .001)**	29.9 vs. 25.9 months (HR 0.75)
TH3RESA [281]	III	T-DM1	Third line metastatic or more	T-DM1 vs. TPC	602	67 (40 T-M1/27 TPC)	31%	6.2 vs. 3.3 months (HR :0.528; **P<0.001)**	22.7 vs. 15.8 months (HR: 0.68, **P =0.0007)**

Table 1.6 continued

Trial	Phase	Drug	Line	Treatment	N	Brain Metastases	ORR	mPFS	mOS
DESTINY BREAST 03 [275]	III	T-DXd	Second line metastatic	T-DXd vs. T-DM1	261	82 (39 T-M1 / 43 T-DXd)	79%	28.8 vs. 6.8 months (HR 0.33; P < 0.0001)	Data not mature
HER2CLIMB [282]	II	Tu	Third line metastatic or more	C + T + Tu vs C + T	612	291 (198 C + T-Tu / 93 C + T)	40.6%	7.6 vs. 4.9 months (HR 0.57; **P < 0.0001)**	24.7 vs. 19.2 months (HR 0.73; **P =0.004)**
NALA [235]	III	N	Third line metastatic or more	N + C vs. L + C	621	101 (51 N + C / 50 L + C)	32.8%	8.8 vs. 6.6 months (HR 0.76; **P= 0.003)**	24 vs 22.2 months (HR 0.88; P = 0.21)
SOPHIA [283]	III	M	Third line metastatic or more	Ch + M vs Ch + T	536	Treated	22%	5.8 vs, 4.9 months (HR 0.76; **P = 0.033)**	21.6 vs. 21.9 months (HR 0.95; P = 0.62)

AI, aromatase inhibitor; **C**, capecitabine; **Ch**, chemotherapy; **HR**: Hazard ratio; **L,** lapatinib; **M**, margetuximab; **ORR**, median overall response rate; **mBC**: metastatic breast cancer; **mOS**, median overall survival; **N**, neratinib; **NE**, not estimable; **P,** pertuzumab; **T**, trastuzumab; **T-DM1**, trastuzumab duocarmazine; **Tu**, tucatiniband; **TPC**, treatment of physician's choice.

1.6.11 The Resistance to Anti-HER2 Treatments

Despite the advances in HER2-positive BC targeted therapy, long-term results from the adjuvant pivotal trials indicated that approximately 15%-31% of patients experienced disease relapse [220-222]. Moreover, the development of CNS metastases in 5% of the patients remains an unmet need [270]. In this section, the main mechanisms of resistance to anti-HER2 targeted therapy are summarized [284] (**Figure 1.12**).

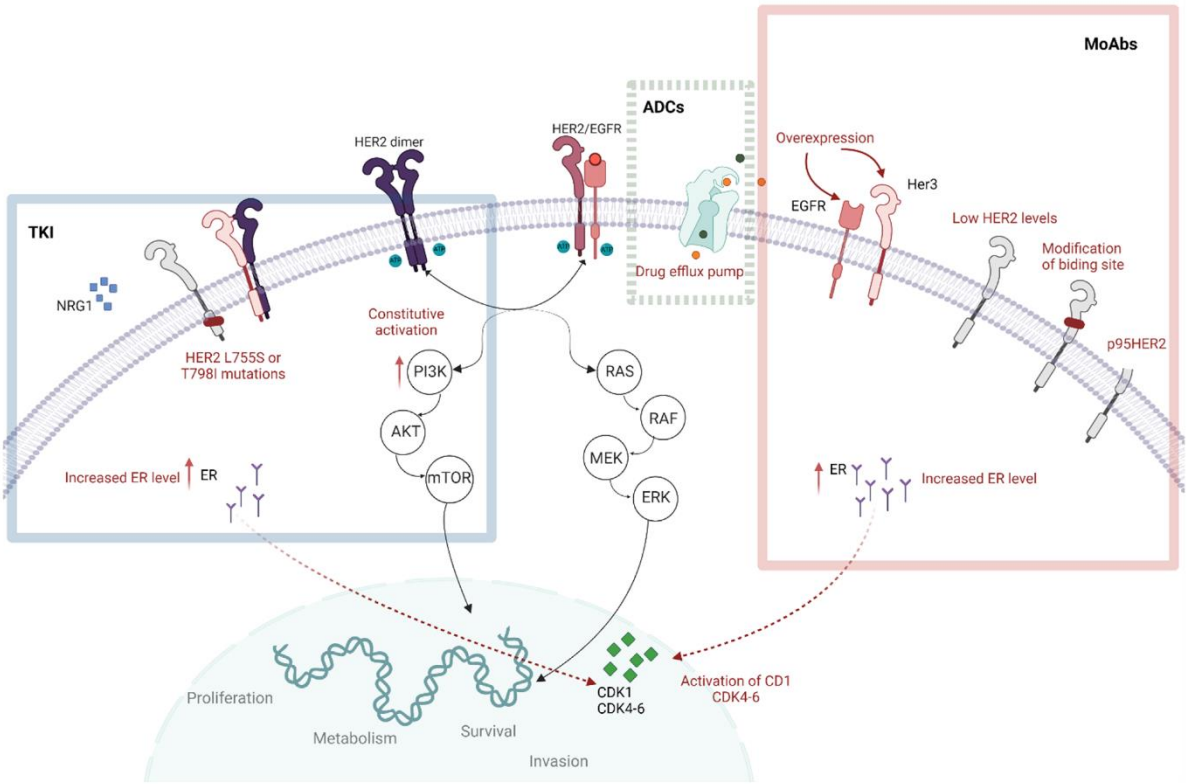


Figure 1.12: Mechanism of resistance to anti-HER2 targeted therapy. (1) Resistance to monoclonal antibodies (right, red box). Low HER2 expression, changes in the extracellular binding domain, and constitutive activation of the PI3K pathway can lead to resistance. Overexpression of receptor tyrosine kinase (RTKs) can promote the formation of HER2–EGFR and HER2–HER3 heterodimers, activating the pathway. Resistance to antibody-drug conjugates (ADCs) is also common, with drug efflux pumps reducing the intracellular cyto-

toxic action of ADCs. Resistance to TKIs is also common, with low HER-2 expression, activation of CD1 and CDK4-6, increased ER, constitutive activation of the PI3K pathway, and overexpression of NRG1. (2) Resistance to ADCs (centre, green box), and TKIs is shared among other drug classes, with some unique escapes. ADCs' cytotoxic action can be reduced by drug efflux pumps on cell walls. TKIs' binding site binding site mutations, such as L755S and T798I, confer specific resistance, preventing them from blocking HER2 function. Abbreviations: ADCs: antibody-drug conjugates; EGFR: epidermal growth factor receptor; HER2: human epidermal growth factor receptor 2; ER: oestrogen receptor; NRG1: neuroregulin 1; CDK: cyclin dependent kinase [285].

1.6.11.1 Impaired Binding to HER2

1.6.11.1.1 Low HER2 levels

HER2 protein overexpression (IHC 3+) and *HER2* gene amplification are key indicators of tumour dependence on HER2 signalling [165], which is linked to sensitivity to anti-HER2 therapies. Tumours with an IHC score of 3+ show the highest sensitivity to treatment, while those with lower scores (1+ or 0) are generally resistant to treatments like Trastuzumab [174].

1.6.11.1.2 HER2 receptor variants or molecular masking

Variants of the HER2 receptor, such as p95HER2, which lacks the extracellular domain, may impair the binding of antibodies like Trastuzumab, leading to resistance. While some studies suggest a link between p95HER2 and resistance, others report benefits from treatments in cases expressing this variant, making its role in resistance uncertain. Additionally, HER2Δ16, another variant, shows conflicting results regarding its impact on Trastuzumab resistance. The membrane-associated protein MUC4 may also obstruct Trastuzumab from binding to HER2, although this mechanism requires further exploration. [140, 286-291]. **Table 1.7** summarises the mechanism of resistance to each anti-HER2 therapy drug.

1.6.11.2 Altered intracellular signalling.

1.6.11.2.1 Other intracellular mechanisms potentially involved in resistance to anti-HER2 therapy consist in

- Aberrant activation of the tyrosine kinase Sarcoma gene (*SRC)*, which is placed downstream of several RTKs, including HER2; notably, *SRC* inhibition restores in vitro and in vivo sensitivity to trastuzumab [292].
- Overexpression of Cyclin E, which binds cyclin-dependent kinase 2 (CDK2) and promotes the G1/S cell cycle transition. Interestingly, cyclin E is overexpressed in about 20% of HER2-positive BC and is associated with a worse patient prognosis. Based on this evidence, CDK2 inhibitors promise to improve the efficacy of anti-HER2 treatments [293].

1.6.11.2.2 Constitutive activation of the PI3K/AKT/mTOR pathway

Persistent activation of the phosphoinositol 3 kinase (PI3K)/AKT/ mammalian target of rapamycin (mTOR) signalling pathway can undermine the effectiveness of trastuzumab by bypassing its inhibitory effects. Mutations in PI3KCA or low levels of PTEN have been linked to resistance, and inhibitors targeting these pathways have shown promise in restoring sensitivity to treatment. [294-298]. Consistent with these findings, pharmacological inhibitors of PIK3CA (copanlisib, alpelisib) or mTOR (everolimus) sensitise cancer cell lines to trastuzumab [299-301]. Notably, about 30% of human HER2-positive BCs bear somatic alterations in PI3K/AKT/mTOR pathway genes, with *PIK3CA* mutations occurring in 20–23% of primary tumours [302].

1.6.11.3 Cross-signalling to HER2

1.6.11.3.1 HER2 heterodimers

HER2 can form heterodimers with other receptors like EGFR and HER3, enabling tumour cells to maintain HER2 signalling despite antibody treatment. This cross-signalling complicates treatment by reactivating HER2 pathways even when most HER2 receptors are blocked [303-305]. Other HER2 dimerization partners include insulin-like growth factor-1 receptors 1 and 2 (IGFR 1/2), the hepatocyte growth factor (HGF) receptor c-MET, EphA2 [306-309].

1.6.11.4 Activation of cyclinD1-cyclin-dependent kinase 4/6 (CDK 4/6) axis

Overexpression of cyclin D1/CDK4 or mutations in CDK4 contribute to resistance to anti-HER2 therapies in HER2-positive BC. Studies in mouse models have shown that the absence of cyclin D1 protects against HER2-driven tumours [310], and CDK4/6 inhibitors synergise with anti-HER2 treatments [311]. A quadruple combination therapy involving anti-HER2 treatment, palbociclib, and fulvestrant has shown promising results in HER2-positive ER-positive BC, indicating the potential of targeting the cyclin D1-CDK4/6 axis in combination with HER2 inhibitors and endocrine therapies [312, 313].

1.6.11.5 Escape from ADCC

The efficacy of trastuzumab partly relies on antibody-dependent cellular cytotoxicity (ADCC). However, overexpression of proteins like Neuromedin U (NmU) can reduce ADCC effectiveness, leading to resistance. The use of immune checkpoint inhibitors may help overcome this resistance [314-316].

1.6.11.6 HER2 gene mutations

Mutations in the *HER2* gene, particularly in regions critical for kinase activation, can lead to resistance against therapies like Lapatinib. However, newer drugs such as neratinib show promise in overcoming resistance caused by specific HER2 mutations. [317, 318].

1.6.11.7 HER2 heterogeneity

Intra-tumour heterogeneity of HER2 expression has also been associated with reduced activity of trastuzumab-based treatments in the neoadjuvant setting, possibly reflecting the presence of cell clones that express low HER2 levels and are not HER2-dependent. Details are mentioned in section 1.6.7

Table 1.7: Mechanisms of resistance to anti-HER2 agents [284]

Anti HER2 agent(s)	Mechanism of resistance	Factors involved
Trastuzumab	- Impaired HER2 binding	Low HER2 levels, Splicing variants (p95HER2; Δ16 HER2).
	-Parallel/downstream pathways	PI3KCA mutations, PTEN loss
	-Enhanced lipid metabolism	FASN
	-ER signalling	ER-PR expression
	-Cell cycle regulation	Cyclin D1-CDK 4/6 expression
	-Escape from ADCC	Poor binding to CD16A
Lapatinib	-HER2 signalling	*HER2* mutations
	-Cell cycle regulation	Cyclin D1-CDK 4/6 expression
	-Parallel/Downstream pathways	PI3K/AKT/mTOR pathway alterations
	-ER signalling	ER-PR expression
T-DM1	-Impaired HER2 binding	p95HER2; MUC4 expression
	-Parallel/downstream signalling	*NRG, HER2-HER3*, *PIK3CA* mutations
	-T-DM1 internalization/release	*SLC46A3, MDR1*
Trastuzumab plus Lapatinib	-Impaired HER2 binding	Low HER2 levels/ *HER2* mutations
	-FGFR1 signalling	*FGFR1* amplification
	-Downstream pathways	*PI3KCA* mutations,
	-ER signalling	ER-PR expression
	-Cell cycle regulation	Cyclin D1-CDK 4/6 expression
Trastuzumab + Pertuzumab	-Altered intracellular pathways	*PIK3CA* mutations
	-HER2 signalling	*HER2* mutations

T-DM1: Trastuzumab emtansine, **ER**: Oestrogen receptor ; **PR**: progesterone receptor; **ADC**: antibody drug conjugate; **FGFR1**: fibroblast growth factor receptor 1

1.6.12 Role of ER in response to anti-HER2 therapy (triple positive BC)

The crosstalk between the ER and HER2 signalling has also attracted a great deal of attention and has been studied in several clinical trials [261, 266, 319-321]. Both HER2 and ER drive BC proliferation by a complex network of molecular signalling processes [322]. The complexity of response to anti-HER2 therapy varies among the different ER expression groups, as reported in the literature. ER-negative / HER2-positive tumours have shown higher response rates compared to ER-positive/HER2-negative tumours [323] . However, some studies suggest that ER-positive tumours also exhibit a good response to anti-HER2 targeted therapy [324]. On the other hand, some studies found no relationship between ER status and response to anti-HER2 therapy [246]

The distribution of HER2-E subtype and activity of HER2 oncogenic signalling seems to be heavily influenced by ER status, with HER2-E subtype representing only 30 % of molecular subtypes within HER2-positive/ HR-positive BC [57, 264, 321, 325, 326], some authors even claimed that HER2-E subtype is predominantly ER-negative [326]. According to St. Gallen Expert Consensus, HER2-positive tumours are divided into two classes, a Luminal B-like subtype that features ER and/or PR expression and a HER2-E-like, which does not express both HR [256]. Several clinical trials and studies highlighted the bidirectional crosstalk between HER2 and ER when both receptors are expressed in BC cells [261, 266, 319-321, 327-329], and these reports concluded that HER2-positive tumours differ in main clinicopathological features and natural history of disease depending on HR expression.

1.7 Digital Pathology and Artificial intelligence

Histopathology has undergone major changes, first with the introduction of IHC, and latterly with genomic medicine. We argue that a third revolution is computational pathology (CPATH), including both digital pathology (DP) and artificial intelligence (AI). CPATH is defined as a branch of pathology analysing wide range of pathology images data and metadata for better disease understating [330].

DP includes the process of digitising histopathology slides using whole-slide scanners as well as the analysis of these digitised whole-slide images (WSI) using computational approaches [331]. The introduction of digitalised WSI technology has attracted the greatest attention of pathologists/clinicians and the use of DP is now becoming commonplace [331-334].

1.7.1 Digital Pathology and WSI Applications

WSI provide the possibility of viewing and manipulating pathology samples on a computer screen in a way comparable to a conventional microscope [335]. Moreover, WSI boasts many advantages over glass slides and a conventional microscope, including easy image accessibility, sharing, annotating and amenability to automated image analysis, which is believed to improve the objectivity and productivity within pathology practice. These features facilitated WSI integration in different pathology applications, mainly used for education, consultation, frozen section diagnosis, quality assurance, clinicopathological conferences and research [336, 337].

Several validation studies have shown that the diagnostic performance using WSI is comparable to that of a conventional microscope [335, 338, 339]. Since

2017, the FDA has approved the use of commercial WSI platforms, facilitating the use of DP as a tool for primary diagnosis [340-342].

1.7.2 Digital Image Analysis

Digital image analysis (DIA) refers to the process of extracting meaningful information and quantitative data from digital images using computational techniques. It involves the application of various algorithms and methods to analyse the visual content of images, identify patterns, and extract relevant features. It also has the potential to enhance the precision and reproducibility of pathology and improve BC diagnosis [343]. DIA offers a more efficient and standardised approach to mitotic counting. Advanced algorithms can be developed to automatically detect and quantify mitotic figures within digitised histopathological images.

DIA has shown high levels of reproducibility and accuracy in breast pathology [344]. It also focuses on quantifying biomarkers determined by IHC [345]. Several software solutions for breast pathology have emerged, such as ImageJ, and Qu Path [346] with most utilising scanned WSIs [347]. Many pathology departments are incorporating WSIs into their histology laboratory workflow. DP has enabled remote consultation, telepathology, interactive presentations of tumour features in multidisciplinary team conferences, advanced research methods, and improved histopathology education[348]. Recently, the food and FDA has approved the introduction of WSIs for digital surgical pathology. As a result, the demand for advanced image analysis software is on the rise [349].

1.7.3 Artificial intelligence applications

The widespread utilisation of WSI technology for primary breast pathology diagnosis paves the way for the integration of AI-based tools. AI is a broad field of research focused on designing computer systems that simulate human intelligence. Machine learning (ML) is a subfield of AI that develops algorithms enabling computers to adapt and solve problems based on data, without requiring explicit programming.

ML systems learn from provided data by applying statistical methods to identify patterns. These algorithms can be viewed as mathematical models that establish relationships between observed variables, referred to as features or predictors, and outcome variables, known as labels or targets [350, 351]. The observed variable and the output labels can be simple scalars, such as age, weight, and gender of a patient, to a more primitive observation, such as images of histopathology slides. However, as the relationship between the observed feature variables and the desired outcome labels becomes more complicated (such as mapping raw pixel values of images to their semantic label), the sophistication of the ML algorithms will have to grow to match the complexity of the relationship (**Figure 1.13).**

1.7.3.1 Diagnostic Applications

Regarding AI-assisted diagnostic applications, the initial step in diagnosing BC involves detecting invasive tumour cells, determining the tumour type, and assessing its extent. Researchers have utilised AI and ML techniques for various diagnostic applications.

ML algorithms have also shown promise in diagnosing LN metastasis, outperforming pathologists. Bejnori et al. reported that the algorithms outperformed a panel of 11 pathologists in a simulated time-constrained diagnostic setting [352].

In addition to tumour identification, AI and ML methods have been used to characterize invasive breast tumours and address the subjectivity and low concordance rates associated with histologic grading. While various features can describe histological components, such as tubular formation and mitotic count, much of the focus in this field has been on mitosis detection due to its prognostic significance, despite being a labour-intensive task.

Through using several approaches such as object recognition, detection and segmentation, current evidence indicates that computer vision algorithms may be capable of extracting several features from WSI to make a diagnostic prediction [347, 353, 354] .

These include AI algorithms that can provide diagnosis without input from pathologists. Examples include screening algorithms that can identify normal tissue (colonic, gastric biopsies, prophy-lactic and reduction breast specimens and so on) and provide automated reports on such cases.

1.7.3.2 Biomarker Status Determination

Automated quantification of IHC staining intensity, receptors and other markers scoring is attracting a lot of interest, and more recently, efforts have been made to predict BC biomarkers directly from the haematoxylin and eosin (H&E) slides [355].

ER, PR, HER2, and ki67 are usually assessed using IHC to determine therapy options offered to the patient [356]. Although the IHC techniques used are well validated, there remains significant inter-observer variability in manual biomarker status assessment [357, 358], suggesting an opportunity for ML-based systems to assist pathologists.

Couture et al. implemented feature-based and deep learning (DL) models to predict ER status and achieved an 84% accuracy when tested on H&E tissue microarray (TMA) images [355]. In a related study, Shamai et al. developed a DL system to predict multiple biomarkers, including ER and PR, with a high accuracy of 92% for ER status in high-confidence cases [359]. Other groups generated IHC-stained Ki-67 images using conditional Generative adversarial networks (GANs). Senaras et al created 15 real and 15 synthetic images of BC pathology for five experts, and their mean accuracy in distinguishing them was 47.3% [360].

In breast pathology, 10 cellular features introduced by Osareh et al. [361] into ML that were identified by an expert breast pathologist to differentiate between malignant and benign tumours using images of fine-needle aspiration biopsy samples [361].

1.7.3.3 Prognostic and Predictive Applications

One of the most important potential applications of AI in pathology is to predict patient prognosis and response to specific therapy based on morphological features [362, 363]. Image-based AI tools can provide a novel classification system that is based on clinical relevance according to outcome and response to therapy, and correlate a set of features out of a myriad of features related to

tumour cell morphology, architecture, stroma and microenvironment, and presence of LVI, as well as correlate all these features to defined endpoints of clinical relevance such as probability of recurrence or metastasis and degree of response to specific therapy [364].

1.7.3.4 AI and assessment of tumour microenvironment

Tumour infiltrating lymphocytes (TILs) have been considered one of the cancer hallmarks, with remarkable predictive importance [365]. Recent studies using ML based algorithms applied to histopathological images provided encouraging results. Development of ML algorithms for automated computational TILs assessment to allow precise, rapid and less exhaustive workflow is what is currently needed [366]. AI will not only reduce inter-pathologist disagreement but will add more information that cannot be assessed by human eye.

Apart from the evaluation of lymphoid infiltrates, stromal alterations are often subtle and difficult to characterize and quantify by light microscopy alone. Emerging data suggest that automated pattern recognition systems could be used to characterize stromal changes. For example, in a computer-generated automated analysis of routinely prepared H&E stained BC tissue sections, Beck, Sangoi [90] found that characteristics of the stroma correlated with BC survival and proved to be more prognostic than epithelial features. Creating an automated digital tool for recognizing and analysing tumour-related stroma could be valuable in pathology, aiding in assessing tumour boundaries, detecting cancer field effects, or gauging the potential of DCIS to progress to invasion post-treatment, should residual neoplastic cells persist. Developing robust al-

gorithms to differentiate between patterns of normal stroma and tumour-associated stroma in histopathology images is challenging. This challenge arises partly because clear morphological criteria for distinguishing tumour-associated stroma have yet to be established.

1.7.4 Artificial intelligence and assessment of HRE2 status

Different approaches have been applied in HER2 IHC AI algorithms. Some AI algorithms segment tumour cells, classify each cell into a different staining category, and then calculate to obtain a final score. Other AI algorithms evaluate the connectivity of HER2-stained membrane to determine HER2 IHC score [367]. Studies have used such AI algorithms to accurately determine HER2 IHC score and to discriminate HER2-positive and HER2 cases [367-369].

Wang et al developed an automated cellular imaging system that showed a higher correlation with HER2 status determined by FISH compared to the manual assessment of IHC slides [370]. In a similar approach, Rexhepaj et al designed a nuclear detection algorithm for quantifying IHC staining of ER and PR expression, which correlated well with manual quantification [371]. Skaland et al used DIA software and showed 100% concordance between algorithmic prediction and consensus clinical status assessment for HER2 IHC [372].

Oliveira, Ribeiro Pinto [373] developed a CNN model based on multi-instance learning to classify HER2-negative or HER2-positive from H&E images, and their trained model was tested on the CIA-TCGA-BRCA dataset, yielding an accuracy of 83.3%. However, they only classified HER2-negative and HER2-positive but not classified the four statuses of HER2. Lu, Toss [374] proposed a GNN model-SlideGraPh+, which not only predicted the DAB density of H&E

stained WSIs but also predicted the HER2 status according to the DAB density.

Finally, the ASCO/CAP guidelines have acknowledged AI algorithms as diagnostic modalities to evaluate HER2 IHC, and the CAP has published guidelines to facilitate the adoption of AI algorithms into clinical practice [141, 375].

Notably, AI algorithms have been developed to assist pathologists in detecting, classifying, and counting HER2 signals in cells of interest, and excellent concordance between manual scoring and AI scoring of HER2 FISH has been detected [376]. The benefits of using AI to analyse HER2 FISH include improved efficiency and productivity because manual counting of HER2 FISH signals is time consuming [377-381].

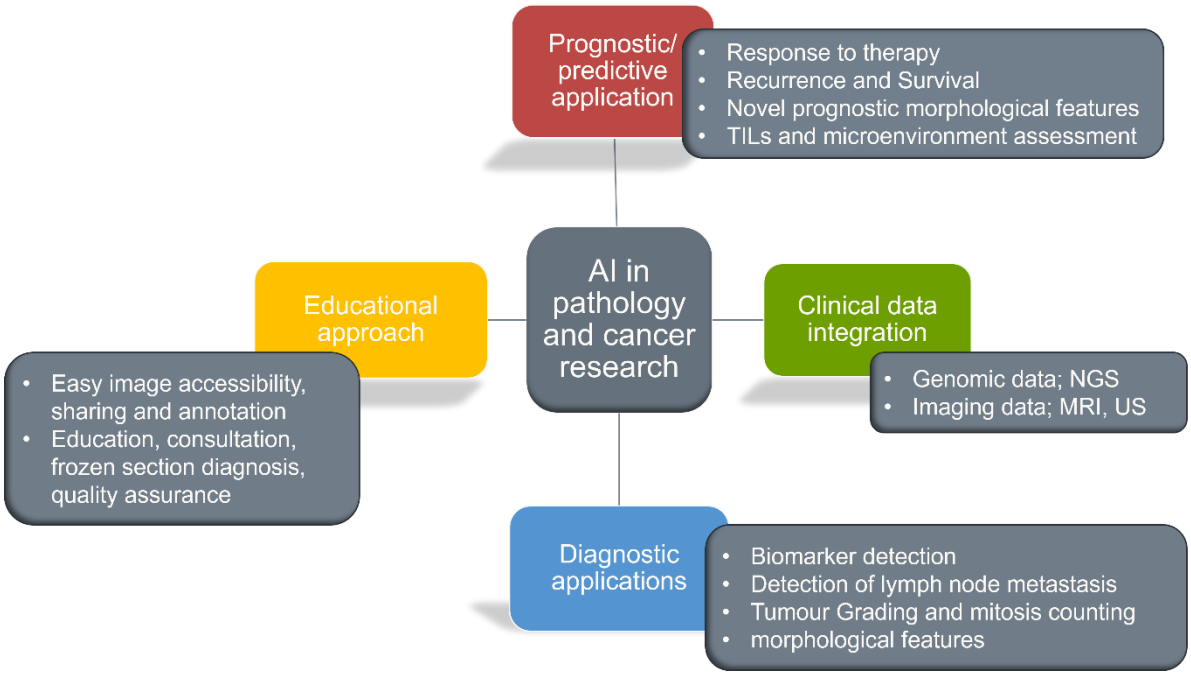


Figure 1.13: Diagram illustrating the main applications of digital pathology and AI in pathology. AI, artificial intelligence; NGS, next-generation sequencing.

1.7.5 Challenges to AI application in breast pathology

With the advancement of AI applications in breast pathology, several challenges remain to be solved.

1.7.5.1 Data and image quality

AI-based approach is markedly dependent on the quantity and quality of the input data. For image-based models, image quality can have a large impact on AI performance. If the scanner cannot produce images at a high enough resolution, the model will not be able to distinguish the details required to make an assessment of tissues. Out of focus is another challenging issue. Scans at high magnification tend to have a limited focusing range, and scanned images cannot be refocused after the fact (unlike slides being observed under the microscope). This becomes problematic when small objects such as mitotic figures are under consideration as refocusing digital images will require a rescan [382].

1.7.5.2 Missing a tissue during scanning

The representation of the WSI on the glass slides remains not fully known, and whether missing tissue in the WSI that is present on the glass slides could result in a misdiagnosis or change the tumour margin from negative to positive remains a concern.

1.7.5.3 Computational efficiency of the analysis methodology and the sensitivity to the parameter settings

Besides the quality of input data, the quality of annotation is equally, if not more, important. For an AI approach to segment biological structures, the performance is dependent on the fidelity of the annotations by expert pathologists in the learning set [383, 384]. If the annotations contain high variability, the supervisory signal to the model will be inconsistent, and the model can expect to fail.

1.8 Hypothesis and Aim of the Work.

1.8.1 Hypothesis

1- CPATH may serve as a robust tool capable of providing an objective assessment of morphological features beyond the human eye, including the spatial distribution of tumour cells, surrounding stromal cells, and the morpho-molecular signature of the oncogenic signalling pathway.

2- The current spectrum of HER2 expression in BC appears to be evolving. We hypothesise that further refinement of the HER2-expression spectrum in BC, in relation to therapy response, may lead to improved patient outcomes. Additionally, the newly recognised entity of HER2-Low BC requires further investigation to elucidate its clinical and molecular characteristics.

1.8.2 Aims

1- Assess the quality of DP performance in routine practice, through assessment of different variables affecting the quality of reporting using WSI including the frequency and nature of missing a tissue on WSI compared to glass slides and its clinical implications, Image quality and the role of quality control (QC) measures in minimising these pitfalls

2- Using AI to study the prognostic role of tumour-associated stroma ratio and spatial distribution in BC
3- Characterisation of the morphometric features of HER2-positive BC that reflect HER2 oncogenic activity using DIA.
4- Differential response of HER2-positive BC patients to anti-HER2 therapy based on HER2 protein expression level and its related mechanisms.
5- Identify a set of genes modulating the response of HER2-positive BC patients to trastuzumab.
6- Study the integrated role of *ER, PR, Ki67, and ERBB2* mRNA expression levels on the response of HER2-positive BC to anti-HER2 therapy.
7- Identify and characterise HER2-Low BC class in routine practice as an individual subtype with setting a cut-off point for HER2-Low offering a potential to improve the reproducibility and concordance among pathologists in scoring this new entity.
8- Decipher the clinical, molecular and immunophenotypic characteristics of HER2-negative and HER2-Low tumours considering HR status.

Chapter 2. Patients And Methods

2.1 Patient cohorts

2.1.1 Nottingham BC cohort

This is a well-characterised cohort of 7,140 patients with invasive BC who were treated at Nottingham City Hospital between 1986 and 2018. The patients were aged 70 years or younger. The management of these patients was uniform based on tumour characteristics determined by the NPI HR and HER2 status.

Patients classified as having an excellent prognosis (NPI score ≤ 3.4) did not receive any additional therapy after primary surgery. However, patients with an NPI score above 3.4 and positive ER status were treated with tamoxifen. Premenopausal patients in this group also received Goserelin (Zoladex). Patients who tested negative for ER and were deemed suitable for chemotherapy received cyclophosphamide, methotrexate, and 5-fluorouracil (CMF) treatment. None of the patients in this cohort received neoadjuvant therapy. HER2-positive patient received adjuvant trastuzumab. A subset of HER2-positive patients in our cohort were diagnosed before the era of targeted anti-HER2 therapy and treated with chemotherapy with/without tamoxifen.

The cohort's clinical history, tumour characteristics, and outcomes were prospectively recorded and regularly updated. Clinical details included patient age at diagnosis, menopausal status, tumour size, tumour grade, tumour type, NPI, nodal stage, and the presence of LVI [385]. ER, PR, HER2, and Ki67 data were available as previously published [386-389]. Hormonal and HER2 statuses were assessed according to the ASCO/CAP guidelines [165]. The Ki-67 score was calculated by visually evaluating the ratio of the number of positively stained tumour cells to the total number of malignant cells evaluated. The Ki-

67 score is expressed as a percentage and is an indicator of IHC-based tumour proliferation [390] and was defined as high when ≥14% of tumour cells showed nuclear positivity [391]. The recorded outcomes included (BCSS), which denotes the time in months from the primary surgery until BC-related death. Additionally, distant metastasis-free survival (DMFS) was recorded, representing the time in months from the primary surgery to the occurrence of distant metastasis and recurrence-free survival (RFS) was defined as the time from the date of curative surgery to the time of recurrence event [392]. **Table 2.1** provides a comprehensive summary of the clinicopathological characteristics observed within the Nottingham cohort.

2.1.1.1 Neoadjuvant cohort

A total of 766 invasive BCs who received neoadjuvant chemotherapy (NACT) and/or neoadjuvant anti-HER2 therapy with subsequent therapeutic surgery between 2013 and 2020 were also investigated. Patients were treated at Nottingham University Hospitals NHS Trust. Patients were considered eligible for anti-HER2 therapies if their tumours showed HER2 IHC score of 3+, or 2+ with *HER2*/CEP17 ratio ≥2.0 regardless of *HER2* copy number (CN) or if the *HER2* gene CN was ≥6, as recommended by UK guidelines and ASCO/CAP guidelines [141, 161]. Treatment was given according to institutional guidelines. Patients were divided into two groups according to the neoadjuvant treatment received: chemotherapy alone and chemotherapy with anti-HER2. **Table 2.1** summarises the clinicopathologic data of the neoadjuvant cohort.

Table 2.1: Frequency of clinicopathological parameters of Nottingham BC series.

Parameter	Nottingham series		Neoadjuvant Cohort	
	Number	(%)	Number	(%)
Age at diagnosis				
≥ 50 years	5183	(72.0)	408	(64.4)
< 50 years	1957	(28.0)	226	(36.5)
Menopause status				
Premenopausal	2274	(31.8)	NA	
postmenopausal	4866	(68.2)		
Tumour size				
≥ 2cm	2687	(38.0)	NA	
<2cm	4453	(62.0)		
Grade				
1	1299	(18.0)	65	(8.6)
2	3030	(42.0)	504	(66.3)
3	2811	(40.0)	191	(25.1)
Tubule formation			NA	
>75%	574	(8.0)		
25%-75%	2050	(29.0)		
<25%	4516	(63.0)		
Pleomorphism			NA	
1	168	(2.4)		
2	2805	(39.3)		
3	4167	(58.3)		
Mitosis			NA	
1	3688	(52)		
2	1300	(18.0)		
3	2141	(30.0)		
Histological Tumour type				
Invasive duct carcinoma NST	4475	(63)	661	(86.7)
Invasive lobular carcinoma	785	(11.0)	57	(7.4)
Other tumour types	1880	(26.0)	44	(5.7)
Lymph node metastasis			NA	
No	4725	(66.0)		
Yes	2402	(34)		
Lymph node stage			NA	
1	4725	(66.2)		
2	1849	(26.0)		
3	553	(7.8)		
Lymph vascular invasion			NA	
No	5483	(77.0)		
Yes	1657	(23.0)		
Nottingham prognostic index				
Good	2870	(40.0)	NA	
Moderate	3340	(47.0)		
Poor	911	(13.0)		
Oestrogen receptor status				
Negative	**1440**	**(20.5)**	223	(29.2)
Positive	**5581**	**(79.5)**	540	(70.8)

Table 2.1 continued

Parameter	Nottingham series		Neoadjuvant Cohort	
	Number	(%)	Number	(%)
Progesterone receptor status				
Negative	2382	(35.9)	318	(41.7)
Positive	4251	(64.1)	444	(58.3)
HER2 status				
Negative	5728	(86.9)	343	(66.1)
Positive	865	(13.1)	176	(33.9)
Ki67 Index				
<14%	1776	(49.5)	NA	
≥14%	1813	(50.5)		
Molecular Classes			NA	
Luminal A	1602	(35.3)		
Luminal B	1666	(36.7)		
HER2-enriched	338	(7.5)		
Triple negative	930	(20.5)		
Adjuvant Chemotherapy			NA	
No	5102	(71.5)		
Yes	2035	(28.5)		
Adjuvant Endocrine therapy			NA	
No	2692	(38.0)		
Yes	4400	(62.0)		
Adjuvant anti-HER2 therapy			NA	
No	6319	(93.5)		
Yes	438	(6.5)		
Neoadjuvant anti-HER2therapy				
No			639	(83.3)
Yes			128	(16.6)
Neoadjuvant endocrine therapy				
No			317	(41.3)
Yes			450	(58.7)
Pathological response				
No			336	(74.3)
yes			116	(25.7)

NST: non special type. *Some data are missing from some parameters. **NA**: Not applicable

2.1.1.2 Exemplar Breast Cohort

Pathlake's BC exemplar project is a subset of the Nottingham cohort (**Section 2.1.1**) that included primary invasive ER-positive/HER2-negative BC cases and aims to develop a novel prognostic algorithm for patients with early-stage BC **Chapter 4)**. This algorithm leverages the power of AI to extract features from digitised images and create a risk score for patient stratification. This cost-

effective and time-saving tool can predict disease outcomes and guide patient management decisions. The study utilises a large cohort (n=1968) of primary invasive ER-positive/HER2-negative BC cases diagnosed and treated at Nottingham City Hospital, UK. Ninety-three per cent of patients received endocrine therapy, while clinically fit patients received chemotherapy. Notably, none of the patients received neoadjuvant therapy. Clinical data and tumour characteristics were collected, including patient age at diagnosis, histological tumour type, grade, size, LN status, NPI, and LVI status. Data on ER, PR, HER2, and Ki67 were obtained from a previously published study [385]. Outcome data included BCSS, DMFS, and RFS. Pseudonymised patient tissue samples were provided, with one representative FFPE tissue block containing adequate tumour tissue chosen per case. The Nottingham cases were then divided into a discovery set (n=1027) and a validation set (n=941) using a stratified random distribution of events. The cut-off values generated in the discovery set will be applied to the validation set for further analysis.

2.1.1.3 Oncotype DX cohort

This is a subset of the Nottingham cohort (**Section 2.1.1**) and included a well-characterised cohort of patients (n=363) who had undergone Oncotype DX testing between 2014 and 2018 as part of the routine clinical care at Nottingham City Hospital NHS Trust, UK, as per National Institute for Health and Care Excellence (NICE) guidance for early-stage BC [393], was included. This cohort was mainly utilised to refine the definition of HER2-Low tumours **(Chapter 9)**. Data on clinicopathological characteristics were collected retrospectively from patients' electronic records. In this cohort, patients had newly diagnosed BC with ER-positive/HER2-negative, LN negative or pN1a disease (one to

three involved nodes), underwent surgery with curative intent and were assigned clinically as the intermediate-risk group for adjuvant chemotherapy (NPI = 3.4–5.4) [393]. Selection of the block for Oncotype DX testing was based on a histological review of all tumour blocks, with the most representative of invasive tumour tissue and/or higher-grade component selected. Blocks with extensive DCIS or extensive necrosis are avoided as much as possible, so the neoplastic cells represent the invasive components. As all cases in our study had tumour blocks with adequate invasive tumour tissue, as they were surgical excision specimens, no minimum quantum (e.g. 100 invasive tumour cells) was used for selection. The Oncotype DX test is validated on needle core biopsies [394] so a small amount of tumour tissue can be considered sufficient. If the Oncotype DX test fails for any reason, including insufficient tumour tissue, a different block can be selected if available, or repeating the subsequent excisional specimen would be recommended. Transcriptomic data on *HER2* mRNA expression was available for this cohort within the recorded Oncotype DX report [395] which was carried out as part of the patients' clinical care for management**.** Briefly, mRNA levels were obtained from tumour samples extracted from FFPE tissue using high-throughput, RT-qPCR. Normalised expression measurements were calculated as the mean cycle threshold (CT) for the 5 reference genes minus the mean CT of triplicate measurements for each individual gene.

2.1.2 Transcriptomic cohort

2.1.2.1 Molecular Taxonomy of Breast Cancer International Consortium (METABRIC) cohort

This is a previously conducted study that involved a cohort comprising 1980 fresh-frozen samples of primary BC obtained from tumour banks in the UK and Canada. Both DNA and RNA were isolated from these samples and used for CN/genotype analysis and transcriptional profiling, respectively. The quality of the extracted DNA was assessed using agarose gel electrophoresis, while the integrity of RNA was evaluated using the Agilent 2100 Bioanalyzer Nanochip. DNA probes were hybridised to Affymetrix SNP 6.0 arrays at AROS Applied Biotechnology, and the resulting data were analysed. Biotin-labelled complementary RNA (cRNA) was generated from the total RNA using the Illumina Totalprep RNA amplification kit and hybridised onto Illumina Human HT-12 v3 platforms. The gene expression raw data obtained was pre-processed and normalised as previously described [396]. In this cohort, patients who tested positive for ER and/or were negative for LN involvement did not receive adjuvant chemotherapy **(Table 2.2).** However, patients who were ER-negative and had positive LN status were offered adjuvant treatment. Notably, none of the patients with HER2 positivity received anti-HER2 targeted therapy with trastuzumab.

2.1.2.2 The Cancer Genomic Atlas Breast Cancer (TCGA-BRCA) cohort.

The Cancer Genomics Browser of the University of California Santa Cruz (UCSC) was used, it provides access to the images and clinical data of The Cancer Genome Atlas (TCGA) database, which can be found on their website (https://genome-cancer.ucsc.edu/) and was used in Wang, Jensen [397] study. H&E images (n=1070) were obtained from excision specimens from different institutions across the United States and scanned using various scanners. Clinical data were available for 854 cases, and these were retrieved from the Cancer Genomics Browser of the University of California Santa Cruz website (https://genome-cancer.ucsc.edu). Comprehensive clinical data, including age, tumour size, grade and its components, histological tumour subtypes, pathological stage, ER/PR status, LVI, and Ki67 score, were extracted from the TCGA cohort. OS, BCSS and RFS data were also included in the analysis. All images were downloaded from the cBioPortal website and viewed on Aperio ImageScope [398]. To access the TCGA-BC RNAseqV2 gene expression and clinical data, TCGA Data Portal was utilised. This portal provides the necessary data for analysis, including normalised gene expression values and clinicopathological characteristics such as age, gender, tumour location, histological type, and TNM stage **(Table 2.2).**

2.1.2.3 Breast Cancer Gene-Expression Miner v4.0 (BC-GenExMiner v4.0)

BC Gene-Expression Miner v4.0 (BC-GenExMiner v4.0) is available at https://bcgenex. This dataset consists of transcriptomic data from a large, pooled cohort of patients, totalling 10,872 BC patients. The BC-GenExMiner v4.0 platform offers three statistical mining modules for analysis.

The first module is the prognostic module, which enables the assessment of the prognostic impact of candidate gene expression in BC. It achieves this through the application of univariate Cox regression proportional hazards models and the generation of Kaplan-Meier plots to visualize survival outcomes based on gene expression levels. The second module is the expression module, which can examine the expression levels of candidate genes in relation to various clinicopathological variables, such as nodal status, HR status, and molecular subtypes. The final module is the correlation module which provides the ability to calculate Pearson correlation coefficients between the expression levels of the candidate gene and other genes of interest. Furthermore, it can perform subgroup analyses by dividing the cohort into sub-populations based on different clinicopathological variables, such as nodal status, HR status, or molecular subtypes [399].

2.1.2.4 ROCPLOT online dataset for response to therapy

The ROC plotter is for breast, ovarian, and colorectal cancer patients and glioblastomas. The custom plotter generates a ROC plot for user-uploaded data. ROC plot online tool is capable of linking gene expression and therapy re-

sponse using transcriptome-level data. It was also used to validate the predictive role of the selected biomarkers in response to anti-HER2 therapy. Published gene expression data of 36 publicly available datasets were integrated with treatment data into a unified database. Response to therapy was determined using either author-reported pathological complete response data (n = 1,775) or relapse-free survival status at 5 years (n = 1,329). Treatment data includes chemotherapy (n = 2,108), endocrine therapy (n = 971) and anti-HER2 therapy (n = 267) [400]. The transcriptomic database includes 20,089 unique genes and 54,675 probe sets. Gene expression and therapy response are compared using receiver operating characteristics and Mann-Whitney tests.

Table 2.2: Frequency of clinicopathological parameters of the METABRIC and TCGA cohorts.

Parameter	METABRIC series (1980)		TCGA cohort (854)	
	Number	(%)	Number	(%)
Patient Age				
≤ 50 years	424	(21)	231	(27.0)
> 50 years	1556	(79.)	623	(73.0)
Tumour size*				
≤ 2cm	622	(32)	151	(24.8)
> 2cm	1331	(68)	459	(75.2)
Tumour grade*				
1	170	(9)	79	(20.8)
2	770	(41)	145	(38.3)
3	952	(50)	155	(40.9)
Nodal Stage*			NA	
1	1035	(53)		
2	622	(31)		
3	316	(16)		
Vascular invasion*				
Definite	1207	(62)	559	(65.5)
Negative/Probable	736	(38)	295	(34.5)
Oestrogen receptor status*				
Negative	474	(24)	185	(22.5)
Positive	1506	(76)	639	(77.5)
Progesterone receptor status*				
Negative	940	(48)	272	(33.0)
Positive	1040	(52)	551	(67.0)
HER2 status*				
Negative	1733	(87)	569	(80.5)
Positive	247	(13)	138	(19.5)
Nottingham prognostic index				
Good	680	(34)	NA	
Moderate	1101	(56)		
Poor	199	(10)		
PAM50 molecular subtyping	724	(36.4)	405	(52.9)
Luminal A	488	(24.7)	141	(18.4)
Luminal B	329	(16.7)	56	(7.3)
HER2-Enriched	240	(12.2)	133	(17.4)
Basal like	199	(10.1)	30	(3.9)
Normal like				

* Some data are missing from the online website; NA: Not available

2.2 Construction of tissue microarray (TMA)

The TMA technique brings revolutionary changes in high-throughput analysis by being able to handle up to several hundred samples in one slide with sub-

sequent application of techniques such as IHC to allow a diverse range of biomarkers to be studied [401]. Using TMAs saves a considerable amount of time and reagents while attaining more standardised laboratory conditions [402]. TMAs can make working with and evaluating IHC and other staining protocols faster and easier [403]. The steps of the TMA production included the collection of the study cohort to be arrayed, preparation of the recipient array blocks, designing the array grids, construction of the individual array blocks, and preparation of the array block for sectioning [404]. The initial tasks of preparing donor blocks and TMA design are the most critical parts of TMA construction and are, therefore, quite time-consuming. TMA construction was performed mainly by the author.

2.2.1 Collection of the study cohort, preparation of the donor blocks and their corresponding slides

Searching for HER2-positive cases was carried out through different data storage pathology systems. A representative FFPE tumour block (donor) for each patient's specimen was retrieved from the tissue block archives. Priority was given to blocks containing viable tumour tissue that were not frequently sectioned for previous studies (not less than 4mm in depth). A fresh full-face section of 4 micrometres (µm) thickness was cut from each block and stained with H&E and each slide was reviewed by the author using light microscopy to confirm the presence of the tumour and to identify the most representative areas suitable for array sampling. In cases where the block did not contain any tumour, insufficient tumour, or was thinner than 4mm, an alternative archive block for the patient was retrieved. Some cases were omitted from the arrays

because either the block was thin or contained no/insufficient tumour with no alternative blocks in the archive.

Digital slide scanning with a 'Pannoramic' digital slide scanner (250 Flash III, 3DHISTECH®, Budapest, Hungary), followed by marking the representative tissue regions, was carried out **(Figure 2.1**), using 'Slide Viewer' software v 2.5.0 (3D HISTECH®, Budapest, Hungary). The Slide Viewer enabled me to view the scanned slides and to mark the areas of interest (those non-necrotic with high tumour burden). Block layout design using the TMA Grand Master software v 2.8 (3D HISTECH®, Budapest, Hungary), followed by digital slide overlay and marker transfer, and finally punching from donor block into recipient block, was performed.

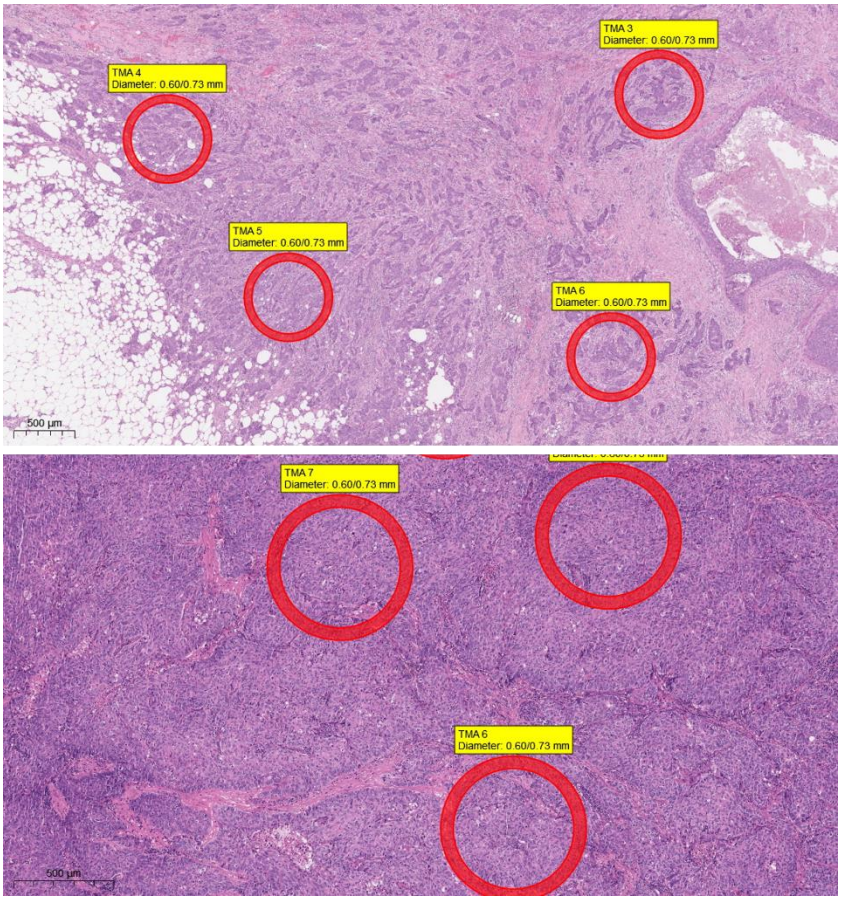


Figure 2.1: Marking of invasive breast cancer using 0.6mm circle diameter using slide viewer software.

2.2.2 Preparation of the recipient array blocks

Recipient blocks were prepared by using freshly poured empty paraffin blocks (5–10 mm deep) into which the tissue array cores were extruded. The recipient block was prepared by pouring molten (56–58°C) regular paraffin wax into a mould, after which a tissue cassette was placed on top [404]. The complex was cooled on ice until hardened. The wax was checked for the presence of air bubbles, striations or stress marks, and fault lines, and it was ensured that wax covered the entire base of the cassette without surplus wax on the edges or back of the cassette. The block was trimmed smooth to ensure a flat surface using a microtome [405]. This step was performed with the help of the group technicians.

2.2.3 Construction of the individual array blocks

The ‘TMA Grand Master® (3D HISTECH®, Budapest, Hungary) was used for automated TMA production with 0.6mm [405]. Donor blocks were loaded, and automatic donor block labelling and aligning with the image was used. This was done by the author.

2.2.4 Designing the Array Grids

Selection of the TMA layout was made by selecting the layout editor in the TMA grandmaster software v 2.8 (3D HISTECH®, Budapest, Hungary). The creation of a new layout, followed by the insertion of a new layout name, was performed. Block size was inserted as a standard of 24x35mm. The core size was

set up to 0.6mm. Three replicates were prepared, where possible, to allow for backup and compensate for core loss if needed. Blocks were distinguished by version number and manually added to the block later. Cores in each subarray were arranged at a centred distance, and the subarrays were separated by a single gap for orientation and macroscopic identification of the TMA block. Additional orientation cores from normal kidney, liver and tonsil tissues were included outside of the geometric margin of the array on the top and bottom left-hand side. The orientation cores served as positive internal experimental controls.

Great care was taken during the documentation of both the donor block and the TMA position of each individual core. An array map grid was produced for each array block. Each grid contained the patients' unique identifier and was arranged in the same sequence corresponding to its position in the array block. All the former steps were performed by the author.

2.2.5 Preparation of the array block for sectioning

TMA blocks were heated at 37°C for 20 minutes to facilitate adherence and annealing of the tissue cores to the walls of the recipient holes and to make the wax flexible to handle. After warming the block, a clean glass microscope slide was placed on top of TMA blocks and gently pushed all tissue cores into the block to pave them with the surface and to smoothen the block surface. Using a microtome, 4µm sections were cut from TMA blocks onto permanent positively charged glass slides (Surgipath, X-tra™ Adhesive, Peterborough, UK), using the standard microtome sectioning technique. The initial section from each block was stained in H&E for QC purposes to ensure histology and

efficient construction steps **(Figure 2.2).** This step was performed with the help of the group technicians.

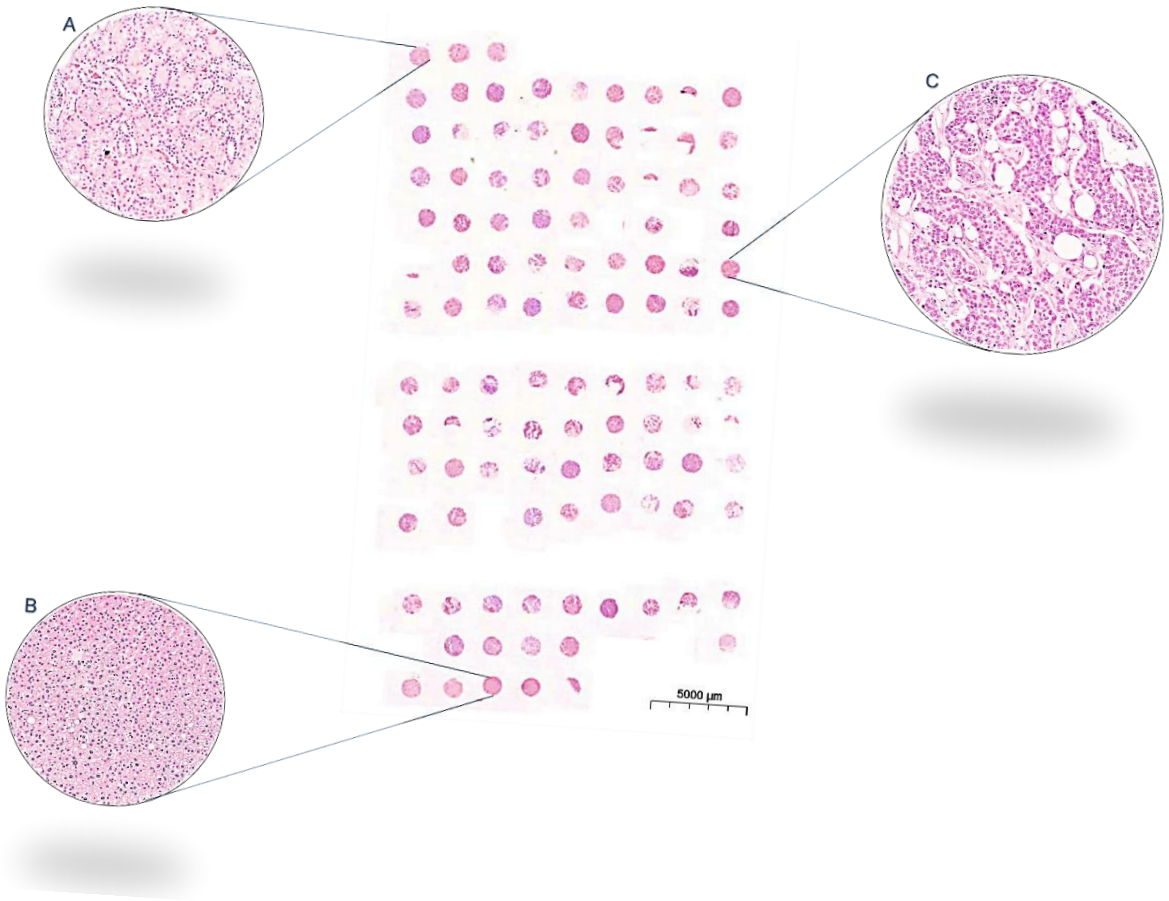


Figure 2.2: H&E sections of HER2-positive TMA. The grid represents an overview of 0.6mm needle core diameter TMA. A and B represent orientation cores from normal kidney and liver, respectively, included outside of the geometric margin of the array on the top and bottom left-hand side. C: core from invasive breast cancer.

2.3 Biomarkers data

The study analysed several molecular biomarkers relevant to BC, which had been previously studied in the Nottingham cohort. These biomarkers included HRs such as ER and PR, as well as HER2, cell proliferative marker Ki-67 and Androgen receptor (AR). HER2 staining in diagnostic practice was completed

on the Ventana Benchmark ULTRA IHC automated staining system using the Ventana PATHWAY anti-HER-2/neu, Rabbit Monoclonal ready-to-use primary antibody in combination with Ventana detection kits. Cases with borderline protein expression underwent FISH analysis as part of the patient's routine diagnostic pathway. HER2 scoring follows the recommendations from ASCO/CAP guidelines and UK guidelines [161, 165]. ER IHC staining was carried out following a standard protocol, the 4µm sections were prepared, and slides were processed through pre-diluted Tris-based buffer with a basic pH (Roche, Ventana) for 64 minutes at 95°C for antigen retrieval, an anti-ER rabbit monoclonal antibody SP1 clone (Roche) was applied and incubated for 16 minutes. ER and PR positivity was assessed according to ASCO/CAP guidelines if ≥1% of the invasive tumour cell nuclei were immunoreactive [406]. IHC was used to assess Ki-67, which was carried out on full-face sections. AR IHC was carried out by a former researcher and data were retrieved from the Nottingham biomarker library.

2.3.1 BC molecular subtypes in Nottingham cohort

BC molecular subtypes in the Nottingham cohort were determined based on tumour immunohistochemical profiling [407, 408], which resulted in luminal HR-positive: ER+ and/or PR+), HER2-positive class (HER2-positive regardless of the expression of other markers and Triple Negative subtype: ER-negative, PR-negative and HER2-negative [409].

2.3.2 Selection of biomarkers for this research

In this study, HER2 IHC staining was carried out on a subset of the Nottingham cohort. We followed the standard HercepTest guidelines (Dako) to evaluate the

immunoreactivity of HER2. According to these guidelines, a score of 0 or 1+ indicated negative and/or low HER2 staining, while a score of 3+ indicated positive HER2 staining. Cases with a score of 2+ were considered equivocal. In cases with equivocal HER2 status, CISH was used to quantify *HER2* gene amplification using a kit called HER2 CISH pharmDx from Dako, and the assessment was done according to the ASCO guidelines [165]. Details on the CISH technique will be discussed in **section 2.7**.

According to the scientific context, HER2 staining was carried out on both TMA sections and full-face resection specimens in this study.

Additional biomarkers influencing the response of HER2-positive patients to trastuzumab-based treatment (TATA-box Binding Protein Associated Factor 10 (TAF10) and Branched Chain Amino Acid Transferase 1 (BCAT1) were identified. These genes were chosen via differential gene expression analysis (DGE) and were found to be enriched in cell lines sensitive or resistant to trastuzumab. The protein expression of these genes was evaluated using IHC to detect their antibodies on TMA sections. Details on gene selection are mentioned in **Section 2.11** and **Chapter 7.**

2.4 Validation of antibody Specificity

2.4.1 Western blotting (WB)

Western blotting was used to validate the specificity of antibodies involved in the immunostaining. Western blotting was applied to whole cell lysates of cervical/ BC cell lines (HeLa, MCF7, MDA-MB-231, MDA-M-157 and SKBR3).

2.4.1.1 Cell lines and preparation of cell lysates.

Cell lysates were prepared using cell lines obtained from the American Type Culture Collection, Rockville, MD, USA. MCF7, MDA-MB-231 cells were cultured in Roswell Park Memorial Institute (RPMI-1640) medium (GE Healthcare Life Science, AE25719279, South Logan, Utah), and SKBR3 cells were grown in McCoy's 5A medium (Sigma Life Science, SLCB4463, USA) while HeLa cells were cultured in Dulbecco's Modified Eaglemedium (DMEM) (Sigma Life Sciences, RNBH6547, UK). All media were supplemented with 10% fetal bovine serum (FBS) (Sigma-Aldrich, UK). Cells were maintained in a 37°C humidified incubator with 5% carbon dioxide (CO_2).

Cells were grown until 80 to 90% confluent. Respective culture medium was discarded, and cells were washed twice with sterile Dulbecco's Phosphate BufferedSaline (DPBS) (Sigma Life Science, RNBH8631, UK), in order to remove the medium residue. Thereafter, cells were detached by adding trypsin (Sigma Life Science, 29259717, USA); a serine protease, which breaks down protein bounds to allow a gentle dissociation of cells from the tissue culture flasks and incubatedat 37°C for ≤ 5 minutes. Following this, cells were checked under the microscope to ensure they were detached, and fresh media was added to neutralize the detached cells, followed by centrifugation at 1000 rpm for 5 minutes. Cell pellets were re-suspended in fresh media, and cells were counted (the aim is a concentration of 1×10^7 cells/mL, which is roughly equal to 1µg of protein/1 µl). To count viable cells, a Neuber Haemocytometer was used; where a mixture was prepared by adding Trypan Blue (a substance that stains the non-viable cells in blue) to the cell suspension (with a 1:1 ratio). 20µl

of Trypan Blue/ cell mix was loaded under acoverslip on the haemocytometer and only viable cells were counted in the central(5x5) grid, using light microscopy. All counts were carried out in duplicate and thenumber of cells per ml was achieved by multiplying the average cell count by dilution factor (2) $x10^4$. After determining the cell count, the cell suspension was centrifuged at 1000 rpm for 5 minutes and the cell pellet was placed on ice. To lyse the cells, each $1x10^7$ cell pellet was re-suspended in 1 ml of RIPA lysis buffer (25mM Tris, 150mM sodium chloride, 1% Nonidet P-40, 1% sodium deoxycholate and 0.1% Sodium Dodecyl Sulfate (SDS) (Thermo Scientific, #89901) and protease inhibitor (Roche, Complete Mini Protease Inhibitor Cocktail tablets, #04693124001). After 15 minutes of incubation on ice, cell lysis was centrifuged at4°C at 13000 rpm for 10 minutes. Finally, the supernatant was collected and stored at -20°C until use.

2.4.1.2 Sample preparation and gel electrophoresis.

Samples of approximately 30 µl volume were prepared by adding 20 µg of proteinlysates, 7.5 µl of NuPAGE/ Bolt LDS Sample Buffer (4x) (Novex Life technologies)and 3 µl of NuPAGE/ Bolt Reducing Agent (10x) (Novex Life technologies,NP0009). After mixing, samples were heated at 100°C for 5 minutes and placed on ice. Following that, samples were loaded onto NuPAGE/Bolt Bis-Tris protein gel(4-12%) (Novex Life Technologies, NW04120BOX) in 20x MOPS SDS running buffer (Novex Life Technologies). The PageRuler™ Plus Prestained Protein Ladder (Thermo Scientific) was used as a molecular weight standard and gels were run at 150 volts for 90 minutes or 160 volts for 60 minutes for NuPAGE or Bolt gels, respectively.

2.4.1.3 Protein transfer

After electrophoresis, proteins were transferred to Polyvinylidene difluoride (PVDF) membrane (Merck Millipore, R9DA13833, Ireland) and electro-blotting wasperformed at 25 Volt for 60 minutes in 20x NuPAGE/ Bolt transfer buffer (Novex Life Technologies), which was prepared by adding 1x NuPAGE/Bolt transfer bufferwith 10% methanol and 0.1% NuPAGE/Bolt Antioxidant (Novex Life Technologies).

2.4.1.4 Blocking and antibody probing

The membrane was blocked in blocking buffer, using 5% milk powder (Marvel Original Dried Skimmed Milk, Premier Food Groups Ltd, UK) in Phosphate Buffer Saline (PBS) (Oxoid, Hampshire, UK) containing 0.1% Tween-20 (Sigma) for one hour at room temperature. After blocking, the membrane was incubated with primary antibodies at 4°C overnight, using the optimal dilutions detailed in **Table 2.3**. 1:5000 mouse monoclonal anti-β-actin primary antibody (Sigma-Aldrich, A5441) was included as a positive control. After washing with PBS + 0.1% Tween-20, 3 x 5 minutes each, the membrane was incubated for 60 minutes at room temperature with 1:1000 anti-rabbit or anti-mouse monoclonal horseradish peroxidase (HRP) conjugate (Dako, Carpinteria, CA, USA) was applied as a secondary antibody. n

2.4.1.5 Detection using Enhanced Chemiluminescence (ECL)

ECL was used to visualise protein bands using MagicMark™ XP Western Protein Standard (Invitrogen) as a molecular weight standard. For the detection, the following steps were carried out in the dark room, the membrane was incubated with ECL detection reagent (GE Healthcare, UK) for 1 minute and then

removed from the solution and placed in a plastic pouch, making sure to remove air bubblesand excess reagent. Following that, the membrane pouch was placed into a cassette and a film sheet (Kodak Bio Max Film) was overlaid on the membrane pouch for 10 minutes. The film was soaked in developer (Sigma Aldrich, UK) for 1minute, placed in fixing solution (Sigma Aldrich, UK) for 1 minute, then washed inwater until the background was clear, and allowed to dry overnight.

2.4.2 Peptide Blocking

Peptide blocking was employed to evaluate the specificity of the primary antibody used in the IHC staining. This technique involves pre-incubating the primary antibody with a molar excess of a peptide harbouring the identical amino acid sequence as the target antigen. Two antibody solutions were prepared: one containing the primary antibody pre-incubated for the same duration as the antibody at a ratio of 5:1 to 10:1 blocking peptide ("blocked antibody solution"), and a control solution containing the primary antibody alone ("control antibody solution"). Tissue sections were then incubated with either the blocked antibody solution or the control solution. Subsequent steps followed the standard IHC protocol, including secondary antibody incubation, detection, and analysis.

A significant reduction or complete absence of staining in the sections incubated with the blocked antibody solution, compared to the control sections, indicated specific binding of the primary antibody to the target antigen. This confirmed observation arises because the free-blocking peptide is competitively bound to the antibody's binding site, preventing it from recognizing and

attaching to the target antigen present within the tissue sections. The inclusion of peptide blocking in the IHC protocol served to strengthen the validity of the primary antibody's specificity towards the protein of interest, ensuring confidence in the interpretation of the staining patterns observed in the tissue samples (**Table 2.3).**

2.5 Immunohistochemistry

IHC is a widely used technique in both diagnostic and research fields. It is based on the concept of detecting antigens (proteins) through the process of antigen-antibody binding in biological tissues. It allows the examination of differentially expressed proteins in tissues and the understanding of their distribution and cellular localisation. In this study, IHC was performed using a Novolink polymer detection system (Leica Biosystems, RE7150-K). Staining was carried out on 4µm thick tissue sections.

Steps of the IHC technique

2.5.1 Optimisation of primary antibody

All primary antibodies were optimised, using BC TMA sections, to ensure appropriate staining, with no or minimal backgroundstaining. Optimisation of the staining conditions for each antibody under study was performed by changing several variables in the staining protocol until the optimum result was obtained. These variables include 1- dilution of the antibody, starting with the dilution recommended by the supplier datasheet plus three or four dilutions around (i.e., above and below the recommended one, e.g., in case of recommended 1: 100 dilution, other dilutions including 1:50, 1:25, 1:150, 1:200 were tried). 2-

Antigen retrieval solution: microwave pre-treatment in citrate buffer at pH 6.0, or water bath pre-treatment.

Therefore, the optimum conditions for staining of different antibodies used in the current study were carefully chosen based on the information from previous publications using the same antibody clone, antibody suppliers' datasheets and the previous experiences of our laboratory. Ideally, an antibody with specific staining of the cells showing immunoreactivity within the specific cellular location (membranous, cytoplasmic, or nuclear) with no or minimal background staining would allow the most accurate evaluation of its protein expression status. This was obtained by finding the optimum antibody concentration by applying serial dilutions of the antibody to sequential sections of breast tissue.

2.5.2 Slide heating, Deparaffinisation and Rehydration

Slides were placed on a 60°C hotplate for 20 minutes, to melt the paraffin and maintain firm fixation of the BC tissue on the slides. The slides were then allowed to cool for 5 minutes and placed in an auto stainer machine (Leica Biosystems), where they were de-waxed, in two xylene baths for 5 minutes each, followed by three changes of industrial methylated spirit (IMS) (100%, Thermo Fisher Scientific, M/4450/25) two minutes each. The slides were then rehydrated in water for 3 x 5 minutes.

2.5.3 Antigen retrieval

Heat-induced antigen epitope retrieval was performed in citrate buffer (1M sodiumcitrate at pH 6.0) for 30 minutes using a water bath preheated to 90c followed by cooling under running tap water for 5 minutes.

2.5.4 Applying Leica Max Polymer Detection Kit

The following steps were accomplished manually either by using Sequenza trays,to stain full-face sections, or a flatbed for the TMA sections. For Sequenza staining,slides were loaded into Sequenza plates (Thermo Scientific) under the surface of tap water, making sure that they were free of air bubbles, and placed into Sequenza trays. Subsequently, slides were washed twice with Tris Buffered Saline(TBS, PH 7.6). When flatbed staining was used, slides were placed onto a flatbed tray and a hydrophobic barrier pen was applied across the width of the slides to limit the wetting area and ensure reagents were confined to the TMA cores. Slides were washed two times with TBS-T (TBS pH 7.6, containing 0.1% Tween 20). Therest of the steps are the same in both ways, with one difference, which is the useof TBS for washing in the Sequenza staining method, while TBS-T was used when the flatbed staining was applied. Endogenous peroxidase activity was blocked by applying a peroxidase block (Novolink kit) for 5 minutes. Slides were rinsed with TBS/TBS-T for 2 x 5 minutes, followed by application of protein block (Novolink kit) for 5 minutes. After another TBS/TBS-T wash, sections were incubated with the primary antibody, optimally diluted in Leica antibody diluent (Lieca, Biosystems, UK, RE AR9352). Incubation times differed between 30 miutes – 2hours at room temperature and overnight at 4°C **(Table 2.4)**. Slideswere washed with TBS/TBS-T for 2 x 5 minutes and incubated with Post Primary Block (Novolink kit) for 30 minutes followed by another washing step. Novolink polymer (Novolink kit) was added for 30 minutes and 3, 3'Diaminobenzidine (DAB) working solution (1:20 DAB chromogen in DAB substrate) (Novolink kit), for 5 minutes, was applied. Before and after adding the DAB, slides were washed twice with TBS/TBS-T

for 5 minutes. Slides were counterstained with Novolink Haematoxylin for 6 minutes.

2.5.5 Dehydration and mounting

Slides were dehydrated by placing them in the autostainer machine, where they were immersed in IMS for 3 x 2 minutes, then cleared in xylene for 2 x 5 minutes. Finally, slides were mounted, with a glass coverslip, using Dibutylphthalate Polystyrene Xylene (DPX) (BDH, Leica Microsystems, Newcastle, UK), and left to dry overnight at room temperature

Table 2.3: Validation of biomarkers used in the current research

Antibody	Validation of specificity	Molecular Weight	Concentration	Supplier
TAF10	Peptide Blocking	NA	TAF10 recombinant protein at concentration of 10:1	Novus Biologicus
BCAT1	Western blotting	~43kDa	1:2000	Invitrogen
AR	Western blotting	~110kDa	1:10000	Santa Cruz Biotechnology
β-actin	Western blotting	~42 kDa	1:5000	Sigma

Table 2.4. Details of the antibodies used in this research.

Antibody	Supplier	Species	Code/ clone	Dilution for IHC	Antigen retrieval	Incubation period for IHC	Positive control for IHC	IHC localisation	Cutoff values
ER	Ventana	Rabbit monoclonal	SP1		Microwave	16 Min	Internal/normal breast tissue	Nuclear	Negative (0), Positive (≥1%)
PR	Agilent	Mouse monoclonal	PgR636	1:150	Microwave	30 Min	Internal/normal breast ducts	Nuclear	Negative (0), Positive (≥1%)
AR*	Santa Cruz Biotechnology	Mouse monoclonal	AR-N20, sc-816,	1:40	Microwave	60 Min	kidney	Nuclear	Low <10% High≥10%
HER2	DAKO	Rabbit polyclonal		1:400	Water bath	30 Min	BC tissue	Membranous	Negative (<10%), Positive (≥10%)
Ki67*	DAKO	Mouse Monoclonal	MIB-1	1:100	Microwave	1 hour	Tonsil tissue	Nuclear	Negative (<14%) positive (≥14%)
TAF10	Novus Biologicus	Rabbit polyclonal	NBP1-80706	1:50	Water bath	Overnight	Kidney	Nuclear	Positive>195 Negative<195
BCAT1	Invitrogen	Mouse monoclonal	OTI3F5	1:100	Water bath	1 hour	Endometrium	Cytoplasmic	Positive>195 Negative<195

*Carried out by a former researcher; NA: Not applicable

2.5.6 Positive and negative controls

Positive and negative controls were included in all IHC experiments. Positive control tissues were selected based on antibodies' supplier recommendations or through choosing specific tissues, which showed high expression of the target proteins, in addition to Human Protein Atlas (http://www.proteinatlas.org/). Negative controls were included, whereIHC staining was carried out on BC tissues with the omission of primary antibodies.

2.5.7 Assessment of IHC staining

Stained sections were scanned to produce high-resolution digital images (0.45 µm/pixel) using Pannoramic's digital slide scanner (250 Flash III, 3DHISTECH®, Budapest, Hungary) at 20x magnification. Digital slides were viewed using Slide Viewer version 2.5.0. TMA cores were evaluated semi-quantitatively using a modified histochemical score (H- score) [410], where the intensity of staining andthe percentage of stained invasive BC cells were both considered. For the stainingintensity, a score index of 0, 1, 2 and 3 is consistent with negative, weak, moderate, and strong staining, respectively. The percentage of the positively stained tumour cells was estimated subjectively. The final H-score was calculated by multiplying the percentage of positive cells (0- 100) by the intensity (0- 3), producing a total range of 0- 300. All non-representative cores were excluded from scoring, such as cores that contain <15% tumour cells relative to the whole core area, cores that show only stroma or normal breast tissue and cores that were folded during processing or staining. Prior to TMA staining, all biomarkers of interest were stained in full-face BC tissue sections

to assess the staining pattern and thus ensure that TMA coresare representative of the whole tumour. All cases were scored without foreknowledge of patients' clinical or outcome data.

Scoring tissue stained by HER2 was performed using HercepTest [165] , according to the manufacturer's recommendation: DAKO protocol (DAKO Corporation, Glostrup, Denmark). Each core was placed into one of four categories (0, 1+, 2+, or 3+). Tumours with a complete absence of membrane staining, or in which membrane staining is observed in <10% of the tumour cells, were scored as 0. Those with faint/barely perceptible, incomplete membranous staining detected in >10% of tumour cells were classified as 1+. Tumours with weak to moderate complete membranous staining in >10% of the tumour cells were classified as 2+, while those with strong, complete membranous staining in >10% of the tumour cells were classified as 3+. Assessment of the other selected biomarkers was done by the semi-quantitative H score (TAF10, BCAT1).

2.5.8 Setting up cut-off points

All biomarkers' expression data, at mRNA and protein levels, was dichotomised to identify a cut-off point which enables parsing the cohort into two categories; expression levels > the identified cut-off point represent high expression group, while values ≤ the cut-off point reflect the low expression group. Dichotomisation was determined using x-tile bioinformatics software (version 3.6.1, Yale University, USA) [411]. This software works on splitting a single

patient cohort into two sub-populations, training, and validation sets. The optimally significant cut-off point, based on the prediction of BCSS, is determined in a training group and validated in the second group.

2.6 RNA extraction and reverse transcriptase quantitative polymerase chain reaction (RT-qPCR)

2.6.1 Formalin fixed paraffin embedded block retrieval and sample preparation

A cohort of HER2-positive cases was compiled, including both anti-HER2 naïve patients and those who had received targeted anti-HER2 therapy. Outcome data with a sufficient number of events to allow for robust statistical analysis was also required. To minimise bias, the clinicopathologic parameters of patients in the treated and untreated groups were matched. Tumour blocks were retrieved from archival repositories, with four blocks available per case. Freshly cut H&E sections were prepared from each tumour block, followed by a detailed pathological review of the representative H&E-stained slides (from the resection specimen). The slide containing the highest proportion of tumour cells, with minimal DCIS, was selected for RNA extraction. The inclusion criterion for tumour content was a minimum of 20% tumour cells.

2.6.2 RNA extraction.

Extracting high-quality RNA from FFPE tissues remains a significant challenge for researchers due to the inherent limitations imposed by formalin fixation [412]. This routine histological procedure, crucial for preserving tissue morphology, significantly complicates RNA isolation. Formalin fixation induces crosslinking between cellular components, including RNA and proteins, which

hampers efficient RNA extraction and compromises the integrity of RNA molecules[413]. Additionally, RNA yield from FFPE samples is typically lower compared to fresh tissues, necessitating the optimisation of extraction protocols and the use of specialised techniques to acquire sufficient RNA for downstream analyses.

Given these challenges, two different RNA extraction protocols were tested on 25% of the cohort to determine the optimal method for FFPE samples. RNA concentration and purity were compared between the two assays, and the protocol yielding the highest-quality RNA was subsequently applied to the remaining samples. The extraction methods tested were the RNXtract® Nucleic Acid Extraction Kit IVD (BioNTech Diagnostics GmbH) and the Qiagen RNeasy FFPE kit. By comparing these techniques, the goal was to identify the most effective approach for obtaining high-quality RNA from FFPE tissue samples, facilitating accurate molecular analysis.

For each assay, four consecutive 5-µm-thick FFPE sections were cut using a standard microtome (Reichert-Jung Hn40, Leica Instruments). Two sections (totalling 10 µm in thickness) were placed into separate 1.5-mL microcentrifuge tubes (Starlab). One tube was designated as a backup, while both tubes were stored at 4 °C until RNA extraction commenced.

2.6.2.1 The RNXtract® Nucleic Acid Extraction Kit

It employs germanium-coated magnetic beads technology in order to segregate RNA from FFPE material with preference over DNA. This kit purifies nu-

cleic acid from FFPE samples by using lysis buffer and protease K sequentially. The unique buffer system of this kit provides a suitable condition for magnetic beads to bind nucleic acid efficiently and specifically. The unique washing system provides the nucleic acid with high purity, stable quality and free of protein, nuclease, and other impurities. This kit does not need to use deparaffinisation reagent to remove paraffin.

2.6.2.1.1 Lysis and Incubation

Paraffin sections were transferred to the bottom of a 1.5 mL centrifuge tube, and 150 µl of lysis buffer was added to the FFPE sections. The samples were then incubated in thermomixer 1 for 30 minutes at 80°C and 1,200 rpm, followed by incubation in thermomixer 2 for 10 minutes at 65°C without shaking. Samples were centrifuged for 3-5 seconds to collect material at the bottom of the tube. A 50 µl proteinase K solution was added to the sample, which was then incubated in thermomixer 2 for 30 minutes at 65°C and 1,200 rpm.

2.6.2.1.2 Magnetic Bead Capture

Following incubation, the sample was centrifuged for 3-5 seconds, and 800 µl of Binding Buffer was added. The liquid was transferred to a new 1.5 mL centrifuge tube. Mag Beads (40 µl) were added to the tube and incubated in a thermomixer at 1,200 rpm for 15 minutes at 20℃ or room temperature (RT). After incubation, the tube was centrifuged briefly for 3-5 seconds, and then placed in a magnetic rack. Upon magnetic collection of the beads, the supernatant was carefully removed with a pipette and discarded.

2.6.2.1.3 Wash Steps

Wash Buffer 1 (850 µl) was added to the tube, and the tube was vortexed or inverted until the Mag Beads were completely suspended. The tube was centrifuged, and the supernatant was discarded following magnetic bead collection. This process was repeated for Wash Buffers 2 and 3.

2.6.2.1.4 Elution and RNA/DNA Extraction

Elution Buffer (40 µl) was added to the tube, vortexed for 15 seconds, and centrifuged briefly to collect the mag beads. The eluate was then transferred to a new 1.5 mL nuclease-free centrifuge tube. RNA/DNA could be used immediately or stored at -80℃ for future use.

2.6.2.2 Qiagen RNeasy FFPE kit

The extraction process was performed according to the RNeasy FFPE Kit user manual. Extraction was performed with DNase I digestion.

Before starting,

- Thoroughly clean the workspace with RNase-Away and allow to air dry for 2 minutes.
- Preheat the thermos-mixers/heating blocks to 56°C and 80°C respectively.
- Prepare ice in a box.

2.6.2.2.1 Deparaffination

For each sample section, 1 ml of Roti-Histol was added. The samples were then vigorously vortexed for 10 seconds and centrifuged at full speed for 2 min.

The supernatant was carefully removed by pipetting without disturbing the pellet. Subsequently, 1 ml of ethanol (96-100%) was added to the pellet, mixed by vortexing, and centrifuged at full speed for 2 min. Again, the supernatant was carefully removed without disturbing the pellet. Final centrifugation at full speed for 1 min was performed, followed by the careful removal of any residual ethanol using a fine pipet tip. The lid was left open, and the samples were incubated at room temperature (15-25°C) for 10 min or until all residual ethanol had evaporated.

2.6.2.2.2 Sample Lysis

For sample lysis, 150 µl of Buffer PKD was added to each sample, and the mixture was vortexed. Then, 10 µl of proteinase K was added and gently mixed by pipetting up and down. The samples were incubated at 56°C for 15 min, followed by an additional incubation at 80°C for 15 min. After incubation on ice for 3 min, the samples were centrifuged for 15 min at 20,000 x g (13,500 rpm). The supernatant was transferred to a new 2 ml microcentrifuge tube without disturbing the pellet, and RNA purification from the supernatant was continued.

2.6.2.2.3 RNA Purification

To the supernatant, DNase Booster Buffer equivalent to a tenth of the total sample volume (16 µl) and 10 µl of DNase I stock solution were added. The mixture was inverted to mix, and the tube was briefly centrifuged to collect residual liquid from the sides. Incubation was carried out at room temperature for 15 min. Then, 320 µl of Buffer RBC was added to adjust binding conditions, and the lysate was thoroughly mixed. Subsequently, 1200 µl of ethanol (100%)

was added to the sample, and it was mixed well by pipetting. Without centrifugation, 700 µl of the sample, including any precipitate, was transferred to a RNeasy MinElute spin column placed in a 2 ml collection tube. Centrifugation was performed for 15 s at 28,000 x g (210,000 rpm), and the flow-through was discarded. The binding step was repeated until the entire sample had passed through the RNeasy MinElute spin column. Then, 500 µl of Buffer RPE was added to the spin column, followed by centrifugation for 15 s at 28,000 x g (210,000 rpm). The flow-through was discarded, and this step was repeated once more. Afterward, 500 µl of Buffer RPE was added again, and the spin column was centrifuged for 2 min at ≥8000 × g (210,000 rpm) to wash the spin column membrane. The collection tube with the flow-through was discarded. The RNeasy MinElute spin column was placed in a new 2 ml collection tube, and the lid of the spin column was opened. Centrifugation was performed at full speed for 5 min, and the collection tube with the flow-through was discarded. Then, the spin column was placed in a new 1.5 ml collection tube,

Finally, 40 µl of RNase-free water was added directly to the spin column membrane. Centrifugation was carried out for 1 min at full speed to elute the RNA and the RNA eluates were stored in 1x100 µl aliquots at -80°C.

2.6.3 Assessment of RNA concentration

As destruction of mRNA integrity in FFPE samples is well established [150, 155, 156], we compared the concentration of RNA extract from both extraction method. We utilised Qubit™ RNA high sensitivity (HS) assay Kit, (Invitrogen, ThermoFisher, cat. No. Q32852) on a Qubit™ 4 Fluorometer. It is a powerful tool for accurately quantifying RNA samples with high sensitivity and specificity

across a wide dynamic range. The assay is accurate for initial sample concentrations from 0.2 ng/µL to 200 ng/µL, providing an assay range of 4−200 ng. It employs fluorescent-based quantification technology, offering several advantages over traditional spectrophotometric methods, such as enhanced sensitivity, minimal interference from contaminants, and compatibility with challenging sample types.

The required number of Qubit™ tubes for standards and samples was set up. Two standards are necessary for the Qubit™ RNA HS assay. Thin-wall, clear, 0.5-mL PCR tubes (Cat. No. Q32856) were exclusively used for the Qubit™ 4 Fluorometer. The tube lids were labelled. It was ensured not to label the side of the tube to avoid interference with the sample read. Each standard tube lid was labelled correctly. Calibration of the Qubit™ Fluorometer necessitated the insertion of standards into the instrument in the correct order.

Preparation of the Qubit™ working solution involved diluting the Qubit™ RNA HS reagent 1:200 in Qubit™ RNA HS buffer. A clean plastic tube was used for each preparation of the Qubit™ working solution. It was emphasised not to mix the working solution in a glass container.

Qubit™ working solution was added to each tube to achieve a final volume of 200 µL. The volume of Standard assay tubes required 190 µL of working solution, and 10 µL Qubit™ standard were added to the appropriate tube, while user sample assay tubes required 199 and 1 µL RNA. The tubes were vigorously vortexed for 3–5 seconds. All tubes were allowed to incubate at room temperature for 2 minutes before proceeding to read standards and samples.

Reading Standards and Samples with the Qubit™ 4 Fluorometer, on the home screen, the RNA assay type was selected, and RNA High Sensitivity was chosen. Standard #1 was inserted into the sample chamber, and the reading was initiated by touching Read standard. After completion, Standard #1 was removed. Standard #2 was then inserted into the sample chamber, and the reading was initiated. After completion, Standard #2 was removed. Run samples was selected to proceed with sample readings.

2.6.4 mRNA quantification with RT-qPCR

The expression levels of *ERBB2, ESR1, PGR and MKI67* were determined by RT-qPCR using the CE-marked MammaTyper® assay (Ref CC01010, Cerca Biotech GmbH) on Applied Biosystems® 7500 Fast Real-Time PCR system with software version 2.3.

The MammaTyper® assay kit includes three assay mixes, and an enzyme mix for RT-qPCR, provided in 260 µl volumes and ready to use. The enzyme mix contains a buffered solution with reverse transcriptase, DNA polymerase, and dNTPs. It also includes a buffered solution containing specific control RNA (0.1 pg/µl) as a positive control and one negative (no-template control; NTC) external control to qualify the RT-qPCR process. The kit uses two internal reference genes (*B2 macroglobulin, B2M, and Calmodulin 2, CALM2*) for assessing sample validity and normalisation.

Assay mix 1 (90 µl, ready to use) measures *ERBB2* and *ESR1* and contains DNA oligonucleotides with qPCR TaqMan probes. Assay mix 2 (90 µl, ready to use) measures *MKI67* and the first housekeeping reference gene, *B2M*,

and includes DNA oligonucleotides and qPCR TaqMan probes. Assay mix 3 (90 µl, ready to use) measures *PGR* and the second housekeeping reference gene, *CALM2*, and also contains DNA oligonucleotides and qPCR TaqMan probes.

RT-qPCR steps

To prepare for the test execution, several essential steps must be completed before initiating the real-time PCR reaction. First, the work area is thoroughly decontaminated to prevent cross-contamination and eliminate any risk of exposure to RNA-degrading enzymes or reagents. The MammaTyper® reagents are thawed on ice while being shielded from strong light exposure. Once thawed, the reagents are gently inverted to ensure a homogeneous mixture, followed by a brief centrifugation to collect any remaining material. The enzyme mix is then allowed to equilibrate to room temperature for two minutes to reduce its viscosity.

The next steps involve preparing instrument-specific 96-well plates and sealing covers, along with providing ice for the reagents and PCR cooling rack. PCR reactions are prepared, with marker determination performed in triplicate. For each assay mix, a master mix is created in 1.5 ml reaction vessels, with the volume calculated based on the number of samples and controls, incorporating a 15% pipetting margin. The enzyme mix, added last due to its high viscosity, is pipetted 5-10 times to ensure thorough mixing. After a quick vortex and centrifugation, the master mixes are placed on ice.

For the RT-qPCR reaction, each well of the 96-well plate contains a total reaction volume of 10 µl, consisting of 7.5 µl of assay-specific master mix, 2.5 µl of RNA eluate (sample), or 2.5 µl of positive control (PC) or water (negative control, NC) in the corresponding wells (**Figure 2.3**).

	1	2	3	4	5	6	7	8	9	10	11	12
A	P1	P1	P1	P1	P1	P1	P1	P1	P1	PC	PC	PC
B	P2	P2	P2	P2	P2	P2	P2	P2	P2	PC	PC	PC
C	P3	P3	P3	P3	P3	P3	P3	P3	P3	PC	PC	PC
D	P4	P4	P4	P4	P4	P4	P4	P4	P4	---	---	---
E	P5	P5	P5	P5	P5	P5	P5	P5	P5	---	---	---
F	P6	P6	P6	P6	P6	P6	P6	P6	P6	NC	NC	NC
G	P7	P7	P7	P7	P7	P7	P7	P7	P7	NC	NC	NC
H	P8	P8	P8	P8	P8	P8	P8	P8	P8	NC	NC	NC

Figure 2.3: Layout of the 96 well plate. Each colour columns represent triplicates of one master mix; yellow is master mix 1 for assessment of *ERBB2* and *ESR1*, blue is master mix 2 for assessment of *MKI67* and *B2M* reference gene and red is master mix 3 for assessment of *PGR* and *CALM2*, the other reference gene. Each sample "P" and distributed in the wells from 1 to 9, so each gene is assessed in triplicates. PC: is positive control included in the kit. NC is the negative control which is RNASE free water. Eight patients' samples can be assessed per kit.

The reaction was performed following the manufacturer's protocol with 40 cycles of amplification. The preamplification product was diluted 1:5. The RT-qPCR reactions were run for 5 min at 50 °C, 20 sec at 95 °C, followed by 40 cycles of 15 s at 95 °C and 1 min at 60 °C (**Figure 2.4**).

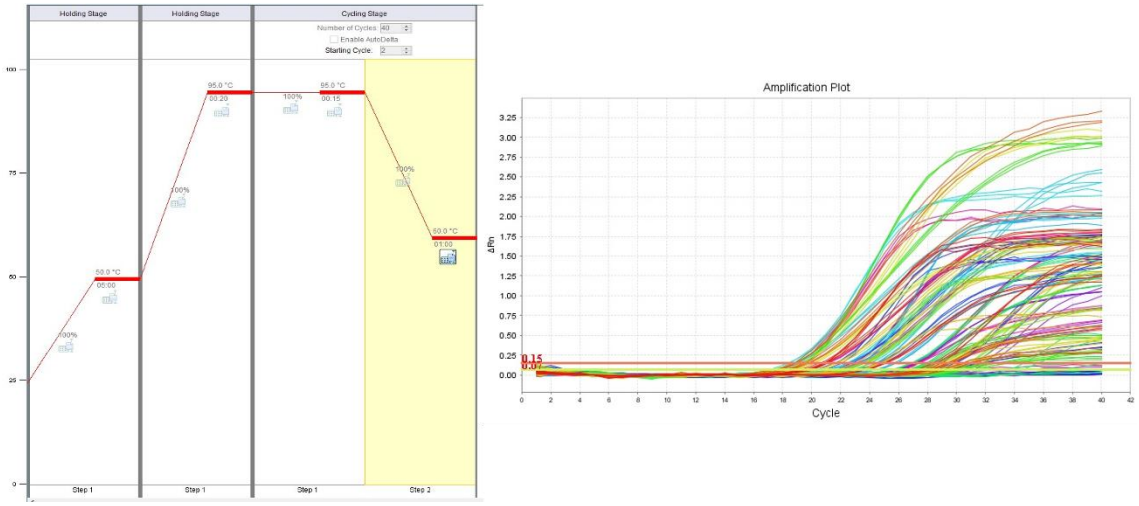


Figure 2.4: Figure showing RT-qPCR run temperature setting (left side) and the amplification curves after 40 cycles of gene amplification (right side)

2.7 Chromogenic in situ hybridisation (CISH)

This was done by a previous PhD student, and data was available in the Nottingham data library. *HER2* gene amplification is primarily detected by in situ hybridisation, and CISH is an introduced alternative method to FISH [414]. The performance of CISH in HER2 testing has rarely been tested in series studies, so it is aimed to characterise HER2 status using IHC and CISH and assess its prognostic value in a large and well-annotated cohort. *HER2* gene amplification was determined by CISH using the ZytoDot 2C SPEC *ERBB2/*CEN 17 Probe Kit, (ZytoVision®, Germany). TMA sections were deparaffinised and incubated for ten minutes (at 70°C on thermal plate) followed by dewaxing in xylene (2×five minutes), and then serial ethanol dilutions (each five minutes). Incubation of the slides with hydrogen peroxide (H2O2) (3%, for five minutes) is followed by washing in distilled water (D.W) Treatment of the slides by pre-heated pre-treatment solution EDTA (PT2) for 15 minutes was performed, fol-

lowed by immediate transfer into D.W (2×two minutes each). Enzymatic digestion was carried out by drop-wise application of pepsin solution (ES1) to the tissue sections and incubation for five minutes at room temperature (RT) in a humidity chamber. After a wash in D.W., slides were dehydrated with graded ethanol, followed by air drying. A ready-to-use DNA probe (ZytoDot 2C SPEC ERBB2/CEN 17 Probe, PD12) was applied to the slides (10µl per slide) and cover-slipped (22x22mm) and then sealed with a layer of rubber cement. The sections were denatured on a thermal plate (80°C for five minutes), and hybridisation was carried out overnight at 37°C in a humidity chamber. After hybridisation, the cover slip was removed, and slides were washed twice (each five minutes) with wash buffer SSC (WB1) (first washed at room temperature, and the second heated to 75°C). After two washes in D.W. (one minute each), slides were immersed into 1x wash buffer TBS (prepared using WB5). The HER2 probe was detected by sequential incubation with anti-digoxigenin DIG/DNP-Mix (AB14) for 15 minutes (at 37°C in a humidity chamber), peroxidase polymer horseradish peroxidase HRP/AP-Polymer-Mix (AB13) for 15 minutes (at 37°C in a humidity chamber), AP-Red Solution B (SB6b) for 15 minutes (at room temperature) and HRP-Green Solution A (SB7a) for 15 minutes (at room temperature). Counter-staining was achieved by Nuclear Blue Solution (CS2) for two minutes followed by washing and dehydration in absolute ethanol followed by xylene. Covering the slides (22x22mm cover slips) using Alcoholic Mounting Solution (MT4) and air-dry slides for 30 minutes was the final step.

2.7.1 Interpretation of CISH

Interpretation of CISH was performed using a Nikon microscope equipped with an x63 objective lens. At least 20 malignant, non-overlapping cell nuclei were scored to assess the *HER2* gene CN. Chromosome 17 (represented by the red signals) (**Figure 2.5**) was used as an internal control, particularly in the low *HER2* gene CN cases, as per the recommended protocol. *HER2* gene amplification was defined as six or more signals per nucleus or when clusters (clumps of aggregated green signals) were identified in the cell nuclei in more than 50% of tumour cells [165]. If the average copy number was ≥4 to <6 per nucleus (equivocal), another 20 tumour cells were enumerated, and the final average copy number of the case was calculated from the total of 40 cells. This was carried out by the author on the already stained slides.

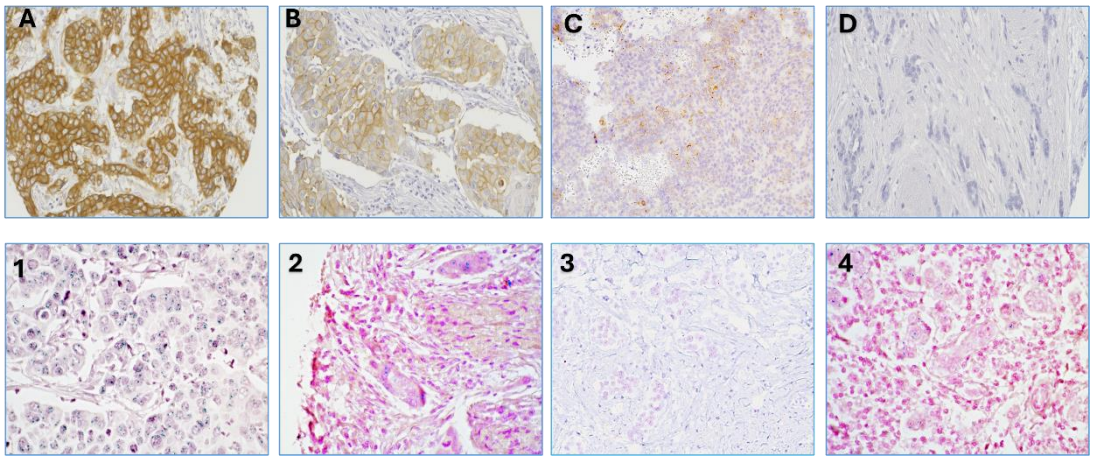


Figure 2.5: Different HER2 IHC scores and their corresponding CISH results. A) HER2 IHC 3+ with CISH amplification (1); B) HER2 IHC2+ with CISH amplified (2); C) HER2 1+ non amplified CISH (3), D), HER2 IHC0 with no CISH amplification (4)

2.8 Whole slide image quality control (QC)

To maximise the role of WSI in further research projects, we carried out a detailed QC check for 40.000 scanned WSIs. Four slides per each tumour case underwent a thorough QC. The purpose of this QC was to determine whether the slides were suitable for scanning and could meet specific criteria for passing or failing. These criteria included checking for slide or coverslip cracks, air bubbles, poor staining, presence of ink, folded sections, or absence of tumour tissue. The selection of these cases also depended on the availability of tissue FFPE blocks and the abundance of tumour tissue within the blocks. Cases that failed QC, were repeated either on preparation level or scanning level.

All scanning was carried out at x40 magnification equivalent to 0.25um/pixel resolution. WSIs were visualised by specific viewer software (Philips Image Management System IMS, Aperio image scope version 12.4.3 and 3DHistech case viewer Version 2.4), respectively. In each image we have assessed missing tissue frequency, the image quality and resolution and the role of applying various QC measures in lowering the WSI rejection rate.

Data on the scanned digital image failure rates before and after the application of QC measures performed during routine scanning were collected. WSI QC included macro-evaluation of pre-analytic slide artefacts that should have been resolved before scanning. Protocols were applied for glass slide QC including glass slides should be intact (not broken or cracked), appropriately stained and dried, clean without any ink markings, properly placed coverslips without hanging over the edge of the glass slides, and air bubbles were to be absent; the

glass slide label should be flat and not extending past the slide edge or covering tissue on the slides. Small air bubbles over the tissue section or varied size air bubbles away from the tissue section are usually acceptable in examining slides using the conventional microscope as they do not affect the morphology. However, during WSIs acquisition using digital scanners, these air bubbles produce uneven slide surface and hence the produced image usually shows areas of tissue out of focus which will affect the overall WSI quality. Additional real-time QC was performed by the scanner that provided user interface messages including barcode detection failures, no tissue detection, macro focus image failure, or image quality errors. Post-scan QC measure included a review of the WSI to visualise utilising the image thumbnails to ensure all tissue present on the glass slide was scanned. Poor WSI quality resulting from a glass slide quality was an indication for reprocessing of the glass slides (e.g., recutting, remounting, re-staining or re-placing the coverslip properly) whereas failed scanning of an adequate glass slide during scanning errors such as out of focus or obvious missed tissue was an indication of rescanning.

The clinical significance of the missing tissue and WSI quality was evaluated. The impacts assessed included any change in the recognition of tissue type examined, identification of the lesion, classification of the lesion, tumour type, grade, tumour stage (LN metastasis, tumour size) and surgical resection margin distance and completeness of excision. For the clinical significance of the missed tissue on the IHC stained slides, we evaluated the change of Ki67 and PR final score between glass slides and WSI.

2.8.1 Comparison of the missing tissue between glass slide and WSIs

We compared each WSI with their corresponding glass slides. The image thumbnail (the low-resolution whole section view) was used to evaluate whether the missed tissue was obvious and easily detected by the pathologist or not. In each image the missing tissue was assessed regarding; 1) The percentage of the missed tissue in relation to the whole tissue (percentage of missing tissue= $\frac{area\ of\ missed\ tissue\ in\ mm}{total\ tissue\ aera\ in\ mm}$). Multifocal missed tissue areas were summed up and the final total percentage was estimated. 2) Missing tissue type i.e., fatty tissue, normal breast lobules and ducts or any pathological lesions. The latter was classified into invasive tumour and its type, in situ components and atypical proliferative lesions including ductal and lobular, and benign lesions such as intraductal papilloma, fibroadenoma and radial scar. 3) The site or location of the missed tissue in relation to the whole tissue section (i.e. peripheral, central or multifocal). 4) Cofounders including specimen types (e.g., excision specimens, or core biopsy), the relation between time of the implementation of the digitalisation service and missing tissue frequency and the type of stain. in addition, the relation between the frequency of missing tissue and scanning time and image file size was evaluated using the 3 scanners.

2.9 Annotation and development of machine learning algorithm.

Annotation is the process of marking and labelling specific regions and structures within BC tissue samples. This process involved identifying and delineating areas of interest, including tumour regions, stromal components, normal tissue, and other relevant features. After completing the annotation process, a machine learning algorithm was developed to analyse the annotated data. This algorithm was designed to learn patterns and relationships within annotated images and to make predictions or classifications based on these patterns.

2.9.1 Digital scanning of slides:

For all selected cases, FFPE tumour tissue blocks were retrieved, and three sections were cut and stained with H&E, Ki67 and PR. The resulting slides were scanned at 40x magnification using Philips IntelliSite Ultra-Fast Scanner, Philips Digital Pathology Solutions, the Netherlands, and Panoramic 250 Flash III: 3D Histech, Budapest, Hungary, generating high-resolution WSIs. The model was trained on images from both scanners and random brightness/contrast, median blur and colour jitter augmentations were carried out. One representative WSI was used for each case where the largest tumour burden is present. This step was performed with the help of the group technicians.

2.9.2 Whole slide annotations

The reviewed slides (H&E, PR, and Ki67 stained slides of each case) were uploaded to an online annotation software called WASABI (https://wasabi.dcs.warwick.ac.uk), where a group of six pathologists per-

formed an exhaustive region and cell-level annotations using various annotation tools. Each type of tissue was annotated with a unique colour code and annotation style **(Figure 2.6 and Figure 2.7)**

Regional annotations involved invasive and in situ tumour areas, TAS, and normal breast tissue (terminal duct lobular units) regions. Cell annotations included tumour cells with various morphologies and degrees of pleomorphism, mitotic figures, stromal cells either fibroblasts or myofibroblasts, normal epithelial cells and TILs Areas of necrosis, calcification and tissue/image artefacts were also annotated and excluded from final image processing (**Figure 2.8)**.

For each WSI, two pathologists were assigned to independently annotate different morphological features of BC in a blinded manner to train the algorithm. The algorithm accurately detected each of these structures with high precision. Subsequently, the algorithm predicted the detected features of each patch (the

WSI was divided into smaller patches) independently from the whole case.

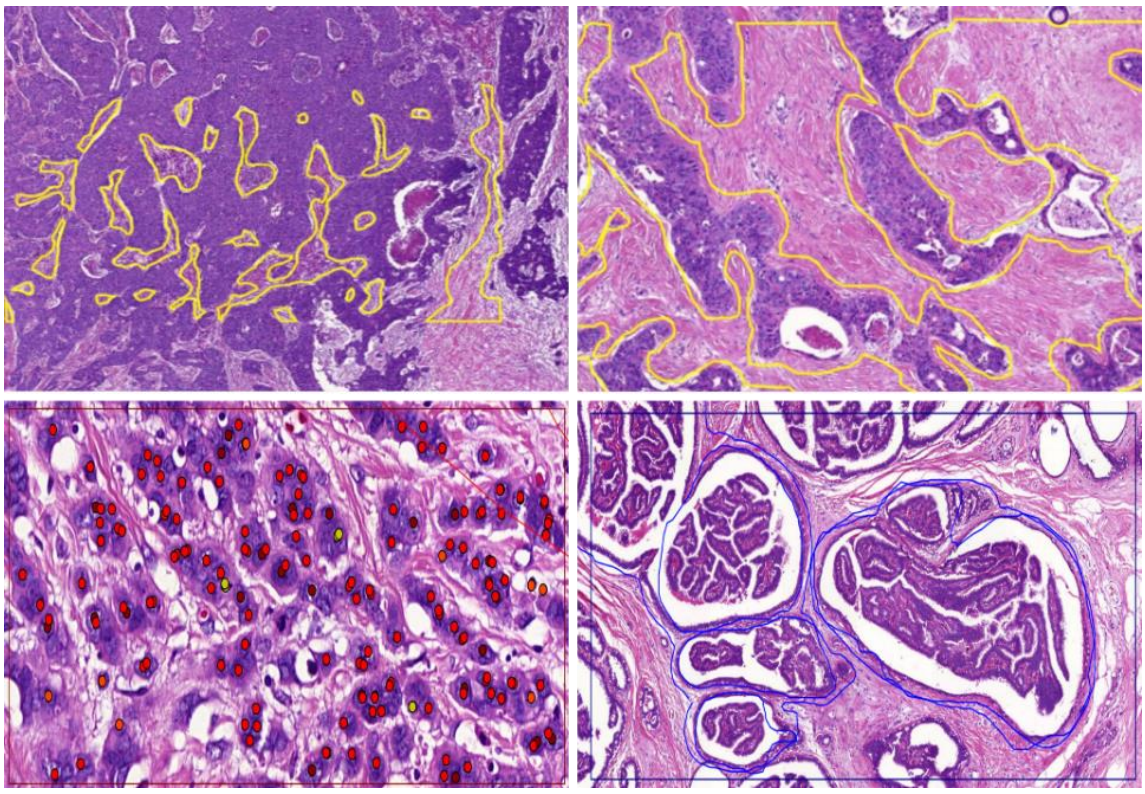


Figure 2.6: H&E-stained BC sections showing regional and cell-level annotations. The regional annotations encompass different areas within the tissue, including invasive and in situ tumour regions, tumour-associated stroma (TAS), and normal breast tissue, level annotations highlight specific cellular components including tumour cells with degrees of pleomorphism, mitotic figures, stromal cells such as fibroblasts or myofibroblasts, normal epithelial cells, and TILs.

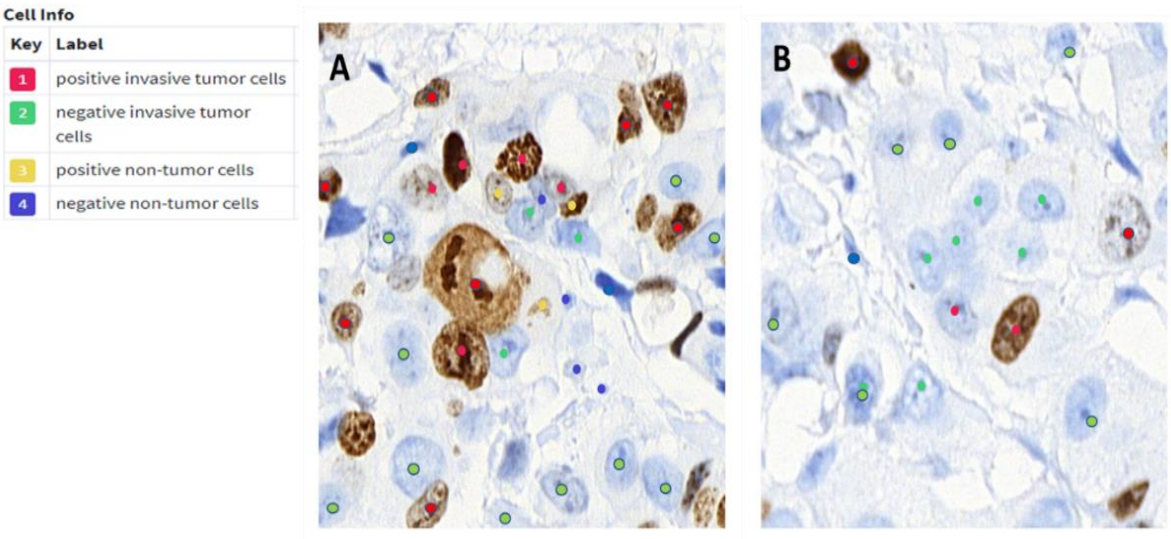


Figure 2.7: Cellular annotations of Ki 67 and PR were performed separately, where positive and negative tumour cells were annotated as well as positive and negative non-tumour cells: Ki 67 stained BC sections showing cell level annotation, where specific cells within the tissue are labelled using coloured dots. The red dots represent positively stained tumour cells, the green dots denote negatively stained tumour cells, the yellow dots are used to label positively stained non-tumour cells and the blue dots are used to label negatively stained non-tumour cells.

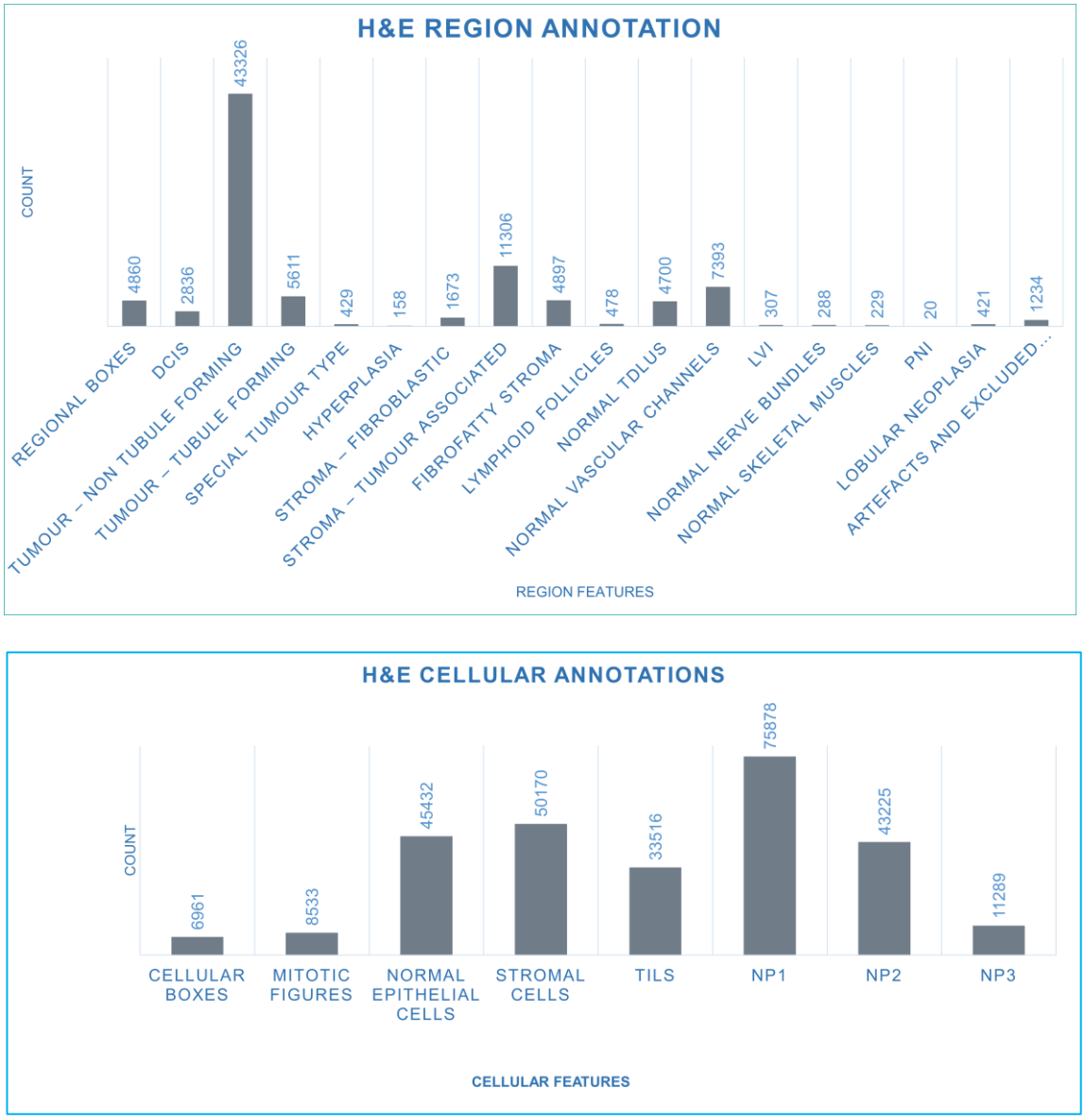


Figure 2.8 : Bar chart showing the total number of annotated morphological features used for the training of machine learning algorithms, both on regional and cellular levels.

2.9.3 Deep learning-based feature computing

To generate different features related to TAS, in situ and invasive tumour, a deep learning (DL) based pipeline is proposed **(Figure 2.9A).** First, tissue mask was generated for a WSI using image thresholding and morphological operations. A Convolution Neural Network (CNN) based model (CNN_{DCIS})

[415] filtered out *in situ* regions from the tissue so that they were excluded from the calculation of invasive tumour and stromal features. CNN_{Nuc} [416] segmented and classified different types of nuclei including those of tumour, stromal and normal epithelial cells within the TDLUs. Tumour and stromal nuclei were then used to generate nuclei related features. CNN_{Reg} [417] segmented stromal and other regions (non-ROIs) where the stromal regions were further restricted to TAS via morphological operations.

2.9.4 Nuclei segmentation/classification and nuclear features

To segment and classify different types of nuclei, an in-house developed state-of-the-art nuclei segmentation and classification model (HoVer-Net) [416] was employed. A pretrained version of the model [418] was fine-tuned to get CNN_{Nuc} on the target dataset. Parameters for the fine-tuning process were as follows: patch size: 256 × 256 pixels; learning rate: 0.0001 (initial two epochs), 0.00001 (3rd epoch onwards) and batch size of 8. During inference on a WSI, a nuclei mask was generated by mapping the type/class of each detected nucleus at its centroid in a five-times down-sampled WSI **(Figure 2.9 B).** A cooccurrence matrix (CM) was then created for tumour and stromal nuclei **(Figure 2.10).** Based on the CM, different features were calculated, including tumour and stroma nuclei heterogeneity, cell cooccurrences, tumour-to-stroma nuclei ratio, tumour-to-stroma nuclei cooccurrence, and heterogeneity.

2.9.5 Region segmentation and region features.

The U-Net model [417] (referred here by CNN_{Reg}) was adapted by adding two additional encoding/decoding blocks for semantic segmentation of stromal and other non-ROI regions **(Figure 2.9C)** and was trained on the annotated regions

to generate segmentation masks for the WSIs. Training parameters for CNNReg was as follows: patch size= (512 × 512) with 96 pixels context on all sides; batch size =8; learning rate= 0.01 (initial five epochs), 0.001 (epoch 6-10), 0.0001 (epoch 11-30); momentum 0.9; loss cross-entropy. Other settings included: normalised input to [0-1] and different augmentations (random brightness/contrast, random rotate, median blur) trained with values of 0.5. As CNN_{Reg} segmented out stromal regions irrespective of them being associated with tumour, therefore to restrict to TAS only the following steps were taken: 1) Tumour regions segmented by CNN_{DCIS} were combined with stromal regions segmented by CNN_{Reg}; 2) Mask size was reduced by a factor of seven to ensure fast processing; 3) Tumour regions were dilated to capture the TAS with a disc of radius 8 pixels followed by filling the holes with a disc of radius 32 pixels; 4) Stroma captured in the dilated tumour regions was considered as TAS for further feature calculation. Different features were calculated from in situ, tumour and TAS regions. The features included region areas, their ratios with each other, stroma to tumour ratio (STR) and heterogeneity in terms of tumour-stroma patches.

2.9.6 Defining the morphological features

Using annotated data and a DL pipeline, features related to tumour and stroma were calculated for each case from several patches (each measuring 62 micrometres) of WSIs. A hexagonal tiling approach was used to extract these features, and a comprehensive quantification of tumour features was performed based on these hexagonal grid analytics, which were then subsampled into a grid to compute the total number of variables. A co-occurrence matrix

was generated to produce Haralick texture indicators, enabling the quantification of morphological features in the form of uniformity measures.

2.9.7 AI-based STR quantification and spatial distribution.

STR was calculated using surface area and cell count. The surface area ratio was calculated as: STR= TAS area / (TAS area + Tumour area) × 100 **(Figure 2.9C)**The cell count ratio was calculated as the ratio of total stromal cell count to total tumour cell count in the WSI. Similarly, an automated score for the quantification of STR spatial distribution **(Figure 2.9D)** in the context of tumour cells was calculated and expressed as spatial co-occurrence. Spatial cooccurrence quantified the cooccurrence of two or more structures (such as tumour cells with stromal cells) within a certain distance in a patch of size 256 × 256 pixels. CMs were constructed and different features were calculated using python library*. STR intratumoural heterogeneity and contrast were calculated from these CM. STR heterogeneity measures how heterogeneous a WSI is in terms of the occurrences of tumour and stromal nuclei together which ranges from 0 (highly homogeneous) to 1 (highly heterogeneous). STR contrast measures local changes over the WSI and it ranges from 0 (a constant image) to 1 (size of CM). To assess the validity and reliability of the DL detection algorithm, visual assessment of STRin WSI was performed and estimated blindly and the concordance between DL and visually assessed ratio was carried out on 10% of the cases **(Figure 2.9E)**.

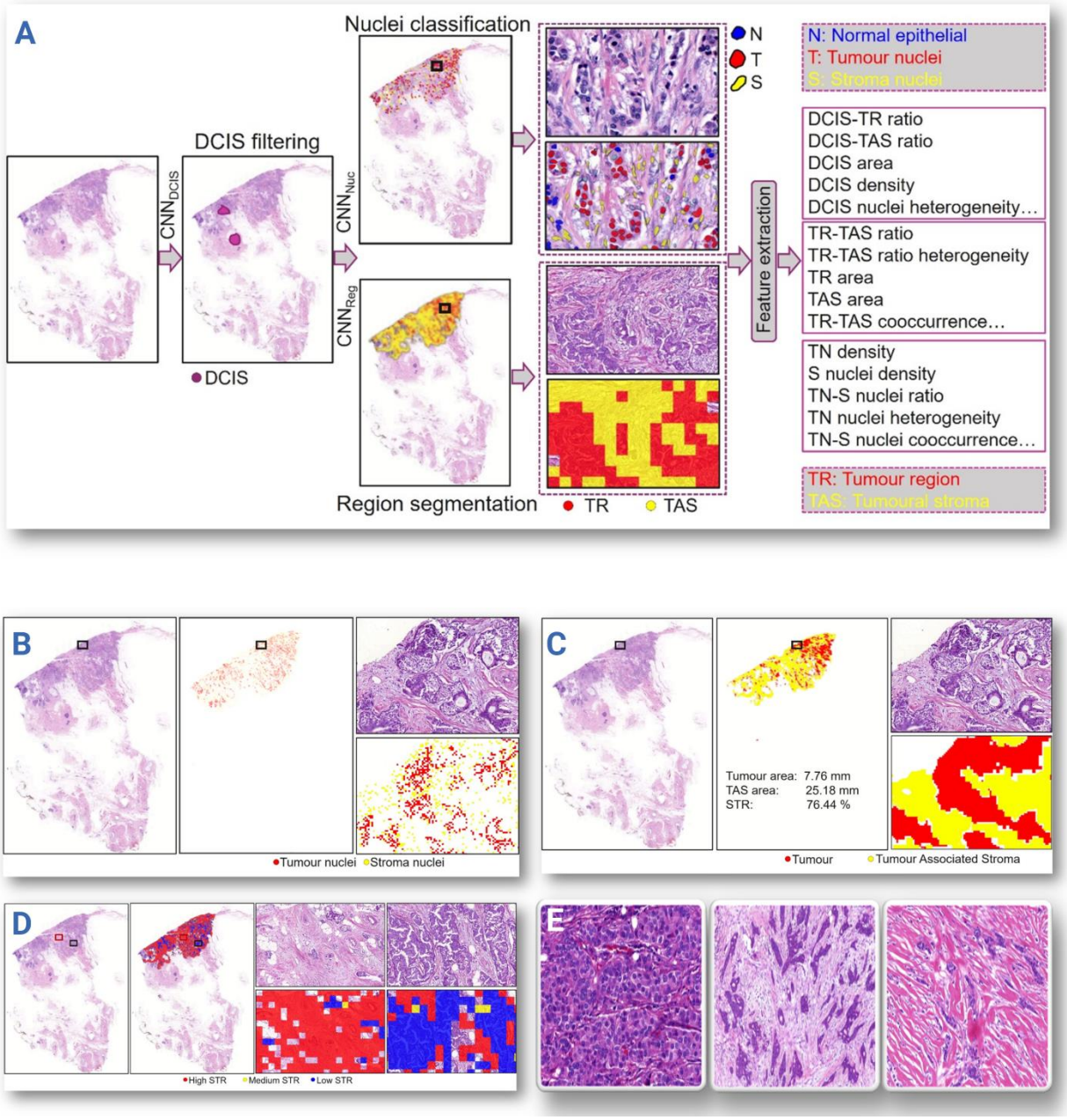
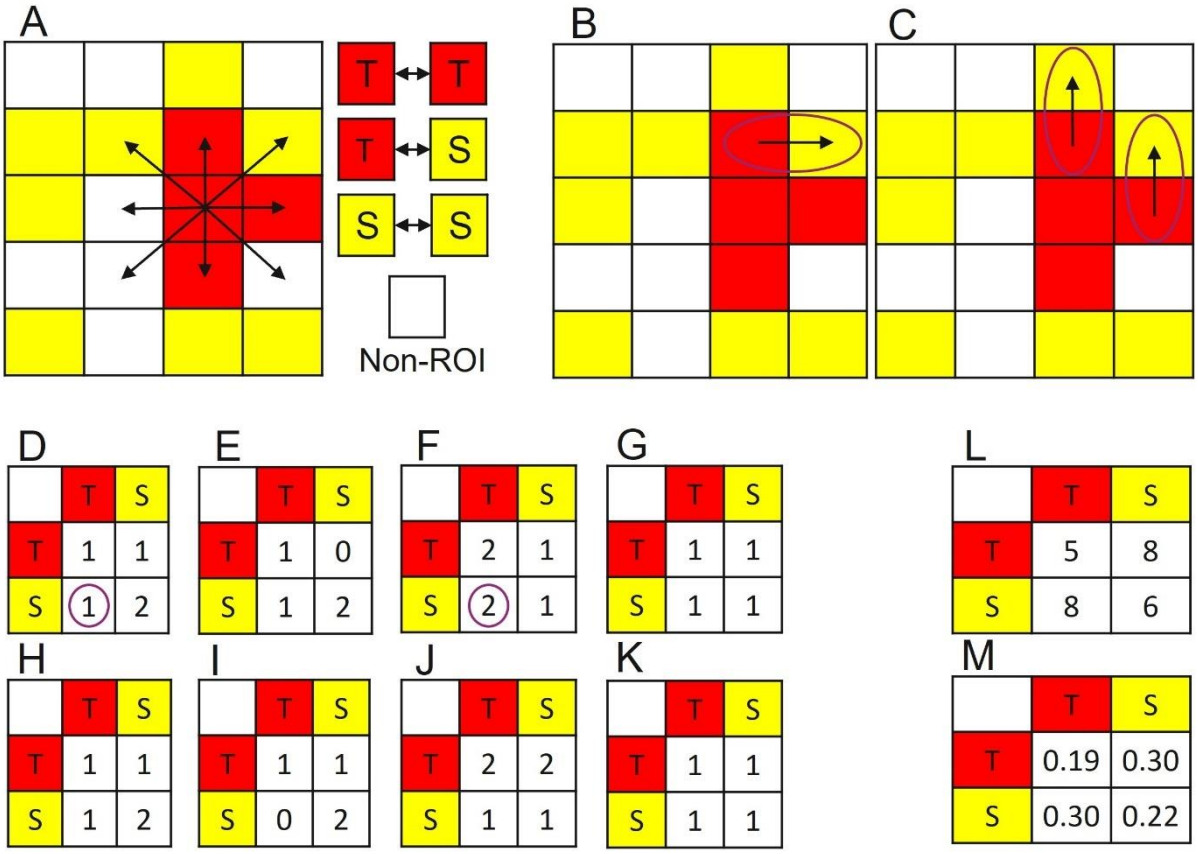


Figure 2.9: Graph illustrating deep learning (DL) based feature computing. A: DL pipeline for feature generation. Ductal carcinoma in situ (DCIS) is filtered out by CNNDCIS before CNNNuc performs nuclei segmentation and classification and CNNReg performs region segmentation for extracting different features. B Nuclei map generation for quantifying nuclei cooccurrences. Each detected nuclei type is mapped at its centroid in five times down sampled whole slide image. C: Tumour and tumour associate stroma (TAS) regions segmentation. The resulting regions are then used to calculate STR. D: Heatmap for stromal cell to tumour cell ratio measured in 256 × 256 pixels patches. E: Visual subjective

assessment of STR into low (left), medium (Middle) and high (right). STR: Stroma to tumour ratio.



`skimage.feature.texture.greycoprops(P, prop='contrast')`

Calculate texture properties of a GLCM.

Compute a feature of a grey level co-occurrence matrix to serve as a compact summary of the matrix. The properties are computed as follows:

- 'contrast': $\sum_{i,j=0}^{levels-1} P_{i,j}(i-j)^2$

Contrast: Measures local changes in the co-occurrence matrix (CM). Range = [0 (size(CM)-1)^2]. Contrast for a constant image is 0.

- 'homogeneity': $\sum_{i,j=0}^{levels-1} \frac{P_{i,j}}{1+(i-j)^2}$

Heterogeneity: 1-homogeneity. Homogeneity measures the closeness of the distribution of elements in the CM to the CM diagonal. Range = [0 1]. Homogeneity is 1 for a diagonal CM.

Figure 2.10: Number of times predicted tumour nuclei (T) neighbour with stroma nuclei (S) at a distance of one cell hop on any of the 8-direction shown (A). S occurring to the right (i.e., at angle 0) of T is 1 and is shown by an ellipse in B

(and circled in D). Similarly, S occurring above (i.e., at angle 90) T is 2 and is shown by an ellipse in C (and circled in F). Such occurrences can be calculated at 8 different angles (0, 45, 90, 135, 180, 225, 270, and 315 shown in D, E, F, G, H, I, J and K, respectively) and then summed to get total occurrences (L). Note: to get the sum of occurrences of the same entity for example T with T, the total occurrences are divided by 2. The resulting values are then normalised (i.e., each value in the table is divided by the total sum of the values) and the resulting table – termed Co-occurrence Matrix (CM) (M) is then used to calculate different features such as contrast and heterogeneity.

2.10 Digital Image Analysis (DIA)

DIA involves the application of various image processing techniques to analyse images, enabling quantitative measurements, feature extraction, and pattern recognition. We utilised QuPath image analysis software version 4.3 [346] to extract and analyse cyto-morphological features potentially associated with HER2 positivity in BC. This allowed us to perform cellular classification, measure fine nuclear and cellular structures, and evaluate parameters related to spatial distribution, as described in the following sections.

2.10.1 Image acquisition and scanning

Fresh H&E-stained sections of FFPE tissue blocks of surgical excision specimens from each case were prepared and scanned with Pannoramic 250 Flash III: 3DHistech, Budapest, Hungary (0.19 ml/pixel) with 0.25 µm/pixels at x20 magnification. To ensure image quality, a series of QC measures were applied to the scanned images, including checks for the presence of sufficient and representative tumour tissue, out of focus areas, and the absence of tissue or staining artefacts. Cases that did not meet these QC criteria were excluded from the analysis.

2.10.2 Image preprocessing

Colour normalisation and stain separation through an unsupervised algorithm using colour deconvolution were carried out as previously published [419, 420]. This was performed to obtain a more accurate calculation of H&E stain optical density (OD) within tumour cells and to improve cell and nuclear segmentation.

2.10.3 Cellular and Nuclei segmentation and classification

This was carried out using Cellpose and Stradist extensions within QuPath [421, 422]. For each case, 3 different areas (2000x2000 pixels each) were annotated. Areas selection was based on the highest tumour cellularity within the WSI, which in turn was identified through the density maps algorithm. The model semantically segmented both cells and nuclei. An object classifier was trained using several annotated areas from different slides on differentiating tumour and immune cells, and the trained classifier was then applied to all cases. Areas were strictly selected not to include any stromal cells. The cellular and subcellular measurements identified by the model included nuclear dimensions (area, length, diameter), nuclear haematoxylin density, cell area, cytoplasmic area, nuclear/cytoplasmic ratio (N/C ratio) and nuclear/cell ratio. Features related to nuclear circularity were excluded as the Stardist tool add smoothing features to the nuclei membrane would affect the accuracy of the measurements.

2.10.4 Spatial distribution and arrangement of tumour cell

For that we applied the Delaunay 2D model [346, 423]. Delaunay triangulation is a geometric method used to partition a set of points (nuclei) in a plane (usually in 2D space) into non-overlapping triangles. The key characteristic of a Delaunay triangulation is that no nuclei in the dataset is inside the circumcircle (the circle that passes through all three vertices) of any triangle in the triangulation. Delaunay mean distance is a measure of average spacing or separation between nuclei in WSI based on Delaunay triangulation. It can provide insights into the spatial characteristics of the tumour nuclei. **Figure 2.11** summarises WSI analysis. The performance of the software was checked throughout the segmentation, classification and spatial distribution steps for each WSI to ensure accuracy of the extracted features and cases that failed human assisted QC were excluded.

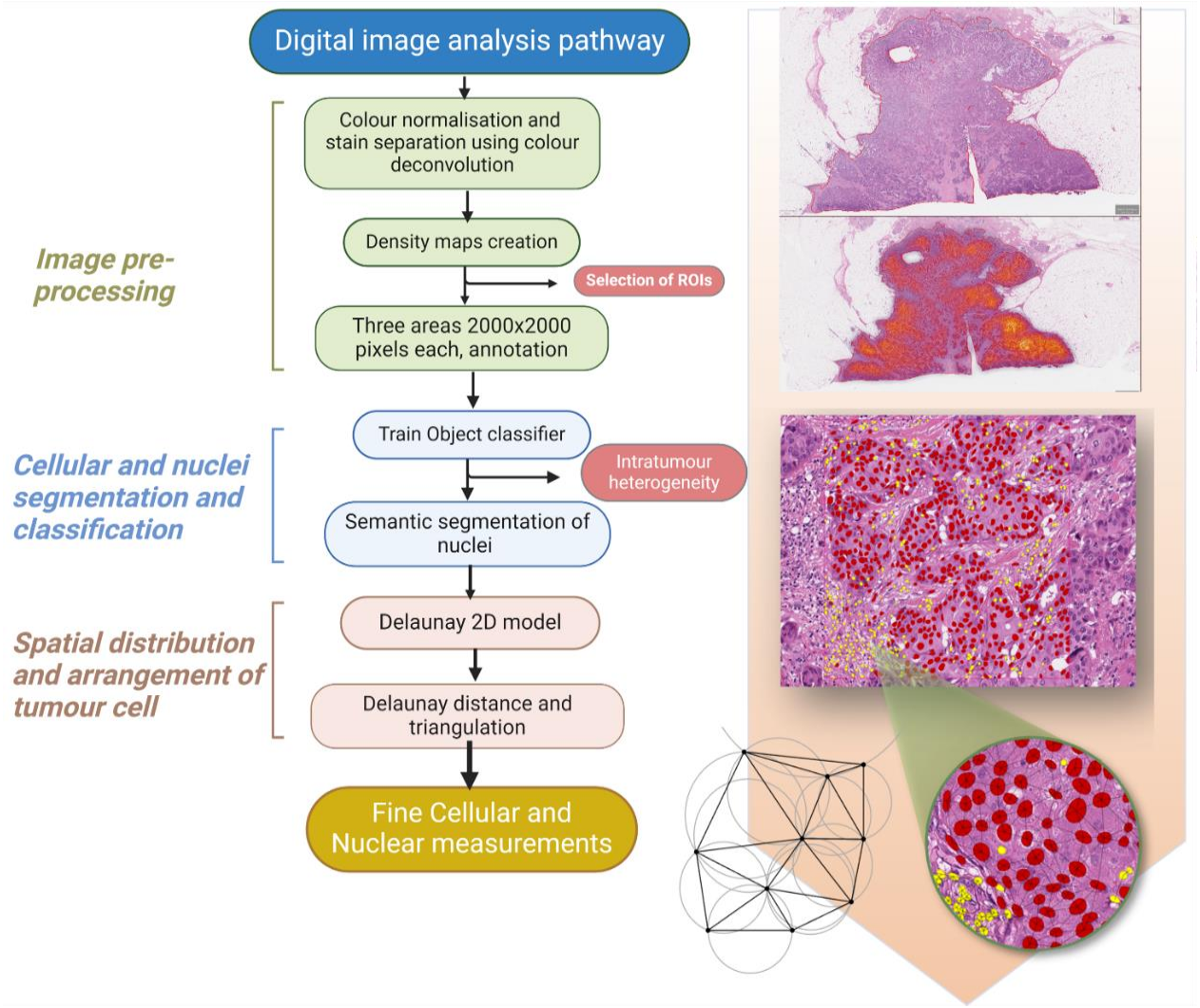


Figure 2.11: Schematic illustration summarising the digital image analysis workflow. ROIs: regions of interests

2.11 Bioinformatics

Bioinformatics is a scientific subdiscipline that involves the application of computer technology and computational methods to analyse biological data, including DNA and amino acid sequences, as well as various annotations related to those sequences [424]. By integrating clinical and morphological information with gene expression data, potential biomarkers and molecular pathways associated with HER2 activity, response and resistance to therapy can be identified.

2.11.1 Gene Expression Omnibus dataset

An extensive search was carried out in the National Centre for Biotechnology Information (NCBI) gene expression omnibus (GEO) dataset looking for preclinical trials, and experiments investigating genes regulating trastuzumab response/resistance in HER2-positive tumours either on homo sapiens BC cell lines or xenografts. The raw sequencing data for this study was retrieved from the National Centre for Biotechnology Information's GEO repository under accession numbers; GSE136300, GSE55005, GSE161420, GSE121105 and GSE60182. GEO serves as a public repository for curated gene expression datasets. To access the raw sequencing reads associated with this GEO dataset, the European Nucleotide Archive (ENA) was utilised. ENA collaborates with GEO to provide an alternative access point for sequencing data. By searching the GEO record for Sequence Read Run (SRR) identifiers, we were able to locate the relevant Illumina HiSeq data within ENA. The SRR identifiers uniquely identify each sequencing run deposited in the NCBI Sequence Read Archive (SRA). ENA's user-friendly interface allowed for the download of

FASTQ files containing the raw sequencing reads. This was done by the author. Adapters were removed, and low-quality reads (phred <30) were removed using Trim Galore[425] which is a bioinformatics tool specifically designed for processing sequencing data, particularly RNA-Seq data generated by Illumina sequencing platforms. The resultant reads aligned to the GRCh38 version of the human reference genome using STAR [426], and gene expression was quantified using Feature Counts. The DESeq2 tool in R software (version 3.4.3; https://cran.r-project.org/) was used for differential analysis of gene expression between trastuzumab sensitive and / resistant cell lines (BT474) before and after treatment with trastuzumab. The significantly differentiated expressed genes showed dysregulation with an absolute log-fold change (|log FC|) greater than 1 and a false discovery rate (FDR) below 0.05 when comparing trastuzumab-sensitive versus resistant cell lines. Common differentially expressed genes (DEGs) between conditions were identified using Venn diagrams. This was carried out under the supervision of prof Nigel Mongan.

2.11.2 Identification of valid DEGs and their functional analysis

BC-related microarray data downloaded from TCGA and METABRIC databases were processed using R software (version 3.4.4; https://cran.r-project.org). Our main objective was to investigate the panel of genes' functioning HER2 oncogenic signalling pathway and genes upregulated in HER2-Low tumours. Therefore, we intended to search for DEGs between different HER2 IHC categories; HER2-positive, HER2-Low and HER2-negative. DEGs were defined as genes (|logFC|) > 1 and FDR below 0.05 when comparing each of the two HER2 categories. The analysis of DEGs was conducted using the R

package "limma," which stands for linear models of microarray data. The DEGs were then visually represented using hierarchical clustering, heatmaps and principle component analysis through ClustVIS online tool [427].

2.11.3 Functional and pathway enrichment analyses of DEGs.

The list of up- and down-regulated DEGs obtained from our analysis was further investigated using overrepresentation analysis (ORA) and Kyoto Encyclopaedia of Genes and Genomes (KEGG) pathway analysis. These analyses were performed on webgestalt.org. [428], a web-based platform known for its functional enrichment analysis capabilities. This analysis allowed us to gain insights into the underlying enriched molecular pathways, biological processes, cellular components and molecular functions associated with the observed gene expression changes. An FDR threshold of less than 0.05 was set to ensure the result's reliability, indicating that only pathways with a statistically significant enrichment were considered, minimising the likelihood of false-positive findings.

2.11.4 Construction of the protein-protein interaction (PPI) network and identification of hub genes

To understand the functional relationships between DEGs, we constructed a protein-protein interaction (PPI) network utilising the Search Tool for the Retrieval of Interacting Genes/Proteins (STRING) database [429]. STRING offers a wealth of information on both known and predicted protein interactions, aiding in deciphering the functional interplay between the DEGs.

Next, to identify key players within this network, we employed the cytoHubba plugin for Cytoscape software (version 3.7.2) [430]. Specifically, the Maximal

Clique Centrality (MCC) algorithm was used to pinpoint hub nodes highly connected proteins likely to exert significant influence on the network. Additionally, the clustering coefficient algorithm of cytoHubba helped us rank all genes based on their network connectivity and potential importance. Finally, the top 10 genes with the highest scores were designated as hub genes, signifying their potential to play critical regulatory roles in BC biology.

2.12 Statistical analysis

Statistical analysis was performed using Statistical Package for Social Sciences (SPSS) software Version 27.0 (SPSS Inc., Chicago, IL, USA). GraphPad PRISM software Version 7.0 (GraphPad Prism Inc., San Diego, CA, USA) was used to plot graphs and analyse some of the generated data. p-value <0.05 was considered significant.

2.12.1 Conventional Statistical Approach

2.12.1.1 Univariate analysis with clinicopathological parameters

Analysis of continuous variables was performed using the appropriate statistical test (e.g. t-test, Mann-Whitney U test, ANOVA test). Chi-squared analyses were used for inter-relationships between categorical variables (e.g. biomarker expression and clinicopathological variables). Inter-class correlation coefficient (ICC) was used for inter-rater concordance (as continuous values) and Kappa test for the concordance rate as a categorical value.

2.12.1.2 Univariate analysis with outcome

Survival estimates for patients' were analysed by the Kaplan-Meier method with significance determined by the log rank test. This analysis included BC-

specific deaths, cases still alive, and censoring cases for those who were lost to follow-up or died of other causes The study endpoints ranged between 5 years to 20-year BCSS or DMFS.

2.12.1.3 Multivariate analysis with patients' outcome

Multivariate analysis was performed by Cox proportional hazard analysis to test for confounders and prognostic or predictive independency of the studied biomarker from standard prognostic/predictive factors.

All statistical analyses were performed by the author

2.12.2 Other analysis

2.12.2.1 Artificial neural network models (ANN)

Extreme gradient boosting "XGBoost model to identify the most effective feature combinations with the highest accuracy in predicting HER2 positivity. XGBoost model is an ensemble machine learning algorithm that is widely used to handle tabular data and excels in predictive modelling, classification, and regression tasks. XGBoost works by training a number of decision trees. Each tree is trained on a subset of the data, and the predictions from each tree are combined to form the final prediction [431, 432]

We used XGBoost model to predict the most important set of features in predicting HER2 morphometric signature and also link this to a prognostic index.

We studied each morphometric feature contribution into the final prediction by applying Recursive Feature Elimination (RFE) which is an iterative algorithm

that systematically removes less important features from the dataset based on model feature importance **(Figure 2.12).**

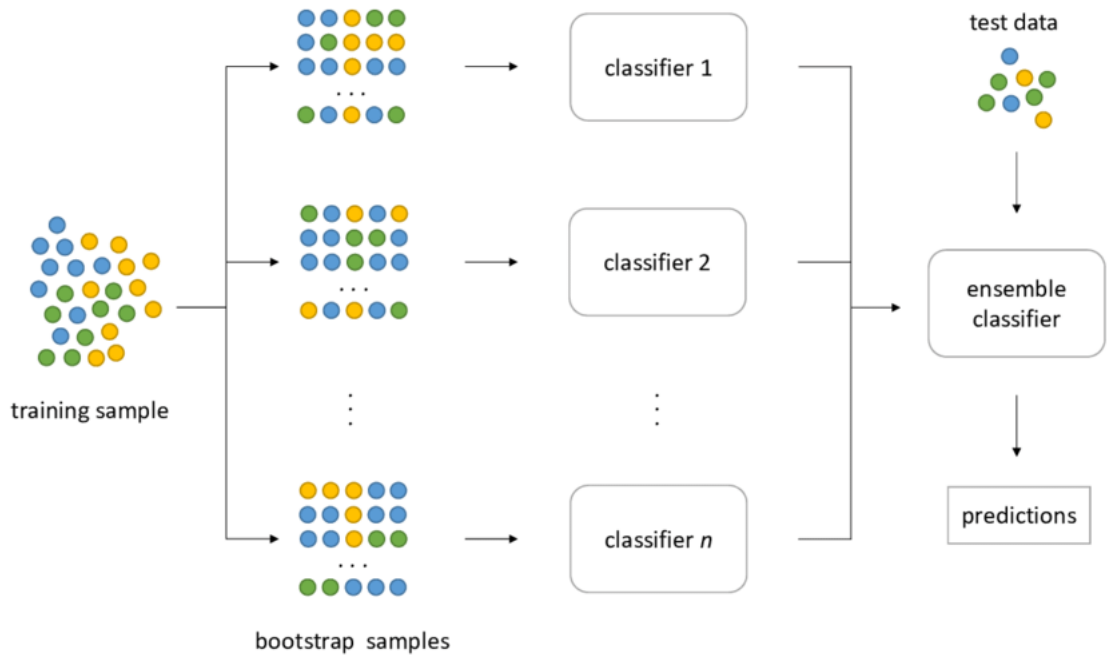


Figure 2.12: XGBoost architecture: It's an ensemble of classifiers where each classifier is focused on the mistakes made with the previous classifier.

Then, we aimed to establish a link between extracted HER2 morphometric features (covariates) and time to recurrence in HER2-positive BC patients following adjuvant anti-HER2 therapy. We enrolled the morphometric signature both alone and combined with clinicopathological parameters (ER, PR status, and tumour size), to develop the optimal prognostic index (clinic-morphometric) for predicting recurrence time after anti-HER2 therapy. Results were compared to models based solely on HER2 IHC score and on clinico-HER2 IHC score, which included the same clinical parameters along with HER2 IHC score.

Survival analysis is a type of regression problem, but with a twist. It differs from traditional regression by the fact that parts of the training data can only be partially observed as they are censored. Formally, each patient record consists of a set of covariates $x \in \mathbb{R}^d$, and the time $t > 0$ when an event occurred or the time $c > 0$ of censoring. Since censoring and experiencing and event are mutually exclusive, it is common to define an event indicator $\delta \in \{0; 1\}$

and the observable survival time $y > 0$. The observable time y of a right censored sample is defined as

$$y = \min(t, c) = \begin{cases} t & if\ \delta = 1 \\ c & if\ \delta = 0 \end{cases}$$

For our model we used survival gradient boost (SGM) model with the partial likelihood loss of Cox's proportional hazards model. Therefore, the objective is to maximize the log partial likelihood function, but replacing the traditional linear model $x^T\beta$ with the additive model $f(x)$:

$$arg\min_f \sum_{i=1}^{N} \delta_i \left[f(x_i) - \log\left(\sum_{j \in R_i} e^{f(x_j)} \right) \right]$$

Rather than predicting a single point in time of an event, the prediction step in survival analysis focuses on predicting a function: either the survival or hazard function. The survival function S(t) returns the probability of survival beyond time, whereas the hazard function h(t) denotes an approximate probability that an event occurs in the small-time interval under the condition that an individual would remain event-free up to time.

For evaluation of the model accuracy, we used the concordance index (c-index). It is a measure of rank correlation between predicted risk scores $\hat{f}$ and observed time points y. We also used time-dependent receiver operator characteristics (ROC) curve. Given a time point t, we can estimate how well our model can distinguish subjects who will experience an event by time t (sensitivity) from those who will not (specificity). The final area under the ROC curve (AUC) score is the mean score of the cumulative/dynamic AUC at a given list of time points. . For evaluation of the model accuracy, we used the concordance index (c-index). It is a measure of rank correlation between predicted risk scores $\hat{f}$ and observed time points y. For all tests, p<0.05 (two-tailed) was considered statistically significant.

2.12.2.1.1 K-means clustering

The K-means technique aims to partition the data into k-groups such that the sum of squares from points to the assigned cluster centres is minimised. To refine the definition of HER2-Low tumours according to mRNA level, *HER2* mRNA values were classified, using k-means, into 2 clusters based on their similarity of expression across multiple HER2 scoring parameters. Then ANN model (NeuroSolution version 7.0, NeuroDimension, Gainesville, FL with a range of hidden nodes in three layers, with a Levenburg Marquardt algorithm and a TanH activation function) was used to set cut off point for defining HER2 1+. Predictions of trained models were examined to determine predicted probability of K-means cluster membership. These were examined to determine a probabilistic cut point for HER2 score 1+.

2.12.2.1.2 Receiver operator characteristics (ROC) curve

We used the ROC curve to evaluate the accuracy of the developed models. It is a graphical representation used to evaluate the performance of a binary classification model. It plots the True Positive Rate (TPR), also known as sensitivity or recall, against the False Positive Rate (FPR) at various threshold settings [433]. The TPR represents the proportion of actual positives correctly identified by the model, while the FPR represents the proportion of actual negatives incorrectly classified as positive. The AUC is a single scalar value summarizing the overall performance of the classifier; an AUC of 1.0 indicates a perfect model, while an AUC of 0.5 suggests a model with no discriminatory power, equivalent to random guessing [434]. The ROC curve is particularly useful in comparing different models and selecting the optimal threshold for classification, as it provides a clear trade-off between sensitivity and specificity. This makes it an essential tool for evaluating the effectiveness of predictive models in various fields, including medical diagnostics, machine learning, and risk assessment [435].

With the exception of ANN and XGBBOST model, all the statistical analyses were performed by the author.

2.12.3 Ethical approval

This study was approved by the Nottingham Research Ethics Committee, REC 19/YH/0293 –“Refining the prognosis of and breast cancer precursor lesions for personalised therapy” , IRAS ID 266925.

Statement of author contribution to this work

This study included the integration of various research methods and techniques, the author carried out the majority of the work as follows:

Wet Lab Work

The author performed TMA blocks for the HER2-positive cohort and completed immunohistochemical staining, optimisation, assessment, and scoring. Biomarker selection and validation were conducted through WB and peptide blocking. The author also carried out RNA extraction and RT-qPCR-related studies.

Digital Image Analysis

The author was responsible for image acquisition, processing, cellular and nuclear segmentation using DIA software, morphometric feature extraction, measurements, and statistical analysis.

AI Studies

The author conducted WSI QC, whole-slide extensive annotation, and data analysis of the identified DL-extracted features. The DL model was completed by computer scientist collaborators at Warwick University.

ANN models were developed in collaboration with a statistician.

Bioinformatics related work

For bioinformatics-related studies, the author carried out validation of DEG through various web tools, as well as all subsequent pathway enrichment,

PPI, and hub gene-related analyses. The main DGE analysis was conducted by Prof Nigel Mongan.

For all the observational studies, the author collected and reviewed the data through accurate inclusion and exclusion criteria. The author also carried out all data analysis and interpretation of results.

Chapter 3. The Performance of Digital Pathology in Clinical Practice

3.1 BACKGROUND

The advent of digitalised WSI technology has drawn considerable interest within the pathology community. DP for primary diagnosis is increasingly becoming standard practice, transforming the field with its various advantages [332, 334, 436, 437]. This trend towards digitalisation has been propelled by governmental funding and the recent approval of WSI devices for primary diagnosis by the FDA [438]. The implementation of this advanced technology not only allows for remote reporting with flexible working hours and ensures uninterrupted service delivery even during crises like the COVID-19 pandemic, but it also facilitates second and expert opinion reporting [331]. Moreover, DP serves as a foundation for deploying AI-based algorithms, which can potentially improve diagnostic precision and efficiency.

Moreover, the implementation of WSI has shown to not only match but occasionally surpass the diagnostic capabilities of traditional microscopy. This is particularly true in cases requiring detailed analysis and quantification of tissue features, where digital tools and algorithms can provide enhanced visualisation and measurement capabilities ([439]. The reproducibility of DP diagnoses also benefits from the ability to easily share digital slides among pathologists for second opinions, thereby improving diagnostic confidence and reducing variability.

3.2 INTRODUCTION

Digitising an entire glass slide is intricate and involves multiple steps, requiring the integration of advanced scanner hardware, robotics, and software systems. Achieving optimal-quality WSIs is contingent on the proficiency of skilled

operators who manage the scanning process and stringent QC protocols that are implemented from the time the specimen is received. These protocols encompass fixation, processing, and slide preparation before the actual scanning and acquisition of WSIs [440].

The concordance between DP-based diagnosis and traditional microscopy diagnosis has been a significant area of research, aiming to validate the reliability and accuracy of DP. Studies have demonstrated high levels of agreement between the two modalities, supporting the use of DP in routine diagnostic practice. One such study by Williams and Treanor [441] found that the concordance rate between DP and traditional glass slide diagnosis was over 95% for a range of pathological conditions, indicating that DP can reliably replicate the diagnostic outcomes of traditional methods. Similarly, a study by Hanna, Reuter [442] involving a large cohort of cases across multiple pathology subspecialties reported an overall concordance rate of 96.3%, further validating the diagnostic accuracy of DP. However, ensuring the precise representation of tissue in WSIs compared to their glass slide counterparts is essential for the routine use of DP, as it allows for accurate diagnoses and the ability to share complex cases for second opinions.

Maintaining both glass slides and WSIs in regular practice is not cost-effective and demands additional resources. Despite this, pathology laboratories are unlikely to discontinue the storage of glass slides in favour of exclusively using digitised WSIs without robust evidence demonstrating that WSIs are fully representative of the original glass slides. Such evidence needs to be compelling enough to alter national guidelines. Additionally, to facilitate the extensive adoption of slide scanning in routine histopathology, it is important for scanner

manufacturers to develop high-speed, high-throughput scanners that can manage the volume of slides produced by contemporary laboratories while ensuring high image quality. An automated scanning process is crucial to achieve this, and it must be designed to avoid errors, such as missing low-density tissues like adipose tissue.

3.3 HYPOTHESIS

In this study, we hypothesised that not all tissue on glass slides is accurately represented on digitised WSIs, particularly in fatty tissue-rich organs, which pose significant scanning challenges due to their pale nature and reduced contrast. Using histopathology WSIs acquired from various breast lesions as a prototype model of fatty tissue-rich organs, we evaluated this hypothesis across multiple scanners, breast specimen types, and scanning protocols. The study emphasises the role of QC measures in minimising these pitfalls and ensuring high-quality digital representations.

3.4 AIMS OF THE STUDY

- Assess the representation of digitised WSIs to evaluate how well WSIs represent the corresponding glass slides in histopathology.
- Evaluate clinical implications of missing a tissue using digitised WSIs compared to traditional glass slides.
- Focus on various breast lesions, different specimens, both resection and core biopsy, and different staining techniques, both IHC and H&E, as models to assess scanning quality, given the challenges posed by fatty tissue with reduced contrast.

- Compare multiple scanners and protocols: to evaluate the performance across multiple scanners, breast specimen types, and scanning protocols.
- Role of QC measures in minimising scanning pitfalls and ensuring high-quality WSIs

3.5 MATERIAL AND METHODS

This study involved a total of 40,160 WSIs from breast resections and biopsies, divided into two groups:

Main Study Cohort (Group 1): This cohort consisted of 22,160 WSIs (22,000 H&E images and 160 IHC stained slides scanned by the Philips Intellisite UltraFast Scanner (Amsterdam, Netherlands) (Scanner A) from breast patients at Nottingham University Hospitals, United Kingdom (UK), between March 2020 and January 2021. The cohort included a diverse range of breast excisions, such as normal tissue from reduction and re-excision specimens, benign lesions, atypical proliferations, and malignant lesions, both in situ and invasive tumours.

Group 2 Cohort: This cohort included 18,000 historical H&E WSIs of invasive BC scanned for various research purposes by the Nottingham Breast Pathology Research Group. The WSIs were scanned using two different devices: 10,000 images were acquired from the Aperio AT2 – High Volume Scanner (Leica Microsystems (UK) Ltd) (Scanner B), and the remaining 8,000 WSIs were scanned using the Pannoramic 250 FLASH III 2.0 (3DHistech, Budapest, Hungary) (Scanner C) (**Figure 3.1)** This cohort aimed to study the frequency of missing tissue in WSIs produced by different scanning approaches (with or

without human input during scanning) and assess the clinical impacts of missing tissue on tumour and resection margin assessments. Human input in this cohort included manual orientation and outline annotation of focus points in Scanner B, and adjusting specimen threshold settings in Scanner C. The specimen threshold level ranged between 0 and 255, with a default value of 220. Lower threshold values (more sensitive scanning) resulted in more areas being captured, taking more time and producing larger file sizes. Higher threshold values (less sensitive scanning) resulted in faster scanning. Details are provided in **Section 2.8.**

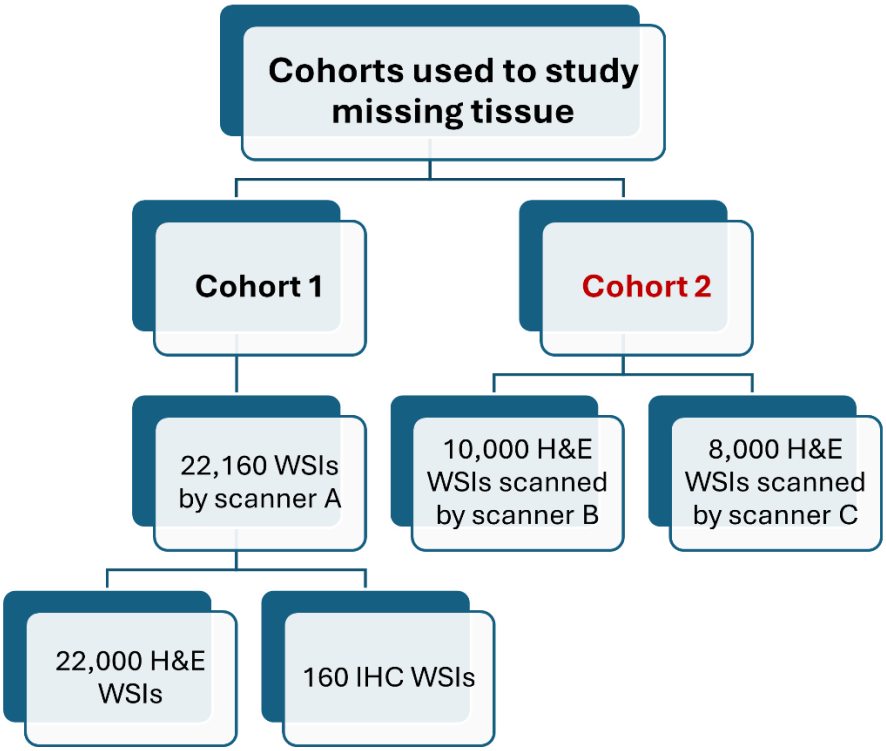


Figure 3.1: Schematic illustration of the study cohorts. WSI: whole slide image; IHC: immunohistochemical

All scanning was performed at a magnification of 40x, corresponding to a resolution of 0.25 µm per pixel. The WSIs were reviewed using dedicated viewer

software: Philips Image Management System IMS, Aperio Image Scope version 12.4.3, and 3DHistech Case Viewer version 2.4. For each image, we evaluated the frequency of missing tissue, the image quality and resolution, and the effectiveness of various quality control measures in reducing the rejection rate of WSIs.

3.5.1 Missing tissue in WSIs compared to glass slides

We assessed the presence of missing tissue WSIs compared to their corresponding glass slides. A pathologist examined low-resolution WSI thumbnails to identify discrepancies. When missing tissue was detected, we estimated the percentage and type of missing tissue (such as fatty tissue, normal structures, or lesions) and noted its location within the section. Additionally, we investigated factors that might influence missing tissue, including specimen type (excision vs. core biopsy), timing of DP implementation, stain type, and scanning time/file size for the three scanners used in the study. This comprehensive evaluation aimed to pinpoint the potential limitations of WSIs in comparison to traditional glass slides (**Section 2.8).**

3.5.2 WSI Quality Control

QC encompasses several steps, from checking glass slides for defects before scanning (cracks, stains) and real-time scanner checks (tissue presence, focus) to reviewing final WSIs for missing tissue. The study then goes beyond QC to assess the clinical impact of missing tissue and WSI quality on diagnosing lesions, tumour characteristics, and surgical margins. It even considers the impact on protein analysis using IHC. This thorough approach ensures reliable diagnoses based on digital slides **(section 2.8).**

3.5.3 Statistical Analysis

IBM-SPSS statistical software 27.0 (SPSS, Chicago, IL, USA) was used for statistical analysis. Descriptive Statistics i.e., Arithmetic mean (x) was used as a measure of central tendency, Standard deviation (SD) was used as a measure of dispersion, Percentage (%), Range and Median. Fisher's exact test (F.E.) and Chi-square ($\chi 2$) were used to compare between qualitative data. Differences were considered statistically significant when ($P<0.05$).

3.6 RESULTS

3.6.1 Missing Tissue Characteristics

In this study, 19% of all WSIs from cohort 1 showed a variable degree of missing tissue and the mean proportion of the missed tissue was 13%, range 1%-70% **(Table 3.1).** In 49% of cases, the missing tissue was <5% while in the majority of cases (82%), the missing tissue was < 20%. Only 1% showed >50% of tissue loss **(Table 3.2).** In all cases, the missed tissue was fibrofatty tissue with or without minute vasculatures (100%).

Table 3.1: Characteristics of the whole slide images (WSI) scanned in the routine diagnostic practice and showed missing tissues (number=4268)

Parameters	Cases with Missing Tissue	
	Number	%
Type of missed tissue		
Fat and blood vessels	4268	100
Normal Ducts/ TDLUs	1760	41.2
Benign lesions	0	0
In situ carcinoma	0	0
Invasive Carcinoma	0	0
Site of Missed Tissue		
Peripheral only	3337	78.2
Central and Peripheral	931	21.8
Type of specimens		
Resection specimens	4268	100
Core Needle biopsy	185	0
Date of Scanning		
Early*	2068	48.5
Late	2200	51.5
Change in the final diagnosis		
Yes	0	0
No	4268	100

TDLU: Terminal duct lobular unit. *First 3 months after installation and the use of the scanner

Table 3.2: Detailed analysis of the proportion of missing tissue in all cases within cohort 1, scanned during routine diagnostic practice

Proportion of missing tissue	Number of cases	Per cent out of total studied cases	Per cent out of missing tissue cases	Cumulative Per cent
1%	760	3.5	17.8	17.8
2%	401	1.8	9.4	27.2
3%	191	0.9	4.5	31.7
4%	106	0.5	2.5	34.2
5%	615	2.8	14.4	48.5
6%	21	0.1	.5	49.0
7%	85	0.4	2.0	51.0
8%	64	0.3	1.5	52.5
10%	572	2.6	13.4	65.8
12%	43	0.2	1.0	66.8
15%	250	1.2	5.9	72.8
17%	21	0.1	.5	73.3
20%	358	1.6	8.4	81.7
30%	250	1.2	5.9	87.6
35%	64	0.3	1.5	89.1
40%	127	0.6	3.0	92.1
50%	212	1.0	5.0	97.0
60%	85	0.4	2.0	99.0
70%	43	0.2	1.0	100.0
Total cases with missing tissue	4268	19.4	100.0	
Total studied cases	22000	80.6		

Only 8% of cases showed missed small normal breast ducts and/or lobules, in addition to the missing fatty tissue ***(*Figure 3.2 and Figure 3.3*).*** All the missed ducts were peripherally located and surrounded by fat. The largest missed ter-

minal lobular duct unit (TLDU) was 1.5mm in maximum diameter and the largest duct that was missed on scanning was measured 830µm in maximum diameter. The missed tissue was allocated peripherally in 78% of the cases, while 22% of cases showed centrally and peripherally located missed tissue. None of the examined core needle biopsy specimens (n=185) revealed missed tissue when compared to the corresponding glass slides.

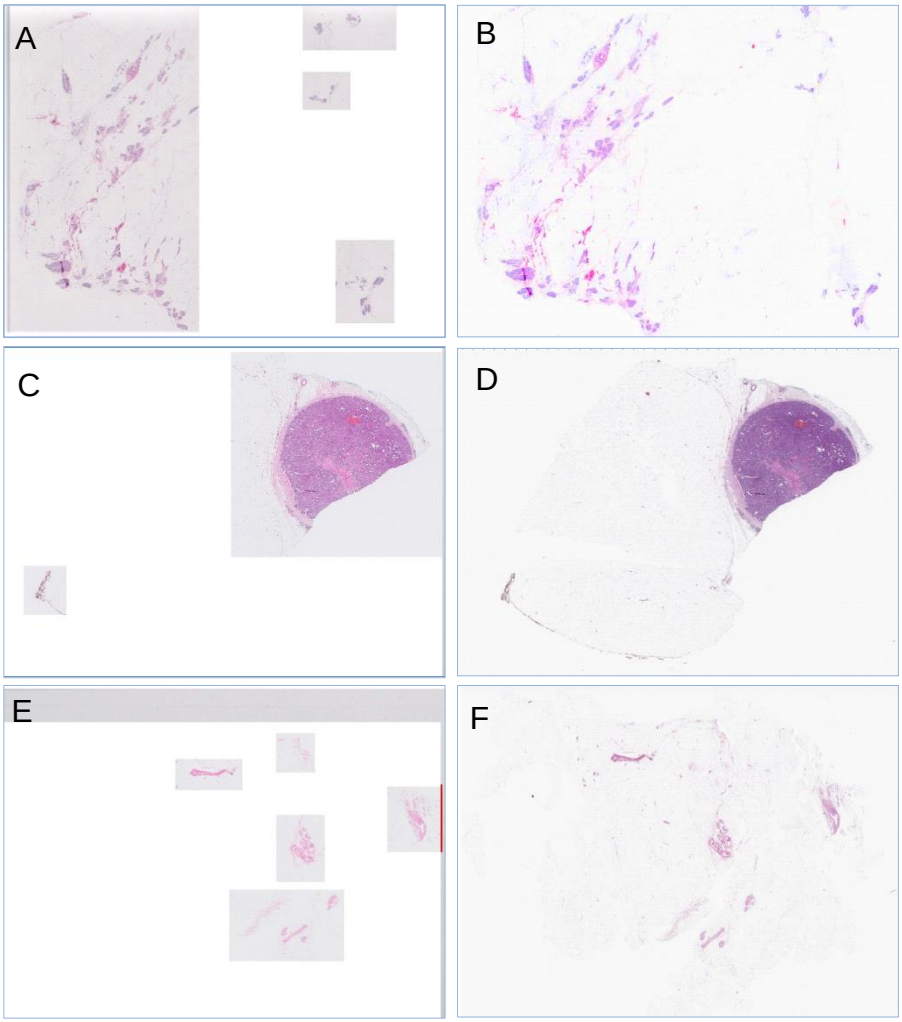


Figure 3.2: Examples of missed tissue in WSI (left) compared with the corresponding glass slides (right).

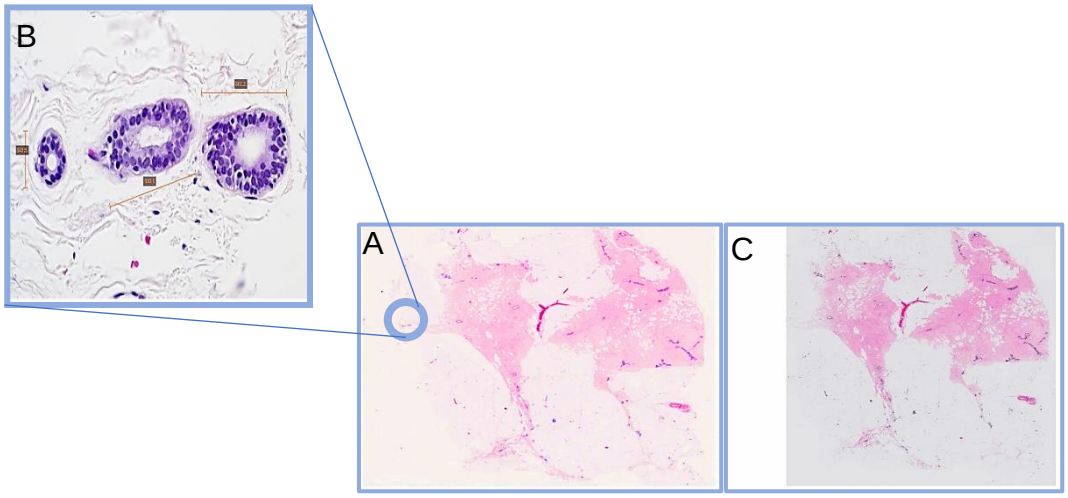


Figure 3.3: Example of WSI missing normal breast duct at the periphery of the slides. A): overview image of a slide that was fully scanned, B): High power of the normal breast terminal lobular duct unit on a glass slide (x40 light microscope) present at the periphery of the slide and was missed upon scanning (C). The terminal lobular duct measured 1.5mm at its largest diameter.

Focusing on WSIs of invasive BC tissue sections only (from both cohorts 1 and 2), The mean proportion of missing tissue for the 3 scanners collectively was 9%. None of the WSIs with missing tissues resulted in a change in the final diagnosis, i.e., differentiating benign from malignant lesions, changing tumour grade or stage. However, there was an underestimation of the distance to margins when the missed tissue was peripherally allocated. 12% of cases revealed a reduction of distance to the actual margin, and the reduction ranged from 1mm to 8mm. In all cases, the margins were inked, facilitating the identification of the defects and that a missing part of the tissue was present opposite to the tumour, particularly when it was close (1mm). Importantly, none of the cases was reported as tumour on ink (positive margin) as a result of missing tissue on WSI; thus, no subsequent re-excision was performed.

Regarding WSIs of the IHC stained tissues, 16% of the cases showed a degree of missing tissue. The mean proportion of missed tissue was 6% and ranged between (2% to 10%) The missed tissue was fat in all cases with occasional normal breast TLDUs. There was no change in the final score between the glass slide and WSI, except in one case stained with Ki67 (0.6%) that showed missing few invasive tumour cells infiltrating fat and resulted in a reduction of the Ki67 score from 15% on a glass slide to 12% on WSI when we considered average ki67 expression in whole slide, while when we considered the expression on hot spot, there was no difference on the final score. In either scoring method, this did not affect the final scoring category of the cases, as the cut-off of positivity used was 10%.

3.6.2 Quality Control Data

During the early implementation of the scanning service, the WSI scanning failure rate was 20%. Failed image quality was related to poor quality issues, including pixelated or out of focus images or failed scanning **(Figure 3.4I**). Poor quality images that necessitate rescanning partially related to suboptimal glass slide qualities, including tissue folding, cracking, uneven stain distribution and/or air bubbles ***(*Figure 3.4II*)***.

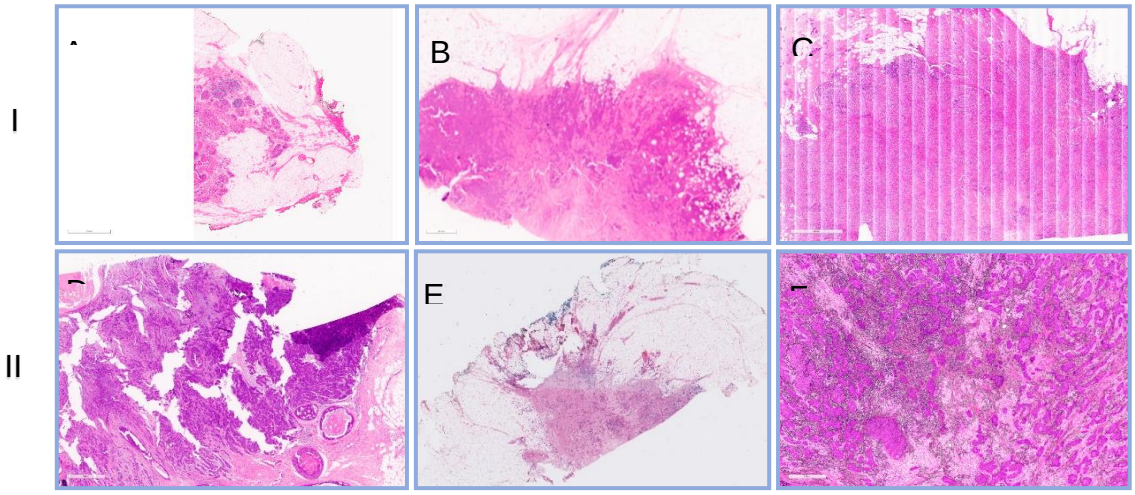


Figure 3.4: Examples of different quality control categories on failed WSIs.

Following three months after applying strict QC measures to both glass slides and WSI, the scanned image failure rates decreased to 2% ***(*Figure 3.5 and Figure 3.6)**. Although there was a significant reduction in WSIs failure rate ($p<0.05$) after applying the QC measures, there was no significant difference in the frequency of missing tissue and the time to implementation of the digitalisation service ($p>0.05$).

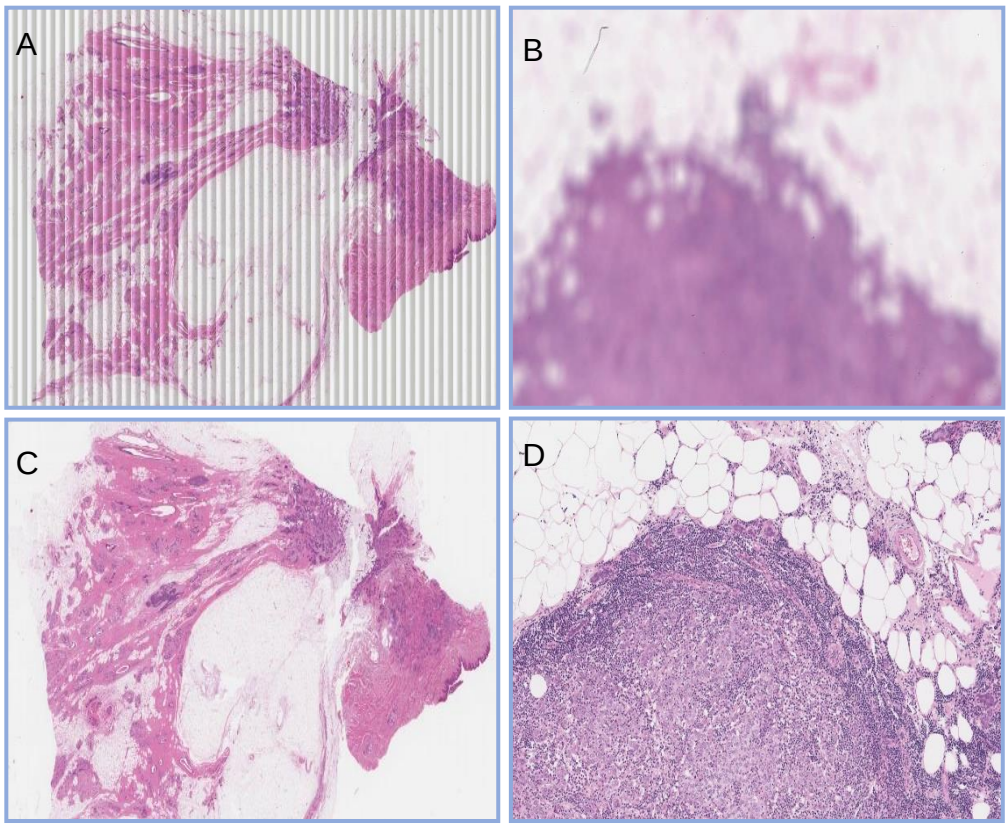


Figure 3.5: Role of quality control in improving digitalised image quality; Failed images before (A, B) and after quality control (C, D). A: shows longitudinal scores, B: is out of focus.

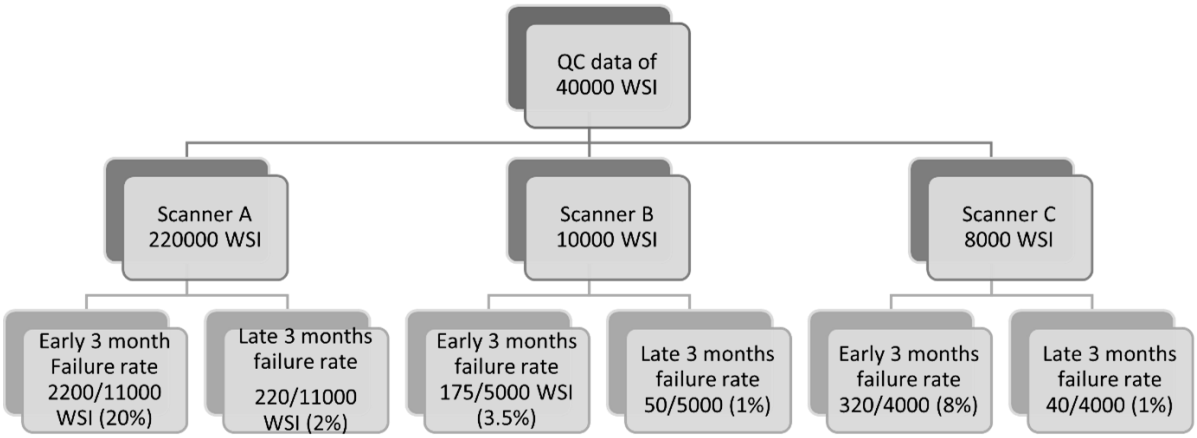


Figure 3.6: A flowchart demonstrates the WSI failure rate before and after the application of quality control measures for the three studied scanners.

3.6.3 Missing tissue and confounders

The average time consumed to scan each slide by scanner (A) was 60 seconds (range 30-90 seconds), and the average image file size was 1.2GB (range 1.1-1.4 GB) **(Table 3.3)**. Scanning time for one slide in scanner B ranged between 7-9 minutes (average 8 minutes), including time required for manual orientation and outline annotation of the focus points, and the average image size was about 1.5 GB (range 1.4-1.7 GB). For scanner C, when using a low specimen threshold setting, the average scanning time was 2.5 minutes (range 3-4 minutes), and the average image file size was 1.7 GB (range 1.5-1.8 GB). For the high specimen threshold setting (the time for each slide scanning ranged between 1-2 minutes, and the average image file size was 800 MBs **(Figure 3.7).** The specimen threshold level setting ranges between 0 and 255. The default value is 220. Smaller values (low threshold) result in more sensitive scanning, with more areas to be captured, but also more time and a larger file size. High threshold values result in less sensitive, faster scanning.

Table 3.3: Relation between missing tissue and both the scanning time and average image file size with their impact on the clinical final diagnosis

Studied Scanners	Scanning Time	Average image file size	Missing tissue/ Type	Out of Focus images	Impact on the final clinical diagnosis
Scanner A	0.5-1.5 minutes	1.2 GB	Yes/ Fat	No	No effect
Scanner B	7-9 minutes	1.5 GB	No	No	No effect
Scanner C					
High Specimen threshold	1-2 minutes	800 MB	Yes/ Fat	No	No effect
Low Specimen threshold	3-4 minutes	1.7 GB	No	No	No Effect

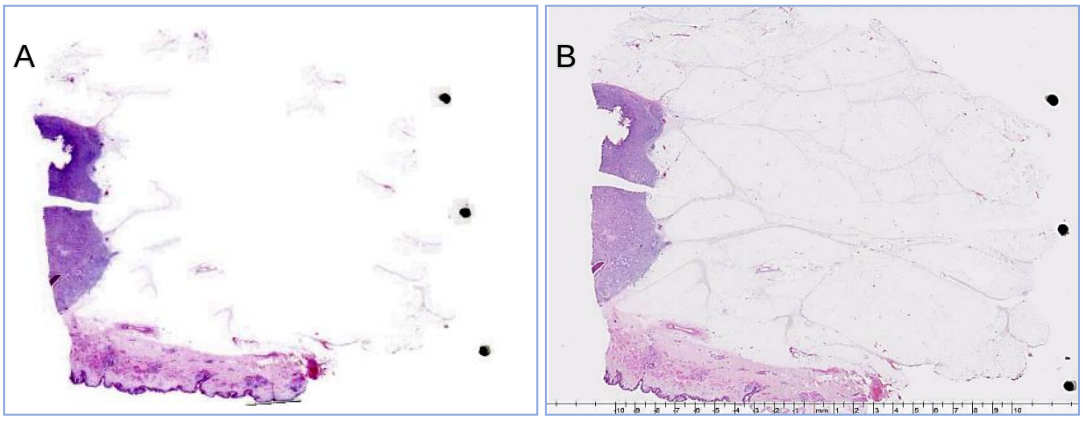


Figure 3.7: Example of an image scanned by the same scanner but at two different settings: A) High specimen threshold scanning with missing most of the fatty tissue on WSI, while B) the image was scanned at low specimen threshold scanning and no missing tissue was detected.

3.7 DISCUSSION

Validation studies have established that WSI is non-inferior to traditional glass slides for routine diagnostic purposes. [439, 443, 444]. As the adoption of DP and WSI technology expands, the development of standardisation and best practice guidelines becomes essential to ensure optimal implementation and application without compromising patient healthcare. [445].

Accurate diagnosis using WSIs relies on the premise that the digital image is an exact reproduction of the scanned glass slide. Any missing diagnostic material in the digital image compared to the glass slide could lead to misdiagnosis and improper patient management. The College of American Pathologists recommends validating WSI for diagnostic use by ensuring that all material on a glass slide is scanned and viewable in the digital image. However, this approach is impractical due to the variable percentage of missing tissue in WSIs, influenced by tissue types, scanners, and pre-scanning processing.

Pathologists often accept glass slides with some missing tissue, provided the slides are interpreted in context with the individual case.

Seeking strict criteria for WSI acceptance could hinder the technology's implementation and its healthcare benefits. Therefore, evidence-based studies showing differences between glass slides and WSIs and their impact on clinical decisions are crucial. While many studies have focused on validating the diagnostic concordance of WSI and light microscopy [446], few have addressed the representation of glass slides in digital images and its clinical impact.

In this study, we aimed to assess the quality of WSI performance in routine practice by evaluating the frequency, nature, and location of missing tissue in WSIs compared to glass slides and their clinical implications. We also examined image quality and the role of QC measures in minimising these issues.

Breast tissue is a perfect model in that it is formed normally of various tissue types and has a broad spectrum of heterogeneous lesions and pathological entities that covers a considerable sector in pathology i.e. well differentiated BC that is mostly glandular could represents gastric tissue, liposarcoma as an example of soft tissue tumours, metaplastic carcinoma as a model of squamous cell carcinoma. It also contains a considerable amount of fatty tissue, which is well known to be difficult for digital scanners to capture due to its pale nature.

The frequency of missing tissue varied among the various cohorts and scanners used in the study. Although direct comparison between the cohorts and the scanner has limitations due to lack of randomisation, this variation can be

related to differences in the composition of the scanned cohort, whether it is primarily faint, loose, fibrofatty tissue or dense tissue. The first cohort was routine clinical practice cases where each contained sections from tumour tissue, normal breast tissue, margins, and various types of lesions, while the second cohort included sections from invasive tumours only, which were selected based on the tumour burden and thus less fatty tissue. The latter cohort was scanned in research setting with different scanning protocols based on the research activities. So, cohort 1 was expected to have more fatty tissue component than cohort 2. Moreover, the in-built functionalities and mechanisms the scanner uses to capture the WSIs are different. Automatic tissue finder algorithms scanner differs from others with human inputs. Fatty tissue was the most frequent tissue to be missed. Fatty tissue is less dense and fainter than the surrounding tissues, so it is easily missed by the scanner detection system, especially in thinner tissue sections and paler staining density [444, 447]. Also, lipocytes are vacuolated empty spaces separated by thin cell membranes/septae so they could be considered as the empty slide white background and hence the scanner camera skips these areas. This could explain why the scanner can capture other faintly stained tissues/structures like mucin pool in mucinous carcinoma for instance as they usually have a bit of colour contrast compared to the background slide white spaces. None of the mucinous carcinomas included in this study showed missed tissue. The small proportion of WSIs with missed TDLU was at the periphery of the tissue section and was surrounded by fatty tissue, and these ducts were minute and widely spaced, which could explain the reason for being missed.

The incidence of missing a tissue was higher when it was peripherally allocated than being centrally present. This could be explained by both the mechanism at which the scanner works and the specimen itself. Scanners with automated algorithms to detect tissues tend to neglect peripherally faint and loose tissue to speed up the scanning process. Also, operators may ignore peripheral fatty tissue during the setting of the scanning area (cropping), and the focus points to reduce the scanning time and image file size. Peripherally situated tissues in larger tissue sections that extend beyond the coverslip are more prone to incomplete scanning than fatty tissue present centrally. Furthermore, fatty stroma among invasive BC is usually infiltrated by the malignant cells and consequently easily detected and less likely to be missed.

Importantly, no pathological breast lesions were included in the non-scanned missed tissue, neither from large resection sections nor core biopsies. That is because WSI captures pre-scans of the whole slide at low resolution, and only tissue detected on the pre-scan is then scanned at high magnification. All previously mentioned breast lesions are easily detected in the low-resolution image and completely scanned on the digital image. None of the studied core biopsies revealed missing tissue which is quite reassuring for the pathologist in reporting during routine clinical practice. This may be due to the nature of core biopsies, as they are basically punched from mass-forming lesions with less fat content. Missing tissue did not affect the final diagnosis of the cases nor the tumour grade or stage. Although 12% of cases revealed a reduction of distance to the actual margin, none of the cases was misidentified as having a positive margin (tumour on ink) [445], and no subsequent re-excision was carried out.

Although these findings could reassure the majority of pathologists that using WSIs in histopathology reporting is optimal, the risk of missing specific lesions that arise in adipose soft tissue, like liposarcoma, needs further investigation. This supports the hypothesis that the guidelines for using WSIs in routine pathology reporting should be individualised based on several factors, as mentioned above, in addition to tissue type. Considering such limitations without generalisation will help faster implementation of the technology.

The frequency of missing tissue in WSI of IHC stained sections was higher than the H&E WSIs, which is expected as IHC sections are usually thinner and using haematoxylin only as a counterstain reduces the tissue contrast; thus, fatty tissue in IHC sections tends to be paler and fainter. Nevertheless, the main missing tissue was fat, which did not affect the assessment of the IHC biomarkers. IHC sections are more liable to tissue folding/loosing during staining, especially from the antigen retrieval method. This uneven tissue surface usually affects the quality of the acquired images with areas out of focus. This could affect the assessment of IHC biomarkers, not due to missed tissue but to difficulty evaluating such hazy areas. Therefore, standard QC measures focusing on the overall quality of the slides, including tissue processing, sectioning quality, and staining quality, should be followed in addition to QC of the scanning process to ensure the highest quality WSI of the IHC stained slides.

An overview image (macro-image) could help pathologists detect missing tissue to determine if the WSI would be enough for diagnosis, especially if the missing tissue proportion is low or they need to return to glass slides if the missed tissue is peripherally located and would affect surgical margin measurement.

In this study, we compared the frequency of missing tissue and the image quality within the first three months of digitalisation of the department and the following three months to assess the impacts of early implementation of the technology and full application of the QC measures in routine practice. There was an improvement in the image quality and a reduction in WSI failure rates following the initial implementation period. The image failure was categorised into tissue-related factors such as folding and scores, faint and blurred WSI, and scanning errors, i.e., longitudinal scores, incomplete scanning or out-of-focus areas. Issues related to slide preparation and microtomy were solved by properly calibrating microtomes, changing tissue thickness from 2.5um to 4um and re-staining faint slides. [448]. Proper cleaning of slides, as well as avoiding extensions of tissue fragments beyond the coverslips, minimises missing parts of the tissue near the edges of the slide [440]. Other image failure causes were poor quality scan, and this was solved by rescanning the slides. Our findings indicated that QC measures were successful in reducing the image failure rates. However, the missing tissue frequency was not significantly improved over time even with the adoption of these strict QC measures. This could be explained by the nature of the tissue and the scanner's performance and its ability to detect low-density and faint tissue rather than the quality of the slides' preparation.

Although strict QC measures can reduce scanned image failure rates, they may add costs to the digitising process in terms of staff, time, and that the WSI can be considered as an additional financial burden on pathology laboratories. Unlike digitisation of radiology, WSI technology in pathology is considered an additional rather than a replacement technology WSI will not be able to create

digitalised WSI without the creation of the glass slides. However, we must highlight that the return on investment measures in WSI in pathology are mainly related to changing the geographically fixed workload of glass slide reporting to a fully flexible workflow that can be delivered electronically. Just as with mail communications, this change has multiple benefits and efficiencies to be exploited, including sharing workload between multiple pathologists, centres and regions, rapid and convenient peer review of cases, reporting remotely from the host laboratory, 24-hour working and, easy access to archived material. More importantly the promise of AI algorithms that can result in a paradigm shift in the field of pathology [347, 449] can only be delivered to a digitised workflow.

In our study, a negative correlation between the frequency of missing tissue and both the scanning time and the image file size was observed. Also, scanners without human input during scanning had a shorter scanning time, but the highest frequency of missing tissue as it tends to ignore faint tissue during scanning to speed up the process.

In conclusion, missing tissue on breast WSIs is observed with variable frequency. Fatty tissue is frequently missed but is of little diagnostic consequence. Improving scanning algorithms and increasing the tolerance towards slide margins can potentially improve the performance and user confidence in the technology. Balancing between WSIs quality and scanning time/image file size should be considered. Similar to glass slide preparation, adequate QC measures can reduce WSI failure rates and diminish the potential clinical implications of missing tissue on WSIs**.**

Chapter 4. Assessment of BC stroma features using AI

4.1 BACKGROUND

BC is a complex and heterogeneous disease and is a leading cause of cancer related deaths worldwide [2]. Prognostic stratification of BC using conventional morphological features and advanced genetic profiles plays a key role in patients' management decision-making. Alterations in the TME are increasingly recognised as important drivers of tumour maintenance and progression [450]. Emerging evidence shows that the STR defined as the relative volume TAS in relation to neoplastic epithelial cells, has an independent prognostic value in several solid tumours, including BC [2, 91, 96, 451-458]. TAS is usually assessed through visual examination of H&E stained sections, or more special techniques using polarised, photon laser, fluorescence microscopes or IHC stains [459, 460]. However, these methods are time-consuming, subjective, not standardised, difficult to quantify and incorporate with other morphological features, and often carried out on a small area of tumour tissue. For these reasons their integration into routine practice is challenging [461, 462]. There are also limitations to the human visual capacity to discern complex morphological features within the tumour cells and tissues and surrounding TME.

Reliable assessment is essential for patient stratification and follow-up, necessitating an automated method for objective and standardised STR quantification with high reproducibility. The growing adoption of DP workflows also highlights the need for automated evaluation methods with standardised protocols [463, 464]. Automated histopathological analysis enhances both efficiency and consistency compared to traditional methods [465]. Although some studies have explored computational image analysis to classify stroma and tumour

epithelial cells in small tissue samples for STR assessment [463, 466], a fully automated STR evaluation applicable to WSI remains unavailable [462, 466].

4.2 INTRODUCTION

The tumour mass comprises not only a heterogeneous mix of cancer cells but also various resident and infiltrating host cells, secreted factors, and extracellular matrix (ECM) proteins, collectively known as the tumour microenvironment [467]. Malignant transformation of cancer cells is often accompanied or preceded by changes in the surrounding stroma. Carcinoma-associated fibroblasts, activated by the tumour microenvironment, play a significant role in ECM-related changes, including increased ECM synthesis and remodelling of ECM proteins by proteinases [468]. Carcinoma-associated fibroblasts, activated by the tumour microenvironment, play a significant role in ECM-related changes, including increased ECM synthesis and remodelling of ECM proteins by proteinases [469, 470]. The altered ECM subsequently influences tumour progression through architectural and signalling interactions [471]. This tumour stroma, an essential component of cancer tissue, consists of various cell types such as fibroblasts, immune cells, vasculature cells, and the extracellular matrix [472]. Research indicates that tumorigenesis is heavily influenced by interactions between cancer cells and stromal elements. This interaction could be a defensive attempt by the host to combat tumour cells, exerting antagonistic biological forces **(Figure 4.1)**. Alternatively, it may benefit the tumour by promoting neovascularisation and restricting access to host lymphocytes, macrophages, and other immune regulatory cells [473-478]. Numerous studies have linked specific stromal characteristics to tumour aggressiveness and patient outcomes [477, 479-481]. As a result, the development of the stroma is now

recognised as playing a supportive role in tumorigenesis, and these stromal changes can be utilised as prognostic or predictive biomarkers [468].

A few studies have applied computational image analysis for the assessment of STR in BC. However, these prior studies were performed on TMA sections or applied on a small area of tumour [453, 482, 483]. Therefore, clinicopathological, biological and prognostic values of STR showed inconsistent results among studies even within the relatively molecularly uniform luminal/HER2-negative BC subtype [96, 452, 454, 456, 482]. Some reports indicate that stroma-rich luminal/HER2-negative BC tumours have a worse prognosis than stroma-poor tumours [96, 451, 456], while other reports demonstrated the opposite [454, 482]. Such discrepancies may not only relate to the heterogeneity of BC but also to the subjectivity and variation in the STR assessment used previously. In the era of increasing use of DP in clinical practice, AI-based assessment of complex morphological features may provide a promising alternative technique to identify several stromal features from WSI [331, 333, 334, 464, 465, 484].

Invasive tumour size is a key prognostic factor that represents a component of the Nottingham prognostic index [485]. However, the density of tumour cells within small size tumours might be an omitted aggressive factor. Tumour cell density refers to the number of cancer cells in a specific tumour tissue area, and it has been associated with tumour proliferation rates and metastatic potential. The accurate assessment of these features through automated methods can improve the precision of tumour characterisation and prognostication. By integrating tumour cell density and size measurements with STR analysis,

AI-based algorithms can provide a comprehensive evaluation of tumour morphology, enhancing the overall prognostic accuracy and aiding in more tailored treatment strategies.

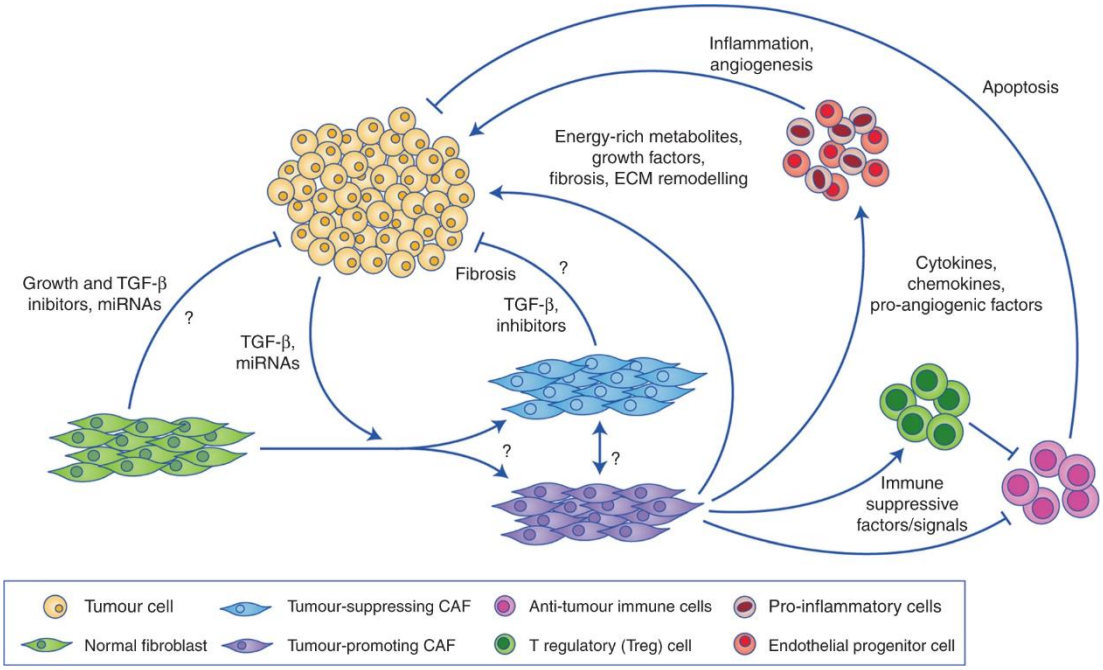


Figure 4.1: Roles of Carcinoma Associated Fibroblasts (CAFs) in Tumorigenesis. Tumour cells and the surrounding CAFs, interact to create a microenvironment that can either promote or suppress tumorigenesis. Tumours can stimulate normal fibroblasts to transform into CAFs, yet the biological mechanisms that dictate whether these fibroblasts adopt tumour-promoting or tumour-suppressing roles are still unclear. Tumour-promoting CAFs enhance tumour growth, survival, and metastasis both directly and indirectly by influencing other tumour-associated stromal cells. Conversely, both normal fibroblasts and CAFs have been observed to inhibit or slow down tumorigenesis. [486].

4.3 HYPOTHESIS

In this study, we hypothesised that an AI-based algorithm can be developed to reliably assess tumour and stromal morphological features from BC WSI, including STR, the spatial distribution of stroma relative to tumour cells, and tumour cell density.

4.4 AIMS OF THE STUDY

- Develop an AI-based algorithm to assess STR and spatial distribution of stroma in WSI of ER-positive, HER2-negative luminal BC.
- Evaluate the reliability of the AI-based algorithm compared to traditional assessment methods.
- Investigate the prognostic significance of the AI-derived STR and spatial distribution of stroma features in a large cohort of patients with long-term follow-up.
- Stablish a parameter that better represents tumour burden, which combines tumour size and tumour cell density, and compare its prognostic value compared to tumour size only.

4.5 MATERIALS AND METHODS

This study was conducted as part of the PATHLAKE project, a major initiative aimed at advancing the use of AI in DP and medical imaging. It is part of a network of five Centres of Excellence in the UK, a UK Centre of Excellence in DP and medical imaging. Nottingham University aimed to develop an AI-based tool to predict the prognosis of BC patients from H&E-stained features. In collaboration with the computer science team at Warwick University, UK, the experimental work included cohort characterisation, WSI acquisition, extensive region and cellular annotation, algorithm development, and quantification of the stroma-tumour ratio and spatial distribution. The DL algorithm and feature quantification were performed by the AI team at Warwick University. The author was responsible for tissue annotation, tumour burden assessment, visual

STR evaluation, and all statistical analyses. Other H&E features, such as tumour-infiltrating lymphocytes, mitosis count, and intratumor heterogeneity, were also assessed through the AI algorithm. Although the author contributed to other studies, the main focus was on assessing BC stroma-related features.

4.5.1 Cohort characteristics and image acquisition

A large cohort (n=1,968) of ER-positive and HER2-negative BC was included. Detailed clinicopathological parameters were available including patient age at diagnosis, tumour size and grade, NPI, LN stage, LVI and PR status. Ninety-three per cent of patients received adjuvant endocrine therapy, while 7% of the patients were endocrine therapy naïve. Outcome data including BCSS defined as the time from the initial diagnosis to the time of BC-related death, and DMFS defined as the time from surgery to development of distant metastasis, were collected and calculated as detailed in **section 2.1.1.2**. The cases were divided into a discovery (n=1027) and an internal test set (n=941) using stratified random sampling, making sure enough events were available in both sets.

4.5.2 Tissue and Cellular Annotation

Extensive annotation of tumour and stromal cells at region and cell levels was carried out by experienced pathologists as previously described [487] as described in **Sections 2.9.1 and 2.9.2**

4.5.3 Deep learning-based feature computing

This DL pipeline analyses BC tissue in WSIs. First, it separates tissue from the background and removes non-invasive regions. Then, it identifies and classifies different cell nuclei (tumour, stroma, normal) and segments the TAS area. Finally, it extracts features based on these various elements **(Section 2.9.3).**

4.5.4 Nuclei segmentation/classification and nuclear features

To segment and classify different types of nuclei, an in-house developed state-of-the-art nuclei segmentation and classification model (HoVer-Net) [416] was employed. Details are mentioned in **Section 2.9.4.**

4.5.5 Region segmentation and region features.

The U-Net model [417] (referred here by CNN_{Reg}) was adapted by adding two additional encoding/decoding blocks for semantic segmentation of stromal and other non-ROI regions and was trained on the annotated regions to generate segmentation masks for the WSIs **(Section 2.9.5)**.

4.5.6 Stroma tumour ratio quantification and spatial distribution

STR was calculated using surface area and cell count. The surface area ratio was calculated as STR= TAS area / (TAS area + Tumour area) × 100 **(Figure 4.2).** The cell count ratio was calculated as the ratio of total stromal cell count to total tumour cell count in the WSI. Similarly, an automated score for the quantification of STR spatial distribution in the context of tumour cells was calculated and expressed as spatial co-occurrence. Spatial cooccurrence quantified the cooccurrence of two or more structures (such as tumour cells with stromal cells) within a certain distance in a patch of size 256 × 256 pixels. CMs were constructed, different features were calculated using python library. STR intratumoral heterogeneity and contrast were calculated from these CM. STR heterogeneity measures how heterogeneous a WSI is in terms of the occurrences of tumour and stromal nuclei together and how close the distribution of elements in the CM to the CM diagonal which ranges from 0 (highly homogeneous) to 1 (highly heterogeneous). STR contrast measures local changes

over the WSI and it ranges from 0 (a constant image) to 1 (size of CM). Details are mentioned in **Section 2.9.7.**

4.5.7 Visual assessment of STR

To evaluate the validity and reliability of the DL detection algorithm, a visual assessment of the STR in WSI was performed on 10% of the cases. Using the same WSI used for AI-based stroma assessment, the author subjectively estimated the percentage of stromal tissue in relation to tumour tissue. The analysis was carried out using Slide Viewer software v2.5.0 (3D HISTECH®, Budapest, Hungary). Currently, there is no standardised approach for STR assessment, and various methods have been implemented previously[454, 488]. We adopted this method to align with the DL algorithms' approach. The visual assessment was conducted independently of the DL score, and the concordance between the DL and visually assessed ratios was then evaluated.

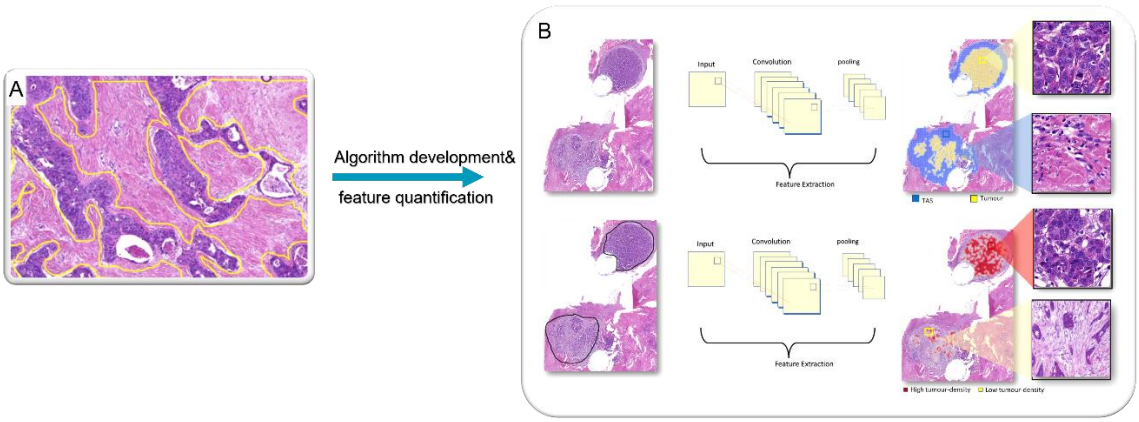


Figure 4.2: Graphical illustration of tumour associated stroma (TAS) features extraction using deep learning model. A: represent TAS annotation, followed by multiple convolutional neural network development.

4.5.8 Assessment of tumour burden

Tumour burden, defined as the effective tumour cell mass instead of the absolute tumour size, was calculated by multiplying tumour size in centimetres by the density of tumour cells obtained from the ratio of mean tumour to stromal cells count, as given below:

$$Tumour\ burden = Tumour\ size \times \frac{mean\ of\ patch\ tumour\ cells\ count}{mean\ of\ patch\ stromal\ cells\ count}$$

4.5.9 Statistical Analysis

IBM-SPSS statistical software 27.0 (SPSS, Chicago, IL, USA) was used for statistical analysis. Frequency and distribution of all assessed features were described in detail. The level of agreement between visual and automated scores was assessed using ICC. Association between clinicopathological parameters and both the continuous and categorical values of the assessed features was carried out using Mann-Whitney Kruskal-Wallis, and Chi-square ($\chi 2$) tests. Each feature was dichotomised, into low and high for outcome analysis based on X-tile software version 3.6.1 (Yale University, New Haven, CT.[411]) using BCSS as end point. Cut-off values were calculated on the discovery split using X-tile software with BCSS as end point and then applied on the test cohort. Kaplan Meier curves and log-rank test were used to assess significance between low and high groups against patient's outcome. Cox-regression analysis was performed for univariate and multivariate analysis, and hazard ratios were calculated. A p-value of less than 0.05 (two-tailed) was considered significant in all the statistical tests

4.6 RESULTS

The baseline DL extracted features characteristics are described in **Table 4.1 and Table 4.2.** summarises the baseline patient' and tumour characteristics, including the assessed STR features in both discovery and test cohorts. The mean age of patients was 59 years (range 20 to 88) and 60 years (range 30-90) in the discovery and tests sets, respectively, while the mean tumour size was 1.8 cm (range 0.15 to 9 cm) and 1.7cm (range 0.3 to 10 cm), respectively. The median follow-up duration for BCSS and DMFS was 104 and 102 months, respectively, in the discovery set and 102 and 99 months, respectively, in the test set. The baseline DL extracted features are summarised in **Table 4.2.**

A high degree of concordance was obtained between the visual assessment of STR and DL model (ICC=0.7, $p<0.001$).

Table 4.1: Summary of tumour associated stroma (TAS) extracted features with their descriptions.

AI extracted Features		Description	Median (range)
Tumour density related features	**WSI tumour cell count**	Total number of tumour cells in WSI	28024 (7560 – 73556)
	WSI tumour density H-H cooccurrence	Number of times a high tumour density patch cooccur with high tumour density patch. Threshold is the mean for the individual WSI	1254 (50 – 46351)
	WSI tumour density H-L cooccurrence	Number of times a high tumour density patch cooccur with low tumour density patch. Threshold is the mean for the individual WSI	2119 (61 – 55009)
	WSI tumour density heterogeneity	Heterogeneity between high tumour density (above the mean threshold of individual WSI) patches and low-tumour-density (below threshold) patches. Calculated from Cooccurrence matrix (CM).	0.6 (0 – 1)
	Tumour burden	Tumour size (cm) multiplied by tumour cells density obtained from mean tumour to stromal cells count ratio $= Tumour\ size\ x \frac{mean\ of\ tumour\ cells\ count\ \ in\ WSI}{mean\ of\ stromal\ cells\ count\ in\ WSI}$	0.49 (0.01-4.67)
Stromal related features	**Stromal cell count**	Number of stromal cells in r WSI	10134 (3093 – 27165)
	Stromal TILS	Number of immune cells in tumour associated stroma	4892 2003 -11441
	WSI high stromal density patches	Percentage of stroma patches* with stroma density above the mean threshold for the individual WSI	0.42 (0 – 0.66)
	WSI low stromal density patches	Percentage of stroma patches with stroma density below or equal to the mean threshold for the individual WSI	0.58 (0 – 0.74)

Table 4.1 continued

	AI extracted Features	Description	Median (range)
	WSI H-H stromal density cooccurrence	Number of times a high stromal density patch cooccur with high stromal density patch. Threshold is the mean for the individual WSI	8572 (4465- 14289)
	WSI H-L stromal density cooccurrence	Number of times a high stromal density patch cooccur with low stromal density patch. Threshold is the mean for the individual WSI	13622 7436 - 22798
	WSI H-H stromal density cooccurrence score	WSI H-H stromal density cooccurrence / (WSI H-H stromal density cooccurrence + WSI H-l stromal density cooccurrence	0.38 (0.05 – 0.41)
	WSI H-L stromal density cooccurrence score	WSI H-l stromal density cooccurrence /(WSI H-H stromal density cooccurrence + WSI H-l stromal density cooccurrence	0.62 (0.3 – 0.7)
	WSI stromal density heterogeneity	Heterogeneity between high stroma density (above the mean threshold of individual WSI) patches and low-stroma-density (below threshold) patches. Calculated from Cooccurrence matrix (CM).	0.72 ± .056
Stroma to tumour Ratio quantitative features	**ST surface area Ratio**	Stroma to tumour area ratio = TAS patches / (TAS patches + tumour patches) ×100	74 (13.7 - 90)
	ST mean count Ratio	Mean of stromal cell count / mean of tumour cell count across all the patches in a WSI	40 (5.0 – 70)

Table 4.1 continued

	AI extracted Features	Description	Median (range)
Stroma to tumour ratio spatial distribution related features	**WSI ST ratio H-H cooccurrence score**	WSI H-H STR cooccurrence / (H-H STR cooccurrence + H-L STR cooccurrence)	0.69 (0.01 - 1)
	WSI ST ratio H-L cooccurrence score	WSI H-L STR cooccurrence / (H-H STR cooccurrence + H-L STR cooccurrence)	0.31 (0.01 – 0.34)
	WSI ST ratio contrast	Contrast between high stroma to tumour ratio (above the mean threshold of individual WSI) patches and low stroma to tumour ratio (below threshold) patches. Calculated from Cooccurrence matrix (CM). It measures local changes in the co-occurrence matrix (CM). Range = [0 (size(CM)-1)^2]. Contrast for a constant image is 0.	0.27 (0.01-0.5)
	WSI ST ratio heterogeneity	Heterogeneity between high stroma to tumour ratio (above the mean threshold of individual WSI) patches and low stroma to tumour ratio (below threshold) patches. Calculated from Cooccurrence matrix (CM). Homogeneity measures the closeness of the distribution of elements in the CM to the CM diagonal. Range = [0 1]. Homogeneity is 1 for a diagonal CM.	0.12 (0.01 – 0.25)

WSI: whole slide image; **H-H**: high to high; **H-L**: high to low; **TILs**: tumour infiltrating lymphocytes

* Standard patch size =62 µm

Table 4.2: Patients and tumour characteristics

Parameters	Discovery set (n=1027)	Test set (n=941)	P value
	N (%)	N (%)	
Age at diagnosis (years)			X^2=2.1 0.26
< 50	225 (22)	193 (21)	
≥ 50	802 (78)	747(79)	
Menopause			X^2=2.04 0.16
Pre	280 (27)	230 (24)	
Post	747 (73)	711 (76)	
Tumour size (cm)			X2=2.3 0.18
< 2.0	699 (68)	671 (71)	
≥ 2.0	328 (32)	270 (29)	
Histologic tumour type			X2=1.2 0.74
IDC NST	571 (56)	522 (56)	
Invasive lobular carcinoma	134 (13)	126 (13)	
*Other special types	61 (6)	66 (7)	
Mixed NST and special types	261 (25)	227 (24)	
Histological tumour grade			X^2=0.8 0.67
1	242 (24)	238 (25)	
2	564 (55)	504 (54)	
3	221 (21)	199 (21)	
Tubule formation score			X^2=0.02 0.98
1	101 (10)	92 (10)	
2	333 (32)	308 (33)	
3	593 (58)	541 (57)	
Pleomorphism score			X^2=3.2 0.15
1	14 (2)	10 (1)	
2	506 (49)	501 (53)	
3	507 (49)	430 (46)	
Mitosis score			X^2=2.0 0.36
1	728 (71)	681 (72)	
2	172 (17)	136 (15)	
3	127 (12)	124 (13)	
Lymphovascular Invasion			X^2=1.18 0.27
No	853 (83)	798 (85)	
Yes	174 (17)	143 (15)	
Lymph node status			X^2=4.7 0.04
Negative	750 (73)	727 (77)	
Positive	277 (27)	214 (23)	
PR Status			X^2=.06 0.11
Negative	201 (20)	180 (19)	
Positive	826 (80)	761 (81)	

Table 4.2 continued

Parameters	Discovery set (n=1027)	Test set (n=941)	P value
	N (%)	N (%)	
NPI risk group			
Low risk	547 (53)	537 (57)	X^2=4.4
Intermediate risk	429 (42)	371 (39)	0.82
High risk	51 (5)	33 (4)	
Adjuvant therapy			
Endocrine therapy only	1821 (93)		
Endocrine naive	147 (7)		
****Stroma to Tumour Ratio**			
low	643 (63)	543 (58)	X^2=0.47
High	384 (37)	398 (42)	0.54
****H-H STR spatial co-occurrence score**			
Low	879 (86)	803 (85)	X^2=0.05
High	148 (14)	138 (15)	0.85
****H-L STR spatial co-occurrence score**			
Low	305 (30)	284 (30)	X^2=0.57
High	722 (70)	654 (67)	0.46
****Intratumor STR spatial contrast**			
Low	295 (29)	271 (29)	X^2=0.08
High	732 (71)	670 (71)	0.8
****Intratumor STR spatial heterogeneity**			
Low	310 (30)	336 (36)	X^2=0.95
High	717 (70)	605 (64)	0.34
****Tumour Burden**			
Small	767 (75)	715 (76)	X^2=0.57
Large	260 (25)	226 (24)	0.46

IDC NST: Invasive duct carcinoma on no special types**; NPI:** Nottingham prognostic index**; PR:** Progesterone receptor **H-H STR spatial co-occurrence score: high STR patches cooccurrence with high STR patches; H-L STR spatial co-occurrence score:** high STR patches cooccurrence with low STR patches.

* Other types include invasive tubular and mucinous carcinoma

**Parameters were categorised into high/low and small/large based on cut-off based on X-tiles software.

4.6.1 Cell density, STR and spatial distribution

The median density of tumour cells was significantly higher than the density of the stromal cells in both the discovery (30683 cells/mm2 compared to 11190 cells/mm2) and the test cohorts (26870 cells/mm2 vs 9804 cells/mm2) ($p<0.001$) **(Figure 4.3A).** There was a significant positive correlation between stromal cells and tumour cells counts ($r=0.96$, $p<0.001$) (**Figure 4.3B)**.

In the whole cohort, the mean stroma to tumour surface area ratio was 0.74 and the median stroma tumour cell counts ratio was 0.40. The percentage of patches with high STR (above the mean threshold for individual WSI) was higher than patches with low STR (70% vs 30%) ($p<0.001$). The frequency of homogenous spatial co-occurrence of high STR patches with another high STR patch was higher (H-H STR co-occurrence score 0.69 compared to a score of 0.31 for H-L co-occurrence. Similar findings were detected for STR heterogeneity and contrast within WSI 0.12 and 0.25, respectively **(Figure 4.3C).**

The frequency of homogenous spatial co-occurrence of high STR patches with another high STR patch was higher (H-H STR co-occurrence score 0.69 compared to a score of 0.31 for H-L co-occurrence. Similar findings were detected for STR heterogeneity and contrast within WSI 0.12 and 0.25, respectively.

Regarding the spatial distribution of stromal cells in relation to tumour cells, heterogeneous stromal cells' spatial distribution was high compared to homogenous distribution. This was identified by the median value of high-low (H-L) stromal cooccurrence frequency (13622, 0.6 cooccurrence score) compared to high-high (H-H) stromal density patches cooccurrence frequency (8572, 0.4

occurrence score). In addition, WSI stromal cell density heterogeneity score was high (0.7).

The spatial distribution of tumour cells also tends to be heterogeneous. This was evident from the increased H-L tumour density patches cooccurrence (2219, 0.45 co-occurrence score) and tumour density heterogeneity score (0.6).

Furthermore, homogenous tumour cell density spatial distribution (increased H-H tumour density spatial distribution) was associated with worse outcomes ($p<0.001$), and high tumour density heterogeneity score was associated with better patients` survival ($p=0.005$) in both the discovery and test cohorts.

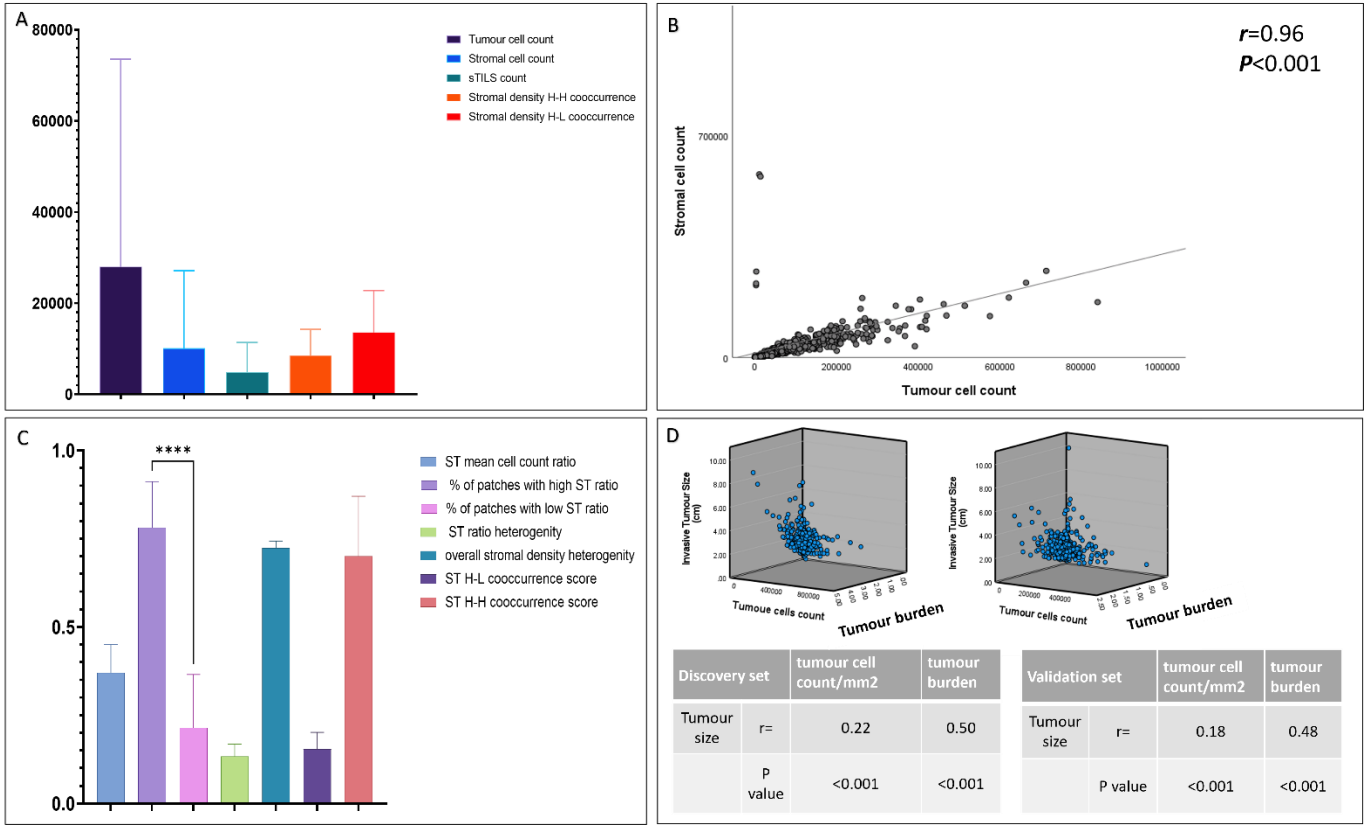
4.6.2 Association between STR ratios and tumour behaviour

In the discovery cohort, high STR (as both continuous and categorical variable) was significantly associated with other parameters of better tumour behaviour including low tumour grade ($p<0.001$), high tubule formation ($p=0.04$), low pleomorphism and low mitotic scores ($p<0.001$), and good NPI group ($p<0.001$). High STR was significantly associated with lobular BC subtype ($p<0.001$)**.** Similar results were obtained in the test cohort. Tumours with high stroma tumour cell count ratio tend to be of low tumour grade ($p=0.001$) **(Table 4.3, Table 4.4 and Figure 4.4).**

4.6.3 Impact of tumour burden on tumour behaviour

There was strong positive correlation between tumour cell density, and tumour size ($p<0.001$**) (Figure 4.3D).** In this study, both tumour size and tumour cell density were used to estimate tumour cell burden and eliminate the impact of the stromal component. The mean tumour burden was 0.3 in both cohorts and

ranged between 0.01 to 6.95. and 0.01 to 2.2 in the discovery and test sets, respectively. In both the discovery and test sets, larger tumour burden, showed significant correlation with aggressive tumour behaviour including high tumour grade, high mitotic count, high pleomorphism ($p<0.001$), invasive duct carcinoma of NST subtype, poor NPI index, presence of LVI ($p<0.001$) and LN metastasis ($p<0.004$). **(Table 4.5, Table 4.6 and Figure 4.4).**



Discovery set		tumour cell count/mm2	tumour burden
Tumour size	r=	0.22	0.50
	P value	<0.001	<0.001

Validation set		tumour cell count/mm2	tumour burden
Tumour size	r=	0.18	0.48
	P value	<0.001	<0.001

Figure 4.3: Summary of distribution of assessed tumour and stroma features. A: Bar Chart displays the mean values ± standard deviation (SD) for tumour cell count, stromal cell count, stromal immune cells (sTILS), and the spatial co-occurrences of stromal cells. B: Scatter Plot shows a significant correlation between tumour cell counts and stromal cell counts (p<0.001). C: Bar Chart summarises the mean values ± SD of stroma-to-tumour ratio (STR) related features, highlighting a significant difference between the percentage of patches with high stroma and those with low stroma. D: 3D Scatter Plot reveals a significant correlation between tumour size, tumour cell density, and tumour burden (p<0.001). H-H: High to high co-occurrence, H-L: High to low co-occurrence score.

Table 4.3: Correlation between stroma-tumour ratio and clinicopathologic parameters

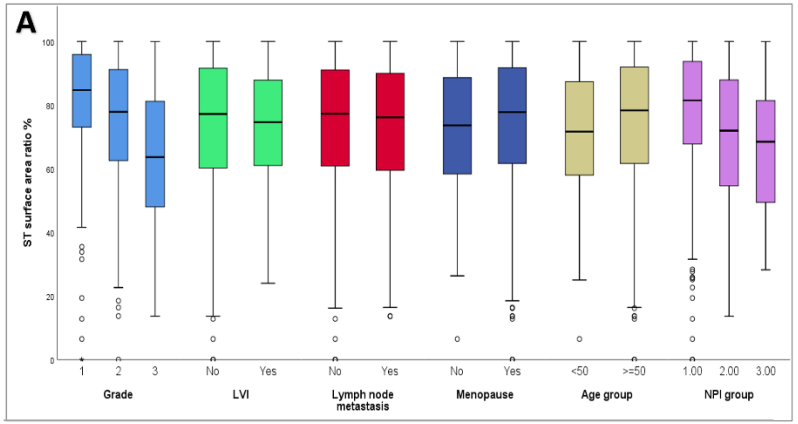
Parameter	Discovery Cohort (n=1027)			Test Cohort (n=941)		
	Low STR	High STR	P value*	Low STR	High STR	P value *
Age Groups						
<50 years	15 (24)	9 (18)	X^2=5.5	125 (22)	67 (18)	X2=1.49
≥50 years	486 (76)	314 (82)	**0.019**	451 (78)	297 (82)	0.25
Menopause						
Pre	185 (29)	95 (25)	X^2=1.9	148 (26)	81 (22)	X^2=1.43
Post	458 (71)	288 (75)	0.17	428 (74)	283 (78)	0.24
Tumour size group						
<2 cm	421 (66)	278 (73)	X^2=5.6	404 (70)	267 (73)	X^2=1.12
≥2 cm	222 (35)	105 (27)	**0.019**	172 (30)	97 (27)	0.3
Grade						
1	124 (19)	118 (31)		113 (20)	125 (34)	
2	339 (53)	225 (59)	X^2=49.6	298 (52)	206 (57)	X^2=60.7
3	180 (28)	40 (10)	**<0.001**	165 (29)	33 (9)	**<0.001**
Tubule Formation						
1	52 (8)	49 (13)	X^2=6.1	33 (6)	59 (16)	
2	211 (33)	122 (32)	**0.04**	198 (34)	110 (30)	X^2=27.7
3	380 (59)	212 (55)		345 (60)	195 (54)	**<0.001**
Pleomorphism						
1	4 (1)	10 (3)		2 (0.3)	8 (2)	
2	269 (42)	237 (62)	X^2=50.1	259 (45)	242 (67)	X^2=53.2
3	370 (8)	136 (35)	**<0.001**	315 (54.7)	114 (31)	**<0.001**
Mitosis						
1	398 (62)	330 (86)		366 (64)	315 (87)	
2	134 (21)	37 (10)	X^2=71.1	105 (18)	30 (8)	X^2=60.3
3	111 (17)	16 (4)	**<0.001**	105 (18)	19 (5)	**<0.001**
Tumour type						
NST	411 (64)	159 (42)		388 (67)	133 (37)	
ILC	53 (8)	81 (21)	X^2=63.3	39 (7)	87 (24)	X^2=109.7
Special types	27 (4)	34 (9)	**<0.001**	23 (4)	43 (12)	**<0.001**
Mixed NST and Special types	152 (24)	109 (28)		126 (22)	101 (28)	
LVI						
No	529 (82.3)	323 (84)	X^2=0.72	473 (82)	325 (89)	X^2=8.9
Yes	114 (18)	60 (16)	0.44	103 (18)	39 (11)	**0.003**
Lymph node Status						
Negative	460 (72)	289 (76)	X^2=1.8	440 (76)	286 (79)	X^2=0.60
Positive	183 (29)	94 (24)	0.19	136 (24)	78 (21)	0.43
PR status						
Negative	127 (20)	73 (19)	X2=0.7	96 (17)	84 (23)	X^2=5.9
Positive	516 (80)	310 (81)	0.81	480 (83)	280 (77)	**0.017**
NPI risk groups						
Low	309 (48)	238 (62)		291 (51)	246 (68)	
Intermediate	293 (46)	135 (35)	X^2=21.9	260 (45)	110 (30)	X^2=26.9
High	41 (6)	10 (3)	**<0.001**	25 (4)	8 (2)	**<0.001**

NST: Non-special type**, ILC:** Invasive lobular carcinoma**; LVI: l**ymphovascular invasion**; NPI:** Nottingham prognostic index**; PR:** Progesterone receptor. Parameters were categorised into high/low and small/large based on cut points extracted from X-tiles software.

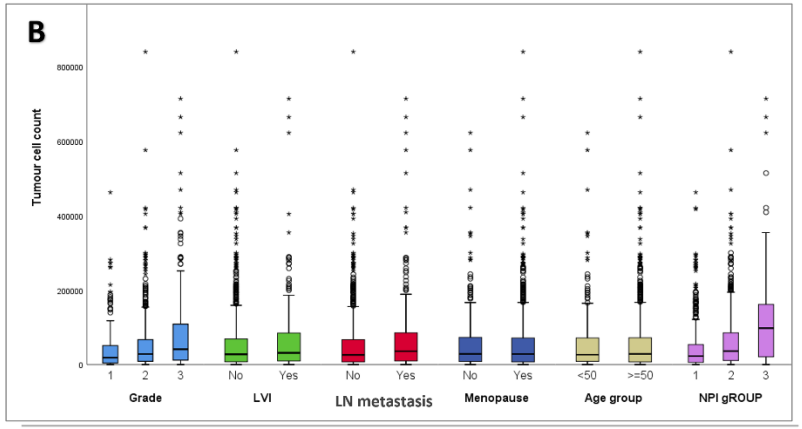
Table 4.4: Correlation between stroma-tumour ratio and clinicopathologic parameters in the endocrine treated only patients.

Parameter	Discovery Cohort (n=941)			Test Cohort (n=878)		
	Low STR	High STR	P value *	Low STR	High STR	P value *
Age Groups						
<50 years	147 (24)	57 (17)	X^2=7.14	119 (22)	58 (18)	X2=2.09
≥50 years	459 (76)	278 (83)	**0.008**	430 (78)	271 (82)	0.17
Menopause						
Pre	175 (29)	77 (31)	X^2=3.7	143 (26)	70 (21)	X^2=2.53
Post	432 (71)	257 (77)	0.065	406 (74)	259 (79)	0.12
Tumour size group						
<2	396 (65)	230 (69)	X^2=1.2	381 (69)	235 (71)	X^2=0.41
≥2	211 (35)	104 (31)	0.28	168 (31)	94 (29)	0.5
Grade						
1	110 (18)	93 (28)		99 (18))	101 (31)	
2	319 (53)	202 (61)	X^2=40.9	286 (52)	196 (60)	X^2=53.7
3	178 (29)	39 (11)	**<0.001**	164 (30)	32 (10)	**<0.001**
Tubule Formation						
1	46 (8)	40 (12)		28 (5)	48 (15)	
2	193 (32)	100 (30)	X^2=5.1	185 *34)	97 (29)	X^2=23.7
3	368 (60)	194 (58)	0.08	336 (61)	184 (56)	**0.001**
Pleomorphism						
1	2 (0.3)	5 (1)		2 (0.4)	4 (1)	
2	253 (41.7)	203 (61)	X^2=37.6	241 (44)	217 (66)	X^2=44.2
3	74 (58)	126 (38)	**<0.001**	306 (55.6)	108 (33)	**<0.001**
Mitosis						
1	367 (61)	284 (85)		340 (62)	281 (85)	
2	131 (22)	35 (11)	X^2=63.1	105 (19)	30 (9)	X^2=56.3
3	109 (18)	15 (4)	**<0.001**	104 (19)	18 (6)	**<0.001**
Tumour type						
NST						
ILC	397 (65)	145 (43)		380 (69)	128 (39)	
Special types	49 (8)	72 (22)		38 (7)	81 (25)	
Mixed NST and Special types	20 (3) 141 (23)	27 (8) 90 (27)	X^2=59.6 **<0.001**	21 (4) 110 (20)	34 (10) 86 (26)	X^2=97.5 **<0.001**
LVI						
No	502 (83)	282 (84)	X^2=0.46	449 (82)	295 (90)	X^2=9.9
Yes	105 (17)	52 (16)	0.52	100 (18)	34 (10)	**0.002**
Lymph node Status						
Negative	430 (71)	244 (73)	X^2=0.52	416 (62)	252 (77)	X^2=0.08
Positive	177 (29)	90 (27)	0.50	133 (24)	77 (23)	0.81
PR status						
Negative	117 (19)	65 (19)	X2=0.005	91 (17)	75 (23)	X^2=5.19
Positive	490 (81)	269 (81)	1	458 (83)	254 (77)	**0.027**
NPI risk groups						
Low	283 (47)	192 (58)		268 (48)	213 (65)	
Intermediate	284 (47)	132 (39)	X^2=12.8	256 (47)	108 (33)	X^2=21.9
High	40 (6)	10 (3)	**0.002**	25 (5)	8 (2)	**<0.001**

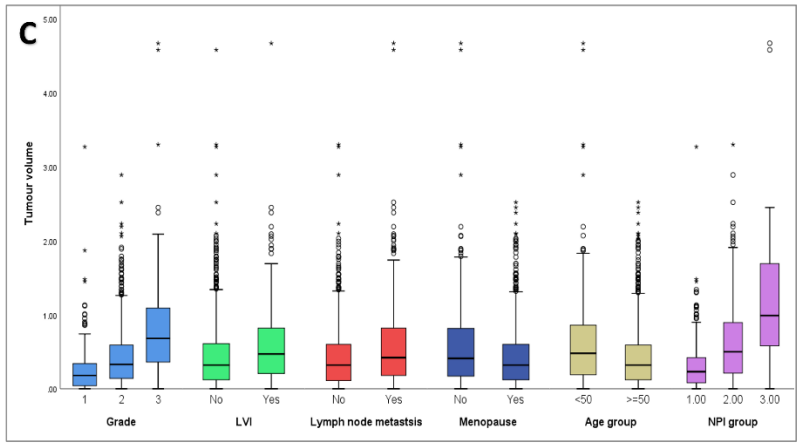
NST: Non-special type**, ILC:** Invasive lobular carcinoma**; LVI: l**ymphovascular invasion**; NPI:** Nottingham prognostic index**; PR:** Progesterone receptor. Parameters were categorised into high/low and small/large based on cut points extracted from X-tiles software.



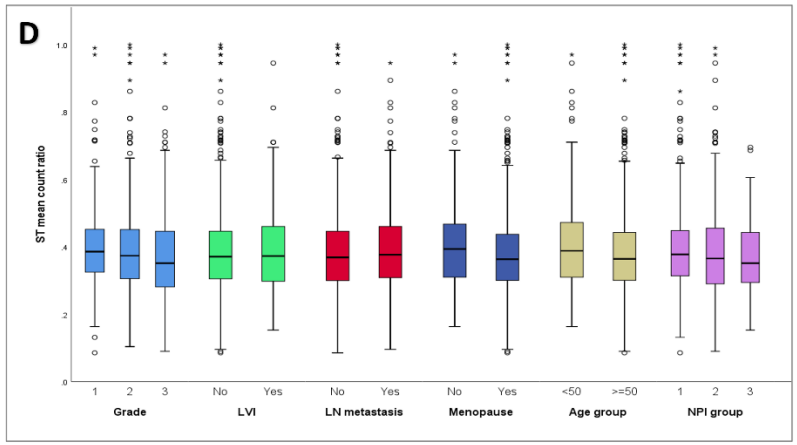
Test	127.8	144338	175343	164515	141555	54.1
P value	<0.001	0.07	0.153	0.026	0.001	<0.001



Test	35.24	141702	166349	17251	158782	40.3
P value	<0.001	0.042	0.008	0.41	0.764	<0.001



Test	205.9	122636	150694	150000	127916	202.6
P value	<0.001	<0.001	<0.001	<0.001	<0.001	<0.001



Test	13.1	151543	170752	153100	140000	5.9
P value	0.001	0.95	0.11	<0.001	0.001	0.05

Figure 4.4: Box plot chart demonstrating the correlation between continuous values of stroma to tumour surface area ratio (STR) (A), Tumour cell count (B), tumour burden (C) and stroma to tumour cells count ratio (D).

Table 4.5: Correlation between tumour burden and tumour density with clinicopathologic parameters

Parameter	Discovery set						Test set					
	Low tumour density	High tumour density	P value*	Small tumour burden	Large tumour burden	P value*	Low tumour density	High tumour density	P value*	Small tumour burden	Large tumour burden	P value*
Age Groups												
<50 years	191 (21)	34 (29)	X^2=3.9	45 (21)	180 (22)	X^2=0.1	169 (20)	24 (23)	X^2=0.4	129 (18)	64 (29)	X^2=11.8
≥50 years	718 (79)	83 (71)	0.057	171 (79)	630 (78)	0.66	667 (80)	81 (77)	0.52	586 (82)	162 (71)	**0.001**
Menopause												
Pre	238 (26)	42 (36)	X^2=5.0	54 (25)	226 (28)	X^2=0.7	201 (24)	29 (28)	X^2=0.65	161 (23)	69 (31)	X^2=6.3
Post	672 (74)	75 (64)	**0.03**	162 (75)	585 (72)	0.4	635 (76)	76 (72)	0.47	554 (78)	157 (69)	**0.013**
Tumour size												
<2	645 (71)	54 (46)	X^2=29.1	601 (78)	97 (14)	X^2=149.0	615 (74)	56 (53)	X^2=18.6	580 (81)	89 (40)	X^2=141.3
≥2	265 (29)	63 (54)	**<0.001**	166 (22)	162 (63)	**<0.001**	221 (26)	49 (47)	**<0.001**	135 (19)	137 (60)	**<0.001**
Grade												
1	225 (25)	17 (15)	X^2=35.8	67 (31)	175 (22)	X^2=28.4	221 (26)	17 (16)	X^2=23.5	220 (31)	18 (8)	X^2=148.3
2	514 (57)	50 (42)	**<0.001**	130 (60)	434 (53)	**<0.001**	457 (55)	47 (45)	**<0.001**	407 (57)	96 (43)	**<0.001**
3	171 (19)	50 (43)		19 (9)	202 (25)		158 (19)	41 (39)		88 (12)	112 (49)	
Tubule Formation												
1	95 (10)	6 (5)	X^2=7.1	23 (11)	78 (10)	X^2=0.8	87 (10)	5 (5)	X^2=3.5	85 (12)	7 (3)	X^2=39.1
2	284 (31)	49 (42)	**0.03**	74 (34)	259 (32)	0.67	270 (32)	38 (36)	0.17	258 (36)	49 (22)	**<0.001**
3	531 (58)	62 (53)		119 (55)	474 (58)		479 (57)	62 (59)		372 (52)	170 (75)	
Pleomorphism												
1	14 (2)	0 (0.0)	X^2=19.8	6 (3)	8 (1)	X^2=24.2	7 (1)	3 (3)	X^2=24.5	9 (1)	1 (0.5)	X^2=51.3
2	469 (52)	37 (32)	**<0.001**	134 (62)	372 (46)	**<0.001**	468 (56)	33 (31)	**<0.001**	427 (60)	74 (33)	**<0.001**
3	427 (46)	80 (68)		76 (35)	431 (53)		361 (43)	69 (66)		279 (39)	151 (66)	

Table 4.5 continued

Mitosis												
1	676 (74)	52 (44)	**X^2=56.7**	188 (87)	540 (67)	**X^2=35.3**	628 (75)	53 (51)	**X^2=34.3**	590 (83)	90 (40)	**X^2=158.3**
2	144 (16)	28 (24)	**<0.001**	19 (9)	15 (19)	**<0.001**	115 (14)	21 (20)	**<0.001**	75 (11)	61 (27)	**<0.001**
3	90 (10)	37 (32)		9 (4)	118 (15)		93 (11)	31 (30)		50 (7)	75 (32)	
Tumour type												
NST	488 (54)	83 (71)	X^2=6.0	109 (51)	462 (57)	X^2=3.4	461 (55)	61 (58)	X^2=0.887	365 (51)	156 (70)	X^2=30.0
ILC	127 (14)	7 (6)	**0.014**	34 (16)	100 (12)	0.33	119 (14)	7 (7)	0.35	111 (16)	15 (7)	**<0.001**
Special types	58 (6)	3 (3)		13 (6)	48 (6)		64 (8)	2 (2)		60 (8)	6 (3)	
Mixed types	237 (26)	24 (21)		60 (28)	201 (25)		192 (23)	35 (33)		179 (25)	46 (21)	
LVI												
No	771 (85)	82 (70)	X^2=15.8	193 (89)	660 (81)	X^2=7.7	721 (86)	77 (73)	X^2=12.1	631 (88)	164 (74)	X^2=28.3
Yes	139 (15)	35 (30)	**<0.001**	23 (11)	151 (19)	**0.006**	115 (14)	28 (27)	**<0.001**	84 (12)	62 (27)	**<0.001**
Lymph node Status												
Negative	689 (76)	61 (52)	X^2=29.3	165 (76)	585 (72)	X^2=0.21	658 (79)	69 (66)	X^2=9.0	570 (80)	154 (69)	X^2=11.3
Positive	221 (24)	56 (48)	**<0.001**	51 (24)	226 (28)	1.57	178 (21)	36 (34)	**0.004**	145 (200	72 (31)	**0.001**
PR status												
Negative	168 (19)	33 (28)	X^2=6.25	141 (18)	60 (32)	X^2=2.81	148 (18)	32 (31)	X^2=10.0	134 (19)	45 (20)	X^2=0.23
Positive	742 (81)	84 (72)	**0.018**	626 (82)	199 (77)	0.10	688 (82)	73 (70)	**0.003**	581 (81)	181 (80)	0.63
NPI risk groups												
Good	520 (57)	27 (23)	X^2=72.0	150 (69)	397 (49)	X^2=29.3	499 (60)	38 (36)	X^2=35.2	496 (69)	40 (18)	X^2=190.3
Intermediate	359 (40)	70 (60)	**<0.001**	61 (28)	368 (45)	**<0.001**	316 (38)	55 (52)	**<0.001**	207 (29)	165 (73)	**<0.001**
Poor	31 (3)	20 (17)		5 (2)	46 (6)		21 (12)	12 (11)			21 (9)	

NST: Non-special type**, ILC:** Invasive lobular carcinoma**; LVI: l**ymphovascular invasion**; NPI:** Nottingham prognostic index**; PR:** Progesterone receptor. Parameters were categorised into high/low and small/large based on cut points extracted from X-tiles software.

* Significant p values are in bold.

Table 4.6: Correlation between tumour burden and clinicopathologic parameters in the endocrine-treated patients

Parameter	Tumour burden in discovery cohort (n=941)			Tumour burden in test Cohort (n=878)		
	Small	Large	P value*	Small	Large	P value*
Age Groups						
<50 years	129 (19)	75 (30)	X^2=12.7	118 (18)	62 (28)	X^2=9.5
≥50 years	561 (81)	176 (70)	**<0.001**	541 (82)	157 (72)	**0.003**
Menopause						
Pre	167 (24)	85 (34)	X^2=9.7	150 (23)	66 (30)	X^2=5.3
Post	524 (76)	165 (66)	**0.003**	511 (77)	151 (70)	**0.023**
Tumour size						
<2 cm	531 (77)	94 (38)	X^2=126.7	528 (80)	88 (40)	X^2=127.3
≥2 cm	160 (23)	156 (62)	**<0.001**	131 (20)	131 (60)	**<0.001**
Grade						
1	186 (27)	17 (7)		183 (28)	19 (8)	
2	409 (59)	111 (44)	X^2=138.4	389 (95)	92 (42)	X^2=134.3
3	96 (14)	122 (49)	**<0.001**	87 (13)	108 (50)	**<0.001**
Tubule Formation						
1	80 (12)	6 (2)		69 (11)	9 (3)	
2	220 (32)	73 (29)	X^2=21.4	235 (36)	46 (21)	X^2=33.5
3	391 (57)	171 (68)	**<0.001**	355 (54)	164 (76)	**<0.001**
Pleomorphism						
1	7 (1)	0 (0.0)		7 (1)	1 (0.5)	
2	389 (55)	75 (30)	X^2=50.6	385 (58)	73 (34)	X^2=41.3
3	304 (44)	175 (70)	**<0.001**	269 (41)	143 (65.5)	**<0.001**
Mitosis						
1	555 (80)	95 (38)		535 (81)	87 (39)	
2	101 (15)	66 (26)	X^2=190.8	75 (11)	61 (28)	X^2=146.3
3	35 (5)	89 (36)	**<0.001**	49 (7)	71 (33)	**<0.001**
Tumour type						
NST	365 (53)	177 (71)		355 (54)	155 (71)	
ILC	101 (15)	20 (8)		104 (16)	15 (7)	
Special types	43 (6)	4 (2)	X^2=27.8	49 (7)	6 (3)	X^2=23.6
Mixed	182 (26)	49 (20)	**<0.001**	151 (23)	43 (20)	**<0.001**
LVI						
No	593 (86)	191 (76)	X^2=11.7	581 (88)	160 (74)	X^2=26.3
Yes	98 (14)	59 (24)	**0.001**	80 (12)	57 (26)	**<0.001**
Lymph node Status						
Negative	524 (76)	150 (60)	X^2=22.8	515 (78)	153 (70)	X^2=6.6
Positive	167 (24)	100 (40)	**<0.001**	144 (22)	66 (30)	**0.013**
PR status						
Negative	126 (18)	57 (23)	X^2=2.41	124 (19)	43 (20)	X^2=0.13
Positive	565 (82)	193 (77)	0.13	537 (81)	174 (80)	0.68
NPI risk groups						
Good	428 (62)	46 (18)		442 (67)	40 (18)	
Intermediate	250 (36)	167 (67)	X^2=165.6	205 (31)	158 (72)	X^2=168.3
Poor	13 (2)	37 (15)	**<0.001**	12 (2)	21 (10)	**<0.001**

NST: Non-special type**, ILC:** Invasive lobular carcinoma**; LVI: l**ymphovascular invasion**; NPI:** Nottingham prognostic index**; PR:** Progesterone receptor. Parameters were categorised into

high/low and small/large based on cut points extracted from X-tiles software. * Significant p values are in bold.

4.6.4 Impact of STR, tumour burden and spatial distribution related features on patient outcome

-Both in the discovery and test cohorts, high STR was significantly associated with better outcomes in terms of prolonged BCSS (p=0.003) and DMFS (p=0.008) (**Figure 4.5 and Figure 4.6**). Higher STR was a significant predictor of better patients' survival in terms of prolonged BCSS and DMFS when the cases were grouped based on menopausal status, tumour grade, NPI, and LN status **(Figure 4.5).**

In the endocrine-treated patients, high STR was predictive of prolonged BCSS (HR:0.44, 95% CI: 0.29-0.66, p=0.02) and DMFS (HR:0.5, 95% CI: 0.35-0.72, p<0.001), however in the non-treated subgroup, the association between STR ratio and patient's outcome was not significant.

Larger tumour burden was associated with worse outcomes in terms of shorter BCSS and DMFS (p<0.001) both in the discovery and test sets (**Figure 4.6 and Figure 4.7**, respectively). Furthermore, large tumour burden was associated with a high risk of distant metastasis (HR:2.4, 95% CI: 1.77 -3.72, p<0.003) and shorter BCSS (HR:2.4, 95% CI: 1.75- 3.4, p<0.006) in a subgroup of patients who received adjuvant endocrine therapy. Larger tumour burden was also associated with worse patient survival in a subgroup of patients with less aggressive tumour behaviour like low tumour grade, negative LLN status and good NPI (**Figure 4.7)**.

Cases with high intratumor STR heterogeneity and contrast scores, as well as increased H-L STR spatial co-occurrence, were associated with shorter BCSS

(p=0.02, p=0.007 and p=0.027, respectively). In the same context, patients with homogenous STR distribution (Increased H-H STR spatial co-occurrence score) had better survival in terms of prolonged BCSS (p=0.036) **(Figure 4.8, Figure 4.9).** Same results were confirmed in the test cohort (**Figure 4.10).**

ST cell count ratio was not associated with outcome either in the discovery or in the test cohorts.

In a multivariate Cox regression model, when cases were adjusted for tumour grade, LN status, LVI and other significant clinicopathologic parameters, large tumour burden was an independent predictor of poor patient BCSS. However, the absolute tumour size did not show significance. Similarly, in a model adjusted for the same clinicopathologic parameters, STR was an independent predictor of longer patient survival. However, when both STR and tumour burden were compared against each other, only tumour burden was a significant independent predictor of patient outcome (**Figure 4.11, Figure 4.12 and Figure 4.13)**

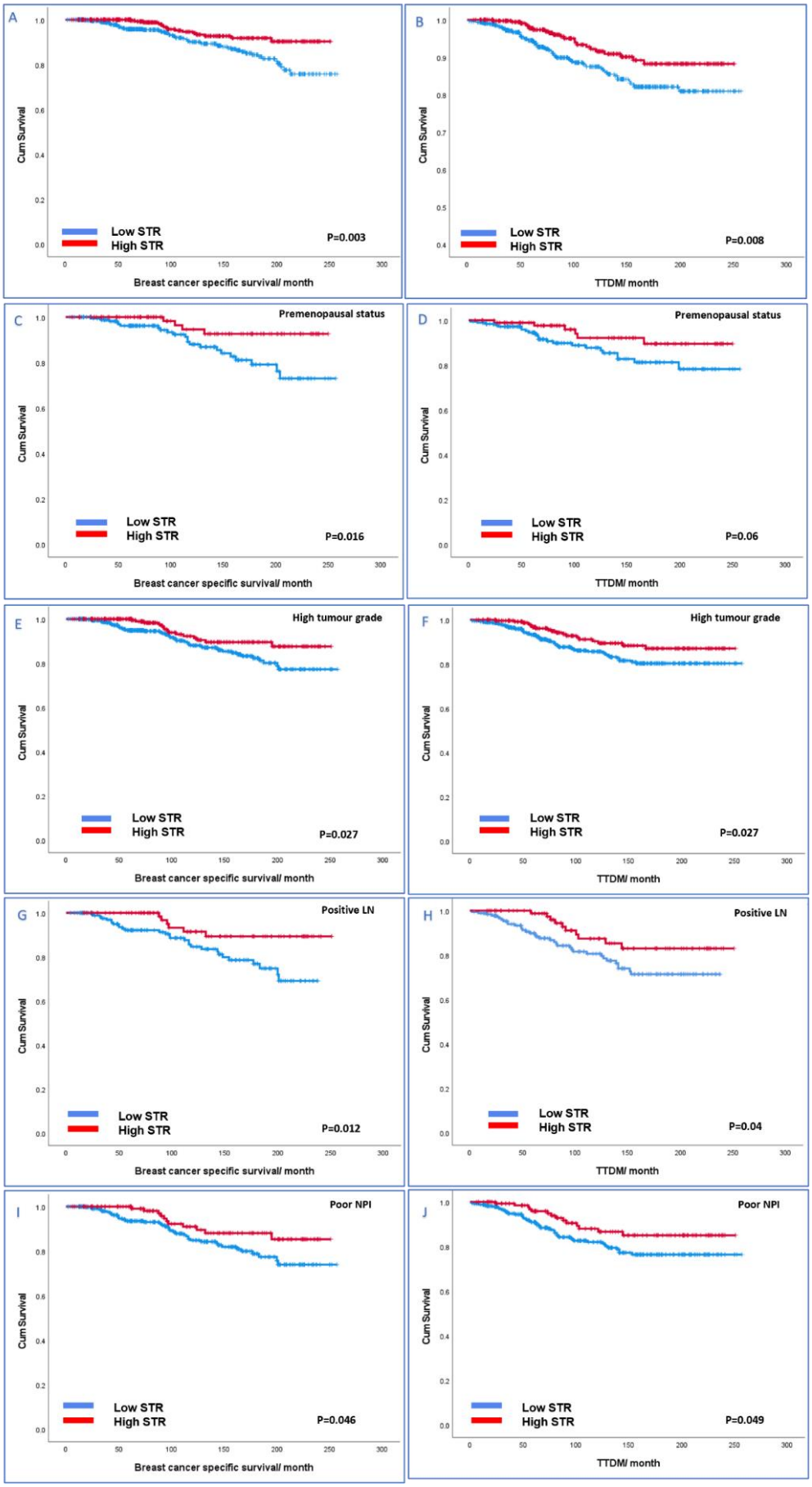

A
Cum Survival
Low STR
High STR
P=0.003
Breast cancer specific survival/ month
B
Cum Survival
Low STR
High STR
P=0.008
TTDM/ month
C
Premenopausal status
Cum Survival
Low STR
High STR
P=0.016
Breast cancer specific survival/ month
D
Premenopausal status
Cum Survival
Low STR
High STR
P=0.06
TTDM/ month
E
High tumour grade
Cum Survival
Low STR
High STR
P=0.027
Breast cancer specific survival/ month
F
High tumour grade
Cum Survival
Low STR
High STR
P=0.027
TTDM/ month
G
Positive LN
Cum Survival
Low STR
High STR
P=0.012
Breast cancer specific survival/ month
H
Positive LN
Cum Survival
Low STR
High STR
P=0.04
TTDM/ month
I
Poor NPI
Cum Survival
Low STR
High STR
P=0.046
Breast cancer specific survival/ month
J
Poor NPI
Cum Survival
Low STR
High STR
P=0.049
TTDM/ month

Figure 4.5: Kaplan Meier curves showing significant correlation between high stroma to tumour surface area ratio (STR) with better patients' survival in the discovery cohort; both in breast cancer specific survival (A), and distant metastasis free survival (B) and in subgroup of patients with aggressive tumour behaviour as premenopausal (C,D); high tumour grade (E,F); lymph node metastasis (G,H) and poor Nottingham prognostic index (I,J).

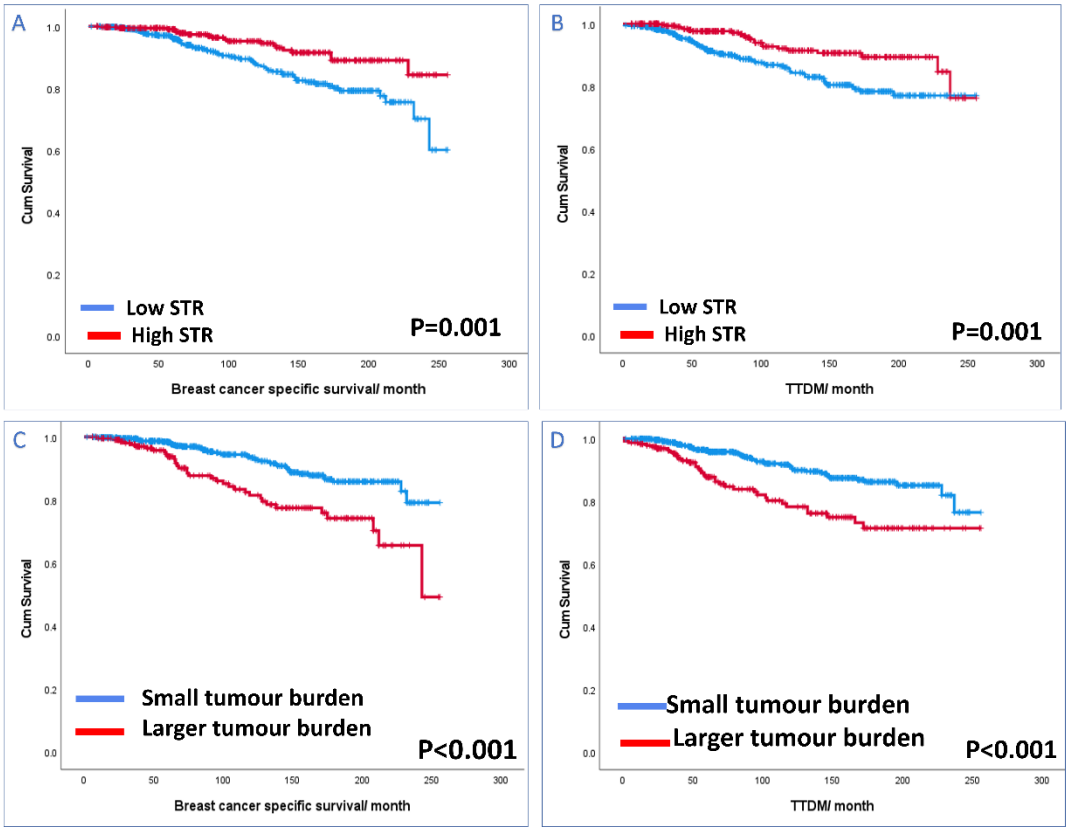


Figure 4.6:Kaplan Meier curves showing significant correlation between high stroma to tumour surface area ratio (STR) with better patients' survival in the test cohort; both in breast cancer specific survival (A), and distant metastasis free survival (B). and the significant association between high tumour burden and wore patient's outcome (C, D).

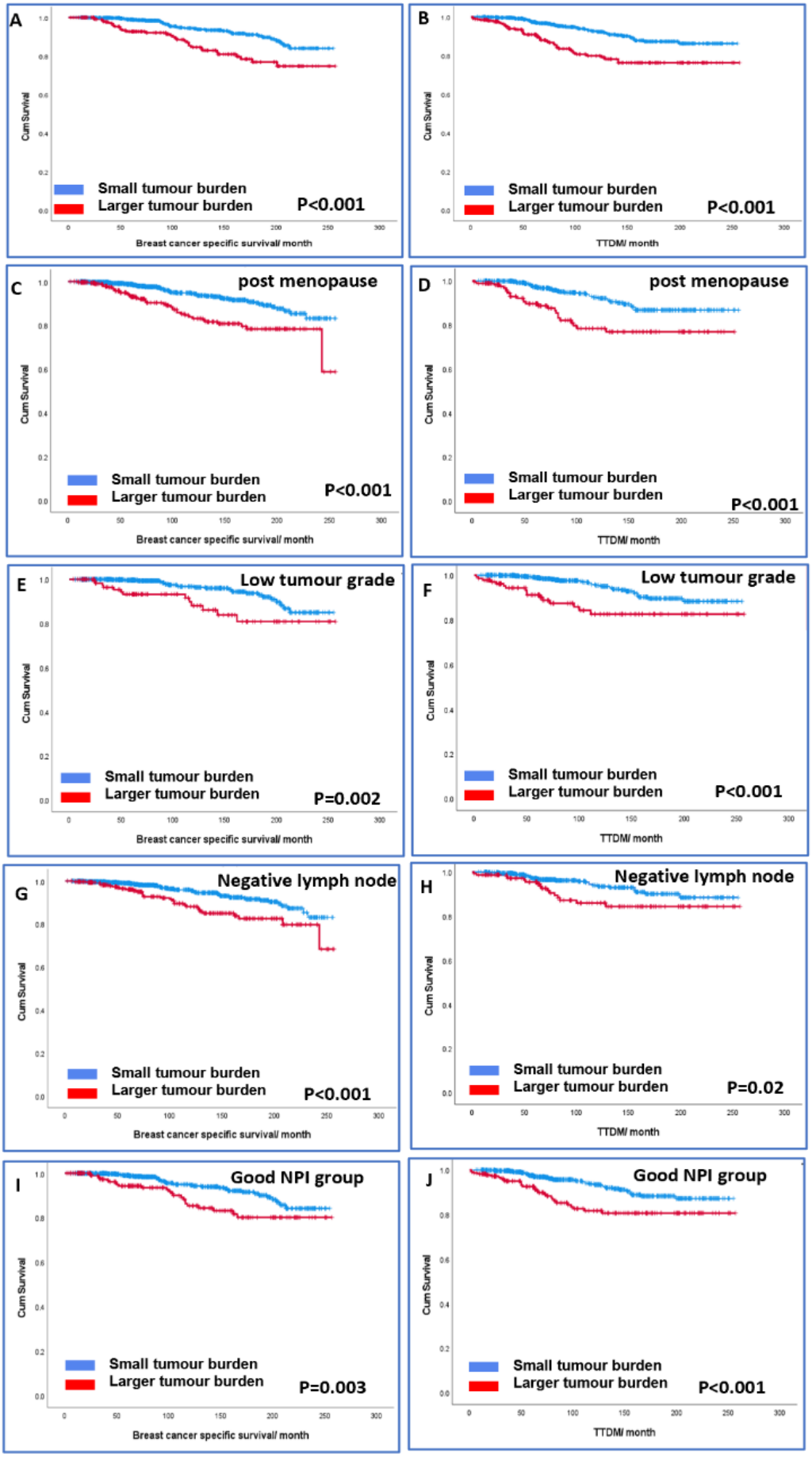

A
Cum Survival
Small tumour burden
Larger tumour burden
P<0.001
Breast cancer specific survival/ month
B
Cum Survival
Small tumour burden
Larger tumour burden
P<0.001
TTDM/ month
C
post menopause
Cum Survival
Small tumour burden
Larger tumour burden
P<0.001
Breast cancer specific survival/ month
D
post menopause
Cum Survival
Small tumour burden
Larger tumour burden
P<0.001
TTDM/ month
E
Low tumour grade
Cum Survival
Small tumour burden
Larger tumour burden
P=0.002
Breast cancer specific survival/ month
F
Low tumour grade
Cum Survival
Small tumour burden
Larger tumour burden
P<0.001
TTDM/ month
G
Negative lymph node
Cum Survival
Small tumour burden
Larger tumour burden
P<0.001
Breast cancer specific survival/ month
H
Negative lymph node
Cum Survival
Small tumour burden
Larger tumour burden
P=0.02
TTDM/ month
I
Good NPI group
Cum Survival
Small tumour burden
Larger tumour burden
P=0.003
Breast cancer specific survival/ month
J
Good NPI group
Cum Survival
Small tumour burden
Larger tumour burden
P<0.001
TTDM/ month

Figure 4.7: Kaplan Meier curves showing significant correlation between larger tumour burden with worse patients' survival in the discovery cohort; both in breast cancer specific survival (A), and distant metastasis free survival (B) and in subgroup of patients with less aggressive tumour behaviour as postmenopausal (C,D); low tumour grade (E,F); negative lymph node metastasis (G,H) and good Nottingham prognostic index (I,J).

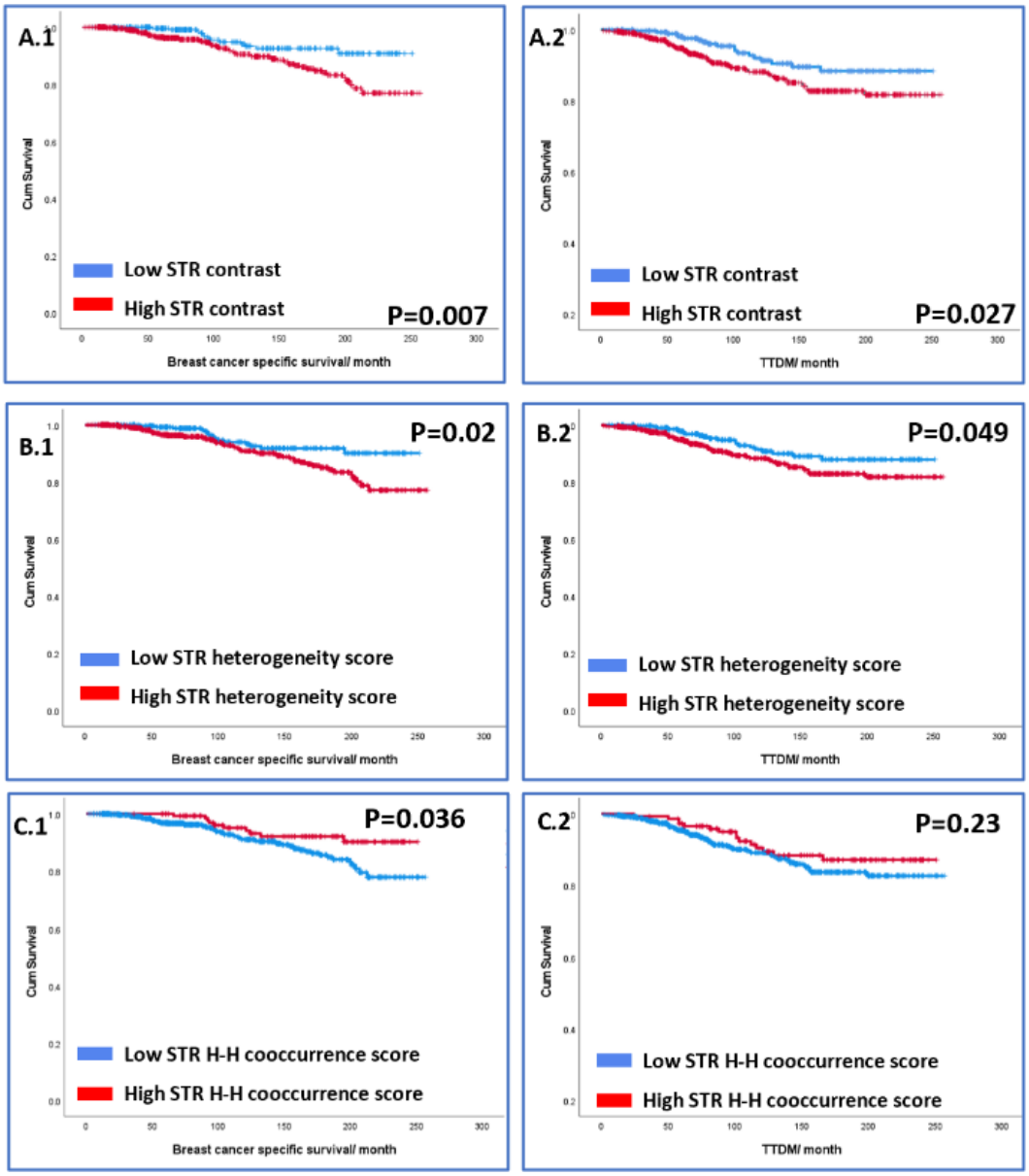


Figure 4.8: Kaplan Meier curves demonstrating effect of stroma to tumour ratio (STR) spatial intratumor contrast (A1,2), heterogeneity (B1,2) and spatial cooccurrence (C1, C2) on breast cancer specific survival and distant metastasis free survival in the discovery cohort. TTDM: time to distant metastasis

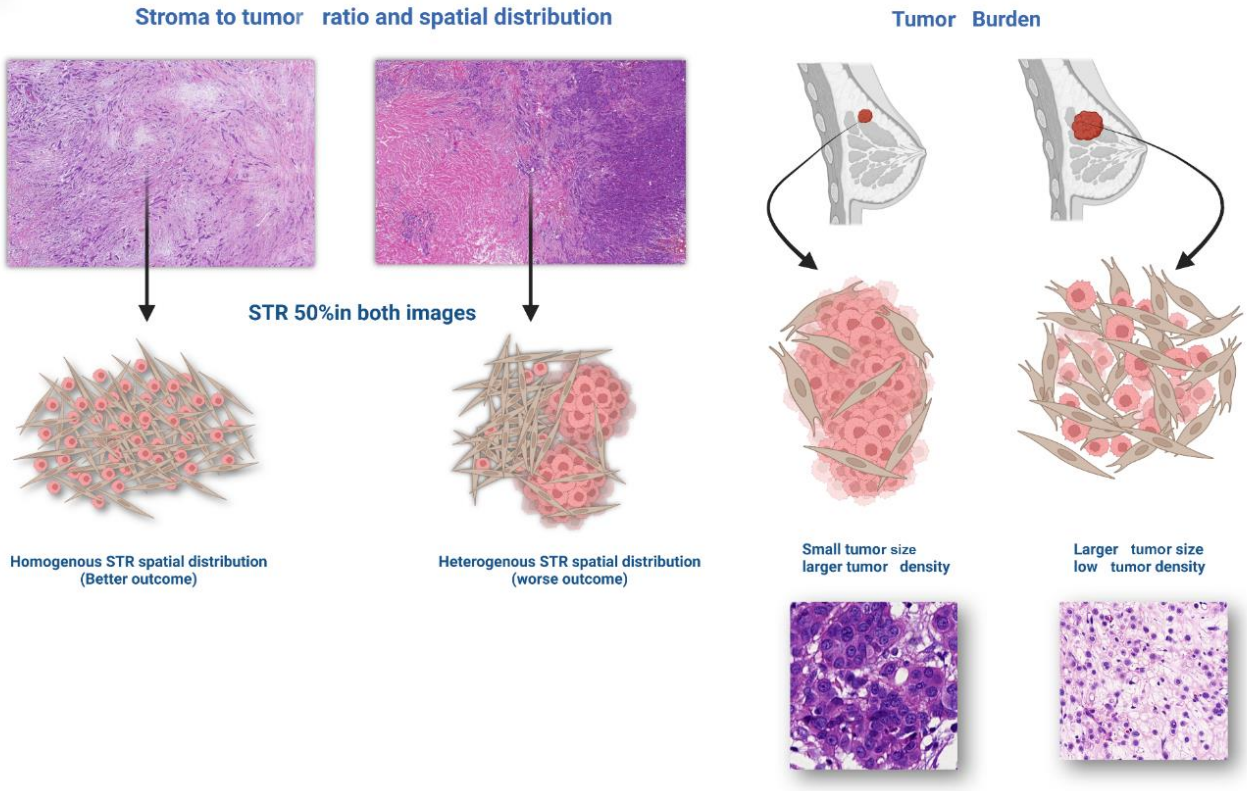


Figure 4.9: Illustrated diagram showing the difference between Stroma tumour ratio and spatial distribution as well as the value of tumour burden.

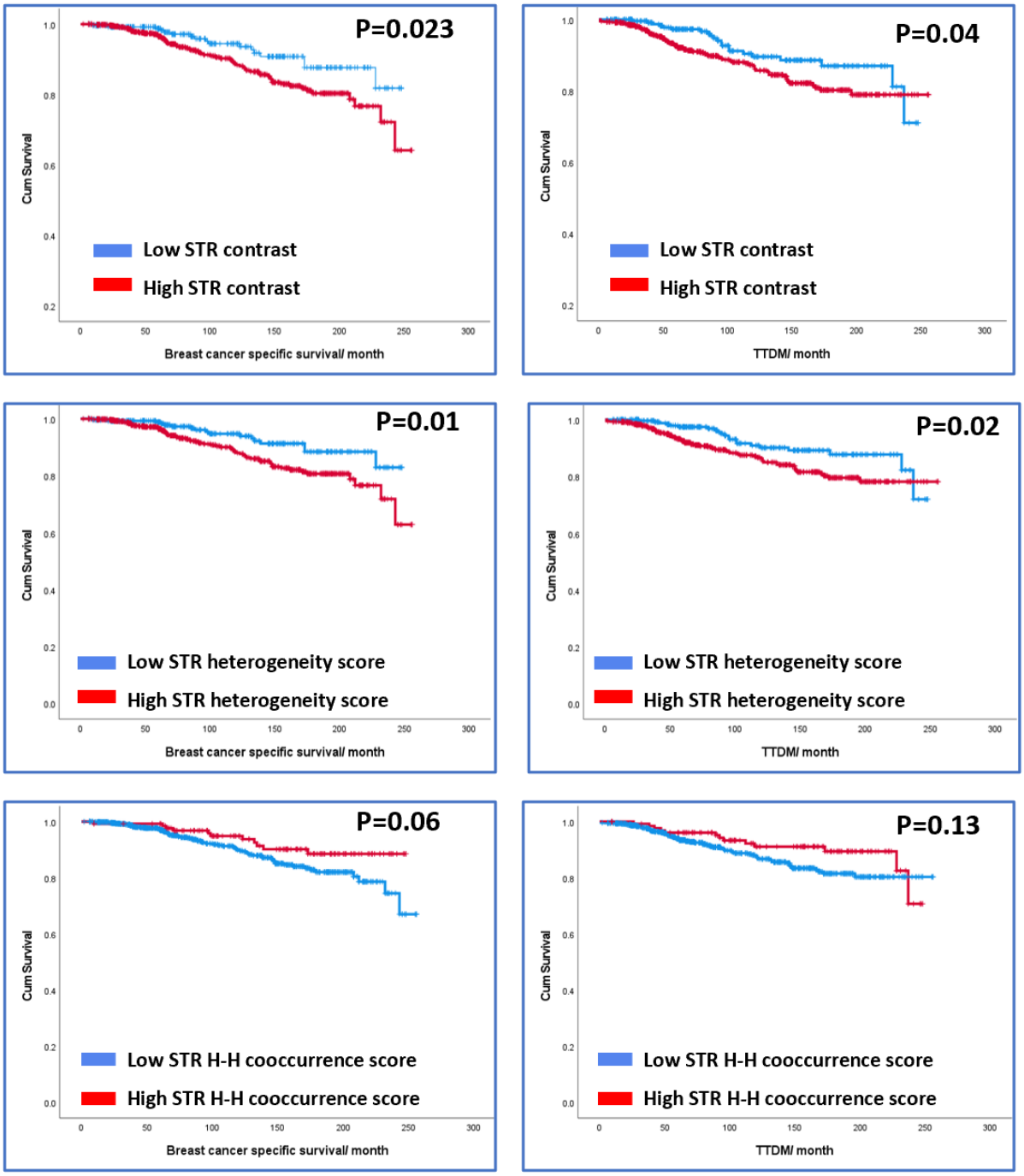


Figure 4.10: Kaplan Meier curves demonstrating the effect of stroma to tumour ratio (STR) spatial intratumor contrast (A1,2), heterogeneity (B1,2) and spatial cooccurrence (C1, C2) on breast cancer specific survival and distant metastasis-free survival in the test cohort. TTDM: time to distant metastasis

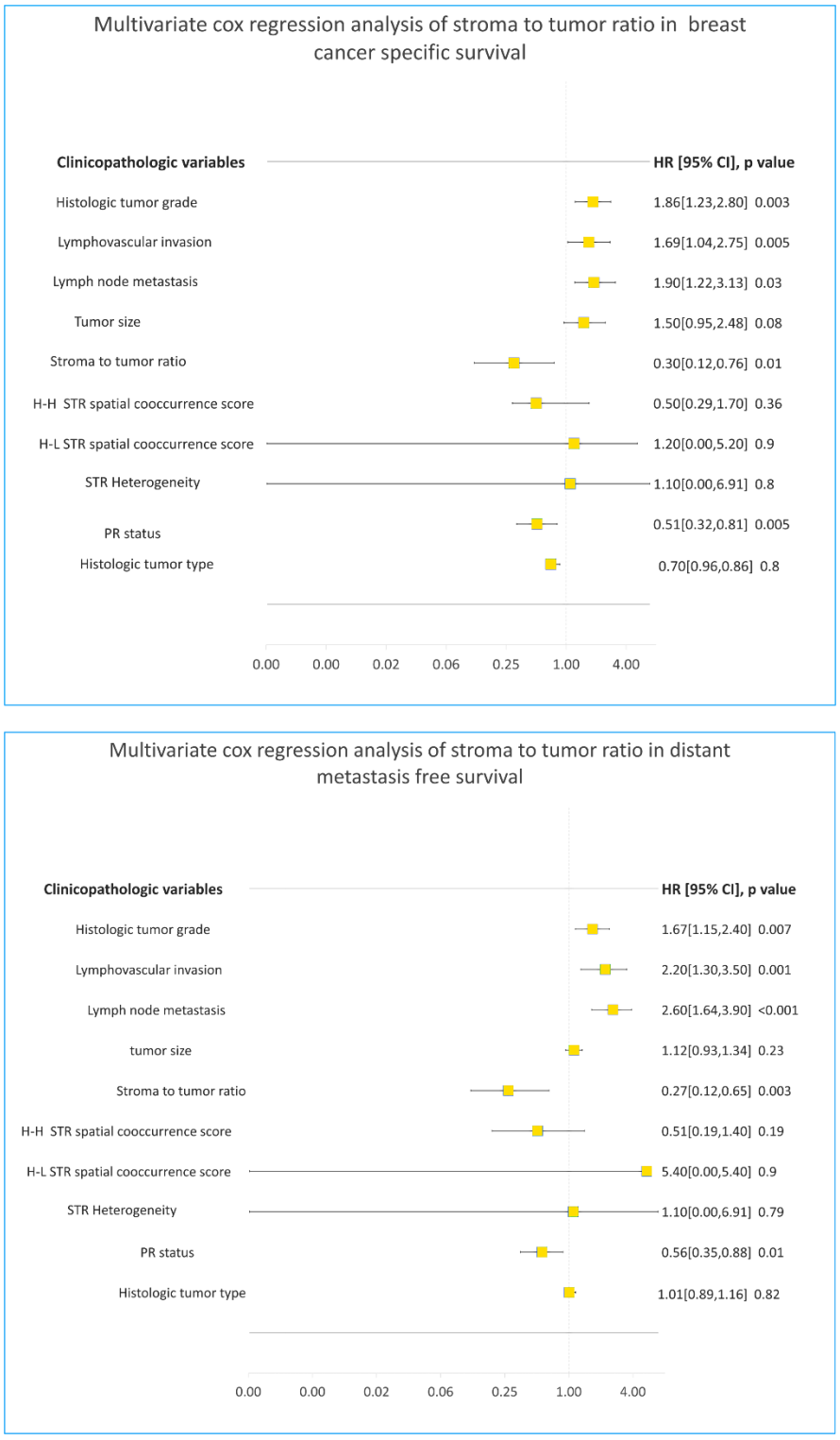


Figure 4.11: Forest plot illustrating the multivariate Cox regression model for stroma to tumour ratio (STR) adjusted for the clinicopathologic parameters showing that STR is an independent predictor of patient outcome.

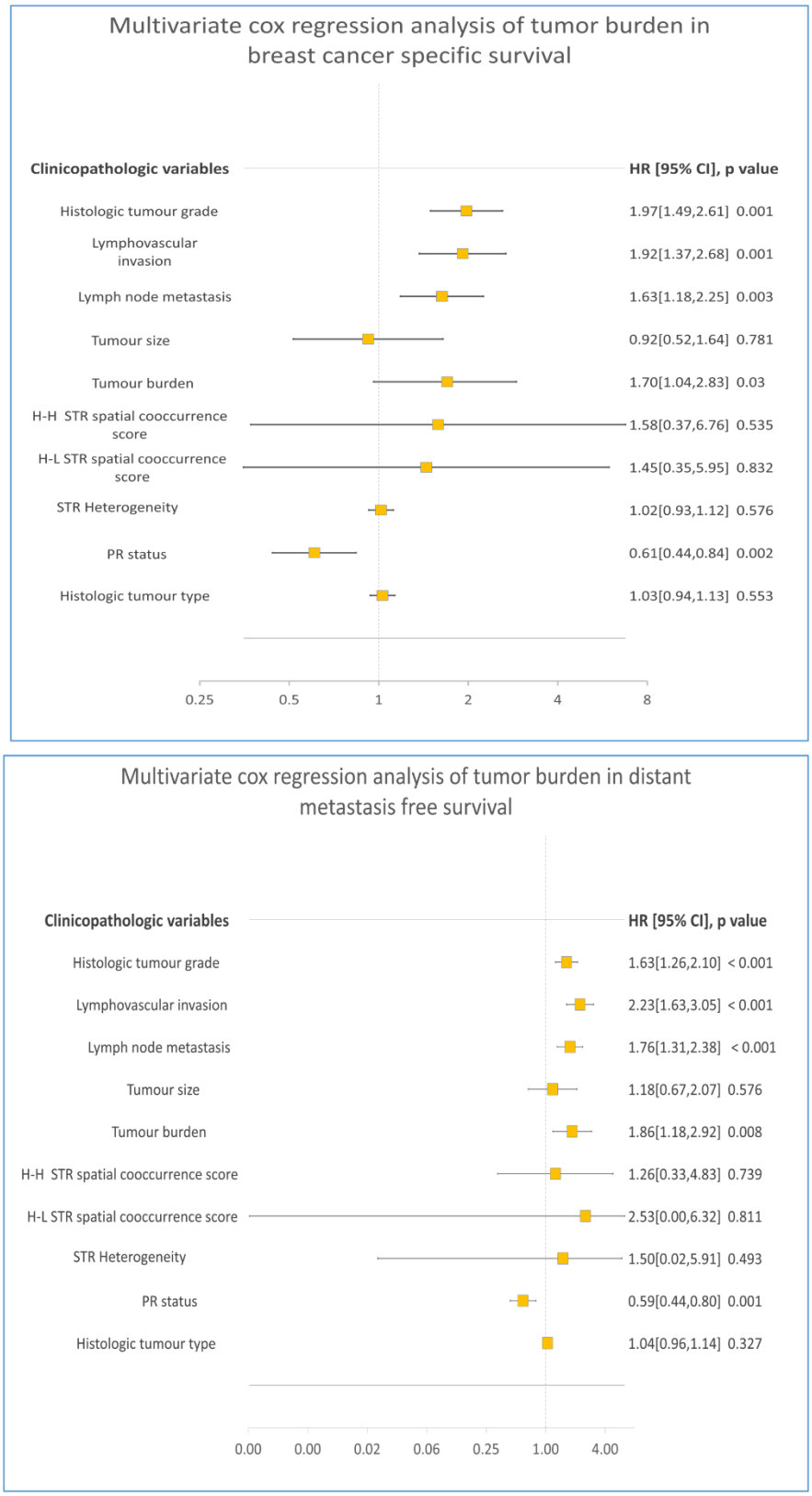


Figure 4.12: Forest plot illustrating the multivariate Cox regression model for tumour burden adjusted for the clinicopathologic parameters showing that tumour burden is an independent predictor of patient outcome.

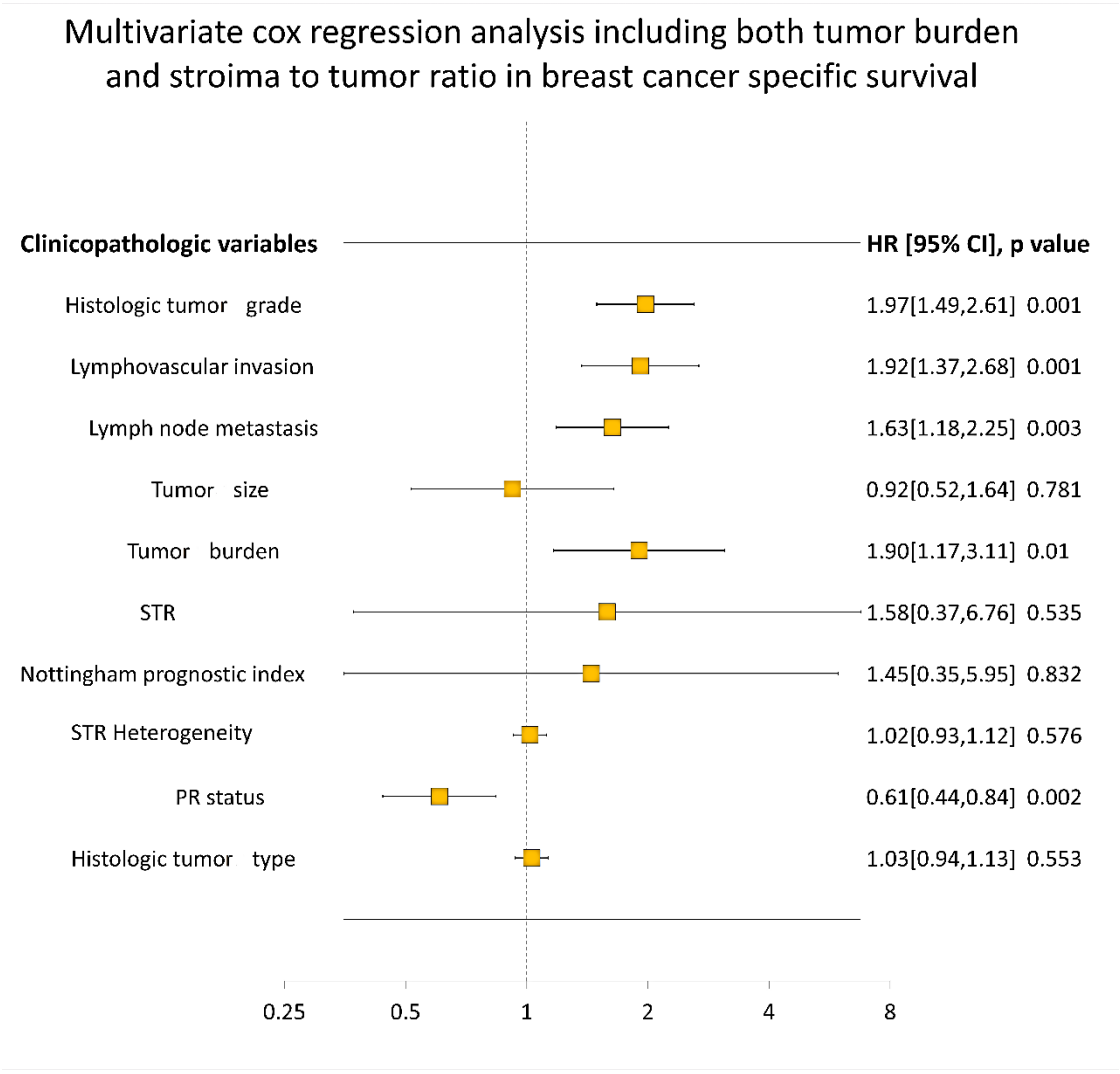


Figure 4.13: Forest plot illustrating the multivariate Cox regression model including both tumour burden and STR and showing that tumour burden is an independent predictor of patients' outcome and STR is not.

4.7 DISCUSSION

Recently, TAS has been gaining much interest, and it proved to be of prognostic significance in different solid tumours, including BC [453, 482, 488]. However, no standardised approach has been agreed for accurate and reproducible TAS assessment. Assessment of STR has been carried out through different approaches, from traditional subjective visual assessment of H&E stained slides, special stains, and polarising microscope to digitalised image analysis on WSIs [96, 451, 454, 459, 460, 482, 483]. Using the power of AI algorithms can revolutionise traditional pathology and decipher the important histologic tumour features that are unavailable in molecular profiling or omics data and beyond the technical limitations of standard light microscopy. The spatial context of tumour and stromal cells is one of these features [489, 490]. Previous research has focused on the prognostic effect of STR; however, the results were not always consistent in different molecular subtypes, especially luminal BC [96, 451, 452, 454, 456, 482, 491]. In this study, we aimed to provide a standardized, objective, and comprehensive method for assessing TAS and its spatial distribution. We focused on luminal BC to avoid the confounding effect of other molecular classes, using a large number of cases with available clinicopathological, management, and follow-up data.

Although a good concordance was obtained for the visual assessment of STR and AI-based assessment, the traditional method was less standardized, time-consuming, and could not calculate the spatial distribution.

The first step toward a DL model to quantify the STR based on WSI of colorectal cancer tissue has also been taken [492] and proved that AI automated assessment of STR ratio holds great opportunities. In BC, most studies have

adopted either the traditional visual assessment of STR using a predefined cut-off point or focused on a narrow-filed area of the slide, and both methods are less standardised with much subjectivity and interobserver discordance [461, 462]. Other studies that implemented digitalised approaches for assessment of STR, either used complex 300 points counting on 9 mm^2 area or DIA software on TMA sections [453, 454, 482, 483]. Our study is the first to our knowledge that applied AI developed algorithm on WSI of full-face BC cases to assess STR together with the spatial heterogeneity of stromal and tumour cells.

We found that high STR is a significant prognostic parameter and is associated with better prognosis in ER-positive and HER2-negative early BC patients. Our results are consistent with those of both Downey and colleagues and Millar and colleagues [454, 482] who reported that high stroma was associated with better tumour behaviour and prolonged patients' survival. However, controversial results about the role of stroma in ER-positive BC have also been reported [96, 451, 454, 456, 482]. This may be attributable to the lack of standardized techniques in STR assessment. Cancer-associated fibroblasts (CAFs) were originally presumed to represent a homogeneous population uniformly driving tumorigenesis, united by their morphology and peritumoral location. However, recent single cell RNA-seq data led to a better understanding of CAF biological functions, and now it is widely appreciated that CAFs form a group of highly heterogeneous populations which has the capacity to promote or inhibit cancer [486, 493, 494].

Current conventional approaches to the assessment of the TME do not adequately consider the spatial-level cellular distribution, co-organization, and cell-

cell interaction. With the emergence of CPATH, DL and AI-based spatial TME analyses of pathology images could revolutionize our understanding of the highly heterogeneous and complex molecular architecture of the TME. A number of studies have shown that the spatial colocalization of immune and cancer cells could lead to prognostic biomarkers for BC [495], and is a good predictor in colorectal cancer patients [496]. However, the role of stromal cell distribution as a component of tumour microenvironment has not been studied. The spatial distribution of stromal cells in relation to tumour cells is also another prognostic factor to be considered in BC patients. The current work revealed that the spatial co-localization of high STR areas close to each other in a homogenous distribution within the tumour is a good predictor of patients' survival. In the same context, STR intratumor heterogeneity carries a poor prognosis for ER positive and HER2-negative BC patients. This could be explained by the suppressive role played by CAF in luminal BC as they tend to secrete TGF-B inhibitors that induce fibrosis and prevent tumour cell proliferation [486]. However, the exact mechanism of complex cellular crosstalk between cancer cells and stromal cells is an area of active interest and not fully understood yet. High STR was not only a good prognostic parameter in luminal BC patients, but also a predictive factor for response to endocrine therapy as well. These results were confirmed by Brechbuhl, and colleagues who reported that CAF in ER-positive BC maintains ER expression and sustains oestrogen-dependent proliferation and sensitivity to tamoxifen [497]. Most of the endocrine naive patients were of grade 1 or 2, so cases were adjusted for low tumour grade upon performing the analysis. It is worth mentioning that this was a historical cohort

when patients with indolent behaviour features were not treated with endocrine therapy, as currently, all ER-positive patients receive endocrine therapy.

Although the differentiation between prognosis and response to therapy can be only confirmed in the context of randomised clinical trials of the specific therapy, in the context of our study we considered the outcome of patients treated with endocrine therapy is based on response to the treatment and patients without events are classified as responders and patients who developed events are classified as non-respondent.

High tumour density and/or homogenous distribution of tumour cells was associated with worse tumour behaviour and decreased patient survival in terms of shorter BCSS and DMFS. This is consistent with our findings, which show that when tumour cells are uniformly surrounded by stromal cells in a homogenous high STR, patients have better survival. This might be explained by the ability of stromal cells to interrupt the tumorigenic signals released by tumour cells. This does not take place when stromal cells are absent and tumour cells are in close proximity to one another. However, this has to be verified, and further investigation is needed.

To date, tumour size has been the primary parameter used to represent tumour mass. However, absolute tumour size may not accurately reflect tumour cell density, which is a crucial factor in assessing tumour burden. In this study, we propose a novel tumour burden parameter that integrates tumour size with the ratio of tumour cells to stromal cells, providing a more comprehensive repre-

sentation of effective tumour mass. Our findings suggest that this adjusted tumour burden metric demonstrates a stronger association with prognosis than tumour size alone, reinforcing its potential clinical relevance.

The methodology developed for tumour burden assessment leverages DIA and DL applied to WSI. By enabling precise quantification of tumour cell density, these advanced computational techniques overcome the limitations of traditional histopathological assessment, which relies on subjective visual estimation. The practical implementation of this approach in routine pathology practice would require integration into existing digital pathology workflows. This could be achieved through automated pipelines that process WSI, extract morphometric features, and generate tumour burden scores in real time, aiding pathologists in refining prognostic assessment and therapeutic decision-making.

Despite its potential, the clinical relevance of tumour burden assessment must be critically examined. Is it truly an improvement over conventional tumour size measurement? Emerging evidence suggests that incorporating cellular density into tumour burden estimation offers prognostic advantages. While some previous studies have attempted to refine tumour size as a measure of burden, they have often focused on volumetric assessments or histological grading rather than integrating computationally derived tumour-stroma ratios [498-500]. Furthermore, multifocality presents a unique challenge in tumour burden estimation, as multiple tumour foci may contribute variably to overall disease burden. Future studies should explore whether our proposed tumour burden metric can be adapted to account for multifocal tumours and whether it retains prognostic significance across different breast cancer subtypes.

Ultimately, this work underscores the necessity of a more precise tumour burden assessment and highlights the role of AI-driven pathology in advancing oncological diagnostics. Further validation in larger cohorts and comparative analyses with existing tumour burden models will be essential to establish its utility in clinical practice.

Through using a high throughput AI tool, STR and tumour burden were significant biomarkers for risk stratification of patients with aggressive tumour behaviour for better-personalised therapy. To conclude, deep learning is a reliable method for STR assessment but also the spatial arrangement of stromal and tumour cells in addition to tumour cell density. Spatial distribution and heterogeneity of TAS are worthy to be considered during the assessment of STR. A variable based on tumour size and adjusted for the ratio of tumour cells to stromal cells (tumour density based on mean cell counts, not the ratio of surface stromal and tumour surface areas) shows a more significant association with prognosis than absolute tumour size does.

Chapter 5. Morphometric Signature for HER2 Activity and response to therapy

5.1 BACKGROUND

HER2 oncogenic activity should ideally correlate with protein overexpression levels. However, HER2 positivity definition is based on clinical response to anti-HER2 therapy and was extended to include BC with equivocal protein expression (HER2 IHC score 2+) with evidence of *HER2* gene amplification using ISH techniques [39, 501]. Advanced genomic sequencing and pathways studies showed that only 65% of clinically defined HER2-positive tumours are classified as HER2-E using intrinsic molecular subtype classification [399, 502, 503], suggesting clinical, pathologic and molecular heterogeneity related to HER2 expression level. Therefore, the current definition of HER2 positivity in BC may neither fully reflect the spectrum of oncogenic activity of *HER2* signalling pathways that drive BC growth, differentiation and behaviour nor the clinical and biological heterogeneity within these tumours.

5.2 INTRODUCTION

HER2-E BC has the highest *ERBB2* mRNA expression, and HER2 protein overexpression and is associated with higher pCR rates following anti-HER2-based regimens [504-508].

The morphological features of a tumour are the end product of the activity of a specific set of genes working individually or in combination [509-513]. Correlation between morphometric features and the molecular profiles, including molecular aberrations, has been previously reported in different tumours including BC [514-519]. Therefore, an accurate assessment of morphometric features of tumour cells could provide insights into molecular and biological

cancer signatures and potentially reflect the activity of key driver genes rather than measuring the existence or level of expression of these genes.

Recently, there has been an increasing interest in leveraging the power of AI to identify HER2 status in BC from tumour morphology using the digitalised H&E-stained slides [374, 520-526]. Despite being a promising tool, the majority of these AI algorithms utilise an unsupervised approach without consideration of the biological relevance of the analysed features or HER2 heterogeneity. Current approaches have also failed to explain the molecular basis of their results and have not provided information on how specific predictions are made or elucidate the potential ramifications on therapeutic response [220, 527].

5.3 HYPOTHESIS

We hypothesised that clinically diagnosed HER2-positive BC could be further refined using morphometric features extracted from digital image analysis to reflects HER2 oncogenic activity and response to therapy.

5.4 AIMS OF THE STUDY

- Assess the role of DIA tool and visual-based assessment in defining a set of biologically relevant morphological features that are statistically correlated with HER2 protein over-expression.
- Develop a morphometric signature that can reflect HER2-positive tumours with active oncogenic activity and validate it using HER2-E PAM50 molecular subtype.
- Evaluate the prognostic and predictive validity of the developed morphometric signature.

- Create a web tool that can be utilised clinically as an ancillary tool in the prediction of HER2-E status.

5.5 MATERIALS AND METHODS

5.5.1 Study cohorts

A. *Discovery cohort*: A well-characterised cohort of 289 invasive BC cases presented to Nottingham University Hospitals was investigated. Cases were selected as a subset of the Nottingham cohort (**Section 2.1.1**) based on inclusion and exclusion criteria. This cohort included two subsets: 1) HER2-positive cases defined as HER2 IHC score 3+ and IHC score 2+ with *HER2* gene amplification (n=164), 2) a control group of HER2-negative BC (n=125), including both TNBC and luminal subtypes (ER-positive/HER2 IHC 0 and 1+) of matched tumour type, grade and stage. All cases in both subsets were invasive breast carcinoma of non-special type with tumour grade 2 or 3**. Figure 5.1** represents a schematic illustration of cohort selection and characterisation.

One representative section with adequate tumour content was selected for each case. Clinicopathological data, including age at diagnosis, histological tumour grade, tumour size, axillary LN status, LVI, NPI, HR, and HER2 status, were available from patients records. ER and PR positivity was defined according to ASCO/CAP guidelines, which stipulate a requirement for positive IHC staining in ≥1% of the invasive tumour cell nuclei [406]. HER2 staining had been completed on the Ventana Benchmark ULTRA IHC Automated staining system using the Ventana PATHWAY anti-HER-2/neu (4B5) rabbit monoclonal ready to use primary antibody in combination with Ventana detection kits as part of patient diagnostics. HER2 scoring was carried out following ASCO/CAP

guidelines and UK guidelines [141, 161]. *HER2* gene amplification status, where available, was obtained from patient records.

Treatment regimens and long-term patients' follow up were collected. Patients with HER2-positive BC were treated with adjuvant anti-HER2 therapy. Patients' response to therapy was monitored through DMFS, **Section 2.1.1**

B. *Test cohort:* Cases from TCGA were included as a test cohort *(n=71)*. Only cases with available Virtual histologic slides, HER2 IHC score and PAM50 molecular subtype were included. PAM50 molecular subtypes and their corresponding normalised RNA-seq gene expression values were downloaded from HTTPS://PORTAL.GDC.CANCER.GOV/. This cohort was utilised as an independent external test cohort to validate the reliability of extracted features and also to assess the enrichment of identified features within HER2 status and HER2-E molecular subtype, **Section 2.1.2.2**.

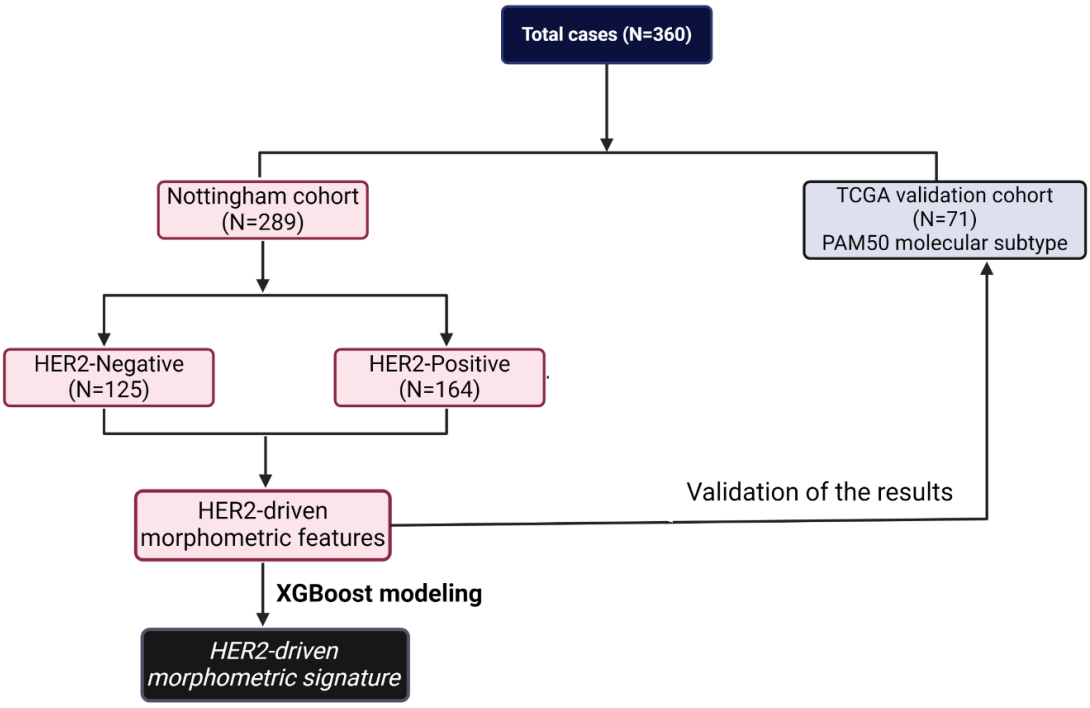


Figure 5.1: Schematic illustration summarising the characteristics of the study cohort.

5.5.2 Image acquisition and morphometric digital image analysis

- Fresh H&E-stained sections were scanned at high resolution using the Pannoramic 250 Flash III scanner. All 360 digital images underwent QC and were analysed using QuPath software. The analysis included colour normalisation, stain separation, and cellular segmentation to extract biologically relevant morphometric features such as cell count, nuclear dimensions, and nuclear/cytoplasmic ratios. Spatial distribution was assessed using the Delaunay 2D model. For objective evaluation of intra-tumoral heterogeneity in HER2-positive cases, we computed the variance in the assessed features from annotated areas within each case. Cases were grouped according to ER status. The intra-tumoral heterogeneity was proven if a significant feature variance was detected between the two groups of HER2-positive tumours stratified by ER status **(Figure 5.2)**. Details are mentioned in **Section 2.10.**

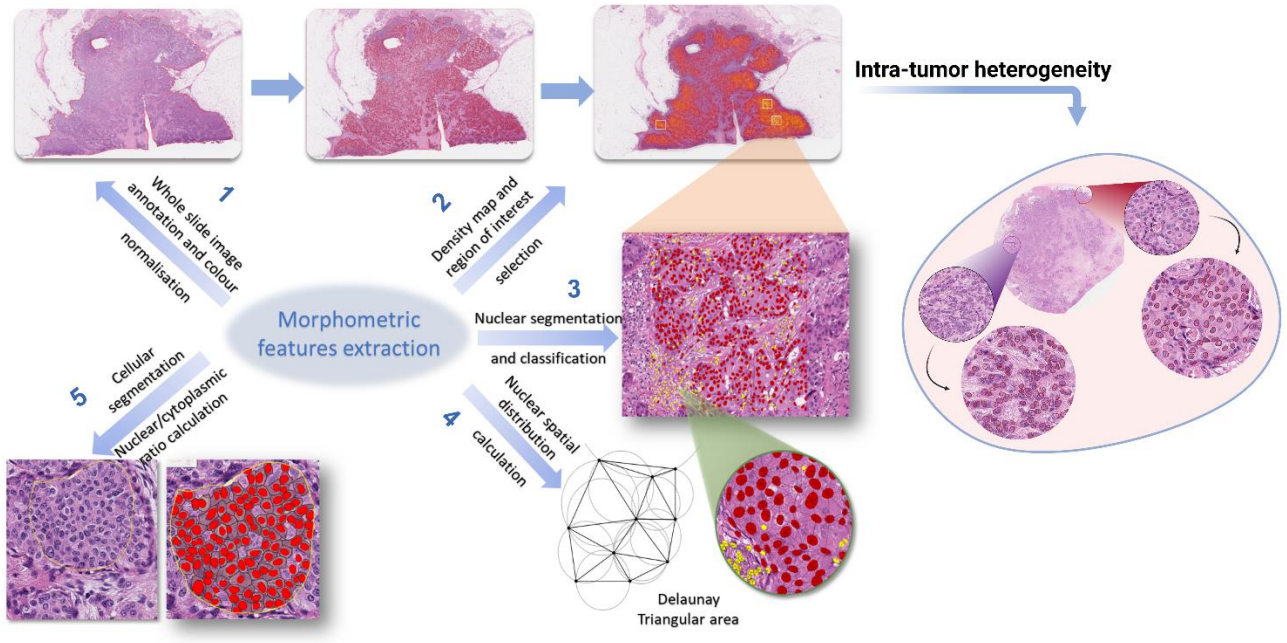


Figure 5.2: A graph that summarises the process used in image processing to extract morphometric features and evaluate intra-tumour heterogeneity. Step 1 involved colour normalisation of the entire slide image and tumour cell detection. Step 2 involved creating a density map to identify the regions with the

highest tumour density. Density maps were used to select the region of interest (ROI), and three annotation areas of 2000 by 2000 pixels each were made. Step 3: After nuclear annotations and object classifier training, segmented nuclei were divided into nuclei related to tumours and immune cells. Step 4: The Delaunay 2D spatial function was used to calculate the internuclear distance. Step 5: The nuclear/cell ratio was calculated, and cells were detected using the Cellpose plugin. The variance of morphometric characteristics inside each annotated ROI within the same tumour was used to measure intra-tumour heterogeneity.

5.5.3 Visual-based assessment

Additional features considering tumour cell architecture and patterns, which could not be analysed through an image analysis approach, were assessed through visual eyeballing assessment. The assessed parameters were based on published literature that addressed different morphological tumour patterns, cellular architecture and arrangement and their clinical significance, if present [528-532]. To guarantee high reproducibility, the scoring was carried out by three experienced pathologists (NA, SM, AI), who were totally blind to the clinicopathological and molecular profiles of these cases.

The assessed parameters included:

- Tumour architecture: Six different tumour architectural (cellular arrangement) patterns were evaluated: large solid sheets, tumour strands, small, nested clusters/groups of cells (alveolar-like pattern), large, nested clusters/groups separated by thin intervening fibrous septa, large trabecular sheets and acinar/tubular pattern. The proportion of each pattern was considered, and the predominant pattern was assigned and included in the analysis (**Figure 5.3 left panel)**.

- Cellular morphology: cellular features were categorised based on cell shape, nuclear to cytoplasmic (N/C) ratio, cytoplasmic quality and cell membrane distinction into hepatoid-like cells (large polygonal and surrounded by abundant pale, glassy cytoplasm and tumour cells are arranged in a cobblestone-likes structure), spindling with elongated nuclei, or no special feature (**Figure 5.3 right panel**).
- Cytoplasmic eosinophilia: The intensity and pattern of cytoplasmic staining were assessed as pale/foamy/glassy vs. deep eosinophilic and clear cytoplasm.
- Distinction of the cellular membrane (defined or indistinct).
- Intra-tumour heterogeneity was evaluated by examining the existence of mixed patterns paired with cytoplasmic and membrane characteristics. Mixed architectural heterogeneity refers to tumour architecture heterogeneity accompanied by a shift in cellular pattern. Cases with less than 50% of a single predominant pattern were classified as mixed heterogeneous patterns and given a positive or negative score. Tumours with more than 50% of a single predominant pattern were allocated to this pattern.

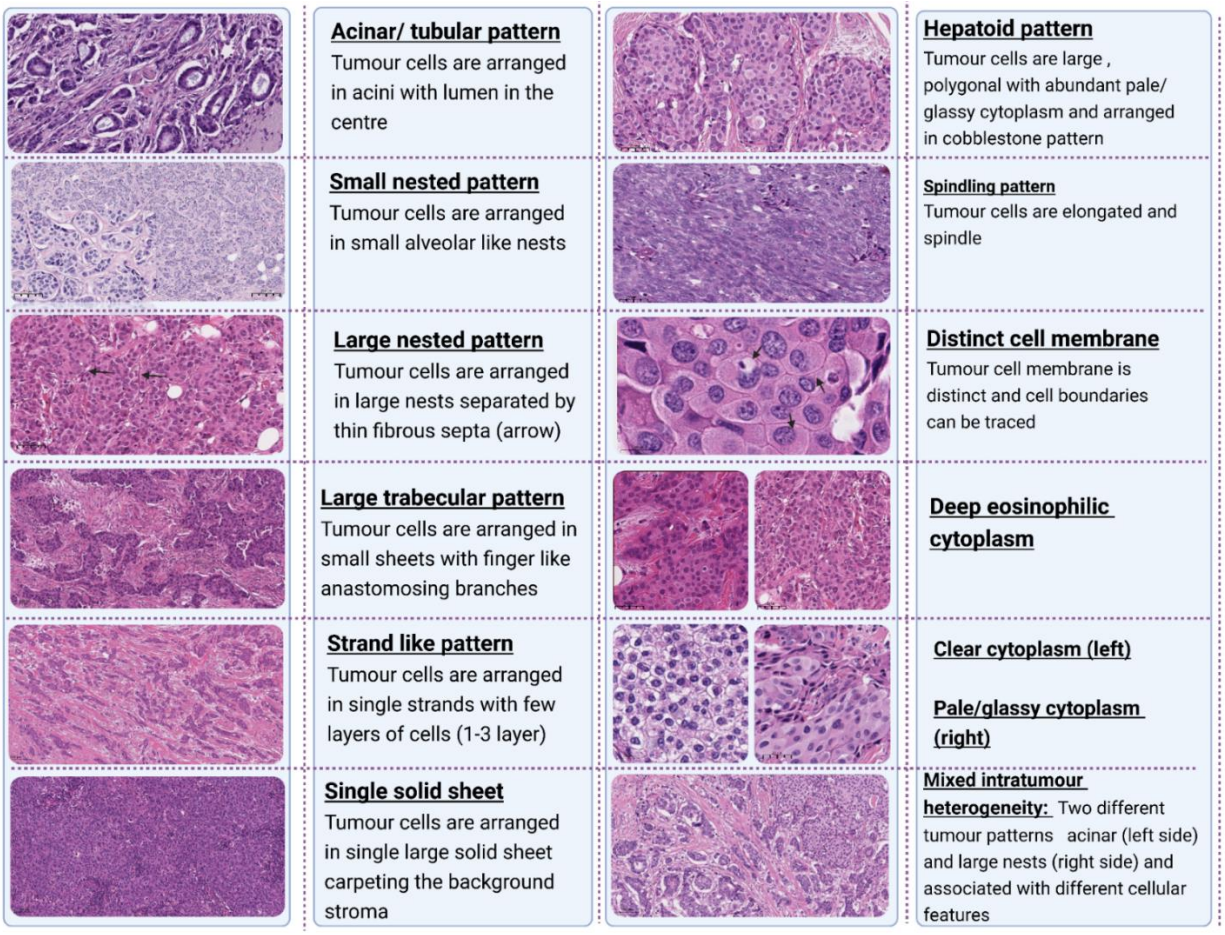


Figure 5.3: A graph summarising different visually assessed features of tumour cell patterns (left panel) and architecture (right panel)

5.5.4 Identification of HER2 driven morphometric features

Out of the total assessed features (both visual and image analysis), we identified the set of features highly associated with HER2 IHC score 3+ tumours, representing the prototype of HER2 protein overexpression, compared to HER2-negative and HER2 with equivocal expression tumours. Then we expanded the comparison to include both HER2-positive subtypes (3+ and 2+ amplified) and all HER2-positive cases against HER2-, considering the role of ER status. Data was validated in the HER2-E molecular subtype from TCGA cohort.

5.5.5 Development of a single HER2-driven morphometric signature.

Then, from the total identified significant set of features, we aimed to develop a single HER2-driven morphometric signature that could reflect HER2-positive tumours with evident HER2 oncogenic activity and, hence, a better response to anti-HER2 therapy. For that, we harnessed the power of ANN through the extreme gradient boosting "XGBoost model to identify the most effective feature combinations with the highest accuracy in predicting HER2 positivity (**Section 2.12.2).**

The significant morphometric features alone and in combination with HR status and HER2 IHC score were used as the input parameters. The obtained signature evaluation metrics included accuracy, precision, recall, and F1-score, and its performance was compared against *ERBB2* mRNA using the AUC measuring the sensitivity and the specificity.

The signature with the highest accuracy was then selected for further analysis. Each case had a probability score ranging from 0-1, cases were then classified into HER2 morphometric signature positive/negative, according to cut point predefined using AUC, and its potential clinical significance was assessed through its ability to detect patients who would benefit the most from anti-HER2 therapy using the DMFS as a surrogate. This model was trained on the discovery cohort, which was split into training (80%) and cross-validation (20%) sets. The TCGA cohort was used as an independent test cohort as detailed in **Section 2.12.2.** The ANN model was developed by a computer scientist; however, the author carried out all subsequent analyses and validations.

5.5.6 Differential gene expression and pathway enrichment analysis

To further test the histo-morphometric signature score, DGE and pathway enrichment analysis between cases with high and low scores in TCGA validation cohort, were carried out. RNA-seq data was obtained from TCGA gene expression profile and the DESeq2 tool in version 1.1, IDEP software [533], http://bioinformatics.sdstate.edu/idep11/) was used for data normalisation and DGE analysis. The significantly differentiated expressed genes were defined as log2 fold change (≥±1) and FDR <0.05 between high and low score groups. The web-based gene set enrichment analysis tool (WebGestalt) [428] was used to explore significantly enriched pathways based on the identified DEGs in cases with high HER2-driven histo-morphometric signature.

5.5.7 HER2 risk of recurrence prognostic index

We aimed to establish a link between extracted HER2 morphometric features (covariates) and time to recurrence in HER2-positive BC patients following adjuvant anti-HER2 therapy, and accordingly, patients will be divided into high/low risk of recurrence according to the onset of recurrence. We enrolled HER2 morphometric signature both alone and combined with clinicopathological parameters (ER, PR status, and tumour size), to develop the optimal prognostic index (clinic-morphometric) for predicting time to recurrence after anti-HER2 therapy. Results were compared to models based solely on the HER2 IHC score and on the clinical-HER2 IHC score, which included the same clinical parameters along with the HER2 IHC score. Patients were categorised into high-risk if they developed recurrence early in 5-year intervals and low-risk if no DM occurred in 5 years' time, as detailed in **Section 2.12.2.**

5.5.8 Webtool application

We developed a web application that provides personalised HER2 signature predictions as a probability score. This tool visually represents the key features associated with the HER2-morphometric signature. By analysing these features, the application estimates the likelihood of a patient being HER2-positive, with a probability score ranging from 0 to 1, indicating their potential responsiveness to HER2-targeted therapies. Users can input the relevant parameters, and the tool utilises the XGBOOST classifier to predict the probability of HER2-positivity for each case. The following clinical and histologic variables serve as inputs: total detected nuclei, immune cell/tumour cell ratio, nuclear area variance, nuclear length, nuclear maximum diameter, spatial distribution parameters, cell area, N/Cytoplasmic ratio, and nuclear cell ratio (**Figure 5.4).**

5.5.9 Statistical analysis

Statistical package of social science (IBM-SPSS) statistical software v. 28.0 (SPSS, Chicago, IL, USA) was used to perform the statistical analyses. We computed the descriptive data (mean, median, range and SD) for the extracted morphometric features of tumour cells and nuclei. Differences among HER2-positive and HER2-negative tumours and other molecular subtypes was carried out using Mann-Whitney and Chi-square tests. Independent Samples t-Test was used when comparing means between two independent groups. Interobserver agreement was calculated through Fliess kappa test, which determines the level of agreement between two or more raters [534]. Silhouette score was utilised to measure the accuracy of hierarchical clustering analysis.

Outcome analysis was assessed using univariate and multivariate cox regression models and Kaplan–Meier curves and the log-rank test. For evaluation of the model accuracy, we used the concordance index (c-index). It is a measure of rank correlation between predicted risk scores. For all tests, $p<0.05$ (two-tailed) was considered statistically significant.

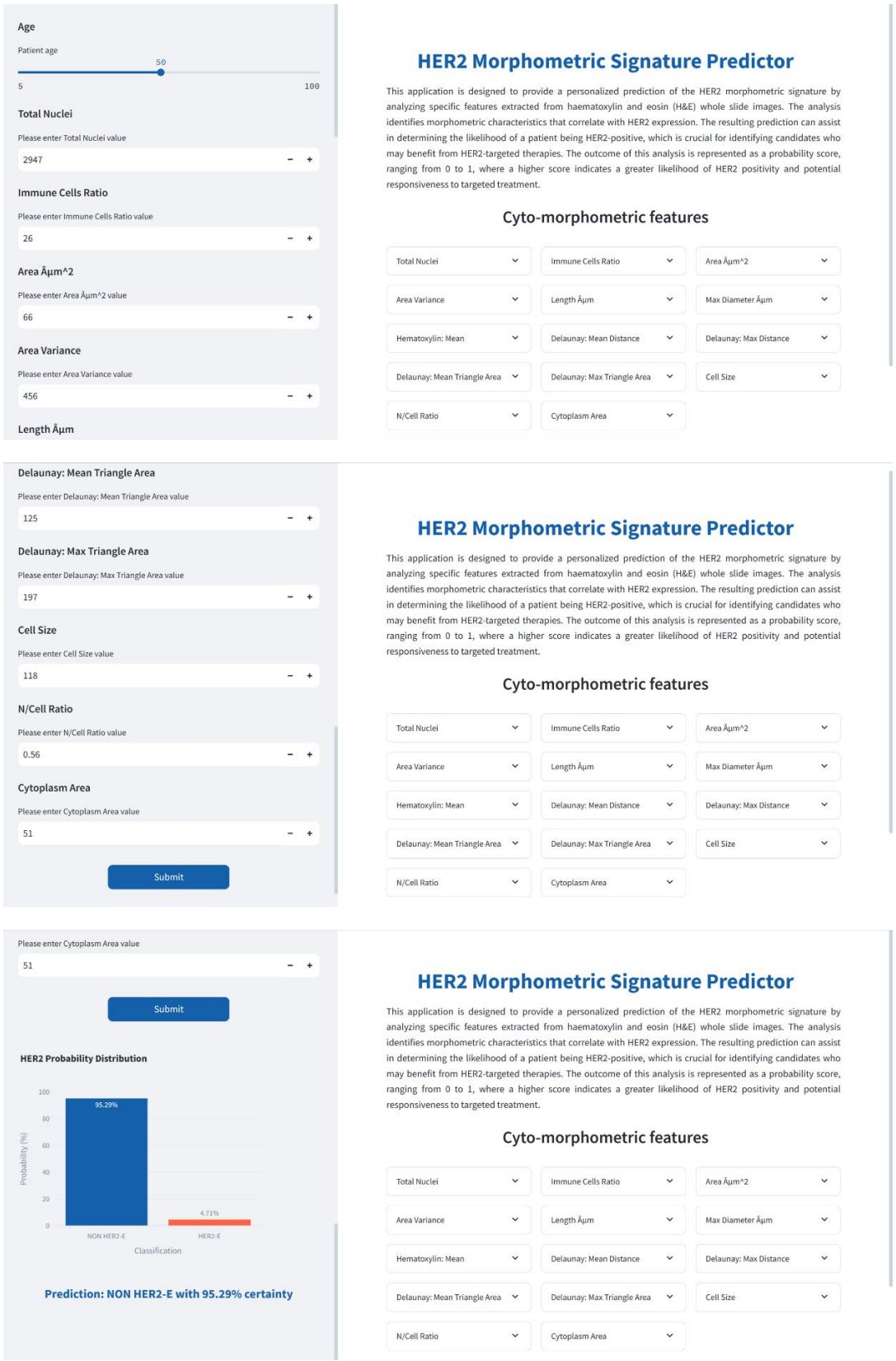


Figure 5.4: Screenshots from HER2-morphometric signature web tool

5.6 RESULTS

5.6.1 Basic Cohort Description

The total number of enrolled cases was 360, including 289 BC cases in the Nottingham discovery cohort and 71 in the TCGA test cohort. **Table 5.1** summarises the baseline patient and tumour characteristics. In the discovery and test sets, respectively, the mean age of patients was 51 years (range 28-78) and 54.60 years (range 22-80).

Table 5.1: Baseline patients and tumour characteristics

Parameters	Discovery set (n=289)		Test cohort (n=71)	
	N	%	N	%
Age at diagnosis (years)				
< 50	127	43.9	30	42.3
≥ 50	162	56.1	41	57.7
Menopause				
Pre	136	47.1	NA	
Post	153	52.9		
Tumour size (cm)				
< 2.0	152	52.6	21	19.4
≥ 2.0	137	47.4	50	80.6
Tubule formation				
2	34	11.8	19	11.9
3	255	88.2	52	88.1
Pleomorphism				
1	16	5.5	0	0
2	46	15.9	20	15.0
3	227	78.5	51	85.0
Mitosis				
1	124	42.9	8	16.3
2	45	15.6	8	16.3
3	120	41.5	33	67.3
Lympho-vascular Invasion				
No	183	63.3	42	59.2
Yes	106	36.7	29	40.8

Table 5.1 continued

Parameters	Discovery set (n=289)		Test cohort (n=71)	
	N	%	N	%
Lymph node status				
Negative	155	53.6	NA	
Positive	134	46.4		
HER2 IHC status				
Negative	125	43.3	27	38
Positive	164	56.7	44	62
HER2 IHC scores				
0/1+	95	32.8	15	21
2+/non-ISH amplified	30	10.1	10	14
2+/ISH amplified	46	16.3	19	27
3+	118	40.8	27	38
ER Status				
Negative	136	47.1	35	48.5
Positive	153	52.9	36	51.5
PR Status				
Negative	179	61.9	41	58.3
Positive	110	38.1	30	42.7
PAM50 molecular subtype				
Luminal A	NA		5	7.0
Luminal B			20	28.2
HER2-Enriched			27	38.0
Basal like			18	25.4
Normal like			1	1.4
NPI risk group				
Low risk	24	8.3	NA	
Intermediate risk	193	66.8		
High risk	72	24.9		
Adjuvant anti-HER2 therapy				
No	26	18	0	0.0
Yes	118	82	36	100

IHC: immunohistochemical expression**, ER**: Oestrogen receptor; **PR**: Progesterone receptor; **ISH**: in situ hybridisation; **NPI**: Nottingham prognostic index. Some cases are missing.

5.6.2 Characterisation of HER2 driven morphometric features

5.6.2.1 Image analysis

In total, ~914024 nuclei were assessed, including both tumour and immune cells. The total number of the extracted high throughput subcellular morphometric features was 40**,** however, only 18 features have meaningful biological and statistical relevance, demonstrated significant associations with HER2-positive compared to HER2-negative tumours, and were employed for all subsequent analyses (**Table 5.2, Table 5.3, and Table 5.4)**. These features included tumours with lower tumour cell density, larger nuclear and cellular area, open-phase nuclear chromatin, high variability in nuclear size, and tumours with widely spaced, less overlapped tumour nuclei ($p<0.001$).

Table 5.2: Summary of the extracted morphometric features using digital image analysis software

	Cyto-morphometric Feature	Description	Mean	
			HER2-negative	HER2-positive
Quantitative criteria	Average total detected nuclei/case	Total number of segmented nuclei in 3 annotated areas	38834	30730
	Tumour nuclei/case	Average number of tumour nuclei detected within annotated areas by the object classifier algorithm	2577	2080
	Immune cells/case	Average number of immune cell nuclei detected within annotated areas by the object classifier algorithm	1278	987
	Immune cells/tumour cells	The ratio of immune cell nuclei to the total detected nuclei	31.0	16.6
Nuclear Dimensions	Nuclear area µm 2	The area occupied by single segmented tumour cell nuclei using Stardist algorithm	55.2	60.8
	Nuclear area standard deviation µm*	The dispersion of segmented nuclei area in relation to the mean. Low, or small, standard deviation indicates data are clustered tightly around the mean, and high, or large, standard deviation indicates data are more spread out.	19.1	22.0
	Nuclear area variance*	Variance is the average squared deviations of nuclear areas from the mean	406.9	570.1
	Nuclear length (perimeter) µm	The length of single cell nuclear membrane	27.1	28.4

	Nuclear max diameter μm	Maximum diameter of single cell nuclear membrane	10.0	10.4
	Nuclear min diameter μm	Minimum diameter of single cell nuclear membrane	7.0	7.3
Nuclear basophilia	Nuclear Haematoxylin: Mean	Mean nuclear Haematoxylin optical density in single tumour cell	0.49	0.38
	Nuclear Haematoxylin: Median	Median nuclear Haematoxylin optical density in single tumour cell	16.1	17.9
	Nuclear Haematoxylin: Min	Minimum nuclear Haematoxylin optical density in single tumour cell	10.6	11.5
	Nuclear Haematoxylin: Max	Maximum nuclear Haematoxylin optical density in single tumour cell	23.8	27.0
	Nuclear Haematoxylin: Standard deviation	Nuclear Haematoxylin optical density standard deviation in single tumour cell	0.24	0.20
Spatial distribution analysis	Delaunay: Mean distance	It is the mean of distance where no point (nuclei) lies within the circumcircle of any line formed. Larger distance means that the tumour nuclei are widely separated from each other (less overlap)	16.6	18.6
	Delaunay: Median distance	It is the median of distance where no point (nuclei) lies within the circumcircle of any line formed	16.1	18.0
	Delaunay: Max distance	It is the maximum of distance where no point (nuclei) lies within the circumcircle of any line formed	23.8	27
	Delaunay: Min distance	It is the minimum of distance where no point (nuclei) lies within the circumcircle of any line formed	10.6	11.6
	Delaunay: Mean triangle area	It is the mean of triangulated network area where no point (nuclei) lies within the circumcircle of any triangle formed. Larger area means that the tumour nuclei are widely separated from each other (less overlap)	108.1	134.0
	Delaunay: Max triangle area	It is the maximum of triangulated network area where no point (nuclei) lies within the circumcircle of any triangle formed	171.1	213.5
Tumour cluster Nuclear Dimensions	Cluster mean: Nuclear area μm^2	The area occupied by the segmented tumour cell nuclei cluster	54.7	57.9
	Cluster mean: Nuclear length μm	The length of nuclear membrane measured in tumour cluster	26.9	27.4
	Cluster mean: Nuclear max diameter μm	Maximum diameter of nuclear membrane measured in tumour cluster	9.9	10.1
	Cluster mean: Nuclear min diameter μm	Minimum diameter of nuclear membrane measured in tumour cluster	7.0	7.1
Tumour cluster Nuclear basophilia	Cluster mean: Nuclear Haematoxylin: Mean	Mean nuclear Haematoxylin optical density measured in tumour cluster	0.49	0.39
	Cluster mean: Nuclear Haematoxylin: Median	Median nuclear Haematoxylin optical density measured in tumour cluster	0.42	0.37
	Cluster mean: Nuclear Haematoxylin: Min	Minimum nuclear Haematoxylin optical density measured in tumour cluster	0.016	0.006
	Cluster mean: Nuclear Haematoxylin: Max	Maximum nuclear Haematoxylin optical density measured in tumour cluster	1.18	1.1

	Cluster mean: Nuclear Haematoxylin: Std.Dev.	Nuclear Haematoxylin optical density standard deviation measured in tumour cluster	0.24	0.17
Tumour cluster Spatial distribution analysis	Cluster mean: Delaunay: Mean distance	It is the mean of distance where no point (nuclei) lies within the circumcircle of any line formed, calculated for tumour cluster	16.6	18.5
	Cluster mean: Delaunay: Median distance	It is the median of distance where no point (nuclei) lies within the circumcircle of any line formed, calculated for tumour cluster	16.12	17.8
	Cluster mean: Delaunay: Max distance	It is the maximum of distance where no point (nuclei) lies within the circumcircle of any line formed, calculated for tumour cluster	23.8	27.5
	Cluster mean: Delaunay: Min distance	It is the minimum of distance where no point (nuclei) lies within the circumcircle of any line formed, calculated for tumour cluster	10.6	11.2
	Cluster mean: Delaunay: Mean triangle area	It is the mean of triangulated network area where no point (nuclei) lies within the circumcircle of any triangle formed for the whole tumour cluster. Larger area means that the tumour nuclei are widely separated from each other (less overlap)	107.9	132.2
	Cluster mean: Delaunay: Max triangle area	It is the maximum of triangulated network area where no point (nuclei) lies within the circumcircle of any triangle formed, calculated in tumour clusters	170.4	219.9
	Cell Area μm^2	The mean area of cells detected using Cellpose algorithm	100.6	123.0
	Nuclear/Cell ratio	The ratio of nuclear area to cell area	0.54	0.51
	Cytoplasm area μm^2	cell area-nucleus area	49.8	62.1
	Nuclear/Cytoplasmic ratio	The ratio of nuclear to cytoplasmic areas	1.2	1.1

Table 5.3: Correlation between different HER2 immunohistochemical scores and cyto-morphometric features in the discovery cohort

	HER2 IHC 3+			HER2 IHC 2+				HER2-negative		
	ER-negative (n=60)	ER-positive (n=58)	P value[a]	ISH positive (n=46)	ISH negative (n=30)	P value[b]	P value[c]	ER-positive/HER2 0/1+ (n=46)	Triple-negative (n=49)	P value[d]
	Mean±SD	Mean±SD		Mean±SD	Mean±SD			Mean±SD	Mean±SD	
Average total detected nuclei	2802±689.2	3192±904.9	**0.009**	3278±998	3203.1±1560	0.13	0.32	3830.3±1116	4265.5±685	**<0.001**
Average tumour nuclei	1861±550.1	2218±577.9	**0.001**	2191.1±656	2236.4±1083	0.20	0.65	2720.9±931.1	2564.5±186	**<0.001**
Average immune cells	934±537	934±735.6	0.8	1063.3±868	966±712	0.99	0.66	1061.2±879.2	1583.1±192	**0.045**
Immune cells/total cells ratio	32.9±13.0	28.1 ±13.4	**0.08**	30.6±15.1	28.1±12.8	0.91	0.60	27.3±17.1	35.4±17.1	0.828
Nuclear area μm^2	64.5±12.9	57.9± 9.6	**0.004**	60.5±16.3	58.3±10.6	0.33	0.85	50.9±7.7	58.4±10.0	**<0.001**
Nuclear area standard deviation	24.5±10.6	19.4 ±6.9	**0.002**	21.4±10.6	19.8±7.2	0.54	0.50	17.1±5.5	21.4±6.8	**0.009**
Nuclear area variance	713.5	420.6	**0.005**	572.4	446.2	0.54	0.50	321.2	491.2	**0.009**
Nuclear length μm	29.1±2.7	27.8 ±2.2	**0.006**	28.2±3.1	27.8 ±2.5	0.41	0.77	26.4±3.1	27.5±2.2	**<0.001**
Nuclear max diameter μm	10.7±.05	10.1±0.8	**0.006**	10.4±1.2	10.3 ±0.94	0.52	0.67	9.8±2.2	10.0±0.9	**<0.001**
Nuclear min diameter μm	7.5±0.6	7.23±0.61	**0.013**	7.2±0.8	7.2 ±0.61	0.26	0.87	6.8±0.5	7.1±0.5	**<0.001**
Nuclear haematoxylin optical density	0.35±0.1	0.39±0.1	0.74	0.37±0.1	0.34 ±0.1	0.72	0.19	0.68±0.8	0.4±0.1	**<0.001**
Delaunay: Mean distance	19.4±32.	17.9±2.4	**<0.001**	18.4±3.5	18.7±2.7	0.18	0.43	15.7±2.4	16.5±2.3	**<0.001**
Delaunay: Mean triangle area	145.3±33.4	122.8±33.7	**<0.001**	133.2±51.2	135.6±37.6	0.22	0.46	96.7±24.8	107.7±32.8	**<0.001**
Delaunay: Max triangle area	228.6±57.3	197.47±64.2	**0.003**	213.9± 96.8	223.8±73.1	0.24	0.29	156.9±43.6	163.7±63.6	**<0.001**

Table 5.3 continued

	HER2 IHC 3+			HER2 IHC 2+				HER2-negative		
	ER-negative (n=60)	ER-positive (n=58)	P value[a]	ISH positive (n=46)	ISH negative (n=30)	P value[b]	P value[c]	ER-positive/HER2 0/1+ (n=46)	Triple-negative (n=49)	P value[d]
	Mean±SD	Mean±SD		Mean±SD	Mean±SD			Mean±SD	Mean±SD	
Cell area um²	129.0±35.0	121.1±34.0	0.22	117.1±45.9	117.9±29.6	**0.01**	0.33	94.1±20.5	NA	**<0.001**
Nuclear/Cell ratio	0.51±0.09	0.50±0.1	0.51	0.54±0.09	0.51±0.11	**0.01**	0.13	0.55±0.08	NA	**0.095**
Cytoplasm Area	65.5±31.9	63.8±33.4	0.77	56.6±35.9	60.4±27.9	**0.007**	0.19	43.1±17.1	NA	**0.001**
Nuclear/Cytoplasmic ratio	1.1±0.49	1.08±0.6	0.80	1.28±0.45	1.12±0.48	**0.01**	0.12	1.3±0.4	NA	**0.072**

ER: Oestrogen receptor; **ISH**: Insitu hybridisation, **SD**: standard deviation

Independent Samples t-Test was used when comparing means between two independent groups

P value[a]: P value between HER2 IHC 3+/ER-negative and HER2 IHC 3+/ER-positive

P value[b]: P value between HER2 IHC 3+ and HER2 IHC 2+/ISH+

P value[c]: P value between HER2 IHC 2+/ISH+ and HER2 IHC 2+/ISH-

P value[d]: P value between HER2-positive (HRE2 IHC 3+ and 2+/ISH positive) and HER2-negative

Table 5.4: Description of the biologically relevant morphometric features in TCGA cohort.

Morphometric features	HER2-E	Luminal B	Luminal A	TNBC*
	Mean±SD/ Median (range)	Mean±SD/ Median (range)	Mean±SD/ Median (range)	Mean±SD/ Median (range)
Average total detected nuclei/case	3217 (1711-11097)	3593 (1847-12401)	3325 (2086-3989)	3495 (1732-4840)
Average tumour nuclei/case	1935 (1144-7240)	2446 (871- 9688)	1491 (1034-2019)	2383 (1233-3817)
Average immune cells/case	1292 (226-3857)	1146.9 (307-2713)	1834 (1052-2391)	1112 (361-2354)
Immune cells/total cells ratio	0.38±0.17	0.33±0.15	0.54±0.05	0.32±0.15
Nuclear area μm^2	62.5±11.9	61.5±9.4	47.5±2.1	56.37±8.6
Nuclear area SD	24.8±9.9	21.8±6.1	15.8±4.6	20.03±6.6
Nuclear area variance	748.2	513.8	268.4	441.5
Nuclear length μm	28.9±2.6	28.7±2.0	25.5±0.71	27.6±2.2
Nuclear max diameter μm	10.8±1.02	10.6±0.72	9.4±0.35	10.2±0.9
Nuclear min diameter μm	7.3±0.67	7.3±0.63	6.46±0.11	7.02±0.15
Nuclear Haematoxylin OD	0.48±0.16	0.52±0.18	0.47±0.15	0.42±0.15
Delaunay: Mean distance	21.4±3.8	17.6±1.9	17.5±2.5	17.14±1.8
Delaunay: Mean triangle area	147±51	128.1±25.0	127.6±39.0 1	113.3±24.5
Delaunay: Max triangle area	218 68.6	198.6±47.1	176.2±57.1	169.02±39.2
Cell area um²	139±36.07	118.3±32	77.9±13.8	99.5
Nuclear/Cell ratio	0.47±0.12	0.52±0.18	0.6230.4±13.30	0.3742
Cytoplasm Area	77.3±34.3	57.0±31.8	30.4±13.3	46.4280
Nuclear/Cytoplasmic ratio	1.01±0.66	1.5±1.1	1.8±0.8	1.4206

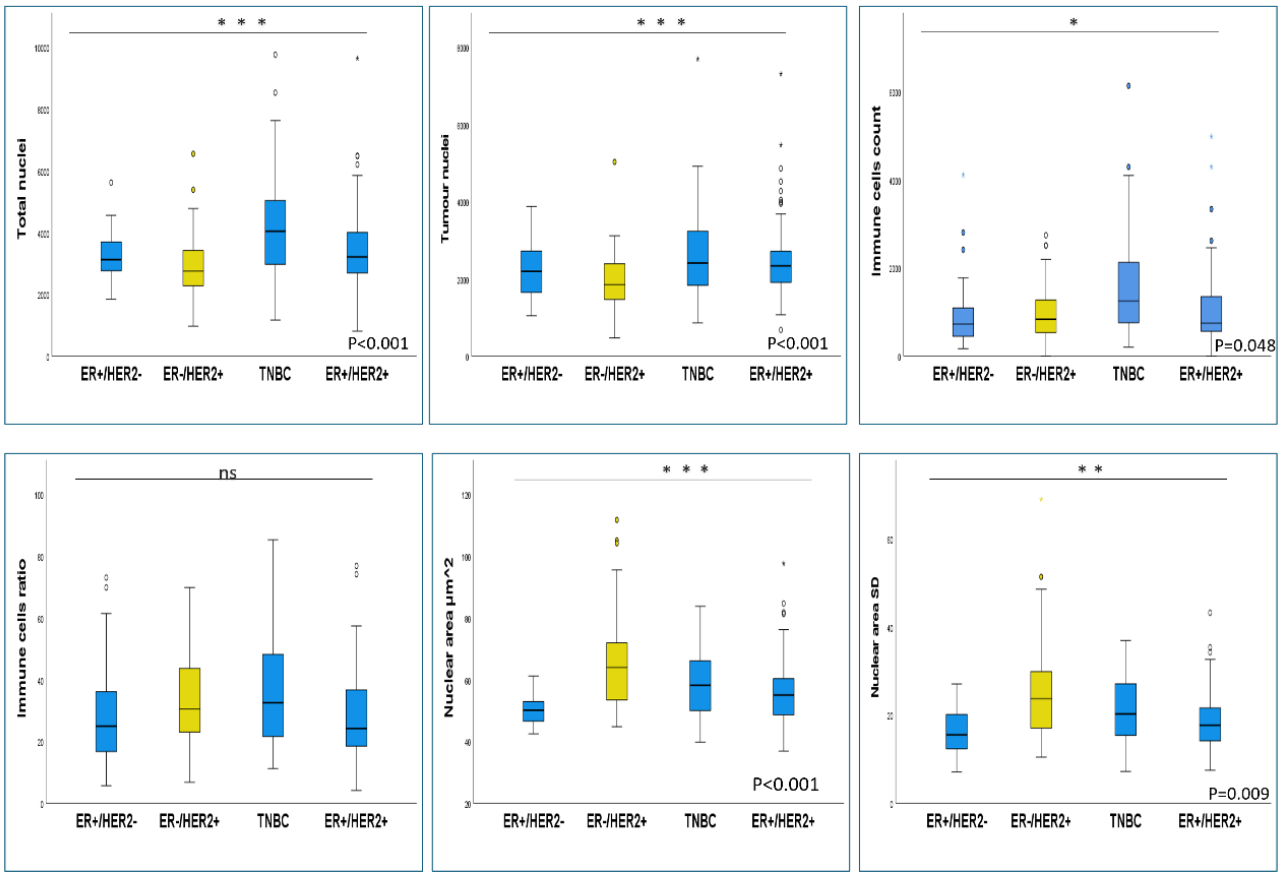
HER2-E: HER2-enriched, TNBC: Triple-negative breast cancer; **SD:** Standard deviation**; OD:** Optic density. * TNBC include both basal and normal-like subtypes

In both discovery and test cohorts, categorisation of HER2-positive cases according to HER2 IHC scores, tumours with HER2 IHC3+ showed the highest enrichment of the identified morphometric features and were significantly different from HER2-positive tumours with borderline protein expression. Within HER2 2+ tumours, no statistically significant difference in the assessed morphometric features was identified between *HER*2 gene amplified and non-amplified **(Table 5.3).** HER2-positive /ER-negative tumours were more enriched with HER2-driven morphometric features compared to HER2-positive /ER-positive tumours **(Table 5.3 and Figure 5.5 A-C)**

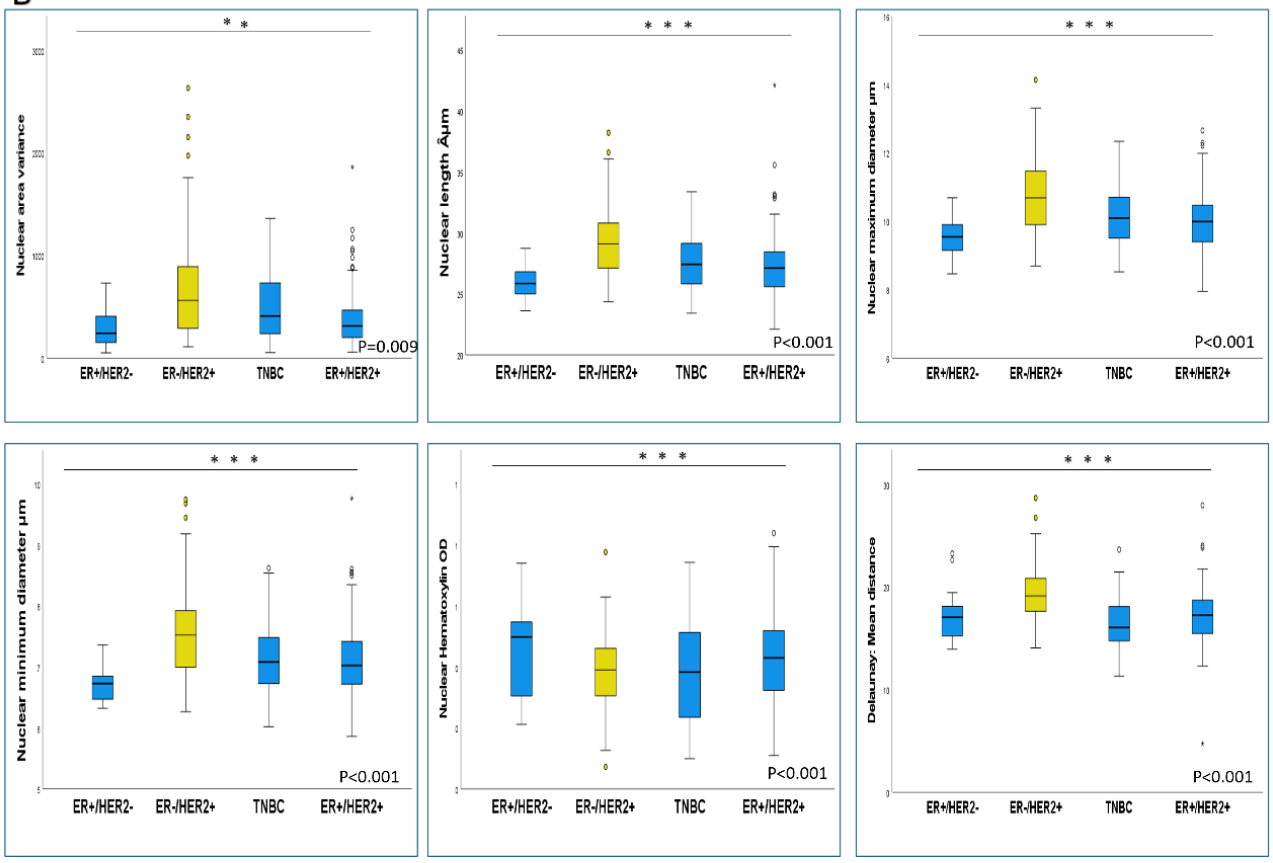
In the TCGA cohort, HER2-E subtype was significantly associated with most of HER2-driven morphometric features (15/18) compared to clinically HER2-positive / non HER2-E on PAM50 assay (**Figure 5.6 A-C**).

The hierarchical clustering of the cases in the discovery cohort using HER2-driven morphometric features as the clustering input yielded clearly defined clusters with the highest enrichment of the features obtained in HER2 IHC3+/ER-negative, and the silhouette score reached 0.65. Similar results were observed in the TCGA cohort, where the highest enrichment was seen in the HER2-E PAM50 molecular subtype with a 0.53 clustering score and compared favourably to the 0.40 clustering score obtained when applying HER2 oncogenic signalling pathway genes [224] as the clustering input instead of the morphometric features (**Figure 5.7)**. For better presentation of the heatmap, we included only the features that are positively correlated with HER2-positive tumours (10 features), excluding negatively correlated ones, to highlight the most relevant associations.

A


Total nuclei
* * *
P<0.001
Tumour nuclei
* * *
P<0.001
Immune cells count
*
P=0.048
Immune cells ratio
ns
Nuclear area µm^2
* * *
P<0.001
Nuclear area SD
* *
P=0.009
ER+/HER2-
ER-/HER2+
TNBC
ER+/HER2+

B


Nuclear area variance
* *
P=0.009
Nuclear length Âµm
* * *
P<0.001
Nuclear maximum diameter µm
* * *
P<0.001
Nuclear minimum diameter µm
* * *
P<0.001
Nuclear Hematoxylin OD
* * *
P<0.001
Delaunay: Mean distance
* * *
P<0.001
ER+/HER2-
ER-/HER2+
TNBC
ER+/HER2+

C

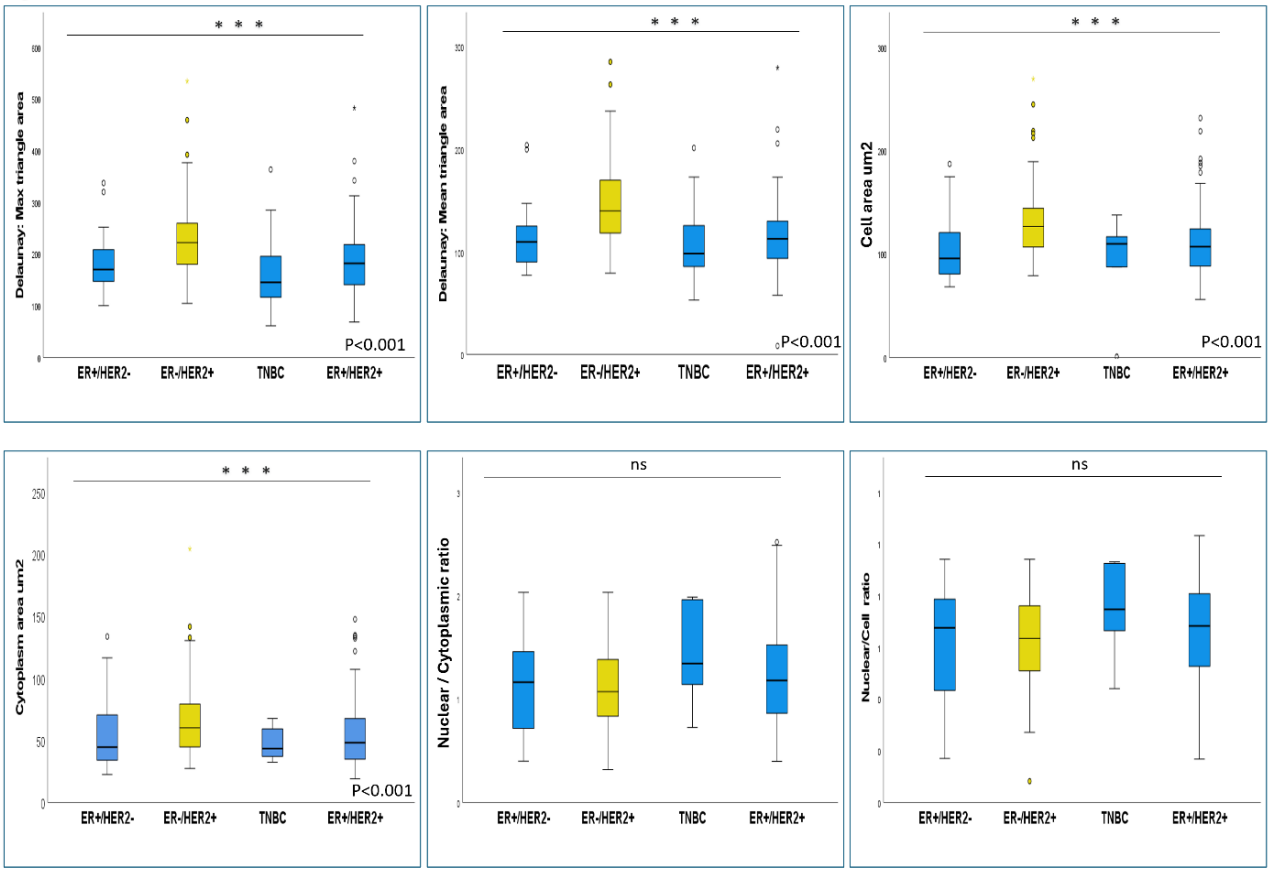
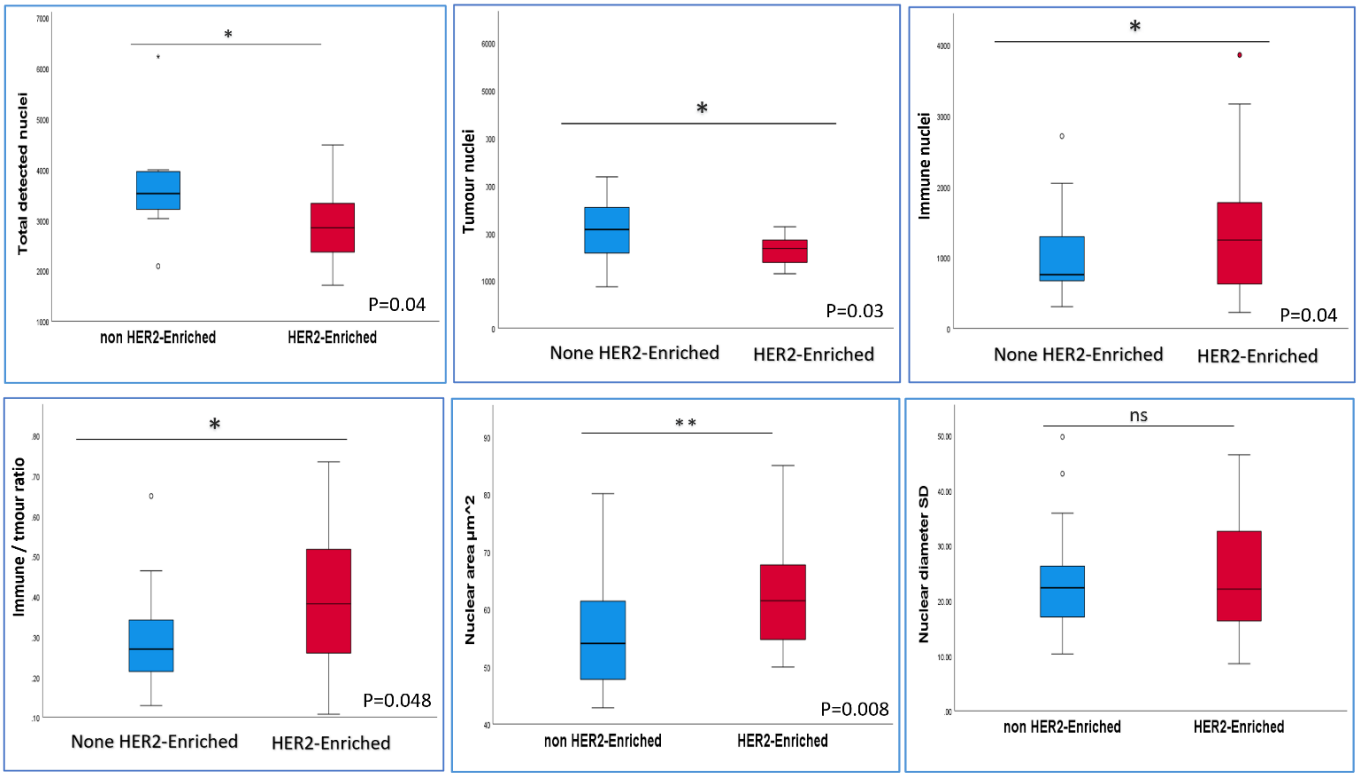
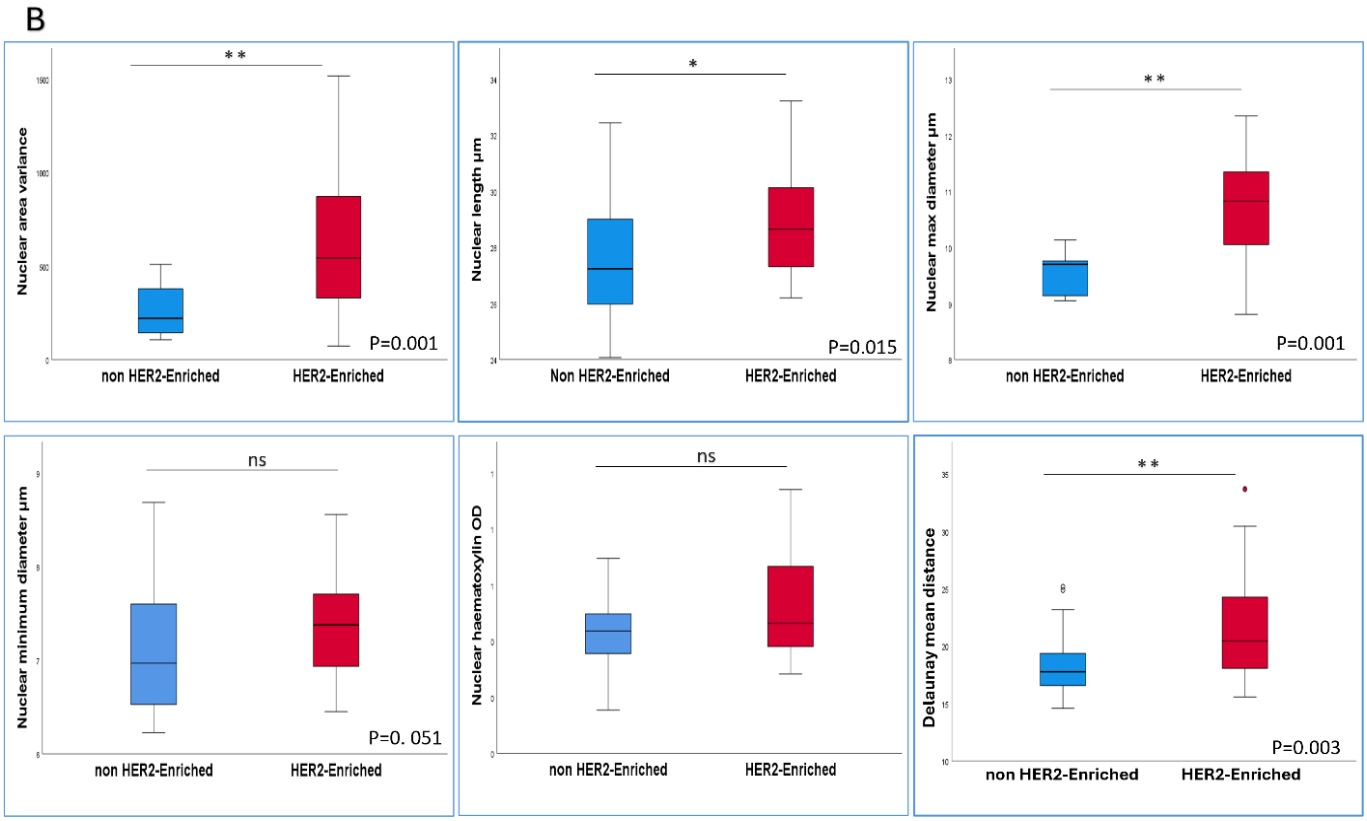


Figure 5.5: Box plot chart summarising the correlation between the significant morphometric features in the discovery cohort and different HER2 classes

A


Total detected nuclei
*
P=0.04
non HER2-Enriched
HER2-Enriched
Tumour nuclei
*
P=0.03
None HER2-Enriched
HER2-Enriched
Immune nuclei
*
P=0.04
None HER2-Enriched
HER2-Enriched
Immune / tmour ratio
*
P=0.048
None HER2-Enriched
HER2-Enriched
Nuclear area µm^2
**
P=0.008
non HER2-Enriched
HER2-Enriched
Nuclear diameter SD
ns
non HER2-Enriched
HER2-Enriched

B


Nuclear area variance
**
P=0.001
non HER2-Enriched
HER2-Enriched
Nuclear length µm
*
P=0.015
Non HER2-Enriched
HER2-Enriched
Nuclear max diameter µm
**
P=0.001
non HER2-Enriched
HER2-Enriched
Nuclear minimum diameter µm
ns
P=0. 051
non HER2-Enriched
HER2-Enriched
Nuclear haematoxylin OD
ns
non HER2-Enriched
HER2-Enriched
Delaunay mean distance
**
P=0.003
non HER2-Enriched
HER2-Enriched

C

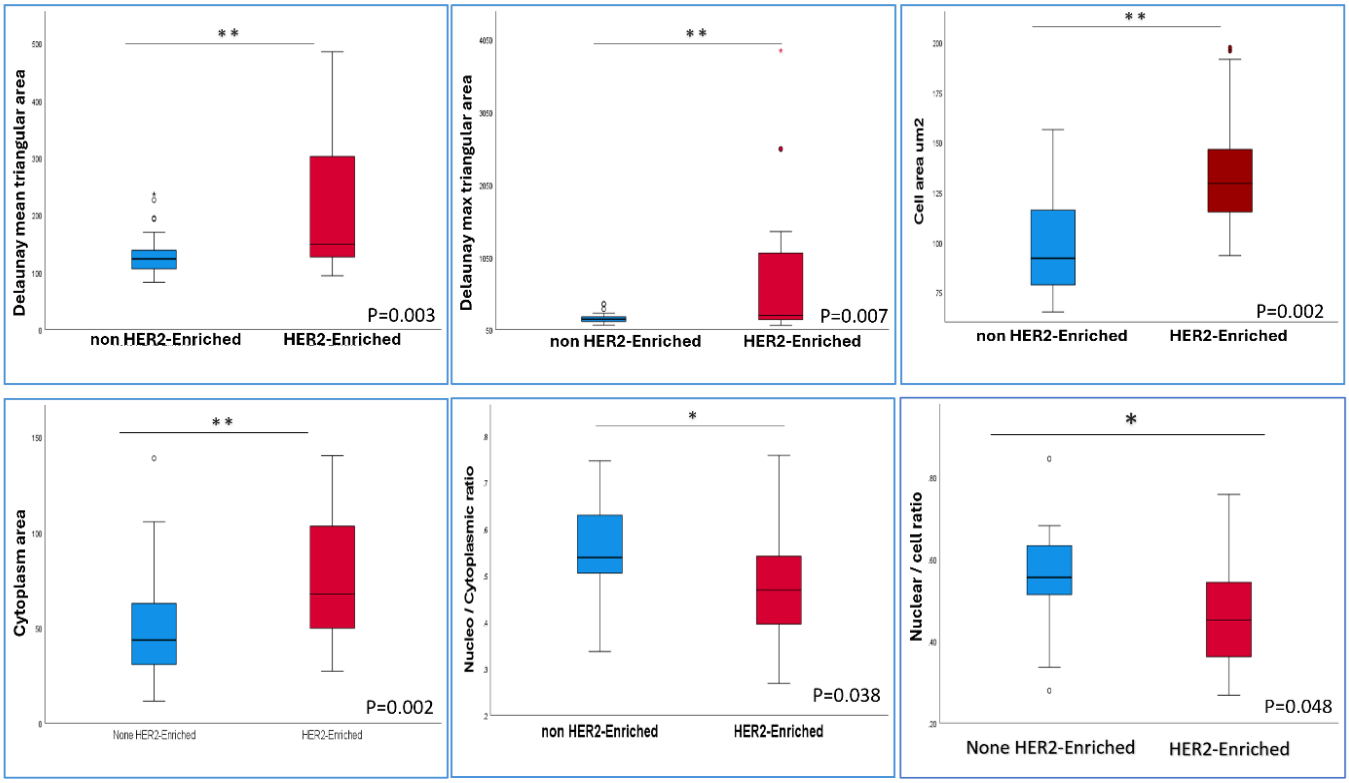


Figure 5.6:Box plot showing the correlation between the preidentified morphometric features and PAM50 HER2-enriched molecular subtype in the test cohort

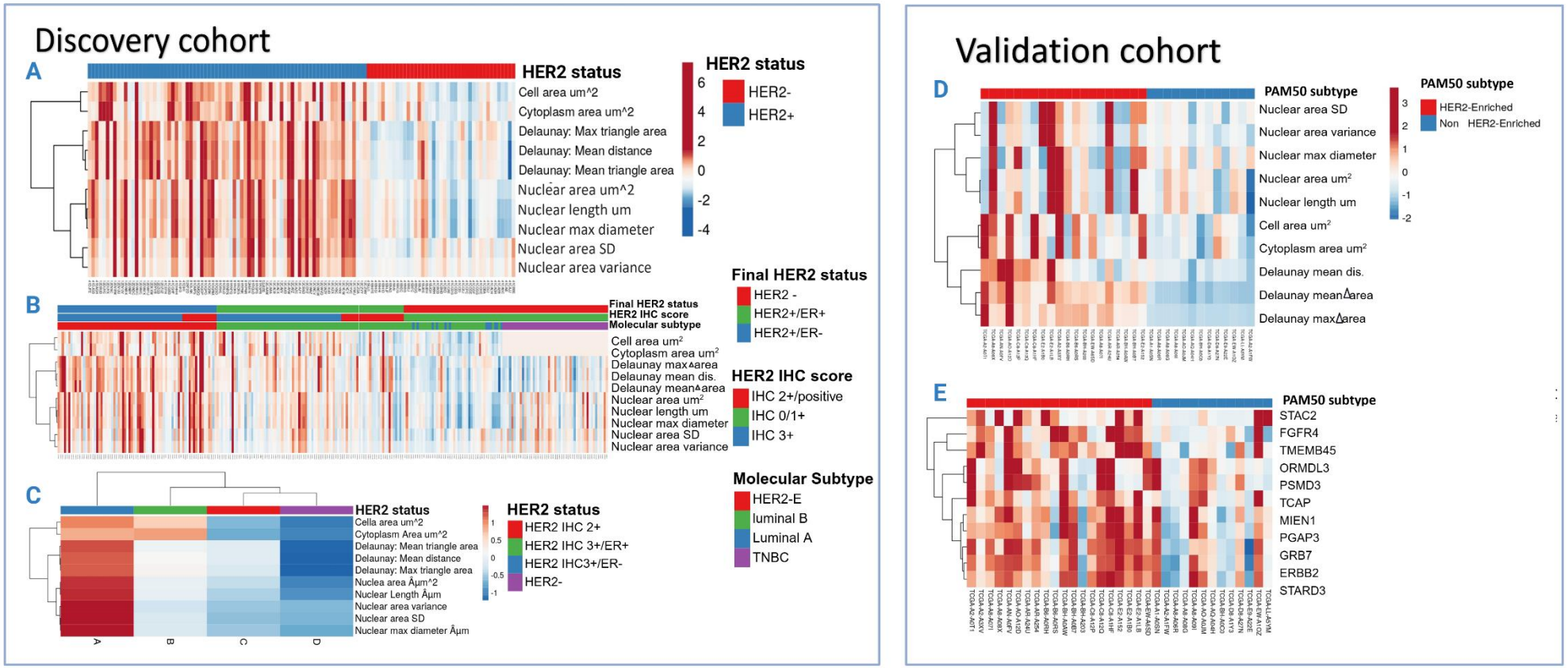


Figure 5.7: A heatmap showing how cases in the discovery and test cohorts were grouped hierarchically based on HER2-driven morphometric characteristics. A: The morphometric features allowed for a distinct separation of HER2 positive and negative. B: The panel shows the same cohort split up by ER status and HER2 IHC score. When compared to other classes, HER2 IHC3+/ER-negative tumours had a much higher enrichment of morphometric characteristics. C: Shows how the instances are grouped according to the morphometric feature's summed means for each class. Similar to HER2 oncogenic signalling genes (E), HER2-driven morphometric characteristics in the test cohort effectively segregated the PAM50 molecular subtype into HER2-E and non-HER2-E (D).

5.6.2.2 Correlation between morphometric features and clinic-pathological and molecular parameters

In HER2-positive tumours, larger internuclear spatial distribution parameters and larger cell and cytoplasmic areas were significantly associated with an increased number of metastatic LNs. Poor NPI was significantly associated with high tumour cell density and less immune/tumour cell ratio. Higher ER% in HER2-positive cases were significantly associated with decreased nuclear-related dimensions (area, length, diameter, variance) (r= - 0.4, P=0.001) and decreased intercellular spatial distances (r= - 0.34, p=0.002) (**Figure 5.8A**).

In the test cohort, there was a significant positive association between *ERBB2* mRNA and larger internuclear spatial distance (r=0.55, p<0.001), features related to larger cell and cytoplasmic area (r=0.43, p=0.01 and r=0.32, p=0.02), respectively, and less nuclear/cytoplasmic ratio (r= -0.29, p=0.03) as presented in the correlation matrix **(Figure 5.8B)**. In contrast, high *ESR1* mRNA level was significantly associated with decreased nuclear-related dimensions (p=0.01) and decreased intercellular spatial distances (p=0.02).

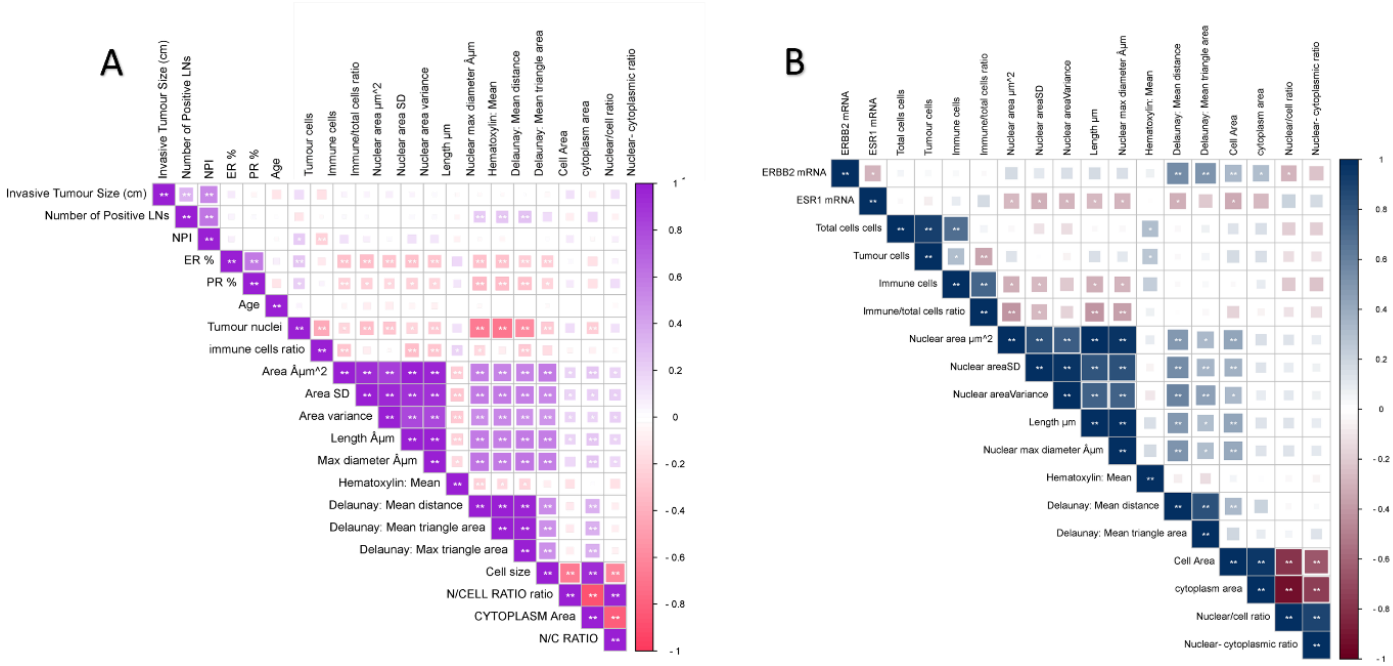


Figure 5.8: A correlation matrix demonstrates the correlation between the significant HER2 morphometric features and tumour clinicopathological parameters (A) and both *ERBB2* mRNA and *ESR1* mRNA expression levels in HER2-positive tumours (B). * Represents significant p value<0.05, ** when p value <0.01.

5.6.2.3 Visual assessment of tumour features

Seventeen visually assessed features encompassing detailed architectural and cellular morphologies that were not analysed using image analysis were evaluated. The overall inter-observer agreement was 0.75 (excellent), which entailed 0.79 for tumour architecture, 0.82 for cellular patterns, and 0.71 for both cytoplasmic eosinophilia and cell membrane distinction.

Four main features were significantly associated with HER2 positivity. Regarding tumour architecture, nested tumour pattern (both small and large) (50%) was the main one that significantly associated with HER2-positive tumours (p<0.001)., compared to large trabecular tumour pattern (18%) and large solid sheets of tumour cells. The latter was more predominant in TNBC (4% vs 30%

for HER2-positive and TNBC, respectively). For cellular patterns, a significant association was found between HER2-positive tumours and cells exhibiting polyhedral shape (p=0.03), abundant pale and foamy cytoplasm (p<0.001), and cells with distinct cellular membrane (p<0.001), compared to HER2-negative tumours (**Figure 5.9)**

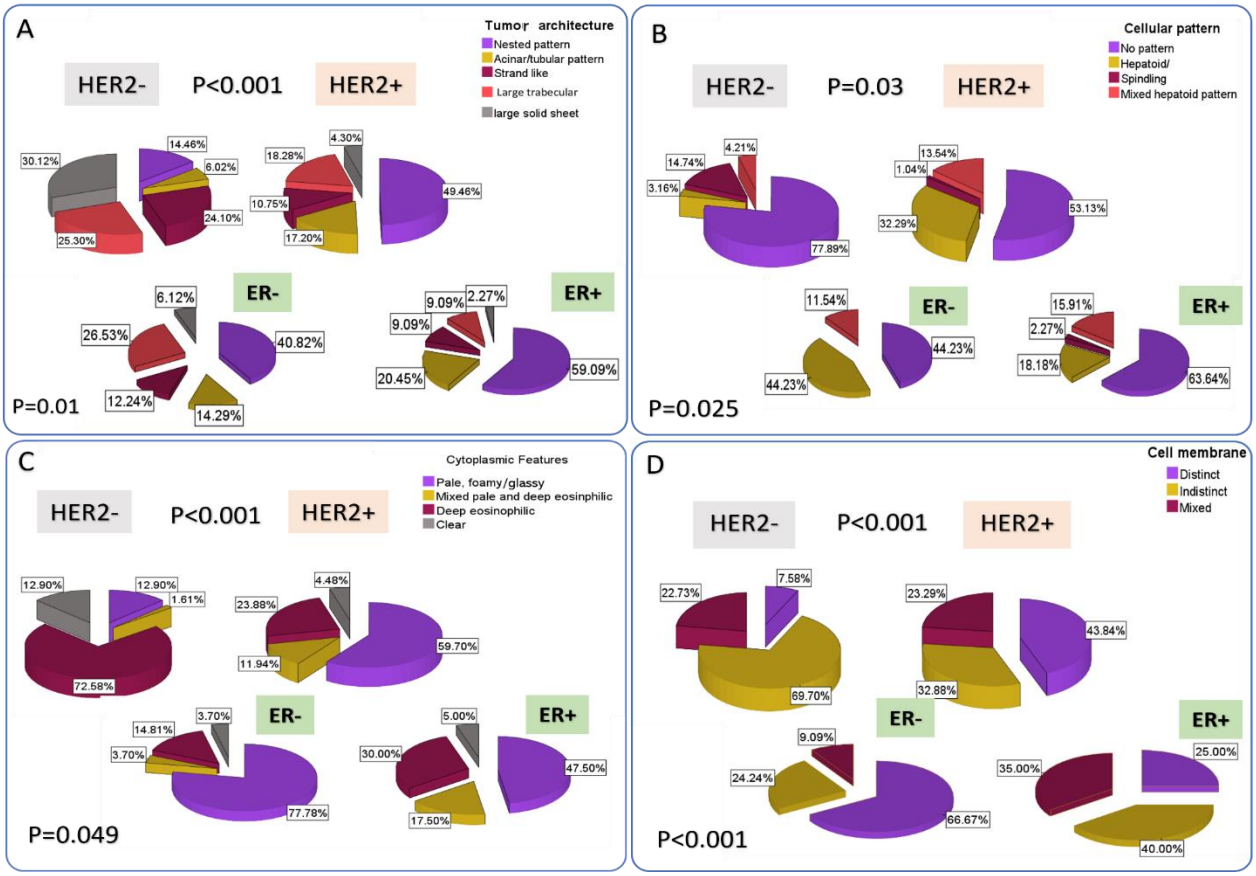


Figure 5.9: Pie chart summarising the distribution of the visually assessed features between HER2 + and HER2-negative tumours. HER2-positive tumours are significantly associated with nested tumour architecture (A), hepatoid like cellular pattern (B) with pale eosinophilic cytoplasm (C) and distinct cell membrane (D). Within HER2-positive tumours, a significant difference was also seen in the visually assessed features between ER- and ER+ cases. HER2+: HER2-positive; HER2-: HER2-negative, ER-:ER-negative; ER+: ER-positive

Through visual-based assessment of intra-tumour heterogeneity, 35% of HER2-positive tumours have mixed tumour architectures associated with heterogenous cellular patterns, “mixed architecture heterogeneity”, 12% showed mixed cytoplasmic features, 23% showed mixed cell membrane patterns. Upon stratifying HER2-positive cases according to ER status, intra-tumour mixed architecture heterogeneity and mixed cell membrane pattern were significantly associated with HER2-positive /ER-positive compared to HER2-positive /ER-negative tumours (p=0.007, p<0.001 and p=0.007, respectively).

Assessment of the features variance among different annotated tumour areas within the same case revealed that the features variance within HER2-positive /ER-negative tumours was significantly less than its corresponding within HER2-positive /ER-positive regarding, nuclear area median difference (2.1 vs 7.5, p=0.02), nuclear area SD median difference (1.02 vs 4.3, p=0.003), and nuclear area variance mean difference (68.3 vs 122, p=0.017) (**Figure 5.10).**

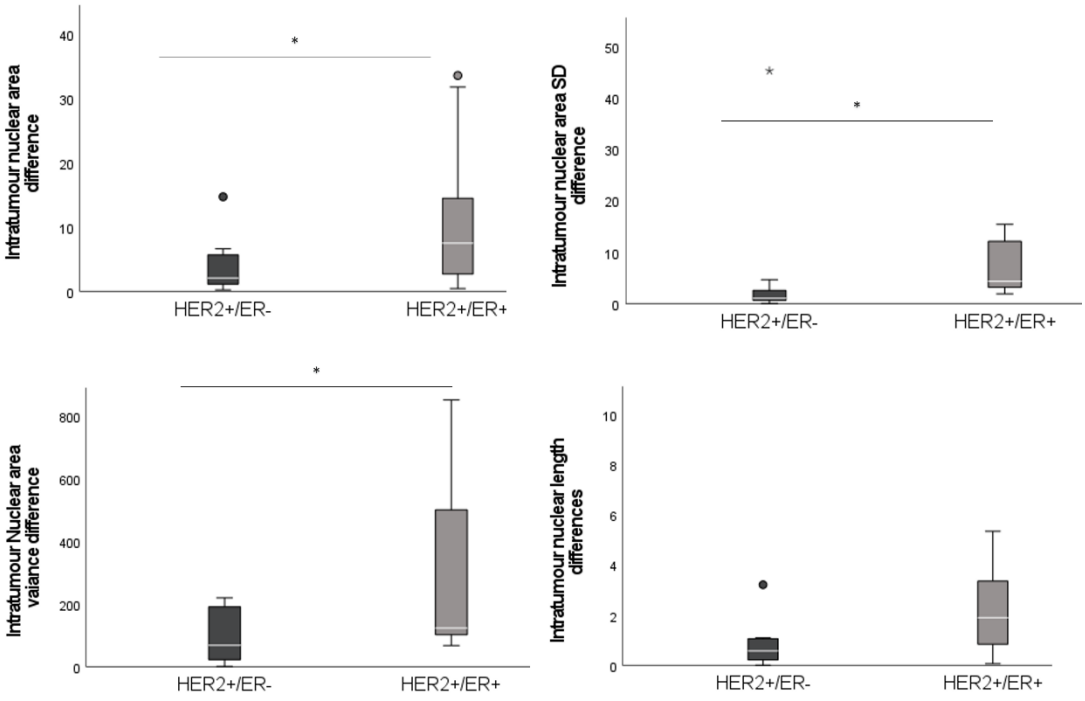
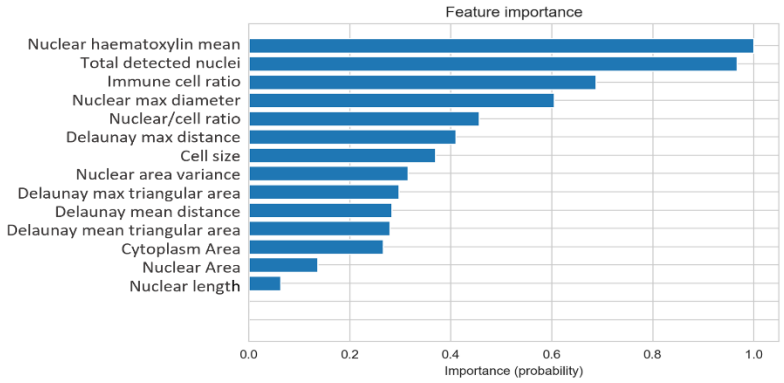


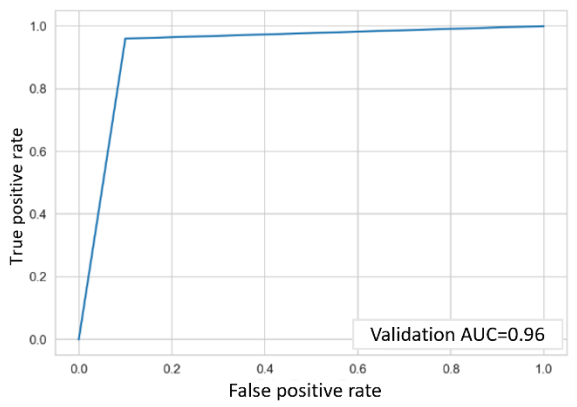
Figure 5.10: Box blot chart demonstrating intratumor heterogeneity represented by feature variance among annotated areas in HER2+ cases adjusted for ER status. HER2+: HER2-positive; ER-positive: Oestrogen receptor-positive; ER-: ER-negative.

5.6.3 HER2-driven morphometric signature and response to anti-HER2 therapy.

We ended up with 22 (18 images analysis-based and 4 visually assessed) features that are significantly correlated with HER2-positive tumours. For the development of a morphometric signature that can be used in clinical practice, a gradient boosting classifier was employed. The model was trained using continuous, non-parametric image analysis features only, as incorporating visually assessed categorical features could potentially affect the model's performance. This signature was able to predict HER2-positive tumours with 95% accuracy (AUC=0.96) in the cross-validation set and 83% (AUC=0.82) in the external test cohort (**Figure 5.11**), in comparison to *ERBB2* mRNA (AUC=0.80). Out of the 18 cyto-morphometric features, the model selected 14 based on their relevance and contribution to improving model accuracy, as demonstrated in **Figure 5.11.**



Dataset	Accuracy	Sensitivity (recall)	Specificity	Precision	F1-score	AUC
Validation	95%	93%	96%	90%	91%	0.96
Test	82%	82%	82%	84%	82%	0.82



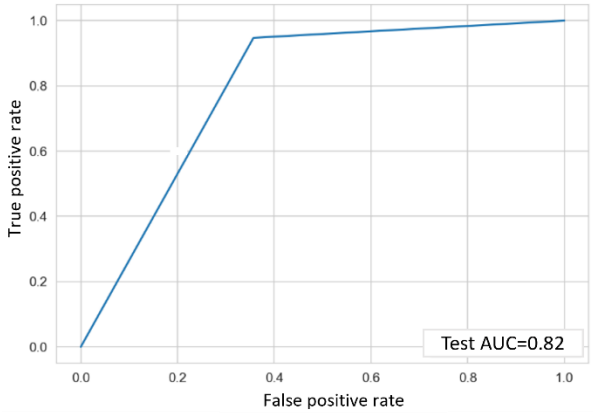


Figure 5.11: HER2 morphometric signature component and its performance. The receiver operator characteristics curves (ROC) highlight the signature accuracy in the cross validation and external test cohort. AUC: Area under the curve.

According to the probability score obtained from the model, cases were divided into either morphometric signature positive or negative. HER2-positive patients treated with adjuvant anti-HER2 therapy who had BC with positive HER2-morphometric signature had significantly longer DMFS (p=0.007, p=0.004 in the discovery and test set, respectively) **(Figure 5.12).** Contrasting this, the subset of HER2-positive patients who did not receive anti-HER2 therapy showed a significantly higher risk of recurrence when their BC displayed a positive HER2 morphometric signature (p=0.048)

In a multivariate analysis, HER2 morphometric signature was an independent predictor of prolonged DMFS post adjuvant anti-HER2 therapy when adjusted for tumour size, LN status and LVI and HER2 IHC score (HR:0.4, p=0.026, 95%CI: 0.18-0.89).

Pathway enrichment analysis revealed enrichment with ERBB signalling pathway (FDR =0.03) with upregulation of *ERBB2* gene in positive HER2-driven morphometric signature class **(Table 5.5**).

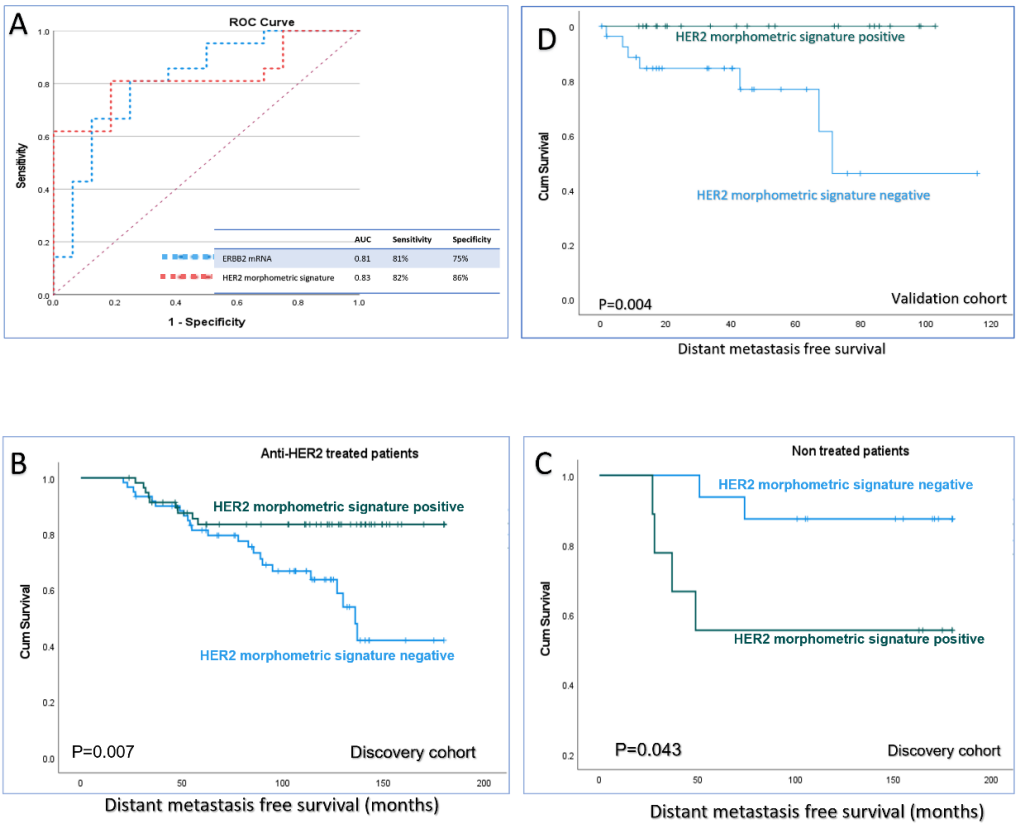


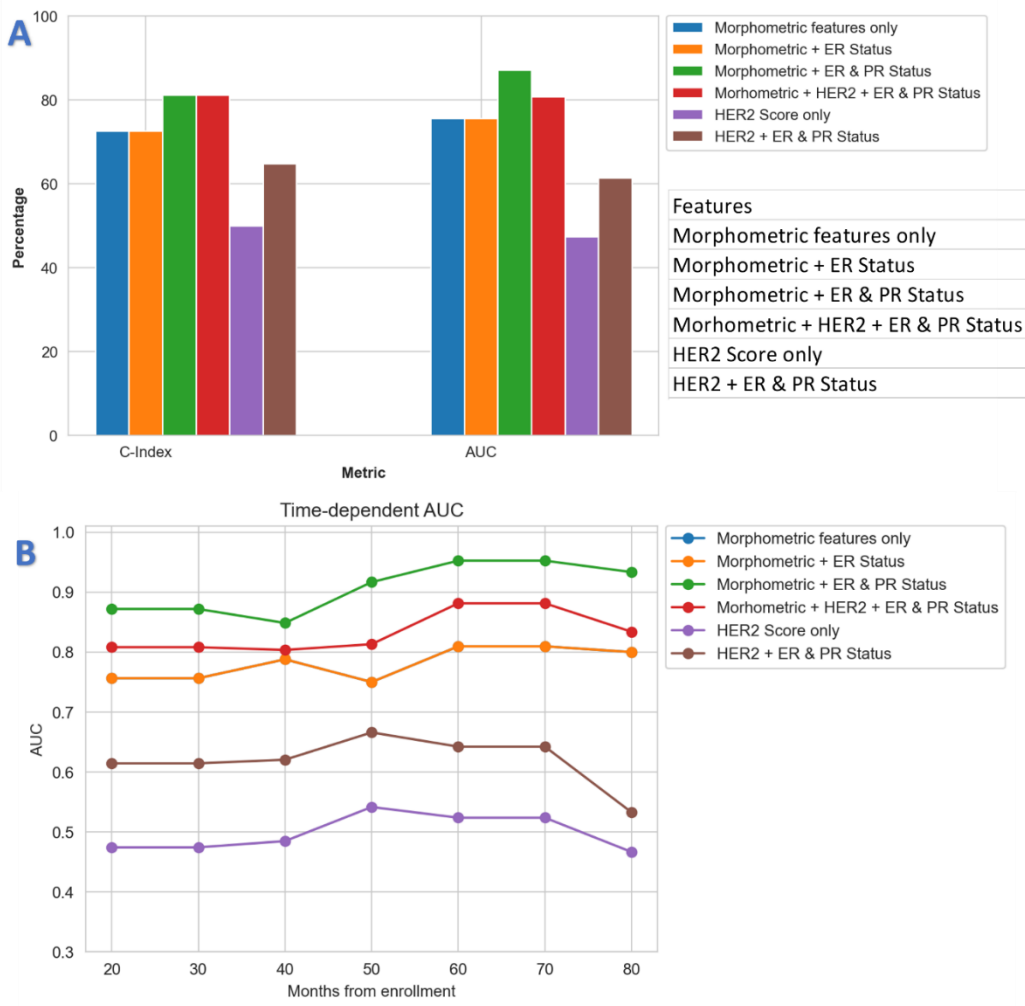
Figure 5.12: A graph demonstrating the performance and clinical significance of HER2 morphometric signature. A: Receiver-operator characteristics curve comparing between HER2 morphometric signature and *ERBB2* mRNA in the prediction of HER2-E subtype. B, D: Kaplan Meier curve showing better response of HER2 morphometric signature positive patients to anati-HER2 therapy with prolonged distant metastasis-free survival in discovery and test cohorts, respectively. While in non-treated HER2 morphometric signature-positive tumours had a higher frequency of distant metastasis (C).

Table 5.5: Pathway enrichment analysis of HER2-morphometric signature positive vs HER2-morphometric signature negative cases

Gene Set	Description	Size	FDR
hsa01522	Endocrine resistance	98	0.0028299
hsa05224	Breast cancer	147	0.0048011
hsa05205	Proteoglycans in cancer	201	0.0081827
hsa05213	Endometrial cancer	58	0.027888
hsa05223	Non-small cell lung cancer	66	0.027888
hsa04917	Prolactin signalling pathway	70	0.027888
hsa01521	EGFR tyrosine kinase inhibitor resistance	79	0.030446
hsa04012	ErbB signalling pathway	85	0.030836
hsa05215	Prostate cancer	97	0.035670
hsa05200	Pathways in cancer	526	0.042924

5.6.4 HER2-positive BC patient risk of recurrence prognostic index

HER2 IHC score (3+ versus 2+ amplified) based prognostic index shows moderate accuracy AUC=0.47) in predicting the risk of patients' recurrence, while the morphometric features achieved an AUC of 0.75. When the HER2-driven morphometric features were combined with ER and PR status (clinico-morphometric prognostic index) this achieved the highest accuracy in the prediction of risk of early recurrence in HER2-positive BC patients with C index=0.81, AUC =0.87 in the test cohort. This was better than the combined HER2 IHC score plus ER and PR status score, which achieved AUC of 0.61 **(Figure 5.13**).



Features	C-Index	AUC
Morphometric features only	0.726563	0.756417
Morphometric + ER Status	0.726563	0.756417
Morphometric + ER & PR Status	0.8125	0.871797
Morhometric + HER2 + ER & PR Status	0.8125	0.808104
HER2 Score only	0.5	0.474352
HER2 + ER & PR Status	0.648438	0.614468

Figure 5.13: HER2 risk of recurrence prognostic index. A: A bar chart demonstrating the average accuracy of each prognostic index in the test cohort. B: A time-dependent ROC curve highlighting the AUC of each index at a given time point. Both charts show that "morphometric features +ER &PR status "is the most accurate index.

5.7 DISCUSSION

HER2-positive BC constitutes approximately 15%-20% of all BC cases [535]. HER2-E BC is characterised by the highest levels of *ERBB2* mRNA, total HER2 protein, suggesting that this group has the highest activation of the HER2 signalling pathway [325, 502, 507]. However, not all clinically HER2-positive positive cases are HER2-E subtype and only 65 % fall into that category [325, 502]. Currently, every HER2-positive BC patient is eligible for anti-HER2 therapy regardless of HER2-E status, yet, the response rate varies, with 20% of patients experiencing recurrence and metastasis post-adjuvant therapy [220, 527]. Identification of HER2-positive tumours with active HER2 oncogenic activity through a clinically applicable and cost-effective tool is mandatory for the prediction of patients who would benefit the most from HER2 signalling pathway targeting therapy, both in the neoadjuvant and adjuvant settings [57, 264, 326, 507, 536]. Building upon the established morpho-molecular signature across various tumours [514-519], our aim was to delineate a collection of clinically pertinent histo-morphometric features. These features aim to reflect the extent of HER2 signalling pathway activity and establish connections between these features and response to anti-HER2 targeted therapy, incorporating digital image analysis and culminating in the development of a clinically feasible and cost-effective tool. To the best of our knowledge, there have been no prior studies aimed at characterising the activity of the HER2 oncogene, using the tumour morphological features and response to therapy.

We were able to identify a set of features highly associated with HER2-positive tumours as well as the HER2-E intrinsic subtype. Those features included large polygonal cells with larger nuclei, open phase nuclear chromatin that was

evident through the pale nuclear haematoxylin OD, more abundant pale eosinophilic cytoplasm, which reduced N/C ratio, less tumour cell density, higher immune/tumour cell ratio and wider internuclear spatial distances. This aligns with previous reports that stated that active *HER2* signalling pathway stimulate downstream cascade, increasing cell proliferation and modulation in chromatin structure to yield an open-phase chromatin [537].

We also found that HER2-positive tumour cells tend to have distinct cellular membrane and are arranged in small nested/alveolar-like patterns rather than single solid sheets that were predominant in TNBC. This was previously reported by Denisov and colleagues, who performed pathway analysis of transcripts that were differentially expressed in the different morphological structures of breast tumours and found that tumours arranged in small nests showed more considerable association with *ERBB2* pathway [531]. TNBC cells were reported to have a syncytial pattern with ill-defined cell borders compared to HER2-positive and luminal tumours [538] which was also evident in our study.

HER2-driven morphometric features were highly predominant in HER2 IHC 3+/ER-negative BC cases compared to HER2 IHC3+/ER-positive and HER2 IHC 2+ with evidence of *HER2* gene amplifications. This agrees with previous reports that stated that HER2 protein overexpression (IHC score 3+) is the key driver of *HER2* oncogenic activity and is highly enriched with *HER2* signalling pathway genes compared to borderline HER2-positive BC with evidence of gene amplification [224, 228].

The distribution of HER2-E subtype and activity of *HER2* oncogenic signalling seems to be heavily influenced by ER status, with HER2-E subtype representing only 30 % of molecular subtypes within HER2-positive / HR-positive BC [57, 264, 321, 325, 326], some authors even claimed that HER2-E subtype is predominantly ER-negative [326]. According to St. Gallen Expert Consensus, HER2-positive tumours are divided into two classes, a Luminal B-like subtype that features ER and/or PR expression and a HER2-E-like, which does not express both HR [256]. Several clinical trials and studies highlighted the bidirectional crosstalk between HER2 and ER when both receptors are expressed in BC cells [261, 266, 319-321, 327-329], and these reports concluded that HER2-positive tumours differ in main clinicopathological features and natural history of disease depending on HR expression. More specifically, HER2-positive /ER-negative tumours are more likely to present with high histologic grade and higher tumour stage, less likely to first relapse in bone and more likely to recur in brain, than HER2-positive /HR-positive [539].

The identified morphometric signature reflected both HER2-E, representing the oncogenic activity of the *HER2* signalling pathway, as well as high *ERBB2* mRNA and HER2 protein levels that represent therapeutic targets. This could explain the high accuracy obtained from the HER2-driven morphometric signature model in predicting the response of HER2-positive BC patients to HER2 pathway targeting therapy, superseding HER2 IHC score-based risk of recurrence model. The value of combined HER2-E subtype with *ERBB2* mRNA expression levels and better prediction response to anti-HER2 therapy was previously reported [507, 540].

Combining ER and PR morphometric features improved the accuracy of the risk of recurrence model. This agrees with several clinical trials and meta-analyses that demonstrated a strong association between HR status and pCR [231, 261, 508] and patient outcomes [224].

HER2 intra-tumour heterogeneity is a well-known phenomenon in BC, defined as the coexistence of subpopulations of tumour cells with different HER2 clones. This has been reported in up to 40% of BC and is more frequently associated with HR positivity and poor prognosis and was proposed to be a potential mechanism for anti-HER2 resistance [41, 541]. This was obvious in the current study, where HER2-positive /ER-positive tumours were significantly associated with high intra-tumour variance compared to HER2-positive /ER-negative tumours.

Recent advances in DP and AI have empowered us to analyse fine subcellular architectural and morphometric characteristics of tumours, offering a more comprehensive understanding of the disease. Previous studies that employed AI algorithms to predict HER2 status and response to therapy exhibited promising results [39, 374, 520-526]. However, the majority of these algorithms utilised an unsupervised data analysis approach to predict HER2 positivity rather than oncogenic signalling activity, and also lack clear explainability of the used morphological features and their clinical relevance. In contrast, our approach, which employed a biologically relevant and explainable set of morphometric features, could be used as a complementary tool for training AI algorithms in order to obtain more reproducible results. Our study had some limitations including the small number of external test cohort, but we were limited by the cases with HER2-E PAM50 molecular subtyping in TCGA dataset. We believe

that the data in this work could be validated on a larger cohort and even used for training deep learning algorithms.

In conclusion, tumour morphometric features could reflect *HER2* oncogenic activity in BC and hence response to HER2 pathway targeting therapy. The crosstalk between ER and HER2 impacted HER2 signalling activity and was reflected in the HER2-driven morphometric features and intra-tumour heterogeneity. HER2 IHC3+/ER-negative tumours were highly enriched in the HER2-driven signature among HER2-positive tumours. In clinical practice, the developed HER2-morphometric signature is a robust tool that could be used as a prognostic and a predicative indicator of HER2 oncogenic signalling activity, aggressive tumour behaviour and hence the response to HER2 pathway targeting therapy.

Figure 5.14 is a graphical illustration summarising our study

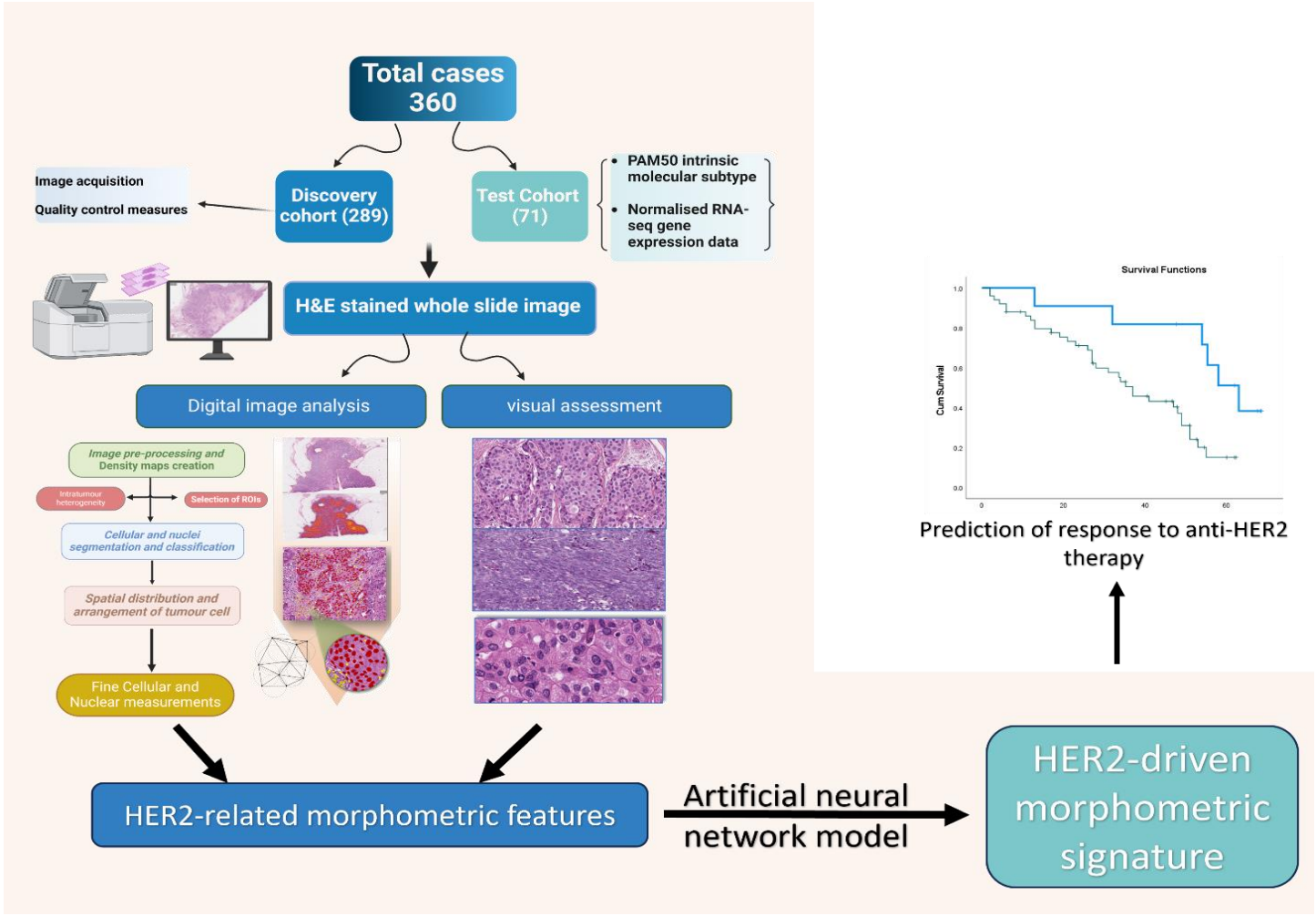


Figure 5.14: Graphical illustration summarising our study

Chapter 6. Biological and clinical characterisation of HER2-positive breast cancer

6.1 INTRODUCTION

The response rate in HER2-positive BC patients is not uniform, and predictors of response are variables and complex including protein expression level, *HER*2 gene copy number level and others [227, 320, 321].

A meta-analysis study showed that the pCR rate in HER2-positive BC after neoadjuvant therapy varied from 15 to 45% [323]. In other studies, the pCR rates ranged from 26 to 40%[262, 266, 542]. The variability in response rate among HER2-positive BC patients urged the researcher to question the actual driver of HER2 positivity is it the intensity of HER2 protein expression or the gene amplification level. Recent studies have found that pCR is better in HER2-positive BC cases overexpressing HER2 protein (IHC score 3+) than those with borderline protein expression level (IHC score 2+ with gene amplification) [228, 242, 243, 245, 246]. Furthermore, patients with HER2 IHC 3+ were reported to have longer survival than those with IHC 2+/Amplified, when treated with anti-HER2 therapy [159]. In studies comparing the response rate in relation to *HER2* gene amplification levels, some studies have indicated that the therapeutic response to anti-HER2 therapy correlates with the level of *HER2* gene amplification [542-546]. However, no association between *HER*2 gene copy number and survival was identified [266, 542, 547, 548]. In the NeoALTTO phase III clinical trial, a significant association between *HER*2 gene copy number and pCR was reported [549], but the effect of *HER2* gene amplification status ceased to have predictive value when HER2 protein expression level was considered [549]. Within the HER2 IHC2+/Amplified class, Dowsett

et al. [550] found no association between *HER*2 gene copy number or *HER*2/*CEP*17 ratio and outcome.

The crosstalk between the ER and HER2 signalling has garnered significant attention due to its implications for BC treatment and prognosis. This interaction has been extensively studied in several clinical trials, which have provided insights into the molecular underpinnings and therapeutic outcomes of HER2-positive BC [261, 266, 319-321]. Both HER2 and ER contribute to BC proliferation through a complex network of signalling pathways involving various molecular mechanisms that regulate cell growth, differentiation, and survival [322].

The complexity of the response to anti-HER2 therapy varies significantly among different ER expression groups, as documented in the literature. ER-negative HER2-positive tumours have demonstrated higher response rates to anti-HER2 therapies compared to ER-positive/HER2-positive tumours, suggesting a differential impact of ER status on treatment efficacy [323]. This observation is further supported by studies indicating that ER-negative tumours are generally more aggressive and more responsive to certain chemotherapies and targeted therapies, including those targeting HER2 [324].

However, the relationship between ER status and response to anti-HER2 therapy is not straightforward. While some studies suggest that ER-positive tumours can also respond well to anti-HER2 therapies, especially when combined with hormonal treatments, other research indicates that ER-positive status may be associated with a less robust response to these therapies [324]. For instance, a study by Chen, Chen [246] found no significant relationship

between ER status and the efficacy of anti-HER2 therapy, highlighting the need for a more nuanced understanding of these interactions.

Additionally, the impact of ER status on the response to anti-HER2 therapy within different HER2-positive IHC classes has not been fully elucidated. It remains unclear how ER expression influences therapeutic outcomes in patients with varying levels of HER2 protein expression and gene amplification. Further research is needed to dissect the role of ER in modulating HER2-driven signalling pathways and to identify potential biomarkers that could more accurately predict response to therapy.

Recent advances in molecular profiling and high-throughput technologies offer new opportunities to explore these complex interactions in greater detail. By integrating genomic, transcriptomic, and proteomic data, researchers can gain a deeper understanding of the crosstalk between ER and HER2 signalling and its implications for treatment resistance and disease progression. This knowledge could ultimately inform the development of more personalized and effective therapeutic strategies for HER2-positive BC patients.

6.2 HYPOTHESIS

In this study, we hypothesised that HER2 protein overexpression is the gold standard in predicting the response to anti-HER2 targeted therapy rather than the level of gene amplification. Patients' outcomes and responses to therapy in the neoadjuvant settings were used as our gold standard to prove or decline this hypothesis.

6.3 Aims of the Study

6.3.1 Evaluate the impact of HER2 protein expression levels on treatment response and outcomes

- To compare the pCR rates between HER2 IHC 3+ and HER2 IHC 2+/Amplified BC patients undergoing anti-HER2 therapy.
- To assess survival outcomes in patients with HER2 IHC 3+ versus HER2 IHC 2+/Amplified BC treated with anti-HER2 therapy.

6.3.2 Investigate the role of *HER2* gene amplification levels:

- To analyse the correlation between *HER2* gene amplification levels and therapeutic response in BC patients receiving anti-HER2 therapy.
- To determine if *HER2* gene amplification levels alone can predict survival outcomes or if they lose predictive value when HER2 protein expression levels are considered.

6.3.3 Examine the interaction between ER status and HER2 signalling:

- To explore how ER status (ER-positive vs. ER-negative) affects the response to anti-HER2 therapy within each HER2-positive IHC class.

6.3.4 Decipher clinical, biological, and molecular signatures:

- To characterise the clinical, biological, and molecular signatures of HER2-positive IHC classes, focusing on DGE and pathway enrichment analysis.

6.3.5 Enhance personalised treatment strategies:

- To integrate findings from molecular profiling and high-throughput technologies to inform the development of more personalised and effective therapeutic strategies for HER2-positive BC patients.
- To identify potential biomarkers that could predict response to anti-HER2 therapy more accurately, aiding in the optimisation of treatment plans.

By achieving these aims, the study seeks to provide a more nuanced understanding of the determinants of response to anti-HER2 therapy, ultimately contributing to improved patient outcomes in HER2-positive BC.

6.4 MATERIALS AND METHODS

6.4.1 Study Cohort

A total of (n=10.135) invasive BC cases were initially included in this study and comprised multiple large cohorts:

- The first cohort comprised Nottingham University Hospitals (NUH) BC patients (*n*=7485). Details about this cohort are mentioned in **Section 2.1.1.**
- The second cohort was available from the publicly available BC datasets (PABCD), including TCGA, https://identifiers.org/cbioportal:brcatcga) BC cohort (*n*=855), a subset of the METABRIC, https://identifiers.org/cbioportal:brcametabric) (*n*=289) and GEO, https://www.ncbi.nlm.nih.gov/gds) (*n*=136).

  For NUH, TCGA and METABRIC, clinicopathological data, including age at diagnosis, tumour size, histological tumour grade, axillary LN status, histologic tumour type, LVI, NPI, HER2 IHC scores (0-3), *HER2* gene amplification, HR

status (including ER and PR in addition to long term follow up data was extracted from patients records. Data about treatment regimen (chemotherapy and anti-HER2) in the adjuvant settings were available from the NUH cohort, while intrinsic molecular subtypes were available through the PAM50 classification and integrative cluster subtypes in TCGA and METABRIC cohorts, respectively, as detailed in **Section 2.1.2**.

- The third cohort was derived from the previously published multicentre (MC) study of HER2-positive BC patients [227] (*n*= 1370). From that cohort, data about neoadjuvant therapy, pCR, HER2 IHC scores, *HER2* gene amplification, *HER2*/*CEP17* ratio, HR status, histologic tumour grade on the core biopsy and histologic tumour type were available. That cohort was enriched for HER2 IHC 2+/Amplified cases to assess the differential response between both HER2-positive categories in the neoadjuvant settings (**Section 2.1.1.1**).

6.4.2 CISH

- CISH assay in the NUH cohort was carried out by a former PhD student on a large number of BC cases with variable HER2 IHC scores (from 0-3+) as detailed in **Section 2.7**. Interpretation of CISH assay and *HER2* gene amplification status was carried out by the author and following ASCO/CAP guidelines [165] (**Section 2.7.1)**

  Cases without HER2 IHC score and/or gene amplification status were excluded, and the final number of cases enrolled in this study was 7254 patients, of which 1054 received neoadjuvant anti-HER2 therapy and 751 cases had data on pCR (**Figure 6.1**)

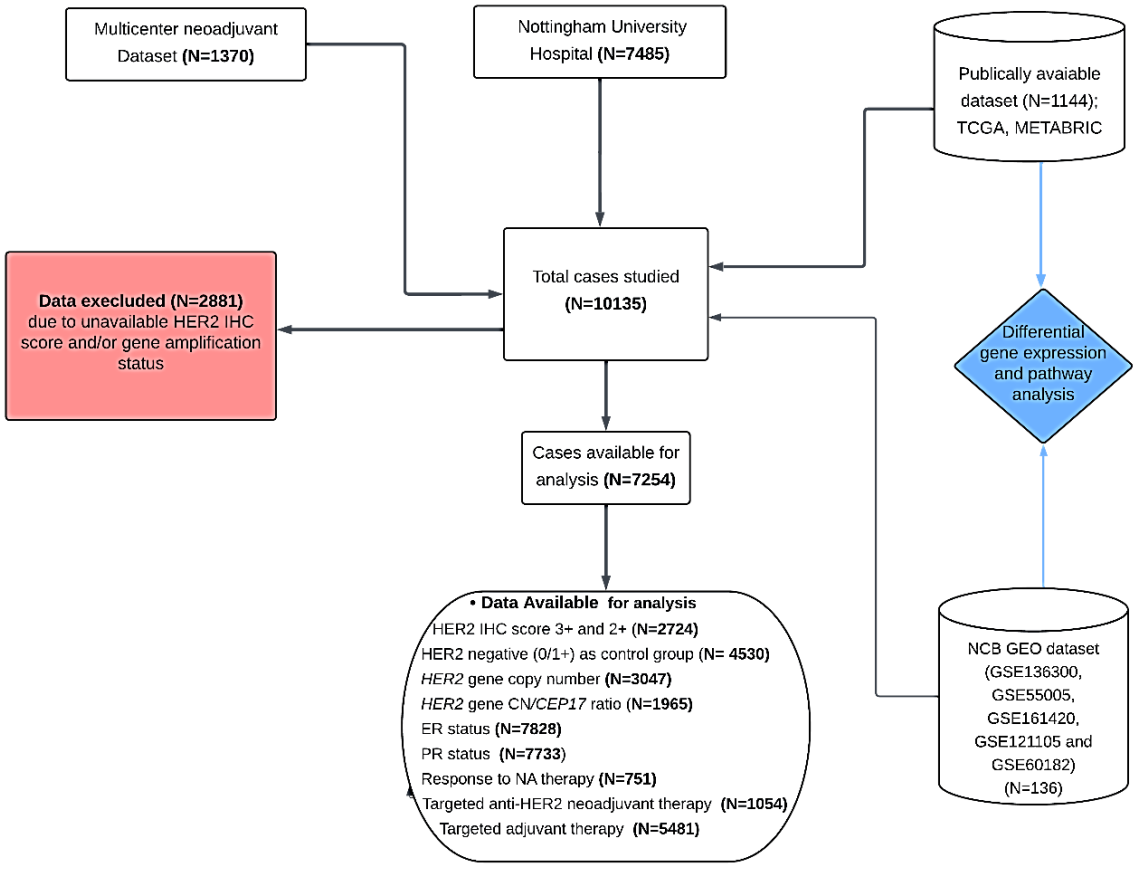


Figure 6.1: Schematic illustration of different cohorts used for this study. Cases with HER2 status only (positive/negative) and without HER2 IHC score and/or *HER2* gene amplification status were excluded from the study.

6.4.3 HER2 and HR IHC staining

HER2 and HR IHC staining was completed as part of the routine diagnostic pathway, as mentioned in **Section 2.3**. ER and PR positivity were assessed according to ASCO/CAP guidelines if ≥1% of the invasive tumour cell nuclei are immunoreactive [406]. HER2 IHC was scored in all included cohorts as positive (IHC 3+), equivocal (score 2+) or negative (score 1+/0). IHC score 2+ patients were tested for *HER2* gene amplification by FISH or CISH [141, 161].

HER2 cases with equivocal protein expression were considered positive if the HER2 gene copy number was ≥ 6.0 and/or the HER2/*CEP17* ratio was ≥ 2.0

[141]. HER2-negative BC cases defined as HER2 IHC score 2+/non amplified, and those with IHC scores 1+ and 0 were used as control groups.

6.4.4 Assessment of pathological response to neoadjuvant therapy

The response to neoadjuvant therapy was evaluated. pCR was defined as no residual invasive carcinoma in both breast and axillary LN s regardless of the presence of residual DCIS (ypT0/is ypN0) [261]. Differences in pathologic response were evaluated according to HER2 protein expression level, *HER2* gene amplification level, ER status and whether patients received anti-HER2 targeted therapy with the NACT.

To investigate the impact of the levels of *HER2* gene amplification on the pathologic response in tumours with equivocal protein expression, cases were stratified into; low (*HER2* gene copy number ≥6.0 - <9.0, and/or *HER*2/*CEP*17 ratio ≥2.0 - <4.0) [141] and high (*HER2* gene copy number ≥ 9.0 and or *HER*2/*CEP*17 ratio ≥ 4.0) amplification status. These cut-offs were based on the median of *HER2* gene copy number or *HER2/CEP17* ratio within the HER2 IHC 3+ group, which was used as a benchmark for gene amplification level in this study.

6.4.5 HER2-positive BC patients' outcome in the adjuvant settings

The correlation between HER2-positive BC classes and patients' outcomes was assessed in the combined NUH, TCGA and METABRIC cohorts. For those who received adjuvant anti-HER2 therapy using BCSS, defined as the time from the initial diagnosis to the time of BC-related death, and DMFS, defined as the time from surgery to development of distant metastasis.

6.4.6 Differential Gene Expression Analysis

HER2-positive IHC classes were identified from PABCD. DGE analysis between HER2 IHC 3+ vs IHC 2+/Amplified was carried out, and the molecular characteristics of both HER2-positive classes were analysed using gene set enrichment (GSEA) and pathway analysis. RNAseq counts were obtained from the TCGA-BRCA RNAseqV2 dataset [551]. We also accessed the METABRIC cohort on cBioPortal website [396, 552] for gene expression and clinical data. The web-based gene set enrichment analysis tool (WebGestalt) [428] was used to explore significantly enriched pathways based on the identified DEGs in HER2 2+/ISH amplified samples. Details are mentioned **in Section 2.11.1**

ER signalling pathway-related genes were identified from the Reactome pathway website reactome.org, and their enrichment among HER2-positive classes was also assessed. A heatmap was constructed for illustration of the results using ClustVis website [427]

6.4.7 Gene Expression Omnibus dataset

This was carried out to identify a set of genes responsible for HER2 pathway signalling activity as well as genes responsible for response/resistance to targeted anti-HER2 therapy.

An extensive search was carried out in the NCBI GEO dataset looking for preclinical trials, and experiments that investigated genes regulating trastuzumab response/resistance in HER2-positive tumours either on homo sapiens BC cell lines or xenografts. The raw sequencing data for this study was retrieved from the National Centre for Biotechnology Information's GEO repository under accession numbers GSE136300, GSE55005, GSE161420, GSE121105 and

GSE60182 and were exploited as discovery cohorts to identify DEGs. These datasets were composed of 136 samples divided as follows: 40 HER2-positive and trastuzumab-sensitive cell lines (BT474) and PDX samples, 57 HER2-positive and trastuzumab-resistant cell lines and PDX samples) and 12 samples HER2-positive BT474 cell lines undergone HER2siRNA knockdown **(Table 6.1)**. All these samples were processed using the Illumina HiSeq tool. Samples with irrelevant information (n=25) were removed before analysis. Further details are mentioned in **Section 2.11.1**

6.4.7.1 HER2 oncogenic pathway signalling genes.

The DEseq2 tool in R software (version 3.4.3; https://cran.r-project.org/) was used for differential analysis of gene expression. DGE was carried out on in HER2-positive samples before and after HER2 knockdown by siRNA. We integrated our results with gene expression analysis of different HER2 IHC scores (HER2 IHC 3+ vs IHC 2+/Amplified and HER2 IHC2+/non amplified) from TCGA and METABRIC cohorts to identify differences in expression of HER2 signalling pathway genes between different classes of HER2 protein expression.

6.4.7.2 Anti-HER2 targeted therapy response/resistance genes

DGE in both drug-sensitive and resistant HER2-positive samples pre- and post-HER2 inhibition by trastuzumab was carried out. shrinkage estimation for dispersions and fold changes to empower the stability and interpretability of estimates. The significantly differentiating genes were identified using log2 fold change (≥±1) and FDR < 0.05 between high and low score groups, and valid DEGs were visualised via Venn graphs. Details are in **Section 2.11**

Table 6.1: Summary of GEO datasets used in this study.

GEO dataset	Study title	Platform	Overall samples
GSE60182	Integrative transcriptome-wide analyses reveal critical HER2-regulated mRNAs and lincRNAs in HER2-positive BC	Illumina HiSeq 2000	12
GSE121105	RNA sequencing of BT474 cells treated with trastuzumab or trastuzumab + pertuzumab and BT474-derived cells resistant to trastuzumab or trastuzumab + pertuzumab	Illumina HiSeq 2000	21
GSE136300	Deep sequencing of GSK-126 treated HER2-positive PDX tumours	Illumina HiSeq 2500	4
GSE55005	mRNA profiling reveals determinants of trastuzumab efficiency in HER2-positive BC.	Illumina HiSeq 2000	63
GSE161420	Divergent resistance mechanisms to HER2-targeted therapies in BC (bulkRNA-Seq and Exome-Seq)	Illumina NextSeq 500	36

6.4.8 Statistical Analysis

Statistical package of social science (IBM-SPSS) statistical software v. 28.0 (SPSS, Chicago, IL, USA) was used to carry out the statistical analysis. Correlations between HER2 IHC scores, pCR and clinicopathologic parameters were analysed using Chi-square ($\chi 2$) test, Fisher's exact test, Kruskal–Wallis where appropriate. Univariate and multivariable logistic regression analyses were performed to investigate the association of each variable with pCR and the effect of other confounders. Odds ratios and 95% CIs were calculated for each variable. Outcome analysis was assessed using Kaplan–Meier curves and the log-rank test. The difference between gene expression among two groups was calculated through t-test or ANOVA using GraphPad software. For

all analyses, a P value of <0.05 (two-tailed) was considered statistically significant

6.5 RESULTS

Table 6.2 summarises the demographic and pathological characteristics of the included cohorts. In the whole cohort, the median value of *HER2* gene copy number was 2.0 (range 0.8 - 440) and *HER2/CEP17* ratio was 1.5 (range 0.42 - 32). When HER2-positive BC was stratified based on IHC classes, in the HER2 IHC 3+, the median *HER2* gene copy number was 9.0 (range 2 - 440) and the median *HER2/CEP17* ratio was 4.0. In HER2 IHC 2+/Amplified, the median *HER2* gene copy number was 4.4 (range 1.7-370), and *HER2/CEP17* ratio was 2.3, respectively. Eighty per cent of HER2 IHC2+ were ER positive compared to 60% in HER2 IHC 3+.

There was a significant correlation between HER2 IHC 3+ and features characteristic of aggressive tumour behaviour, including larger tumour size, higher tumour grade, high NPI risk group, positive LN status and ER and PR negativity (P<0.001). These associations were maintained when IHC 3+ tumours were compared to IHC 2+/Amplified BC (**Table 6.3**).

Table 6.2: Descriptions of the basic clinicopathologic parameters in our cohort

Parameter	Cohorts for outcome analysis (NUH / TCGA / METABRIC)		Patients from neo-adjuvant cohort	
	N	**%**	***N***	**%**
Age at diagnosis (years)				
< 50	1631	24.6	392	31.7
≥ 50	4995	75.4	843	68.3
Tumour size (cm)				
< 2.0	3745	59.0	NA	
≥ 2.0	2637	41.0		
Tumour grade				
1	1079	17.6	88	6.5
2	2828	46.0	884	65.4
3	2240	36.4	379	28.1
Lymph node status				
Negative	4554	70.0	NA	
Positive	1902	30.0		
Histologic tumour type				
IDC-NST	4310	65.2	1239	90.6
ILC	798	12.1	80	5.9
Other types	1500	22.7	48	3.5
Lymphovascular Invasion				
No	4998	79.0	NA	
Yes	1340	21.0		
NPI risk group				
Good	1627	47.0	NA	
Moderate	1504	43.0		
Poor	345	10		
HER2 IHC score				
3+	550	9.3	149	10.9
2+/Amplified	254	4.3	384	28.0
2+ ISH non amplified	796	13.5	591	43.0
1+/0	4284	72.9	246	18.1

Table 6.2 continued

***HER2* gene copy number**				
<6.0	**2491**	**81.8**		
≥6.0 - <9.0	**279**	**9.2**		
≥9.0	**277**	**9.0**		
***HER2/CEP17* ratio**				
<2.0	1386	70.5		
≥2.0 - <4.0	538	27.4		
≥4.0	41	2.1		
ER status				
Negative	1208	18.2	309	25.0
Positive	5386	81.7	925	75.0
PR Status				
Negative	2193	33.4	447	38.0
Positive	4365	65.6	728	62.0
PAM50 molecular classes				
Luminal A	513	49.0		
Luminal B	221	20.0		
HER2-Enriched	86	8.0	NA	
Basal-like	184	18.0		
Normal like	48	5.0		
Integrative Cluster subtype				
Non-HER2 cluster	253	88.0	NA	
HER2 cluster	35	12.0		
Type of neoadjuvant therapy				
Chemotherapy only	NA		744	70.6
Anti-HER2 + chemotherapy			310	29.4
Adjuvant Chemotherapy				
No	4101	64.7	NA	
Yes	2234	35.3		
Adjuvant anti-HER2				
No	6122	95.4	NA	
Yes	504	4.6		
Response to neoadju therapy				
No or partial response	NA		557	74.0
Pathologic complete response			194	26.0

NUH: Nottingham university hospital; **IDC-NST:** Invasive duct carcinoma non-special type**; ILC:** Invasive lobular carcinoma**; ER:** Oestrogen receptor**; PR:** Progesterone receptor**; NPI:** Nottingham prognostic index, **IHC:** immunohistochemistry; **CEP17**: Centromeric probe for chromosome 17; some cases are missing within each parameter as they were collected from different datasets

HER2 IHC 3+ tumours showed significant association with HER2-E molecular subtype as compared to 2+/Amplified (64% versus 25% respectively; P< 0.001). Contrasting this, when *HER2* gene copy number or *HER2/CEP17* ratio was considered, no correlation with HER2-E molecular subtype was detected **Figure 6.2.** Moreover, when HER2 IHC 2+ with high *HER*2 gene amplification level (≥ 9.0 copies) is compared to HER2 IHC 3+, HER2-E molecular subtypes and HR negativity continue to exhibit a statistically significant association with the HER2 IHC 3+ category (P=0.01, P=0.03 and P=0.008 for ER and PR, respectively).

6.5.1 Differential response of HER2-positive classes to therapy in the neoadjuvant setting

Overall, pCR rate in the whole neoadjuvant BC cohort was 26%, while in HER2-positive tumours it was 36%. When stratified based on HER2 classes, HER2 IHC 3+ tumours had significantly higher pCR than IHC 2+/Amplified (57% vs 22%) ***(***P< 0.001). In the whole HER2-positive tumour cohort, no significant difference in pCR rates between BC patients with low (< 9.0) and high (≥ 9.0) *HER2* gene copy number levels was identified (P=0.13). The same was found for patients with *HER2/CEP17* ratios ≥ 2.0 - < 4.0 or ≥ 4.0. Moreover, patients with HER2 IHC 2+ tumours and high *HER2* gene amplifi-

cation level had lower pCR rate when compared with all HER2 IHC 3+ tumours regardless of their gene amplification levels (17% vs 57%, P=0.001). Considering the whole spectrum of HER2 expression, there was a significant positive association between pCR and HER2/CEP17 ratio (P=0.0.03). However, significance was lost within patients with IHC 2+/Amplified tumours (P=0.5). **Figure 6.3** summarises pCR at different *HER* gene copy number amplification levels scenarios.

Table 6.3: Correlation between clinicopathologic parameters and HER2 IHC scores

Parameter	Cohorts for outcome analysis (NUH/TCGA/METABRIC)							Patients from Neoadjuvant cohort				
	IHC 3+	IHC 2+/Ampli-fied	IHC 2+/non ampli-fied	IHC 0/1+	*P* value[a]	*P* val-ue[b]	*P* value[c]	IHC 3+	IHC 2+/Ampli-fied	HER2-nega-tive	*P* val-ue[a]	*P* val-ue[b]
	N (%)	*N* (%)	*N* (%)	*N* (%)				*N* (%)	*N* (%)	*N* (%)		
Age at diagnosis												
<50 years	177 (32)	76 (30)	163 (20)	1007 (23)	X^2=30.8	X^2=2.40	X^2=9.7	63 (42)	113 (31)	215 (30)	X^2=53.4	X^2=6.4
≥50 years	373 (68)	178 (70)	633 (80)	3277 (77)	**<0.001**	0.121	**0.002**	86 (58)	256 (69)	501 (69)	**0.01**	**<0.011**
Tumour size												
<2 cm	300 (56)	134 (55)	444 (58)	2567 (61)	X^2=8.51	X^2=0.15	X^2=0.93	N/A	N/A	N/A		
≥2 cm	234 (44)	111 (45)	319 (42)	1648 (39)	**0.036**	0.698	0.34					
Tumour grade												
1	6 (1)	14 (6)	121 (17)	844 (21)	X^2=229	X^2=27	X^2=50.6	2 (2)	19 (5)	66 (8)	X^2=2.02	X^2=10.6
2	146 (29)	94 (40)	388 (54)	1977 (48)	**<0.001**	**<0.001**	**<0.001**	86 (61)	267 (71)	529 (64)	0.15	**<0.001**
3	358 (70)	126 (54)	214 (30)	1302 (32)				52 (37)	92 (24)	235 (28)		
LN Status												
Negative	331 (62)	152 (62)	565 (73)	2998 (71)	X^2=28.6	X^2=0.01	X^2=11.6	N/A	N/A	N/A		
Positive	202 (38)	94 (38)	207 (27)	1238 (29)	**<0.001**	0.933	**0.001**					
Tumour type												
IDC NST	490 (89)	214 (85)	536 (68)	2592 (61)	X^2=232	X^2=10.3	X^2=47.8	142 (96)	359 (94)	735 (88)	X^2=13.9	X^2=0.4
ILC	24 (5)	7 (3)	103 (13)	560 (13)	**<0.001**	**0.006**	**<0.001**	3 (2)	17 (4)	60 (7)	**0.001**	0.52
Other types	34 (6)	32 (12)	155 (19)	1126 (26)				3 (2)	7 (2)	38 (5)		
LVI												
No	365 (70)	173 (71)	639 (81)	3331 (82)	X^2=54.8	X^2=0.10	X^2=10.8	N/A	N/A	N/A		
Yes	156 (30)	70 (29)	149 (19)	732 (18)	**<0.001**	0.749	**0.001**					
ER status												
Negative	228 (41)	55 (22)	92 (12)	675 (16)	X^2=246	X^2=30	X^2=16.4	66 (45)	50 (17)	193 (24)	X^2=39.5	X^2=37.13
Positive	321 (59)	199 (78)	704 (88)	3609 (84)	**<0.001**	**0.001**	**<0.001**	82 (55)	238 (83)	604 (76)	**<0.001**	**<0.001**
PR status												
Negative	350 (65)	101 (40)	198 (25)	1279 (30)	X^2=290	X^2=42.3	X^2=21.2	92 (62)	81 (32)	273 (35)	X^2=42.7	X^2=33.8
Positive	193 (36)	152 (60)	597 (75)	2991 (70)	**<0.001**	**0.001**	**<0.001**	56 (38)	170 (68)	502 (65)	**<0.001**	**<0.001**

Table 6.3 continued

NPI risk groups											
Low	69 (22)	52 (33)	301 (49)	1205 (50)	***X²*=113**	***X²*=7.67**	***X²*=13**	N/A	N/A	N/A	N/A	N/A
Intermediate	186 (59)	84 (54)	250 (41)	984 (41)	**<0.001**	**0.022**	**0.002**					
High	60 (19)	21 (13)	61 (10)	203 (9)								
PAM50 classes											
Non HER2 cluster	47 (51)	37 (84)	117 (98)	444 (97)	*X²*=190	*X²*=13.7	*X²*=10.2	N/A	N/A	N/A	N/A	N/A
HER2 cluster	45 (49)	7 (16)	3 (2)	15 (3)	**<0.001**	**<0.001**	**0.002**					
PAM50 classes											
Luminal A	19 (21)	15 (34.1)	68 (56.7)	226 (49)								
Luminal B	23 (25)	15 (34.1)	25 (20.8)	103 (22)	*X²*=0.96	*X²*=2.03	*X²*=1.42	N/A	N/A	N/A	N/A	N/A
HER2 E	45 (49)	7 (15.9)	3 (2.5)	15 (3)	0.327	0.154	0.232					
Basal	2 (2)	6 (13.6)	19 (15.8)	88 (19)								
Normal like	3 (3)	1 (2.3)	5 (4.2)	27 (7)								
Integrative Cluster subtype	6 (20.7)	7 (63.6)	5 (62.5)	218 (98.6	*X²*=156	*X²*=6.70	*X²*=0.02	N/A	N/A	N/A	N/A	N/A
Non HER2 cluster	23	4 (36.4)	3 (37.5)	3 (1.4))	**<0.001**	**0.010**	0.96					
HER2 cluster	(79.3)											
Type of neoadjuvant therapy	N/A	N/A	N/A	N/A	N/A	N/A	N/A					
Chemotherapy only								30 (20)	99 (39)	654 (100)	*X²*=464	*X²*=16.3
Anti-HER2 + chemo								119 (80)	150 (61)	0 (0.0)	**<0.001**	**<0.001**
Adjuvant anti-HER2 therapy												
No	261 (48)	119 (47)	780 (98)	4284 (100)	*X²*=2375	*X²*=0.03	*X²*=408	N/A	N/A	N/A	N/A	N/A
yes	289 (52)	135 (53)	16 (2)	0 (0.0)	**<0.001**	0.87	**<0.001**					
Response to therapy												
No or partial response	N/A	N/A	N/A	N/A	N/A	N/A	N/A	67 (43)	127 (78)	363 (90)	*X²*=105	*X²*=36.9
pCR								88 (57)	35 (22)	43 (10)	**<0.001**	**<0.001**

LN: Lymph node status**; IDC NST:** Invasive duct carcinoma **non**-special type**; ILC:** invasive lobular carcinoma**; LVI:** lymphovascular invasion**; pCR**: Pathologic complete response; **ER:** Oestrogen Receptors**; PR:** Progesterone receptor, **NPI:** Nottingham prognostic index; **HER2-E**: HER2 enriched. **a**: p value across all HER2 IHC scores; **b**: p value of significance between HER2 IHC 3+ and 2+/Amplified; **c**: p value of significance between HER2 IHC 2+/Amplified and 2+/non amplified. Significant p value is in bold. Some cases are missing within each parameter as they were collected from different datasets.

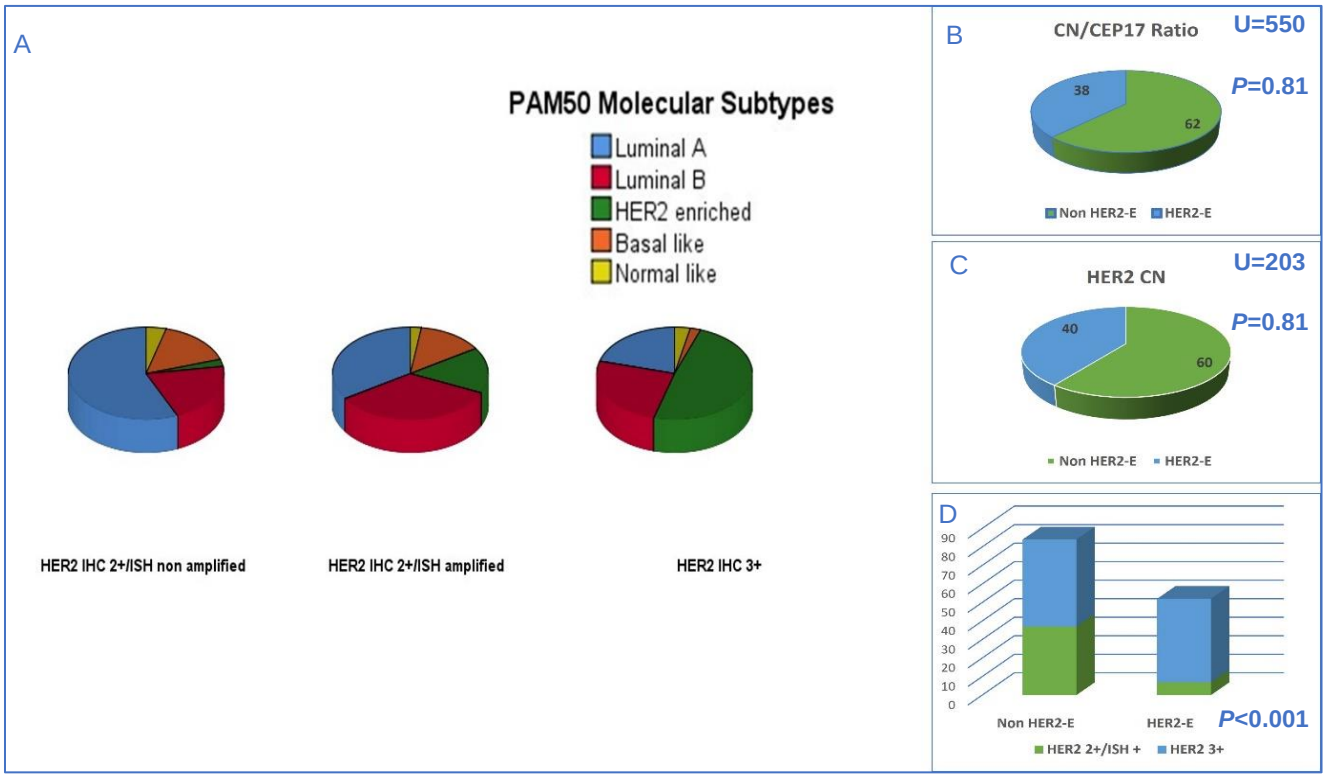


Figure 6.2: Graphical chart illustrating the distribution of PAM50 intrinsic molecular subtypes among HER2 IHC scores (A). Correlation between HER2-E molecular subtype in PAM 50 molecular subtype among HER2-positive classes and HER2/CEP17 ratio (B), HER2 gene copy number (C) and HER2 protein expression level (D). U: value of Mann Whitney test.

ER-positive tumours were significantly associated with lower rate of pCR among HER2-positive patients (33% with pCR vs 67% with no response). Within HER2 IHC 3+ BC patients, there was no statistically significant association between ER status and pCR rates, unlike BC patients with HER2 IHC 2+/Amplified where negative ER status was significantly associated with increased pCR rates (P< 0.001) **(Table 6.4 and Figure 6.4)**

Among IHC 2+/Amplified tumours, the pCR following NACT alone was 13% compared to 39% for HER2 IHC 3+ tumours. Following anti-HER2 therapy the pCR in HER2 IHC 3+ patients was augmented (57%) compared to 21% in IHC 2+/Amplified patients (**Figure 6.4)**

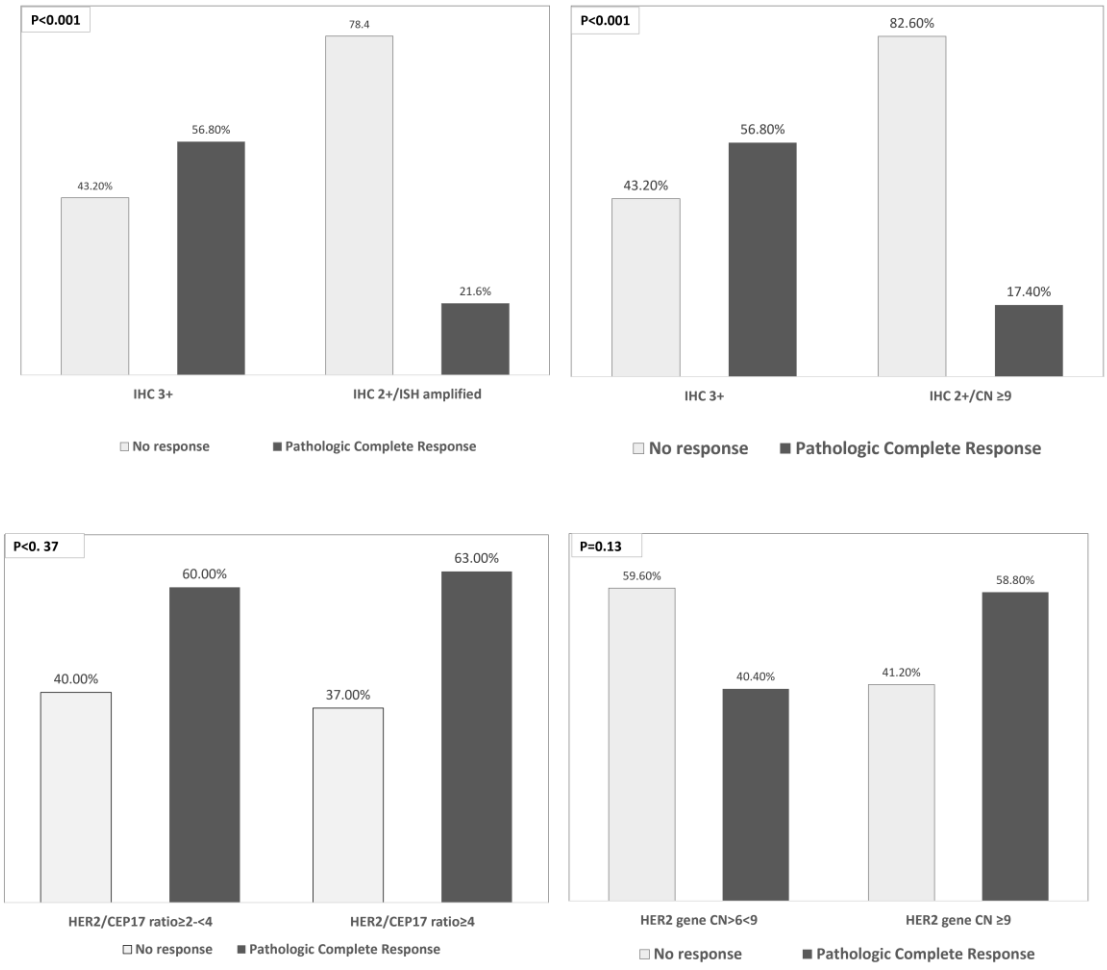


Figure 6.3: Bar chart describing the difference in pCR between HER2 IHC 3+ and 2+/Amplified based on different levels of HER2 gene amplification.

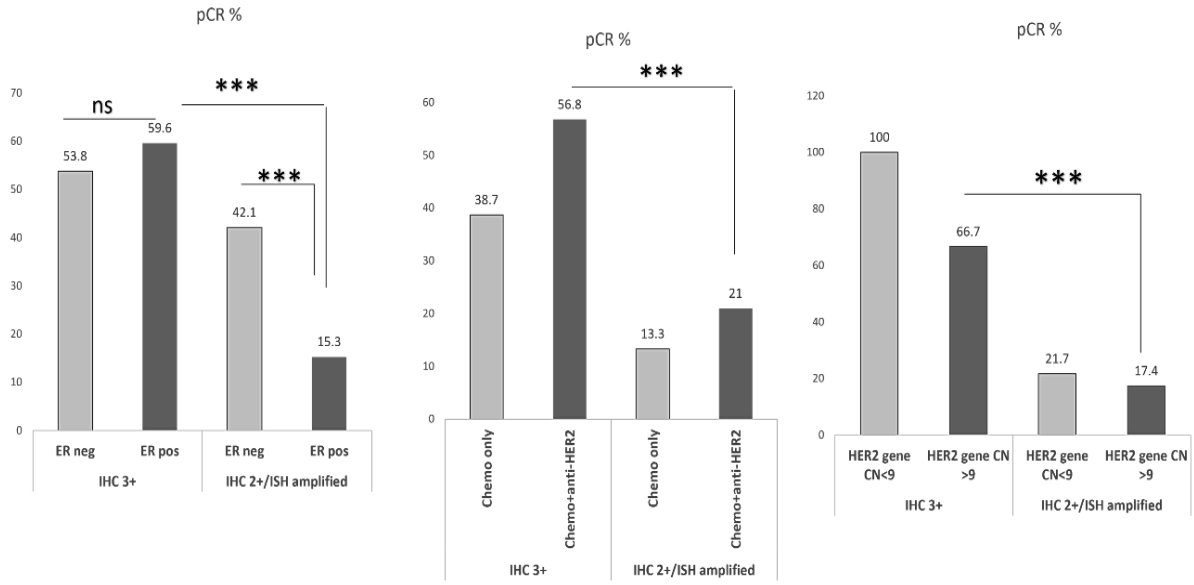


Figure 6.4: Bar chart describing the difference in pCR between HER2 IHC 3+ and 2+/Amplified based on ER status and type of therapy.

Table 6.4: Comparison between pathologic complete response-related factors within each HER2-positive category

Parameter	HER2 IHC 3+ (n=155)			HER IHC 2+/Amplified (n=162)		
	No response (*N*=67)	**pCR (*N*=88)**	***P* value**	**No response (*N*=127)**	**pCR (*N*=35)**	***P* value**
Age at diagnosis						
<50 years	24 (35.8)	40 (45.5)	1.456	51 (40.2)	14 (40)	X^2=0.00
≥50 years	43 (64.2)	48 (54.5)	0.252	76 (59.8)	21 (60)	1
Tumour grade*						
1	1 (1.5)	1 (1.3)	X^2=1.8	2 (1.6)	0 (0.0)	**X^2=8.2**
2	43 (66.2)	41 (54.7)	0.172	71 (58.2)	11 (32.4)	**0.004**
3	21 (32.3)	33 (44.0)		49 (40.2)	23 (67.6)	
Tumour type						
IDC NST						
ILC	64 (95.5)	82 (94.3)	X^2=0.1	118 (93.7)	34 (97.1)	X^2=0.63
Other special	2(3.0)	3 (3.4)	0.924	8 (6.3)	1 (2.9)	0.426
types	1(1.5)	2 (2.3)		0 (0.0)	0 (0.0)	
ER status						
Negative	30 (45.5)	35 (39.8)	X^2=0.4	22 (17.3)	16 (45.7)	**X^2=11.6**
Positive	36 (54.5)	53 (60.2)	0.513	105 (82.7)	19 (54.3)	**0.001**
PR status*						
Negative	41 (62.1)	50 (56.8)	X^2=0.4	35 (36.8)	16 (53.3)	X^2=2.57
Positive	25 (37.9)	38 (43.2)	0.62	60 (63.2)	14 (46.7)	0.109

IDC: invasive duct carcinoma, **NST:** Non-special type**, ILC:** invasive lobular carcinoma **pCR:** Pathologic complete response**; ER:** Oestrogen Receptors**; PR:** Progesterone receptor**;** * Some cases are missing within each parameter as they were collected from different datasets

Multivariate logistic regression model for factors affecting pathologic response among BC patients with over and equivocal HER2 protein expression revealed that HER2 IHC 3+ is an independent predictor of pCR over *HER2* gene amplification level; (OR, 18.00; 95%CI, 89.07-2.66; P= 0.004). Also, histologic tumour grade and ER status were an independent predictor of pCR (OR, 3.12; 95%CI, 1.60-6.00; P=0.001), (OR, 0.35; 95%CI, 0.18-0.67; P=0.001, for grade 3 and ER-positive tumours, respectively (**Figure 6.5).**

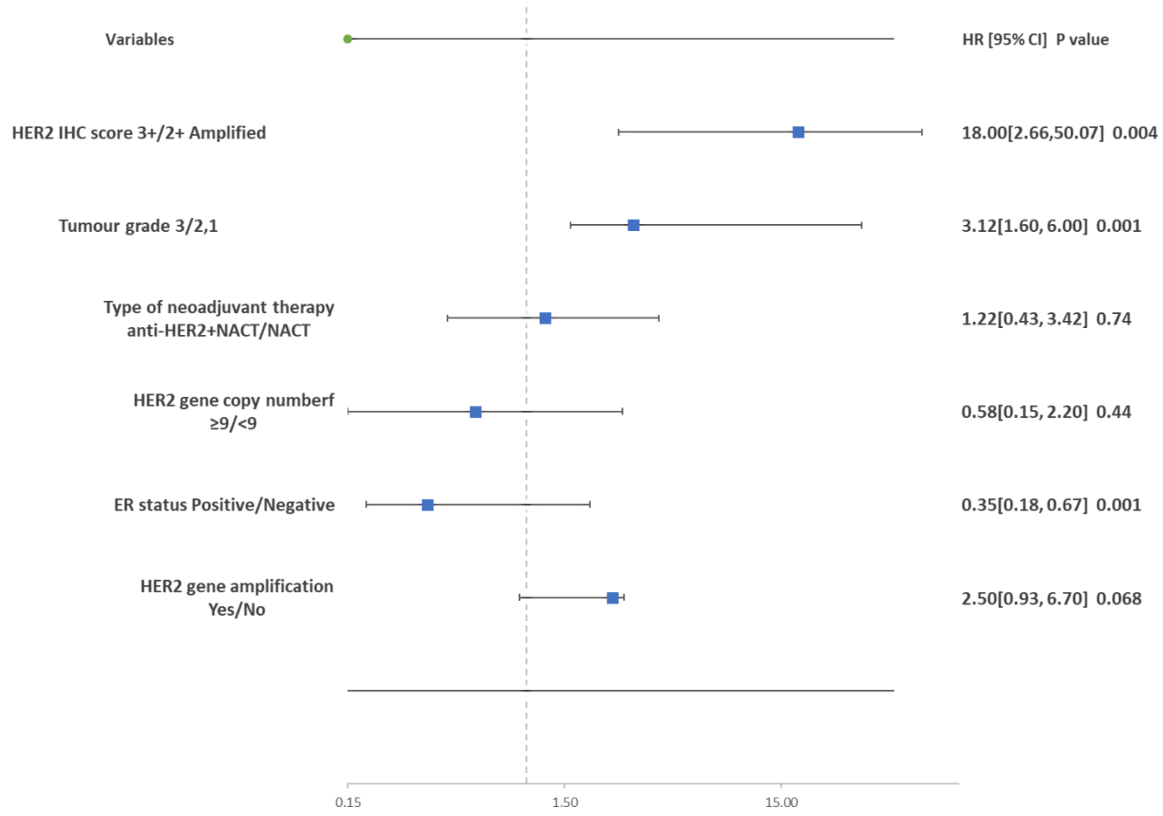


Figure 6.5: Forest plot of multivariate regression model demonstrating independent predictors of pathologic complete response between HER2 IHC 3+ and IHC 2+/Amplified. Significance value p<0.05.

6.5.2 HER2-positive groups and patients' survival.

In the chemotherapy-only treated (anti-HER2 therapy-naive) patients, HER2 IHC 3+ BC patients had significantly shorter BCSS (mean value 84 months) compared to patients with IHC 2+/Amplified tumours (mean value 119 months), (P=0.01). Following anti-HER2 therapy, the mean BCSS of HER2 IHC 3+ increased to 110 months close to IHC 2+/Amplified patients (P=0.23) **(Figure 6.6)**

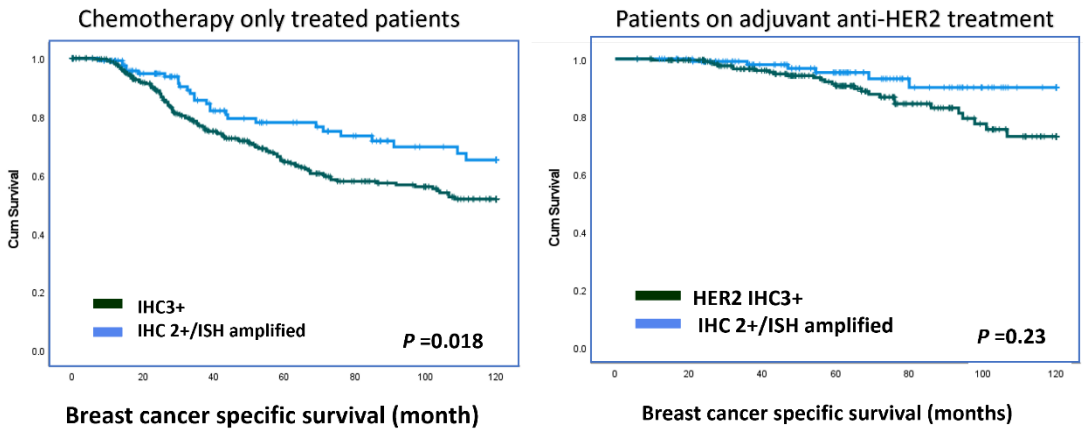


Figure 6.6: Kaplan-Meier curves showing differences in breast cancer-specific survival in HER2-positive BC patients upon administration of adjuvant anti-HER2 therapy. HER2 IHC 3+ patients who did not receive adjuvant anti-HER2 therapy have significantly worse survival compared to patients with HER2 IHC 2+/Amplified tumours (left side). No such difference between both HER2 + positive classes was detected upon treatment with anti-HER2 therapy (right side).

Among HER2 3+ BC patients, administration of adjuvant anti-HER2 in addition to chemotherapy significantly increased 10-year survival (P< 0.001 and P=0.006, for BCSS and DMFS respectively). However, in patients with HER2 IHC 2+/Amplified tumours, no significant difference in survival was observed (P=0.08 and P= 0.14, respectively) (**Figure 6.7**)

When cases were stratified based on ER expression, patients with ER-negative and HER2 IHC 2+/Amplified BC showed improved outcome upon treatment with anti-HER2 therapy (BCSS P=0.02). However, no similar improvement in the outcome was observed in the ER-positive HER2 IHC 2+/Amplified BC patients' group after receiving of anti-HER2 therapy (BCSS P=0.47) (**Figure 6.7)** Contrasting this, in IHC 3+ BC patients, the association between longer survival and anti-HER2 therapy was observed in both ER-negative and

ER-positive groups (BCSS P<0.001 and P= 0.005, for ER-negative and ER-positive, respectively).

6.5.3 Molecular profile of HER2-positive classes and its impact on response to therapy

DEGs regulated by HER2 knockdown, response, and resistance to trastuzumab were obtained from the GEO datasets. Through using screening thresholds of FDR< 0.05 and log 2-fold change|≥2.0, a total of 4960 DEGs (comprising 944 genes significantly downregulated and 4016 significantly upregulated by HER2 knockdown). 1209 genes (49 downregulated and 1160 upregulated) by trastuzumab therapy in the responsive cell lines. Also, 1094 genes were identified from DEG analysis of trastuzumab-resistant samples (111 upregulated genes and 983 downregulated). Also, DEGs of HER2 IHC 3+ vs IHC 2+ with HER2 amplification BC cases composing the TCGA database revealed 595 significantly upregulated genes in IHC 3+ and 248 significantly downregulated genes.

Genes responsible for both HER2 oncogenic signalling pathway and response to trastuzumab therapy were identified through subsequent intersection of DGE using the Venn Diagram package, 450 common DEGs were obtained.

6.5.4 Differential expression of genes responsible for HER2 oncogenic signalling

We next performed an analysis to identify genes responsible for *HER2* oncogenic signalling pathway and response to trastuzumab therapy among the 2 HER2 IHC classes (HER2 IHC3+ and 2+/Amplified) as well as in the 2+/non-amplified tumours. HER2 oncogenic signalling pathway genes were significantly enriched in HER2 IHC 3+ compared to HER2 2+/Amplified (**Figure 6.8, Table 6.5 &Table 6.6).** However, differential expression of these genes was not as significant between the two classes of equivocal HER2 protein expression (2+/Amplified and 2+/non-Amplified).

Differential analysis of genes responsible for resistance to trastuzumab therapy between HER2 IHC3+ and 2+/Amplified groups revealed 82 genes; of them, 46 genes were significantly enriched in IHC 2+/Amplified (**Figure 6.9)**. The predictive validity of those genes was tested through an online database, rocplot.org. Ten genes were significantly associated with no pathologic response to anti-HER2 therapy in HER2-positive BC **(Figure 6.10 and Table 6.7**).

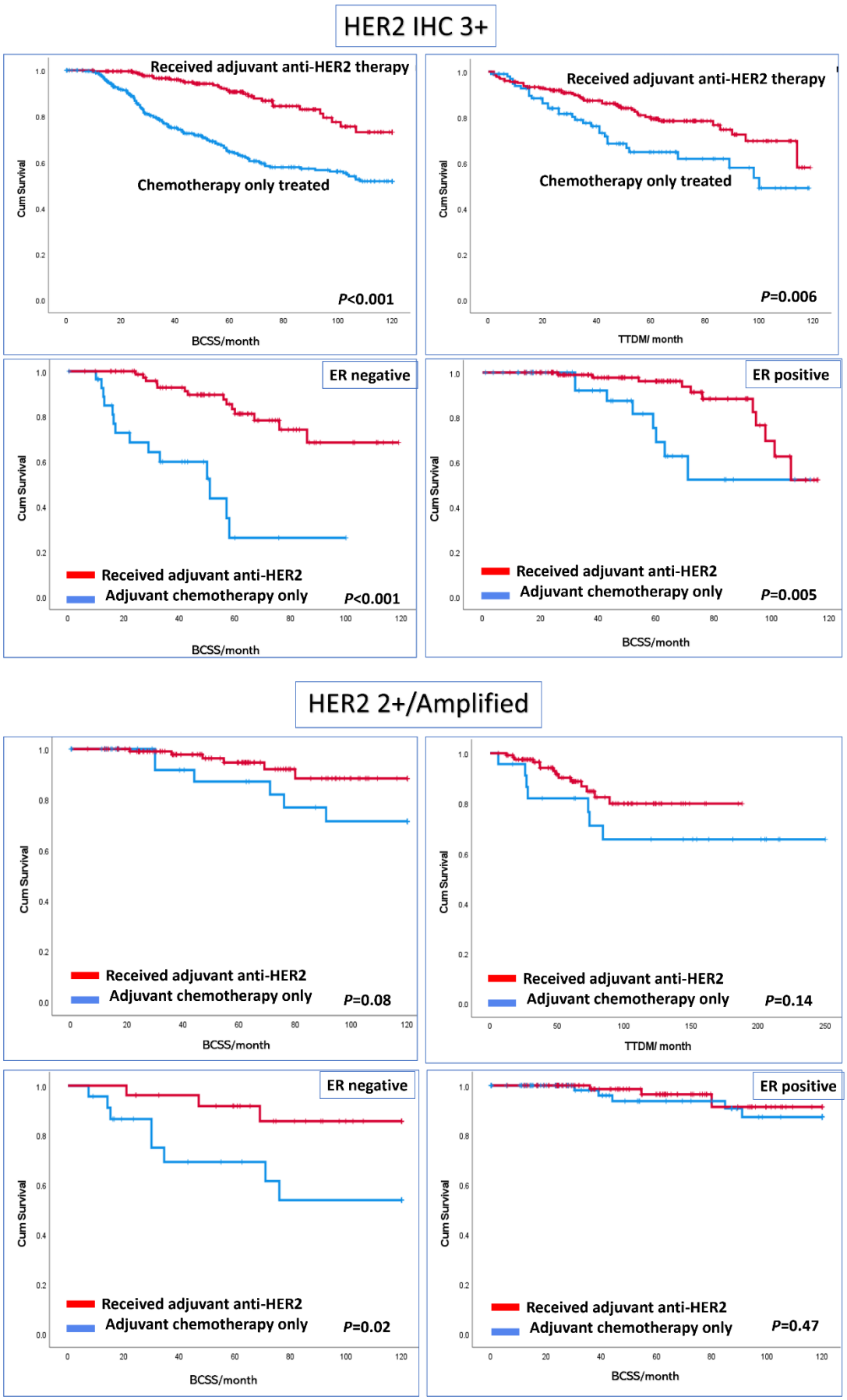

HER2 IHC 3+
Received adjuvant anti-HER2 therapy
Chemotherapy only treated
P<0.001
BCSS/month
Received adjuvant anti-HER2 therapy
Chemotherapy only treated
P=0.006
TTDM/ month
ER negative
Received adjuvant anti-HER2
Adjuvant chemotherapy only
P<0.001
BCSS/month
ER positive
Received adjuvant anti-HER2
Adjuvant chemotherapy only
P=0.005
BCSS/month
HER2 2+/Amplified
Received adjuvant anti-HER2
Adjuvant chemotherapy only
P=0.08
BCSS/month
Received adjuvant anti-HER2
Adjuvant chemotherapy only
P=0.14
TTDM/ month
ER negative
Received adjuvant anti-HER2
Adjuvant chemotherapy only
P=0.02
BCSS/month
ER positive
Received adjuvant anti-HER2
Adjuvant chemotherapy only
P=0.47
BCSS/month
Cum Survival

Figure 6.7: Survival curves showing differences in breast cancer and distant metastasis free survivals in HER2-positive BC patients upon administration of adjuvant anti-HER2 therapy. I: Kaplan-Meier curves showing the effect of addition of anti-HER2 to chemotherapy in adjuvant settings among HER2 IHC3+ patients and IHC 2+/Amplified (II). The impact of ER status on response to adjuvant anti-HER2 therapy within each group is also illustrated.

ER signalling pathway genes were significantly enriched in HER2 IHC 2+/Amplified class compared to HER2 IHC 3+ (P=0.008) (**Figure 6.11). Table 6.8** summarises the mean values of ER signalling pathway genes between BC patients with over and equivocal protein expression.

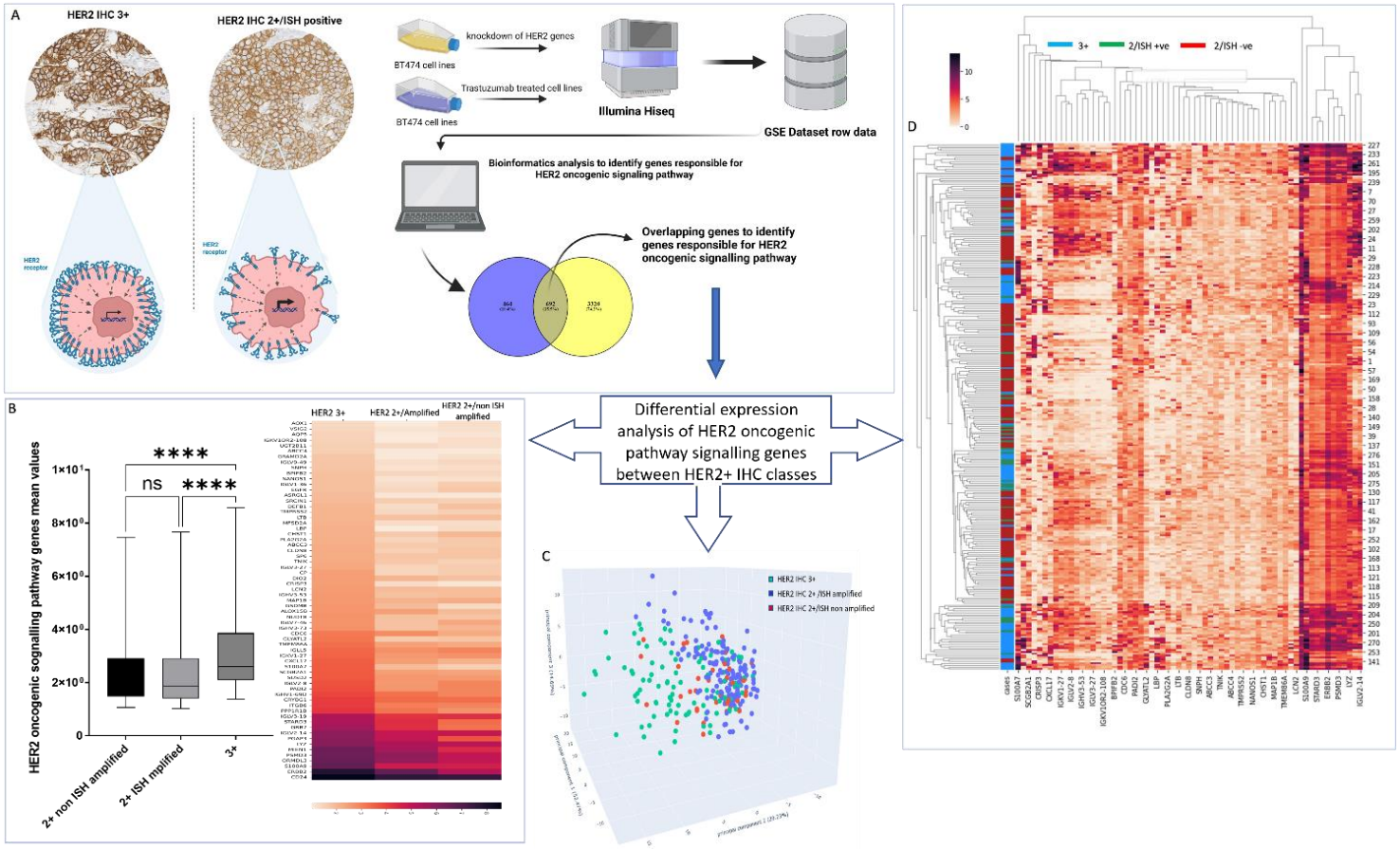


Figure 6.8: An illustrated diagram summarising the workflow that was carried out to identify the differential expression of HER2 oncogenic signalling pathway genes between HER2-positive IHC classes. A: The row data was extracted from GEO dataset and the bioinformatics analysis was carried out to identify genes responsible for HER2 oncogenic pathway and response to therapy. B: The mean values of the normalised reads of HER2 signalling genes were significantly enriched in HER2 IHC 3+ tumours compared to HER2 IHC 2+ tumours regardless of the amplification status. C, D: Unsupervised clustering analysis and heatmap illustrating the expression of HER2 oncogenic pathway genes among HER2-positive classes.

Table 6.5: Mean value of normalised reads of HER2 oncogenic pathway genes among HER2 IHC 3+ and IHC 2+ breast cancer cases

Genes	IHC 2+/ISH non-amplified	IHC 2+/Amplified	IHC 3+	*Genes*	IHC 2+/ISH non amplified	IHC 2+/Amplified	IHC 3+
CD24	7.4615	7.6577	8.5838	***ABCC3***	1.669	1.6861	2.2082
ERBB2	5.2044	6.6107	7.8527	***PLA2G2A***	1.6977	1.4536	2.1894
S100A9	4.6286	4.7450	6.6438	***CHST1***	2.0393	1.6975	2.1505
ORMDL3	5.0041	5.732	6.5724	***LBP***	1.3337	1.0422	2.1429
PSMD3	4.9683	5.840	6.4538	***MFSD2A***	1.2873	1.2820	2.1255
MIEN1	4.3863	5.444	6.4521	***LTB***	1.9119	1.8215	2.1068
LYZ	5.1293	5.357	5.9919	***TMPRSS2***	1.5916	1.4147	2.090
PGAP3	3.7096	4.922	5.8954	***DEFB1***	1.8682	1.3294	2.077
IGLV2-14	4.9534	4.923	5.8599	***SRCIN1***	1.5559	1.6315	1.957
GRB7	3.24343	4.297	5.5325	***ASRGL1***	1.0624	1.117	1.952
STARD3	3.3451	4.330	5.3596	***EGFR***	1.7506	1.4155	1.896
IGLV3-19	4.3034	4.241	5.3131	***IGLV1-36***	1.6407	1.328	1.893
PPP1R1B	2.6944	3.203	4.2062	***NANOS1***	1.2242	1.1895	1.873
ITGB6	2.93654	3.032	4.0918	***BPIFB2***	1.3989	1.4302	1.868
CRYBG1	3.3329	3.355	4.0699	***SNPH***	1.271	1.2044	1.798
PADI2	2.9143	2.612	3.8154	***GRAMD2A***	1.2293	1.0974	1.762
SUSD2	2.575	2.662	3.6183	***ABCC4***	1.0744	1.0434	1.595
SCGB2A1	2.3750	2.497	3.6054	***UGT2B11***	1.2706	1.3802	1.578
S100A7	1.5936	1.958	3.5876	***AQP5***	1.1408	1.0704	1.507
CXCL17	2.1131	2.504	3.5830	***AOX1***	1.2584	1.0256	1.377
IGLL5	2.9630	2.748	3.4171	***MAP1B***	2.2384	2.1365	2.601
TMEM86A	2.2627	2.450	3.3155	***IGHV3-53***	1.9278	1.8492	2.598
GLYATL2	1.7846	1.668	3.1624	***LCN2***	1.9057	1.9540	2.546
CDC6	2.2706	2.789	3.1424	***CRISP3***	1.1029	1.3118	2.5161
NUDT8	1.7997	1.854	2.6816	***DIO2***	1.8305	2.089	2.508
ALOX15B	1.938	2.4753	2.653	***CP***	1.660	1.4308	2.495
GSDMB	1.3816	1.9366	2.650	***TNIK***	1.5515	1.7174	2.266
CLDN8	1.7842	1.5182	2.231	***SP6***	1.7843	1.785	2.247

Table 6.6: Differential expression of HER2 oncogenic signalling pathway genes in HER2 3+ and 2+/ISH amplified.

Gene	HER2 IHC 3+ vs IHC 2+/ Amplified				
	Log2FC	Adj. p-value	*Gene*	Log2FC	Adj. p-value
LBP	4.741056	9.96E-12	***LCN2***	1.536031	0.048597
CRISP3	3.902653	4.63E-06	***ITGB6***	1.535789	0.000576
DEFB1	3.372316	3.51E-09	***ABCC3***	1.506255	1.56E-05
S100A7	3.220169	0.004167	***SP6***	1.408002	0.000021
GLYATL2	3.064741	7.58E-07	***PADI2***	1.402397	0.005749
IGLV3-19	2.801293	2.58E-06	***VSIG2***	1.365056	0.034212
BPIFB2	2.731642	0.000291	***GSDMB***	1.351141	0.000317
CP	2.689685	2.24E-05	***AOX1***	1.344447	0.0008
UGT2B11	2.521447	0.037629	***GRB7***	1.339957	5.57E-05
IGLV3-27	2.237817	0.00169	***MFSD2A***	1.309924	0.000958
PPP1R1B	2.215686	0.000411	***DIO2***	1.308746	0.001205
SCGB2A1	2.129114	0.00377	***ORMDL3***	1.27925	2.58E-06
AQP5	2.124416	0.011231	***SUSD2***	1.270081	0.004116
IGLV2-8	2.067049	0.000563	***CHST1***	1.26561	0.009022
IGKV1-27	2.051071	0.001045	***SRCIN1***	1.235233	8.48E-05
IGHV3-73	2.01872	0.001912	***CRYBG1***	1.226516	7.44E-05
ALOX15B	1.945205	0.005243	***PSMD3***	1.222795	1.11E-06
IGLV2-14	1.893144	0.003128	***ERBB2***	1.216641	0.000295
ABCC4	1.832871	2.39E-08	***TMPRSS2***	1.197538	0.004663
IGLV1-36	1.830154	0.011526	***NUDT8***	1.184327	0.005719
ASRGL1	1.807777	3.15E-06	***LTB***	1.130501	0.040735
SNPH	1.771015	0.000113	***MAP1B***	1.124583	0.000134
IGLV9-49	1.759752	0.036443	***LYZ***	1.122603	0.023888
CLDN8	1.740505	0.001261	***TNIK***	1.122322	0.002179
PLA2G2A	1.714593	0.020045	***GRAMD2A***	1.120088	0.017956
IGLV7-46	1.69965	0.00972	***TMEM86A***	1.10309	0.000128
IGLL5	1.668707	0.008595	***MIEN1***	1.099839	0.000667
IGHV1-69D	1.668479	0.027451	***PGAP3***	1.042058	0.000581
IGKV1OR2-108	1.664184	0.010735	***STARD3***	1.038876	0.000061
S100A9	1.641824	0.048763	***CD24***	1.03626	0.019456
CXCL17	1.608782	0.046585	***CDC6***	1.03592	0.004091
NANOS1	1.58542	1.93E-05	***EGFR***	1.000987	0.042764
IGHV3-53	1.550831	0.024154			

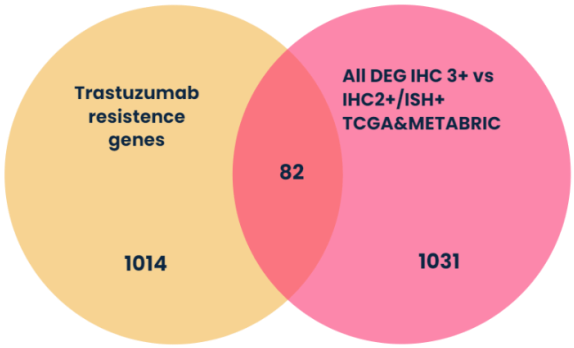


Figure 6.9: Venn diagram illustrating the intersection between trastuzumab-resistance genes in their differential expression in HER2-positive subclasses in both TCGA and METABRIC cohorts.

Table 6.7: Genes for resistance to therapy in HER2 2+/Amplified

Genes	Log2Fold changes IHC2+/Amplified VS HER2 IHC 3+	FDR	*Genes*	Log2Fold changes IHC2+/Amplified VS HER2 IHC 3+	FDR
KRT16	3.03621	2.62E-05	***FLII***	1.564564	0.01269
KRT17	2.84517	7.79E-07	***BAMBI***	1.567909	0.010412
FCRLB	2.51001	7.18E-07	***FRAS1***	1.574527	0.019385
TPRG1	2.27369	2.53E-05	***PCP4***	1.58675	0.018471
FGFBP1	2.14199	0.048339	***FOLR1***	1.596118	0.010412
KLK10	1.79999	0.024767	***UNC13D***	1.596917	0.012287
CCNP	1.6049	0.000376	***FAM38A***	1.621081	0.006492
LDHD	1.55399	1.02E-05	***CTGF***	1.652197	0.001156
GDAP1	1.35895	0.001707	***MESP1***	1.690179	0.000711
DMKN	1.35245	0.003005	***EDN1***	1.690971	0.000753
CCDC85A	1.26083	0.003935	***PHLDA1***	1.69106	0.000552
PCDH18	1.04167	0.066471	***TRIM47***	1.693506	0.000557
KCNK15	1.02264	0.058536	***EXOC7***	1.702787	0.000301
OSGIN1	1.01689	0.007347	***ZDHHC11***	1.72964	0.000225
HSPB8	1.01302	0.079203	***BASP1***	1.739613	8.15E-05
FBXO33	1.514362	0.044517	***EGR1***	1.786544	1.92E-05
ACOT4	1.515967	0.037636	***CLDN3***	1.822926	6.65E-06
ACOX3	1.535079	0.026506	***ITGB4***	1.975066	1.81E-08
CXCL14	1.538414	0.021672	***CITED4***	1.281697	1.91E-15
GOLGA7	1.540341	0.01962	***NPYIR***	1.943626	1.39E-35
GALK1	1.542148	0.019205	***GJA1***	2.147364	1.93E-05
SALL4	1.547727	0.031215	***JUN***	1.7	0.0006
DHRS3	1.551162	0.017118	***ESR1***	1.16844	0.04

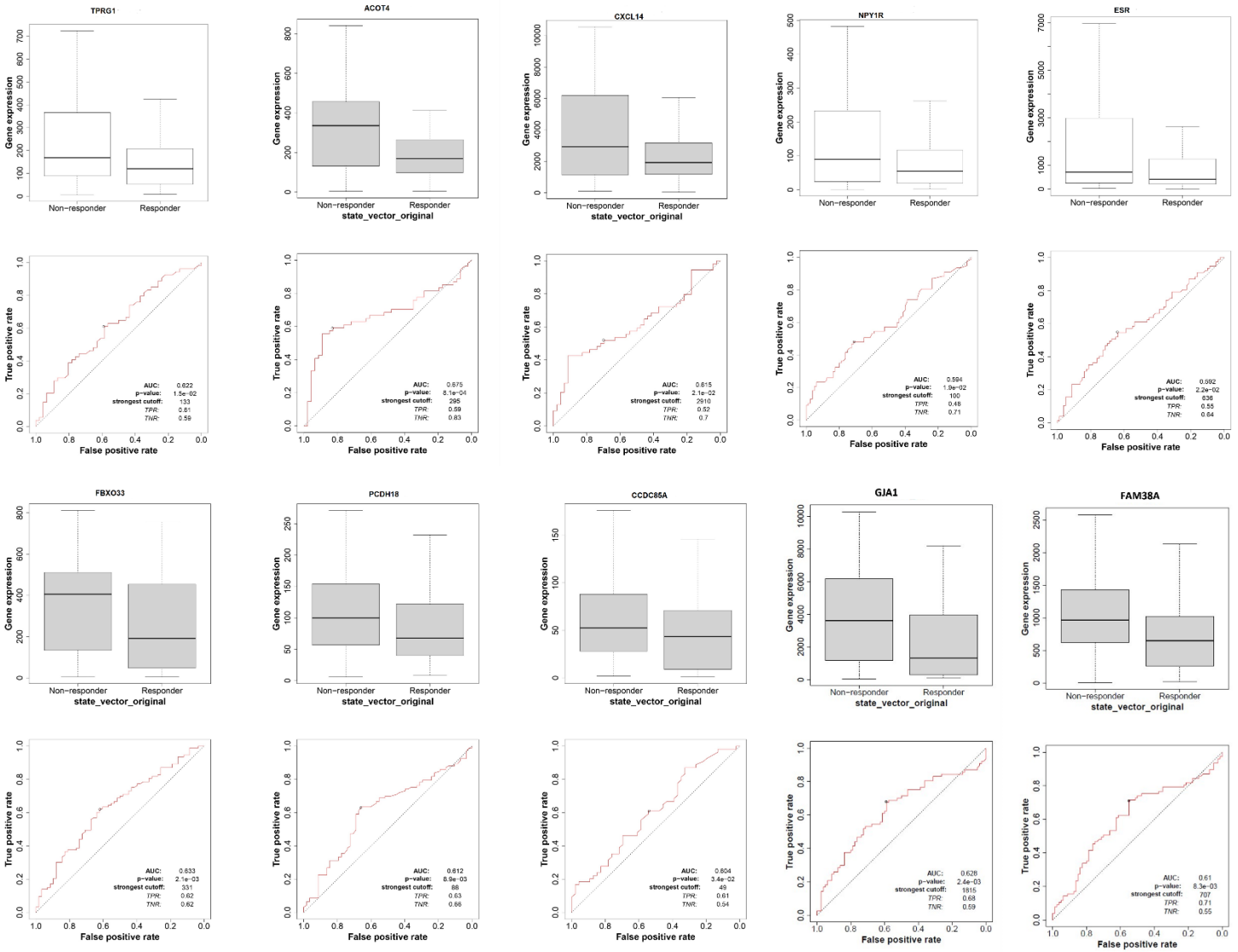


Figure 6.10: Genes identified as predictive of poor response to anti-HER2 therapy in HER2 IHC2+/Amplified breast cancer.

Table 6.8: Expression of ER signalling pathway genes in HER2-positive categories

Gene	HER2 IHC 3+		HER2 IHC 2+/Amplified	
	Mean	**SD**	**Mean**	**SD**
ESR1	5725.482	7459.408	13266.43	13670.6
GATA3	8644.592	6209.894	12202.46	8345.588
TFF3	6490.957	15816.61	10208.77	27969.83
RAD21	9105.409	5640.645	9615.069	11628.28
PTGES3	7516.685	2971.963	8010.854	1823.391
FOXA1	6911.944	2788.464	7089.799	3185.01
TFF1	4100.04	9078.617	5021.493	12122.48
MED1	8596.128	10076.01	4778.073	6702.224
KPNA2	4666.776	4219.439	4044.338	2381.597
FOS	3294.074	3902.395	3535.249	4497.916
RUNX1	3540.17	1688.837	3475.748	1838.463
SP1	3065.08	788.0137	3339.583	1044.204
SMC1A	3491.888	1469.37	3234.176	1174.405
JUN	3915.974	3187.352	3055.394	2404.769
ZNF217	3141.664	1883.507	3051.904	1812.678
HIST1H2AC	1683.527	1221.366	2864.429	1780.165
TLE3	2421.428	1045.821	2779.894	1014.028
STAG2	2304.52	761.9515	2756.544	1152.2
NRIP1	2405.725	1638.737	2747.499	2010.286
JUND	2604.291	2141.055	2661.302	1902.863
KDM4B	2232.925	1629.737	2615.043	1821.578
HDAC1	2241.51	932.0711	2405.738	816.5378
BCL2	1011.037	1000.39	2232.734	2519.243
USF2	2025.941	933.5899	2149.68	1304.95
PRMT1	2180.717	1392.256	2048.148	868.1992
NCOA3	1963.948	975.9478	2023.667	851.9701
MYB	1423.428	1147.441	2005.141	1596.996
GREB1	1211.077	1773.297	1951.057	2551.754
KDM1A	1982.559	702.233	1876.523	797.5676
MYC	1441.253	1066.714	1838.806	1221.984
SMC3	1723.818	559.1047	1737.65	604.2394
GTF2F1	1719.001	577.0501	1719.813	577.1572
PGR	1053.83	2137.447	1513.121	2772.369
NCOA1	1537.453	650.0989	1490.504	681.3695
YY1	1483.167	418.7897	1436.434	361.4866
TNRC6A	1172.639	330.6097	1295.794	500.6958
MOV10	1320.873	560.1504	1223.348	507.076
USF1	1242.066	712.533	1148.351	551.2219
AR	934.5753	887.6541	1060.657	1241.277
TNRC6C	734.2774	452.2206	942.6309	676.3775
STAG1	825.541	329.3487	902.6978	405.6247

KAT5	978.2385	363.5538	893.8402	303.4966
EBAG9	652.0142	248.0344	845.743	448.7483
TNRC6B	851.0509	329.2051	824.6137	354.443
GTF2A2	752.4456	365.8145	719.8842	231.0754
FOSB	791.5344	1220.054	645.366	946.0908
KANK1	593.3999	349.7647	575.1871	270.6319
KCTD6	297.4244	238.6924	495.609	467.2414
GPAM	525.1021	287.3586	456.1648	174.8436
GTF2F2	448.1822	187.6483	451.6812	181.9318
KAT2B	320.9606	157.2357	366.7037	173.4976
GTF2A1	240.5656	135.1905	241.8387	132.4202
TBP	272.7313	84.01856	240.9742	68.46946
TGFA	179.5679	274.4439	187.8069	261.4322
NR5A2	65.19405	46.78028	60.88001	45.85856
CITED1	26.62615	44.41879	17.90006	37.32836

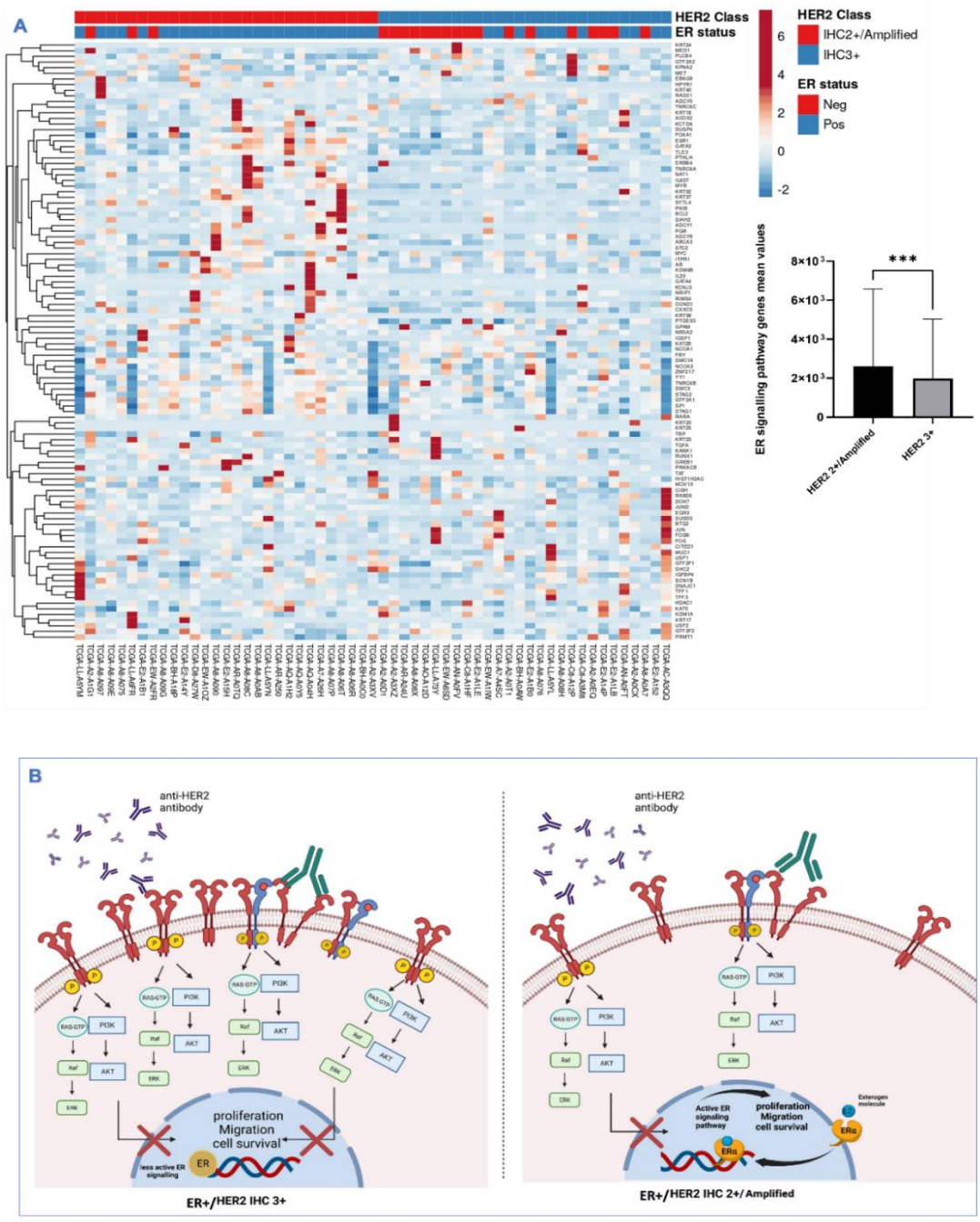


Figure 6.11: An illustrated diagram features two parts. A: presents a heatmap displaying the clustering and distribution of ER signalling genes among HER2-positive IHC 3+ and 2+/Amplified classes, with notable expression in the IHC 2+/Amplified group (p=0.008). B: demonstrates the role of ER positivity in these classes: HER2 IHC 3+ cases primarily rely on HER2-driven oncogenic signalling, where the response to therapy depends on HER2 pathway inhibition. In contrast, ER-positive/HER2 IHC 2+/Amplified cases involve ER pathways, influencing therapy response.

6.6 DISCUSSION

The response of HER2-positive BC patients to anti-HER2 therapy is variable [265, 266, 320, 323, 553-558] and whether the protein expression or the gene amplification levels, when considered together, are the key drivers remains to be confirmed. Although most anti-HER2 targeted therapy exerts their action on HER2 protein and no response is observed in IHC scores 0 or 1+ BC patients, there is high concordance between IHC and *HER2* gene copy number [559] and no response is observed in ISH-negative cases. Moreover, there is an excellent correlation between HER2 IHC 3+ and high *HER2* gene amplification level [164, 560], which may explain why most cases with high amplification levels respond well to anti-HER2 therapy. The main discrepancy is among HER2 IHC 2+ tumours, which typically show borderline gene amplification [228, 535, 559]. These results, together with the finding that 4% of cases with HER2 IHC scores 0 and 1+, show evidence of gene amplification [559], argue against using ISH alone as a predictive of response to anti-HER2 therapy. In addition, the differential response based on interactions between IHC classes and ISH status and the molecular characteristics of these HER2-positive IHC classes is not well-defined. In this study, we aimed to decipher the clinical, biological, and molecular mechanisms involved in anti-HER2 therapy response among these classes.

In our study, the overall pCR rate for HER2-positive BC patients treated with NACT and anti-HER2 therapy was 36%. However, stratifying by IHC classes revealed a significantly higher pCR rate in HER2 IHC 3+ patients compared to HER2 IHC 2+/Amplified patients. While high *HER2* gene amplification was

linked to higher pCR across all HER2 IHC categories, this association disappeared when HER2-positive IHC subgroups were considered. HER2 overexpression (IHC 3+) was an independent predictor of pCR, unlike varying levels of *HER2* gene amplification, reflecting similar findings from the HERA and N9831 trials[548, 550, 561]. These findings are also in line with a number of prior studies that showed HER2 protein overexpression is a strong predictor of anti-HER2 therapeutic response.[159, 228, 242-246, 548, 562]. Other studies have also indicated that the rate of pCR in the subset of patients with evidence of *HER*2 gene amplification in the absence of HER2 protein overexpression was significantly lower (17% vs 66%) [228, 244].

The stronger correlation between HER2 protein overexpression and response to anti-HER2 therapy likely reflects that HER2-driven oncogenic pathways depend on protein overexpression rather than just gene copy number, as seen in HER2 IHC 2+/Amplified tumours. Consequently, patients with equivocal HER2 expression (IHC 2+/Amplified) show limited response to anti-HER2 therapies targeting these pathways. Their clinical outcomes with combined chemotherapy and anti-HER2 therapy do not significantly differ from those with HER2 IHC 2+/Non-amplified tumours treated with chemotherapy alone.

Some studies have shown that the therapeutic response to anti-HER2 therapy is correlated with the level of *HER2* gene amplification [543, 544, 546]. Singer and colleagues [588] evaluated the *HER2/CEP17* ratio and response to therapy, but they did not consider HER2 IHC protein expression in the analysis. Also, Arnold and colleagues[543] compared the response rate between cases with medium and high levels of gene amplification, yet only 1 case was HER2

IHC 2+/Amplified, and the rest of the cases were IHC 3+. Salmon and colleagues [159] demonstrated that trastuzumab efficacy of trastuzumab was consistently observed in both IHC and ISH-positive groups. However, in their study patients with HER2 protein overexpression experienced better survival than those with *HER2* gene amplification but equivocal protein expression.

In the CLEOPATRA Phase III trial, HER2 IHC3+ was associated with improved survival [562]. This is consistent with our study where patients with HER2 IHC3+ benefited from adjuvant anti-HER2 therapy in terms of prolonged BCSS and DMFS compared to HER2 IHC 2+/Amplified BC patients. Previous studies have demonstrated that the level of *HER2* gene amplification is not a prognostic factor in patients with HER2-positive BC treated with anti-HER2 therapy [547, 550]. The N9831 phase III trial assessed disease free survival of patients on adjuvant trastuzumab according to protein expression, *HER2* gene copy number and *HER2/CEP17* ratio. It reported that patients with normal HER2 protein-expressing tumours (0,1,2+) and ISH amplified had no improvement in survival with additional trastuzumab, while patients with IHC 3+ had a significant response to treatment [548].

Some authors have indicated that the level of HER2 protein expression in HER2-positive tumours has no role in clinical management with anti-HER2 therapy [563]. However, that study did not rely on a dichotomous classification (IHC 3+ versus 2+), but instead evaluated HER2 expression as a continuous spectrum. Other studies have proposed that the best approach for selecting patients for anti-HER2 therapy is by assessing HER2 gene amplification through ISH testing, as this might provide a more accurate measure of those who would benefit from targeted therapies. These findings were based on

studies that included tumours with IHC scores of 3+ and 2+, where the ISH-negative group comprised only IHC 2+ tumours. This led to an overemphasis on the importance of ISH testing, potentially inflating its perceived value in determining HER2 status for treatment decisions [564, 565].

Unlike conventional anti-HER2 therapies that block HER2 signalling pathways, HER2-based ADCs like T-DM1 and DS-8201 primarily use HER2 as a target to deliver cytotoxic agents into HER2-expressing cells, and their efficacy is not directly proportional to HER2 protein levels [566]. The Phase III KATHERINE trial demonstrated a differential response to T-DM1 and trastuzumab in HER2-positive BC patients. Patients with HER2 IHC 2+ tumours showed less benefit from trastuzumab compared to IHC 3+ tumours, while the 3-year iDFS rate was similar for both subgroups in the T-DM1 arm, regardless of HER2 expression heterogeneity [567].

In vitro studies comparing trastuzumab and T-DM1 in HER2-positive cell lines have shown that T-DM1 is more effective in both trastuzumab-sensitive and trastuzumab-insensitive cell lines. Additionally, in trastuzumab-resistant xenograft tumour models, T-DM1 was found to induce apoptosis and mitotic catastrophe in vivo. This suggests that T-DM1 can overcome trastuzumab resistance by leveraging its cytotoxic agent delivery mechanism, making it a potent treatment option for HER2-positive breast cancer, even in cases where conventional anti-HER2 therapies are ineffective. [568, 569]. However, the focality of HER2 expression might attenuate T-DM1 activity, which was unable to induce a bystander effect for surrounding HER2-negative cells due to a non-cleavable linker [567]. This issue was resolved through T-Dxd (DS-8201) that proved to overrate T-DM1 in HER2-positive as well as in HER2-Low BC (HER2

IHC 1+ or 2+ without *HER2* gene amplification according to results of DESTINY-Breast04 trial [170, 274]. In that trial, patients with a score of 1+ on IHC analysis and those with a score of 2+ had similar the clinical outcome [170].

Based on experimental and clinical trial data, our findings suggest that the varying responses of different HER2-positive IHC classes to anti-HER2 therapies should be considered when making treatment decisions. Further trials are needed to explore the distinct responses of HER2 IHC 2+/Amplified cases to agents like T-Dxd or T-DM1 compared to trastuzumab and other anti-HER2 treatments. Increasing evidence indicates that the response to anti-HER2 therapies is closely linked to intrinsic molecular subtypes, with HER2-E subtype, identified by RNA-seq, showing a higher likelihood of achieving pCR than other subtypes [570].

Recent systematic review and meta-analysis studies [507, 508, 570-572] concluded that HER2-E biomarker identifies patients with an increased likelihood of achieving a pCR following neoadjuvant anti-HER2-based therapy. Furthermore, in the PAMELA phase 2 trial, they concluded that HER2-E subtype is the predictor of pCR following trastuzumab and lapatinib without chemotherapy in early-stage HER2-positive BC [57]. Not all clinically HER2-positive tumours belong to the HER2-E intrinsic molecular subtype, with only around 50% falling into this category [503]. Tumours with HER2 protein overexpression exhibit significantly higher expression of several RTKs, including *FGFR4, EGFR*, and HER2, as well as genes in the HER2-amplified region on chromosome 17q12-q21, such as *GRB7*. Our study supports these findings, showing that the HER2-E subtype is more associated with HER2 IHC 3+ than IHC 2+/Am-

plified. Additionally, the expression of genes related to HER2 oncogenic signalling was more significant in HER2 IHC 3+, while genes linked to trastuzumab resistance were upregulated in HER2 IHC 2+/Amplified tumours. ER status also emerged as a significant predictive marker, as ER signalling can act as a mechanism of resistance to HER2 inhibition when both receptors are expressed in BC cells [261, 266, 319-321, 327-329]. However, the differential expression of ER within each HER2-positive IHC class and its impact on response to therapy within that class is not clear. In our study, ER positivity was a significant predictor of poorer response to therapy in the whole cohort and in IHC 2+/Amplified, but not in HER2 IHC 3+ patients both in the neoadjuvant and adjuvant settings. This agreed with Harbeck et al [324] study, which showed that in HER2 protein overexpression, HR-positive patients had high pCR rates close to HR-negative patients [324]. In a secondary analysis of the HERA trial, the largest of the adjuvant trastuzumab trials, the role of ER IHC status combined with HER2 IHC levels, in predicting the magnitude of benefit from adjuvant trastuzumab was investigated. The trial showed that patients with ER-positive and HER2-positive with low *HER2* gene copy number derived less benefit from adjuvant trastuzumab with all of these patients receiving endocrine therapy [573]. Also, in a second analysis of NeoALTTO clinical trial which aimed to quantify gene expression levels of *ESR1* and *HER2* and their relation to pCR, it was revealed that high levels of *HER2* and low levels of *ESR1* were associated with higher pCR rates [574] They explained these findings based on the increasing amount of genomic and clinical data reporting that HER2-overexpressing tumours have distinct molecular and clinical profiles [573]. HER2-E subtype, which is predominantly ER-negative, tends to achieve

a higher response to HER2-targeted therapies [326]. In contrast, the luminal B subtype (HER2-positive and ER-positive) shows elevated expression of genes related to the luminal cluster, such as *GATA3, BCL2*, and *ESR1*. As a result, these tumours are primarily driven by ER signalling pathways, with HER2 oncogenic signalling having a more limited role in their progression [399].

Furthermore, the DGE analysis in this study showed that HER2 IHC 2+/Amplified tumours are more frequently ER-positive and enriched with ER signalling pathways and related genes, such as *ESR1* and BCL2, and are less likely to fall into the HER2-E molecular subtype. Treating HER2-positive/ER-positive BC, especially in the HER2 2+/Amplified group, is challenging, as no single treatment or combination suits all patients. Identifying the primary driver of the tumour, whether ER or HER2 signalling, is crucial, although pathway interaction and crosstalk can alter the tumour's behaviour throughout treatment.

In the preclinical setting, it has been shown that the expression of ER and its downstream targets are upregulated in cells with acquired resistance to anti-HER2 therapy [308, 575]. Reactivation of ER expression and signalling, including a switch from ER-negative to ER-positive status, were observed in clinical HER2-positive tumours after neoadjuvant lapatinib treatment [575].

Furthermore, HER2 overexpression affects endocrine therapy responsiveness both to tamoxifen and to oestrogen deprivation by aromatase inhibitors (AI) and ovarian suppression in premenopausal women [575-582].

Combining hormone therapy with anti-HER2 agents has proven beneficial to some specific HER2-positive patients [583, 584], particularly those who have high ER expression. Some ER-positive /HER2-positive tumours behave more

like the luminal A subtype (i.e., ER-driven cancer), and others as HER2-E tumours (HER2-driven cancer) or a combination of both, which require a multi-pronged targeted blockade of both ER and HER2 pathways.

Moreover, preclinical studies suggest that PI3K and CDK4/6 inhibitors could be effective targets acting downstream of both ER and HER2 pathways. The PATRICIA trial, which evaluated palbociclib combined with trastuzumab, with or without endocrine therapy, in HER2-positive advanced BC, showed promising survival outcomes for ER-positive/HER2-positive patients with a PAM50 Luminal A or B subtype treated with trastuzumab[585]. Similarly, the MonarcHER phase II trial demonstrated that the combination of abemaciclib, fulvestrant, and trastuzumab significantly improved PFS compared to standard-of-care chemotherapy plus trastuzumab [586]. In conclusion, BC with HER2 protein overexpression (IHC 3+) appears to be driven by HER2 oncogenic signalling pathway, more HER2-E, which may explain their better response to anti-HER2. Patients with HER2 IHC 2+/Amplified tumours have limited response to anti-HER2 therapy regardless of the *HER*2 gene amplification status, particularly those with ER-positive tumours. Further comparative studies between conventional anti-HER2 therapy and HER2-directed ADC therapy in patients with IHC 2+/Amplified BC could be warranted.

Chapter 7. Modulators of response in HER2-positive BC

7.1 INTRODUCTION

Overexpression of HER2 protein in BC leads to its dimerization with another HER family member. This activates downstream signalling pathways of EGFR, including PI3K/AKT/mTOR, Ras-Raf-MAPK and JNK are triggered to promote cell proliferation, cell invasion, angiogenesis and to protect cells against apoptosis [53, 132, 133].

HER2-positive BCs are primarily treated with either monoclonal antibodies that bind to the HER2 juxta membrane domain IV and heterodimerisation domain II, thereby inhibiting ligand-independent HER2 signalling, downregulating HER2 expression and inducing ADCC [247-249] or other medications that target the HER1, HER2, and HER4 pathways [250, 251] and suppress downstream signalling that involves the MAPK/ERK1/2 and PI3K/AKT pathways [252, 253].

Despite the advances in HER2-positive BC targeted therapy, long-term results from the adjuvant pivotal trials indicated that approximately 15%–31% of patients experienced disease relapse [220-222]. Therefore, prognostic and predictive biomarkers are needed to refine the response to anti-HER2 therapy further. In this chapter, we investigated two genes that might modulate the response of HER2-positive BC to targeted therapy.

TAF10 (TATA-box Binding Protein Associated Factor 10) is a core component of the TFIID complex, a critical element of the general transcription machinery that regulates the expression of numerous genes involved in cellular pro-

cesses such as proliferation, differentiation, and apoptosis [587]. TAF10 interacts with the TATA-box binding protein (TBP) and other transcription factors to help initiate transcription by RNA polymerase II. Beyond its fundamental role in transcription, TAF10 has been shown to play a role in modulating gene expression in various cancer types, often influencing tumour progression and treatment response [588, 589] **(Figure 7.1**)

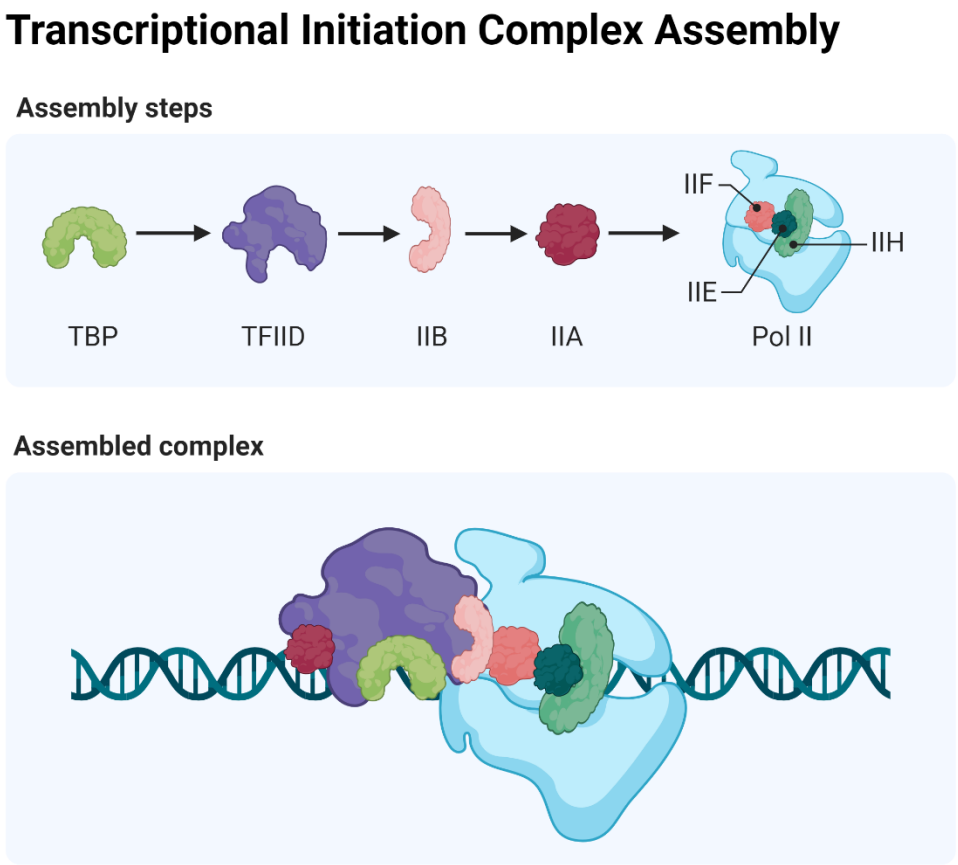


Figure 7.1: Illustration of the transcription association complex. The complex is made up of a number of components, including the enzyme RNA polymerase II (Pol II), TATA Box binding protein (TBP), transcription factor II A (TFIIA), transcription factor II B (TFIIB), transcription factor II D (TFIID), and other general transcription factors (TFIIF, TFIIE, TFIIH). Created by Biorender.com

In cancer biology, TAF10 has been implicated in several malignancies, including hepatocellular carcinoma, colorectal cancer, and glioblastoma. Its dysregulation has been linked to altered expression of genes involved in cell cycle control and DNA repair, processes crucial for cancer development and progression [590-592]. However, the role of TAF10 in BC is yet to be investigated.

Branched-chain amino acid transferase 1 (BCAT1) is a crucial cytoplasmic enzyme responsible for breaking down branched-chain amino acids (BCAA) such as leucine, valine, and isoleucine, which are vital signalling molecules within the PI3K/AKT/mTOR pathway. These amino acids also play significant roles in the metabolism of glucose, lipids, and proteins [593, 594].

There are two main subtypes of human BCAT: BCAT1 and BCAT2. Despite sharing similar substrate specificities, they have different amino acid sequences and protein functions. BCAT1 is a cytoplasmic aminotransferase encoded by the *BCAT1* gene (12p12.1), expressed in specialised tissues like the brain, kidney, and ovary. BCAT2, a mitochondrial enzyme, is encoded by the *BCAT2* gene (19q13.33) and expressed in many tissues except the liver [595].

BCAT1 contributes to the production of energy necessary for mitochondrial ATP synthesis and the formation of various macromolecules [596]. Elevated BCAT1 levels have been linked to tumour growth and poor prognosis across several cancers, including gastric cancer, glioma, liver cancer, and nasopharyngeal carcinoma [597-600]. Additionally, studies have demonstrated that BCAT1 expression is higher in BC tissues, compared to normal breast tissues [601, 602].

BCAT1 expression has been shown to be correlated with HER2-positive BC and luminal B subtypes. Moreover, research has identified BCAT1 as an independent prognostic marker for TNBC[600] However, further comprehensive research is needed to confirm the prognostic and predictive role of BCAT1 expression in HER2-positive BC **(Figure 7.2**).

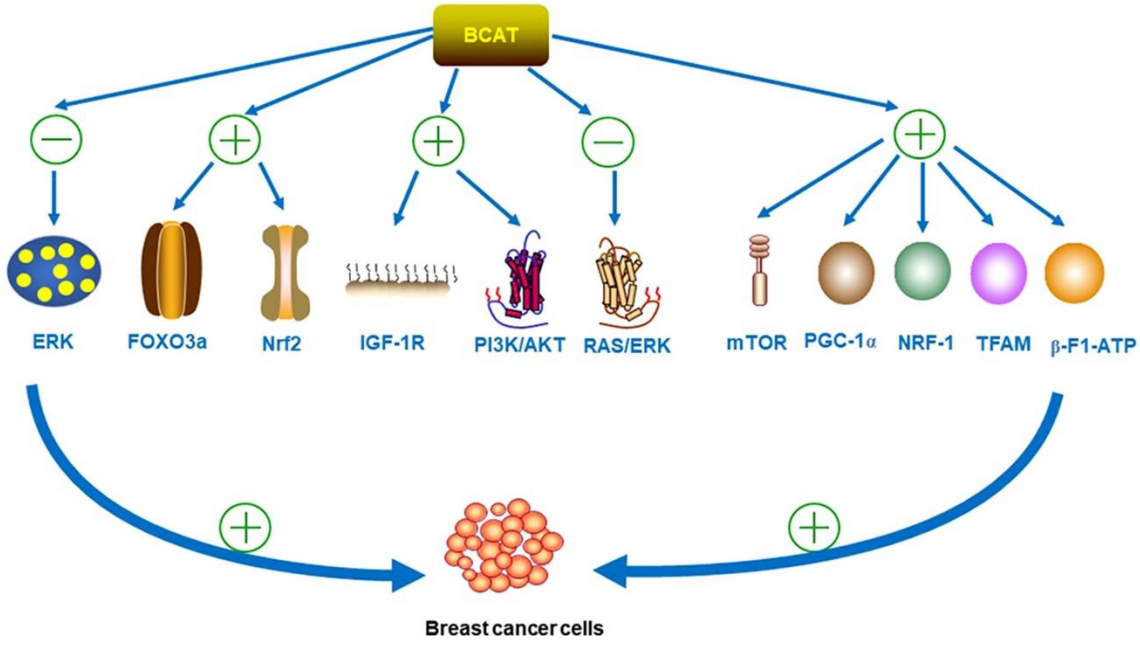


Figure 7.2: Summary of mechanism of action of BCAT1 in breast cancer. BCAT inhibits the phosphorylation of ERK and upregulates the levels of transcription factors FOXO3a and Nrf2 during the development of BC. BCAT1 also activates the PI3K/AKT axis by stimulating the IGF-1R signalling pathway, while down-regulating the RAS/ERK pathway. In addition, BCAT1 also activates mTOR signalling and the expression of PGC-1α, NRF-1, TFAM and β-F1-ATPase, all of which can promote the proliferation, migration and invasion of BC cells. "+" means promotion, "-" means inhibition. [594]

7.2 HYPOTHESIS

The response of HER2-positive BC patients to targeted therapy is variable, and molecular markers can act as indicators for patient stratification. Through DGE analysis of treatment-sensitive and treatment-resistant HER2-positive B

cell lines. This study hypothesised that the expression of *TAF10* and *BCAT1* genes may influence the response of HER2-positive BCs to targeted therapies through regulating gene networks involved in cell proliferation, apoptosis, and tumour progression through their role in transcription regulation and chromatin remodelling.

7.3 AIMS OF THE STUDY

- To investigate the prognostic role of TAF10 and BCAT1 in HER2-positive BC
- To investigate the predictive role of TAF10 and BCAT1 in modulating the response of HER2-positive BC patients to therapy.
- To explore the association between TAF10 and BCAT1 dysregulation and key HER2 signalling pathways (e.g., PI3K/AKT/mTOR and Ras-Raf-MAPK).

7.4 MATERIALS AND METHODS

Our study utilised extensive transcriptomic and proteomic datasets to investigate gene expression and function. The discovery cohort, sourced from the GEO database, was employed to identify a set of candidate genes. These genes were subsequently validated using independent cohorts, which included additional transcriptomic datasets for mRNA-level validation and a proteomic cohort for assessing the prognostic and predictive roles of the selected genes at the protein level.

7.4.1 Discover cohort

7.4.1.1 Gene selection:

Five independent gene expression datasets (GSE136300, GSE55005, GSE161420, GSE121105 and GSE60182) comprising 136 cases were downloaded from the GEO database and exploited as discovery cohorts to identify genes exploited in trastuzumab efficiency in trastuzumab sensitive and trastuzumab-resistant cell lines as detailed in **Section 2.11.1**

7.4.1.2 Differential Gene Expression Analysis

The DESeq2 tool in R software (version 3.4.3; https://cran.r-project.org/) was used to carry out DGE analysis between trastuzumab-sensitive cell lines (BT474) before and after treatment with trastuzumab. This was used to reflect trastuzumab efficiency. Furthermore, the same analysis was carried out between trastuzumab-resistant BT-TR2 cell lines before and after treatment. This was used as a clue for genes responsible for trastuzumab resistance. To avoid false positive results, the overlapping genes from 2 panels were excluded. Details on DGE analysis are mentioned in **Section 2.11.**

A list of the top 10 upregulated genes in each of the trastuzumab-sensitive and trastuzumab-resistant cell lines was identified. Of them, two genes (TAF10 and BCAT1) were selected for thorough evaluation in this study. TAF10 was upregulated in genes responsible for response to trastuzumab in sensitive cell lines. In contrast, BCAT1 was upregulated in the resistant cell line **(Table 7.1).** The selection was based on reviewing the literature, seeking novel genes that can contribute to a better understanding of patient outcomes, and responses

to therapy, the prognostic and predictive significance of these two genes in publicly available gene expression platforms and the antibodies availability for IHC validation through https://www.proteinatlas.org/, https://www.gene-cards.org/, and https://www.uniprot.org/websites.

The expression of *TAF10* and *BCAT*1 at the mRNA and protein levels was correlated with clinicopathological parameters, molecular subtypes, relevant biological markers and patient outcomes. Also, their role in response to anti-HER2 therapy was investigated.

7.4.2 Transcriptomic Validation Cohorts

7.4.2.1 METABRIC dataset

This was used to assess the mRNA expression of the selected genes. This cohort comprised 1980 primary operable invasive BC patients. Clinical history, outcome data and tumour characteristics, including tumour size, tumour grade, LN stage and histological type, were available for this cohort. The intrinsic subtypes of BC (luminal A, luminal B, HER2-enriched, normal-like, and basal-like) were classified based on the PAM50 genes assay. Integrating germline variants, somatic aberrations, and aberration with gene expression data augmented BC classification in this cohort by producing ten integrative clusters. Each cluster represents a distinct genomic landscape, molecular and clinical features and unique ER, PR and HER2 expressions, as detailed in **Section 2.1.2.1.** Gene expression data were pre-processed and normalised as per previous protocols [396]. The study investigated the relationship between mRNA expression and clinicopathological parameters, molecular subtypes, and patient outcomes.

7.4.2.2 The Cancer Genome Atlas

Clinical data were available for 854 cases, and these were retrieved from TCGA of the University of California Santa Cruz website (https://genome-cancer.ucsc.edu). Comprehensive clinical data, including age, tumour size, grade histological tumour subtypes, pathological stage, ER/PR status, LVI, and molecular subtypes, were extracted from the TCGA cohort. BCSS data were also included in the analysis. Details in **section 2.1.2.2**

7.4.2.3 Combined multicentric cohorts:

A multicentre combined cohort consisting of over 7252 patients with early-stage BC was created by including data from 56 publicly available international datasets, using the online tool bc-GenExMiner version 4.0.14 [399]. This dataset offers the possibility to evaluate the clinicopathological and prognostic significance of candidate genes in a large, pooled cohort of BC patients, as detailed in **Section 2.1.2.3**.

7.4.2.4 ROCPLOT online dataset

ROC plot online tool is capable of linking gene expression and therapy response using transcriptome-level data. It was also used to validate the predictive role of the selected biomarkers in response to anti-HER2 therapy. Published gene expression data of 36 publicly available datasets were integrated with treatment data into a unified database, as detailed in **Section 2.1.2.4**.

7.4.3 Proteomic Validation Cohort

7.4.3.1 Nottingham BC cohort

Protein expression was assessed using the Nottingham BC cohort. For this study, HER2-positive cases only (N=466) were assessed for the expression of the selected biomarkers. The clinicopathological profile of the Nottingham BC cohort includes the patient's age, tumour size, tumour grade, LN status, NPI, LVI status and tumour histological types. The HR expression profile and outcome data (BCSS and DMFS) were also recorded. The clinicopathological characteristics, therapeutic regimens and outcome data of this cohort are detailed in **Section 2.1.1.** Patients in this cohort were divided into those who received chemotherapy only and others with trastuzumab-based chemotherapy. The prognostic and predictive role of the selected biomarkers was assessed in the Nottingham cohort.

7.4.4 Western blotting, peptide blocking and IHC

WB was applied to validate the specificity of BCAT1 primary antibody (OTI3F5, MA5-25892, Invitrogen) in a dilution of 1:2000 using whole cell lysates from MCF7, MDA-MB-231, MDA-MB-157, HELA and SKBR3 cell lines. The specificity of TAF10 was confirmed using peptide blocking (TAF10 recombinant protein (NBP1-80706PEP, Novus Biologicus) due to incompatibility of the investigated antibody with WB **(Section 2.4.2**).

IHC staining was performed on TMA sections constructed by the author. This TMA cohort was constructed primarily for the aim of validation of those antibodies. We aimed to construct TMA sections for HER2-positive BC patients

with sufficient data on therapy available for analysis. Details on TMA construction are mentioned in **Section 2.2**. TAF10 IHC was carried out using TAF10 rabbit polyclonal antibody, NBP1-80706, Novus Biologics, in dilution of 1:50 and antibody incubation overnight. BCAT1 IHC was carried out by BCAT1 mouse monoclonal antibody, OTI3F5, Catalog no. MA5-25892, Invitrogen in dilution 1:100 for 1-hour incubation at room temperature. The details of the methodology are described in **Sections 2.3 and Table 2.4.** The Novolink polymer detection kit (Leica Biosystems, Newcastle, UK, RE7230-K) was used for staining visualisation. Mayer's haematoxylin was used for counterstaining. A positive staining control (human tonsil and kidney) was included in each slide. TAF10 and BCAT1 protein expression was initially optimised on full-face positive control tissue (kidney and endometrium, respectively) and full-face BC tissue sections prior to TMA staining.

Biomarker scoring followed REMARK (reporting recommendations for tumour marker prognostic studies) criteria. Stained sections were scanned using Panoramic 250 Flash III (3D Histech, Budapest, Hungary) with high-resolution WSI. Each TMA slide was assessed blindly to the clinicopathological data. Scoring was performed by one observer and validated by another observer who double-scored 20% of the cases.

7.4.5 Statistical Analysis

Statistical tests were performed using the statistical package for the social sciences (IBM SPSS v28). The Chi-square test was used to test the correlation between categorical variables. Gene expression count correlations were tested by Pearson's rank correlation coefficient. ICC was utilised to evaluate

the interobserver concordance. Biomarker gene and protein expression data were categorised based on cut-off point set by X-tiles software using BCSS. Kaplan Meier method and log-rank test were applied to predict the outcome. Multivariate Cox Regression analysis with Hazard ratios and Confidence intervals was used to test for prognostic independence.

7.5 RESULTS

TAF10 and *BCAT1* genes were selected for further validation. **Table 7.1** demonstrated the list of DEGs.

Table 7.1: List of top upregulated genes in trastuzumab resistant and sensitive cell lines

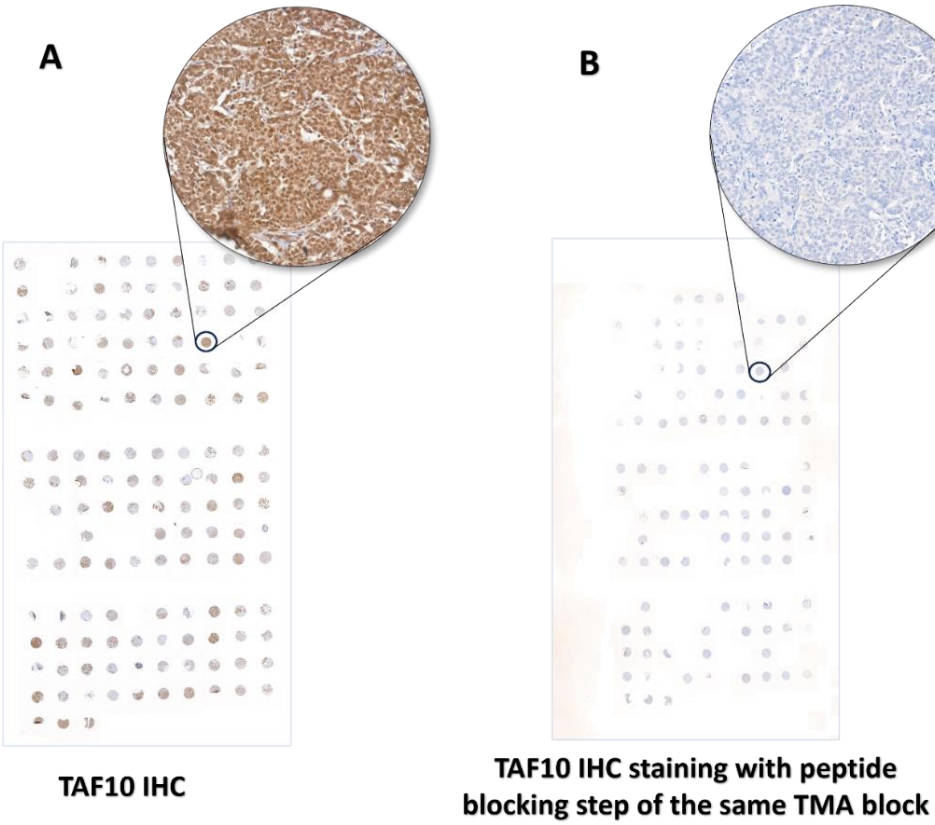
Gene	**Log2fold**	**Adj p value**
Upregulated genes in resistant cell lines		
BCAT1	15.25116	3.2E-15
CLIC3	6.904081	1.26E-08
NUCB1	4.408921	9.71E-23
CCDC85A	3.757367	0.000494
OAS2	3.450129	0.000257
IFIT3	2.359076	0.02404
TBX1	1.876749	0.014482
ACOT4	1.797549	0.000163
KLK10	1.733941	0.002179
CNTD2	1.295493	0.000811
Upregulated genes in resistant cell lines		
FAM9C	18.70147	2.63E-12
KRT17	8.665788	2.98E-05
CLIC3	8.614953	9.65E-07
SRXN1	7.08265	0.000254
CLDN1	5.67566	0.003112
PDXP	3.537912	0.004205
NME2	3.288333	1.8E-05
CRLS1	2.889778	0.000323
TAF10	1.605623	0.001605
NUDT14	1.445568	0.022222

7.5.1 Validation of TAF10 and BCAT1antibodies specificity

Regarding TAF10, complete absence of protein expression was present upon blocking of the antibody with specific TAF10 peptide antigens, Western blotting analysis showed specific bands at the correct predicted size (43kDa) corresponding to BCAT1 protein (**Figure 7.3A-C**).

7.5.2 *TAF10* and *BCAT1* mRNA expression in BC

TAF10 and *BCAT1*mRNA expression levels in BC and matched normal tissues were assessed in the TCGA cohort **(Figure 7.4A and Figure 7.5A**), Both genes revealed significantly higher expression levels in BC tissue compared to normal tissues ($p<0.001$ and $p=0.002$, respectively). Data of TAF10 and BCAT1 mRNA expression was normally distributed and was dichotomised using cut-off points generated from X-tile software, based on the prediction of BCSS. High *TAF10* mRNA expression (log2 intensity >9.2) was observed in 1485/1980 (75%) of the METABRIC cohort. Regarding BCAT1, high mRNA expression (log2 intensity >6.8) was observed in 467/1,980 (24%) of the cases. In the TCGA cohort, normalised reads were accessed from https://xena-browser.net. High *TAF10* levels (791 FPKM) were seen in 379/854 (44.4%), and high *BCAT1* levels (650 FPKM) were seen in 181/854 (21.2%).



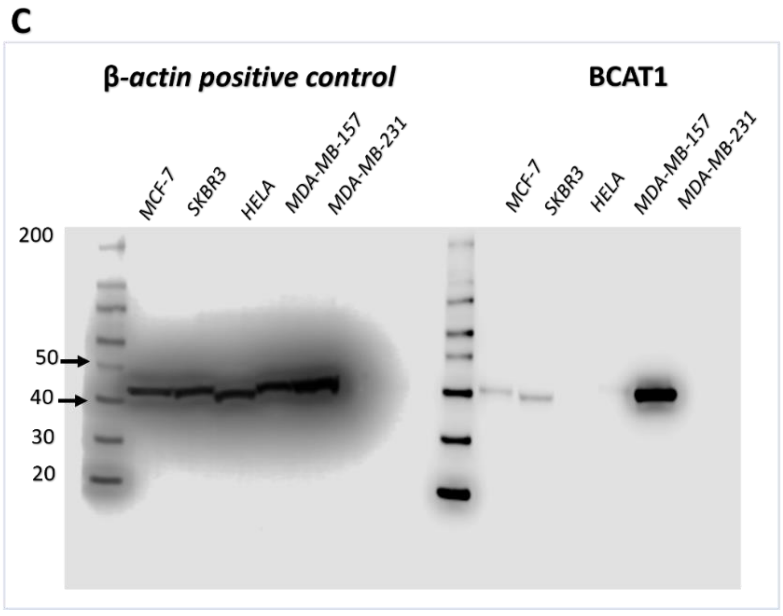


Figure 7.3: Graph showing validation of antibody specificity. A: IHC staining of TAF10 on TMA section. B: IHC staining of TAF10 after incubation with TAF 10 antigen (peptide blocking) of the same TMA section revealed no staining of the antibody. C: WB showing protein expression of BCAT1 antibody at the expected molecular weight (~43kDa) (right) and B-actin was used as a positive control (left).

7.5.3 Association of *TAF10* and *BCAT1* mRNA expression with clinicopathological parameters

There was no significant correlation between *TAF10* mRNA and tumour clinicopathological parameters in the TCGA, METABRIC or combined multicentric cohorts (**Table 7.2** and **Figure 7.4B-D)**. This was also seen when the cohort was dichotomised according to HER2 status.

High *BCAT1* mRNA level was significantly associated with poor prognostic parameters like high tumour grade and poor NPI group. However, no such association was detected in HER2-positive cases. This was found in all transcriptomic cohorts (**Table 7.3 and Figure 7.5B-D**)

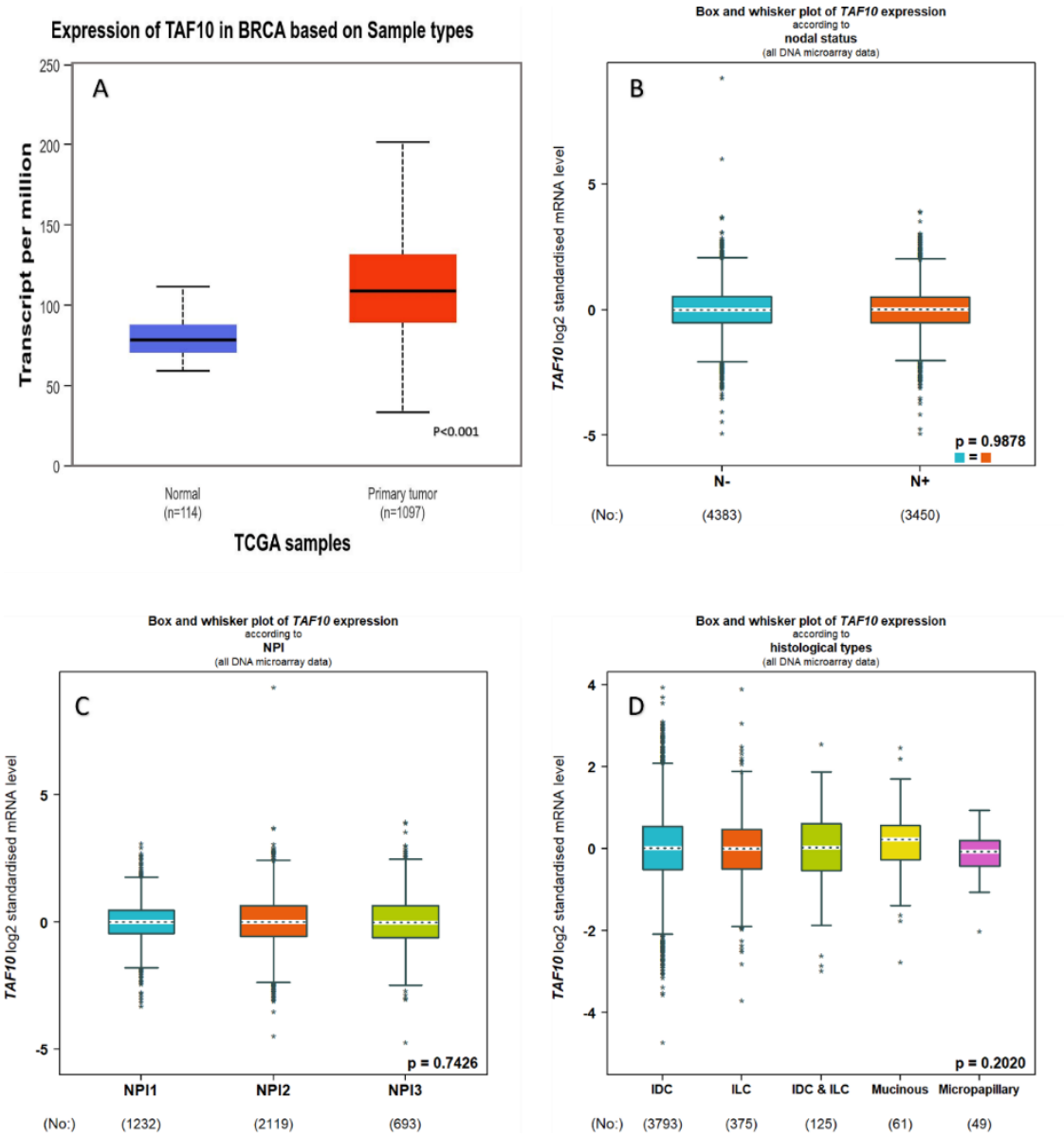


Figure 7.4: Boxplot charts illustrating *TAF10* mRNA expression in normal breast versus cancer tissue (A) and its association with tumour clinicopathologic parameters in the combined multicentric cohort.

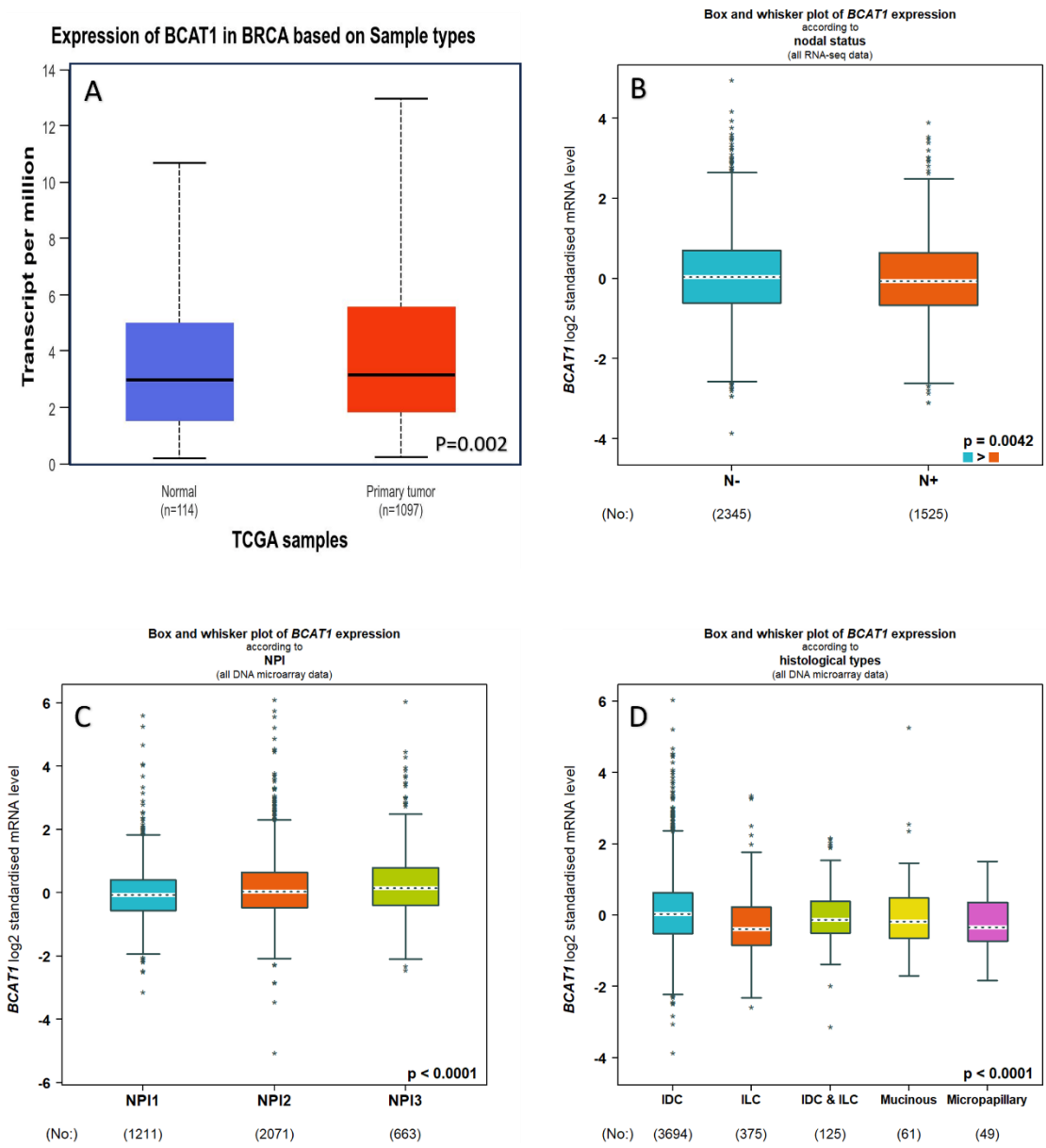


Figure 7.5: Boxplot charts illustrating *BCAT1* mRNA expression illustrating *TAF10* mRNA expression in normal breast versus cancer tissue (A) and its association with tumour clinicopathologic parameters in the combined multicentric cohort.

7.5.4 *TAF10* and *BCAT1* mRNA expression in molecular BC subtypes

In the METABRIC and combined multicentric transcriptomic cohorts, *TAF10* mRNA was significantly associated with HR-positive and HER2-positive tumours (**Table 7.2 and Figure 7.6)**. Regarding the PAM50 molecular subtyping, *TAF10* mRNA were significantly associated with HER2-E molecular subtype ($p<0.001$) in all the studied cohorts **(Figure 7.7 and Figure 7.8).**

Regarding *BACT1* mRNA, it was significantly associated with HR-negative tumours in all the studied cohorts. It also showed a significant association with HER2-positive tumours in the METABRIC ($p=0.002$) and the combined multicentric transcriptomic cohort ($P<0.001$) (**Table 7.3 and Figure 7.9**). *BCAT1* showed a significant association with both HER2-E and Basal-like molecular subtypes compared to luminal and normal-like subtypes **(Figure 7.10**).

Table 7.2: The association between *TAF10* mRNA expression and clinicopathological parameters in the METABRIC and TCGA breast cancer series.

Parameters	METABRIC cohort (n=1980)		TCGA cohort (n=854)	
	Mean Rank	*p*-value	Mean Rank	*p*-value
Age at diagnosis (years)				
< 50	987	0.5	433.11	0.6
≥ 50	966		425.42	
Tumour size (cm)				
< 2	947.8	0.1	305.95	0.5
≥ 2	990.6		305.35	
Tumour grade				
1	895.19		188.49	
2	955.9	0.42	196.74	0.6
3	948		184.46	
Nottingham Prognostic Index				
Good prognostic group	994.10		NA	NA
Moderate prognostic group	980.92	0.5		
Poor prognostic group	1031.22			
Lympho-vascular invasion				
Negative	936.58		421.44	
Positive	993.60	0.05	438.99	0.3
Lymph node stage				
1	977.71	0.7	NA	NA
2	996.20			
3	999.33			
Oestrogen receptor				
Negative	896.23	**<0.001**	401.95	0.4
positive	1020.17		415.56	
Progesterone receptor				
Negative	930.62	**<0.001**	399.69	0.2
Positive	1044.63		418.08	
HER2 status				
Negative	971.63	**<0.001**	342.72	**0.003**
Positive	1122.86		400.50	

Table 7.3: The association between *BCAT1* mRNA expression and clinicopathological parameters in the METABRIC and TCGA breast cancer series.

Parameters	METABRIC cohort (n=1980)		TCGA cohort (n=854)	
	Mean Rank	***p*-value**	**Mean Rank**	***p*-value**
Age at diagnosis (years)				
< 50	973.52	0.8	438.83	0.4
≥ 50	969.13		423.30	
Tumour size (cm)				
< 2	999.88	0.2	324.62	0.12
≥ 2	966.31		299.21	
Tumour grade				
1	869.09		163.27	
2	865.65	**<0.001**	167.03	**<0.001**
3	1025.72		225.12	
Nottingham Prognostic Index				
Good prognostic group	877.77	**<0.001**	NA	NA
Moderate prognostic group	1051.35			
Poor prognostic group	1039.02			
Lympho-vascular invasion				
Negative	1121.60		431.45	
Positive	880.78	**<0.001**	420.02	0.5
Lymph node stage				
1	968.05	0.2	NA	NA
2	1012.39			
3	999.09			
Oestrogen receptor				
Negative	1247.01	**<0.001**	523.99	**<0.001**
positive	909.76		380.22	
Progesterone receptor				
Negative	930.62	**<0.001**	467.47	**<0.001**
Positive	1044.63		384.62	
HER2 status				
Negative	975.20	**0.002**	346.60	**0.05**
Positive	1097.83		384.50	

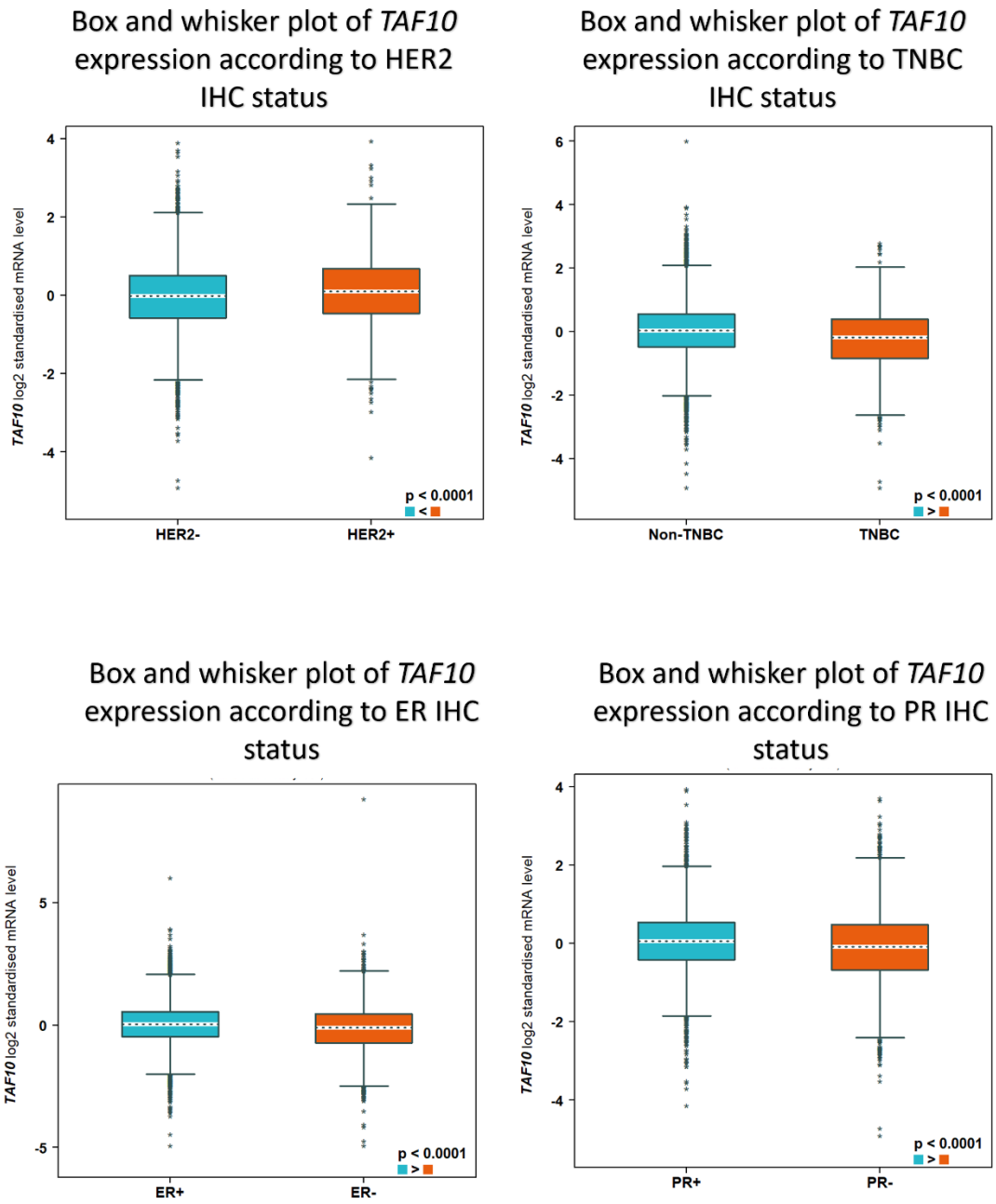


Figure 7.6: Boxplot illustrating the correlation between *TAF10* mRNA and breast cancer hormonal receptor and HER2 status from the combined multicentric transcriptomic cohorts.

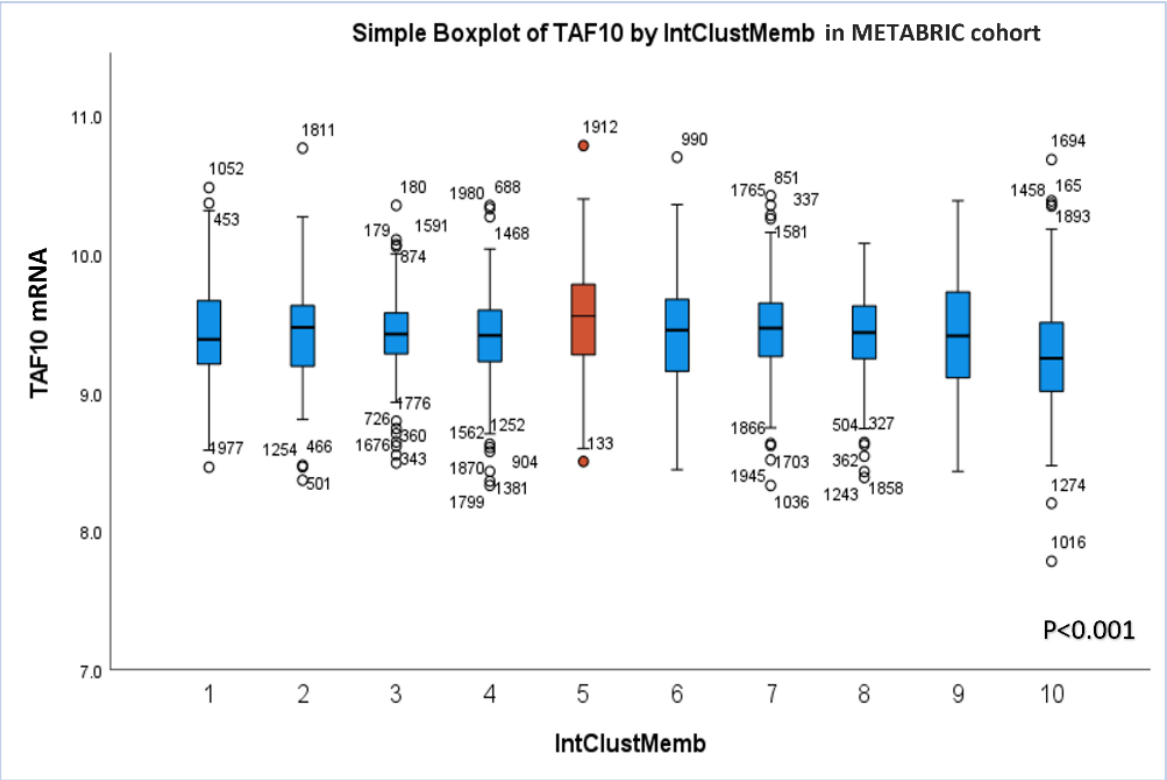
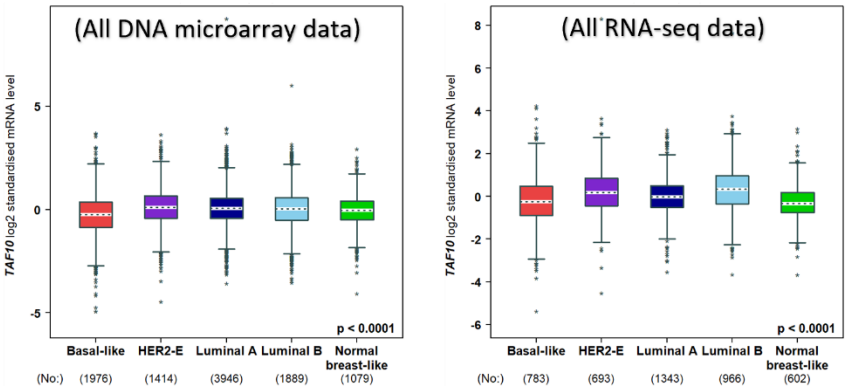
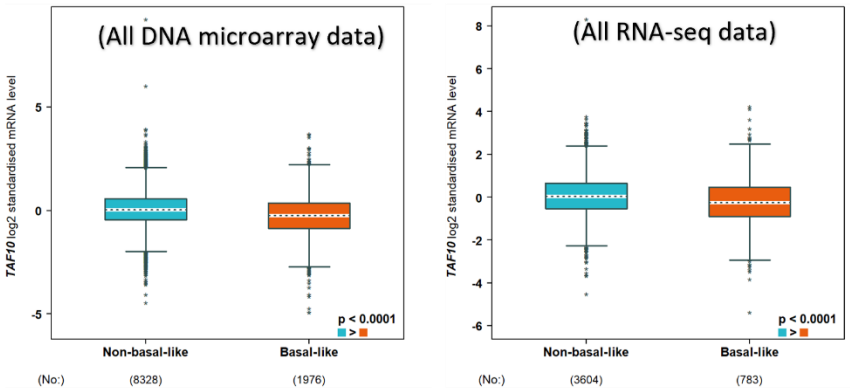


Figure 7.7: Box plot illustrating TAF10 mRNA expression among molecular integrative clusters in METABRIC cohort. Cluster 5, which represents the HER2-positive cluster, shows a significantly high *TAF10* mRNA expression compared with other clusters. IntClustMemb: integrative cluster membership.

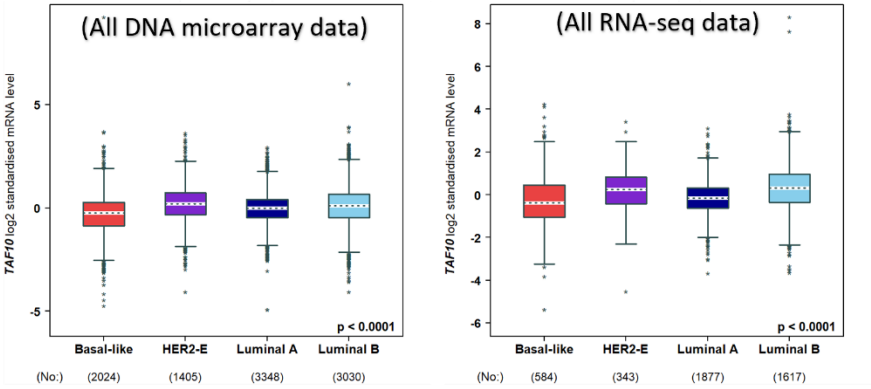
Box and whisker plot of *TAF10* expression according to PAM50 subtype



Box and whisker plot of *TAF10* expression according to PAM50 (basal) subtype



Box and whisker plot of *TAF10* expression according to SCMOD1 subtype



Box and whisker plot of *TAF10* expression according to SCMGENE subtype

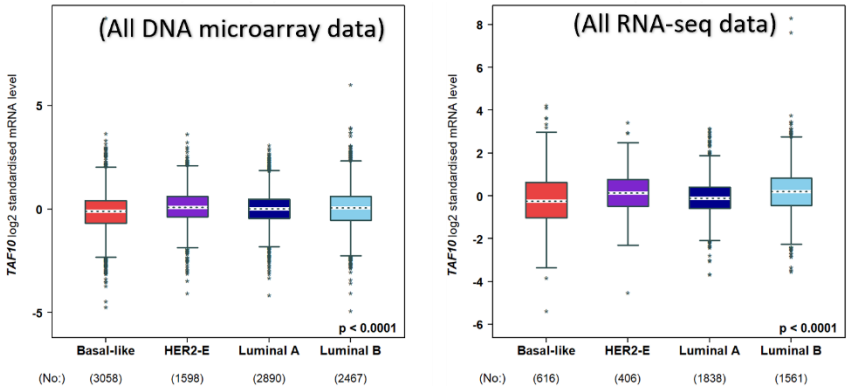


Figure 7.8: Box plot illustrating the association between *TAF10* mRNA and BC molecular subtypes from the combined multicentric cohorts. The graph shows different molecular subtyping platforms, including both DNA microarray (left) and RNA-seq (right) data.

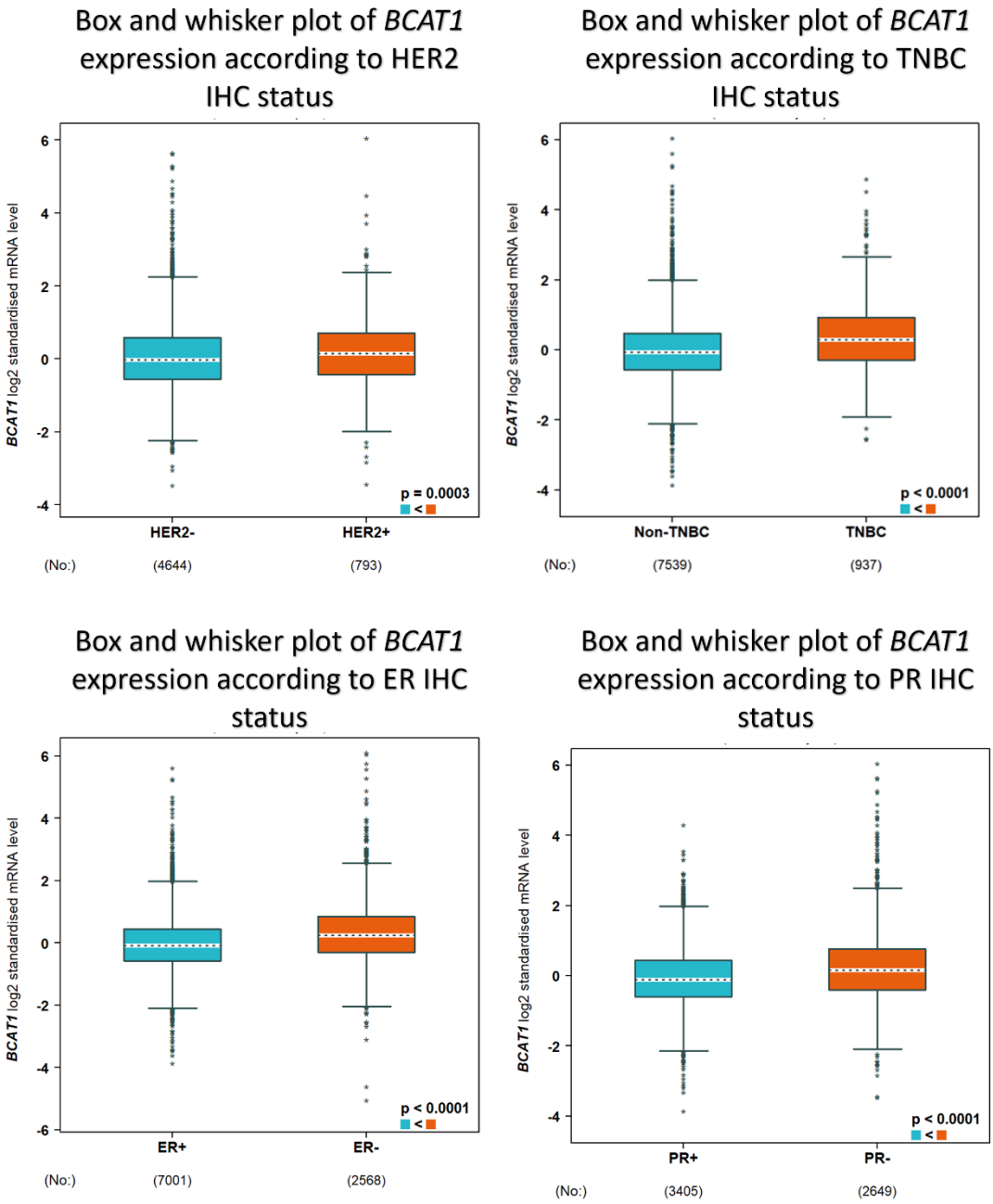
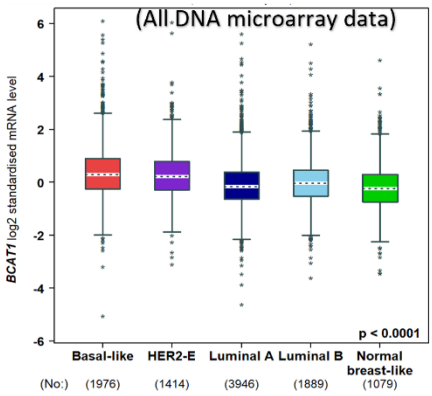
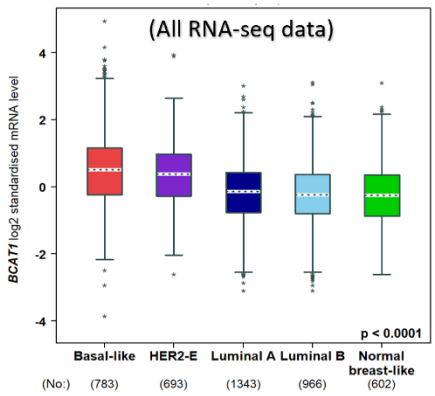


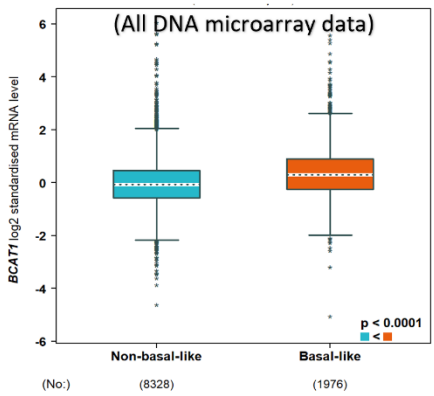
Figure 7.9: Boxplot illustrating the correlation between *BCAT1* mRNA and breast cancer hormonal receptor and HER2 status from the combined multicentric cohorts.

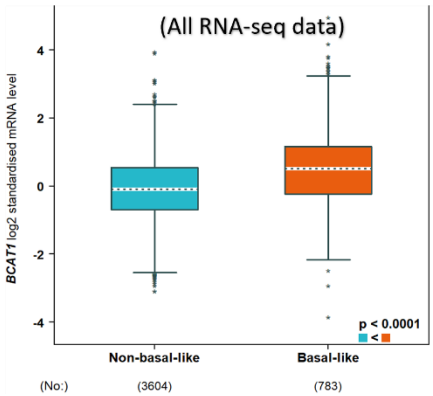
Box and whisker plot of *BCAT1* expression according to PAM50 subtype



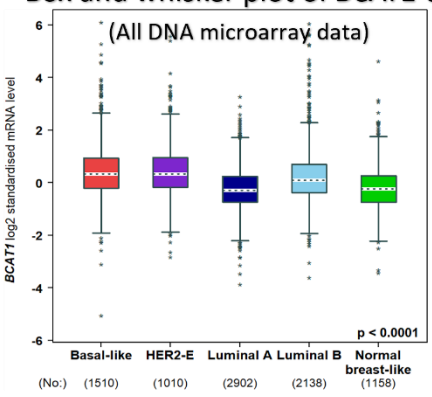


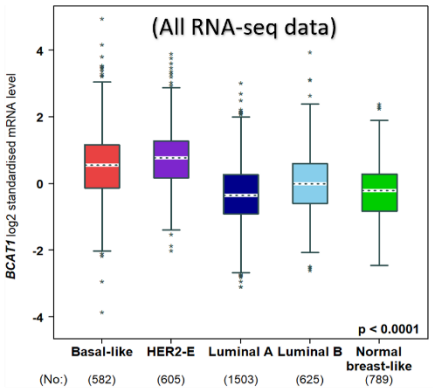
Box and whisker plot of *BCAT1* expression according to PAM50 (basal) subtype



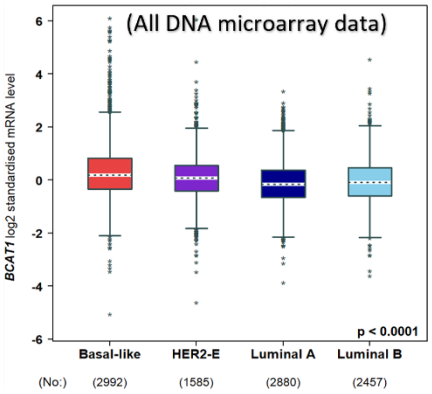


Box and whisker plot of *BCAT1* expression according to Sorlie's subtype





Box and whisker plot of *BCAT1* expression according to SCMGENE subtype



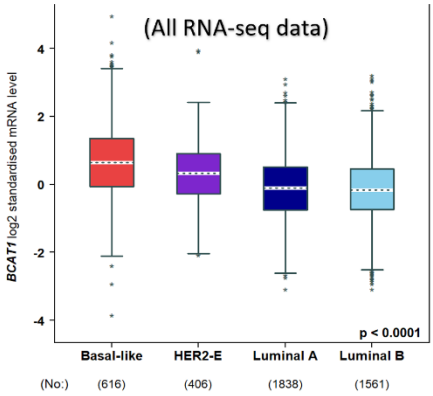


Figure 7.10: Box plot illustrating the association between *BCAT1* mRNA and BC molecular subtypes from the combined multicentric cohorts. A significant association is found in HER2-E and basal-like subtypes compared to other luminal and normal-like subtypes.

7.5.5 *TAF10 and BCAT1* mRNA Expression and patients' Outcome

High *TAF10* mRNA expression was associated with favourable patient outcome in the form of prolonged BCSS survival in all studied cohorts ($p<0.001$, $p=0.02$ and $p<0.001$ in the METABRIC, TCGA and the multicentric cohort, respectively) (**Figure 7.11 A-D).**

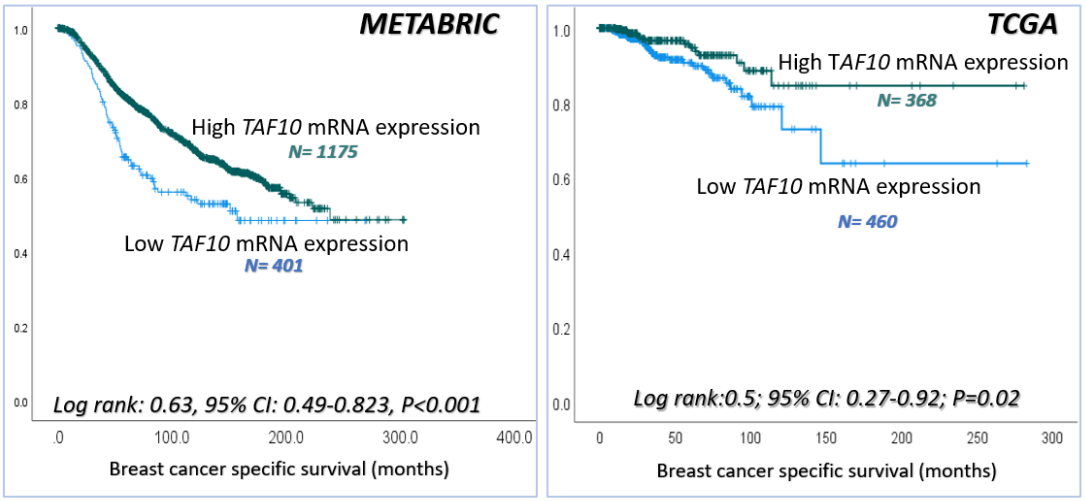
When the cohorts were stratified based on the molecular subtypes, high *TAF10* mRNA expression was associated with prolonged BCSS survival in the PAM50 HER2-E subtype in METABRIC ($p<0.001$) and TCGA cohorts ($p=0.01$) **(Figure 7.12 and Figure 7.13**, respectively). Similar associations were observed in the combined multicentric transcriptomic cohorts **(Figure 7.14)**

In a multivariate Cox regression analysis, high *TAF10* mRNA expression remained an independent predictor of better survival in the METABRIC cohort ($p<0.001$), when adjusted to other prognostic covariates, similar results were observed in the TCGA cohort ($p=0.02$), **(Figure 7.15)**

Conversely, *BCAT1* mRNA expression was associated with poor outcomes in all the studied transcriptomic cohorts with shortened BCSS in the METABRIC, TCGA and the multicentric genomic cohort (**Figure 7.16)**

When the cohorts were stratified according to molecular subtypes, *BCAT1* mRNA was associated with poor patient outcomes in HER2-E in each of the

METABRIC and multicentric cohorts but not in the TCGA cohort **(Figure 7.17** and **Figure 7.18**).



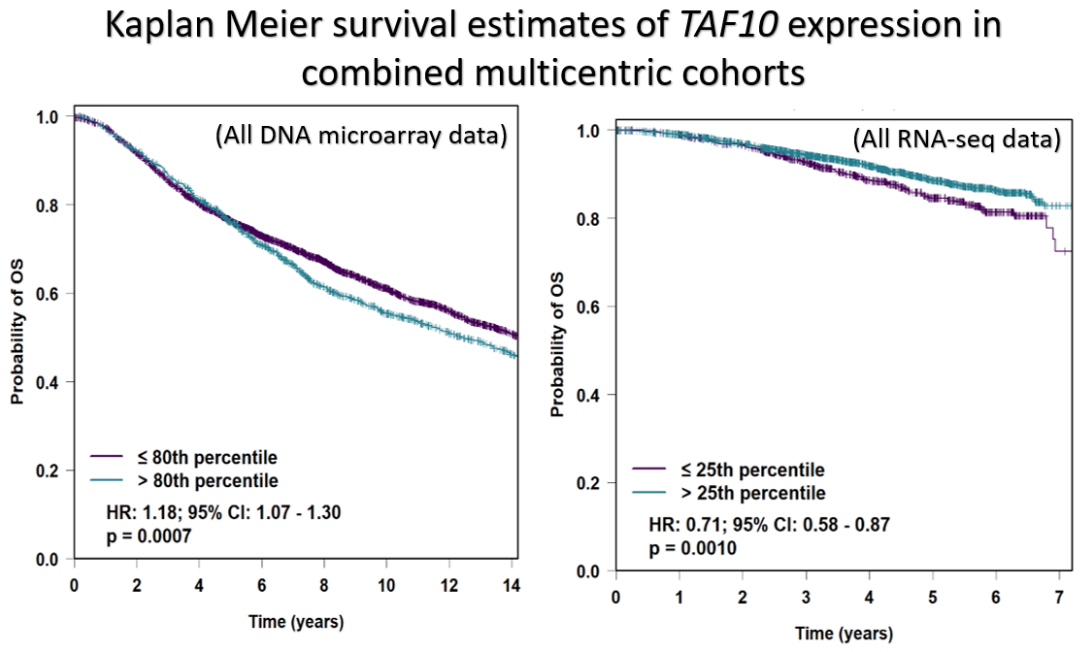


Figure 7.11: Kaplan Meier curves showing the prognostic significance of high *TAF10* mRNA level in patient outcomes in the METABEIC cohort, TCGA cohort and multicentric combined cohort. OS: overall survival

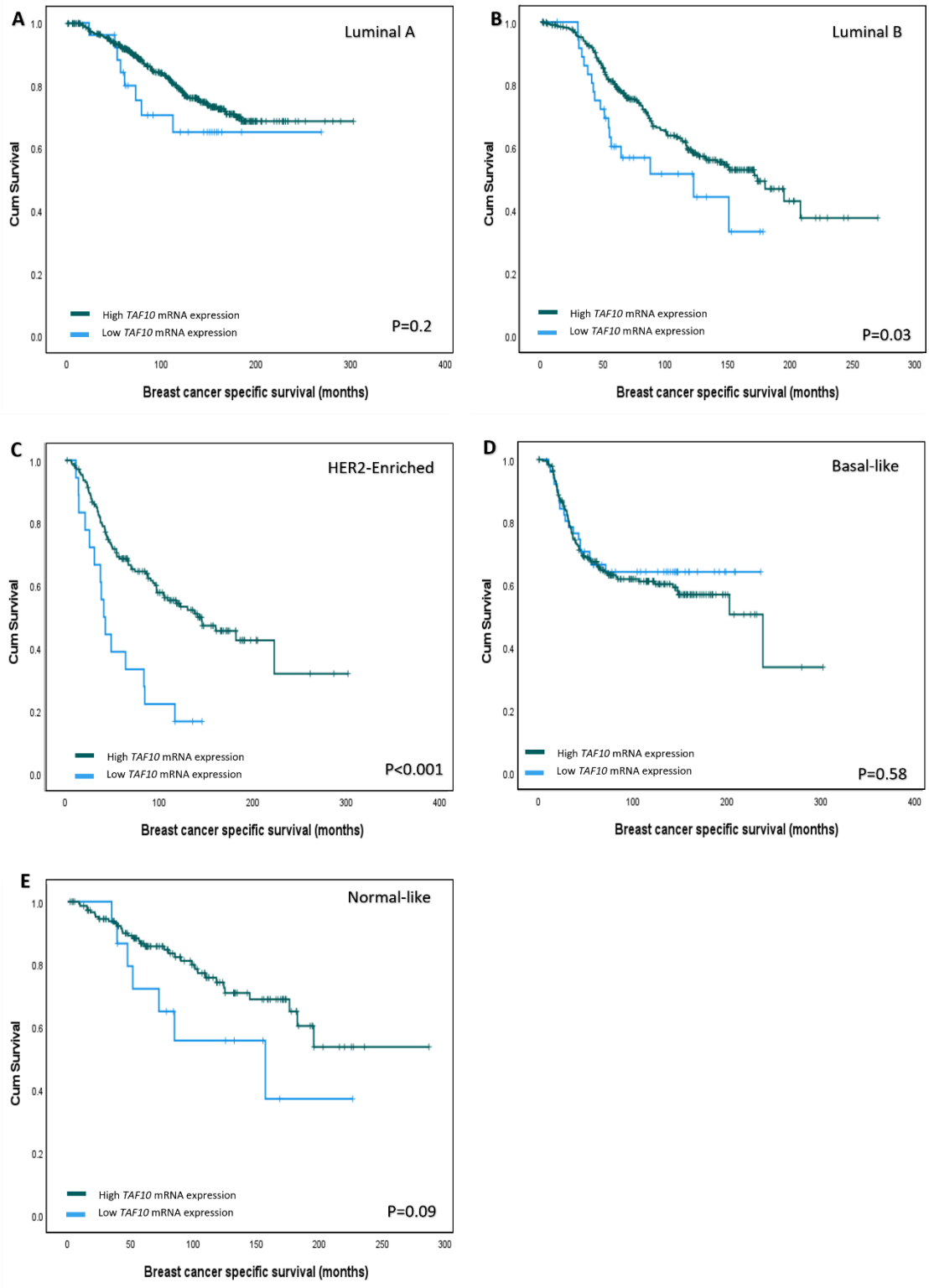


Figure 7.12: Kaplan Meier curves showing the prognostic significance of *TAF10* mRNA level in different molecular subtypes in the METABRIC cohort.

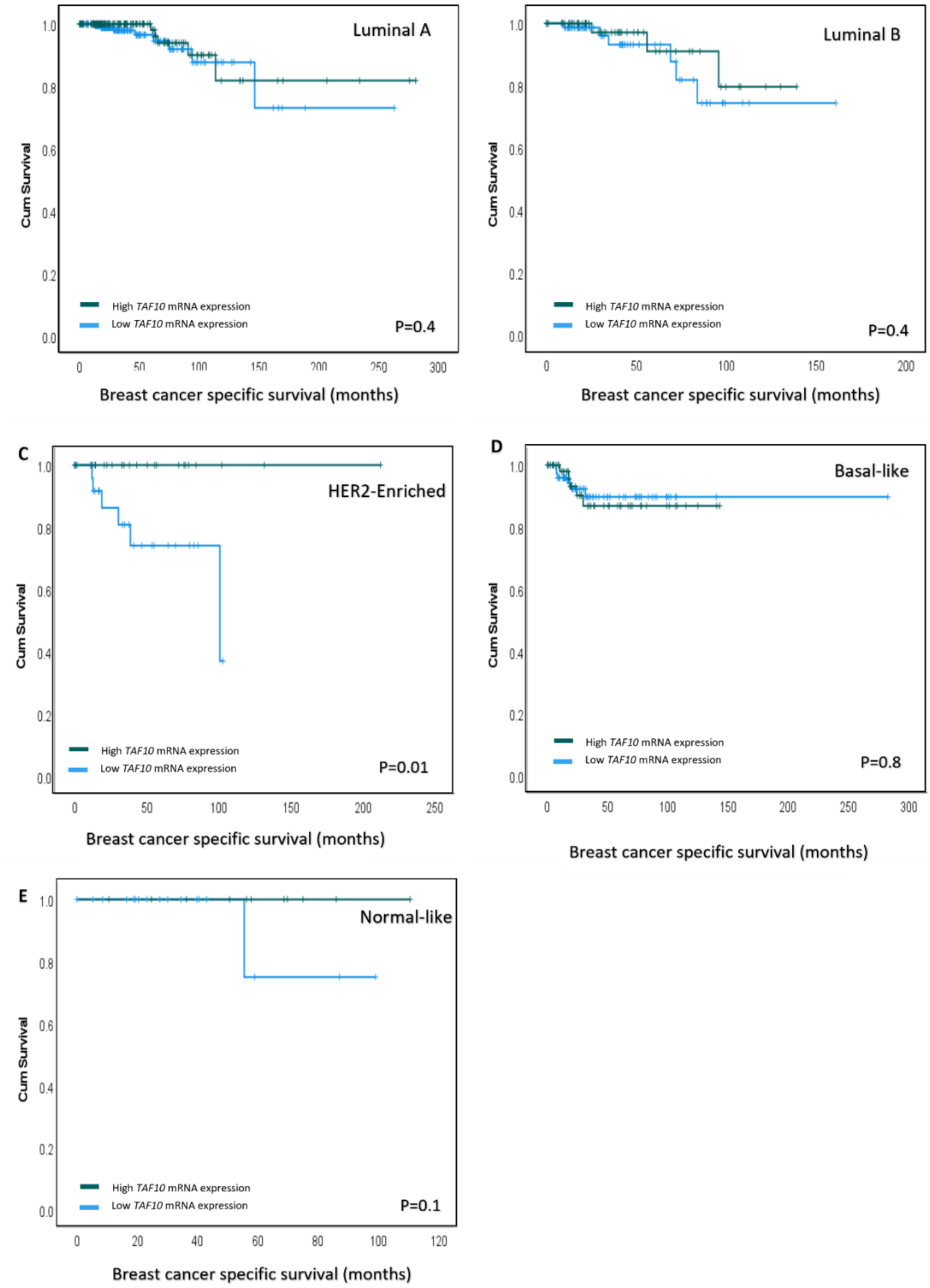


Figure 7.13: Kaplan Meier curves showing the prognostic significance of *TAF10* mRNA level in different molecular subtypes in the TCGA cohort.

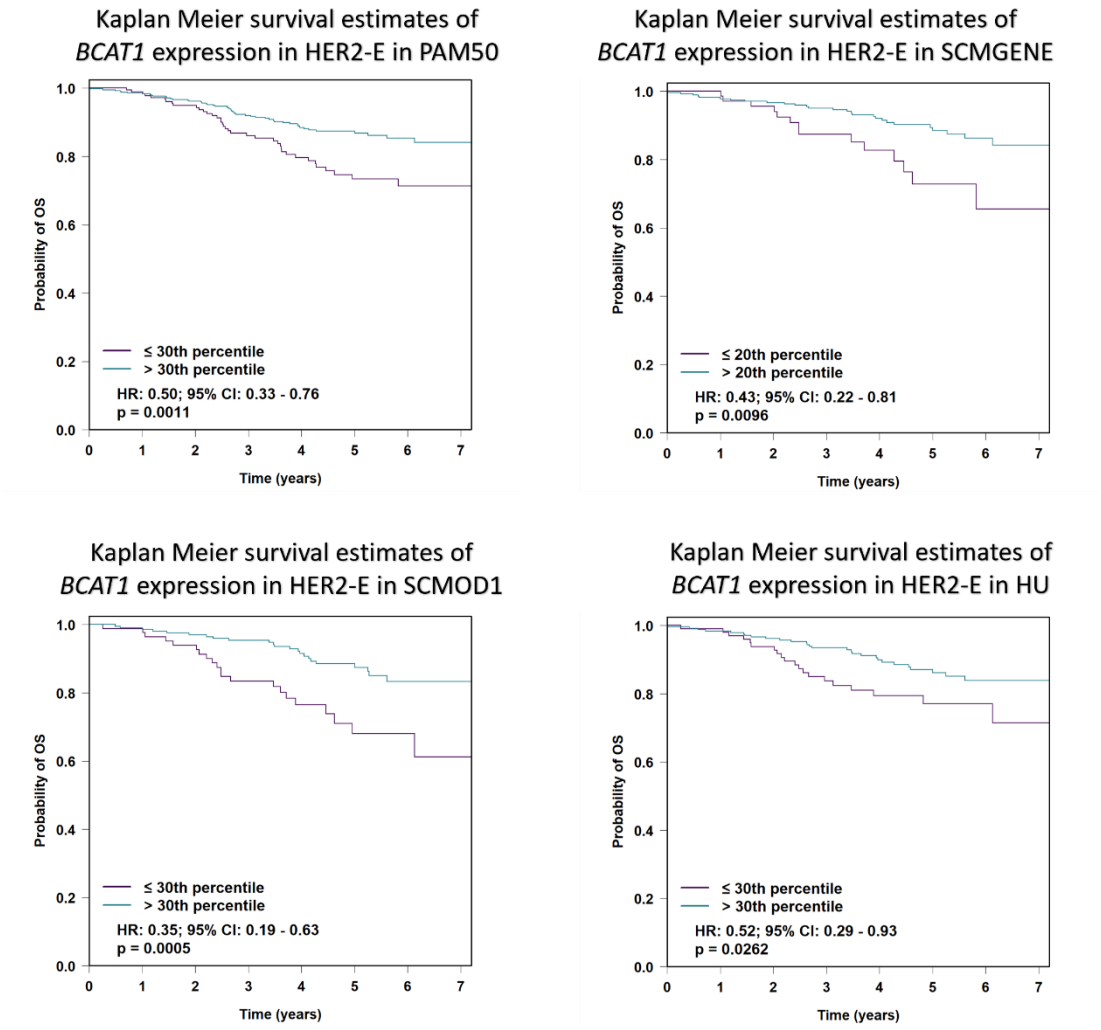


Figure 7.14: Kaplan Meier curves showing the prognostic significance of *TAF10* mRNA level in different molecular subtypes in the combined multicentric cohort. OS: overall survival. HER2-E: HER2 enriched

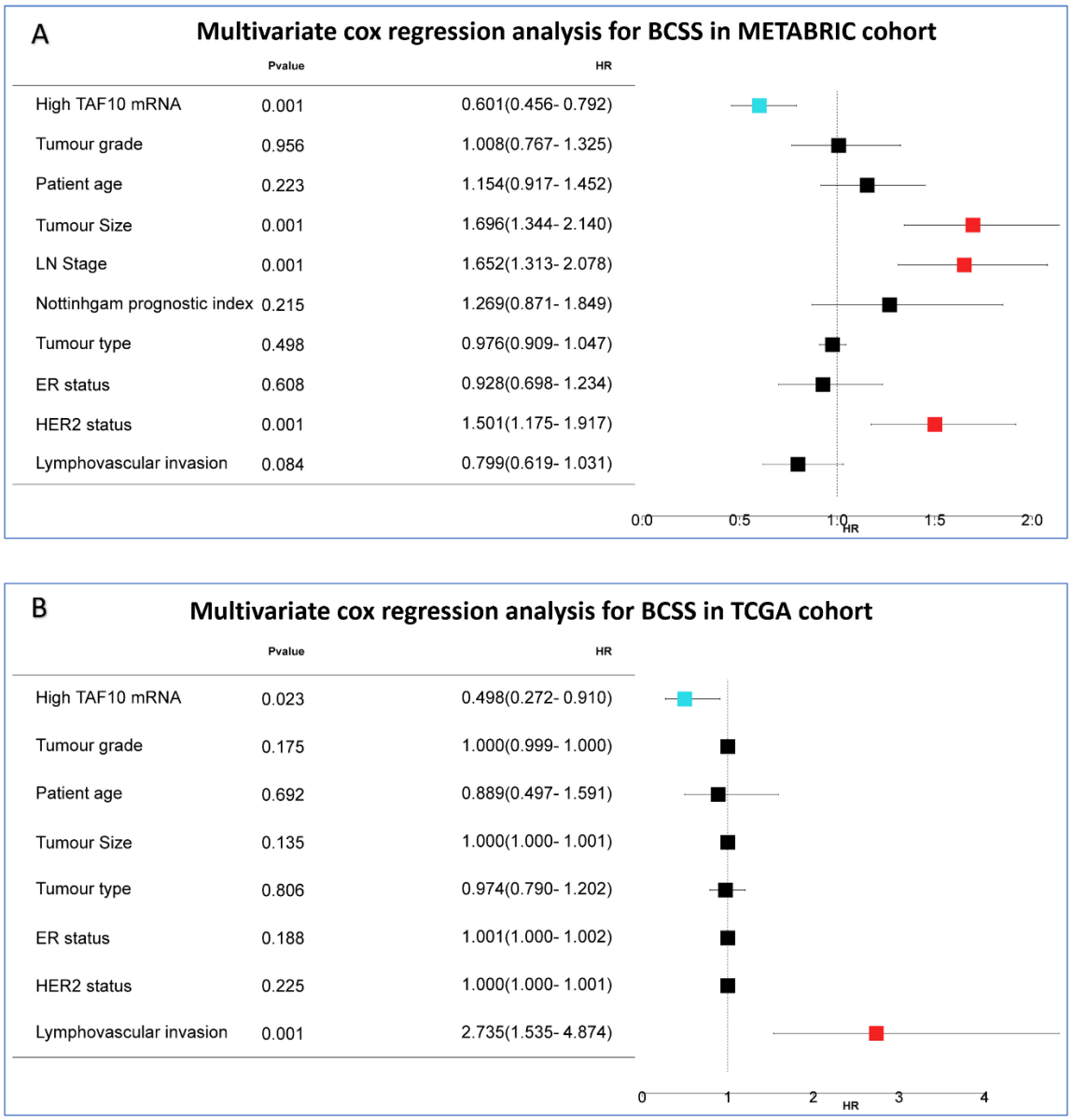
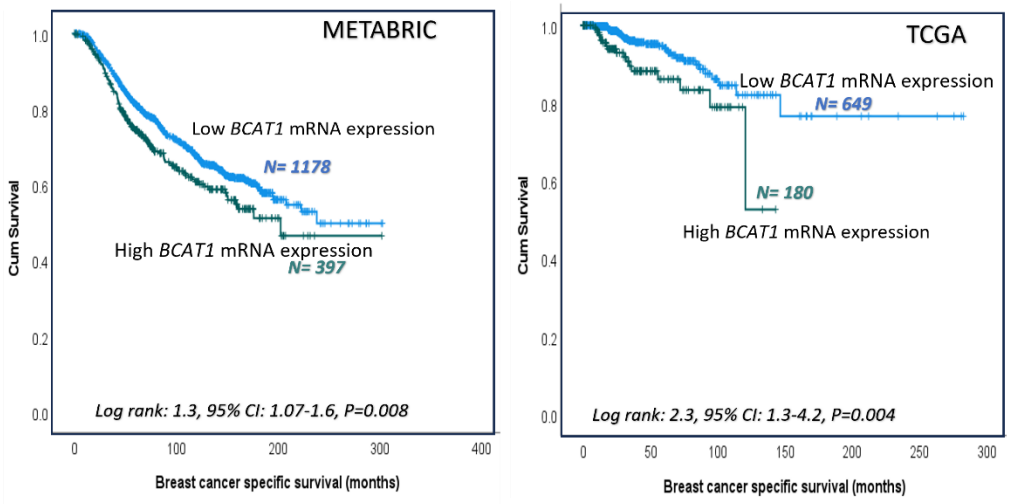


Figure 7.15: Forest plot demonstrating multivariate Cox regression analysis of factors affecting BCSS. *TAF10* mRNA was an independent predictor of better patients survival when adjusted for other tumour clinicopathologic parameters both in METABRIC and TCGA cohort



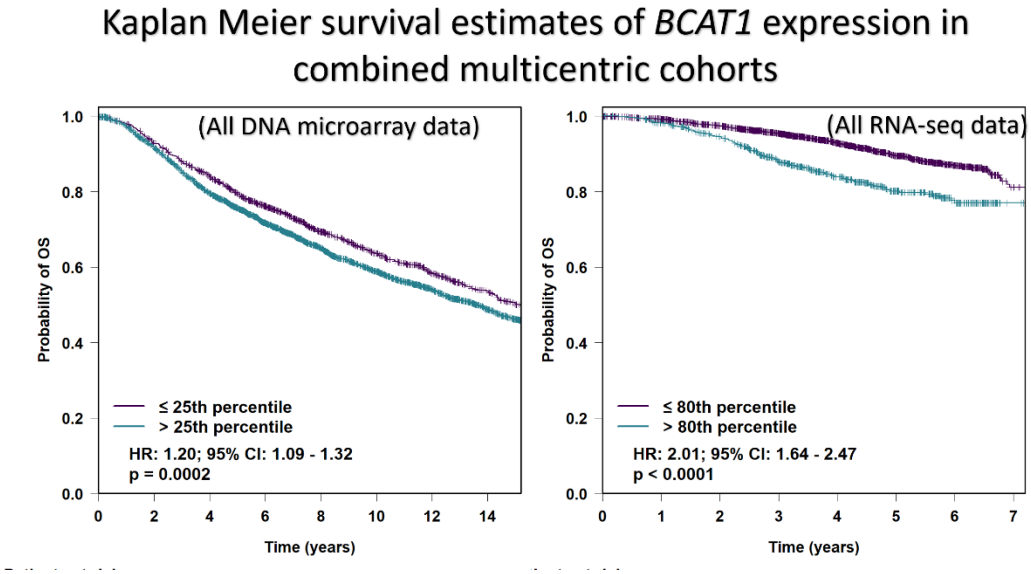


Figure 7.16: Kaplan Meier curves showing the prognostic significance of high *BCAT1* mRNA level in patient outcomes in the METABEIC cohort, TCGA cohort and multicentric combined cohort. OS: overall survival

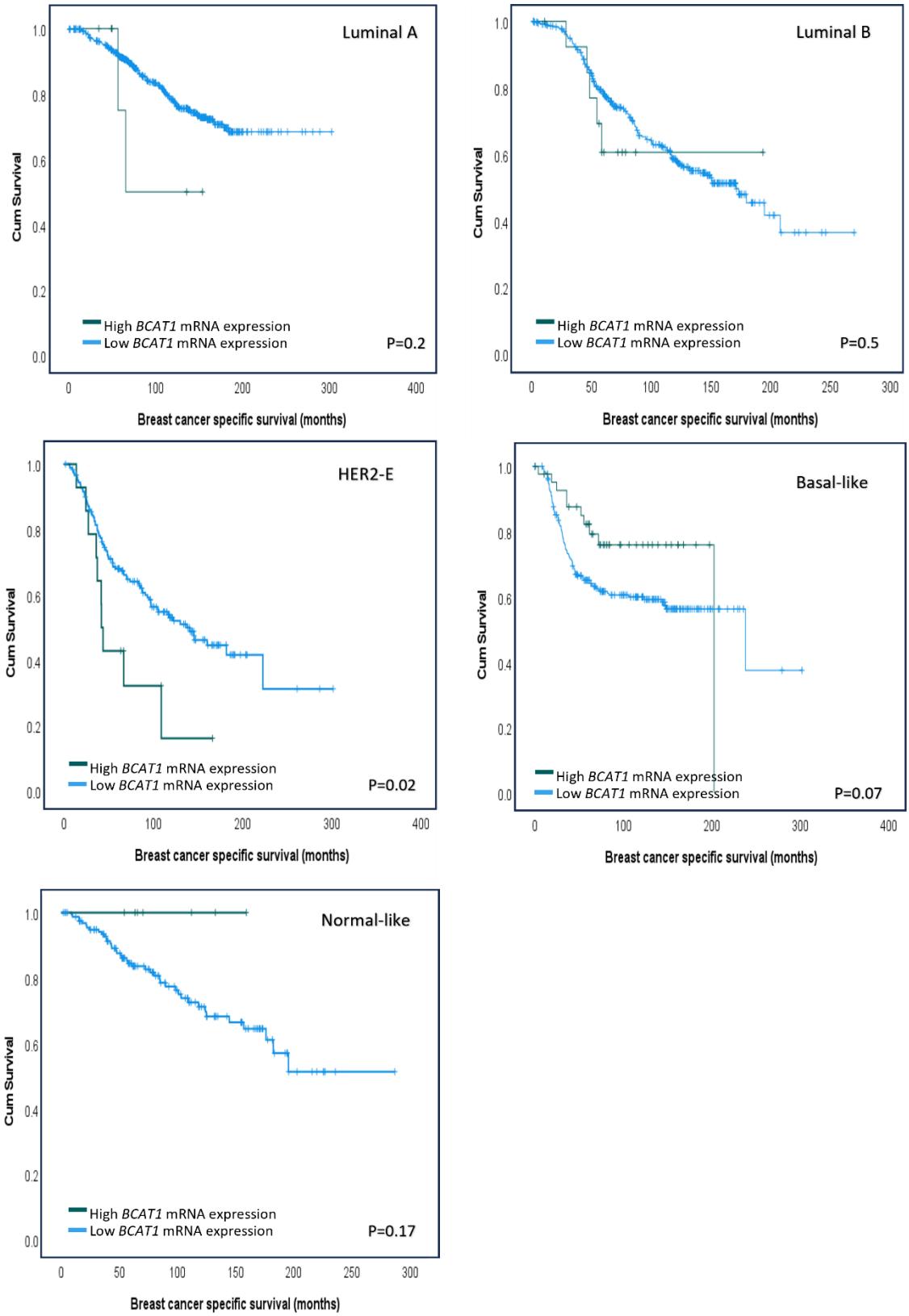


Figure 7.17: Kaplan Meier curves showing the prognostic significance of *BCAT1* mRNA level in different molecular subtypes in the METABRIC cohort.

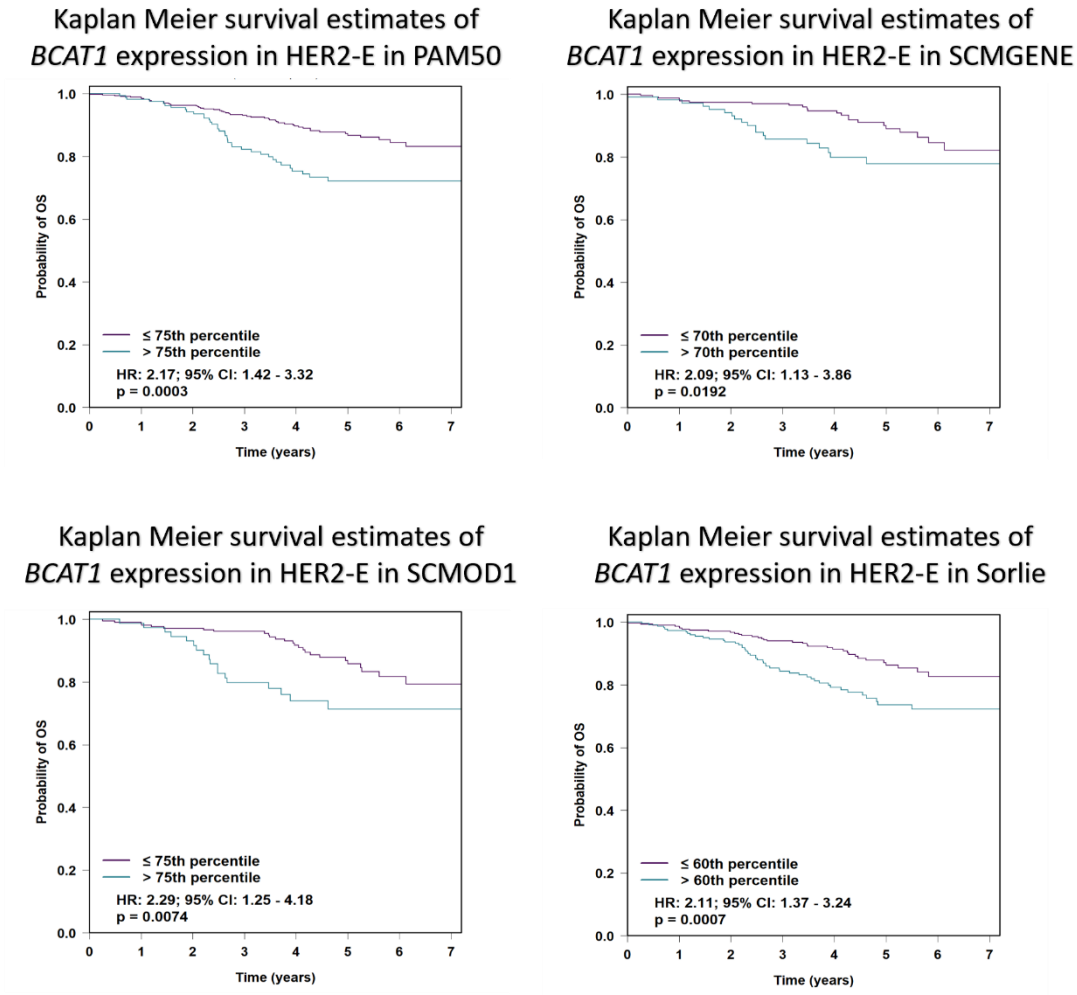


Figure 7.18: Kaplan Meier curves showing the prognostic significance of *BCAT1* mRNA level in different molecular subtypes in the combined multicentric cohort

7.5.6 TAF10 and BCAT1 protein expression

Evaluation of whole tissue sections showed that the staining pattern was homogeneously distributed, thus validating the applicability of IHC detection in TMAs. After the exclusion of uninformative cases (i.e., lost, folded or cores containing scanty tumour cells <15%), a total of 453 tissue cores were included for TAF10 antibody and 464 tissue cores for BCAT1 in the analysis. A high ICC=0.74, p<0.001) and intra-observer (ICC = 0.77, p< 0.001) concordance

were obtained. The cut-off points for TAF10, BCAT1 positivity was set using X-tile software.

TAF10 proteins were expressed mainly in the nucleus of invasive tumour cells, with intensity levels ranging from weak to strong **(Figure 7.19A-C).** Cytoplasmic expression was also observed and scored separately. The median H score of nuclear protein expression was 180 and 107 for cytoplasmic expression. High nuclear TAF10 protein (>195 H-score) was observed in 177/453 (39%) of BC cases.

BCAT1 protein expression in tumour cells was mainly cytoplasmic, with intensity levels ranging from weak to strong **(Figure 7.20 A-C).** The median value of protein expression was 140. High BCAT1 protein (>195 H-score) was observed in 147/466 (31.5%) of BC cases.

7.5.7 Association of TAF10 and BCAT1 protein expression with tumour clinicopathological parameters

High TAF10 nuclear protein expression showed a positive significant association with favourable tumour clinic-pathologic parameters like tumour grade I, small tumour size, good NPI ($p<0.001$) and LN stage N1 **(Table 7.4).** While BCAT1 showed significant correlations with high LN stage **(Table 7.5).**

7.5.8 Association of TAF10 and BCAT 1 protein expression with patient outcome

In the same line with *TAF10* mRNA, patients with tumours showing high TAF10 protein expression demonstrated significantly prolonged survival in terms of

longer BCSS (p=0.02) and DMFS (p=0.004) compared to those with low expression **(Figure 7.21)**

In multivariate Cox regression models, high nuclear TAF10 expression remained an independent predictor of longer BCSS (p=0.04) and DMFS (p=0.01) when considering other prognostic covariates such as tumour grade, size, nodal stage, LVI and HR status (**Figure 7.22).**

BCAT1 protein expression in Nottingham HER2-positive cohort did not show any significant association with patient outcomes**.** Although not statistically significant, dichotomising the cohort based on ER status revealed that high BCAT1 expression was associated with a higher number of events in ER-negative/HER2-positive patients compared with low BCAT1 expression **(Figure 7.23).**

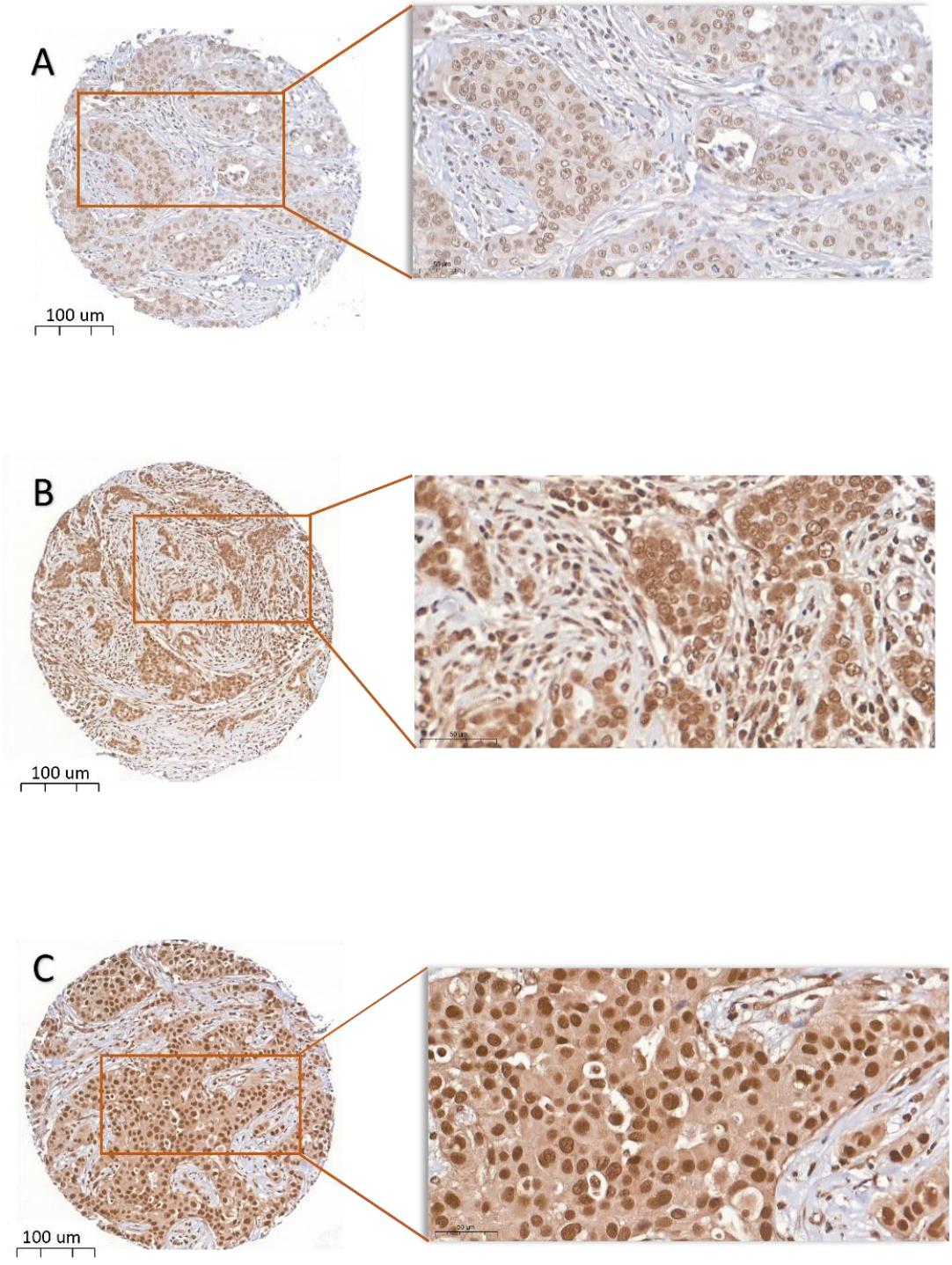


Figure 7.19: Immunohistochemical expression of TAF10 protein in breast cancer TMA sections. Nuclear intensity varied from mild (A) to moderate (B) and strong (C). High power scale bar=50 um. TAF10 also showed cytoplasmic expression.

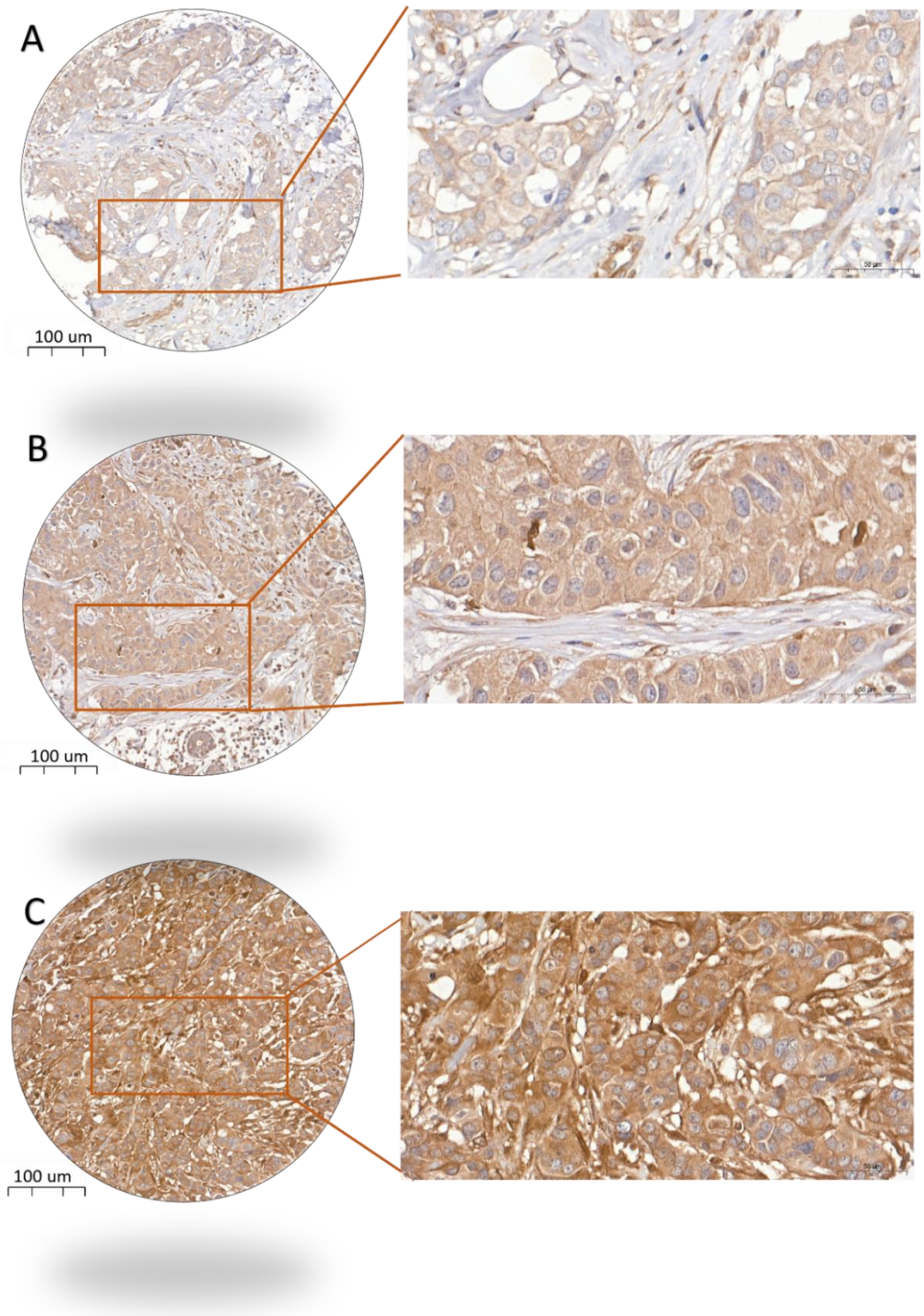


Figure 7.20: Immunohistochemical expression of BCAT1 protein in breast cancer TMA sections. Cytoplasmic intensity varied from mild (A) to moderate (B) and strong (C). The scale bar for the TMA image is 100um, and 50 um.for the high power image

Table 7.4: Correlation between TAF10 protein expression and clinicopathological parameters in Nottingham cohort

Parameter	Low TAF10 expression	High TAF10 expression	Test	TAF 10 H score	P value
	N (%)	*N* (%)	P *value*		
Age at diagnosis					
< 50 years	110 (41)	64 (36)	X^2=0.64	215.97	
≥ 50 years	166 (59)	113 (64)	0.41	233.88	0.16
Menopausal Status					
Pre	118 (43)	69 (39)	X^2=1.83	218.64	
Post	158 (56)	108(61)	0.48	232.87	0.25
Tumour size (cm)				.	
< 2.0	130 (47)	111 (63)	X^2=10.8	246.44	
≥ 2.0	146 (53)	66 (37)	**0.001**	204.90	**<0.001**
Tumour grade					
1	4 (1.6)	6 (3)		296.20	
2	49 (18)	55 (34)	X^2=14.4	264.30	
3	223 (80)	116 (63)	**0.001**	213.51	**<0.001**
Lymph node status					
Negative	142 (51)	90 (51)	X^2=0.17	230.40	
Positive	134 (49)	87 (49)	0.9	223.43	0.57
Lymph node stage					
1	131 (51)	81 (50)		230.40	
2	75 (29)	62 (39)	X^2=7.13	244.91	
3	51 (20)	18 (11)	**0.028**	178.97	**0.002**
Histologic tumour type					
IDC-NST	150 (91)	110 (89)		142.31	
ILC	4 (3)	2 (2)	X^2=1.86	130.08	
Other types	8 (6)	11 (9.0)	0.17	162.76	0.75
LVI					
No	183 (66)	125 (70)	X^2=0.88	231.86	
Yes	93 (34)	52 (30)	0.35	216.68	0.25
NPI risk group					
Good	33 (13)	32 (18)		269.63	
Moderate	153 (55)	108 (61)	X^2=8.12	229.30	
Poor	90 (32)	37 (21)	**0.013**	200.44	**0.002**
ER status					
Negative	121 (43)	48 (27)	X^2=7.36	192.98	
Positive	155 (56)	129 (73)	**0.001**	247.24	**<0.001**
PR Status					
Negative	176 (66)	92 (52)	X^2=10.9	204.10	
Positive	92 (34)	84 (48)	**0.005**	250.53	**<0.001**
HER2 IHC score					
3+	189 (76)	126 (71)	X^2=0.73	229.94	
2+/ISH positive	90 (24)	51 (29)	0.4	220.49	0.47

ER: Oestrogen receptor; **IDC-NST**: invasive duct carcinoma of no special type**; IHC:** immunohistochemistry **ILC**: invasive lobular carcinoma**; LVI**: lymphovascular invasion; **NPI**: Nottingham prognostic index, **PR**: Progesterone receptor Kruskal Wallis test was used to calculate the association between TAF10 continuous score and clinicopathologic parameters. *Some data are missing.

Table 7.5: Correlation between BCAT1 protein expression and clinic-pathological parameters in Nottingham cohort

Parameter	Low BCAT1 expression	High BCAT1 expression	Test	BCAT1 H score	
	N (%)	*N* (%)	*P value*		***P value***
Age at diagnosis					
< 50 years	129 (36.9)	46 (40.4)	X^2=0.44	241.21	
≥ 50 years	221 (63.1)	68 (59.6)	0.51	227.23	0.26
Menopausal Status					
Pre	140 (40)	49 (43)	X^2=.32	239.44	
Post	210 (60)	65 (57)	0.58	227.73	0.35
Tumour size (cm)					
< 2.0	187 (53.4)	55 (22.7)	X^2=0.9	. 231.77	
≥ 2.0	163 (46.6)	59 (51.8)	0.3	233.30	0.9
Tumour grade					
1	9(2.6)	1 (0.9)		172.60	
2	76 (21.7)	22 (19.3)	X^2=1.6	237.98	
3	265 (75.7)	91 (79.8)	0.46	232.67	0.3
Lymph node status					
Negative	183 (52.3)	54 (47.4)	X^2=0.83	232.11	
Positive	167 (47.7)	60 (52.6)	0.39	232.90	0.9
Lymph node stage					
1	183 (52.3)	54 (47.4)		232.11	
2	121 (34.6)	27 (23.7)	X^2=16.2	217.06	
3	46 (13.1)	33 (28.9)	<0.001	262.59	0.04
Histologic tumour type					
IDC-NST	316 (90.3)	97 (85.1)		230.73	
ILC	9 (2.6)	3 (2.6)	X^2=4.09	221.42	
Other types	25 (7.1)	14 (12.3)	0.08	254.63	0. 54
LVI					
No	231 (66)	69 (60.5)	X^2=1.13	229.60	
Yes	119 (34)	45 (39.5)	0.31	237.80	0.5
NPI risk group					
Good	49 (14)	14 (12.3)		233.43	
Moderate	206 (58.9)	59 (51.8)	X^2=3.2	230.60	
Poor	95 (27.1)	41 (36)	0.19	235.78	0.9
ER status					
Negative	143 (40.9)	44 (38.6)	X^2=0.18	215.98	
Positive	207 (59.1)	70 (61.4)	0.7	243.65	0.028

PR Status					
Negative	223 (64.8)	65 (58.6)	X^2=1.4	219.11	
Positive	121 (35.2)	46 (41.4)	0.26	243.32	0.059
HER2 IHC score					
3+	107 (30.6)	35 (30.7)	X^2=0.01	243.52	
2+/ISH positive	243 (69.4)	79 (69.3)	1.0	227.64	0.23

ER: Oestrogen receptor; **IDC-NST**: invasive duct carcinoma of no special type**; IHC:** immunohistochemistry **ILC**: invasive lobular carcinoma**; LVI**: lymphovascular invasion; **NPI**: Nottingham prognostic index, **PR**: Progesterone receptor Kruskal Wallis test was used to calculate the association between BCAT1 continuous score and clinicopathologic parameters. *Some data are missing

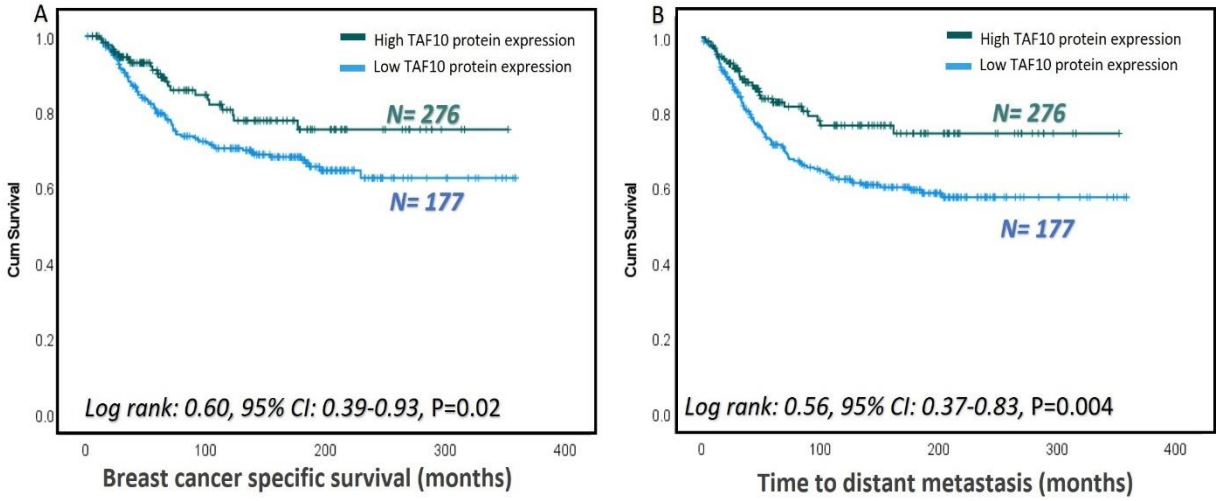


Figure 7.21: Kaplan Meier curve showing the association between TAF10 protein expression and patient outcomes in the Nottingham cohort.

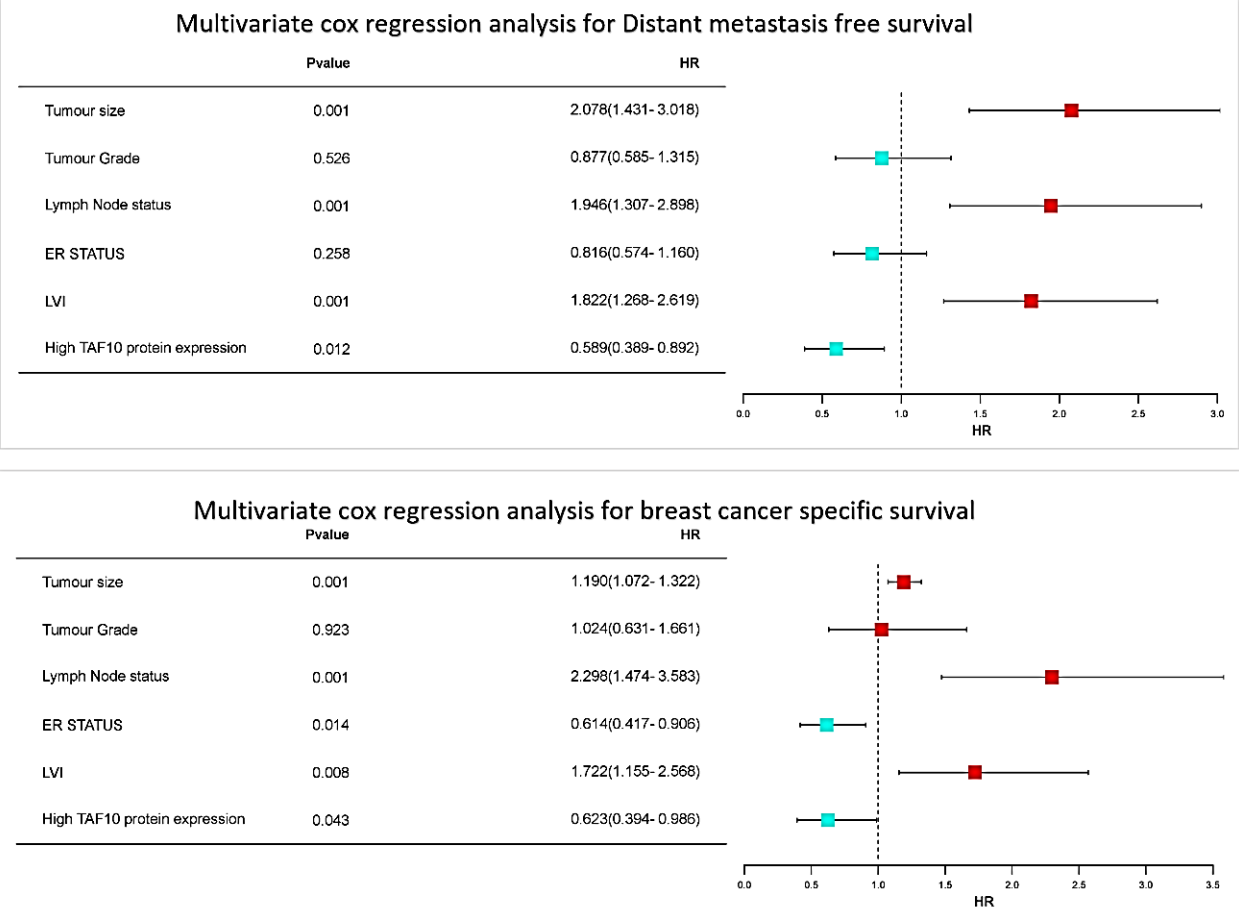


Figure 7.22: Forest plot demonstrating multivariate Cox regression analysis of TAF10 protein expression in predicting patients' survival when adjusted for other tumour clinicopathologic parameters in the Nottingham cohort.

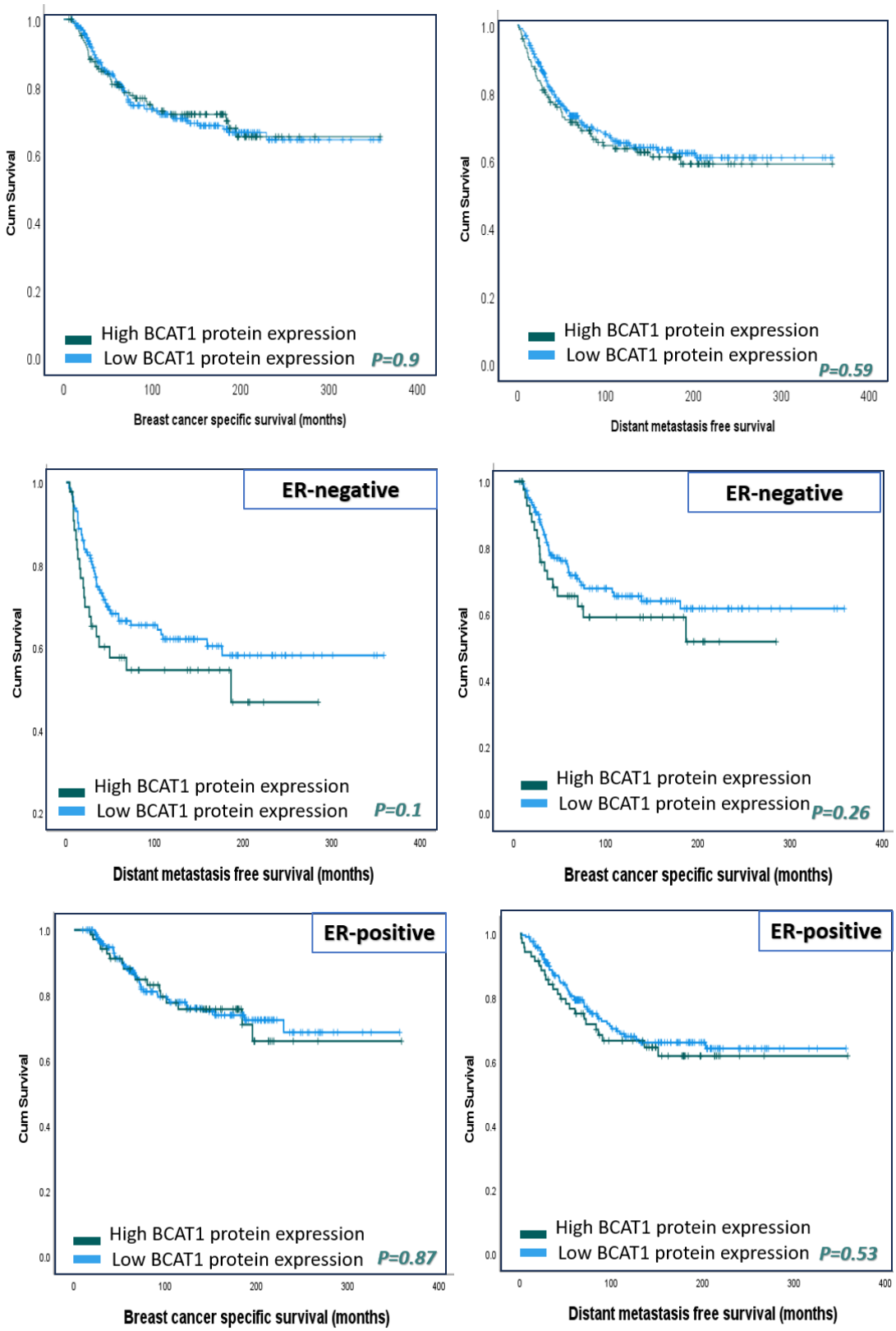


Figure 7.23: Kaplan Meier curve showing the association between BCAT1 protein expression and patient outcomes in the Nottingham cohort. Dichotomising the cohort by ER status revealed better stratification of patients outcomes

7.5.9 Prediction of response to anti-HER2 therapy

In the ROCPLOT dataset, high *TAF10* mRNA level in HER2-positive patients who received anti-HER2 therapy was associated with prolonged 5 years relapse-free survival compared to low *TAF10* mRNA level, while high *TAF10* mRNA level had no significant impact on chemotherapy-only treated HER2-positive BC patients in the same dataset **(Figure 7.24**).

This was further confirmed on the protein expression level in the Nottingham cohort, where high TAF10 nuclear expression was predictive of better response to anti-HER2 therapy, presented by prolonged DMFS and BCSS, compared to low TAF10 nuclear expression. Furthermore, high TAF10 nuclear expression in the treated patients was an independent predictor of prolonged DMFS when adjusted for other clinicopathologic parameters as HR status, tumour grade, tumour size, LN status and LVI (**Figure 7.25)**

Regarding BCAT1 predictive value in HER2-positive BC, high BCAT1 protein expression was significantly associated with poor response to therapy presented by short DMFS (HR: 2.7; 95% CI: 1.5- 4.8; p <0.001) and short BCSS (HR: 2.43; 95% CI: 1.8-5.6; p =0.02) in trastuzumab treated BC patients (**Figure 7.26)**

When BCAT1 expression was adjusted for other clinicopathologic parameters in a multivariate Cox regression model, It was an independent predictor of poor patients response to therapy (HR: 2.6; 95% CI: 1.43 - 4.8; p =0.002) **(Figure 7.27**).

7.5.10 TAF10 cytoplasmic protein expression

There was no significant association between TAF10 cytoplasmic expression and tumour clinicopathologic parameters. Also, no prognostic or predictive significance was detected for cytoplasmic TAF10 in our cohort.

7.5.11 Correlation between *TAF10* mRNA and PI3K/AKT/mTOR signalling genes.

We investigated the correlation between *TAF10* mRNA level and PI3K/AKT/mTOR, RAS/RAF pathway and *HER2* amplicon genes. We found that TAF10 is positively associated with high *ERBB2*, *GRB7* and *STARD3* genes from the HER2 amplicon. Also, a positive association with wild-type TP53 was found. However, *TAF10* mRNA showed a negative correlation with *PIK3CA, AKT3, KRAS, BRAF, MIB1, mTOR and RICTOR* genes.

Regarding *BCAT1* mRNA, a positive correlation was found with *PIK3CA, MIB1, RICTOR, mTOR, BRAF and KRAS* genes. Also, a negative correlation was seen between BCAT1 and *ESR1, GRB7 and TAF10* genes **(Figure 7.28).**

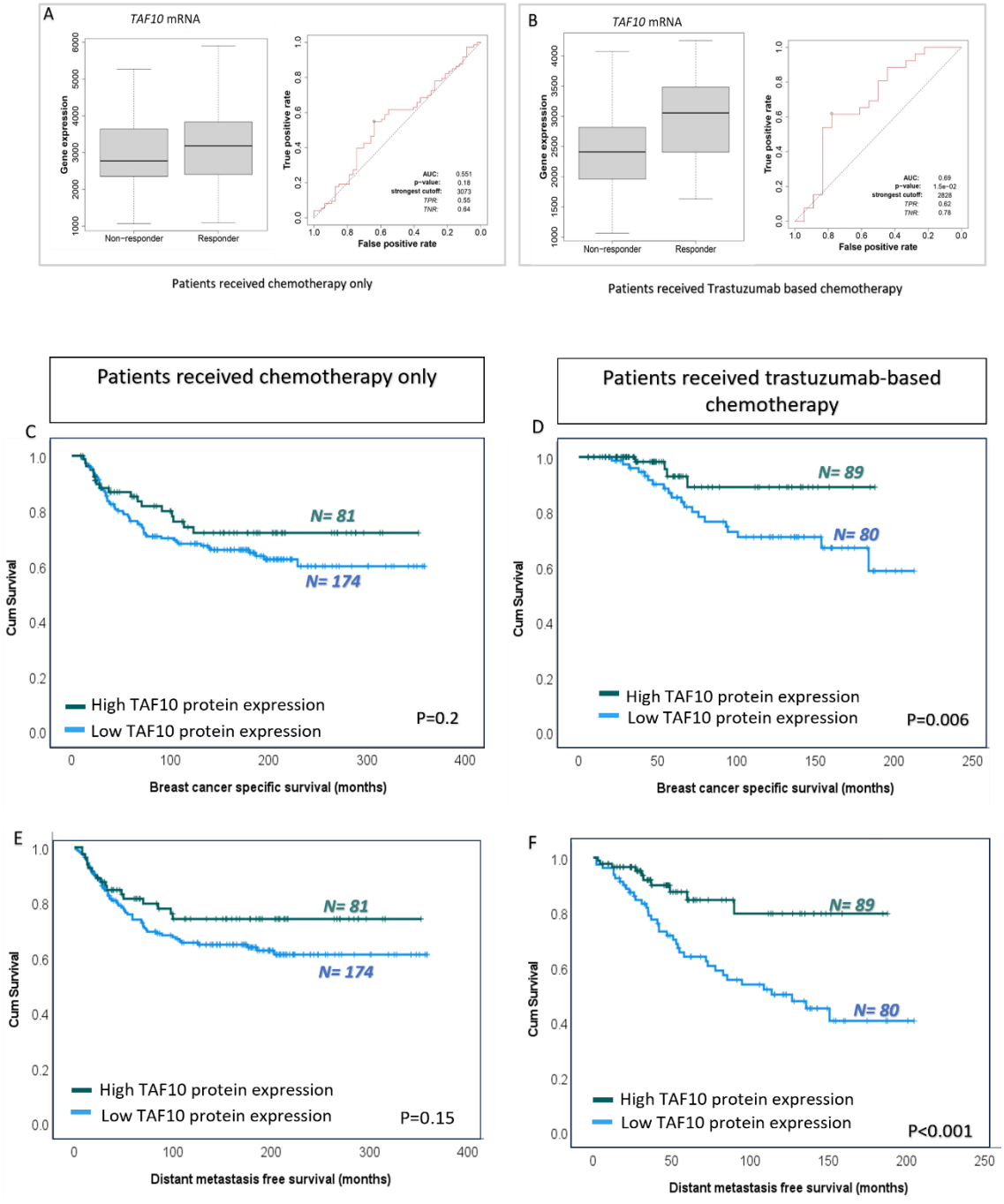


Figure 7.24: Charts showing the predictive role of TAF10 in HER2-positive breast cancer. A, B: Boxplot charts showing the association between *TAF10* mRNA level and relapse-free survival in HER2-positive patients with and without anti-HER2 therapy. C-F: Kaplan Meier curves illustrating the correlation between TAF10 nuclear expression and response to treatment. In chemotherapy only treated cohort, high TAF10 protein levels had no predictive role (C, E). While in patients who received anti-HER2-therapy high TAF 10 nuclear expression is associated with better DMFS and BCSS (D, F).

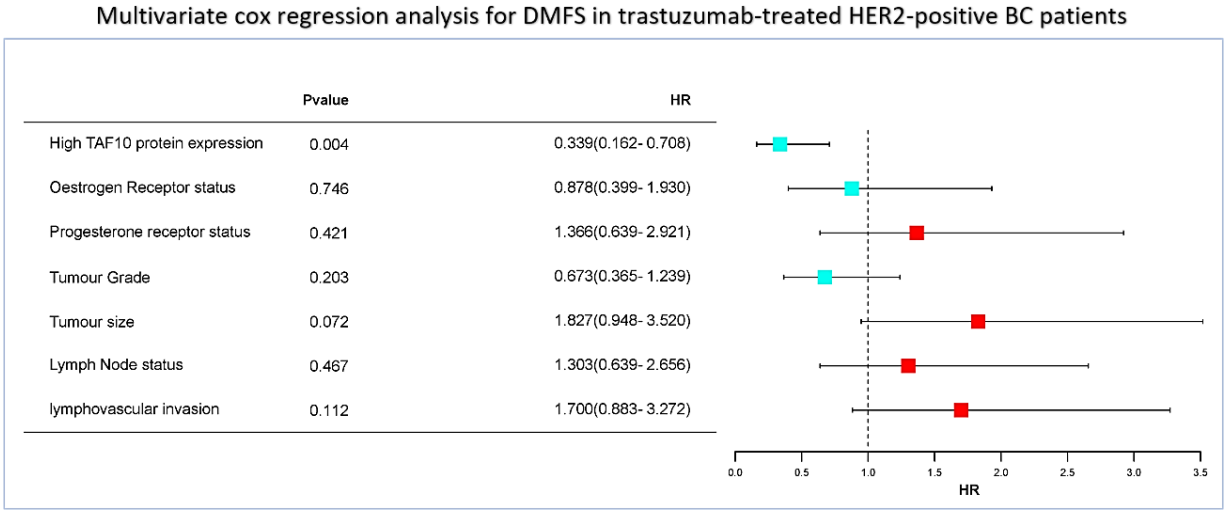


Figure 7.25: Forest plot demonstrating multivariate Cox regression analysis of factors predicting response in patients treated with anti-HER2 therapy. TAF10 protein expression was an independent predictor of prolonged DMFS when adjusted for other tumour clinicopathologic parameters in the Nottingham cohort.

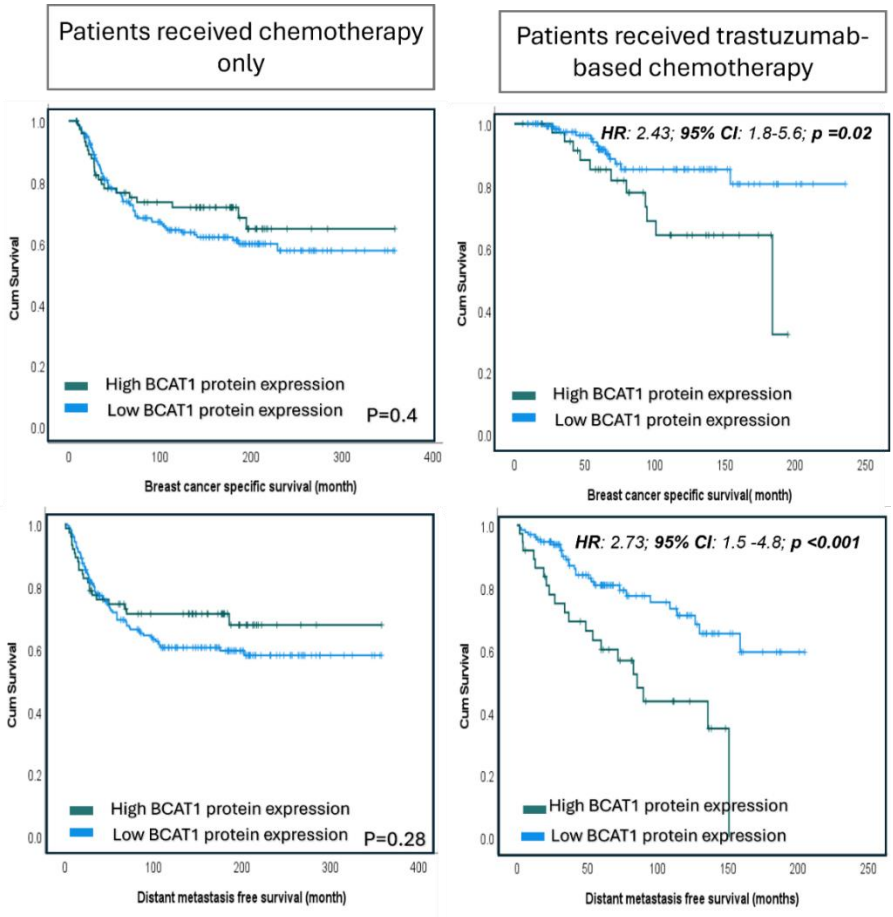


Figure 7.26: Kaplan Meier curves demonstrating the role of BACT1 expression in response to anti-HER2 therapy.

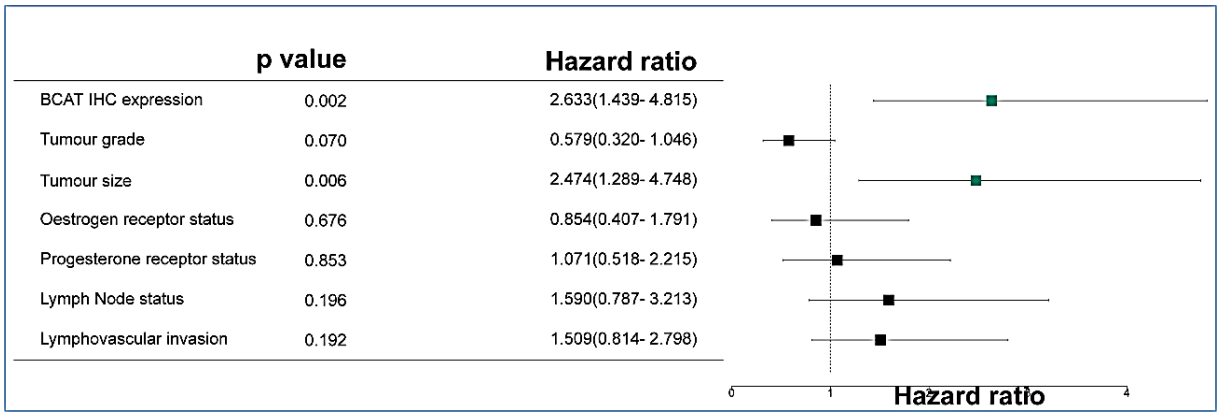


Figure 7.27: Forest plot demonstrating multivariate Cox regression analysis of factors predicting response in patients treated with anti-HER2 therapy. BCAT1 protein expression was an independent predictor of short DMFS when adjusted for other tumour clinicopathologic parameters in the Nottingham cohort.

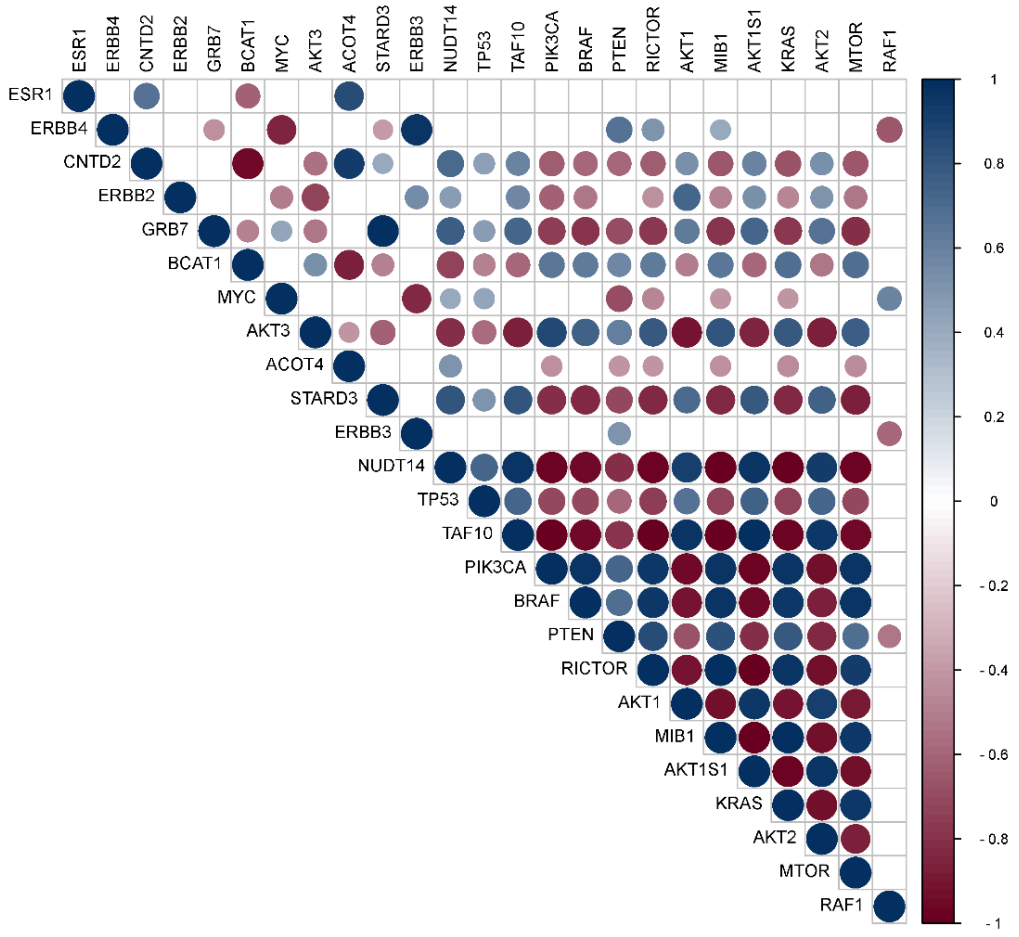


Figure 7.28: A correlation matrix displaying the relationships between the *BCAT1* and *TAF10* genes with other genes in the PI3K/AKT/mTOR pathway and the HER2 amplicon from TCGA cohort. Significant negative correlations are indicated in red, while significant positive correlations are shown in blue. The size of each circle represents the Spearman correlation coefficient (r), with larger circles indicating stronger correlations. Genes without significant correlations are not represented by circles.

7.6 DISCUSSION

This study investigated two genes and their potential role in cancer development and response to trastuzumab therapy in HER2-positive BC.

TAF10, a part of the TFIID complex, is crucial in controlling gene activity, including cancer-related ones. TAF10 exerts its influence by altering transcriptional networks. It can selectively interact with different transcription factors and co-activators to regulate specific sets of genes, depending on the cellular context. This flexibility allows TAF10 to control the expression of oncogenes or tumour suppressors, depending on the tissue or cancer type [603, 604].

Our results suggest that TAF10 is a prognostic and predictive marker that might increase trastuzumab effectiveness in HER2-positive BC patients with prolonged BCSS and DMFS. BCAT1, on the other hand, has a poor prognostic and predictive role in HER2-positive patients with a high risk of recurrence, nodal metastasis and resistance to therapy.

TAF10 is a pivotal player in epigenetic regulation and, further affects transcription and chromatin remodelling influencing cancer cell behaviour [589]. Its interaction with histone acetyltransferase complexes underscores its importance in epigenetic modifications that contribute to cancer development [590, 605].

Given its involvement in fundamental processes governing cell fate, TAF10 is emerging as an important target for understanding cancer biology and potentially for therapeutic interventions.

In the current study, we focused on the interaction between TAF10 and PI3K/AKT/mTOR pathway in addition to genes of HER2 amplicon to explain its role in response to trastuzumab. The PI3K/AKT and mTOR pathway, especially its components *mTOR* and *RICTOR*, plays an important role in cancer cell survival and growth, especially in HER2-positive BC, enabling cancer cells to survive despite HER2 inhibition [606-609].

*RICTOR (*Rapamycin-Insensitive Companion of mTOR*)* is essential for the kinase activity of mTORC2 (the mammalian target of rapamycin complex 2) and plays a crucial role in RTKs downstream signalling. Alterations in RICTOR have been identified in various cancer types, and studies have shown that RICTOR expression is significantly upregulated in invasive BC tissues compared to non-malignant tissues [607]. Its role in tumorigenesis has begun to be unravelled recently [608, 610]. In BC, RICTOR is particularly enriched in HER2-amplified samples and is associated with increased phosphorylation of AKT at Serine473, indicating a potential role for mTORC2 in HER2-driven BC. HER2-amplified BC utilise RICTOR/mTORC2 signalling to promote tumour growth, cell survival, and resistance to HER2-targeted therapies. Inhibiting mTORC2 could, therefore, be a promising therapeutic strategy, especially for eradicating HER2-positive BC that are resistant to HER2-targeted treatments [301, 302, 608, 611-617]. The negative correlation between MTOR/RICTOR and TAF10 suggests that TAF10 could play a role in reducing mTOR activity,

potentially improving response to trastuzumab by decreasing the effects of these resistance-promoting genes.

In addition to the PI3K/AKT/mTOR negative correlation, *TAF10* is significantly associated with low *MIB1* level. This could explain the good prognostic role of TAF10 in BC and presented in our study by low tumour grade and low NPI index group.

A weak positive correlation between *TAF10 and ERBB2* and other HER2 amplicon genes (*GRB7 and STARD3*) suggests that TAF10 may not directly regulate HER2 levels, and the role of TAF10 in the trastuzumab response may lie in pathways beyond HER2 regulation itself. Herein for the first time, we demonstrate the prognostic and predictive role of TAF10 in HER2-positive BC

BCAT1 expression has been linked to tumour progression and poor outcomes in several cancers, such as gastric cancer, glioma, liver cancer, and nasopharyngeal carcinoma [599, 600, 618-620]. Additionally, BCAT1 levels are higher in various BC types, including invasive carcinoma, intraductal carcinoma, and lobular carcinoma, compared to normal breast tissue [601, 602]. However, more extensive studies are still needed to validate the relationship between BCAT1 expression and prognosis in HER2-positive BC.

BCAT1 mRNA was significantly associated with HER2-E and HER2-positive tumours, with significant association of unfavourable tumour behaviour. This was demonstrated in earlier studies [621, 622]. HER2-positive BC shows increased glutamine metabolic activity, with elevated levels of proteins like glutaminase 1 (GLS1) and glutamate dehydrogenase (GDH) leading to tumour

proliferation, growth and metastasis [623-625]. Since transamination of BCAA into glutamine metabolites is mediated by BCAT1, which further enhances their flux into cells, this may explain its poor prognostic role in HER2-positive tumour growth. Our study found that high BCAT1 levels are associated with advanced nodal metastasis, poor response to therapy and shortened DMFS. This was previously reported where high levels of BCAT1 expression were linked with shorter DFS and OS in TNBC, indicating its role in tumour aggressiveness and resistance to therapy [600]. Furthermore, the knockdown of BCAT1 significantly inhibited BC cell growth, suggesting its importance in cancer cell metabolism and proliferation [620].

A possible explanation for the elevated expression of BCAT1 in aggressive tumours, particularly in HER2-positive cases, is its involvement in the PI3K/AKT pathway. BCAT1 enhances the activation of this pathway by promoting insulin-like growth factor 1 receptor (IGF-1R) signalling while concurrently inhibiting the renin-angiotensin system (RAS)/ERK pathway [626].

In the current study, BCAT1 positively correlated with high *mTOR, RICTOR, AKT, KRAS and MIB1 gene expression*. This comes in line with previous studies that concluded that BCAT1 activates the mTOR signalling pathway, which is essential for cellular growth and metabolism [619, 627].

The association between BCAT1 and resistance to therapy has been discussed before. Thewes and colleagues [628] discovered that BCAT1 was upregulated in endocrine resistant ER-positive BC cell lines [628]. In the current work, BCAT1 was also associated with increased resistance to anti-HER2 therapy, which confirms its role in drug resistance. This might be due to the

unopposed activation and signalling of PI3K/AKT pathway, which is one of anti-HER2 therapy resistance mechanisms

No inhibitors for BCAT1 have been developed; however, this work, together with previously published evidence, demonstrates that targeting BCAT1 could offer promising therapeutic potential for HER2-positive BC patients.

This study highlights the potential value of TAF10 and BCAT1 as predictors of anti-HER2 therapy response. More research is needed to better understand TAF10 and BCAT1's role and confirm how they influence the PI3K/AKT/mTOR pathway and other important signalling pathways in HER2-positive BC. Studying how these genes interact with PI3K or mTOR inhibitors could also open new treatment possibilities for overcoming trastuzumab resistance.

Chapter 8. Prediction of response to targeted anti-HER2 therapy using multigene assay

8.1 BACKGROUND

Refinement of HER2 classification for prediction of response to anti-HER2 therapy can improve BC patient's outcomes. The introduction of trastuzumab, the humanised anti-HER2 mAB, and the subsequent development of other anti-HER2 agents (i.e., lapatinib, pertuzumab, T-DM1 and T-DXd) have drastically improved the prognosis of HER2-positive BC patients. Nevertheless, not all patients benefit from these agents and eventually experience recurrence. Extensive translational research has been performed to identify predictive markers for patient treatment selection.

HER2-positivity in BC is currently defined by IHC and ISH in cases with equivocal HER2 protein expression (IHC score 2+). This classification was originally developed to predict the benefit of trastuzumab [159, 165]. However, the traditional definition of HER2-positive BC has recently been challenged, and BC patients with lower levels of protein expression (2+ Amplified) showed limited response to anti-HER2 therapies. The presence of HER2 intratumor heterogeneity also plays a role in influencing the response to anti-HER2 treatments and is associated with poorer patient outcomes [197, 202, 204, 218], a feature that is less likely to be captured when assessing HER2 status on core needle biopsies.

BC is typically classified using global gene expression analysis into intrinsic subtypes, including HER2-E, and HER2-negative classes and the latter includes Luminal A, Luminal B, and basal-like, each associated with distinct

prognoses and varying responses to treatment [41, 42, 629]. In clinical practice, IHC analysis of ER, PR, HER2, and Ki-67 protein expression is commonly used as surrogate markers for these molecular subtypes [391, 505].

However, the IHC evaluation of ER, PR, HER2, and Ki-67 necessitates rigorous standardisation in staining and interpretation processes to account for potential pre-analytical and analytical variables, such as inappropriate fixation, and variability in antibody clones and detection kits [99, 141, 165, 630] and false results cannot be eliminated [192, 195, 631]. Current HER2 assessment also presents challenges, particularly in cases with equivocal protein expression and low level of gene amplification and their response to therapy [141, 377, 632]

Although current guideline recommendations argue against testing HER2 status using mRNA-based techniques, a high correlation between *ERBB2* gene status and HER2 protein levels is documented [150-152]. The possibility to perform *HER2* mRNA testing by RT-qPCR has been extensively evaluated [152-154] and the detection of *HER2* mRNA was successful in >95% of samples [152]. Given that qPCR is quantitative and objective, while IHC is semi quantitative and observer-dependent, we may consider RNA evaluation as a possible option for HER2 assessment. Therefore, further research is needed to determine whether RNA-based testing can be used alongside, or as alternative to, the existing HER2 detection techniques (IHC and ISH) to refine the predictive value of HER2 status.

The response to anti-HER2 therapy is dependent not only on HER2 status, but also on the crosstalk between HER2 and other proteins including hormonal

receptors [308, 575]. Given these challenges, a standardised, robust, reliable, and cost-effective mRNA-based test for *ERBB2* and other key genes ER (*ESR1*), PR (*PGR*), and Ki-67 (*MKI67*), could provide a viable alternative or complement to the current HER2 assessment methodology.

The MammaTyper® multigene assay assesses the expression of 4 biomarkers *ERBB2* (HER2), *ESR1* (ER), *PGR* (PR), and *MKI67* (Ki67), utilising RT-qPCR and classifies BC into molecular classes. Studies have demonstrated that MammaTyper® assay can accurately predict the pCR to NACT, and concordance with IHC for ER and HER2 status have been validated in clinical practice, highlighting its potential to standardise biomarker assessment and improve clinical decision-making in BC treatment [633, 634].

8.2 INTRODUCTION

The variability in response rate among HER2-positive BC patients raised a question regarding the robustness of the current assays used in HER2 assessment. Despite being widely used in clinical practice, IHC assessment in HER2 is subjective with interobserver discordance, especially in the HER2-Low class [192, 195, 631]. Also, within HER2-positive classes, some staining scenarios are difficult to score i.e., strong or moderate incomplete staining in less than 10%. HER2 IHC 2+ tumours are considered positive if there is evidence of HER2 gene amplification by ISH techniques. However, the concordance between ISH results and HER2 IHC score in that class ranges from 60-80% [228, 535, 559].

Despite these advances in HER2-positive BC management, long-term results from the adjuvant pivotal trials indicated that approximately 15%-31% of patients experienced disease relapse [220, 221]. Moreover, the development of CNS metastases in 5% of the patients remains an unmet need [635].

In a previous study that compared different approaches for assessment of HER2 expression on protein and mRNA level and the accuracy of prediction of chemotherapy response in the neoadjuvant GeparTrio trial (NCT00544765), the authors stated that RT-PCR from FFPE tissue might be an additional approach for assessment of this important prognostic and predictive parameter but has to be confirmed by other studies [636].

8.3 HYPOTHESIS

In this study we hypothesised that assessment of *ERBB2* mRNA in combination with *ESR1*, *PGR*, and *MKI67* mRNA levels using the MammaTyper® multigene assay utilising large cohort of BC with long term outcome data can provide better predictive stratification of HER2-positive BC patients to anti-HER2 therapy.

8.4 AIMS OF THE STUDY

- Assess the validity of the MammaTyper® multigene assay in predicting the response of HER2-positive patients to targeted anti-HER2 therapy utilising a large HER2-positive BC cohort with long-term follow-up.
- Compare the predictive performance of the MammaTyper® assay with the current detection method of HER2 status (IHC with or without ISH).

- Assess whether the use of MammaTyper® assay alone or in combination with the current detection methods of HER2 status can improve stratification of HER2-positive BC.

8.5 MATERIALS AND METHODS

8.5.1 Cohort selection and characterisation

A well-characterised HER2-positive BC cohort of 350 cases selected from the Nottingham cohort (**Section 2.1.1**) and were diagnosed at Nottingham University hospitals between (1998-2018) was included. The cohort was divided into 2 groups: a group of patients who received targeted adjuvant anti-HER2 therapy (n=190), and a chemotherapy only treated group where the patients were diagnosed before approval of anti-HER2 therapy (n=160). Clinicopathological parameters, treatment regimens and follow-up data were collected from the data registry.

In both study groups, tumour clinicopathological parameters were matched, particularly aggressive parameters such as tumour grade, LN metastasis, and tumour size. This matching was done to ensure that anti-HER2 therapy would be the primary predictive factor for patient survival. Within the HER2-positive cohort, two molecular subtypes were identified: luminal B-like/HER2-positive (ER-positive, PR-positive/negative, HER2-positive and HER2-positive/non luminal (HER2-positive, ER-negative, PR-negative).

BCSS, defined as the time from initial diagnosis to time of BC related death and DMFS considered as the time from initial diagnosis to any distant metastatic event were calculated. DFS defined as the time from initial diagnosis to any recurrence event were also calculated. Mean patient follow-up was 51

months (IQR: 26 months). The biomarkers were stained as part of routine patient diagnostic workflow and their data status were retrieved from patients records, however Ki67 IHC is not carried out routinely in Nottingham hospitals standard of care. . HER2 staining was completed on the Ventana Benchmark ULTRA IHC automated staining system using the Ventana PATHWAY anti-HER-2/neu (4B5) rabbit monoclonal ready to use primary antibody in combination with Ventana detection kits. Cases with equivocal HER2 protein expression underwent FISH assay for gene amplification assessment. ER and PR IHC staining was carried out following a standard protocol as detailed in **Section 2.3.**

8.5.2 Biomarker evaluation

Percentage of expression and H score assessment was carried out for ER and PR by former researchers, and data were available in Nottingham biomarker library. Also, *HER2* gene copy number for a subset of cases was available (N=81) through CISH assay. Details are mentioned in **Section 2.7.** Cases with qualified FFPE samples and valid MammaTyper® results were included for analysis and comprised 287 HER2-positive cases, (N=159) received trastuzumab, and (N=127) were chemotherapy-only treated patients. (**Figure 8.1).**

8.5.3 Sample preparation and RNA extraction.

Freshly cut H&E sections were prepared from each tumour block, and a pathologic review of a representative H&E-stained slide (resection specimen) ensured the presence of sufficient tumour tissue with at least 20 % tumour cells.

RNA extraction was performed using two different RNA extraction assays on 25% of the cohort. We compared RNA concentration and purity between these two assays, selecting the one with the best RNA yield for use with the remaining samples. The assays used for RNA extraction were the RNXtract® Nucleic Acid Extraction Kit IVD (BioNTech Diagnostics GmbH) and the Qiagen RNeasy FFPE kit. By comparing these methods, we aimed to identify the most effective technique for obtaining high-quality RNA from FFPE tissues, thereby facilitating subsequent molecular analyses.

For each assay, four consecutive 5 µm-thick FFPE sections were cut using a standard microtome (Reichert-Jung Hn40; Leica Instruments). Each pair of sections (totalling 10 µm in thickness) was placed into separate 1.5-mL microcentrifuge tubes (Starlab). One tube was designated as a backup, and both tubes were stored at 4 °C until the extraction process commenced. The steps are detailed in **Section 2.6.2.**

8.5.4 Assessment of RNA concentration

We utilised Qubit™ RNA high sensitivity (HS) assay Kit, (Invitrogen, ThermoFisher, cat. No. Q32852) on a Qubit™ 4 Fluorometer. It is a powerful tool for accurately quantifying RNA samples with high sensitivity and specificity across a wide dynamic range. The assay is accurate for initial sample concentrations from 0.2 ng/µL to 200 ng/µL, providing an assay range of 4−200ng/µL. RNA concentration from 80 cases extracted by the two mentioned RNA extraction assays was compared. The values were recorded in ng/ul. Details are mentioned in **Section 2.6.3.**

8.5.5 mRNA quantification with RT-qPCR

The expression levels of *ERBB2, ESR1, PGR and MKI67* were determined by RT-qPCR using the CE-marked MammaTyper® assay (Ref CC01010, Cerca Biotech GmbH) on Applied Biosystems® 7500 Fast Real-Time PCR system with software version 2.3. With MammaTyper®, reverse transcription of RNA and amplification of cDNA take place successively in one reaction mix. Two internal reference genes (REF) for assessment of sample validity and normalisation; B2 macroglobulin (*B2M*) and Calmodulin 2 (*CALM2*). mRNA quantification was carried out according to the manufacturer protocol [637], as detailed in **Section 2.6.4**. mRNA cut-off for biomarker positivity was predefined to match clinically validated cut-point; ≥1% for *ESR1*, *PGR* positivity. For *MKI67,* we considered the cutoff value for Ki67 IHC from guidelines and evidence from the literature. A majority of the St Gallen's Panel voted that a threshold of ≥20% was indicative of 'high' Ki67 status [51]. Assessment of gene status was carried out using the MammaTyper® Report Generator.

8.5.6 Validation of discordant results

For cases exhibiting discordant HER2 status between IHC protein expression on core biopsy and their corresponding mRNA expression, double validation was performed using two main approaches: 1) reviewing the HER2 status and FISH level in the original patient diagnostic database, and 2) re-staining the discordant cases on full-face excision specimens from the same block used for MammaTyper® mRNA analysis.

For IHC staining, sections were incubated with the rabbit polyclonal antibody against human HER2 (HercepTest antibody, Dako, 1:400 for 30 minutes at room temperature) (**Section 2.3**).

Biomarkers scoring was based on ASCO/CAP and UK guidelines [141, 161]. The final HER2 status of borderline IHC protein expression was assessed based on *HER2* gene amplifications from CISH that were carried out according to the manufacturer protocol [638].

8.5.7 Statistical analysis

Statistical package of social science (IBM-SPSS) statistical software v. 28.0 (SPSS, Chicago, IL, USA) was used to perform the statistical analyses. Correlation analyses were carried out using Chi-square and Mann-Whitney tests where appropriate. Outcome analysis was assessed using univariate and multivariate Cox regression models, Kaplan–Meier curves, and the log-rank test. For all tests, $p<0.05$ (two-tailed) was considered statistically significant. The C-index, or Concordance Index, is a measure of predictive accuracy for risk models; it was calculated using Python software as the proportion of all possible pairs of patients in which the predictions and outcomes are concordant, effectively quantifying the model's ability to discriminate between higher and lower risks."

8.6 RESULTS

8.6.1 Basic clinicopathological parameters of the study cohort

A total of 287 HER2-positive BC cases were enrolled in the study after exclusion of 63 cases. MammaTyper® testing was applied on all full-face resection specimens. Cases were divided into two groups based on the administration

of anti-HER2 therapy; chemotherapy only treated cohort (n=128) and the trastuzumab-based chemotherapy-treated cohort (**Figure 8.1)**. The median *HER2* gene copy number by CISH assay was 8.1 and ranged between (6-14). Clinicopathological parameters in both chemotherapy-only and trastuzumab-based chemotherapy-treated patients are summarised in **Table 8.1.**

8.6.2 Quality of RNA among two extraction assays

Twenty-five per cent (23/90) of cases that underwent RNA extraction using spin column-based assay (Qiagen RNeasy FFPE kit) had very low RNA concentration <0.2ng/ul, and these samples failed amplification on RT-qPCR. However, the failure rate for the mag- beads-based RNA extraction assay (RNXtract® Nucleic Acid Extraction Kit IVD) was 4.4% (4/90 samples). The rest of the cases were extracted using the RNXTRACT assay, and 13 cases in total had low RNA yield not enough for amplification and were excluded from the final analysis **(Figure 8.1).**

8.6.3 *ERBB2* mRNA, *HER2* gene copy number and HER2 IHC score

There was positive correlation between *ERBB2* mRNA and *HER2* gene copy number (R=0.31, p=0.006).

ERBB2 mRNA was significantly higher in HER2 IHC3+ cases compared to HER2 IHC 2+/ISH positive cases (P=1.4e-14). The same result was found when evaluating the *HER2* gene copy number between HER2 IHC 3+ and HER2 IHC 2+/ISH positive cases, however, with a much less significant association (p=0.03).

Regarding correlation with IHC based molecular subtype, *ERBB2* mRNA was significantly associated with HER2-E molecular subtype compared to luminal

B/HER2-positive (p=0.00019), unlike *HER2* gene copy number which showed no significant association (p=0.33) **(Figure 8.2).**

8.6.4 MammaTyper® defined HER2 status

The mean ± SD of *ERBB2* was 42.31 ± 2.25, with a predefined cut point for positivity, MammaTyper® assay identified 251/ 287 (87.4%) cases as HER2-positive, while 36 out of 287 (12.6%) were *ERBB2*-negative including 31/287 (10.6%) HER2-Low cases **(Table 8.2).** Among *ERBB2*-positive cases, 97% exhibited a high *MKI67* proliferative index, and 81% (203/251) of *ERBB2*-positive cases scored 3+ on the IHC assay. Details on mRNA-based biomarkers status and correlation with the clinicopathologic parameters are summarised in **Table 8.2 and Table 8.3.**

Considering MammaTyper® assay defined *ERBB2*-negative cases, 70% (26/36) were HER2 IHC 2+/ISH positive, with a median *HER2* gene copy number of 6.5.

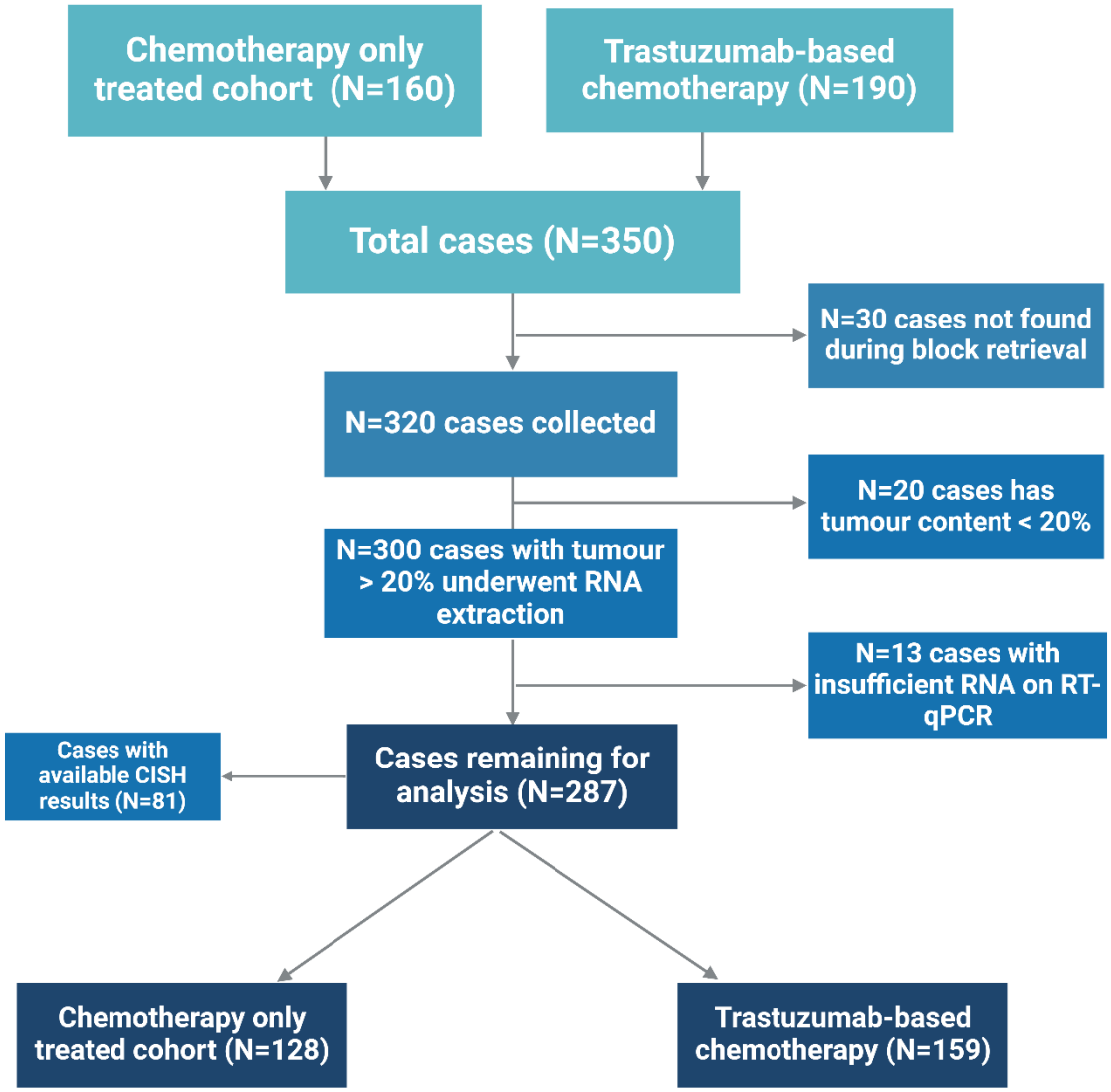


Figure 8.1: Flow chart of the cohort used in the study. RT-qPCR: reverse transcriptase quantitative polymerase chain reaction

Table 8.1: Basic clinicopathological characteristics in both cohorts

Parameter	Whole cohort (n=287)		Chemotherapy only treated (n=128)		Trastuzumab based chemo-therapy (n=159)		*Chi-square (X^2)* P value
Age at diagnosis (years)							
< 50	134	(46.7)	76	(59.0)	58	(36.0)	X^2 =14.9
≥ 50	153	(53.3)	52	(41.0)	101	(64.0)	<0.001
Menopausal Status							
pre	144	(50.2)	81	(63.0)	63	(40.0)	X^2 =15.8
post	143	(49.2)	47	(37.0)	96	(60.0)	<0.001
Tumour size (cm)							
< 2.0	109	(38.0)	45	(35.0)	64	(40.0)	X^2 =0.78
≥ 2.0	178	(62.0)	83	(65.0)	95	(60.0)	0.4
Tumour grade							
1	2	(0.7)	0	(0.0)	2	(1.0)	X^2 =4.1
2	29	(10.1)	9	(7.0)	20	(12.0)	0.13
3	256	(89.2)	119	(93.0)	137	(87.0)	
Histologic tumour types							
Invasive duct carcinoma (NST)	255	(89.0)	116	(91.0)	139	(88.0)	X^2 =6.4
Invasive lobular carcinoma	7	(2.4)	1	(0.8)	6	(3.8)	0.79
Other types	25	(8.6)	11	(8.2)	14	(8.2)	
Lymph node status							
Negative	100	(34.8)	44	(34.0)	56	(35.0)	X^2 =0.02
Positive	187	(65.2)	84	(66.0)	103	(65.0)	0.9
Lymphovascular Invasion							
No	159	(55.4)	63	(49.0)	96	(60.0)	X^2 =3.57
Yes	128	(44.6)	65	(51.0)	63	(40.0)	0.073
NPI risk group							
Good	6	(2.1)	2	(1.6)	4	(2.5)	X^2 =3.3
Intermediate	161	(56.1)	65	(50.0)	96	(60.0)	0.186
Poor	120	(41.8)	61	(47.4)	59	(37.5)	
Oestrogen receptor status							
Negative	130	(45.3)	67	(52.3)	63	(39.6)	X^2 =4.6
Positive	157	(54.7)	61	(47.7)	96	(60.4)	**0.03**
Progesterone receptor							
Negative	192	(67.6)	90	(71.0)	102	(65.0)	X^2 =1.5
Positive	92	(32.4)	36	(29.0)	56	(35.0)	0.25
HER2 IHC score							
IHC 2+	74	(25.8)	91	(71.0)	122	(77.0)	X^2 =1.17
IHC3+	213	(74.2)	37	(29.0)	37	(23.0)	0.28
Molecular subtype							
Luminal B/HER2-positive	157	(55.5)	61	49.2	96	60.4	*X2=3.5*
HER2-positive	126	(44.5)	63	50.8	63	39.6	0.07

NST: non-special type; **NPI:** Nottingham prognostic index**; IHC**: immunohistochemical

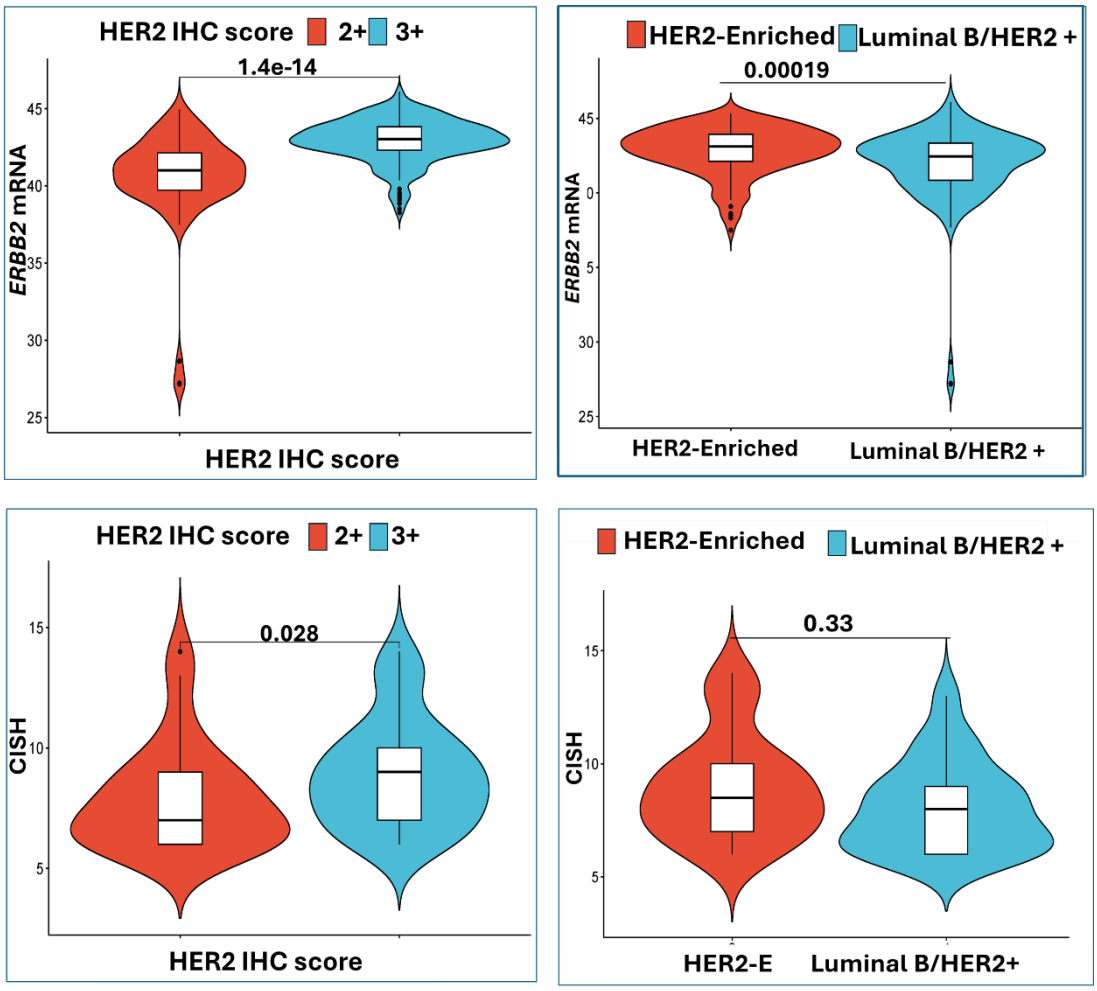


Figure 8.2: Graph describing the correlation between each *ERBB2* mRNA and HER2 gene amplification with HER2 IHC score and molecular class. CISH: Chromogenic in situ hybridisation, HER2-E: HER2 enriched, HER2+: HER2-positive

8.6.5 MammaTyper® assay based molecular subtyping.

According to MammaTyper® RNA-based molecular subtyping, 96/287 cases (33%) were HER2-E molecular subtype compared to 44.5% (126/287) cases from the IHC based molecular subtype (kappa value=0.3, p<0.001). Fifty four per cent were luminal B/HER2-posiive. According to the multigene assay, 8.4% of cases were luminal B/HER2-negaive and 1.4% were luminal A **(Table 8.2 and Figure 8.3)**

Table 8.2: Comparison between the distribution of biomarker status in IHC and mRNA

	IHC defined		mRNA defined	
	N	**(%)**	**N**	**(%)**
Oestrogen receptor status				
Negative	130	(45.3)	104	(36.1)
Positive	157	(54.7)	183	(63.9)
Progesterone receptor*				
Negative	192	(67.6)	154	(54.4)
Positive	92	(32.4)	130	(45.6)
HER2 status				
Negative	0	(0.0)	5	(2.0)
Low	0	(0.0)	31	(10.6)
positive	287	(100)	251	(87.4)
Ki67 proliferation index				
Low	N/A		13	(3.9)
High			274	(96.1)
IHC-based molecular subtyping*				
Luminal B/HER2-positive	157	(55.5)		
HER2-positive	126	(44.5)	N/A	
RNA-based molecular subtype				
Luminal A			4	(1.4)
Luminal B/HER2-negative	NA		24	(8.4)
Luminal B/HER2-positive			155	(54.0)
HER2 Enriched			96	(33.3)
TNBC			8	(2.8)

IHC: Immunohistochemistry**; HER2-E:** HER2 enriched**; TNBC:** triple negative breast cancer

Table 8.3: Correlation between *ERBB2* mRNA status and tumour clinicopathological characteristics

Parameter	*ERBB2*-negative (N=36)		*ERBB2*-positive (N=251)		P value [a]
Age at diagnosis (years)					X^2 =4.12
< 50	11	(30.6)	123	(48.6)	**0.042**
≥ 50	25	(69.4)	128	(51.4)	
Menopausal Status					X^2=1.97
pre	14	(39.0)	130	(51.4)	0.212
post	22	(61.0)	121	(48.6)	
Tumour size (cm)					X^2=2.23
< 2.0	10	(28.0)	100	(39.5)	0.20
≥ 2.0	26	(72.0)	151	(60.5)	
Tumour grade					
1	0	(0.0)	2	(0.8)	X^2 =0.32
2	4	(11.0)	25	(10.1)	0.88
3	32	(89.0)	224	(89.1)	
Histologic tumour types					
Invasive ductal carcinoma (NST)	32	(89.0)	223	(88.7)	X^2 =0.64
Invasive lobular carcinoma	1	(2.7)	6	(2.4)	0.96
Other types	3	(8.3)	22	(8.9)	
Lymph node status					X^2 =0.003
Negative	13	(35.0)	87	(34.7)	1.0
Positive	23	(65.0)	164	(65.3)	
Lympho-vascular Invasion					X^2 =1.52
No	24	(65.0)	135	(54.0)	0.28
Yes	12	(35.0)	116	(46.0)	
NPI group					
good	0	(0.0)	6	(2.4)	X^2 =1.02
Intermediate	22	(61.0)	139	(55.2)	0.95
poor	14	(39.0)	106	(42.3)	
Oestrogen receptor status					
Negative	11	(29.7)	119	(47.6)	X^2 =4.14
Positive	25	(70.3)	132	(52.4)	**0.04**

Table 8.3 continued

Parameter	*ERBB2*-negative (N=36)		*ERBB2*-positive (N=251)		P value [a]
Progesterone receptor					
Negative	19	(51.4)	172	(69.8)	X^2 =4.97 **0.026**
Positive	17	(48.6)	76	(30.2)	
HER2 IHC score					
IHC 2+	26	(73.0)	48	(19.0)	X^2 =48.88
IHC3+	10	(27.0)	203	(81.0)	<**0.001**
***ESR1* status**					
Negative	8	(22.2)	96	(38.2)	X^2 =3.4
Positive	28	(77.8)	155	(61.8)	0.06
***PGR* status**					
Negative	13	(36.1)	143	(57.0)	X^2 =3.4 **0.019**
Positive	23	(63.9)	108	(43.0)	
***MKi67* proliferation index**					
Low <20%	4	(11.1)	7	(2.8)	X^2 =5.8
High ≥20%	32	(88.9)	242	(97.2)	**0.016**
***ERBB2* based HER2 score**					
HER2 0 (negative)	5	(13.5)	0	(0.0)	X^2 =258.8
HER2 1+/2+ non amplified (low)	31	(83.8)	0	(0.0)	<**0.001**
2+ amplified/3+ (positive)	0	(0.0)	251	(100)	
MammaTyper®-based molecular subtype					
Luminal A	4	(11.1)	0	(0.0)	X^2 =285.8 <**0.001**
Luminal B/HER2-negative	24	(66.7)	0	(0.0)	
Luminal B/HER2-positive	0	(0.0)	155	(61.8)	
HER2-Enriched	0	(0.0)	96	(38.2)	
Triple negative breast cancer	8	(22.2)	0	(0.0)	

NST: Non-special type; **NPI:** Nottingham prognostic index; **IHC**: Immunohistochemistry

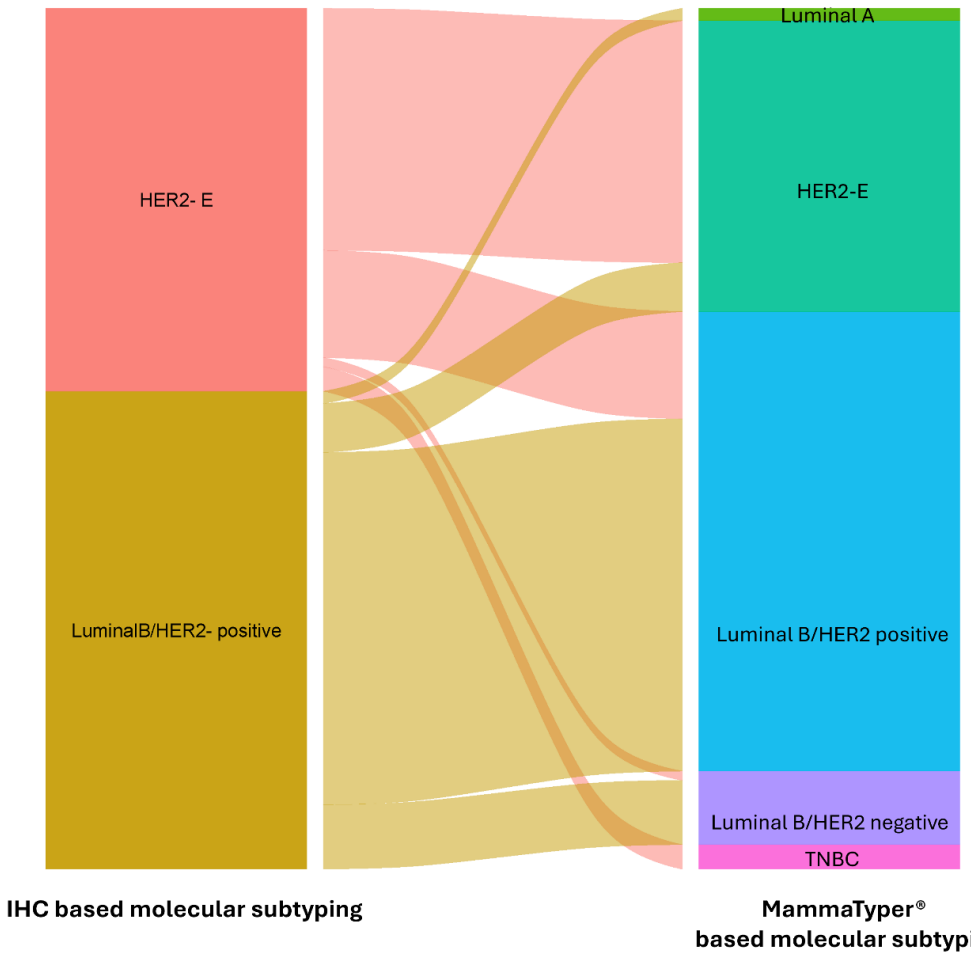


Figure 8.3: Alluvial plot demonstrating the difference in the distribution of molecular subtypes between IHC-based and MammaTyper®-based molecular subtyping. HER2-E: HER2 enriched, TNBC: triple negative breast cancer

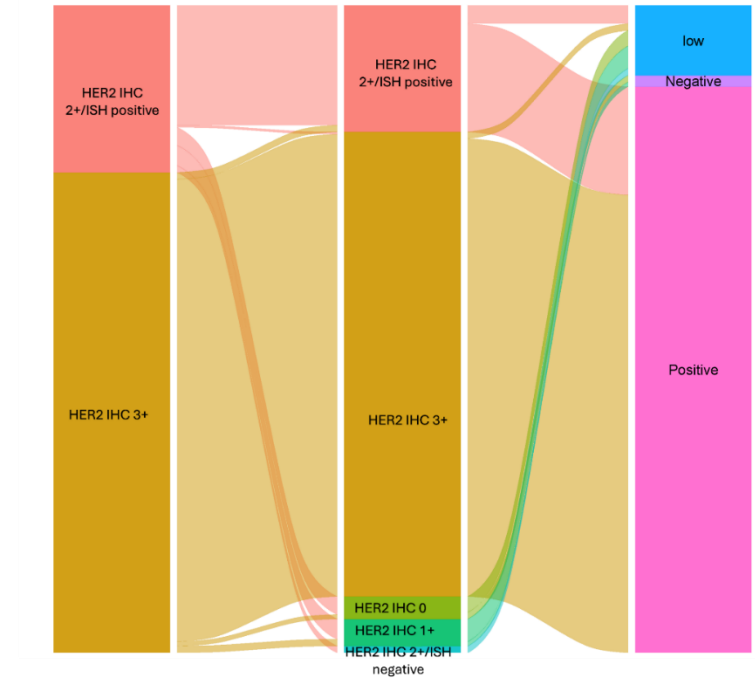
8.6.6 Validation of discordant cases

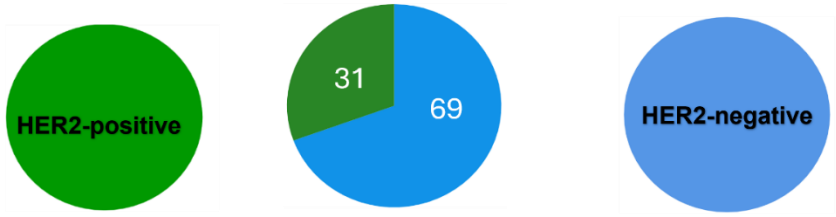
In this study, 36 cases were *ERBB2* negative on MammaTyper® assay, and these comprised 10 cases of HER2 IHC 3+ and 26 cases of HER2 IHC 2+/ISH+.

Upon re-staining of the 36 discordant cases on excision specimens, 25 out of the 36 HER2-positive cases on the prior core needle biopsy were negative on the excision specimens (69%) The remaining 11 cases were confirmed as HER2-positive (3 cases HER2 IHC3+ and 8 cases were IHC 2+/ISH positive **(Figure 8.4**).

Details about the comparison between biomarker status on core biopsy and excision specimen are summarised in (**Table 8.4).** Upon reviewing those 11 cases on patients' clinical records, the 8 HER2 IHC 2+/ISH+ cases showed a very low level of amplification on FISH (average *HER2/CEP17* ratio 2.1), and the 3 HER2 IHC3+ cases showed heterogeneous protein expression (less than 60% of tumour cells).

The concordance between HER2 status on excision biopsy and *ERBB2* mRNA status was excellent (K=0.8, 95% CI: 0.69-0.91, p<0.001).





Core Biopsy IHC		Excision specimen IHC		ERBB2 mRNA	
IHC Score	IHC Status	IHC Score	IHC Status	Score	Status
3+ (N=10)	Positive (N=36)	3+ (N=3)	Positive (N=11)	3+ (N=0)	NA
2+ /ISH + (N=26)		2+ /ISH +(N=8)		2+ /ISH (N=0)	
2+/ISH- and 1+(N=0)	NA	2+/ISH-/1+ (N=15)	negative (N=25)	2+/ISH- and 1+ (N=31)	Negative (N=36)
0 (N=0)	NA	0 (N=10)		0 (N=5)	

Figure 8.4: Alluvial plot of HER2 IHC and *ERBB2* mRNA categories. Alluvial plot showing re-categorisation of HER2 IHC scores by MammaTyper® assay. IHC; Immunohistochemistry, ISH; insitu hybridisation. IHC: Immunohistochemistry; ISH: In situ hybridisation.

Table 8.4: Distribution of HER2 IHC expression of the discordant cases between core biopsy and resection specimen

Core biopsy	Excision specimen				
	HER2/IHC 0	HER2/IHC 1+	HER2/IHC2+	HER2/IHC3+	Total
HER2 IHC 3+	2 (20%)	3 (30%)	3 (30%)	2 (20%)	**10**
HER2 IHC 2+	8 (30.8%)	9 (34.6%)	8 (30.8)	1 (3.8%)	26
Total	10	12	11	3	36

8.6.7 Prediction of HER2-positive BC patients' response to anti-HER2 therapy according to *ERBB2*/HER2 status

Compared to chemotherapy-only treated patients, *ERBB2*-positive patients who received trastuzumab-based chemotherapy had significantly less incidence of early disease recurrence; (HR:0.51; 95%CI: 0.33-0.8; P=0.003) for 5-year DFS and (HR:0.58; 95%CI: 0.36-0.9; P=0.02) for 5-year DMFS with 33% and 15% prolongation in DFS and DMFS, respectively. Additionally, a significantly prolonged 5-year BCSS (HR:0.2; 95%CI: 0.18-0.4; P<0.001) was demonstrated in trastuzumab-treated *ERBB2*-positive patients **(Figure 8.5).**

IHC defined HER2-positive status was also significant in prediction of early recurrence; (HR:0.6; 95%CI: 0.39-0.9; P=0.013) for 5-year DFS and (HR:0.27; 95%CI: 0.15.-0.50; P<0.001) for 5-year BCSS. However, no significant difference was observed in 5-year DMFS among IHC-defined HER2-positive patients treated with anti-HER2 therapy (HR: 0.7; 95% CI: 0.43-1.03; p=0.07) (**Table 8.5).**

Conversely, *ERBB2*-negative patients (36/287) did not show a difference in survival upon the addition of anti-HER2 therapy to chemotherapy (p=0.23) **(Figure 8.6).**

When cases were dichotomised according to ER status, *ERBB2*-positive tumours had prolonged 5-year DFS in both ER-positive and ER-negative tumours **(Figure 8.7).**

Table 8.5: Comparison between patients' recurrence post adjuvant anti-HER2 therapy according to *ERBB2*/HER2 status

Recurrence post adjuvant anti-HER2 therapy	IHC HER2-positive			MammaTyper® *ERBB2*-positive		
	Hazard ratio 95% CI	P value	C index	Hazard ratio 95% CI	P value	C index
5-year DFS	0.6 (0.39-0.9)	0.013	0.90	0.51 (0.33-0.8)	0.003	0.92
5-year DMFS	0.7 (0.43-1.03)	0.07	0.88	0.58 (0.36-0.9)	0.02	0.91

DFS: disease free survival**, DMFS**: Distant metastasis free survival.

8.6.8 Response to therapy according to MammaTyper® Molecular classification

MammaTyper®-based definition of HER2-E molecular subtype significantly predicted the favourable patient response to anti-HER2 therapy with prolonged both 5-year DFS (p=0.012) and 5-year BCSS (p<0.001), unlike IHC-defined HER2-E molecular subtype where the role of anti-HER2 therapy on prediction of early recurrence within those patients was not significant (p=0.18) **(Figure 8.8).**

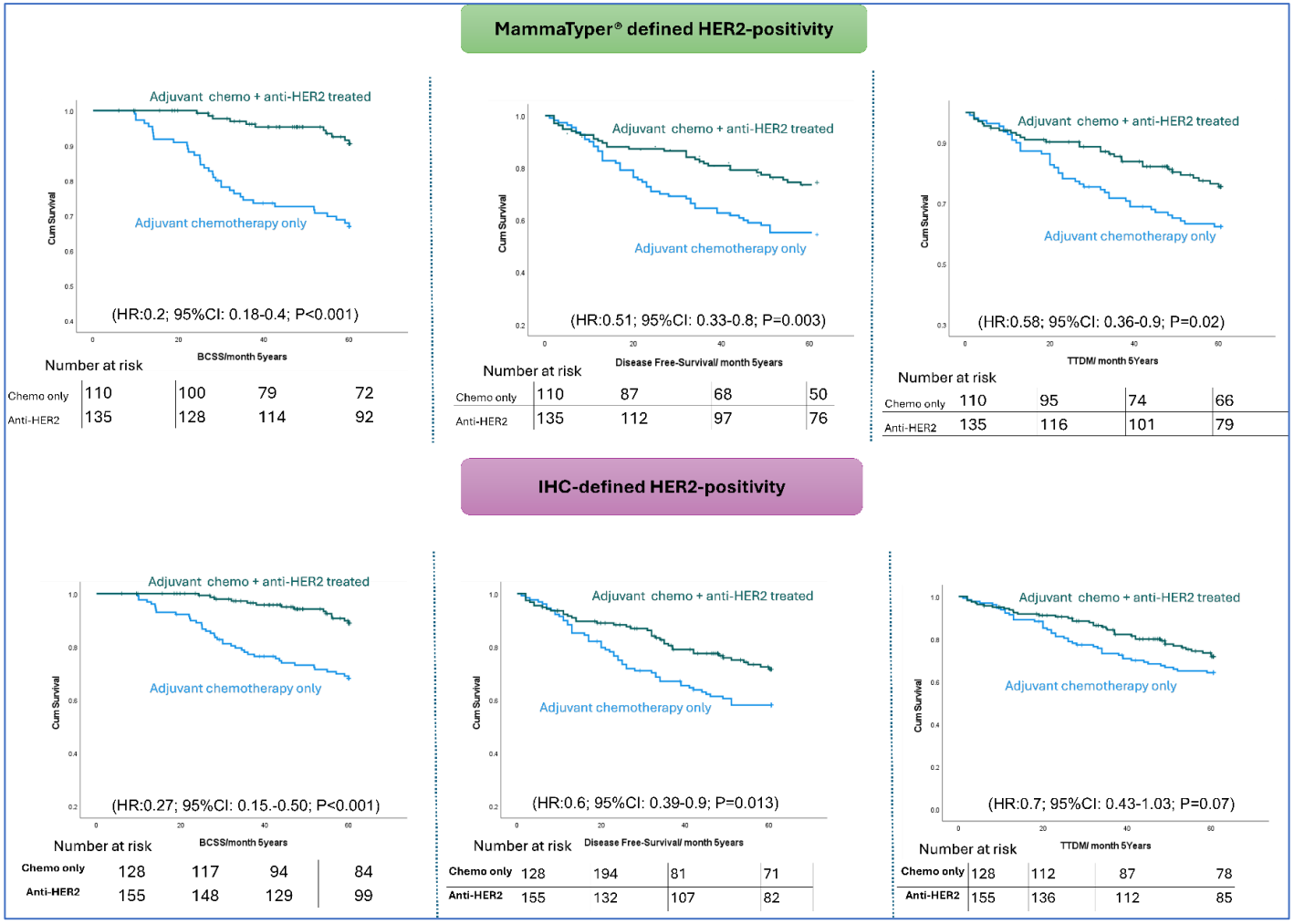


Figure 8.5: Kaplan Meier curves showing the difference between MammaTyper®- defined *ERBB2*-positivity and IHC-defined HER2 positivity in predicting patients' response to therapy. BCSS: Breast cancer specific survival, TTDM: time to distant metastasis, IHC: immunohistochemistry

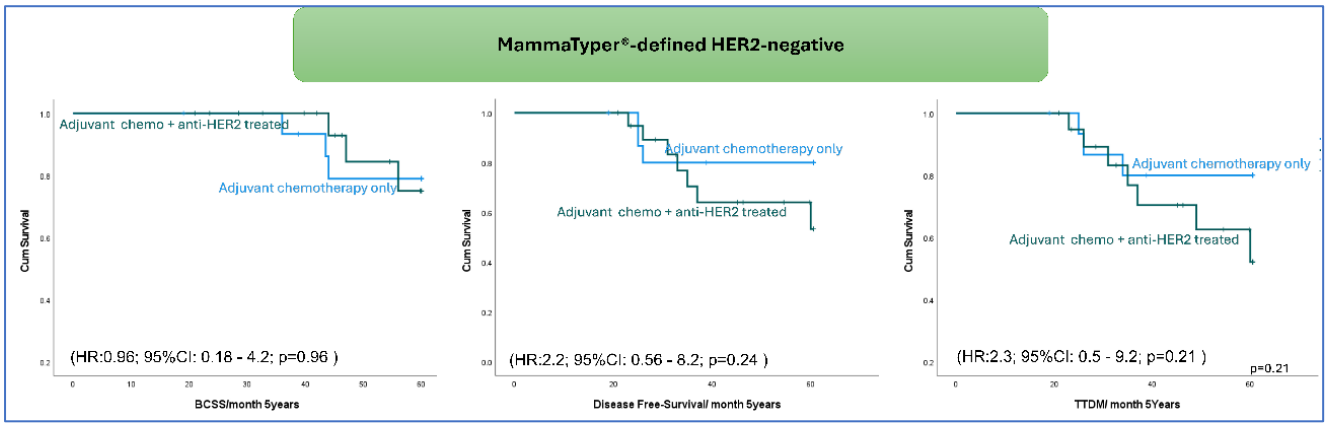


Figure 8.6: Kaplan Meier curves showing the absence of significant difference in the survival outcomes of MammaTyper®-defined *ERBB2*-negative patients upon the addition of anti-HER2 therapy to chemotherapy.

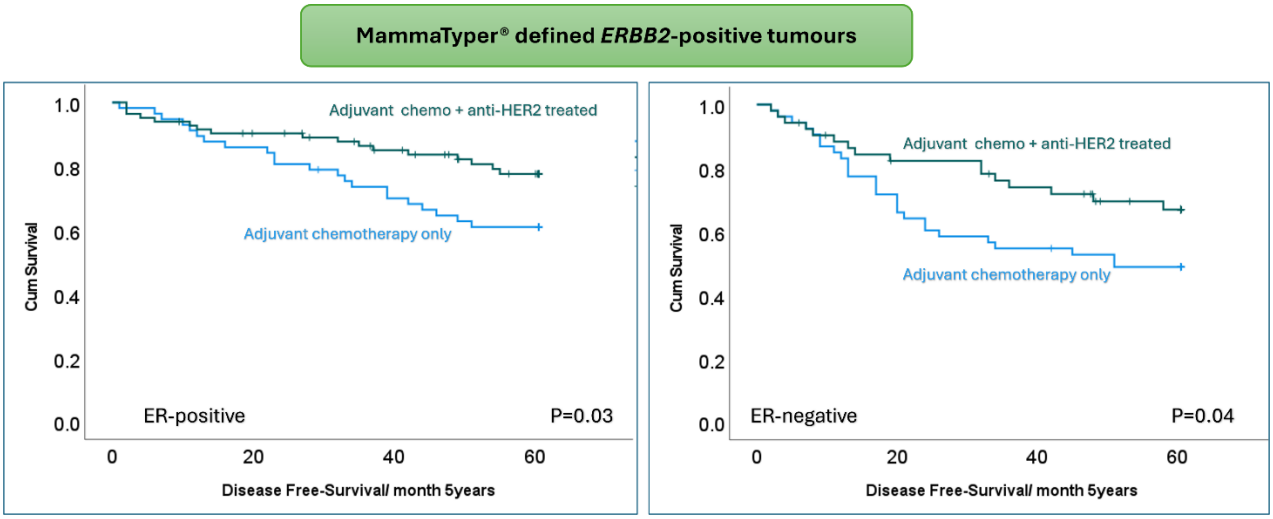


Figure 8.7: Kaplan Meier curves demonstrating response to trastuzumab based therapy in *ERBB2*-positive tumours according to oestrogen receptor status.

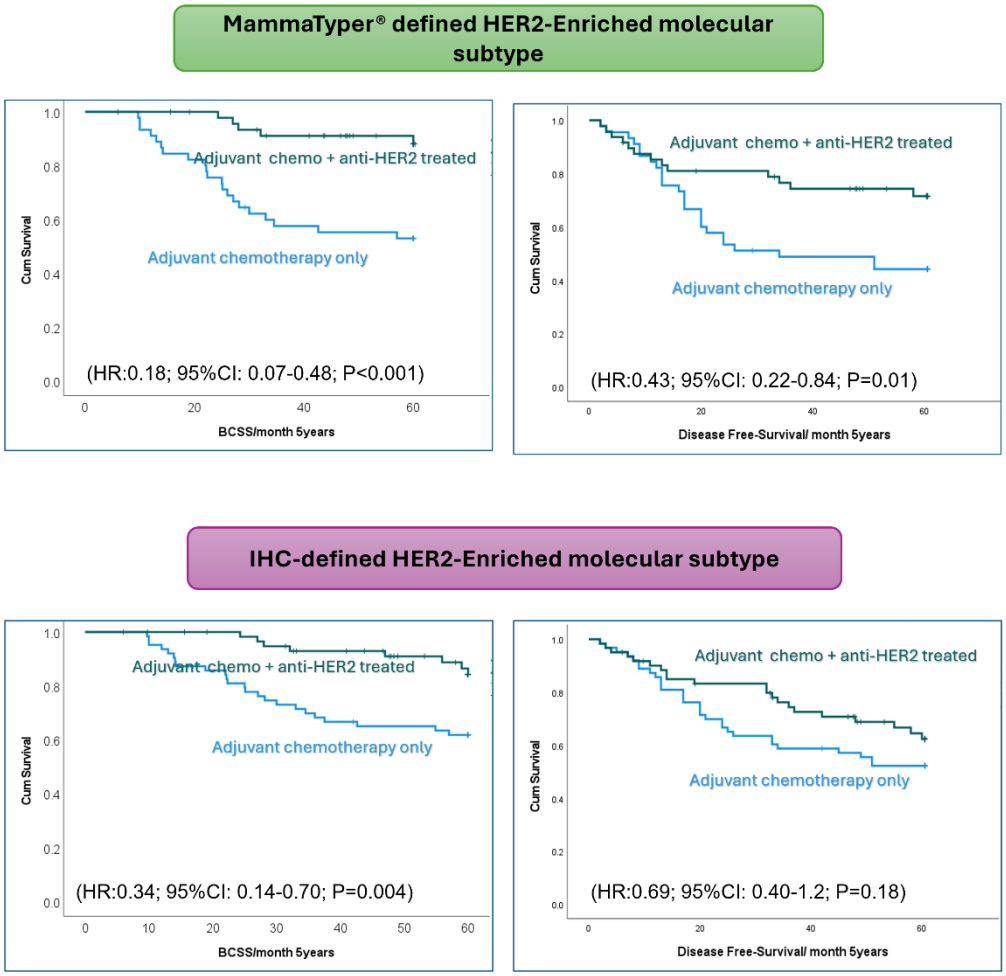


Figure 8.8: Kaplan Meier curves showing the difference in response of HER2-Enriched subtype between MammaTyper® and IHC-based molecular classification.

In a multivariate Cox regression model, when MammaTyper® defined *ERBB2*-positive cases were adjusted for tumour grade, tumour size, LN metastasis, LVI, histological tumour type and ER status, anti-HER2 therapy was an independent predictor of prolonged 5-year DFS (HR: 0.61, 95%CI: 0.38-0.96; p=0.031) and 5-year BCSS (HR: 0.21, 95%CI: 0.18-0.45; p<0.001). While in IHC defined HER2-positivity, anti-HER2 therapy was an independent predictor of better BCSS, but not 5 years DFS (**Figure 8.9**)

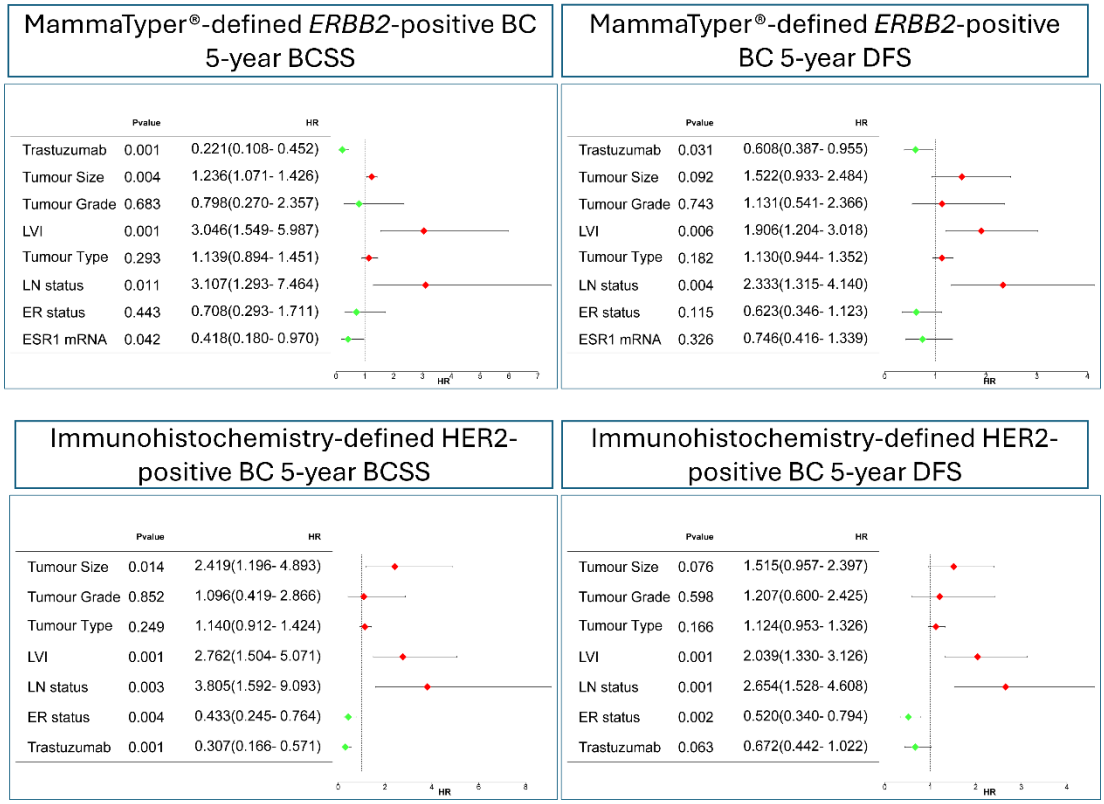


Figure 8.9: Forest plot demonstrating the difference between MammaTyper® / IHC-based definition of HER2 positivity and response to trastuzumab-based represented in 5 years disease-free survival (DFS) and breast cancer-specific survival (BCSS). LVI: lymphovascular invasion; LN: lymph node status; ER: oestrogen receptor

8.6.9 Correlation between mRNA and IHC results

The mean ± SD of *ESR1* and *PGR* mRNA levels were 39.26±2.42 and 34.25±4.3, respectively. The Pearson correlation coefficient between *ESR1* mRNA and ER IHC percentage of expression and ER H score was R=0.75, p<2.2e- 16, and R=0.72, p<2.2e- 16), respectively. *PGR* mRNA also exhibited a high significant correlation with each of PR IHC percentage of protein expression, H score and were as follows (R=0.57, p<2.2e- 16) and (R=0.47, p<9.5e- 15). respectively (**Figure 8.10**).

Regarding the accuracy of MammaTyper® RT-qPCR assay in the assessment of BC biomarkers status, *ESR1 and PGR* mRNA showed high sensitivity of 94% and 87% in the detection of ER and PR status, respectively with overall accuracy of 84% and 80%, respectively (Table 8.6 and Table 8.7)

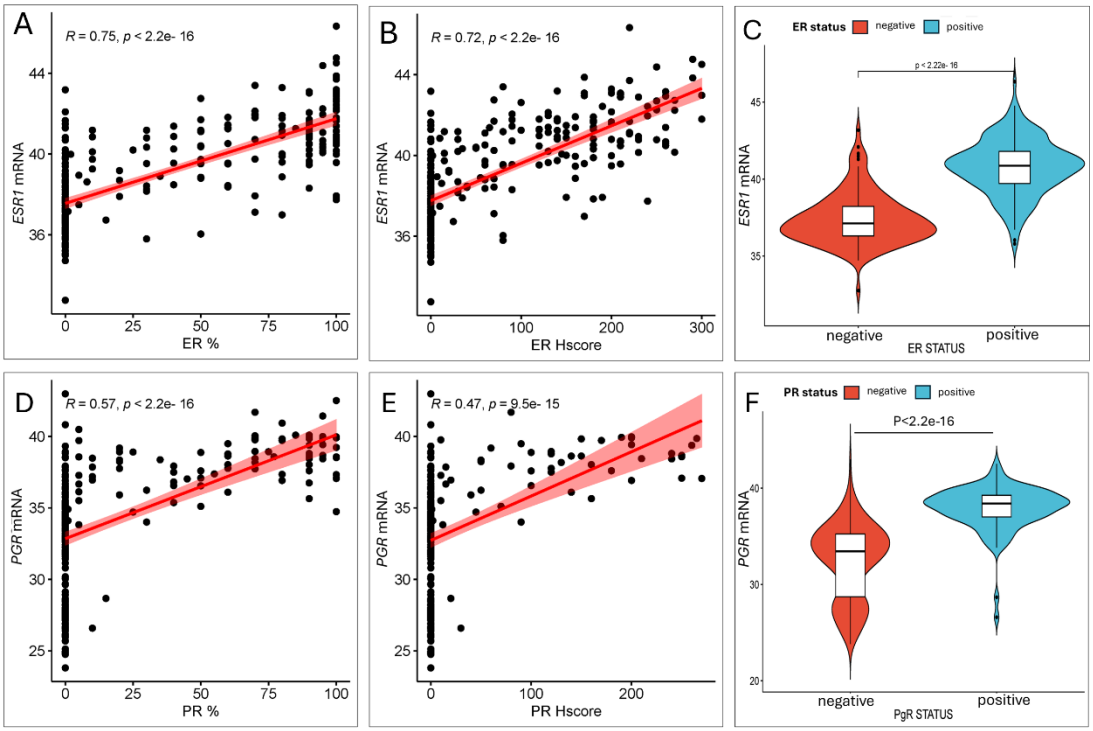


Figure 8.10: Correlation between biomarker protein expression and mRNA level. The top panel represents the correlation coefficient between *ESR1* mRNA and ER IHC percentage (A) and H score (B). C: is a violin plot representing the correlation between *ESR1* mRNA and ER status. The lower panel is the same for *PGR* mRNA and PR IHC protein expression.

Table 8.6: Concordance between immunohistochemistry and mRNA assays in detection of biomarkers status

IHC status	mRNA status	
ER IHC status	***ESR1* status**	
	Positive (183)	Negative (104)
Negative (130)	36 (27.9%)	94 (72.1%)
Positive (157)	147 (93.6%)	10 (6.4%)
PR IHC status	***PGR* status**	
	Positive (130)	Negative (154)
Negative (190)	45 (23.7%)	145 (76.3%)
Positive (97)	85 (90.2%)	9 (9.8%)

ER: Oestrogen receptor**; PR**: Progesterone receptor**; IHC:** Immunohistochemistry

Table 8.7: Accuracy of mRNA in assessment of biomarker status

Gene	Sensitivity	Specificity	PPV	NPV	Accuracy
ESR1	80.3	90.4	93.6	72.3	84%
PGR	65.4	94.2	90.2	76.3	81%

PPV: positive predictive value, **NPV:** Negative predictive value

8.7 DISCUSSION

This study aimed to assess the role mRNA based multigene assay in predicting the response of HER2-positive BC patients to targeted anti-HER2 therapy compared to traditional IHC techniques through using MammaTyper® assay. Our findings indicate that the MammaTyper® assay offers an objective and potentially accurate assessment of HER2 status, with significant implications for treatment outcomes.

The traditional methods of assessing breast biomarkers, including HER2 status, IHC and ISH, have been established and approved by several guidelines. Despite being adopted for several years now, these techniques have their own limitations. Concerns regarding the accuracy and reproducibility of IHC testing persist due to high inter-and intra-laboratory variability, with ER and HER2 testing yielding up to 21.4% false-negative and up to 14.5% false-positive results, respectively [639].

ASCO/CAP guidelines and UK recommendations for HER2 testing have been evolving over the years [141, 160, 161, 630]. However, IHC assessment in HER2 is still subjective with interobserver discordance, especially in the HER2-Low class [192, 195, 357, 631, 640-644]. Also, within HER2-positive classes, some staining scenarios are difficult to score i.e., strong or moderate incomplete staining in less than 10%. HER2 IHC 2+ tumours are considered positive if there is evidence of HER2 gene amplification by ISH techniques. However, the concordance between ISH results and HER2 IHC score in that class ranges from 60-80% [228, 535, 559]. Also, intratumor heterogeneity and its impact on response to therapy is another issue [197, 202, 204, 218].

Although there has been continuous improvement and updates in HER2 assessment and management, long-term results from the adjuvant pivotal trials indicated that approximately 15%-31% of patients experienced disease relapse [220, 221]. Moreover, the development of CNS metastases in 5% of the patients remains an unmet need [635]. These pitfalls perhaps underscore the need for more reliable and reproducible diagnostic tools.

The clinical utility of mRNA assays has been questioned due to potential issues such as mRNA degradation in FFPE tissues and tumour heterogeneity [156, 645]. However, several RT-qPCR multigene assay kits have been clinically validated and proven to be of high performance [632, 633, 646, 647]. MammaTyper® assay demonstrated high sensitivity and specificity in detecting ER, PR, and HER2 statuses through strong correlations with their respective IHC protein expressions. This finding is supported by previous studies that have also reported a high correlation between MammaTyper® assay mRNA expression levels and protein expression detected by IHC [633, 647].

In the current study, *ERBB2* mRNA levels correlated positively with *HER2* gene copy numbers (R=0.31, p=0.006) and were significantly higher in HER2 IHC 3+ cases compared to HER2 IHC 2+/ISH-positive cases. This agrees with previous reports that concluded that RT-qPCR correlates better than FISH with HER2 protein levels and that RT-qPCR may outperform FISH in identifying patients overexpressing HER2 protein [648].

The multigene assay detected 36 cases as *ERBB2*-negative, and upon further validation, 25 cases of them (all HER2 IHC 2+) turned out to be HER2-negative upon staining on excision specimens and/or repetition on the clinical settings. This was further confirmed when none of the discordant *ERBB2*-negative cases achieved benefit from targeted anti-HER2 therapy. False-positive HER2 IHC results have been reported previously [148, 649-651]. Also, false negative results on RT-qPCR have been documented [156, 645]. A key factor for discordance between IHC and mRNA results is the heterogeneity of HER2 expression or amplification within a tumour. This variability can lead to inconsistent results across different tests. Additionally, tumours with low-level amplification can also contribute to these discrepancies [501]That was evident in the current study, where all *ERBB2*-Negative/HER2 IHC-positive cases had a very low level of gene amplification and borderline protein expression. For these reasons, patient response to therapy and overall recurrence were our gold standard for validating such discordance.

In the current study, *ERBB2*-positive cases were significantly associated with prolonged DFS and DMFS. This finding aligns with previous studies where high *ERBB2* expression levels were linked to improved responses to HER2-

targeted therapies in HER2-positive BC patients in both neoadjuvant and adjuvant settings[197, 320, 321, 507, 554, 574, 652]. This association may be explained by the higher *HER2* mRNA expression observed in HER2-E tumours compared to non-HER2-E tumours, as determined by the PAM50 gene signature, which includes *HER2* among its 50 genes [507]. Additionally, higher *HER2* mRNA expression was noted in TRAR-low tumours compared to TRAR-high tumours, indicating that *HER2* mRNA levels may reflect the tumour's dependence on HER2 signalling pathways, thereby predicting trastuzumab response [653]. The predictive value of *HER2* mRNA likely stems from its correlation with the amount of HER2 protein present on BC cell membranes [503].

The study also highlighted the potential of MammaTyper® in molecular subtyping. MammaTyper®-defined HER2-E subtypes showed a significantly better response to anti-HER2 therapy compared to IHC-defined HER2-E subtypes ($p=0.012$ for 5-year DFS, $p<0.001$ for 5-years BCSS). This finding supports the use of mRNA-based molecular subtyping as a superior method for guiding treatment strategies and agrees with previous studies that have suggested that combining HER2-E subtype and *ERBB2* mRNA into a single assay identifies tumours with high responsiveness to HER2-targeted therapy [507].

The field of targeted anti-HER2 therapy has been evolving since the introduction of ADC and HER2-Low tumours. *ERBB2* mRNA expression has been linked to a greater benefit from T-DM1 in several randomised clinical trials for HER2-positive mBC [197, 654-656]. Consequently, current trials aim to set a cut-off point for the *ERBB2* mRNA level in HER2-Low tumours, which is representative of the response to T-DXD.

Future studies should aim to refine these techniques and validate their clinical utility in larger, diverse cohorts. Further research is also needed to evaluate the cost-effectiveness of integrating mRNA-based assays into routine clinical practice and to explore the potential for these assays to guide personalised treatment strategies more effectively. In conclusion, MammaTyper® mRNA multigene assay offers a promising companion to traditional HER2 assessment methods. Its ability to provide an accurate and objective evaluation of HER2 status and molecular subtyping could significantly enhance the prediction of response to anti-HER2 therapy, ultimately improving patient outcomes. However, the integration of mRNA-based assays into routine clinical practice requires further validation and consideration of practical implementation challenges. *ERBB2* mRNA expression may also help address tumour heterogeneity within a single, manageable assay.

Chapter 9. Refining the definition of HER2-Low class in invasive breast cancer

9.1 INTRODUCTION

HER2-Low BC is estimated to account for 40–50% of all BCs [169] and appears to be a heterogeneous disease [177, 501] with regard to its clinical, morphological, immunohistochemical, and molecular characteristics [178-182]. Since the results of the DESTINY-Breast04 trial which introduced the term HER2-Low to the clinical field [170], several clinical trials are ongoing aiming at finding the lower limit at which ADCs can be effective in BC patients with low HER2 expression. DAISY II trial reported a modest level of activity of T-DXd in non-HER2 expressing tumours [172]. However, 48% of the tumours that were HER2 IHC 0 had detectable HER2 expression and were classified as 1+ on external pathology review [172]. Destiny-breast-06 trial results have been revealed with a conclusion that T-Dxd can be effective in tumours displaying some HER2 membrane positivity not insufficient for a designation of IHC score 1+, the so called HER2-Ultralow [171, 657].

Since the publication of the results of the Destiny-Breast04 trial [170], there have been calls for the development of new assays to assess HER2 status with particular emphasis on identifying HER2-Low tumours. The established IHC testing methods (e.g. VENTANA HER2/neu (4B5) assay) are currently used to identify patients with HER2-Low disease in accordance with guideline recommendations [141, 170] and are used in the approved and the ongoing clinical trials (**Table 9.1 and Table 9.2**). We acknowledge that HER2 scoring guidelines, including those developed by the UK and ASCO/CAP [141, 161], have predominantly focused on defining HER2 positivity (3+ or 2+/ISH posi-

tive), with less focus on HER2 IHC scores of 0 and 1+, resulting in low concordance among pathologists in separating those two categories [192, 193]. The emergence of the HER2-Low category has highlighted the importance of adherence to guidelines and ongoing training to improve reproducibility and to ensure accurate recognition of HER2-Low, HER2-ultra-low and HER2 IHC 0 [170]. While new quantitative assays, such as the HERmark BC assay[146, 149], immunofluorescence-based automated quantitative analysis methods [194, 195], quantitative IHC method [196], and assessment of *HER2* mRNA expression levels [197], are being evaluated, any new assay or kit designed for the detection of HER2-Low tumours must undergo rigorous validation through clinical trials before being integrated into clinical practice. In our opinion, current efforts are best directed towards standardisation of the current assays, adherence to the guideline recommendations on pre-analytical and analytical variables for HER2 testing [141, 143, 161, 165], and improve pathologist concordance in categorising HER2 status [658, 659].

Although the ASCO/CAP guideline recommendations provided a comprehensive definition of HER2 staining pattern and the categorisation of cases into 4 IHC scores (0 - 3+), the distinction between IHC scores 0 and 1+ is not sufficiently detailed and lacks relevant evidence, and some scenarios of HER2 expression patterns are missing [141, 161]. This could result in the high discordance rates in HER2 status assessments reported in some studies [148, 660, 661].

Although clinical response can provide the best tool to define the lower limit of the HER2-Low class, the number of recruited patients in such randomised clinical trials, particularly those close to the threshold of positivity, is typically too limited to develop a robust definition. In this study, we have used a large cohort of BC that express low levels of HER2 protein without evidence of *HER2* gene amplification and applied an ANN model to refine the definition of HER2-Low class of BC with an emphasis on distinguishing HER2 score 1+ and 0 categories. We have used the *HER2* mRNA levels as a ground truth to reflect the level of *HER2* gene expression. ANNs can learn and model non-linear and complex relationships [662-666]**.**

9.2 HYPOTHESIS

In this study we hypothesised that refining the definition of the HER2-Low class with precise scoring criteria will lead to better concordance among pathologists and improve the personalisation of ADC therapy for patients with HER2-Low BC.

9.3 AIMS OF THE STUDY

- Assess the current concordance in HER2 IHC scoring among pathologist with a special focus on HER2-Low category.
- Refine the definition of HER2-Low class: To develop a clearer, more straightforward, and applicable approach for interpreting different HER2 expression scenarios in invasive BC, with a particular focus on distinguishing between HER2 IHC score 1+ and score 0.

- Improve scoring concordance: To enhance agreement among pathologists and improve the consistency of HER2 scoring by refining the criteria for the HER2-Low classification.
- Utilise mRNA levels as ground truth: To use *HER2* mRNA levels as a reliable indicator for defining the HER2-Low category, rather than relying solely on patient outcomes, as HER2 is not the driver oncogene at low protein expression levels.

Table 9.1: Overview of the clinical trials on ADC in HER2-Low breast cancer*

Intervention	Target	Study name	Phase	Patient population	Number	Trial status	Key	Key results (or estimated primary completion date)
T-DXd versus physician's choice ChT	HER2	DESTINY-Breast04[170] (randomised, multicentre, two-group, open-label) ***NCT03734029***	III	HER2-Low mBC after 1–2 standard therapies	557 (89% HR+, 11% HR−)	Active, not recruiting		**HR+ patients**, cORR: 52.6% versus 16.3% mPFS: 10.1 versus 5.4mo mOS: 23.9 versus 17.5mo **HR− patients**, cORR: 50.0% versus 16.7% mPFS: 8.5 versus 2.9mo mOS: 18.2 versus 8.3mo **Full population**, ILD: 12.1% versus 0.6%
T-DXd versus physician's choice ChT	HER2	DESTINY-Breast06 [667] (randomised, multicentre, open-label) ***NCT04494425***	III	HR+, HER2-Low (IHC 2+/ISH-, IHC 1+, and IHC>0 0<1+) mBC progressed on ⩾2 lines of ET	866	Complete	PFS	T-DXd significantly improved PFS vs TPC in HER2-low (HR, 0.62 [95% CI 0.51, 0.74], P<0.0001; median, 13.2 vs 8.1 mo). ITT and HER2-Ultralow results were consistent with HER2-Low
T-DXd	HER2	DEBBRAH [668] (multi-centre, open-label, two-stage) ***NCT04420598***	II	Pre-treated HER2-positive/HER2-Low unresectable locally advanced or mBC with untreated BMs or LMC (5 cohorts)	41	complete		ORR-ICb: Cohort 2 (HER2± low): 66.7% Cohort 4 (HER2-Low): 33.3% PFS (both cohorts): 5.7mo
T-DXd	HER2	DAISY[669] (open-label) ***NCT04132960***	II	HER2-positive, HER2-Low, and HER2-null advanced BC	176 (FAS) (72 HER2-Low)	Active, not recruiting		HER2-Low (HER2-null): BOR: 33.3% (30.6%) mPFS: 6.7mo (4.2mo) ILD: n=4 (full population)
T-DXd	HER2	Dose-expansion study [566] ***NCT02564900***	Ib	HER2-Low advanced/mBC refractory to standard therapies	54 (87% HR+,13% HR−)	Active, not recruiting		cORR: 37.0%, mPFS: 11.1mo, mOS: 29.4mo, ILD: 14.8%
T-DXd Combinations (Capivasertib, Anastrozole, fulvestrant)	HER2	**DESTINY-Breast08 [670] (Multicenter, open label, modular, two-part) *NCT04556773***	**Ib/II**	HR+ and HR−, HER2-Low advanced or mBC (Part 2: 5 cohorts)	182 (est.)	Active, not recruiting	AEs	Recommended doses for expansion: T-DXd (5.4mg/kg) Q3W + Anastrozole (1mg QD) or Fulvestrant (500mg Q4Wd) No DLTs reported, both combinations generally well tolerated
T-DXd+ nivolumab	HER2	Two-part, open-label study [671] ***NCT03523572***	Ib	HER2-expressing mBC after standard therapy	Part 2: 45 (16 HER2-Low; 13 HR+)	Active, not recruiting		HER2-Low: ORR: 37.5% mPFS: 6.3mo ILD: 10.4% (full population)

Table 9.1: Overview of the clinical trials on ADC in HER2-Low breast cancer (continued)

T-DXd+ durvalumab+ Dato-DXd	HER2	BEGONIA **[672]** (Two-part, multi-centre, multi-arm, open-label) *NCT03742102*	Ib/II	Untreated, unresectable, locally advanced/ metastatic HER2-Low TNBC (IHC 0 excluded) breast cancer	Five treatment arms - (durvalumab + paclitaxel) vs - (durvalumab +paclitaxel + capivasertib) vs - (durvalumab + paclitaxel + oleclumab) vs -(durvalumab + T-DXd) vs -(durvalumab + Dato-DXd)	Active, not recruiting	cORR: 100% (4/4; only four pts have completed two on-treatment assessments; remaining seven pts still on treatment)
Sacituzumab govitecan versus physician's choice ChT	TROP2	TROPiCS-02 [673, 674] ***NCT03901339***	III	HR+, HER2-advanced BC, heavily pre-treated, ET resistant	543 post hoc analysis: HER2-Low: 283, IHC 0:(217)	(Active, not recruiting	SG versus physician's choice: HER2-Low patients, ORR: 26% versus 12% mPFS: 6.4 versus 4.2 months. IHC 0 patients, ORR: 16% versus 15%, mPFS: 5.0 versus 3.4 months ILD: 0% versus 1% (full population)
Sacituzumab govitecan versus physician's choice	TROP2	ASCENT [675, 676] ***NCT02574455***	III	TNBC (local advanced or mBC) RR to ⩾2 previous ChT regimens	468 (post hoc analysis: HER2-Low: 123, IHC 0: 293)	Completed	SG versus physician's choice (post hoc analyses): HER2-Low patients, ORR: 32% versus 8%, mPFS: 6.2 versus 2.9mo, mOS: 14.0 versus 8.7mo IHC 0 patients, ORR: 31% versus 3%, mPFS: 4.3 versus 1.6mo, mOS: 11.3 versus 5.9mo ILD: n=1 (SG group; full population)

*Source is clinicalTrial.gov, accessed on 5th of August 2024

AEs: Adverse events**; BC**, breast cancer; **BM**, brain metastases; **BOR**, best overall response; **cORR**, confirmed objective (or overall) response rate; **ChT,** chemotherapy; **DOR**: duration of therapy; **ET:** Endocrine therapy **est**., estimated; **FAS**, full analysis set; **HER2**, human epidermal growth factor 2; **HR,** hormone receptor; **IHC**, immunohistochemistry; **ILD**, interstitial lung disease (or pneumonitis); **LMC,** leptomeningeal carcinomatosis**; mBC**, metastatic breast cancer; **mo**, months; **mOS,** median overall survival; **mPFS**, median progression-free survival; **N/A,** not available; **ORR**: overall response rate; **pCR**: pathologic complete response; **R/R**, relapsed or refractory; **SG**, sacituzumab govitecan; **TNBC**, triple-negative breast cancer

Table 9.2: Summary of the ongoing clinical trials for management of HER2 expressing BC*

Intervention	Target	Study name	Phase	Patient population	Number	Key end point	1ry completion date
HER2-Low (early and advanced BC)							
Disitamab vedotin (RC48) vs physician's choice	HER2	Randomised, parallel control, multicentre study ***NCT04400695***	III	HER2-Low mBC, previous use of anthracyclines, and 1–2 systemic ChT regimens	366 (est.)	PFS	December 2024
Disitamab vedotin (RC48)	HER2	Open-label study ***NCT05331326***	II	HER2-positive and HER2-Low mBC with abnormal PAM pathway activation	64 (est.)	PFS ORR	August 2024
Disitamab vedotin (RC48) + penpulimab	HER2	Open-label study ***NCT05726175***	II	Neoadjuvant treatment of HER2-Low early or locally advanced breast cancer	20 (est.)	pCR	August 2024
Sacituzumab govitecan vs physician's choice	TROP2	SASCIA ***NCT04595565***	III	HER2 IHC score 0-1+ or FISH negative, post-neoadj residual disease	1332 (ER+ and ER-)	iDFS	March 30, 2027
Disitamab vedotin (RC48-ADC) +ET	HER2	Rosy ***NCT05904964***	III	1st line endocrine resistant HER2-Low mBC	288(est.)	PFS	March 2028
T-DXd+/− Anastrozole	HER2	TALENT Randomised, open-label, dual-arm ***NCT04553770***	II	Neoadjuvant Early-stage BC HER2-Low HR+	88	pCR	30-Sep-25
T-DXd+ pembrolizumab	HER2	Two-part, open label Study ***NCT04042701***	I	HER2-Low, advanced/ mBC with failure on prior standard therapy	105	pCR	2025
T-DXd	HER2	HER2-PREDICT Multicentre, observational study ***NCT04257162***		Using biological samples from patients treated with DS-8201a in the metastatic setting	180	Optimal ERBB2 mRNA cut-point predictive of T-DXd response	December 2024

*Source is clinicalTrial.gov, accessed on 5th of August 2024 **ER**: Oestrogen receptor; **est**., estimated; **HER2**, human epidermal growth factor 2; **DFI**: Disease free interval; **iDFS**: invasive disease free survival; **IHC**, immunohistochemistry; **mBC**, metastatic breast cancer; **mo**, months; **ORR**: overall response rate; **pCR**: pathologic complete response; **PFS**: progression-free survival; **T-DXd** :trastuzumab deruxtecan; ;**tx**:therapy

9.4 MATERIALS AND METHODS

In the 1st part of this study (discovery set), a subset of cases from the Nottingham cohort was stained by HER2 IHC antibody on TMA sections. Cases were scored according to the existing guidelines and the concordance between the clinical score and our score was carried out. Then, a definition of HER2-Low IHC expression was developed through a detailed assessment of HER2 IHC expression pattern on a subset of cases from the same Nottingham cohort and through using *ERBB2* mRNA level as the ground-truth, a refined definition was developed.

9.4.1 Study cohorts

This study was conducted on a primary invasive BC cohort (n=2910) from patients presenting at NUH NHS Trust. Cohort was enriched for HER2-negative cases as this represents the main challenge to separate them from HER2 IHC 1+. Cases were divided into (n=1547) that were used as a discovery cohort to assess the overall HER2 scoring concordance among pathologist with a specific focus on HER2-Low category. These cases were available on TMA sections and selected from the Nottingham cohort (**Section 2.1.1)**.

The other set (experimental) included (n=363) cases with a HER2 IHC score 0, 1+ and 2+ without gene amplification. This cohort is identified as Oncotype DX cohort (**Section 2.1.1.3**). Transcriptomic data on *HER2* mRNA expression was available for this cohort within the recorded Oncotype DX report [395] which was carried out as part of the patients' clinical care for management**.** Briefly, mRNA levels were obtained from tumour samples extracted from FFPE tissue using high-throughput, real-time, reverse transcription-polymerase

chain reaction. Normalised expression measurements were calculated as the mean CT for the 5 reference genes minus the mean CT of triplicate measurements for each individual gene. *HER2* mRNA level ranged between 5.0-10.8 units with a mean of 9 units.

The clinicopathological data for both cohorts including age at diagnosis, tumour size, histological grade, histologic tumour type, axillary LN status, LVI and NPI were available as detailed in **Section 2.1.1**. ER and PR positivity were assessed according to ASCO/CAP guidelines if ≥1% of the invasive tumour cell nuclei are immunoreactive[406].

9.4.2 HER2 IHC staining

HER2 staining in diagnostic practice was completed on the Ventana Benchmark ULTRA IHC automated staining system using the Ventana PATHWAY anti-HER-2/*neu*, rabbit monoclonal ready to use primary antibody in combination with Ventana detection kits. Cases with borderline protein expression underwent FISH analysis as part of the patient's routine diagnostic pathway.

For the purpose of this study, HER2 IHC staining was conducted on TMA sections of the discovery cohorts (n=1547). Furthermore, validation of discordant HER2 status between core biopsy and Oncotype Dx mRNA in the experimental cohort was carried out on full-face sections, as described below. HER2 staining was completed using HER2 rabbit polyclonal antibody, dilution 1:400, DAKO as detailed in **Sections 2.3 and 2.5**. Gene amplification status for cases with borderline HER2 protein expression was assessed through CISH assay as detailed in **Section 2.7**.

Appropriate positive and negative controls were included for each staining run as per the published guidelines [141, 161]. Protein expression assessment was carried out in routine clinical practice using light microscopy on the diagnostic core needle biopsies. The reported HER2 scoring categories in the clinical setting were retrieved from the patient records.

9.4.3 Detailed re-assessment of HER2 IHC protein expression

HER2 expression in the invasive tumour cells of core biopsy (in the experimental cohort) and TMA sections of the discovery cohort. Each case was re-assessed and presented in detail. This included: 1) Cellular localisation of protein expression (membranous, cytoplasmic or both), 2) Intensity of staining divided into 5 grades (negative, faint, weak, moderate, and strong). In addition to the comparison with the positive and negative controls, the magnification rule was used to guarantee high inter-observer agreement. Strong HER2 staining was assessed as those cases displaying unequivocal membranous staining seen easily at low power magnification (2x or 4x), while unequivocal membranous staining (moderate to weak) was only assigned at medium magnification (10x to 20x, respectively). Faint staining can only be appreciated at 40x magnification, whereas weak staining can be appreciated at 20x magnification.[677]. Cases were assessed using NIKON NI-U Microscope, Nikon UK, Branch of Nikon Europe B.V. UNITED KINGDOM. Different intensities within the same tumour were assessed to reflect the heterogeneity. 3) The percentage of each intensity. 4) Distribution/completeness of membranous staining as either complete circumferential membranous or incomplete lateral or basolateral staining. 5) H score was calculated as follows: % of weak intensity X 1 + % of moderate Intensity X 2+ % of strong intensity X 3). In addition, the % of

faint intensity was assessed and multiplied by 0.5 to produce a total score of 350. Each incomplete membranous staining is multiplied by 0.5, while complete membranous staining is multiplied by 1.

9.4.4 HER2 IHC score interobserver concordance

HER2 IHC score for the TMA sections in the discovery cohort was carried out by the author and validated by another experienced pathologist in the team. This score was then compared with the clinical IHC score commenced in the diagnostic settings. The concordance between HER2 status in general, individual HER2 IHC scores and HER2 status divided into negative, low, positive was then performed.

9.4.5 Validation of HER2 status on resection specimen

Assessment of HER2 status was carried out on core biopsies while *HER2* mRNA level from oncotypeDx analysis was obtained from resection specimens. Thus, for the cases that showed discrepancy between HER2 IHC score and mRNA level (n=30) i.e., high mRNA level and HER2 score 0, or HER2 score 2+ with low mRNA level, repeating HER2 IHC staining on the full-face sections using the same tissue block tested for oncotype DX was performed. Whenever possible, the same tissue block that was used to run the Oncotype DX test, was stained with HER2. The staining protocol was similar to the TMA sections from the discovery cohort as described in **Section 2.3**

9.4.6 Defining cut-off for HER2 score 1+ versus score 0

Following a comprehensive assessment of HER2 expression in the experimental cohort, we aimed to establish a cut-off point to differentiate cases with a HER2 score of 1+ from those with a HER2 score of 0, using *ERBB2* mRNA

as the reference standard. This was achieved through a two-step approach. **(Figure 9.1).**

9.4.6.1 Step 1: K-means clustering

The K-means technique aims to partition the data into k-groups such that the sum of squares from points to the assigned cluster centres is minimised. *HER2* mRNA values were classified, using k-means, into 2 clusters based on their similarity of expression across multiple HER2 scoring parameters. Those cases which had a score of 1+ or 0, were clustered into two groups based on *HER2* mRNA level and the detailed IHC scoring performed. Cluster 1 was defined as HER2 negative (0) while cluster 2 represented HER2 positive (1+). HER2 2+ were excluded from the clustering to avoid data bias.

9.4.6.2 Step 2: Artificial neural network model

ANN model (NeuroSolution version 7.0, NeuroDimension, Gainesville, FL with a range of hidden nodes in three layers, with a Levenburg Marquardt algorithm and a TanH activation function) was used to set cut off point for defining HER2 1+ based on the k-means clusters defined in step 1. A Monte Carlo Cross Validation approach was used to train a population of models and early stopping was undertaken using a randomly extracted unseen cross validation set with subsequent validation on a test set (n=38) which was kept completely blind to training process. Weight regularization was conducted during training.

The model was trained with the detailed HER2 scoring parameters including various intensities (faint, weak, moderate) and distribution of each intensity if present either complete and incomplete in addition to total percentage of positive cells and cytoplasmic staining as input and *HER2* mRNA-based clusters

as an output variable. The ANN model determined which of the input parameters predicted HER2 score 1+ with high level of accuracy. Sensitivity and specificity with the produced response curves was applied to set cut-off for the most participating parameter.

Predictions of trained models were examined to decide predicted probability of K-means cluster membership. These were examined to determine a probabilistic cut point for HER2 score 1+. Model performance was further assessed by finding the AUC of a constructed ROC curve. AUC of 1 were seen across the three cross validation cohorts as well as 100% classification rates.

After setting the cut points, a new refined score for HER2 was developed and applied. To detect the accuracy of our refined score against the clinical score, we used the same neural network to build a discriminating model of both HER2 scores using the clinicopathologic parameters as input units and the HER2 score as an output. The differentiating performance of the ANN models was evaluated with AUC as well as the true and false positivity rates.

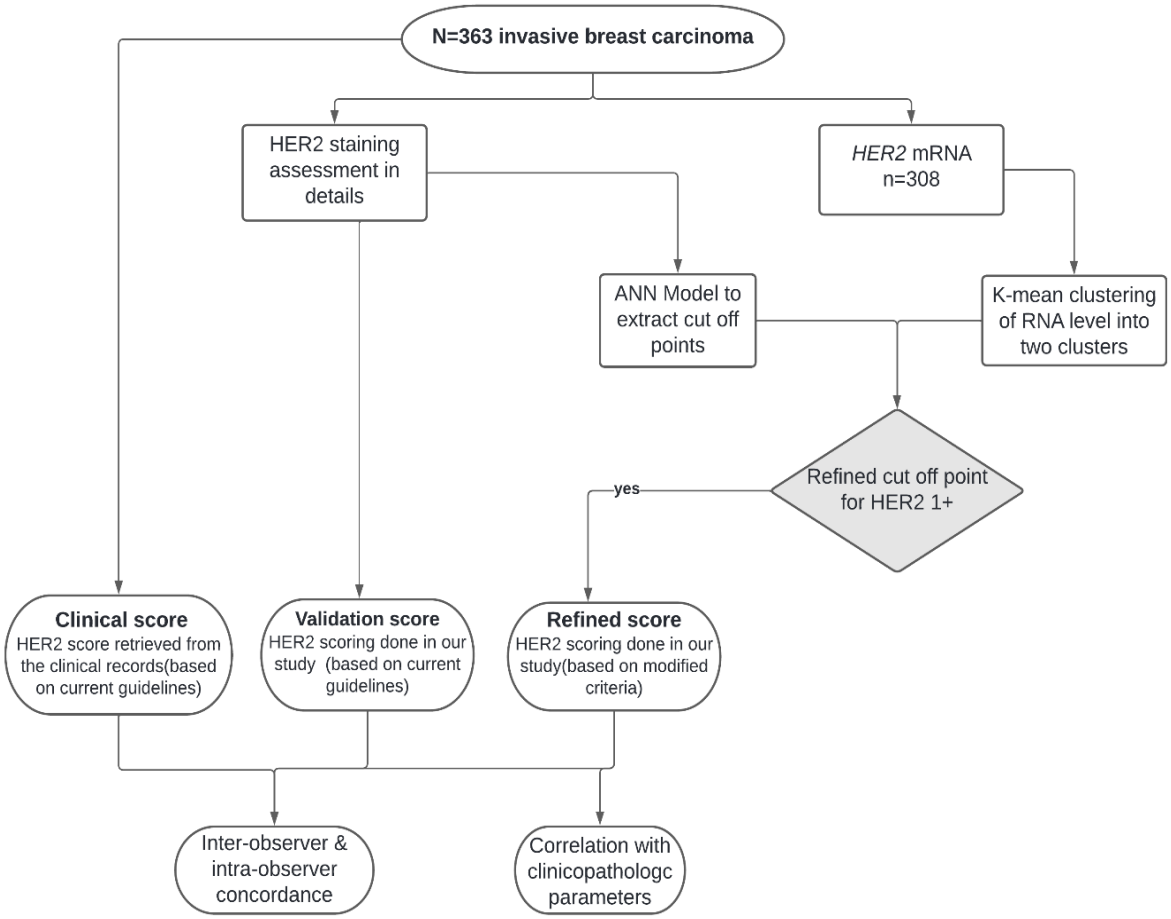


Figure 9.1: Flowchart summarising cohort selection and different steps carried out

To test the reliability of using *HER2* mRNA as a dichotomising variable, we assessed the correlation between *HER2* mRNA, protein level and gene amplification levels in a large independent cohort of primary BCs obtained from two publicly available datasets; TCGA (n=614) and the METABRIC (n=288).

9.4.7 Reliability and reproducibility of the refined HER2 IHC score

The efficiency and reproducibility of the refined HER2 scoring method against the current guidelines were tested. HER2 was scored twice according to the existing ASCO/CAP; once by the clinical team at time of diagnosis and a second score was carried out by experienced pathologists including the author. The agreement between two scores was assessed. Moreover, the inter-observer agreement of the refined score was assessed between both observers and the intra-observer agreement was examined through rescoring the cases again after 3 months washout period.

9.4.8 Correlation between refined HER2 score with the clinicopathological variables

The correlation between the clinicopathologic parameters, including *HER2* mRNA level, HER2 scores including the refined and the original clinical scores was carried out. In addition, *HER2* mRNA k-means clusters were correlated with the other clinicopathologic parameters.

9.4.9 Statistical Analysis

SPSS v.28 was used to carry out the statistical analysis. Correlations were analysed using chi-square ($\chi 2$) test, Fisher's exact test, Kruskal–Wallis and

Wilcoxon rank sum test with continuity correction, where appropriate. The concordance analysis was performed using the Cohen's Kappa test. All differences were considered significant at $p < 0.05$.

9.5 RESULTS

9.5.1 Cohort characterisation

The basic clinical and pathologic parameters of both study cohorts are summarised in **Table 9.3**.For the experimental cohort, the patients mean age at diagnosis was 59 years while the mean invasive tumour size was 2.2 cm (range 0.1-11.5 cm). All cases were ER-positive and HER2-negative.

9.5.2 Concordance in HER2 scoring in the discovery cohort.

Regarding the concordance in assessing HER2 status by IHC, there was perfect interobserver agreement (k=0.98, p<0.001 95%CI: 0.96-1.0) between the clinical score and our score **(Table 9.4).** Then we assessed the agreement upon dichotomising the cases into a 3-tier system of HER2-positive, low and negative, the overall agreement was moderate, and kappa value decreased to K=0.68 (**Table 9.5**). Considering the agreement for each individual HER2 IHC score, the interobserver agreement was moderate (k=0.73). The analysis reveals strong interobserver agreement at the extremes (IHC score 3+ and IHC 0). However, significant discrepancies in intermediate categories were seen. The highest discordance was for IHC score 1+, where 34 cases were scored as IHC 0 in clinical records but as 1+ by the author and only 16% of the cases were agreed between the clinical and the author scores (**Table 9.6).**

Table 9.3: Clinicopathologic characteristics of the study cohort

Parameter	Discovery cohort (n=1547)	Experimental cohort (n=363)
	Number of cases (%)	Number of cases (%)
Age at diagnosis		
< 50 years	456 (29.5)	82 (23)
≥ 50 years	1091 (70.5)	281 (77)
Menopausal status		
Pre	515 (33.3)	101 (28)
post	1032 (66.7)	262 (72)
Tumour size (cm)		
< 2.0	964 (62.3)	167 (46)
≥ 2.0	583 (37.7)	196 (54)
Histologic tumour types		
IDC NST	966 (62.4)	233 (64)
ILC	156 (10.1)	55 (15)
Other types	425 (27.5)	75 (21)
Tumour grade		
1	264 (17.1)	23 (6)
2	648 (41.9)	203 (56)
3	635 (41.0)	137 (38)
LVI		
No	1135 (73.4)	288 (79)
Yes	412 (26.6)	75 (21)
Lymph node status*		
Negative	990 (64.0)	237 (65)
Positive	557 (35.9)	125 (35)
ER Status		
Negative	301 (19.5)	0 (0.0)
Positive	1246 (80.5)	363 (100)
PR status		
Negative	598 (38.7)	50 (14)
Positive	939 (60.7)	313 (86)
HER2 Status		
Negative	1210 (77.8)	126 (34.7)
Low	196 (12.7)	237 (65.3)
Positive	141 (9.1)	NA

Table 9.3

Parameter	Discovery cohort (n=1547)	Experimental cohort (n=363)
	Number of cases (%)	Number of cases (%)
HER2 IHC score		
0	1210 (78.2)	126 (34.7)
1+	186 (12.0)	156 (43.0)
2+/ISH negative	10 (0.6)	81 (22.3)
2+/ISH positive	37 (1.7)	NA
3+	114 (7.4)	NA
NPI prognostic group		
Good	580 (37.5)	49 (14)
Moderate	747 (48.3)	306 (84)
Poor	220 (14.2)	7 (2.0)
Oncotype DX score		
Low risk <18		
Intermediate risk (≥18		180 (50)
<31)		136 (38)
High risk ≥31		47 (13)

ER: Oestrogen receptor**; PR:** progesterone receptor**; IDC NST:** Invasive duct carcinoma non-special type; **ILC**: Invasive lobular carcinoma**; LVI:** lymphovascular invasion**; IHC:** immunohistochemistry**; NPI**: Nottingham prognostic index

Table 9.4: Table summarising Inter-observer concordance for HER2 status in the discovery cohort

Inter-observer concordance for HER2 status in the discovery cohort				
Second Observer	**Clinical Records**			**Kappa Value**
	Negative	**Positive**	**Total**	
Negative	1406 (99.7)	4 (0.3)	1410	**0.98**
Positive	0 (0)	137 (100)	137	
Total	1406	141	1547	

Table 9.5: Inter-observer concordance for HER2 status dichotomised in 3 tier system in the discovery cohort

Inter-observer concordance for HER2 status dichotomised in 3 tier system in the discovery cohort					**Kappa Value**
Second Observer	**Clinical Records**				
	negative	**Low**	**positive**	**Total**	
Negative	1175 (86.8)	178 (13.2)	0 (0.0)	1353	**0.68**
Low	35 (56.5)	18 (29)	9 (14.5)	62	
Positive	0 (0.0)	0 (0.0)	132 (88%)	132	
Total	1210	196	141	1547	

Table 9.6: Inter-observer concordance for HER2 IHC score in the discovery cohort

Inter-observer concordance for HER2 IHC score in the discovery cohort						**Kappa Value**
Second Observer	**Clinical Records**					
	0	**1+**	**2+**	**3+**	**Total**	
0	1175 (86.8)	178 (13.2)	0 (0.0)	0 (0.0)	1353	**0.73**
1+	34 (68.0)	8 (16)	7 (14)	1 (2)	50	
2+	1 (2.0)	0 (0.0)	30 (63.8%)	16 (14)	47	
3+	0 (0.0)	0(0.0)	0(0.0)	97(100)	97	
Total	1210	196	37	114	1547	

9.5.3 Patterns of HER2 protein expression

Of the cases in the experimental cohort, 81% showed a degree of HER2 expression regardless of the pattern and/or the percentage of positive cells. It was observed that each case had a mixture of expression patterns, intensities, and cellular localisation. The most frequent pattern observed was incomplete faint staining which presented in 78% of the cohort followed by complete faint expression which in 58% of cases with or without other patterns of expression. Moderate incomplete staining had the lowest proportion among all patterns of expression (4%). Detailed description of HER2 expression in terms of staining intensities, patterns and percentages are summarized in **(Table 9.7 and Figure 9.2)**

Table 9.7: Description of HER2 expression patterns in the experimental cohort

HER2 expression patterns	Total Cases (n=363)		
	Frequency		Median/Range
	N	(%)	
Complete Faint	209	(58)	5 (0-70)
Incomplete Faint	279	(78)	10 (0-60)
Complete Weak	177	(49)	0 (0-40)
Incomplete weak	184	(51)	2 (0-40)
Complete Moderate	28	(8)	0 (0-30)
Incomplete Moderate	16	(4)	0 (0-15)
Total percentage of positive cells	294	(81)	30 (0-90)
Cytoplasmic expression	135	(37)	0 (0-90)
H score	294	(81)	16 (0.5-105)

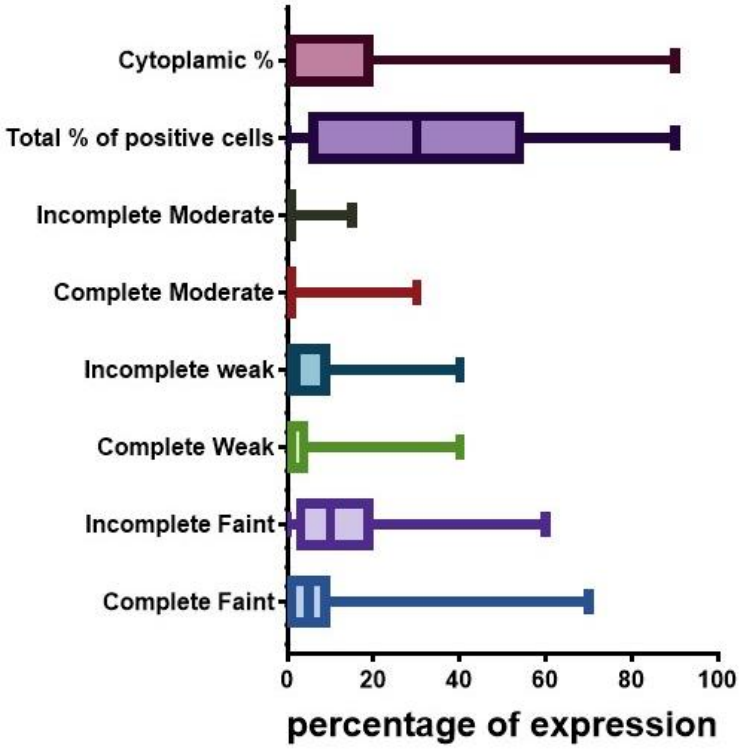


Figure 9.2: Box blot showing different patterns of HER2 expression in HER2-Low category with their median, minimum and maximum values.

9.5.4 Correlation between HER2 IHC score and mRNA level

Discrepancy between HER2 IHC protein expression score on core biopsy and mRNA level was seen in 30/363 (8%) of cases. IHC score 2+ with low mRNA level, as defined based on k mean clustering analysis, was presented in (2/30) cases while the remaining 28 cases had IHC score 0 with high mRNA level. Upon staining those 30 cases on full face tissue sections, all cases that were score 0 on core biopsy were completely negative (score 0) in the invasive tumour cells with weak to moderate staining within the *in situ* component. While the two cases that were score 2+ in core biopsy turned to be completely negative (score 0) on full face sections.

9.5.5 Clustering of *HER2* mRNA

A total of 308 cases with complete data on different HER2 expression patterns and *HER2* mRNA levels were available for k-mean clustering analysis. The dataset was divided into 2 clusters; Cluster 1 (n=109) and Cluster 2 (n=199), based on mRNA level at cut off 8.7units. Based on the new cut off, the mean values ± SD of *HER2* mRNA in HER2 in HER2 IHC 0, 1+ and 2+ was 8.66 ± 0.69, 9.1± 0.66 and 9.4 ± 0.78 (**Figure 9.3**)

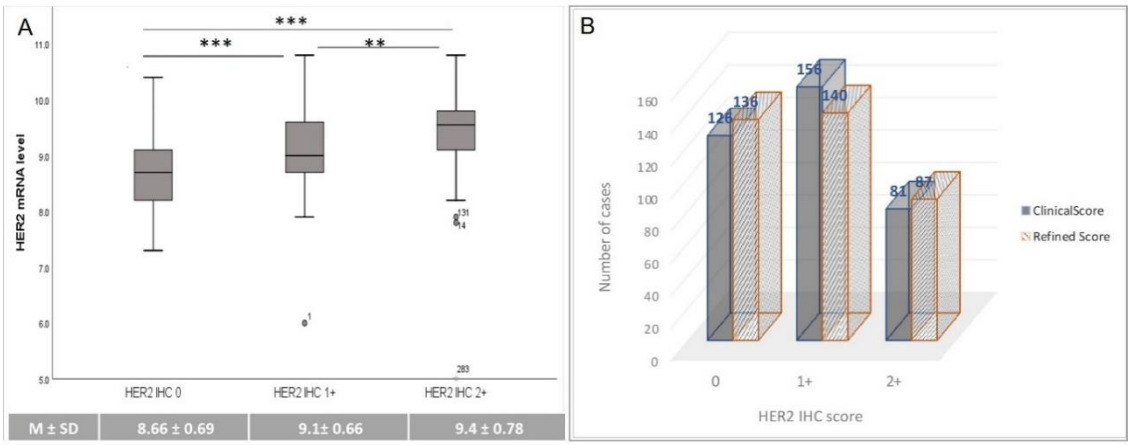


Figure 9.3: A: Box plot demonstrating distribution of HER2 mRNA among HER2 IHC scores. B: Distribution of HER2 IHC scores in the original clinical sore and our score according to refined criteria.

9.5.6 ANN model sensitivity

The parameters that predicted HER2 cluster 2 (equivalent to score 1+) were, faint complete staining at ≥ 20% of invasive tumour cells and/or faint incomplete staining in ≥ 20%, weak complete staining in ≤10%, weak incomplete staining in >10%, moderate incomplete membranous staining in ≤10% of invasive tumour cells. Cytoplasmic staining and total percentage of positive cells did not define the cluster **(Table 9.8 and Figure 9.4).**

Table 9.8: Comparison between HER2 score 1+ definition based on the existing guidelines against the refined criteria

Refined Definition	Existing ASCO/CAP and UK guidelines
*Faint complete and/or faint incomplete in ≥20%	Incomplete membrane staining that is faint/barely perceptible and in >10% of tumour cells
Weak complete ≤10%	
Weak incomplete >10%	
Moderate Incomplete ≤10%	

ASCO/CAP: American Society of Clinical Oncology / College of American Pathologists. *Total Faint staining in tumour cells ≥20%.

Figure 9.5 and Figure 9.6 demonstrates a schematic illustration of different scenarios of HER2 expression in BC and the corresponding score based on the refined criteria compared to the existing guidelines [141, 143, 157, 161].

Based on the new defined cut points for low HER2 IHC scoring, 136/363 (37%) cases were scored 0, 140/363 cases (39%) with score 1+ and 87/363 cases (24%) were score 2+ compared to 126/363 (35%), 156/363 (43%) and 81/87 (22%), for the original scores 0, 1+ and 2+, respectively.

Faint staining intensity was the most predominant pattern in HER2 score 1+ (41/140), followed by weak incomplete staining in >10% of invasive tumour cells and then weak complete staining less than or equal 10% of cells. Exclusive moderate expression either complete or incomplete <10% was not found in HER2 1+ as a unique pattern but was expressed in combination of other patterns (**Figure 9.7and Figure 9.8**). The AUC for the refined score was 0.92 with true positive rate of 92% and false positive rate of 13%. The AUC for the original clinical score was 0.71 with 69% and 34% as true positive rates and false positive rates, respectively **(Figure 9.9).**

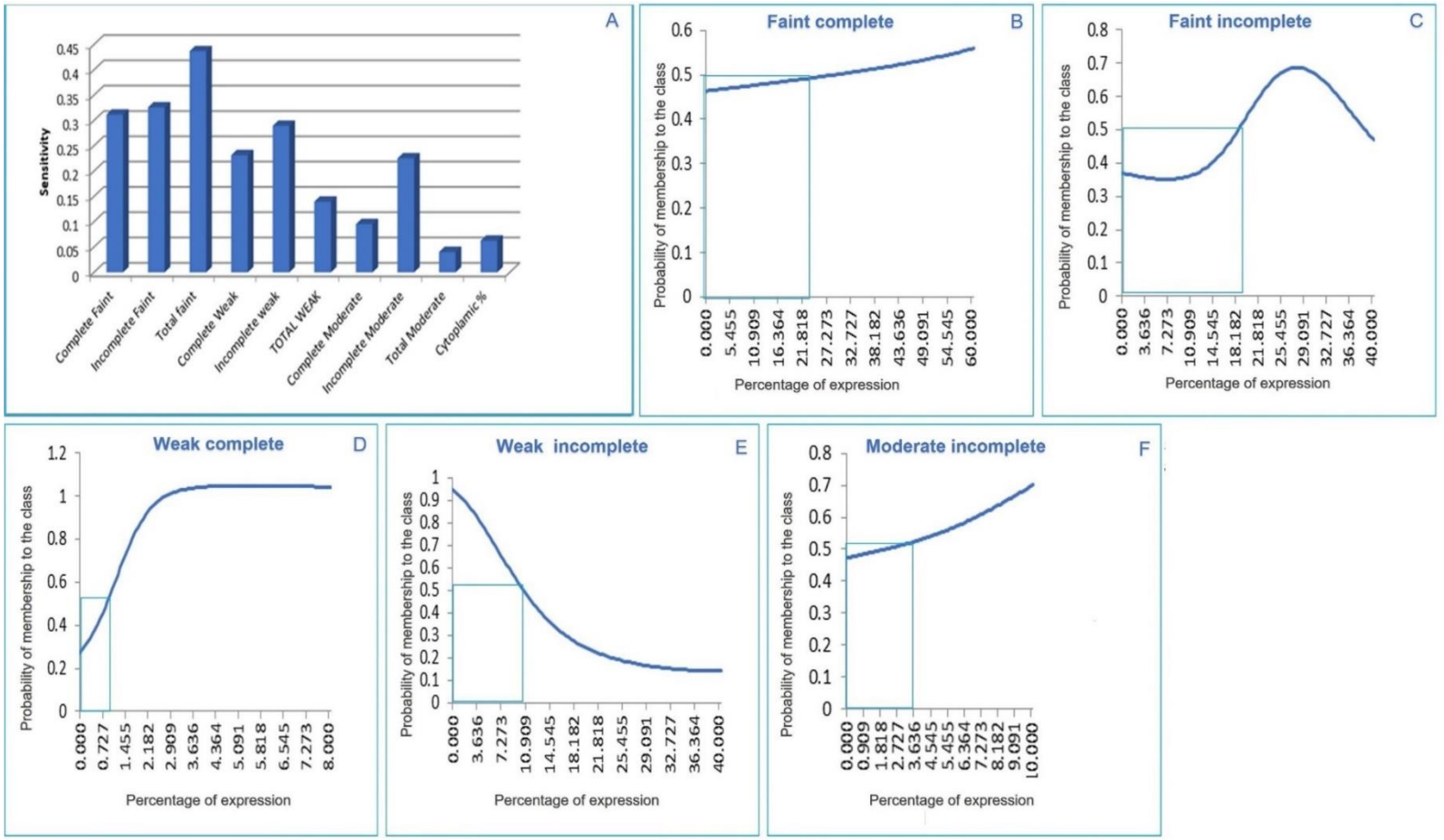
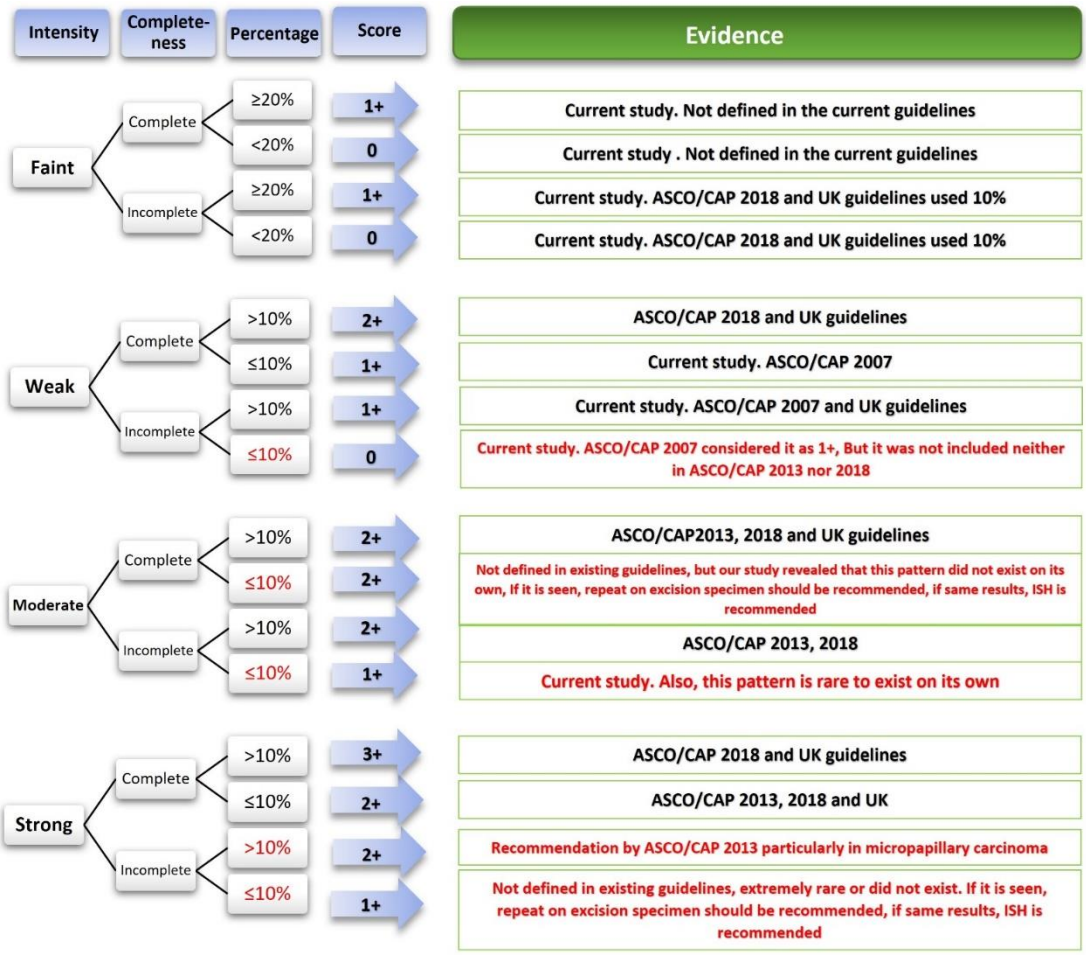


Figure 9.4: Graph showing artificial neural network model prediction of HER2 IHC1+ cut off points. A: Sensitivity analysis curves showing the contribution of each factor to the model and its relation to HER2 1+ cluster. B: Faint complete staining of ≥20% of tumour cells; C: Faint incomplete staining of ≥20%; D: Weak complete staining in ≤10%; E: Weak incomplete staining in >10%, F: Moderate incomplete in ≤10% of tumour cells



***ASCO/CAP*:** American Society of Clinical Oncology / College of American Pathologists.

Figure 9.5: Schematic illustration of different scenarios of HER2 expression in breast cancer and the corresponding score from different existing guidelines.

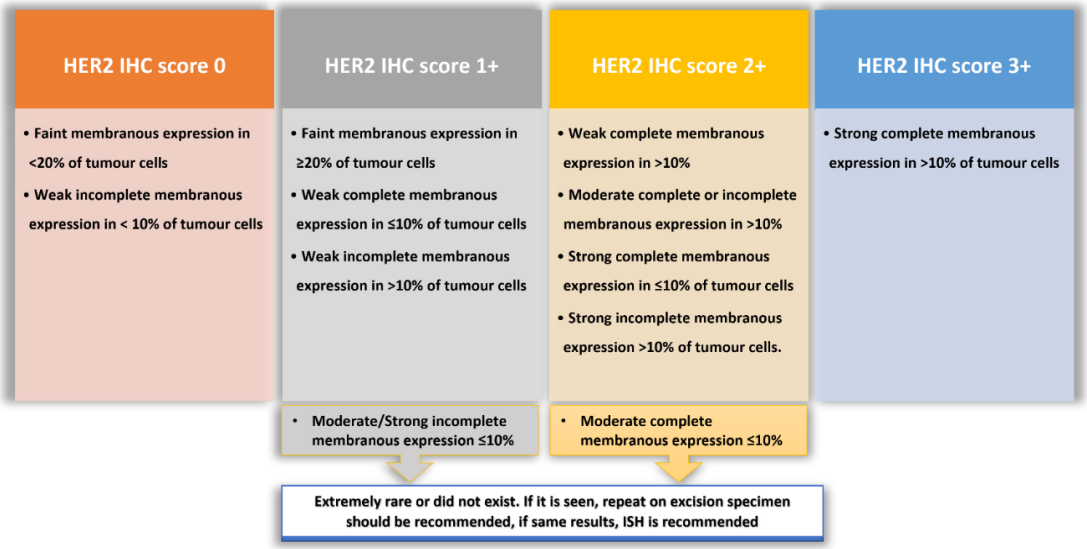


Figure 9.6: Recommended HER2 scoring algorithm based on immunohisto-chemistry-stained slides

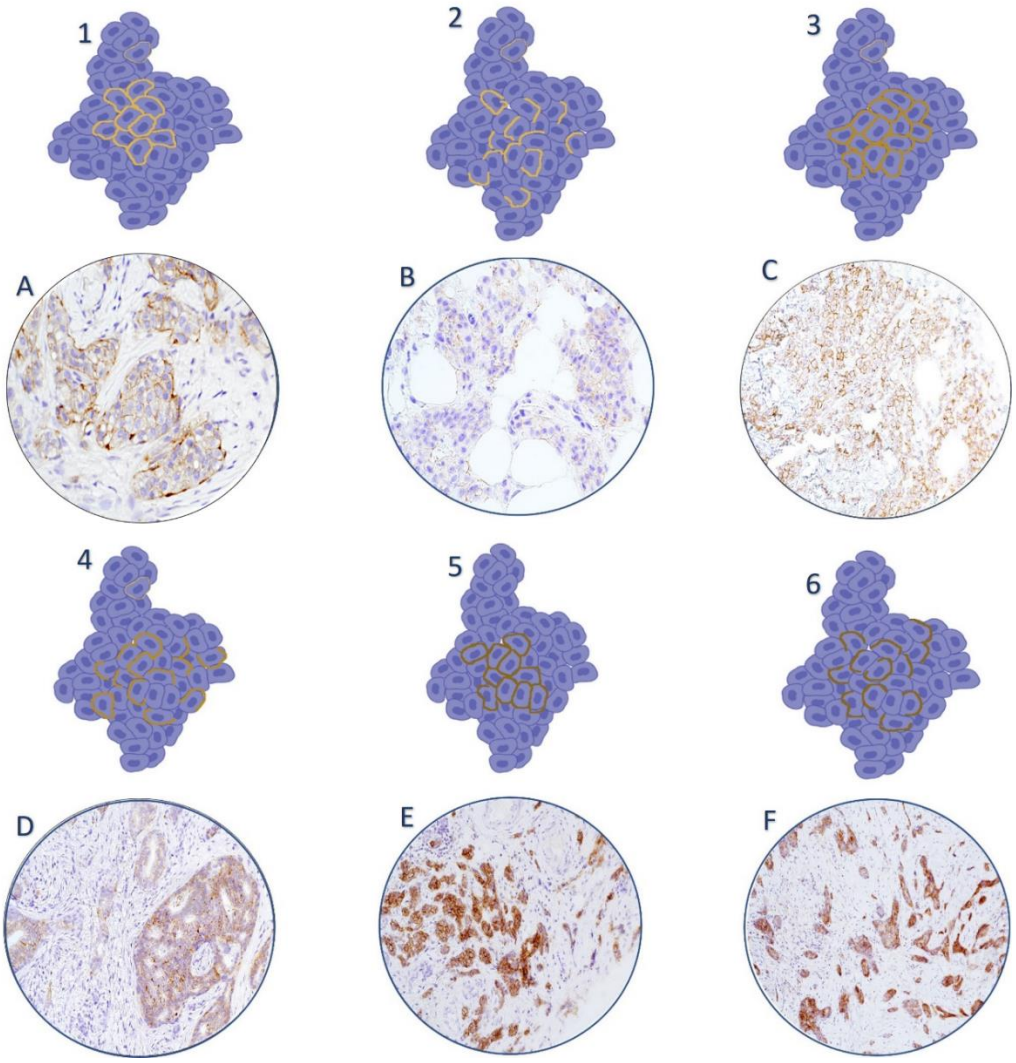


Figure 9.7: An illustrated diagram and photomicrographs showing different HER2 membranous staining patterns and intensities; Faint complete (1, A), Faint incomplete (2, B), Weak complete (3, C), Weak incomplete (4, D), Moderate complete (5, E), Moderate incomplete (6, F).

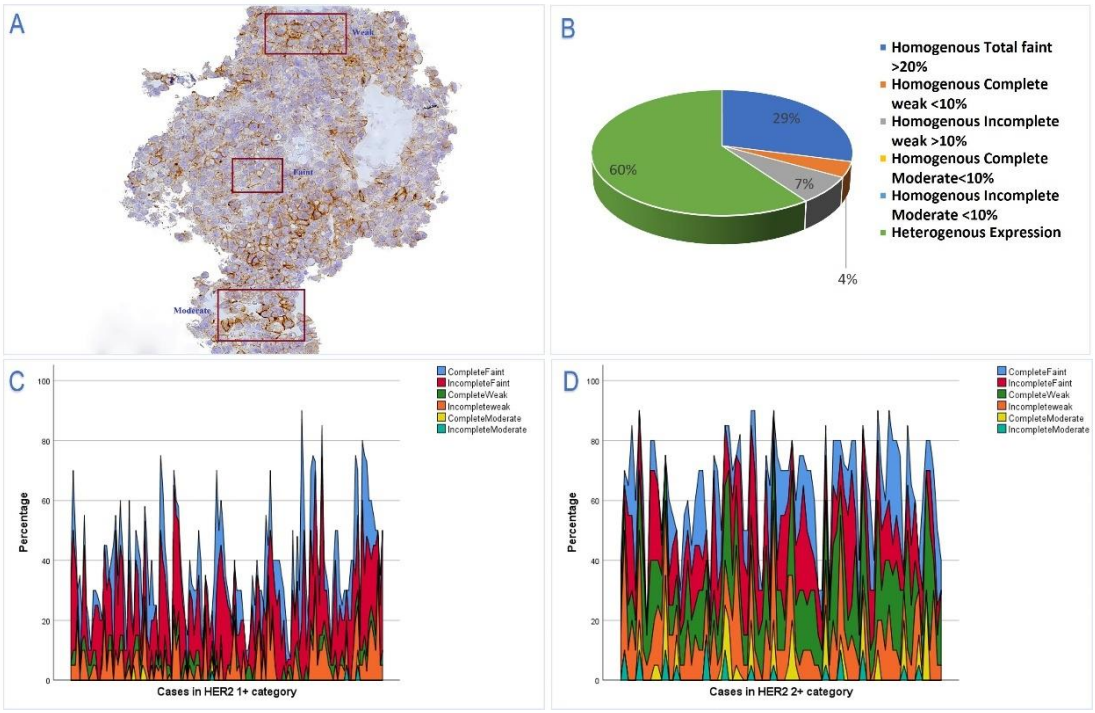
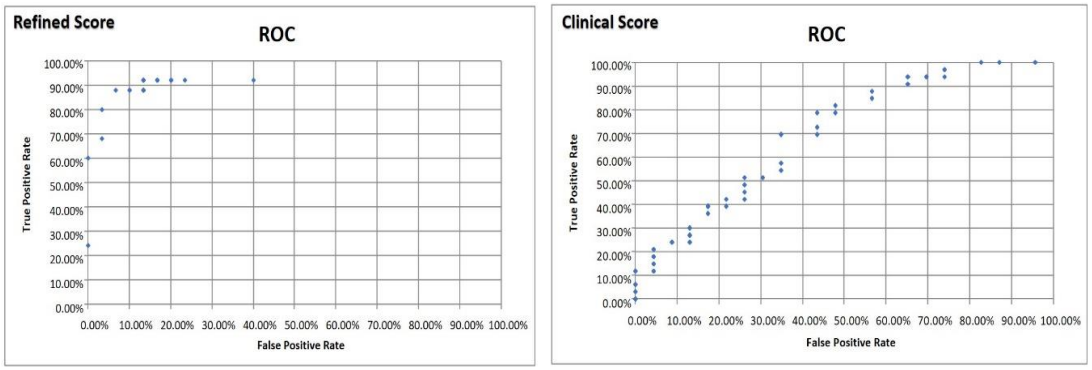


Figure 9.8: Graphical description highlighting degree of Intratumoral heterogeneity within HER2-Low category. A: HER2 IHC stained slide showing different staining intensities within the same tumour; B: Pie chart showing that 60% of HER2 1+ cases were scored based on heterogenous mixed expression patterns, while only 40% were scored based on single homogenous staining. Moderate staining was present in addition to other staining patterns and not alone in HER2 1+ category. Sparklines show multiple combinations of heterogenous patterns in example of HER2 score 1+ (C) and another example of HER2 score 2+ (D).



HER2 IHC Score	AUC	True positive rate	False Positive rate
Refined score	.92	92%	13.3%
Clinical Score	.71	69%	34%

Figure 9.9: Chart illustrating which HER2 score is more accurate in predicting score 1+ based on the true positive and false positive rates obtained from receiver operator characteristics(ROC)- area under the curve (AUC).

9.5.7 Reproducibility of the refined HER2 IHC score

The degree of concordance between the score given on the original clinical settings and the re-defined score upon applying the existing HER2 scoring criteria was substantial (kappa=0.6). Exact score agreement was 79%, while number of discordant cases was 75/363 cases (20%), 47 of them were between IHC score 1+ vs. 0 and the remaining 28 discordant cases were between 1+ vs. 2+. None of the cases showed score 2+ vs. 0 discrepancy. Regarding the refined score, the intra-observer concordance showed perfect agreement (kappa=0.8) with 87% exact score agreement. Furthermore, the interobserver agreement was perfect (kappa=0.9) with 89% exact score agreement. Overall, there were 36/363 cases (10%) with discordance. **Table 9.9** details the agreement levels. There was strong association between H score and HER2 IHC scores (p<0.001).

Table 9.9: Concordance rates of the refined HER2 score

Inter-observer concordance of the refined HER2 score between the 2 observers					
Second observer score	**First observer score**				**Kappa Value**
	0	**1+**	**2+**	**Total**	
0	128 (93.4%)	9 (6.6)	0	137	
1+	8 (5.7)	122 (87.1%)	10 (7%)	140	
2+	0	9 (10.5%)	77 (89.5%)	86	
Total	136	140	87	363	**0.85**
Intra-observer agreement of HER2 score using the refined criteria					
Refined HER2 score (2nd) *	**Refined HER2 score (1st)**				
	0	**1**	**2**	**Total**	
0	124 (92%)	11 (8%)	0	135	
1+	12 (8.3%)	119 (82.6%)	13 (9.1%)	144	
2+	0	10 (12%)	74 (88%)	84	
Total	136	140	87	363	**0.83**

*** Carried out by the first observer after 3 months wash out period from the 1st score.**

9.5.8 The association between various clinicopathological parameters and the refined HER2 score in comparison with the original score

Both HER2 scores showed a statistically significant correlation with LN status and mRNA level **(Table 9.10).** The refined score, but not the original score, showed a statistically significant correlation with the Oncotype DX recurrence score ($p = 0.02$), where score 0 was associated with higher risk Oncotype DX groups. Moreover, there was a statistically significant difference between HER2 IHC 1+ and 2+ using the refined score regarding LN metastasis, where IHC 1+ was associated with LN metastasis. When compared to IHC score 0 cases, there was a statistically significant correlation between HER2-Low cluster and low tumour grade ($p<0.001$), lower pleomorphism score ($p=0.001$) and low mitotic count ($p<0.001$), less DCIS within the tumour ($p<0.001$) and more LN metastasis ($p=0.03$) **(Table 9.11).**

In the transcriptomic cohorts, there was a significant correlation between HER2 mRNA levels and various HER2 IHC scores, both across the entire range of IHC classes (0-3) and specifically within the HER2-Low class. Additionally, a significant correlation was observed between HER2 mRNA levels and HER2 gene copy number in the TCGA and METABRIC cohorts ($p < 0.001$) **(Figure 9.10 and Figure 9.11,** respectively**)**

Table 9.10: Associations between clinicopathologic parameters and HER2 scores (using the refined and the original clinical score)

Parameter	Refined HER2 IHC Score						Clinical HER2 IHC score					
	IHC 0 (N, %)	IHC 1+ (N, %)	IHC 2+ (N, %)	P. Val-ue[a]	P. Val-ue[b]	P. Value[c]	IHC 0 (N, %)	IHC 1+ (N, %)	IHC 2+ (N, %)	P. Val-ue[a]	P. Val-ue[b]	P. Value[c]
Age at diagnosis												
<50 years	36 (44)	24 (29)	22 (27)	X2=3.52	X2=2.20	X2=1.87	26 (32)	43 (53)	12 (15)	X2=1.81	X2=4.50	X2=0.36
≥ 50 years	100 (36)	116 (41)	65 (23)	0.079	0.140	0.170	100 (36)	113 (40)	67 (24)	0.21	0.035	0.548
Menopause												
Pre	35 (34)	44 (44)	22 (22)	X2=1.09	X2=0.98	X2=0.47	37 (37)	40 (40)	24 (23)	X2=0.49	X2=0.59	X2=0.19
Post	101 (38)	96 (37)	65 (25)	0.290	0.320	0.490	89 (34)	116 (45)	55 (21)	0.500	0.440	0.710
Tumour size (cm)												
<2	57 (34)	71 (43)	39 (23)	X2=2.14	X2=0.74	X2=1.47	62 (37)	64 (38)	41 (25)	X2=1.88	X2=2.50	X2=0.67
≥ 2	79 (40)	69 (35)	48 (25)	0.149	0.420	0.230	64 (33)	92 (47)	38 (20)	0.186	0.128	0.440
Histologic types												
NST	87 (37)	86 (27)	60 (26)				82 (35)	95 (41)	56 (24)			
Lobular	20 (36)	23 (42)	12 (22)	X2=0.04	X2=2.82	X2=1.04	19 (35)	29 (53)	7 (13)	X2=0.20	X2=0.92	X2=0.07
Tabular	3 (27)	5 (46)	3 (27)	0.851	0.590	0.900	3 (27)	4 (36)	4 (36)	0.660	0.340	0.930
Special type	23 (40)	23 (40)	12 (20)				20 (36)	24 (43)	12 (21)			
Metaplastic	3 (50)	3 (50)	0 (0)				2 (33)	4 (67)	0 (0)			
Tumour grade												
1	6 (26)	13 (57)	4 (17)				8 (35)	9 (40)	6 (26)			
2	79 (39)	76 (37)	48 (24)	X2=2.58	X2=1.06	X2=1.46	70 (35)	95 (47)	36 (18)	X2=0.82	X2=5.01	X2=0.02
3	51 (37)	51 (37)	35 (26)	0.275	0.302	0.480	48 (35)	52 (38)	37 (27)	0.662	0.080	0.900
Tubule Formation												
1	4 (33)	6 (50)	2 (17)	X2=1.16	X2 =0.04	X2=1.48	4 (33)	5 (42)	3 (25)	X2=3.00	X2=1.17	X2=1.40
2	21 (31)	27 (40)	19 (28)	0.286	0.841	0.480	18 (27)	35 (53)	13 (20)	0.173	0.560	0.240
3	111 (39)	107 (38)	66 (23)				104 (37)	116 (41)	63 (22)			
Pleomorphism*												
2	58 (42)	50 (37)	29 (21)	X2=1.31	X2=0.13	X2=2.20	54 (40)	55 (40)	28 (20)	X2=1.70	X2=0.01	X2=2.00
3	78 (35)	90 (40)	58 (26)	0.268	0.775	0.140	72 (32)	101 (45)	51 (23)	0.219	0.980	0.170
Mitosis												
1	77 (37)	82 (40)	47 (23)	X2=1.62	X2=3.68	X2=0.23	73 (36)	93 (46)	38 (19)	X2=0.08	X2=2.80	X2=0.16
2	32 (36)	38 (43)	19 (21)	0.414	0.159	0.890	30 (34)	36 (40)	23 (26)	0.960	0.243	0.920
3	27 (40)	20 (29)	21 (31)				23 (34)	27 (40)	18 (27)			

Table 9.10 continued

Parameter	Refined HER2 IHC Score						Clinical HER2 IHC score					
	IHC 0 (N, %)	IHC 1+ (N, %)	IHC 2+ (N, %)	P. Value[a]	P. Value[b]	P. Value[c]	IHC 0 (N, %)	IHC 1+ (N, %)	IHC 2+ (N, %)	P. Value[a]	P. Value[b]	P. Value[c]
Associated DCIS												
No	33 (30)	49 (45)	28 (25)	X2=3.87	X2=0.19	X2=3.80	34 (31)	52 (48)	23 (21)	X2=1.33	X2=0.43	X2=0.95
Yes	103 (41)	91 (36)	59 (23)	0.051	0.660	0.053	92 (37)	104 (41)	56 (22)	0.300	0.510	0.340
LVI												
No	104 (36)	115 (40)	69 (24)	X2=1.31	X2=0.28	X2=1.09	101 (35)	121 (42)	65 (23)	X2=0.28	X2=0.71	X2=0.05
Yes	32 (43)	25 (33)	18 (24)	0.298	0.600	0.300	25 (34)	35 (47)	14 (18)	0.662	0.400	0.890
LN Status												
Negative	97 (41)	77 (33)	63 (27)	X2= 7.54	X2=6.57	X2=3.30	93 (40)	95 (40)	48 (20)	X2=5.23	X2=0.09	X2=6.06
Positive	39 (31)	62 (50)	24 (19)	0.008	0.010	0.070	33 (27)	61 (49)	30 (24)	0.023	0.920	0.014
PR status												
Negative	22 (44)	17 (34)	11 (22)	X2=0.93	X2=0.02	X2=1.06	22 (44)	17 (34)	11 (22)	X2=2.52	X2=0.46	X2=2.11
Positive	114 (36)	123 (39)	76 (24)	0.340	0.910	0.300	104 (33)	139 (45)	68 (22)	0.120	0.500	0.150
NPI groups												
Good	21 (15)	16 (12)	12 (14)				21 (43)	17 (35)	11 (22)			
Moderate	115 (38)	121 (39)	71 (23)	X2=3.75	X2=1.39	X2=4.80	104 (34)	136 (45)	64 (21)	X2=2.46	X2=1.36	X2=2.40
Poor	0 (0.0)	3 (43)	4 (57)	0.163	0.490	0.090	1 (14)	3 (43)	3 (43)	0.117	0.508	0.120
Oncotype DX												
Low risk	51 (28)	81 (45)	48 (27)				59 (42)	81 (58)	38 (21)			
Intermediate risk	63 (46)	44 (32)	29 (21)	X2=11.40	X2=0.16	X2=12.71	49 (46)	57 (54)	30 (22)	X2=0.87	X2=0.42	X2=0.56
High risk	22 (47)	15 (32)	10 (21)	0.002	0.920	0.002	18 (50)	18 (50)	11 (23)	0.349	0.810	0.760
***HER2* mRNA clusters**												
Low	64 (59)	35 (32)	10 (9)	X2=16.50	X2=6.45	X2=33.10						
High	51 (26)	84 (42)	64 (32)	<0.001	0.014	<0.001	NA	NA	NA	NA	NA	NA

DCIS: Ductal carcinoma in situ**; NST:** No special type of breast cancer**, LN:** lymph node**; LVI:** lymphovascular invasion, **NPI:** Nottingham Prognostic index; **PR**: Progesterone receptor. * The cohort contained few cases of pleomorphism 1 which have been added to score 2 for statistical analysis purposes to avoid bias.

[a] Significant P values between HER2 IHC score 0 and score 1+; [b] Significant P values between HER2 IHC score 1+ and HER2 score 2+; [c] Significant P values between HER2 IHC score 0 and both HER2 IHC scores 1+&2+ (HER2-Low)

Table 9.11: Clinicopathologic parameters and *ERBB2* clusters

Parameters	*ERBB2*-negative cluster	*ERBB2*-positive cluster	P Value*
	Score 0 (N, %)	Score 1 (N, %)	
Age at diagnosis			X^2=3.36 0.066
<50 years	32 (44)	40 (56)	
≥ 50 years	77 (33)	159 (67)	
Menopausal status			X^2=2.39 0.12
Pree	37 (42)	51 (58)	
post	72 (33)	148 (67)	
Tumour size (cm)			X^2=1.28 0.256
<2	55 (39)	87 (61)	
≥ 2	54 (32)	112 (68)	
Associated DCIS			**X^2=13.04 <0.001**
No	19 (20)	74 (80)	
Yes	90 (42)	125 (58)	
Histologic types			**X^2=7.36 0.007**
IDC NST	84 (43)	113 (57)	
Lobular	10 (20)	39 (80)	
Tabular	1 (11)	8 (89)	
Special type	14 (27)	39 (73)	
Tumour grade			**X^2=28.46 <0.001**
1	3 (15)	17 (85)	
2	42 (25)	126 (75)	
3	64 (53)	56 (47)	
Tubule Formation			X^2=4.31 0.116
1	1 (9)	10 (91)	
2	16 (31)	36 (69)	
3	92 (38)	153 (62)	
Pleomorphism			**X^2=11.93 0.001**
2	28 (24)	91 (76)	
3	81 (43)	108 (57)	
Mitosis			**X^2=33.72 <0.001**
1	36 (21)	134 (79)	
2	41 (51)	39 (49)	
3	32 (55)	26 (45)	
LVI			X^2=0.89 0.345
No	85 (34)	164 (66)	
Yes	24 (41)	35 (59)	
Lymph node Status			**X^2= 4.70 0.030**
Negative	81 (39)	125 (61)	
Positive	27 (27)	74 (73)	
PR status			X^2=0.33 0.57
Negative	18 (39)	28 (61)	
Positive	91 (35)	171 (65)	
NPI groups			X^2=1.92 0.381
Good	11 (26)	31 (74)	
Moderate	95 (37)	163 (63)	
Poor	2 (29)	5 (71)	

DCIS: Ductal carcinoma in situ**; NST:** No special type breast cancer**, LVI:** lymphovascular invasion, **NPI:** Nottingham Prognostic index; **PR**: Progesterone receptor

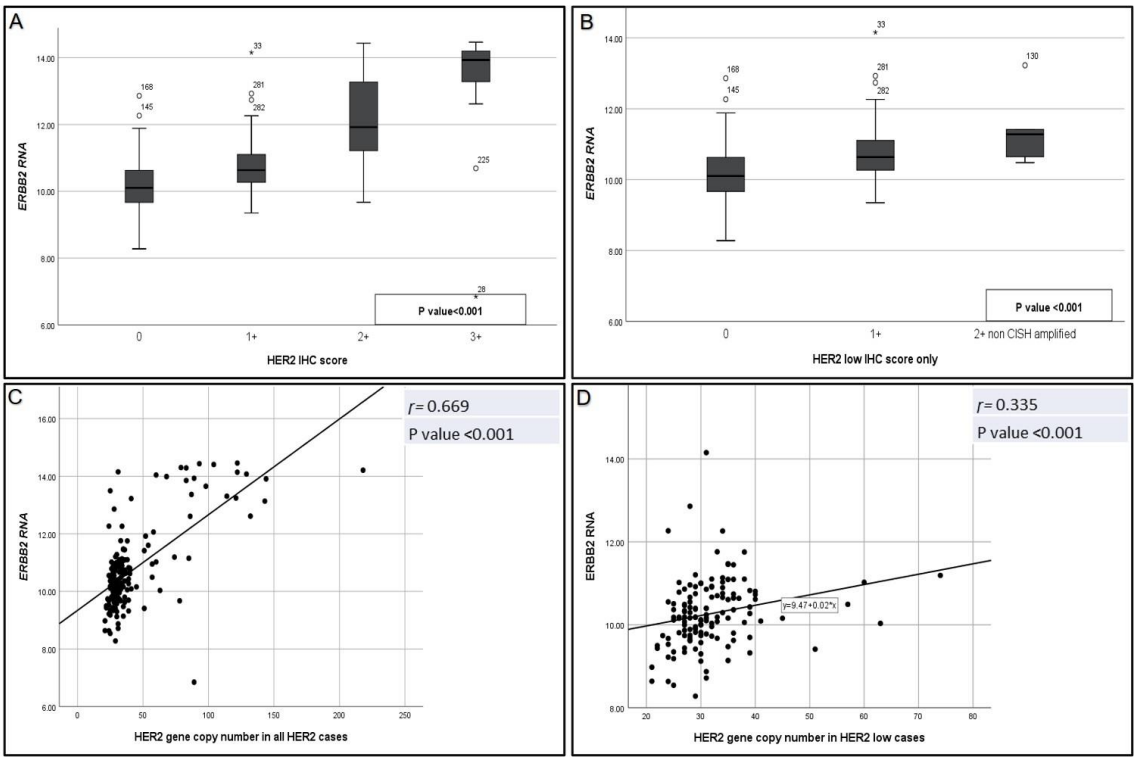


Figure 9.10: Graphs showing relation between *ERBB2* RNA level, HER2 protein level in the form of IHC expression and HER2 gene copy number. A: *ERBB2* RNA level significantly correlates with HER2 IHC scores (0-3+) and HER2-Low cases, B. Positive linear correlation between *ERBB2* RNA level and HER2 gene copy number in all HER2 scores and in HER2-Low cases as shown in C and D, respectively

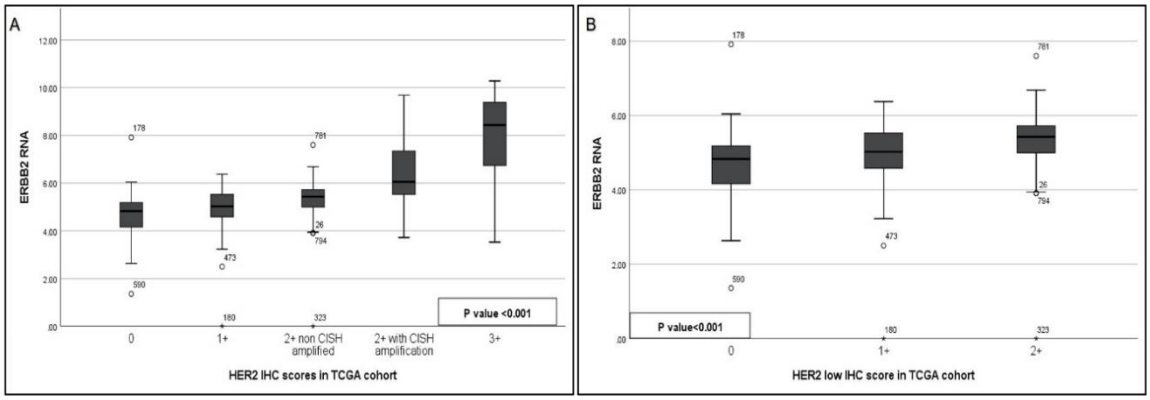


Figure 9.11: Box plot chart showing the significant correlation between HER2 RNA level and HER2 IHC score in TCGA cohort. A: ALL HER2 IHC scores from (0-3+), while B shows HER2-Low cases only

9.6 DISCUSSION

Accurate assessment of HER2 status is integral to the care of patients with BC. Recognizing this the ASCO/CAP HER2 working group released their guideline recommendations on HER2 testing in 2007, which were updated thereafter to provide a clearer guidance for HER2 testing and assessment.

At least 16 scenarios of HER2 expression patterns exist when considering the combination of staining intensity (faint, weak, moderate, and strong), membrane completeness (complete versus incomplete) and the cut-off (e.g.,10%) used to classify the percentage of HER2 in the invasive tumour cells into 2 main categories. However, not all the scenarios have been defined (see below) which in turn led to a degree of subjectivity and discordance in HER2 scoring. Some studies indicated that the concordance rates among pathologists remains low [148, 559, 649, 650], raising a concern regarding the need to refine the scoring criteria. Moreover, the distinction between HER2 IHC score 0 from score 1+, was not clinically relevant, and for practical purposes these two groups have often been combined and/or used alternatively in routine practice. Fernandez et al. demonstrated that the current standard assays utilised in the clinical setting do not efficiently differentiate IHC scores 0 or 1+ and only 26% of these cases had 90% concordance agreement [660]**.** Also**,** Schettini and colleagues showed that multi-rater overall kappa score was 0.7, equivalent to substantial agreement, and almost half of the discordant cases were between IHC score 0 versus 1+ [182].

All previous attempts for the definition aimed at separating HER2-positive from HER2-negative BC for therapeutic and prognostic purposes [141, 143, 161, 678, 679] as patients with tumours that show a low or moderate levels of HER2

protein expression without confirmed gene amplification are currently not candidates to anti-HER2 agents [174]. This category, which accounts for 45-55% of BC, is known as HER2-Low class of BC, which includes an IHC score of 1+ or 2+ with non-amplified *HER2* gene by ISH [169, 178]. With the promising response rate of ADC in HER2-Low BC patients [566, 680-683], we hypothesised that refining the definition of HER2-Low positive class with precise scoring criteria for this group will lead to better scoring concordance levels and better personalization of ADC therapy.

Borderline HER2-Low BC can be demarcated from HER2-positive cases through gene amplification assays, but the lower limit of protein expression beyond which the tumour is considered HER2-negative is not fully identified. In this study, we aimed to refine the definition of different HER2 scoring categories by providing a clearer, easier, and more applicable interpretation approach for different HER2 expression scenarios. We also sought to provide a definition for HER2-Low positive BC by distinguishing HER2 IHC score 1+ from score 0 by using the mRNA expression as ground truth. The rationale behind using mRNA level to dichotomize our cases instead of the patient outcome, is that at this low level of protein expression, *HER2* is not the driver oncogene and the clinical behaviour of the tumour and outcome is typically not dependent on the activation of the HER2 pathways [182, 684]. This was supported by Denkert et al. who demonstrated that there was no difference between HER2-Low and HER2-negative tumours in the triple negative BC cohort [186]**.**

Multiple studies show that rates of concordance for HER2 between core biopsy and excision specimens of 98% to 99% are achievable [685-687]. We have demonstrated that *HER2* mRNA was reliable in reflecting HER2 protein level

both on core biopsy and full-face sections. Our results revealed that *HER2* mRNA is statistically significant in differentiating not only HER2-positive from negative BC, but also in HER2-Low class where it can separate them into two distinct groups, and which are correlated with IHC protein level and gene amplification. Our study also showed that HER2 mRNA significantly correlates with HER2 protein and gene amplification levels supported by data from TCGA and METABRIC cohorts. This was supported in other studies that showed high concordance threshold between *HER2* mRNA and IHC and gene amplification [151, 155, 636, 688, 689]**.** The discrepancy between mRNA level and IHC score that was observed in few cases could be explained by intratumoural heterogeneity, and ratio of malignant to non-malignant cells within tumours, which can dilute the influence of the tumour cells on the result, leading to false-low mRNA level [208, 683]. While false high mRNA level in HER2 score 0 cases was mainly due to the presence of HER2 expression within the *in-situ*.

We had described ten possibilities for the HER2 expression patterns in BC tumour cells related to the staining intensity, localisation, and the circumferential staining completeness. Using a trained ANN model, we identified which pattern has the highest weight to differentiate HER2 score 1+ from score 0 based on the ground truth represented by the mRNA level. We found that at faint intensity, the percentage of expression was more effective than membranous pattern of expression whether complete or incomplete. Based on our data, any faint HER2 protein expression in 20% or more can be considered as IHC score 1+. For weak staining, our results were consistent with the 2007 ASCO/CAP HER2 guidelines [143] and updated UK guidelines [161] in the

definition of HER2 1+ (weak complete staining less than 10% and weak incomplete more than 10%, respectively).

The established algorithm for HER2 scoring according to ASCO/CAP guidelines, encompasses 10 out of the 16 possible scenarios for HER2 expression patterns. In this study, we tried to complete the missing HER2 expression possibilities based on the current study results, data from the various published HER2 scoring guideline recommendations, and our personal experience. Although most of these undefined scenarios are infrequent, like strong incomplete expression and moderate complete less than 10%, providing more objective criteria and adding more guidance to their scoring would improve the concordance rate among pathologists and consequently better HER2 categorization and management decision making.

To guarantee high inter-observer agreement, the magnification rule was also used to define faint staining which is areas showing barely visible expression defined as membranous staining confirmed only at x40, corresponding to faint intensity. This rule is applied and efficient in the assessment of HER2 in gastric carcinoma [677].

Although the H score showed a significant association with the HJER2 scores, we did not include it as a parameter to refine the HER2-Low definition. H score has been used for assessment of HER2 expression in previous studies, yet it is not approved for routine clinical [690-692]. The limitation of using H score is the non-linearity of the score which is due to the heavier weighting of higher intensity staining over lower intensity staining to calculate the score. One more fallacy of using H score in assessment of HER2 expression is that it cannot address faint intensity and completeness of membranous staining. Thus, the

H-score, which was designed as a standard scoring scheme to provide continuous scores, is not well suited for the scoring HER2 in BC [690] and would provide more unclarity to pathologists and clinicians.

Based on the refined score, the proportion of HER2 score 1+ cases decreased by 5% in comparison with the original ASCO/CAP definition that was used in the original scoring in the clinical setting. This could be explained by increasing the cut-off from the 10% used in clinical practice to 10% to 20% in the faint category. From this, we can assume that there could be a false increase in the score 1+ category in the recent guidelines, which may have affected the response rate for ADC in HER2 score 1+ BC patients. The refined score was more efficient in predicting HER2 score 1 + than the current applied score.

The inter-observer agreement between HER2 scores based on existing guidelines showed substantial concordance. This magnitude of concordance is in line with other reproducibility studies [182, 660]. Schettini and colleagues showed that multi-rater agreement was substantial and almost half of the discordant cases were between IHC score 0 versus IHC score 1+ [182]. Moreover, in the Phase 1b T-DXd study, the concordance between local and central pathology was 70% for HER2 IHC score 1+ [566].

The inter- and intra-observer agreement for the two scoring sessions, according to our refined criteria, was near perfect, with a reduction of discordant cases between HER2 scores 1+ vs 0 by more than 70%. These results support the fact that current scoring criteria for HER2 scores 1+ and 0 are subjective and less reproducible among pathologists. Guidelines should be updated or

refined to distinguish between HER2 scores 0 and 1+, especially in the upcoming era of ADC therapy. Recent studies revealed that 40% of patients with HER2-Low BC achieved partial response to T-DXD [241, 566].

The refined score showed stronger association with the clinicopathological parameters than the current applied score. Also, it showed statistical significance with Oncotype DX scores. Our results agreed with both Schettini *et al.,* and Tan *et al.,* who declared that HER2-Low BC is apparently more associated with axillary LN involvement compared to HER2 score 0 tumours [182, 693]**.** Overall, HER2 protein expression and mRNA level in IHC 1+ category was associated with low tumour grade, low mitotic count, special histological types of BC and low risk of recurrence based on Oncotype DX as described in other studies [182, 186, 693].

This study has some limitations including that the mRNA levels were measured on full face sections, whereas the IHC score was assessed on core biopsy. To overcome this issue, we selected cases with conflicting *HER2* mRNA expression and IHC scores and re-stained them on resection specimen blocks. The cohort had low number of outcome events in term of BC related deaths or disease recurrence, so outcome analysis and therapy effects were not feasible in this cohort. Therefore, we have used the mRNA level as our ground truth in classifying patients. . Due to the study design, the cohort did not include ER negative BC. However, this study aimed at refining the scoring of HER2 protein expression rather than assessing its oncogenic effect or its interaction with other proteins, thus we believe that the refined scoring criteria can be generalised and applied to ER negative tumours. In conclusion; this study aimed to discuss refining the HER2-Low positive BC focusing on the distinction between

IHC score 1+ IHC score 0 to provide a more reproducible and non-arbitrary scoring criteria compared with the current definition which is more subjective. *HER2* mRNA level is strongly correlated with HER2 protein expression. Further investigations and clinical trials using ADC in HER2-Low class BC using the refined criteria is warranted.

Chapter 10. Molecular Characterisation of HER2-Low in breast cancer

10.1 INTRODUCTION

The binary categorisation of HER2 expression in BC into HER2-positive tumours, and HER2-negative has evolved. With the introduction of ADCs that target HER2 proteins such as T-DXd [168, 169], the clinical relevance of the traditional HER2 classification is changing. Patients with low levels of HER2 expression, have proved to benefit from these new therapeutics [170, 171]. As the HER2-Low category represents ~45-55% of BC [176, 182], it is important to accurately identify this group of patients for clinical management and to gain further insight into the biology and behaviour of HER2-Low BC.

The success of T-DXd compared with chemotherapy in patients with HER2-Low mBC [170, 694] as well as trastuzumab–duocarmazine in patients with advanced HER2-Low BC [566, 680] has led to the hypothesis that HER2-Low tumours may harbour biological characteristics distinct from HER2-negative luminal and TNBC with distinct clinical properties and potential for new targeted therapies.

The updated ASCO/CAP guidelines [630] stated that there is currently no justification for a new designation of HER2 test results for patients with IHC HER2-Low levels of expression. It was considered premature to create a new HER2-Low category as the implication would be that tumours with HER2-Low behave differently or should be treated differently than tumours that test HER2 IHC 0. However, current evidence based on the Destiny-breast04 clinical trial [170] indicates that patients with HER2-Low BC respond to T-DXd therapy. Furthermore, previous *in vitro* studies have demonstrated a strong quantitative relationship between antigen expression level and intracellular exposure of

ADCs in cancer cells [695, 696]. In line with this, the United Kingdom HER2 guidelines [160] acknowledged the existence of the HER2-Low category.

Data regarding the clinicopathologic characteristics and the prognostic impact of HER2-Low BC are limited, and the published reports are inconsistent. Some studies have reported that HER2-Low tumours are more often HR-positive and are associated with higher tumour histologic grade, higher proliferation rate and increased regional lymph nodal metastases compared to HER2-negative tumours [176, 179, 183-185]. In contrast, others have reported that HER2-Low tumours are associated with a low proliferation index and negative LN status and improved patient outcome [186, 187].

The crosstalk between ER and HER2 signalling has attracted a great deal of attention and has been studied in several clinical trials [261, 266, 319-321], but it remains unclear whether ER or HER2 signalling is the dominant pathway in tumours expressing low levels of HER2. TNBC is a highly diverse and heterogeneous group of tumours associated with a higher risk of local and distant recurrence and poor patient survival [60, 697]. At least six molecular subtypes of TNBC; BL1, BL2, IM, mesenchymal, MSL and LAR have been reported [697]. Among these, the basal-like subtype is the most aggressive and least differentiated while the LAR and IM subtypes are associated with a more favourable prognosis [697, 698]. Chemotherapy is the main treatment option for patients with TNBC in addition to personalised therapies such as immune checkpoint inhibitors in TNBC in the neoadjuvant setting or in patients with programmed death ligand-1 (PDL-1) positive TNBC post-surgery [699, 700]. However, the response to these agents is variable which has prompted researchers to perform further immunophenotyping and genotyping of infiltrating

TILs in TNBC [701]. To date, no useful data have emerged regarding the significance of TILs in TNBC /HER2-negative compared with TNBC HER2-Low BC. We believe that further profiling of TNBC into either HER2-Low or HER2-negative may enable the provision of more effective and alternative personalised therapy for patients with these tumours.

10.2 HYPOTHESIS

We hypothesised that HER2-Low tumours may harbour biological characteristics distinct from HER2-negative luminal and TNBC.

10.3 AIMS OF THE STUDY

- Characterise the HER2-Low category in BC, particularly in luminal and TNBC subtypes, focusing on clinical and pathological characteristics, immunophenotypic signature, and molecular profile.
- Investigate the prognostic impact of HER2-Low status in comparison to HER2-negative and HER2-positive tumours, considering HR status.
- Explore the molecular differences between HER2-Low and HER2-negative tumours, especially within the TNBC subgroup, to understand their distinct molecular profiles and potential therapeutic implications.
- Assess the role of immune cell infiltration and the immunophenotype of HER2-Low tumours compared to HER2-negative TNBC, with an emphasis on identifying unique immunological characteristics.
- Evaluate the potential of AR as a therapeutic target in HER2-Low TNBC, given its association with worse outcomes in this subgroup.

10.4 MATERIALS AND METHODS

10.4.1 Study cohorts and data acquisition:

Two independent datasets have been enrolled in this study.

10.4.1.1 The Nottingham cohort (n=5744) was divided into.

(A1) A BC cohort from patients who had primary breast surgery (n=5115), were diagnosed at the NUH (**Section 2.1.1)**. Documented clinicopathological data included age at diagnosis, histologic tumour type, histological tumour grade, tumour size, axillary LN status, LVI, NPI and HER2 IHC scores (0-3). HR status, including ER and PR, in addition to Oncotype DX score, where available, were retrieved from patient records. ER and PR positivity were defined according to ASCO/CAP guidelines which stipulate a requirement for positive immunohistochemical staining in ≥1% of the invasive tumour cell nuclei [406].

HER2 staining was completed on the Ventana Benchmark ULTRA Immunohistochemistry Automated staining system using the Ventana PATHWAY anti-HER-2/neu (4B5) Rabbit Monoclonal ready-to-use primary antibody in combination with Ventana detection kits as part of the patient diagnostic pathway. The *HER2* gene amplification status, where available, was obtained from patient records (**Sections 2.1.12.3).**

(A2): A BC cohort from patients who received neoadjuvant therapy (n=517) was included to assess possible differences in pCR between those with HER2-Low compared with HER2-negative tumours. HR-negative patients received either anthracycline with taxanes or anthracycline only, while HR-positive patients received neoadjuvant endocrine therapy with or without chemotherapy. None of the patients received T-DXd (**Section 2.1.1.1)**.

(A3) A subset of TNBCs (n=112) was tested using next-generation sequencing (NGS) on representative FFPE tissue and was carried out by a previous researcher, as previously published [702]. Data was used to investigate differentially expressed genes in HR-negative/ HER2-Low vs HR-negative/HER2-negative tumours. This cohort is part of the Nottingham cohort (**Section 2.1.1**).

10.4.1.2 Publicly available dataset (B):

A retrospective cohort of primary BCs extracted from the publicly available BC dataset generated by the TCGA Research Network BC cohort (n=854) was also studied. PAM50 intrinsic molecular subtypes of primary tumour samples and clinicopathological data were downloaded from https://identifiers.org/cbioportal:brcatcga **(Section 2.1.2.2).**

10.4.2 CISH

HER2 CISH was performed using the HER2 CISH PharmDx kit (Dako), as previously described [638], on a subset of the Nottingham cohort (n=1366) and included a wide range of HER2 IHC scores (0-3+). In this study we focused on cases with no *HER2* gene amplification to assess the significance of *HER2* gene copy number in HER2-Low and HER2-negative tumours. Details on CISH assay steps and interpretation are mentioned in **Section 2.7**.

10.4.3 Assessment of stromal TILs

The percentage of stromal TILs (sTILs) on H&E-stained WSIs was scored in a subset of the Nottingham cohort **(Section 2.1.1).** This was carried out by a former researcher, and scores were retrieved from Nottingham Library. TILs were scored into three categories; score 1: <5%, score 2: 5-50% and score 3:

>50%, according to the recommendations of the International TILs Working Group [86].

In the Nottingham cohort (A), HER2 staining in diagnostic practice was completed on the Ventana Benchmark ULTRA IHC automated staining system using the Ventana PATHWAY anti-HER-2/neu, Rabbit Monoclonal ready-to-use primary antibody in combination with Ventana detection kits. Cases with borderline protein expression underwent FISH analysis as part of the patient's routine diagnostic pathway. HER2 scoring follows the recommendations from ASCO/CAP guidelines and UK guidelines [141, 161, 165]. Long-term follow-up data and treatment regimens were extracted from patients' reports. The patients were treated uniformly according to local protocol. HR-positive patients received hormone therapy with or without chemotherapy according to clinical risk or recurrence risk score. TNBC patients received chemotherapy and HER2-positive patients received anti-HER2 therapy with chemotherapy. This cohort was used to profile the clinicopathologic characteristics of HER2-Low tumours and patient outcomes. Cases was then stratified for HR status into HR-positive/ HER2-Low, HR-positive/ HER2-negative, HR-negative/ HER2-Low and HR-negative/HER2-negative and subsequent correlations were performed. None of the patients in the cohort received T-DXd

In the TCGA cohort (**B**), the HER2 IHC stained slides were not available for re-scoring, so the documented original score was considered in the analysis. A 3-tier HER2 scoring system was used in this study: (1) HER2-negative (HER2 IHC score 0), (2) HER2-Low (HER2 IHC score of 1+ or 2+ with a non-amplified ISH), and (3) HER2-positive (HER2 IHC score of 3+ and 2+ with an

amplified ISH score). The clinicopathologic characteristics of HER2-Low tumours were compared with those of the HER2-negative and HER2-positive tumours.

A flow chart of the cohorts enrolled in this study is shown in **Figure 10.1**

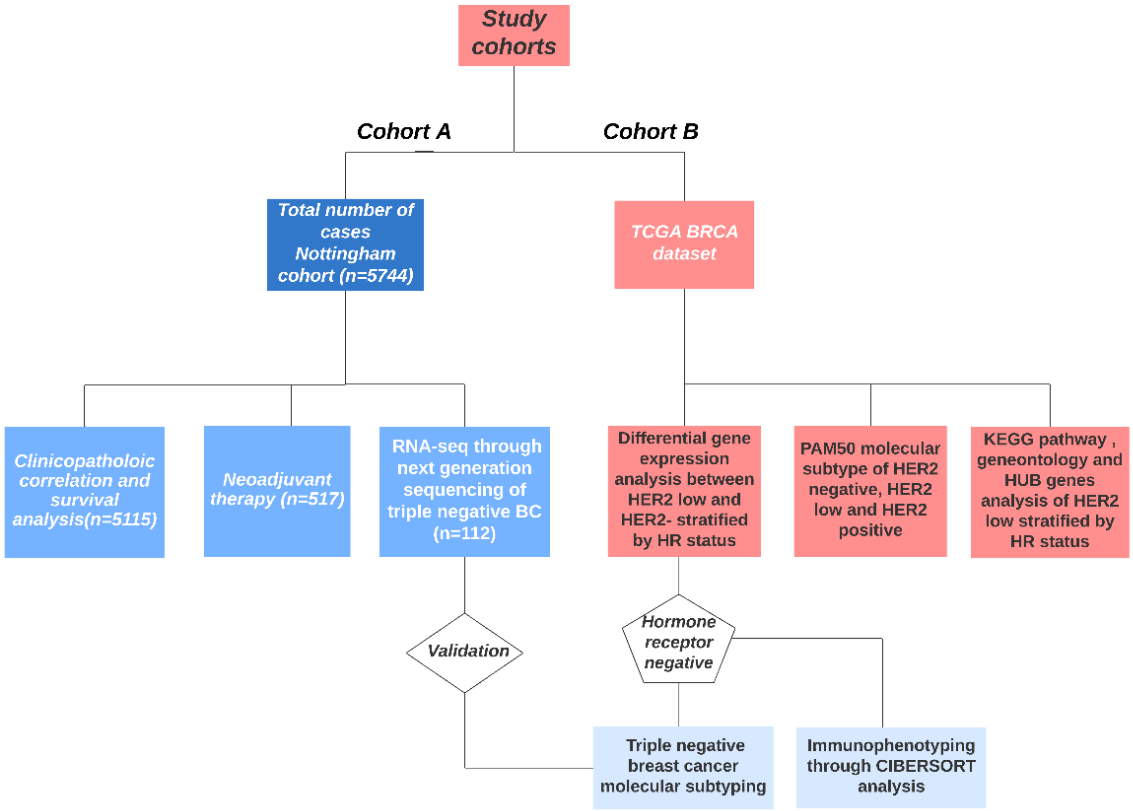


Figure 10.1: Flowchart summarising cohorts enrolled in the study

10.4.4 Differential gene expression analysis and pathway enrichment analysis

Differential expression analysis of genes expressed in HER2-Low tumours was performed with R 3.1.1 Bioconductor package DESeq2 using RNA-seq counts obtained from the TCGA-BRCA RNAseqV2 dataset [551] and from the in-house validation NGS cohort [702, 703]. The following workflow was carried out for the comparison of HER2-Low versus HER2-negative tumours, each

stratified by HR status. Raw read counts were normalised by DESeq2. The magnitude (log2 transformed fold change) and significance (P-value) of differential expression between groups were calculated, and genes with FDR adjusted P-values <0.05 and log2 fold change ±≥1 were considered as significant (**Section 2.11.2**). This part was carried out with the help and supervision of prof Nigel Mongan.

10.4.5 Validation of the results of in-house cohort

Validation of DEGs was performed on the Nottingham NGS TNBC cohort. TNBC cases were divided into HER2-Low and HER2-negative. Raw FastQ sequence reads files were quality assessed and adapter processed using the trim galore wrapper for Fastqc and Cutadapt reads with phred scores >30 retained. The resultant quality trimmed reads were aligned to the hg38 (GRCh38.83) build of the human genome using the STAR aligner [426] Transcript abundance quantification were performed using HTSEQ [704]. Normalization of genes was determined using transcripts per kilobase million (TPM) [705]Only one sample per patient was included in downstream analyses by random selection (**Section 2.11.2**). Professor Nigel Mongan helped and supervised this part.

10.4.6 HER2-Low tumours: Molecular Signature and subtyping

The enrichment of *HER2* oncogenic signalling pathway genes and PAM50 intrinsic molecular subtype within the three HER2 IHC classes, stratified for HR status, was evaluated on the TCGA cohort. Genes were identified from the literature and from a former study (Chapter **6**) [505, 698]. To further decipher

the molecular differences between HR-negative/HER2-Low and HR-negative/HER2-negative tumours, differential expression of the six TNBC molecular subtypes, BL1, BL2, IM, M, MSL and LAR genes, in these two groups was investigated on the TCGA and validated on the Nottingham NGS cohort (A3). TNBC subtype genes were pre-identified as previously published [697].

10.4.7 Immunologic profile and immunophenotyping of HER2-Low tumours

To investigate the role of sTILs in HR-negative/ HER2-Low versus HR-negative/HER2-negative BC, CIBERSORT immunophenotype analysis was carried out to identify differences in immune cell phenotypes using the TCGA dataset (http://cibersort.stanford.edu/). CIBERSORT is a gene expression-based deconvolution algorithm, it uses a set of barcode gene expression values (a "signature matrix" of 547 genes) for characterising immune cell composition. Normalised counts from deseq2 were exported and were used to infer the relative proportions of 22 types of infiltrating immune cells for each category, using the CIBERSORT algorithm as previously reported [706]. Briefly, gene mixture was prepared from the normalised expression values of upregulated genes (adjusted P-values <0.05 and |log2 fold change|≥1) in each HER2 category and data uploaded to the CIBERSORT web portal (http://cibersort.stanford.edu/), with the algorithm run using the default signature matrix at 100 permutations and quantile normalisation disabled. 100 permutations were used as the recommended minimum, but the use of 1000 permutations showed no change in the returned absolute proportion of each cell type.

10.4.8 KEGG and Gene Ontology enrichment analyses of DEGs

To explore the KEGG signalling pathways and GO of HER2-Low tumours, Gene Set Enrichment Analysis (GSEA) was performed using The Database for Annotation, Visualization and Integrated Discovery (DAVID) https://david.ncifcrf.gov/ software for HR-positive/ HER2-Low versus HR-positive/ HER2-negative and HR-negative/ HER2-Low versus HR-negative/ HER2-negative BCs in the TCGA cohort, with a cut-off criterion of adjusted $p<0.05$. KEGG is an encyclopaedia of genes and genomes, which may be used for pathway enrichment analysis of lists of genes [707]. GO annotation contains the three sub-ontologies, biological process (BP), cellular component (CC) and molecular function (MF), that can identify the biological properties of genes and gene sets for all organisms [708].

10.4.9 Protein-protein interaction network construction and hub genes selection

STRING; https://string-db.org/; version 10.5) was applied to construct the PPI network. Acknowledgement of interactions between proteins may provide further understanding of the complex mechanisms of tumour development. A combined score of >0.4 was considered to indicate statistical significance. Cytoscape (version 3.9.1) (22) was used for visualising PPI as detailed in **Section 2.11.4**.

10.4.10 Validation of hub genes

AR gene had the highest rank among other hub genes and was selected for further validation on the protein level. AR protein expression was available on a subset of Nottingham cohort (n=1117). AR IHC was carried out on the TMA

section by a former researcher, and the H score was available in the Nottingham biomarkers library. The author rescored 20% of the cases, and inter-observer concordance was calculated. Details on IHC staining are mentioned in **Section 2.5**. A primary antibody specific for AR (AR-N20, sc-816, Santa Cruz Biotechnology) was validated by western blotting using human cell lines MCF-7 and T47D. The AR antibody was used at a 1:10000 dilution which showed a band at ~110kDa. AR was considered positive based on nuclear expression. AR protein expression was divided into high and low with 10% as our cut off point as previously mentioned [709].

10.4.11 Statistical analysis

Statistical package of social science (IBM-SPSS) statistical software v. 28.0 (SPSS, Chicago, IL, USA) was used to carry out the statistical analysis. Correlations between HER2 IHC scores and clinicopathologic parameters were analysed using Chi-square ($\chi 2$) test and Kruskal-Wallis where appropriate. Univariate and multivariable logistic regression analyses were performed to investigate the association of each variable with HER2 status and the effect of other confounders and to assess factors affecting pCR. Odds ratios and 95% confidence intervals were calculated for each variable. The difference in patients' survival between HER2- and HER2-low tumours using BCSS and DMFS was evaluated using Kaplan–Meier curves and the log-rank test. The univariate and multivariate cox regression analysis was carried out on the whole cohort and also when cases were adjusted for ER status. For all analyses, a P value of <0.05 (two-tailed) was considered statistically significant

10.5 RESULTS

10.5.1 Patients and tumour characterisation

Within (A1) Nottingham cohort, 2196 tumours (43%) were HER2-Low, 2262 (44%) were HER2-negative and 657 (13%) were HER2-positive.

In the HER2-Low category, 91% of tumours were ER-positive compared to 81% in the HER2-negative and 64% in the HER2-positive groups. The mean ± SD of *HER2* gene copy number in the HER2-Low group was 2.2 ± 1.04 copies compared to 2.0 ± 0.34 and 7.6 ± 2.9 copies for HER2-negative and HER2-positive, respectively.

The patients mean age was 61 years (range 25-95) in the overall HER2-Low group. 22% of patients in the HR-negative / HER2-Low group were premenopausal compared with 33% in the HR-negative/HER2-negative group. Further details are summarised in **Table 10.1 and Table 10.2.**

In the neoadjuvant treated patient cohort (A2), 362 of 517 had HER2-Low tumours and 155 had HER2-negative tumours. HR-negative patients (n = 143, 28%) received either anthracycline with taxanes (80%) or anthracycline only (20%), while HR-positive (n=374, 72%) patients received neoadjuvant endocrine therapy with or without chemotherapy. None of the patients received T-DXd. Data regarding response to therapy was available for 296 patients of whom 53 (18%) achieved pCR. In cohort (A3), 90 patients had HER2-negative tumours and 23 had HER2-Low tumours. In the TCGA cohort (B) (n = 854), 47% (405) were HER2-negative, 41% (342) were HER2-Low and 12% (107) were HER2-positive.

Table 10.1: Descriptions of the basic clinicopathologic parameters in Nottingham cohort

Parameter	Primary surgical treated cohort (A1) (n=5115)		Neoadjuvant treated cohort (A2) (n=517)	
	N	%	N	%
Age at diagnosis				
< 50 years	1201	23	Mean+SD= 55.7	
≥ 50 years	3914	77		
Menopausal Status				
Pre-menopausal	1453	28	NA	
post-menopausal	3662	72		
Tumour size (cm)				
< 2.0	3362	66	NA	
≥ 2.0	1753	34		
Tumour grade				
1	911	18	50	10
2	2437	48	337	65
3	1767	34	130	25
Tubule Formation				
>75%	428	8	NA	
10-75	1311	26		
<10%	3376	66		
Pleomorphism				
1	48	1	NA	
2	2062	40		
3	3005	59		
Mitosis score				
1	3067	60	NA	
2	860	17		
3	1188	23		
Lymph node stage*				
1	3464	44	NA	
2	1250	45		
3	375	11		
Lymph node status *				
Negative	3464	68	NA	
Positive	1625	32		

Table 10.1 continued

Parameter	Primary surgical treated cohort (A1) (n=5115)		Neoadjuvant treated cohort (A2) (n=517)	
	N	%	N	%
Histologic tumour types				
IDC NST	3289	64	436	84
ILC	580	11	45	9
Other types	1246	25	36	7
TILS score*				
<5%	1621	72	NA	
5-50%	420	19		
>50%	235	10		
Lympho-vascular Invasion				
No	4182	82	NA	
Yes	933	18		
Nottingham Prognostic index				
Good	2216	44	NA	
Intermediate	2294	45		
Poor	579	11		
Oncotype DX score groups				
Low risk	50	20	NA	
Intermediate risk	156	61		
High risk	49	19		
HER2 IHC status*				
Negative	2262	44	155	30
low	2196	43	362	70
Positive	657	13	NA	
Oestrogen receptor status				
Negative	865	17	143	28
Positive	4250	83	374	72
Progesterone receptor Status				
Negative	1639	32	197	38
Positive	3454	68	320	62
pCR				
No	NA		243	82
Yes			53	18
Type of neoadjuvant therapy				
Chemotherapy only	NA		230	45
Endocrine plus chemo			287	55
Adjuvant Chemotherapy				
No	3432	67	NA	
Yes	1680	33		
Adjuvant Endocrine therapy				
No	1216	24	NA	
Yes	3898	76		

IDC: Invasive duct carcinoma; **NST**: Non-special type; **ILC**: Invasive lobular carcinoma; pCR: pathologic complete response

10.5.2 Clinicopathologic characteristics of HER2-Low BC in cohort A1

HER2-Low tumours were significantly associated with HR positivity and favourable tumour biological behaviour compared to HER2-negative BC. HER2-Low status was significantly associated with high ER H-score compared to HER2-negative and HER2-positive **(Figure 10.2).** When the cohort was stratified according to HR status, the favourable prognostic significance of HER2-Low status was maintained in HR-negative tumours. However, in HR-positive BC, no significant prognostic difference was detected between HER2-Low and HER2-negative status except for the absence of LVI in HER2-Low tumours ($p<0.001$). There was no significant difference in the Oncotype DX recurrence scores between HER2-Low and HER2-negative BC in this group.

Overall, HER2-Low status was significantly associated with low TILs score ($p=0.02$) and the association was maintained in HR-negative subgroups but not in HR-positive tumours **(Table 10.2).** A multivariate logistic regression analysis performed to analyse which clinicopathologic parameters are independently associated with HER2-Low status revealed that only ER positivity was an independent predictor of HER2-Low tumours ($p<0.001$).

No significant association was detected between the *HER2* gene copy number as determined by the CISH assay and the HER2 protein expression level in HER2-Low or HER2-negative tumours.

Table 10.2: Correlation between clinicopathologic parameters and HER2 IHC scores

Parameter	All Cohort					HR positive					HR Negative				
	HER2- N (%)	HER2-Low N (%)	HER2+ N (%)	P value[a]	P value[b]	HER2- N (%)	HER2-Low N (%)	HER2+ N (%)	P value[a]	P value[b]	HER - N (%)	HER2-Low N (%)	HER2+ N (%)	P value[a]	P value[b]
Age at diagnosis															
< 50 years	551 (24)	439 (20)	211 (32)	X^2=12.3	X^2=42.0	410 (22)	394 (20)	142 (34)	X^2=3.4	X^2=38.0	141 (33)	45 (22)	69 (29)	X^2=9.3	X^2=3.4
≥ 50 years	1711 (76)	1757 (80)	446 (68)	**<0.001**	**<0.001**	1430 (78)	1594 (80)	280 (66)	0.06	**<0.001**	281 (67)	163 (78)	166 (71)	**0.002**	0.07
Menopause					X^2=21.9										
Pre	647 (29)	573 (26)	233 (36)	X^2=3.5		505 (27)	527 (27)	162 (38)	X^2=0.4	X^2=3.7	142 (34)	46 (22)	71 (30)	X^2=8.9	X^2=3.7
post	1615 (71)	1623 (74)	424 (64)	0.06	**<0.001**	1335 (73)	1461 (73)	260 (62)	0.54	0.06	280 (66)	162 (78)	164 (70)	**0.003**	0.07
Tumour size									X^2=0.02					X^2=0.1	
< 2.0 cm	1475 (65)	1470 (67)	417 (64)	X^2=1.4	X^2=2.7	1262 (69)	1362 (69)	277 (66)		*X2=1.3*	213 (51)	108 (52)	140 (60)		X^2=2.6
≥ 2.0 cm	787 (35)	726 (33)	240 (36)	0.22	0.1	578 (31)	626 (31)	145 (34)	0.97	*0.25*	209 (49)	100 (48)	95 (40)	0.73	0.12
Tumour grade															
1	449 (20)	444 (20)	18 (2.7)	X^2=30.3		442 (24)	443 (22)	16 (4)			7 (2)	1 (0.5)	2 (1)	X^2=17.7	
2	1048 (46)	1169 (53)	220 (34)		X^2=335	1011 (55)	1127 (57)	175 (42)	X^2=1.8	X^2=224	37 (9)	42 (20)	45 (19)		X^2=0.3
3	765 (34)	583 (27)	419 (64)	**<0.001**	**<0.001**	387 (21)	418 (21)	231 (55)	0.42	**<0.001**	378 (90)	165 (79)	188 (80)	**<0.001**	0.9
Tubule formation															
>75%	210 (9)	207 (9)	11 (1.7)	X^2=0.06	X^2=76.7	209 (11)	206 (10)	9 (2)		X^2=51.6	1 (0.2)	1 (0.5)	2 (1)		
10-75	603 (27)	590 (27)	118 (18)			557 (30)	558 (28)	82 (19)	X^2=4.1		46 (11)	32 (15.4)	36 (15)	X^2=2.9	X^2=0.2
<10%	1449 (64)	1399 (64)	528 (80)	0.97	**<0.001**	1074 (58)	1224 (62)	331 (79)	0.12	**<0.001**	375 (89)	175 (84.1)	197 (84)	0.09	0.85

Table 10.2 continued

Parameter	All Cohort					HR positive					HR Negative				
	HER2-	HER2-Low	HER2+	P val-ue[a]	P val-ue[b]	HER2-	HER2-Low	HER2+	P val-ue[a]	P val-ue[b]	HER -	HER2-Low	HER2+	P val-ue[a]	P val-ue[b]
	N (%)	N (%)	N (%)			N (%)	N (%)	N (%)			N (%)	N (%)	N (%)		
Pleomorphism															
1	33 (1.5)	15 (1.0)	0 (0.0)	X^2=16.		32 (2)	15 (1)	0 (0.0)			1 (0.2)	0 (0.0)	0 (0.0)		
2	951 (42)	1033 (47)	78 (12)	3	X^2=272	936 (50)	1027 (52)	74 (18)	X^2=7.7	X^2=170	15 (3.8)	6 (3)	4 (2)	X^2=0.5	X^2=0.7
3	1278 (57)	1148 (52)	579 (88)	<0.001	<0.001	872 (48)	946 (47)	348 (83)	0.02	<0.001	406 (96)	202 (97)	231 (98)	0.49	0.4
Mitosis score															
1	1369 (61)	1491 (68)	207 (32)	X^2=38.		1330 (72)	1456 (73)	171 (41)			39 (9)	35 (17)	36 (15)		
2	341 (15)	330 (15)	189 (29)	3	X^2=281	273 (15)	283 (14)	110 (26)	X^2=0.4	X^2=179	68 (16)	47 (23)	79 (34)	X^2=14	X^2=6.7
3	552 (24)	375 (17)	261 (40)	**<0.001**	**<0.001**	237 (13)	249 (13)	141 (33)	0.8	**<0.001**	315 (75)	126 (61)	120 (51)	**<0.001**	**0.03**
LN status				X^2=0.0	X^2=32.					X^2=16.					
Negative	1568 (70)	1520 (70)	376 (58)	2	0	1278 (70)	1387 (70)	251 (60)	X^2=0.1	7	290 (70)	133 (66)	125 (54)	X^2=1.1	X^2=6.1
Positive	684 (30)	665 (30)	276 (42)	0.97	**<0.001**	557 (30)	595 (30)	169 (40)	0.83	**<0.001**	127 (30)	70 (34)	107 (46)	0.31	**0.02**
Histologic tu-mour type															
IDC NST	1381 (42)	1329 (61)	579 (88)	X^2=0.0		1003 (40)	1139 (57)	359 (85)			378 (90)	190 (91)	220 (93)		X^2=0.1
ILC	269 (12)	294 (13)	17 (3)	6	X^2=176	266 (15)	287 (14)	13 (3)	X2=4.2	X2=117	3 (1)	7 (3)	4 (2)	X^2=0.8	9
Other types	612 (26)	573 (26)	61 (9)	0.97	**<0.001**	471 (45)	462 (29)	50 (12)	0.06	**<0.001**	41 (9)	11 (6)	11 (5)	0.36	0.75
TILS score															
<5%	445 (70)	993 (76)	183 (56)		X^2=52.	390 (79)	921 (78)	139 (63)		X^2=25.	55 (38)	72 (53)	44 (41)		
5-50%	121 (19)	207 (16)	92 (28)	X^2=7.0	3	74 (15)	171 (15)	51 (23)	X^2=1.3	4	47 (33)	36 (26)	41 (38)	X^2=5.9	X^2=4.4
>50%	69 (11)	112 (8)	54 (16)	**0.02**	**<0.001**	27 (6)	83 (7)	31 (14)	0.4	**<0.001**	42 (29)	29 (21)	23 (21)	**0.02**	0.11
LVI				X^2=18.	X^2=64.				X^2=16.	X^2=38.				X^2=0.1	
No	1829 (81)	1880 (86)	473 (72)	0	9	1496 (81)	1713 (86)	312 (74)	7	8	333 (79)	167 (80)	161 (69)	6	X^2=8.0
Yes	433 (19)	316 (14)	184 (28)	**<0.001**	**<0.001**	344 (19)	275 (14)	110 (26)	**<0.001**	**<0.001**	89 (21)	41 (20)	74 (31)	0.69	**0.005**

Table 10.2 continued

Parameter	All Cohort					HR positive					HR Negative				
	HER2- N (%)	HER2-Low N (%)	HER2+ N (%)	P val-ue[a]	P val-ue[b]	HER2- N (%)	HER2-Low N (%)	HER2+ N (%)	P val-ue[a]	P val-ue[b]	HER - N (%)	HER2-Low N (%)	HER2+ N (%)	P val-ue[a]	P val-ue[b]
NPI risk group															
Low	1001 (44)	1074 (49)	141 (22)			968 (53)	1055 (53)	117 (28)		X^2=94.4	33 (8)	19 (9)	24 (10)		X^2=2.05
Intermediate	1017 (45)	900 (41)	377 (58)	X^2=9.9	X^2=168	714 (40)	761 (38)	233 (56)	X^2=0.1		303 (73)	139 (69)	144 (62)	X^2=1.2	
High risk	234 (10)	211 (10)	134 (21)	0.007	<0.001	153 (8)	166 (8)	70 (17)	0.9	<0.001	81 (19)	45 (22)	64 (28)	0.55	0.36
Oncotype DX score risk groups															
Low	20 (20)	30 (20)				64 (63)	104 (68)								
Intermediate	55 (54)	100 (65)		X^2=5.5		11 (11)	26 (17)		X^2=5.5						
High	26 (26)	23 (15)	NA	0.09	NA	26 (26)	23 (15)	NA	0.06	NA	NA	NA	NA		
ER status				X^2=77.6											
Negative	422 (19)	208 (9)	235 (36)		X^2=266										
Positive	1840 (81)	1988 (91)	422 (64)	**<0.001**	**<0.001**	NA	NA	NA	NA	NA	NA	NA	NA	NA	NA
PR Status				X^2=71.6											
Negative	767 (34)	496 (23)	376 (58)		X^2=293										
Positive	1484 (66)	1697 (77)	273 (42)	**<0.001**	**<0.001**										

HER2+: HER2-positive**; HER2-:** HER2-negative**; LN:** lymph node**; IDC NST:** Invasive duct carcinoma non-special type**; ILC:** Invasive lobular carcinoma; **TILS**: Tumour infiltrating lymphocytes; **LVI:** lymphovascular invasion**; NPI:** Nottingham prognostic index; **ER:** Oestrogen Receptors**; PR:** Progesterone receptor; **NA**: Not applicable **TNBC**: triple negative subtype. **a**: p value across HER-negative and HER2-Low; **b**: p value of significance between HER2-positive and HER2-Low. Significant p values shown in bold.

Some cases are missing within each parameter as they were collected from different datasets.

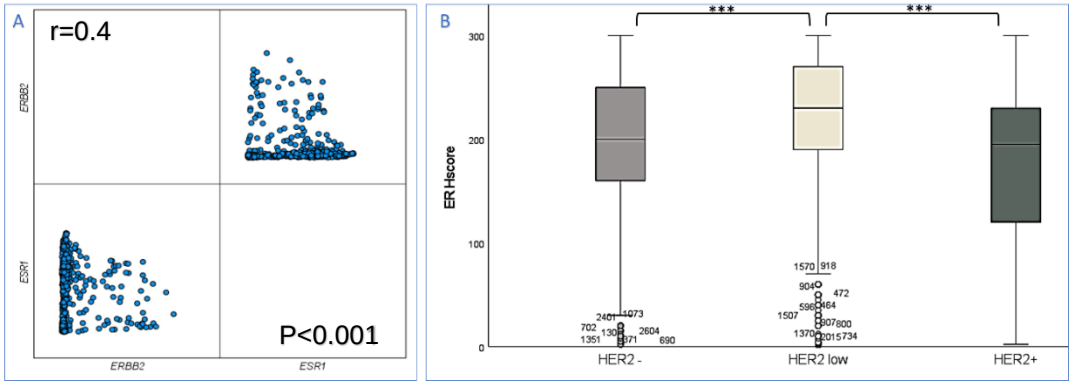


Figure 10.2: A graph illustrating the relation between *ERBB2*, *ESR1* and oestrogen receptor expression in HER2-Low tumours. A: A scatterplot matrix demonstrating the significant positive correlation between *ERBB2* and *ESR1* mRNA levels, The bottom left corner shows the pairwise combination for *ERBB2* and *ESR1* levels in the analysed dataset. B: Box plot showing the correlation between ER H score and HER2 classes. The highest ER H score is in HER2-Low tumours.

10.5.3 Difference in patient outcome between HER2-Low and HER2-negative tumours according to HR status

In cohort A1, HER2-Low BC patients had prolonged BCSS and DMFS (p=0.004 and p=0.009, respectively) compared to HER2-negative patients. In luminal tumours, this significance was lost **(Figure 10.3)** while in HR-negative BC, HER2-Low tumours were associated with improved patient outcomes (p=0.04 for both BCSS and DMFS). In multivariate Cox regression analysis, HER2-Low patients had prolonged DMFS compared to those with HER2-negative BC, adjusted for the significant parameters in univariate analysis (LN status, LVI, and NPI) **(Table 10.3)**. Within the group of patients with HR-negative/ HER2-Low BC, negative LN status was associated with prolonged patient survival (p=0.008 and p=0.006 in BCSS and DMFS respectively). In patients with HR-positive BC, no significant difference in the factors affecting survival between HER2-Low and HER2-negative was detected.

In the neoadjuvant setting (cohort A2), HER2-negative tumours were significantly associated with high pCR rates compared to HER2-Low tumours (74% vs 26%), p<0.001. In HR-negative BC, patients with HER2-negative tumours had significantly higher pCR than those with HER2-Low tumours, p=0.037 following treatment with neoadjuvant chemotherapy. This difference was not observed in HR-positive patients. In the multivariate regression model, HER2 status was an independent predictor of pCR (HR: 3.31, 95%CI: 1.7-6.4, p<0.001) when adjusted for HR status, tumour grade and type of neoadjuvant therapy **(Table 10.4)**

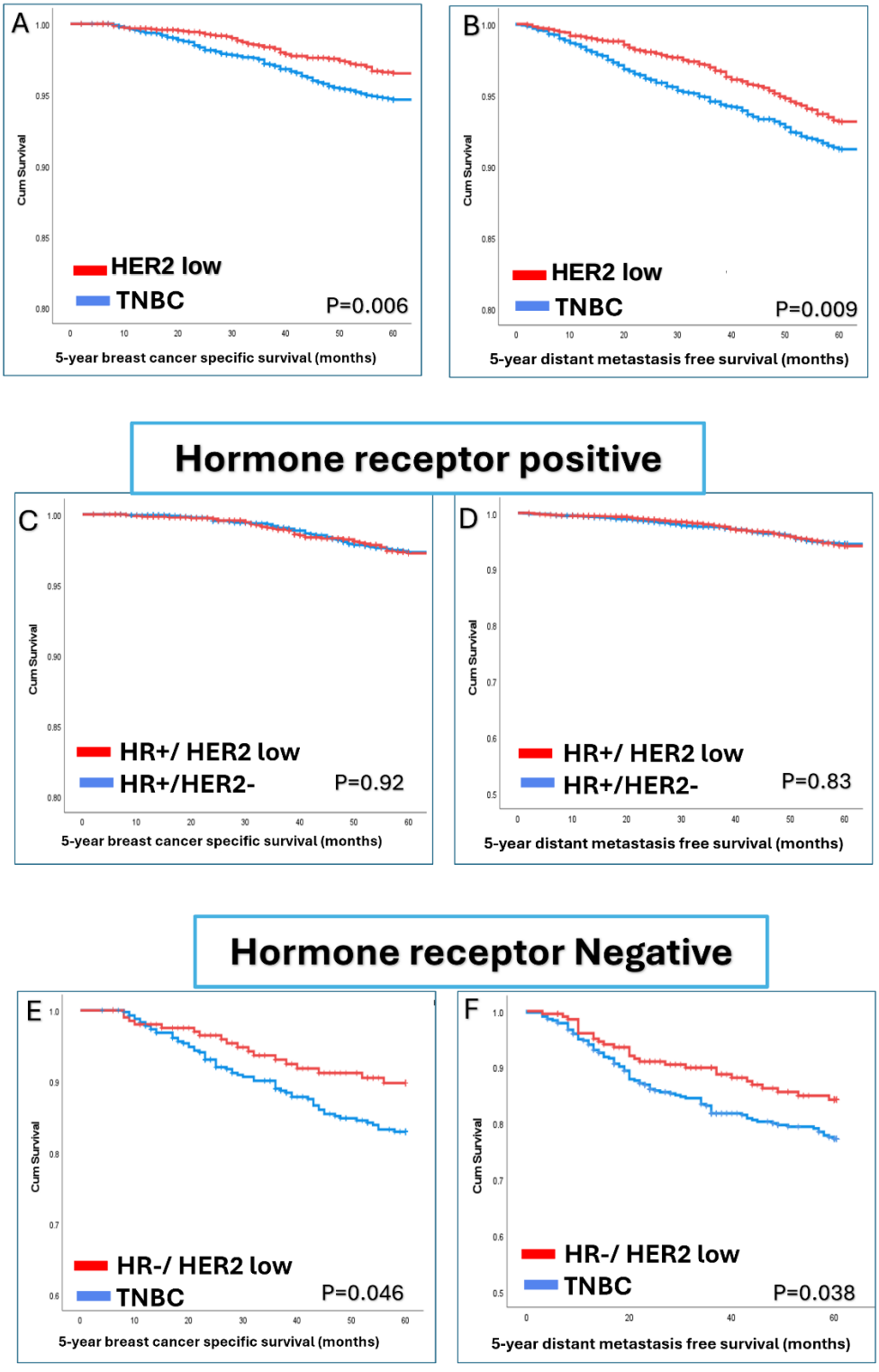


Figure 10.3: Kaplan Meier's curve showing differences in breast cancer specific survival (BCSS) and distant metastasis-free survival (DMFS) between HER2-Low and HER2-negative generally (A&B) and stratified by hormone receptor (HR) status. C&D: No significant difference in patients survival between HER2 Low and HER2-negative in HR positive tumours: E&F: HER2-Low patients had significant improved outcome than HER2-negative in HR negative tumours.

Table 10.3: Difference in patients' outcome between HER2-Low and HER2-negative hormone receptor negative breast cancer

	5 years breast cancer specific survival						5 years distant metastasis free survival					
	Univariate Analysis 5 years			Multivariate Analysis 5 years			Univariate Analysis 5 years			Multivariate Analysis 5 years		
	HR	**95% CI**	**P value**	**HR**	**95% CI**	**P value**	**HR**	**95% CI**	**P value**	**HR**	**95% CI**	**P value**
HER2 status Negative Low	1.73 1	1.02-2.9	**0.04**	1.6 1	0.95- 2.72-	0.05	1.5 1	1.0-2.3	**0.04**	1.52 1	0.99-2.3	**0.049**
Grade 1 2 3	0.0 0.45 1.0	0.0 0.1-1.1	0.22	NA	NA	NA	0.0 0.70 1.0	0.0 0.3-1.37	0.55	NA	NA	NA
LVI Negative Positive	0.26 1.0	0.17 – 0.41	**<0.001**	0.35 1.0	0.21-0.57	**<0.001**	0.38 1.0	0.21-0.44	**<0.001**	0.41 1.0	0.26-0.45	**<0.001**
LN status Negative Positive	0.41 1.0	0.26 - 0.63	**<0.001**	0.94 1.0	0.45-1.35	0.87	0.41 1.0	0.29-0.59	**<0.001**	0.81 1.0	0.45-1.44	0.46
TILS score Score 1 Score 2 Score 3	1.4 1.02 1.0	0.56 - 3.4 0.35-3.1	0.65	NA	NA	NA	1.9 1.8 1.0	0.84-4.1 0.7-4.3	0.27	NA	NA	NA
NPI Good Moderate poor	0.20 0.36 1	0.06-0.66 9.23-0.56	**<0.001**	0.27 0.57 1	0.05-1.36 0.27-1.2	0.2	0.19 0.38 1	007-0.52 0.26-0.56	**<0.001**	0.29 0.644	0.08-1.08 0.36-1.16	0.14
Chemother-apy No Yes	1.3 1	0.47 - 3.7	0.61	NA	NA	NA	1.1 1	0.73-1.6	0.72	NA	NA	NA

HR: Hazard ratio; CI: Confidence interval; **LN:** lymph node**; TILS**: Tumour infiltrating lymphocytes; **LVI:** lymphovascular invasion**; NPI:** Nottingham prognostic index; Significant p values shown in bold.

Table 10.4: Factors affecting pathologic complete response among HER2-Low and HER2-negative BC patients.

	Univariate regression analysis			Multivariate regression analysis		
	Odd's ratio	**95% CI**	**P value**	**Odd's ratio**	**95% CI**	**P value**
HER2 status						
Negative	3.31	1.7-6.4	**<0.001**	2.31	1.14-4.7	**0.02**
Low	1			1		
ER status						
Negative	3.32	1.8-6.2	**<0.001**	1.9	0.96-3.81	0.07
Positive	1			1		
Tumour grade						
1	0.1	0.1 0.2-0.62	**0.002**	0.1	0.1 0.23-0.87	0.06
2	0.34			0.5		
3	1			1		
Neoadjuvant therapy						
Chemotherapy only	0.76	0.15-3.75	0.6	NA	NA	NA
Endocrine + chemo	1					

ER: Oestrogen receptor; **CI:** Confidence interval

10.5.4 HER2-Low molecular signature

In TCGA dataset (cohort B), a positive significant correlation between *ERBB2* and *ESR1* gene (p<0.001, r=0.4) was observed, while *ERBB2* and *MKI67* were negatively correlated to each other (p<0.001) **(Figure 10.2)**.

There was no significant difference between HER2-Low and HER2-negative tumours regarding the expression of HER2 oncogenic signalling pathway genes regardless of HR status, unlike HER2-positive tumours that were enriched for HER2 oncogenic signalling pathway genes (**Figure 10.4)**. PAM50 intrinsic molecular subtyping revealed that 57% of HER2-Low tumours were luminal A intrinsic molecular subtype and 20% were luminal B. In HR-negative tumours, 13% were HER2 enriched, compared to 0.5% in the HR-positive/ HER2-Low group (**Figure 10.5A).**

The differential expression of normalised RNA-Seq reads of PAM50 genes revealed that HR-positive/ HER2-Low and HR-positive/HER2-negative tumours were enriched for luminal A and luminal B genes as expected. HR-negative/HER2-negative tumours were significantly enriched for basal-like genes, while HR-negative/ HER2-Low tumours were enriched for luminal and normal-like intrinsic subtypes genes (*GPR160, MLPH, PGR, KRT14, FOXA1, TMEM45B* and *ESR1*). *ERBB2* gene differential expression was not significantly different in HER2-Low vs HER2-negative tumours regardless of ER status **(Figure 10.5B,C and Table 10.5)**

For further deciphering the molecular differences between HR-negative / HER2-Low and HR-negative/HER2-negative tumours, differential expression of the six TNBC molecular subtypes genes in those two classes was carried out on TCGA dataset and validated on cohort A3. This revealed that HR-negative/ HER2-Low BC tumours are mainly of LAR subtype with significant expression of *AR, APOD, PIP, SPDEF, UGT2B28, SORD, GUCY1A1, HPGD, ELOVL5, and AZGP1* genes in both cohorts (**Figure 10.5 D&E, Table 10.6 and Table 10.7)**, while HR-negative/HER2-negative TNBC are mainly basal-like subtypes.

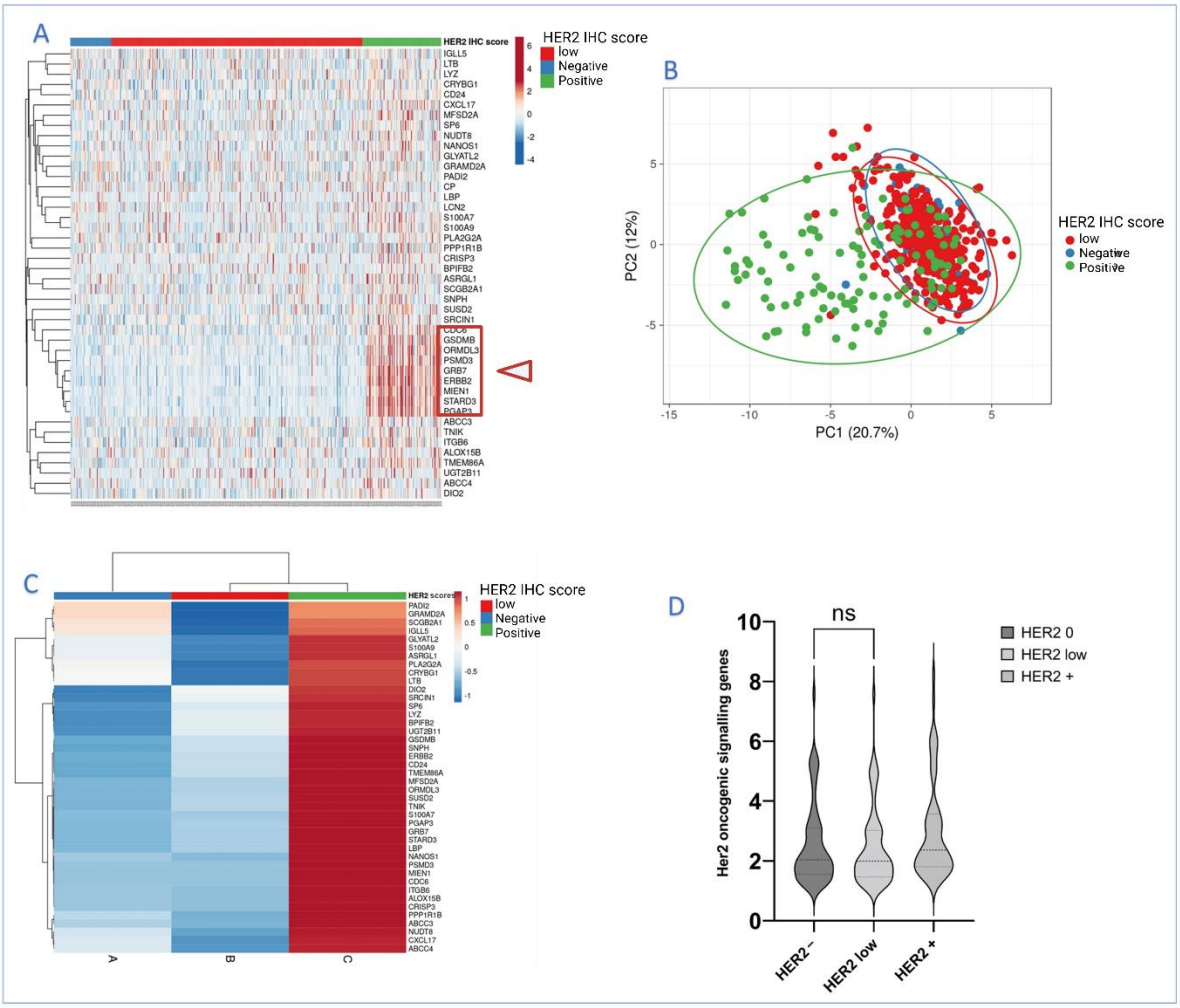


Figure 10.4: Illustrated graph showing differential expression of HER2 oncogenic signalling pathway genes between HER2 -, HER2-Low and HER2-positive breast cancer. A, B: Unsupervised clustering for the normalised values of HER2 oncogenic signalling pathway genes among the 3 HER2 categories. It reveals that no significant difference in the expression of HER2 signalling genes (arrow) between HER2-negative and HER2-Low and both classes are considered as one cluster in the principal component analysis (PCA) (B). C: Heatmap showing the expression of the mean values of HER2 oncogenic signalling pathway genes which is highly enriched in HER2-positive, while no difference between HER2-negative and HER2-Low. D: Violin plot illustrating the non-significant difference between HER2 oncogenic signalling pathway genes between HER2-negative and HER2-Low

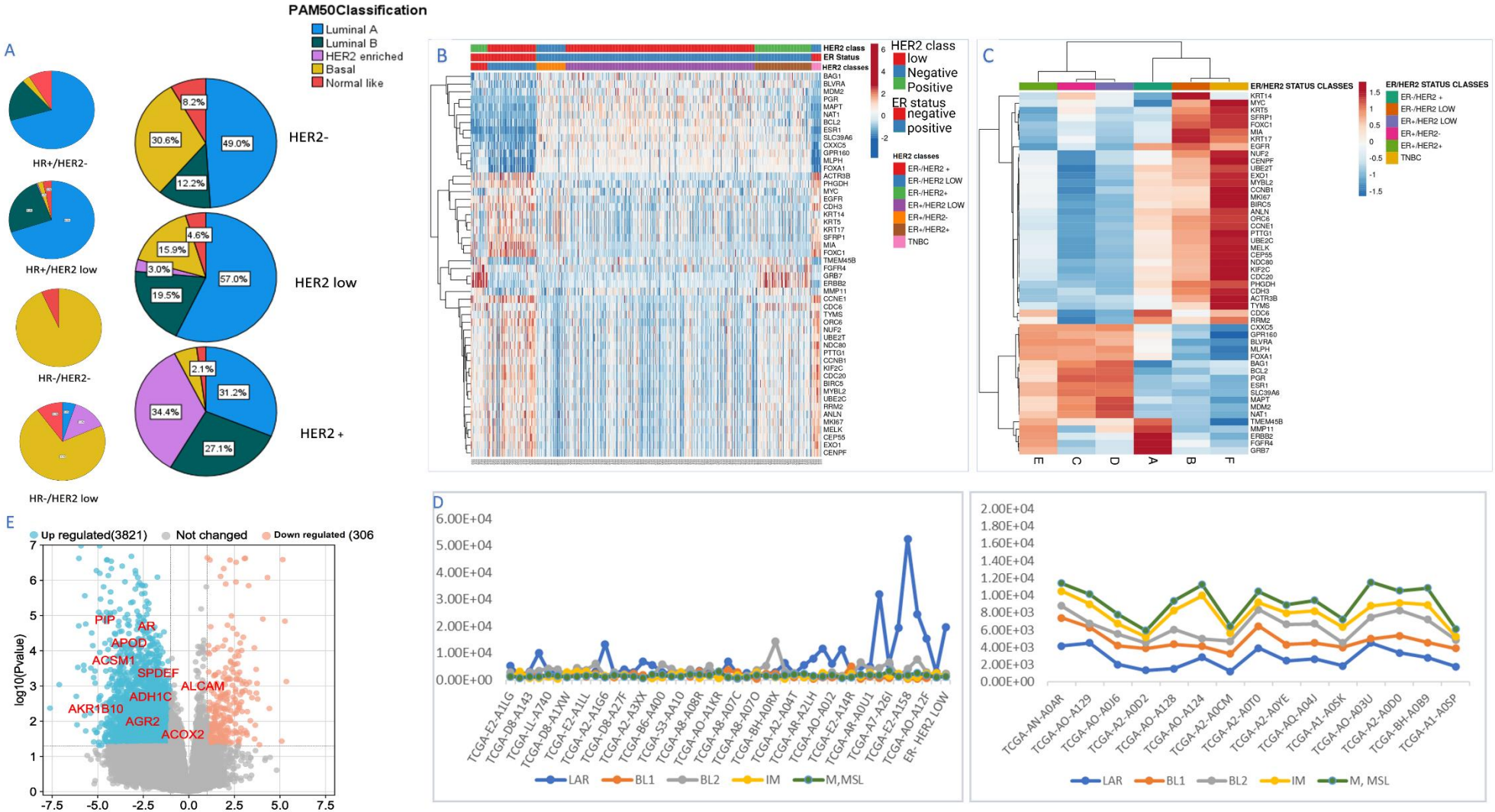

A
PAM50Classification
Luminal A
Luminal B
HER2 enriched
Basal
Normal like
HR+/HER2-
HR+/HER2 low
HR-/HER2-
HR-/HER2 low
HER2-
HER2 low
HER2 +
8.2%
30.6%
49.0%
12.2%
4.6%
15.9%
3.0%
57.0%
19.5%
2.1%
31.2%
34.4%
27.1%
B
HER2 class
low
Negative
Positive
ER status
negative
positive
HER2 classes
ER-/HER2 +
ER-/HER2 LOW
ER-/HER2+
ER+/HER2 LOW
ER+/HER2-
ER+/HER2+
TNBC
C
ER/HER2 STATUS CLASSES
ER-/HER2 +
ER-/HER2 LOW
ER+/HER2 LOW
ER+/HER2-
ER+/HER2+
TNBC
D
LAR
BL1
BL2
IM
M,MSL
M, MSL
E
Up regulated(3821)
Not changed
Down regulated (306
log10(Pvalue)
log2FC
PIP
AR
APOD
ACSM1
SPDEF
ALCAM
ADH1C
AKR1B10
AGR2
ACOX2

Figure 10.5: Distribution of PAM50 molecular subtypes and triple-negative breast cancer molecular subtypes between HER2 categories stratified by hormonal receptor status. A: Differences between HER2 categories regarding PAM50 intrinsic molecular subtype. B, C: Heatmaps illustrating the clustering of PAM50 gene expression among HER2 categories stratified by hormone receptor (HR) status. D: A correlogram summarising the distribution of TNBC molecular subtypes between HER2-Low (left) and HER2-negative (right). The luminal Androgen subtype (LAR) is more predominant in HER2-Low cases compared to HER2-negative, where other triple-negative breast cancer (TNBC) subtypes are most dominant. E: Volcano plot showing differentially expressed genes between HR-/HER2-Low versus HR-/HER2-negative BC. Blue dots stand for significantly upregulated genes in HR-/HER2-Low tumours, while orange dots stand for significantly downregulated genes. Luminal Androgen-like genes are highlighted. BL1: Basal-like 1, BL2: Basal-like 2, IM: Immunomodulatory, M, MSL: Mesenchymal, Mesenchymal stem-like

Table 10.5: Differential expression of PAM50 molecular subtypes genes between HER2-Low and HER2-negative BC in TCGA sample

PAM50 genes	PAM50 molecular subtype	HR-/HER2-negative vs HR-/HER2-Low log2 fold change	adj p value	HR+/HER2-negative vs HR+/ HER2-Low log2 fold change	adj p value
TYMS	BL	0.7818	0.0534	0.1216	0.7393
MYBL2	BL	0.835	0.1648	-0.0626	0.9182
KIF2C	BL	0.4176	0.4138	0.1708	0.6719
ACTR3B	BL	0.2527	0.55	0.0558	0.8793
EXO1	BL	0.3238	0.553	-0.3095	0.3784
UBE2C	BL	0.2927	0.6313	0.2601	0.524
MKI67	BL	0.219	0.6962	0.1161	0.7844
EGFR	BL	-0.2921	0.7293	-0.0052	0.9944
MELK	BL	0.2101	0.73	-0.0287	0.9567
CEP55	BL	0.1706	0.762	0.1454	0.7155
CCNE1	BL	0.2203	0.7838	-1.0824	0.0035
CENPF	BL	0.1276	0.8268	-0.1897	0.6069
ORC6	BL	0.0937	0.8829	0.0222	0.9642
PTTG1	BL	0.077	0.8997	0.2604	0.4475
FOXC1	BL	0.1174	0.9062	0.2791	0.6517
ANLN	BL	0.0456	0.9463	0.1891	0.6459
PHGDH	BL	-0.0079	0.9941	0.2111	0.7141
CDH3	BL, NL	0.3096	0.6944	0.0593	0.9307
MYC	BL,NL	0.3436	0.5023	-0.0172	0.9711
MIA	BL. NL	-1.2078	0.2537	1.0731	0.1004
ERBB2	HER2	-0.6797	0.3053	-0.1038	0.8644
MMP11	HER2	-0.4431	0.5037	-0.1715	0.7458
CDC20	HER2	0.3512	0.5388	0.4064	0.2428
CDC6	HER2	0.3074	0.6352	-0.0613	0.9132
GRB7	HER2	-0.157	0.8459	0.0405	0.9512
MDM2	HER2	-0.0453	0.9232	-0.1059	0.7227
RRM2	HER2	-0.0156	0.9814	-0.037	0.9413
FGFR4	HER2E	-0.6388	0.4508	-0.1784	0.8012
GPR160	LA	-1.5926	<**0.00001**	0.3854	0.1796
PGR	LA	-3.1378	**0.0002**	-0.1348	0.8816
TMEM45B	LA	-2.0281	**0.0021**	0.0925	0.8945
MAPT	LA	-1.1455	0.0835	-0.2601	0.6416
BAG1	LA	0.0995	0.8365	0.0951	0.7754
ESR1	LA,LB	-1.5351	**0.0316**	0.2187	0.7354
FOXA1	LB	-1.7667	**0.0019**	0.1885	0.7236
CXXC5	LB	-0.4965	0.1891	0.1247	0.6968
NAT1	LB	-0.805	0.3312	-0.2616	0.6986
BIRC5	LB	0.3865	0.5026	0.1918	0.663
BLVRA	LB	-0.2387	0.5467	0.307	0.1893
UBE2T	LB	-0.0856	0.8796	0.0796	0.844

Table 10.5 continued

CCNB1	**LB, BL**	**0.2215**	**0.6118**	**0.0238**	**0.9532**
MLPH	NL	-2.1107	<0.00001	-0.0086	0.9883
KRT14	NL	-3.5884	**0.0002**	-0.387	0.6683
BCL2	NL	0.9216	0.0626	0.0684	0.8905
KRT5	NL	-1.1024	0.2932	0.6665	0.3566
KRT17	NL	-0.7918	0.4381	-0.0164	0.9866
SFRP1	NL	-0.3615	0.7454	1.0557	0.0616
SLC39A6	NL	-0.0849	0.9212	0.2765	0.582

LA: luminal A; **LB**: luminal B; **NL**: Normal like; **BL**: basal like; **HER2-E**: HER2 Enriched; **HR+**: hormone receptor-positive; **HR-**: hormone receptor-negative

Table 10.6: Differential expression of TNBC molecular subtypes genes between HER2-Low and HER2-negative in TCGA cohort

A- TCGA genes	6 TNBC subtypes	HR-/HER2-negative vs HR-/HER2-Low Log 2 fold change	adjusted p value
UGT2B28	LAR	-7.57	**<0.0001**
PIP	LAR	-4.60	**<0.0001**
APOD	LAR	-3.28	**<0.0001**
AR	LAR	-2.32	**<0.0001**
SPDEF	LAR	-1.85	**0.0007**
ALCAM	LAR	-1.52	**0.0008**
CAV1	M,MSL	-1.18	**0.0026**
FASN	LAR	-0.94	0.0812
CLDN8	LAR	-0.86	0.3144
BLVRB	LAR	-0.86	**0.0282**
FZD4	M,MSL	-0.81	**0.0224**
TAGLN	BL2	-0.75	0.0919
ZEB1	BL2	-0.73	0.0535
FKBP5	LAR	-0.66	0.2270
FGFR4	LAR	-0.64	0.4508
MMP2	BL2	-0.62	0.1948
TGFB2	M,MSL	-0.60	0.3844
CAV2	M,MSL	-0.60	0.1438
CCND2	M,MSL	-0.59	0.1366
COL5A2	BL2	-0.59	0.2392
THY1	M,MSL	-0.58	0.1354
SMAD6	M,MSL	-0.58	0.0918
COL3A1	BL2	-0.56	0.2954
ZEB2	BL2	-0.49	0.1952
TIE1	M,MSL	-0.48	0.1622
TGFB3	M,MSL	-0.47	0.2644
IRF7	IM	-0.47	0.2906

Table 10.6 continued

KDR	**M,MSL**	**-0.45**	**0.1729**
TWIST1	BL2	-0.41	0.5055
TEK	M,MSL	-0.40	0.3487
TCF4	M,MSL	-0.33	0.4014
EPAS1	M,MSL	-0.31	0.3879
EGFR	BL2	-0.29	0.7293
BMP2	M,MSL	-0.25	0.7308
PER1	M,MSL	-0.24	0.6537
IRF8	IM	-0.22	0.6975
LXN	IM	-0.22	0.5969
DKK3	M,MSL	-0.21	0.6743
CDH1	BL2	-0.21	0.7433
BTK	IM	-0.18	0.6927
DKK2	M,MSL	-0.04	0.9585
SMAD7	M,MSL	0.02	0.9576
DHCR24	LAR	0.03	0.9636
STAT1	IM	0.03	0.9563
EPHA2	BL2	0.04	0.9461
JAK1	IM	0.07	0.8050
LCK	IM	0.08	0.9258
CENPF	BL1	0.13	0.8268
NRAS	BL1	0.15	0.7193
STAT4	IM	0.15	0.8072
ITK	IM	0.21	0.8003
ENG	M,MSL	0.21	0.5124
MKI67	BL1	0.22	0.6962
AURKA	BL1	0.22	0.6838
NFKB1	IM	0.23	0.3461
CTNNB1	M,MSL	0.23	0.3916
AURKB	BL1	0.27	0.6516
JAK2	IM	0.28	0.4098
CENPA	BL1	0.33	0.5674
MYC	BL1	0.34	0.5023
IRF1	IM	0.35	0.3738
BIRC5	BL1	0.39	0.5026
CCNA2	BL1	0.39	0.4261
PRC1	BL1	0.45	0.3070
TTK	BL1	0.47	0.3577
PLK1	BL1	0.54	0.2630
MME	BL2	0.75	0.2448
BUB1	BL1	0.76	0.0839
BCL2	M,MSL	0.92	0.0626

TNBC: Triple negative breast cancer**; HR:** Hormone receptor**; LAR**: Luminal androgen like; **M,MSL**: Mesenchymal, mesenchymal stem like, **BL1**: Basal like 1; **BL2**: Basal like 2; **IM**: Immunomodulatory

Table 10.7: Differential expression of TNBC molecular subtypes genes between HER2-Low and HER2-negative in the overlapping genes between TCGA and NGS cohort (A3)

GENE NAME	TNBC subtype	HR-negative/HER2-negative vs HR-negative/ HER2-Low Log 2 fold change	P value
APOD	AR	-5.8000	**0.0027**
ALCAM	AR	-5.9073	**0.0190**
UGT2B28	AR	-2.6659	**1.87E-08**
AR	AR	-3.9236	**0.0207**
SPDEF	AR	-3.1004	0.0524
PIP	AR	-2.6701	**0.0114**

TNBC: Triple negative breast cancer**; HR:** Hormone receptor**; LAR**: Luminal androgen like

10.5.5 CIBERSORT Immunophenotyping analysis

Within the group of HR-negative/ HER2-Low patients, sTILs score had no significant association with patient survival in contrast to the HR-negative/HER2-negative group where high sTILs scores were associated with prolonged 5-year DMFS (**Figure 10.6 and Table 10.3**).

HR-negative/ HER2-Low tumours contained a higher proportion of anti-tumorigenic T-helper lymphocytes, natural killer (NK) activated cells and tumour associated neutrophils, while HR-negative /HER2-negative tumours were enriched with pro-tumorigenic M0 and M1 macrophages, T cell gamma and delta, activated mast cells, cytotoxic T lymphocytes regulatory T cells (Tregs) and memory CD4 T lymphocytes (**Figure 10.7).**

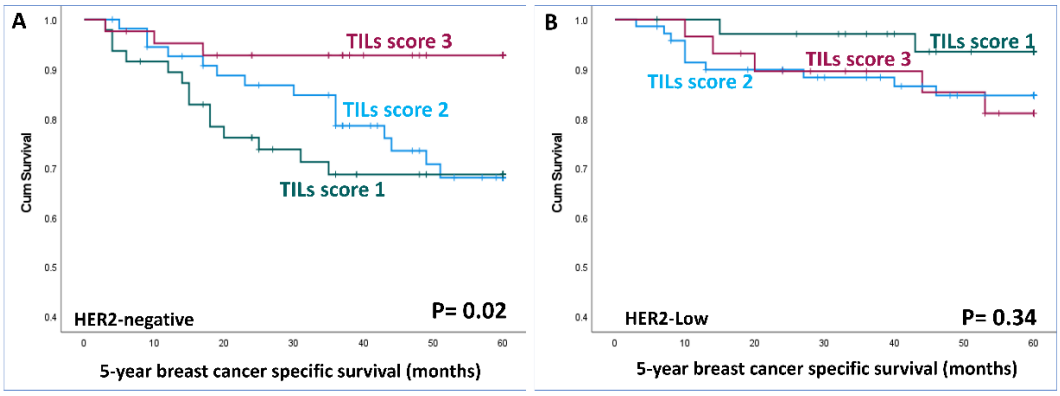


Figure 10.6: Kaplan Meier curve illustrating Tumours infiltrating lymphocytes (TILs) score and patients outcome in (A) HER2-negative and B (HER2-Low) reveals that high TILs score is associated with improved patients DMFS in HER2-negative tumours compared to others of HER2 Low breast cancer.

10.5.6 Gene Set Enrichment Analysis and Gene ontology

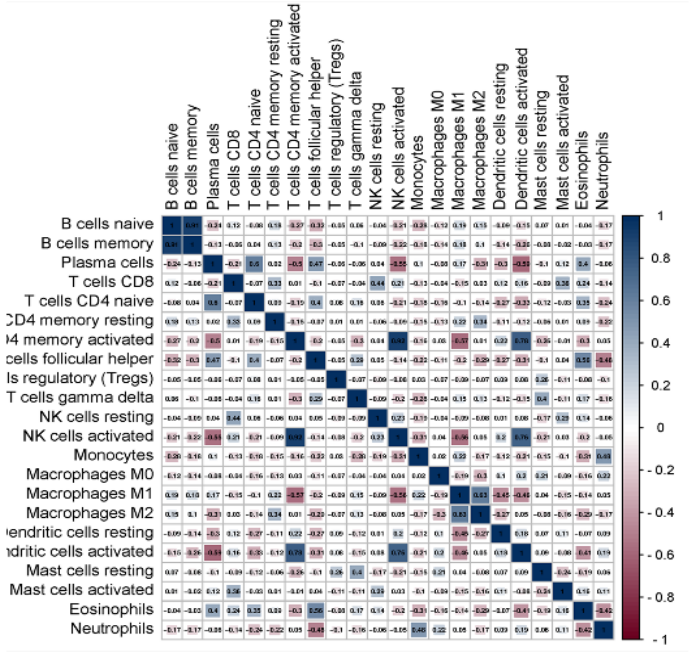
Pathway enrichment analysis showed that the top five significantly enriched pathways between HR-negative/ HER2-Low and HR-negative/HER2-negative tumours are ascorbate and aldarate metabolism, steroid hormone biosynthesis, pentose and glucuronate interconversions, tyrosine metabolism and PPAR signalling pathway. No significantly enriched pathways were detected between HR-positive/ HER2-Low and HR-positive/HER2-negative. Further details on pathway enrichment and GO functions in HR-positive and HR-negative categories are summarised in **Figure 10.8 and Figure 10.9**

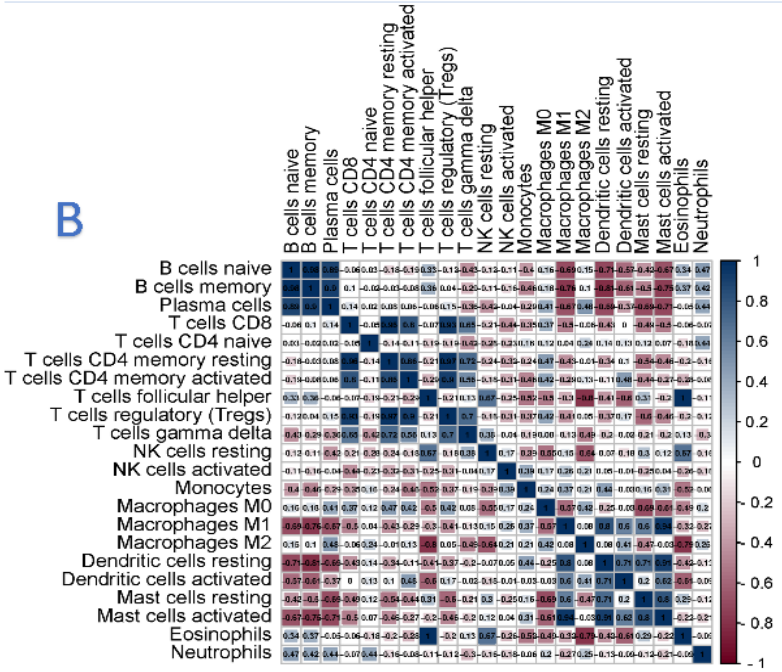
10.5.7 PPI network and hub genes

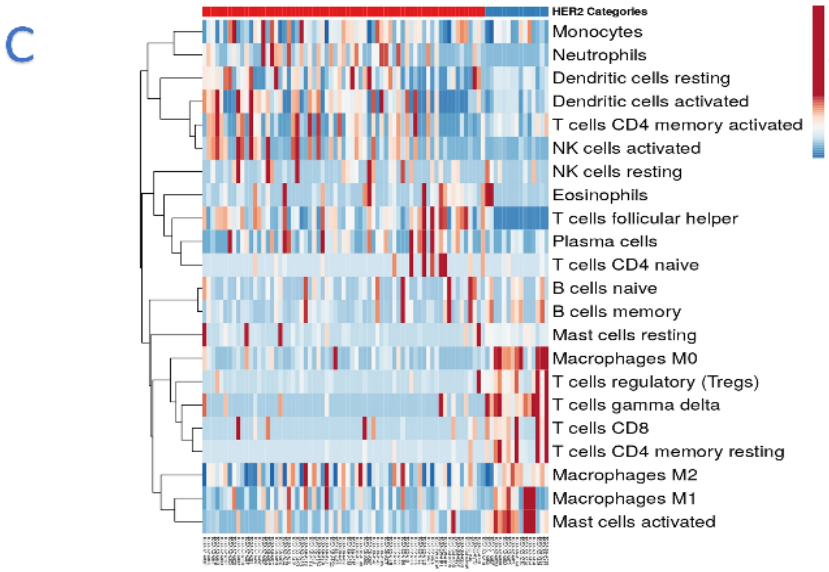
In HR-negative / HER2-Low tumours, the top ten up-regulated hub genes demonstrated by radiality, betweenness and connectivity degree in the PPI network were AR, OPN5, SHH, LEP, PGR, HNF4A, PTGS2, CAV1, CYP3A4 and POMC. Relevant results and further details are shown in **Figure 10.8 and Figure 10.9.**

10.5.8 Immunohistochemical expression of AR

Inter-observer concordance of AR H score was 0.9. The median AR H-score in the overall immune stained cohort was 125 (5-280). This corresponded to 90 (range 5-275) in the HR-negative/ HER2-Low group and 10 (range 5-275) in the HR-negative/HER2-negative group. High AR nuclear expression was significantly associated with HER2-Low tumours compared to HER2-negative-ones both as continuous and categorical score. Within HR-negative /HER2-Low tumours, high AR expression was associated with poor patients outcome (**Figure 10.10)**. Details regarding patients and tumour characteristics are summarised in **Table 10.8**


A
B cells naive
B cells memory
Plasma cells
T cells CD8
T cells CD4 naive
T cells CD4 memory resting
T cells CD4 memory activated
T cells follicular helper
T cells regulatory (Tregs)
T cells gamma delta
NK cells resting
NK cells activated
Monocytes
Macrophages M0
Macrophages M1
Macrophages M2
Dendritic cells resting
Dendritic cells activated
Mast cells resting
Mast cells activated
Eosinophils
Neutrophils
1
0.8
0.6
0.4
0.2
0
- 0.2
- 0.4
- 0.6
- 0.8
- 1


B
B cells naive
B cells memory
Plasma cells
T cells CD8
T cells CD4 naive
T cells CD4 memory resting
T cells CD4 memory activated
T cells follicular helper
T cells regulatory (Tregs)
T cells gamma delta
NK cells resting
NK cells activated
Monocytes
Macrophages M0
Macrophages M1
Macrophages M2
Dendritic cells resting
Dendritic cells activated
Mast cells resting
Mast cells activated
Eosinophils
Neutrophils
1
0.8
0.6
0.4
0.2
0
0.2
0.4
0.6
0.8
- 1


C
HER2 Categories
HR-/HER2 low
HR-/HER2-
6
4
2
0
Monocytes
Neutrophils
Dendritic cells resting
Dendritic cells activated
T cells CD4 memory activated
NK cells activated
NK cells resting
Eosinophils
T cells follicular helper
Plasma cells
T cells CD4 naive
B cells naive
B cells memory
Mast cells resting
Macrophages M0
T cells regulatory (Tregs)
T cells gamma delta
T cells CD8
T cells CD4 memory resting
Macrophages M2
Macrophages M1
Mast cells activated

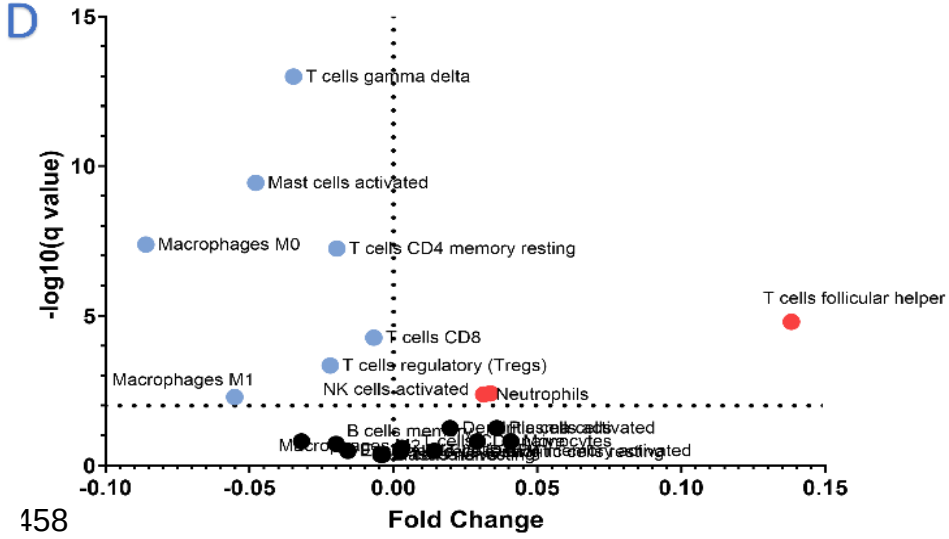
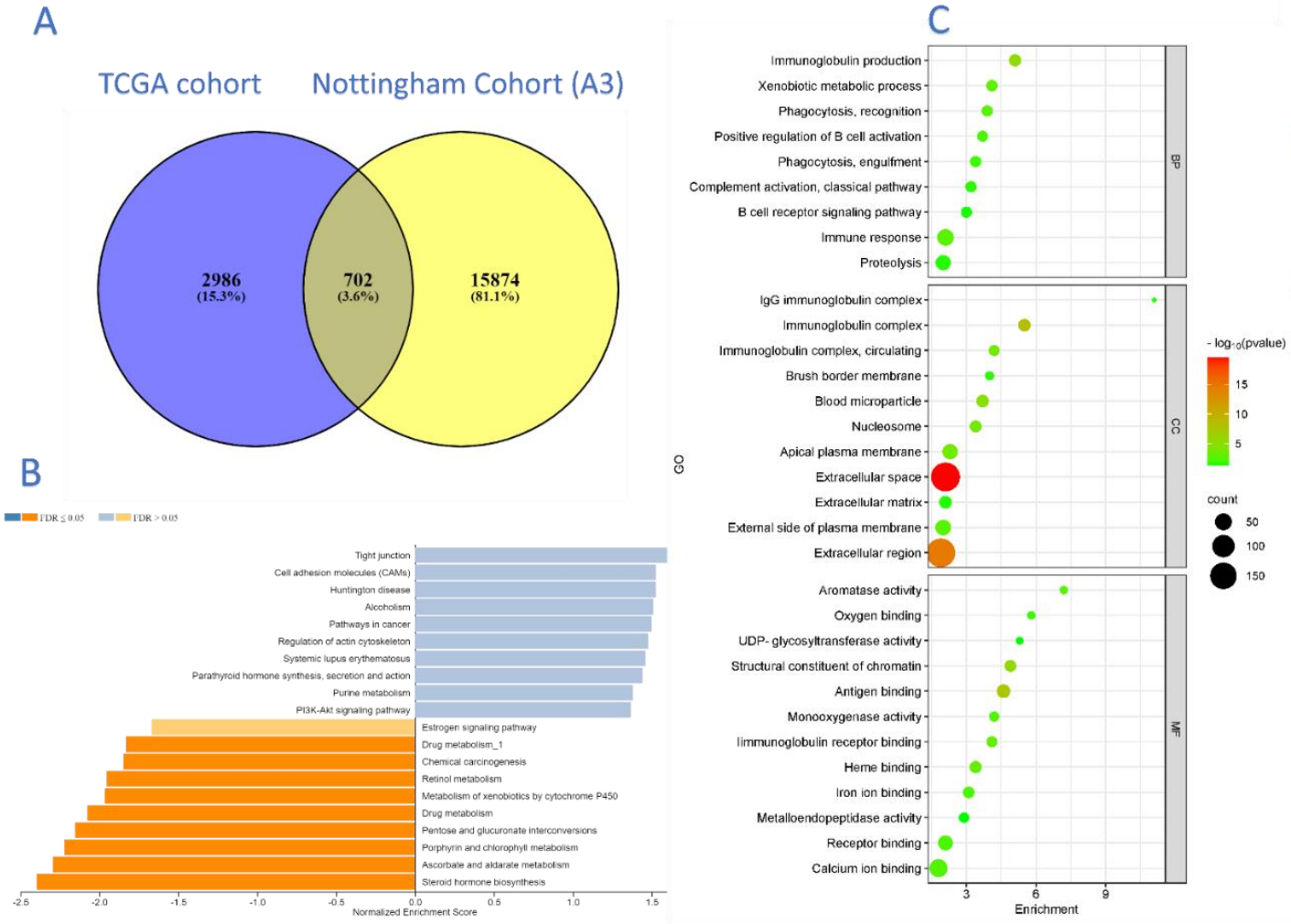

D
-log10(q value)
15
10
5
0
-0.10
-0.05
0.00
0.05
0.10
0.15
Fold Change
T cells gamma delta
Mast cells activated
Macrophages M0
T cells CD4 memory resting
T cells follicular helper
T cells CD8
T cells regulatory (Tregs)
Macrophages M1
NK cells activated
Neutrophils

Figure 10.7: Immunophenotyping of HR-/ HER2-Low (A) and HR-/HER2-negative breast cancer (B) using CIBERSORT analysis. C: Unsupervised clustering between HER2-Low and HER2-negative immunophenotypes. D: Volcano plot showing the distribution of significant immunophenotypes within each HER2 class. Red dots refer to immunophenotypes significantly enriched in HER2 Low BC, while blue dots refer to immunophenotypes significantly enriched in HER2-negative BC. Black dots refer to non-significant immunophenotypes.



Gene	Log2Fold C	P value	Rank
OPN5	2.38	0.03	1
AR	2.32	2.13E-05	2
SHH	2.27	0.01	3
LEP	2.60	0.01	4
PGR	3.14	<0.001	5
HNF4A	2.40	0.01	6
PTGS2	2.81	<0.001	7
CYP3A4	1.94	0.005	8
CAV1	1.18	0.002	9
POMC	1.45	0.04	10

Figure 10.8: Bioinformatics analysis carried out in HR-/HER2 Low BC cases. A: Venn diagram of genes overlapping upregulated genes between TCGA and Nottingham cohort A3. B: KEGG pathways enriched in HR-/HER2-negative BC against HR-/HER2-Low, significant upregulated pathways in HR-/HER2-Low are presented in deep orange with FDR <0.05. C: Diagram illustrating gene ontology (Molecular function (MF), Cellular component (CC) and biological processes (BP)) of the upregulated genes in HR-/HER2-Low BC. D: Protein-protein interaction HUB genes of upregulated genes in HR-/HER2-Low with their rank, log2 fold changes and adj p value. Red colour means high rank with most significant adj p value. FDR: The False Discovery Rate, GO: Gene-ontology

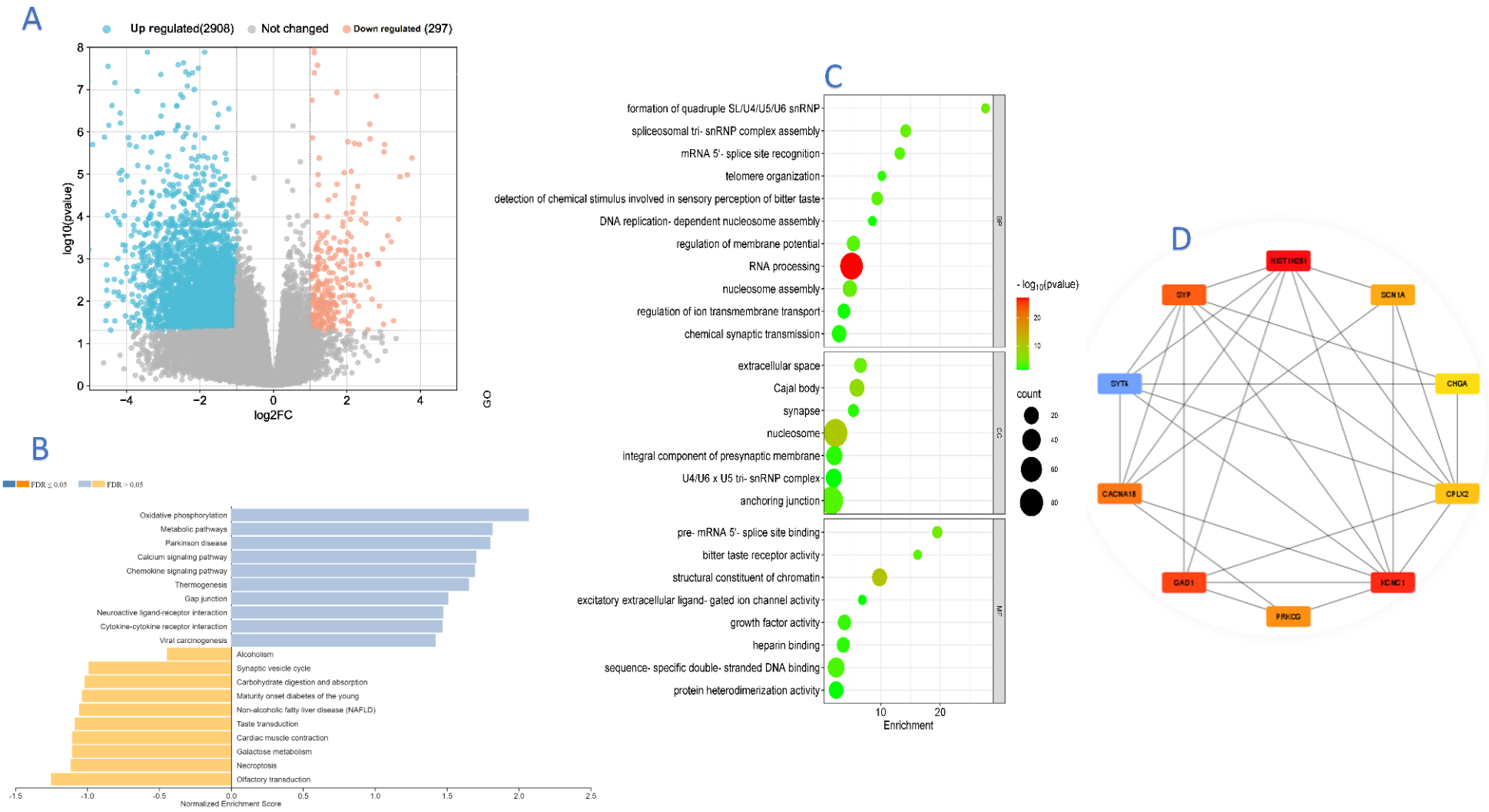

A
Up regulated(2908)
Not changed
Down regulated (297)
log10(pvalue)
log2FC
B
FDR ≤ 0.05
FDR > 0.05
Oxidative phosphorylation
Metabolic pathways
Parkinson disease
Calcium signaling pathway
Chemokine signaling pathway
Thermogenesis
Gap junction
Neuroactive ligand-receptor interaction
Cytokine-cytokine receptor interaction
Viral carcinogenesis
Alcoholism
Synaptic vesicle cycle
Carbohydrate digestion and absorption
Maturity onset diabetes of the young
Non-alcoholic fatty liver disease (NAFLD)
Taste transduction
Cardiac muscle contraction
Galactose metabolism
Necroptosis
Olfactory transduction
Normalized Enrichment Score
C
formation of quadruple SL/U4/U5/U6 snRNP
spliceosomal tri- snRNP complex assembly
mRNA 5'- splice site recognition
telomere organization
detection of chemical stimulus involved in sensory perception of bitter taste
DNA replication- dependent nucleosome assembly
regulation of membrane potential
RNA processing
nucleosome assembly
regulation of ion transmembrane transport
chemical synaptic transmission
extracellular space
Cajal body
synapse
nucleosome
integral component of presynaptic membrane
U4/U6 x U5 tri- snRNP complex
anchoring junction
pre- mRNA 5'- splice site binding
bitter taste receptor activity
structural constituent of chromatin
excitatory extracellular ligand- gated ion channel activity
growth factor activity
heparin binding
sequence- specific double- stranded DNA binding
protein heterodimerization activity
BP
CC
MF
Enrichment
- log10(pvalue)
count
D
HIST1H2BI
SYP
SCN1A
SYT4
CHGA
CACNA1B
CPLX2
GAD1
KCNC1
PRKCG

Figure 10.9: Diagram illustration bioinformatics analysis carried out between HR-positive/HER2-Low and HR-positive/HER2-negative BC cases. A: Volcano plot showing differentially expressed genes between HR-positive/HER2-Low versus HR-positive/HER2-negative BC. Blue dots represent significantly upregulated genes in HR-positive/HER2-Low tumours, while orange dots represent significantly downregulated genes. B: Bar chart showing KEGG pathways enriched in HR-positive/HER2-Low BC, no significant pathways were identified (FDR >0.05). C: Diagram illustrating gene ontology (Molecular function (MF), Cellular component (CC) and biological processes (BP)) of the upregulated genes in HR-positive/HER2-Low BC. D: Graph illustrating protein-protein interaction HUB genes of upregulated genes in HR-positive/HER2-Low; red genes have the highest rank, while blue ones have the lowest rank.

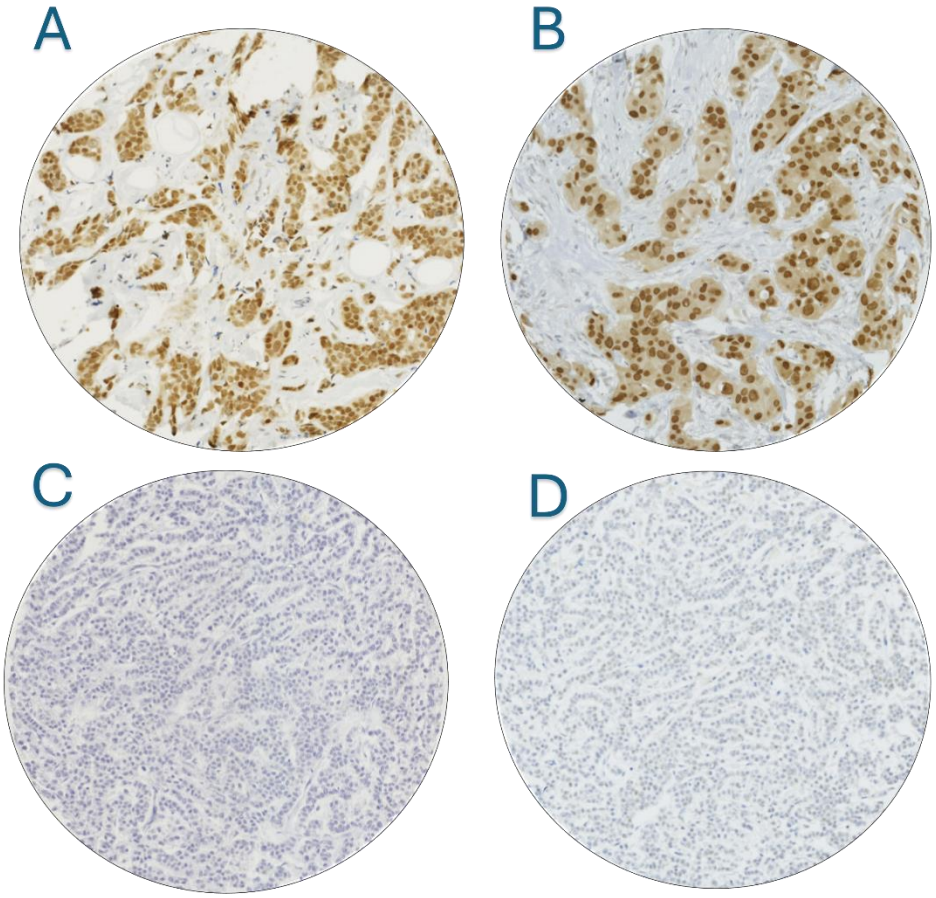


Figure 10.10: Androgen receptor immunohistochemical expression in HER2-Low tumours A&B while C&D are its expression in and HER2-negative BC.

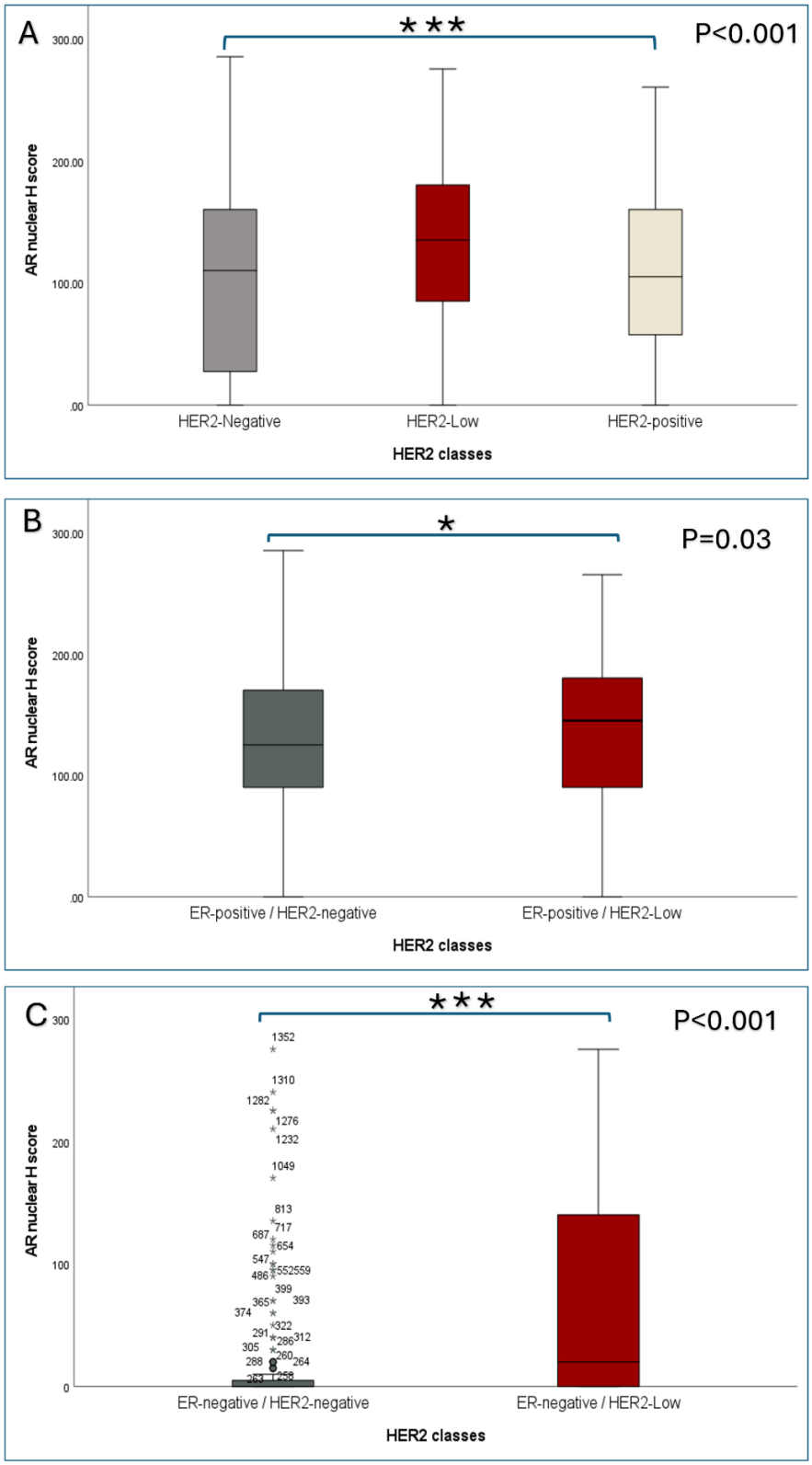


Figure 10.11: Boxplot summarising the expression of AR among HER2 classes with the highest expression in HER2-Low category (A). B: Difference in AR expression between HER2-negative and HER2-Low in ER-positive and ER-negative (C) tumours

Table 10.8: Basic patient and tumour characteristics of Nottingham cases used to assess Androgen receptor immunohistochemical expression.

Parameter	Low AR N (%)	High AR N (%)	Chi square P value
Age at diagnosis			
< 50 years	105 (41)	318 (29)	X^2=14.04
≥ 50 years	151 (59)	780 (71)	<0.001
Menopausal Status			
Pre-menopausal	111 (43)	366 (33)	X^2=9.15
post-menopausal	145 (57)	732 (67)	0.003
Tumour size (cm)			
< 2.0	130 (51)	697 (64)	X^2=14.08
≥ 2.0	126 (49)	401 (36)	<0.001
Tumour grade			
1	11 (4.3)	188 (17)	
2	41 (16)	513 (47)	X^2=159.7
3	204 (79.7)	397 (36)	<0.001
Lymph node status *			
Negative	157 (61.3)	673 (61.3)	X^2=.001
Positive	99 (38.7)	45 (38.7)	=1.0
Tumour types			
IDC NST	229 (89.5)	651 (59.3)	
ILC	4 (1.6)	102 (9.3)	X^2=89.8
Other types	33 (8.9)	345 (31.4)	<0.001
Lympho-vascular Invasion			
No	180 (70.3)	780 (71)	X^2=0.05
Yes	76 (29.7)	318 (29)	=0.82
NPI			
Good	29 (11.3)	431 (39.2)	
Intermediate	175 (68.4)	505 (46)	X^2=72.4
Poor	52 (20.3)	162 (14.8)	<0.001
HER2 IHC status*			
Negative	204 (80)	684 (62.5)	
low	27 (10.6)	271 (24.7)	X^2=30.4
Positive	24 (9.4)	140 (12.8)	<0.001
Oestrogen receptor			
Negative	173 (67.8)	100 (9.1)	X2=443.4
Positive	82 (32.2)	998 (90.9)	<0.001
Progesterone receptor			
Negative	202 (81.5)	332 (30.3)	X^2=220.4
Positive	46 (18.5)	762 (69.7)	<0.001

IDC NST: Invasive duct carcinoma non-special type**, ILC:** invasive lobular carcinoma**, IHC:** immunohistochemistry**; NPI:** Nottingham prognostic index

10.6 DISCUSSION

HER2-Low BC accounts for 40–50% of all BCs [169] and appears to be a heterogeneous disease [177, 501]. The recent development of novel HER2 targeting ADCs, shown to have significant clinical benefit for patients with these tumours, will dramatically revolutionise the treatment landscape of some BCs classified as HER2-negative using the traditional classification system. Our understanding of this potential new BC category continues to evolve with on-going debate regarding its status as a distinct biological entity with a predictable clinical course, specific prognostic and therapeutic implications, and the potential interactive impact of HR status [188-190]. The current study aimed to thoroughly profile the HER2-Low category of tumours with particular emphasis on the potential impact on clinical behaviour, molecular signature and the interaction with and influence of HR status in a large BC series (**Figure 10.12)**.

Some studies have reported that HER2-Low tumours are associated with a more favourable clinical outcome than HER2-negative tumours [186, 187, 693, 710-713] while other authors have demonstrated that HER2-Low BC is not prognostically different from HER2-negative tumours [169, 178]. Our results indicate that, when considered in isolation, HER2-Low tumours are associated with a more favourable clinical outcome, lower histological grade, less mitotic activity and a lower incidence of LN metastases compared to HER2-negative. These tumours also appear to be less responsive to NACT compared to true TNBC (HER2-negative), in agreement with previous studies [179, 186, 712, 714].

In this study, HER2-Low tumours represented 43% of the overall study tumour population, 90% of which were HR-positive. The ER H score was higher in HER2-Low tumours compared to both HER2-negative and HER2-positive, as observed in previous studies [178, 184, 186, 715]. Our results showed that HER2-Low tumours are associated with prolonged survival compared to HER2-negative tumours in unselected patients' population as well as in the HR-negative BC subgroup. These results were in line with multiple previous studies[186, 188-190, 693, 716]. However, this trend was not maintained when results were adjusted for HR positivity, where HER2-Low tumours lost their prognostic significance in terms of the clinic-pathologic parameters or patients' outcomes. These results were also demonstrated by some authors [169, 179, 184]. These findings indicate that the better prognosis of HER2-Low tumours is dependent on HR activity, as demonstrated by the lack of prognostic significance in HER2-Low tumours in HR-positive BC and the association between HER2-Low and luminal phenotype in the HR-negative BC subgroup. Therefore, we conclude that although HER2-Low tumours is a unique therapeutic class of BC that can be treated with specific HER2 based ADC (4), they are not biologically or prognostically a unique class of BC.

HER2 plays an important role in normal cell growth and differentiation. In normal breast epithelial cells, HER2 is expressed at low levels (two copies of the *HER2* gene and up to 20,000 HER2 receptors) [717]. This may indicate that tumours that maintain low levels of HER2 protein are more differentiated while deviation from the normal expression level, either through positive protein expression (IHC 3+), gene amplification in *HER2-positive* tumours or complete loss of expression in HER2-negative BC, is associated with increased tumour

aggressiveness. This deviation is more frequent in HR-negative tumours, while in luminal subtypes HR is the dominant oncogenic driver of BC regardless of HER2 levels.

HER2-Low tumours do not appear to be driven by the HER2 oncogenic signalling pathway. PAM50 molecular subtyping and DGE revealed that neither the *ERBB2* gene nor other HER2 oncogenic signalling pathway genes were significantly enriched in HER2-Low tumours regardless of HR status.

On the contrary, HER2-Low tumours tend to be of luminal molecular subtype if HR -positive and normal-like subtype if HR-negative, in agreement with other studies [178, 182, 184].

Regarding the molecular differences between HER2-Low and HER2-negative BC in the HR-negative tumours, our study showed that HER2-Low tumours exhibit a distinct molecular profile. This was evident through the DGE and pathway enrichment analysis which revealed that HR-negative/HER2-Low tumours are mainly of LAR subtype, with upregulation of luminal androgen-like pathway genes, in particular *AR*, which was also one of the top 10 PPI hub genes and being enriched with fatty acid and steroid hormone metabolism pathways that was previously reported in the LAR TNBC subtype [697]. This accords with the experience of other researchers who observed that HER2-negative and HER2-Low BC exhibit different molecular properties. Yam et al. [718] investigated the molecular differences between HER2-negative and HER2-Low tumours in TNBC patients and demonstrated that HER2-Low was associated with increased AR expression and upregulation of genes associated with fatty acid and steroid hormone metabolism [718]. Other studies showed differences in

resistance drivers between HER2-negative and HER2-Low tumours, mainly in the HR-negative group [719]. An association between AR and HER2 expression has been reported previously [720]. Our results revealed that high AR protein expression was significantly associated with HR-negative / HER2-Low tumours and was a predictor of worse outcome, in accordance with previous studies that demonstrated that AR expression was more frequent inHER2-Low than in HER2-negative BCs [181, 721, 722]. These findings support the hypothesis thatHER2-Low expression is associated with luminal differentiation in TNBC, in keeping with Zhang et al [184] who also concluded thatHER2-Low tumours are less likely to be of basal TNBC subtype. The role of anti-AR inhibitors, e.g., enzalutamide in the treatment of AR+ BC, has been investigated but these have not yet been implemented as therapeutic targets [717, 723-725]. Triana et al [724] reported that enzalutamide demonstrated clinical activity and was well tolerated in patients with advanced AR+ TNBC, but with a clinical benefit rate of only 33%. Based on our findings, the association between AR and HER2-negativelow merits further investigations to evaluate the combination of AR inhibitor and novel anti-HER2 ADC targeted therapy.

The dynamic nature of HER2 expression is an important issue when tumour heterogeneity and low level of expression are considered [726]. In a previous study of 1,119 HR-positive/HER2-negative patients who participated in the phase 3 PENOLOPE-B study and were offered NACT, Denkert and colleagues [727] reported 14% shift from HER2-negative toHER2-Low and a 23% shift fromHER2-Low to HER2-negative in patients who had residual tumours. The heterogeneity ofHER2-Low status was also addressed by Geukens T and co-

authors who demonstrated the presence of intra-patient, inter-metastases heterogeneity ofHER2-Low status in the form of coexistence ofHER2-Low and HER2-negative metastases [728]. Change in HER2 status between primary tumours and matched relapses in either local recurrences or distant metastases was also reported. Recent research findings indicate an increase inHER2-Low tumours during advanced stages. Additionally, they found correlations between these changes and factors such as the time of recurrence [729]. *Bar and colleagues* highlighted the issue of HER2 heterogeneity in repeated biopsies among patients with TNBC and concluded that performing a repeat biopsy at the time of disease progression can enhance the likelihood of obtaining aHER2-Low result [730]. These findings will influence our perspective regarding the reliability of assessing HER2 status in a single tumour sample as a predictive marker for T-DXd treatment, particularly the Destiny-breast04 clinical trial [170] included patients with any HER2-Low sample even if other samples are negative.

Cytotoxic chemotherapy is currently the mainstay of treatment for patients with primary TNBC. In patients with metastatic TNBC with immunohistochemical PD-L1 expression on tumour-associated immune cells, the addition of anti-PD-L1 immunotherapy has been shown to be superior to chemotherapy alone regarding patient survival [731, 732]. The clinical response of patients to these treatments is variable and characterisation of the molecular and immunophenotypic differences between HER2-Low TNBC and pure TNBC may offer insight into the heterogeneity of tumour response. Our study showed that HER2-Low tumours had significantly lower sTILs scores compared to HER2-negative

tumours. This has also been observed by van den Ende et al [185], who reported a significant association betweenHER2-Low status and lower density TILs, despite no significant association betweenHER2-Low status and clinicpathologic features in ER-negative tumours. Regarding immunophenotype, HER2-Low tumours featured aberrant, heterogeneous immune infiltration in patients with HR-negative BC with helper T lymphocytes, activated NK cells and cancer-associated neutrophils being the dominant immunophenotype in contrast to HER2-negative tumours that were enriched for macrophages M0 and M1. Previous studies have demonstrated the role of NK and T helper cells in BC patients with improved survival [733-735]. These findings may have clinical relevance and inform the future development of personalised therapy for patients with HER2-Low BC.

This study has several strengths. It benefits from a substantial clinical cohort, re-assessment of HER2 status in the larger patient cohort, and comprehensive data on patient response to treatment with long-term survival outcomes. Additionally, the study focuses on immunophenotyping and subtyping of TNBC and highlights the distinctions between HER2-Low and HER2-negative BC (true TNBC), with a particular emphasis on exploring the role of AR and its potential therapeutic applications. The study has some limitations. The research is constrained by the historical nature of the patient cohort, with no patients having received T-DXd therapy. Additionally, the study did not include an assessment of HER2 status in the recurrence samples, which may have provided valuable insights into the dynamics of HER2 status and heterogeneity of HER2 expression with disease progression. In conclusion, HER2-Low tumours are fre-

quently HR-positive. HR-positive/HER2-Low tumours exhibit no significant differences from HR-positive /HER2-negative tumours regarding tumour behaviour and patients' outcomes. In HR-negative BC, HER2-Low tumours have improved outcomes but appear to be less responsive to NACT. HR-negative /HER2-negative tumours are enriched with unique immunophenotypes associated with aggressive tumour behaviour. AR is predictive of poor outcomes in HER2-Low TNBC patients and may be a potential therapeutic target.

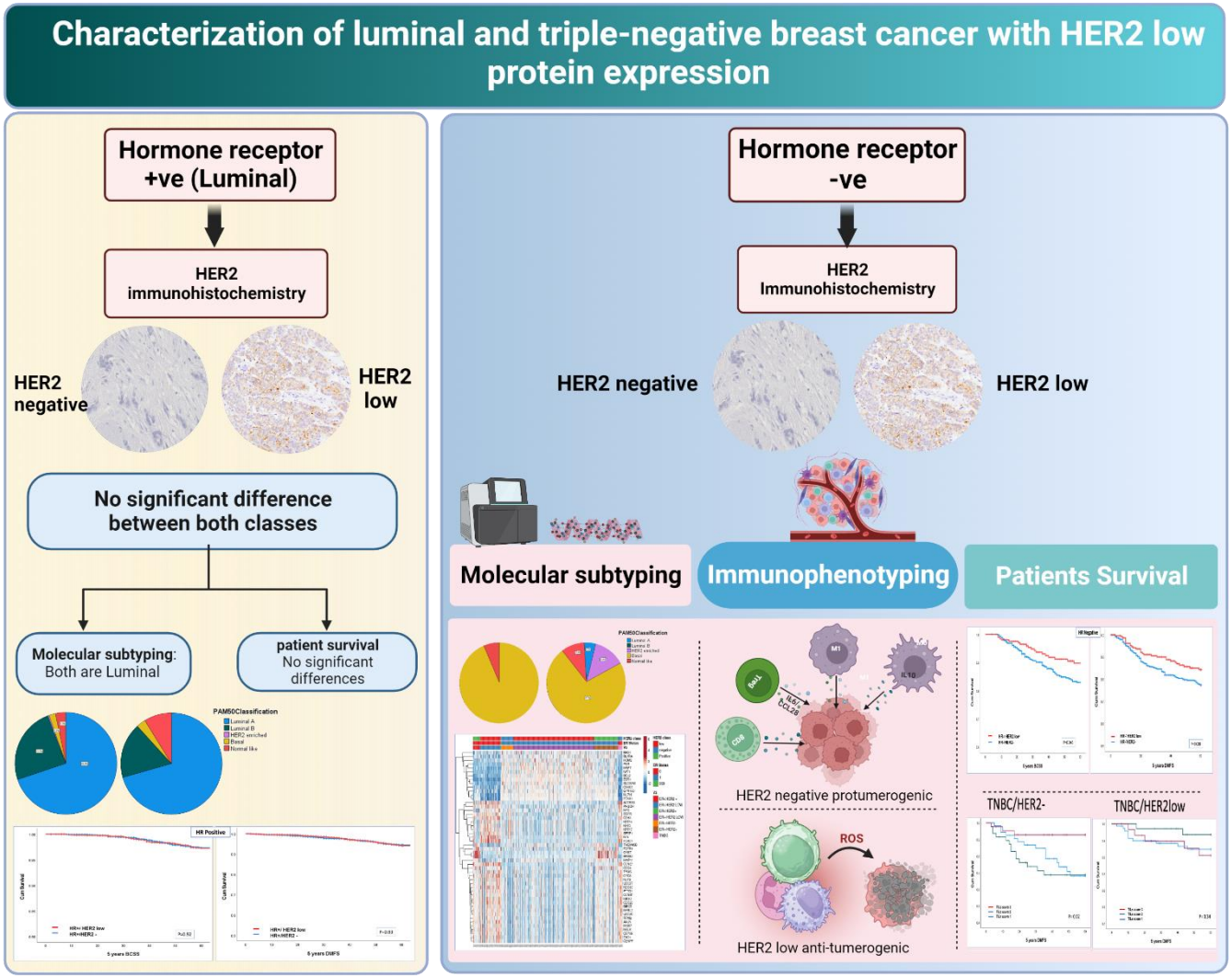


Figure 10.12: Chart summarising the workflow of this study

Chapter 11. General Discussion

11.1 General Background

BC is the most prevalent cancer among women globally and remains a leading cause of cancer-related mortality [1]. It is a heterogenous family of diseases with variable presentation, morphology, molecular features, behaviour and response to therapy. Many studies focused on analysing the molecular patterns of BC in order to group these tumours into classes or entities to assist in clinical management [41-43]. Four clinically relevant molecular subtypes were revealed through comprehensive gene expression profile studies, Luminal A, Luminal B, HER2-E, and TN [45].

HER2 is a critical molecular target in BC, overexpressed in approximately 15-20% of cases [143, 148, 163-165]. The therapeutic stratification of BC based on HER2 expression is rapidly evolving. Despite the increasing success in the management strategies of BC expressing HER2, challenges and evidence gaps persist. The differential response rates to anti-HER2 therapies and the promising results of HER2-based ADCs have also changed our approach to classifying HER2 expressing BC [167-169, 224]. The introduction of the terms HER2-Low and HER2-Ultralow and the current lack of sufficient evidence-based data on the correlation between response to HER2-based ADC and the level of HER2 protein expression requires refining the definition of this new category.

In HER2 overexpressing BC, the growth of tumour cells and, hence, the response to HER2 pathway targeting therapy is mainly driven by the oncogenic activity of the HER2 signalling pathways. To date, patients with BC featuring whether HER2 protein overexpression (IHC 3+) or an equivocal protein level

(IHC 2+) with evidence of *HER2* gene amplification are considered candidates for anti-HER2 therapy [141]. However, the response rate in patients with HER2-positive BC is not uniform. The magnitude of response, measured by the rate of pCR, of HER2 IHC score 3+ tumours ranges from 55 to 70% compared to 17–20% in HER2 2+Ampl [224-228], raising the possibility that HER2 protein overexpression rather than *HER*2 gene amplification is the key driver of response.

Refinement of HER2 classification for prediction of response to anti-HER2 therapy can improve patients' outcomes. The introduction of trastuzumab, the humanised anti-HER2 mAB, and the subsequent development of other anti-HER2 agents (e.g., lapatinib, pertuzumab, T-DM1, and T-DXd) have drastically improved the prognosis of HER2-positive BC patients. Nevertheless, not all patients benefit from these agents and eventually experience recurrence. Extensive translational research has been performed to identify predictive markers for patient treatment selection.

The response to anti-HER2 therapy is dependent not only on HER2 status but also on the crosstalk between HER2 and other proteins, including hormonal receptors [308, 575]. Given these challenges, a standardised, robust, reliable, and cost-effective mRNA-based test for *ERBB2* and other key genes ER (*ESR1*), PR (*PGR*), and Ki-67 (*MKI67*), could provide a viable alternative or complement to the current HER2 assessment methodology.

HER2-Low BC constitutes 40–50% of all BCs [169] and is recognised as a heterogeneous disease [177, 501]. The recent introduction of innovative

HER2-targeting ADCs has demonstrated significant clinical benefits for patients with these tumours, potentially transforming the treatment landscape for BCs traditionally classified as HER2-negative. As our understanding of this emerging category of BC grows, ongoing discussions continue regarding its classification as a distinct biological entity, including its specific prognostic and therapeutic implications and the potential influence of HR status [188-190].

Recently, there has been an increasing interest in leveraging the power of AI to identify HER2 status in BC from tumour morphology using the digitalised H&E-stained slides [374, 520-526]. The application of CPATH alongside advanced molecular techniques would uncover new prognostic indicators in BC and unravel the complexities of HER2 expression, including its biological and clinical characteristics.

11.2 Hypothesis and Aims of the Thesis

This thesis evaluates the integration of computational pathology and advanced molecular approaches in identifying novel BC prognostic parameters and deciphering the complexity of HER2 expression, including its biological and clinical characterisation. It highlights the differential responses to targeted anti-HER2 therapies among HER2-positive subtypes, the role of HR expression, and refines the definition of HER2-Low BC.

Specifically, we aimed to evaluate the utility of DP and AI, particularly WSI and AI-driven analysis, in improving the assessment of BC prognostic markers. We then harnessed the power of integrated molecular and CPATH to develop a

morphometric signature that predicts HER2 activity and response to anti-HER2 therapy, offering a new tool for clinical decision-making.

By enrolling a large, well-characterised clinical cohort with comprehensive clinicopathological, treatment, and outcome data, we sought to unravel the complexity of HER2 expression in BC. We first investigated the biological and clinical implications of HER2-positive BC, including variability in response to targeted therapies, and highlighted the role of HR expression in treatment response. Our study extended to the emerging category of HER2-Low tumours in BC. Our goal was to improve patient stratification for targeted ADCs therapies by improving the definition of HER2-Low tumours. We aimed to improve the classification of this category to boost the reproducibility and concordance among pathologists in scoring HER2-Low BC. Followed by the identification of its molecular, biological, clinical, and immunophenotypic characteristics.

11.3 Cardinal Findings from Each Chapter

11.3.1 Computational Pathology in Clinical Practice

This study aimed to assess the quality of WSI in routine practice by examining the frequency, nature, and location of missing tissue on WSI compared to glass slides, and its clinical implications. The study also explored image quality and the effectiveness of QC measures in reducing these issues. The frequency of missing tissue varied across different cohorts and scanners, with fatty tissue being the most frequently missed due to its less dense and fainter appearance, especially in thinner sections with paler staining [444, 447].

Despite the missing tissue, final diagnoses, tumour grade, and stage were unaffected. Although 12% of cases showed a reduction in the distance to the

actual margin, none were misidentified as having a positive margin, and no re-excisions were necessary [445]. Missing tissue was more common in WSI of IHC stained sections than in H&E WSIs, likely due to the thinner sections and reduced contrast from using only haematoxylin as a counterstain. However, the missing tissue, primarily fat, did not affect the assessment of IHC biomarkers.

Using an overview (macro) image could help pathologists detect missing tissue, determining whether the WSI is sufficient for diagnosis or if glass slides are needed, particularly when missing tissue is peripheral and could affect surgical margin measurement. The study compared missing tissue frequency and image quality before and after QC measures, finding that QC successfully reduced image failure rates. A negative correlation was observed between missing tissue frequency and both scanning time and image file size. Scanners without human input had shorter scanning times but a higher frequency of missed tissue, as they tended to ignore faint tissue to speed up the process.

In addition, this chapter explored the prognostic significance of the tumour-stroma ratio using AI-based analysis. High STR was found to be a good prognostic parameter in luminal BC patients and a predictive factor for response to endocrine therapy, consistent with findings by Brechbuhl, Finlay-Schultz [497]. Moreover, the AI-driven spatial analysis revealed distinct stromal cell distribution patterns correlated with tumour aggressiveness and patient survival.

High tumour density and homogeneous distribution of tumour cells were associated with worse outcomes, whereas patients with uniformly surrounded stro-

mal cells had better survival. These findings highlight the potential of AI in enhancing our understanding of the tumour microenvironment and its role in BC progression.

11.3.2 Morphometric Signature for HER2 Activity and Response to Therapy

This chapter identified key features associated with HER2-positive tumours and the HER2-E intrinsic subtype, including large polygonal cells with larger nuclei, open chromatin, pale eosinophilic cytoplasm, reduced N/C ratio, lower tumour cell density, higher immune/tumour cell ratio, and wider internuclear distances. These findings align with previous reports on the role of active HER2 signalling in promoting cell proliferation and chromatin modulation [537].

HER2-positive tumour cells were often arranged in small nested/alveolar-like patterns rather than the solid sheets typical of TNBC. Denisov, Skryabin [531] similarly found that tumours with small nests were more associated with the *ERBB2* pathway. HER2-driven morphometric features were most prominent in HER2 IHC 3+/ER-negative cases, supporting the idea that HER2 protein overexpression (IHC 3+) drives oncogenic activity more strongly than borderline HER2-positive cases with gene amplification [224, 228].

The identified morphometric signature reflects both the HER2-E subtype and elevated *ERBB2* mRNA and HER2 protein levels, which are key therapeutic targets. This signature model showed higher accuracy in predicting response to anti-HER2 therapy than models based solely on HER2 IHC scores, aligning with previous findings on the value of combining HER2-E subtype with *ERBB2* mRNA levels for better therapy prediction [507, 540].

The study also highlighted HER2 intra-tumour heterogeneity, more common in HER2-positive /ER-positive tumours, which is associated with poor prognosis and potential resistance to anti-HER2 therapy [41, 541].

The development of a HER2-driven morphometric signature offers a novel tool for predicting patient outcomes and guiding treatment decisions. Validation studies confirmed that this signature could predict prolonged DMFS in patients receiving adjuvant anti-HER2 therapy.

11.3.3 Characterisation of HER2-Positive BC

This chapter explored the heterogeneity of HER2-positive BC, focusing on the impact of ER status on therapeutic outcomes. The study aimed to elucidate the clinical, biological, and molecular mechanisms influencing the response to anti-HER2 therapy. The overall pCR rate in HER2-positive BC patients receiving NACT with anti-HER2 therapy was 36%, with a significantly higher pCR rate in HER2 IHC 3+ cases compared to HER2 IHC 2+/Amplified cases. While high HER2 gene amplification correlated with higher pCR rates across all HER2 IHC categories, this association was not observed within individual HER2-positive IHC subgroups. HER2 protein overexpression (IHC 3+) was an independent predictor of pCR, consistent with previous studies [159, 228, 242-246, 548, 562]

The study found that the HER2-E subtype was more strongly associated with HER2 IHC 3+ than with IHC 2+/Amplified, and that genes related to HER2 oncogenic signalling were more significantly expressed in HER2 IHC 3+ tumours. Additionally, genes associated with resistance to trastuzumab were upregulated in 60% of HER2 IHC 2+/Amplified tumours.

ER status also emerged as a significant predictive marker within HER2-positive disease, with ER positivity associated with poorer therapeutic response, particularly in IHC 2+/Amplified tumours, but not in HER2 IHC 3+ patients, both in the neoadjuvant and adjuvant settings [324]. The study also showed that HER2 IHC 2+/Amplified tumours were more likely to be ER-positive, enriched with ER signalling pathways, and less likely to include the HER2-E molecular subtype [326, 736].

11.3.4 Modulators of Response to Targeted Anti-HER2 Therapy

Through comprehensive transcriptomic and proteomic analyses, this chapter identified key modulators, such as TAF10 and BCAT1, that influence the response to anti-HER2 therapy. These genes were shown to correlate with therapeutic outcomes, suggesting their potential as biomarkers for predicting response or resistance to treatment. The identification of these modulators represents a significant advancement in the stratification of HER2-positive patients, enabling more personalised and effective therapeutic approaches.

Using Multigene Assay and prediction of response to therapy

This chapter focused on the use of multigene assays to predict responses to anti-HER2 therapy. The study found a positive correlation between *ERBB2* mRNA levels and HER2 gene copy numbers (R=0.31, p=0.006), with significantly higher mRNA levels in HER2 IHC 3+ cases compared to HER2 IHC 2+/ISH-positive cases. This supports previous findings that RT-qPCR may be more accurate than FISH in assessing HER2 protein levels [648].

ERBB2-positive cases were associated with prolonged DFS and DMFS, consistent with earlier studies linking high *ERBB2* expression to improved outcomes in HER2-positive BC patients [197, 320, 321, 507, 554, 574, 652]. The higher *HER2* mRNA expression in HER2-E tumours, as identified by the PAM50 gene signature, likely explains this predictive value [507, 653].

The study also highlighted the effectiveness of MammaTyper® in molecular subtyping. MammaTyper®-defined HER2-E subtypes demonstrated a significantly better response to anti-HER2 therapy compared to IHC-defined subtypes, supporting the superiority of mRNA-based molecular subtyping for guiding treatment [507].

The multigene assay identified 36 cases as *ERBB2*-negative, with 25 of these cases (all HER2 IHC 2+) confirmed as HER2-negative on IHC. None of these discordant cases benefited from targeted anti-HER2 therapy, reflecting known issues with false-positive HER2 IHC results and the heterogeneity of HER2 expression within tumours [148, 649-651].

11.3.5 Characterisation of HER2-Low tumours

This chapter aimed to refine the classification ofHER2-Low BC to enhance reproducibility among pathologists and improve inter-observer agreement. The refined classification provided a clearer framework for stratifying patients for ADC therapy. The study highlighted distinct biological and clinical characteristics of HER2-Low tumours, which differ significantly from HER2-negative tumours, particularly in relation to HR status.HER2-Low tumours, representing 43% of cases, were predominantly HR-positive (90%) [178, 184, 186, 715]..

These tumours were associated with more favourable clinical outcomes, including lower histological grade, reduced mitotic activity, and a lower incidence of LN metastases compared to HER2-negative tumours [171, 179, 186, 712, 714], though they were less responsive to NACT.

Despite improved BCSS and DMFS in HER2-Low tumours compared to HER2-negative cases, the prognostic significance diminished when adjusted for HR positivity, suggesting HR signalling dominance in these tumours. HER2-Low tumours do not appear to be driven by the HER2 oncogenic pathway. PAM50 molecular subtyping and gene expression analysis showed no significant enrichment of HER2 pathway genes in HER2-Low tumours, with most being of the luminal subtype if HR-positive and normal-like if HR-negative.

In HR-negative cases, HER2-Low tumours exhibited a distinct molecular profile, particularly in the LAR subtype, with upregulation of AR and associated pathways, indicating a luminal differentiation that is absent in pure TNBC. Additionally, HER2-Low tumours had lower sTILs scores and displayed aberrant immune infiltration, which may have future implications for personalised therapy development [185]..

11.4 Conclusion

This thesis presents a comprehensive examination of the complexities surrounding HER2-positive and HER2-Low BC. By integrating DP, AI, and advanced molecular techniques, the research offers new tools and insights for improving diagnostic accuracy, patient stratification, and therapeutic outcomes. The development of a HER2-driven morphometric signature and the

refined classification of HER2-Low BC provides clinicians with valuable resources for personalising treatment and optimising patient care. These advancements represent significant steps forward in the clinical management of BC, particularly in the context of HER2-targeted therapies.

The findings highlight the importance of a multifaceted approach to BC treatment, one that considers the intricate interplay between molecular characteristics, tumour microenvironment, and patient-specific factors. As the field continues to evolve, the integration of computational and molecular approaches will be crucial in driving further innovations and improving outcomes for BC patients.

11.5 Clinical Application of Our Findings

1. The findings from this thesis can be applied clinically to better characterise HER2 expression in patients. Prior to this, validation studies using different sources' cohorts are recommended to assess the reproducibility and reliability of the findings. In the fast-growing era of DP and using AI in pathology, algorithms for STR evaluation can be implemented in clinical settings, which will help in patient risk stratification and personalised management.
2. The developed web tool for the HER2-positive signature can serve as an auxiliary tool for predicting HER2 activity within HER2-positive tumours. Additionally, the identified morphometric features could be used to train AI algorithms for diagnosing HER2-positive cases.

3. The impact of ER expression in reducing the response to targeted anti-HER2 therapy is more pronounced in HER2-positive tumours with borderline protein expression and gene amplification. We believe that comparative studies evaluating the efficacy of ADCs against current therapeutic modalities in HER2 IHC 2+/ISH-positive cases are warranted.
4. The proposed scoring algorithm for HER2 expression in BC would assist in improving the concordance and reproducibility among pathologists, particularly in rare scenarios of HER2 Expression.

11.6 Strengths of the study

1. The study utilised a large cohort of invasive BC patients, with clinicopathological and outcome data meticulously collected, validated, and maintained prospectively. This robust dataset allowed for a strong correlation between the findings of various tissue markers and clinically significant outcomes, as well as IHC-defined intrinsic biological subtypes.
2. The availability of a substantial collection of FFPE blocks, along with comprehensive data on anti-HER2 therapy, enabled the careful selection of tumour-containing blocks for TMA construction, ensuring accurate biomarker staining and evaluation.
3. Automated TMA production facilitated the precise selection and insertion of tumour cores, ensured proper alignment of tissue cores, and allowed for the meticulous recording of sample information, thereby streamlining the subsequent scoring process.
4. Validating AI-extracted data using external validation cohorts further enhanced the robustness of the study's findings.

5. In this study, antibodies were used alongside positive and negative controls, with some antibodies further validated through Western blotting and peptide blocking. Additionally, strict adherence to published guidelines on prognostic marker studies was maintained throughout the process to ensure accurate staining interpretation and reliable statistical correlations.
6. Different statistical methods were employed to determine optimal cut-off points for staining positivity of the markers used, avoiding the use of arbitrary thresholds.
7. Analysing data both as continuous and categorical variables helped confirm the results, enhancing the reliability of the findings.
8. Semi-qualitative results of HER2 protein expression were validated using mRNA and CISH data, which, when combined with HER2 IHC, provided a more accurate assessment of HER2 status.
9. The assessment of morphological features in AI-related studies was conducted on WSI rather than core biopsies, enabling a more comprehensive evaluation of these features.
10. Extensive validation was performed on discordant cases, which included re-staining the same block used for transcriptomic analysis and reviewing clinical records to ensure the robustness and validity of our findings.
11. A pathologist-led approach was used for scoring marker expression rather than relying solely on automated image analysis methods. This approach helped avoid potential errors, such as misclassifying in situ

lesions or normal mammary epithelial cells as hyperplasia, which automated methods might not accurately distinguish.

11.7 Limitations and Weaknesses of the Study

1. This study could have possible limitations; for instance, the subjectivity of staining interpretation and qualitative results of immunohistochemical detection of marker expression. However, I have followed a standard approach to keep these to the minimum.
2. The data were only assessed in one centre, and no multicentre validation was considered.
3. Most of the biomarkers studied showed either nuclear or cytoplasmic expression; however, this does not exclude the possibility that these biomarkers are expressed in other parts of the malignant cells, such as the membrane, mitochondria, or Golgi. Therefore, future studies can highlight the importance of subcellular localisation of these proteins.
4. For this historical patient cohort, relatively old paraffin blocks were used to study tissue marker expression, which might have been exhausted or consumed in some blocks. Moreover, therapeutic regimens used when patients of this study were treated tended to be different from those currently in practice, and many modalities are continually evolving.

11.8 Suggestions and Future Investigations

1. Validation of the morphometric signature across multiple cohorts could facilitate the implementation of this tool for predicting patient response to therapy.
2. Incorporating multigene assays alongside current HER2 assessment methods could enhance the identification of patients who would benefit from anti-HER2 therapy.

3. Although ADCs are becoming increasingly important in the management of HER2-Low tumours, comparative studies are warranted to evaluate the efficacy of ADCs versus existing therapeutic modalities in HER2 IHC 2+/ISH-positive cases. Additionally, investigating the potential role of antiandrogens like enzalutamide in HR-negative/HER2-Low settings could be valuable, particularly in preclinical studies or even in randomised clinical trials.
4. Further functional studies are necessary to validate protein expression results. In vitro knockdown of the identified genes, especially oncogenes, would be valuable in exploring the therapeutic potential of these target genes.
5. Further research is needed to understand TAF10 and BCAT1's role in HER2-positive BC, their interaction with PI3K/AKT/mTOR pathways, and potential treatments for trastuzumab resistance.
6. To emphasise the role of subcellular localisation, it is warranted to measure different cellular components separately through subcellular fractionation.
7. Using more than one core per case in the TMA could improve assessment accuracy, helping to compensate for core loss and address any existing heterogeneity.

11.9 Ongoing work

Assessment of expression of TAF10 and BCAT1 in the whole Nottingham cohort, including all molecular subtypes, is undergoing.

Chapter 12. REFERENCES

1. Wilkinson, L. and T. Gathani, *Understanding breast cancer as a global health concern.* The British journal of radiology, 2022. **95**(1130): p. 20211033-20211033.

2. Sung, H., et al., *Global cancer statistics 2020: GLOBOCAN estimates of incidence and mortality worldwide for 36 cancers in 185 countries.* CA: a cancer journal for clinicians, 2021. **71**(3): p. 209-249.

3. Ferlay, J., et al., *Global cancer observatory: cancer today.* Lyon, France: international agency for research on cancer, 2018. **3**(20): p. 2019.

4. Siegel, R., K. Miller, and A. Jemal, *Cancer Statistics, 2017 CA Cancer J Clin 2017; 67: 7-30.* External Resources Pubmed/Medline (NLM) Crossref (DOI), 2017.

5. Brewer, H.R., et al., *Family history and risk of breast cancer: an analysis accounting for family structure.* Breast cancer research and treatment, 2017. **165**(1): p. 193-200.

6. Washbrook, E., *Risk factors and epidemiology of breast cancer.* Women's Health Medicine, 2006. **3**(1): p. 8-14.

7. Horn, J. and L.J. Vatten, *Reproductive and hormonal risk factors of breast cancer: a historical perspective.* International journal of women's health, 2017. **9**: p. 265.

8. Dall, G.V. and K.L. Britt, *Estrogen effects on the mammary gland in early and late life and breast cancer risk.* Frontiers in oncology, 2017. **7**: p. 110.

9. Rosato, V., et al., *Reproductive and hormonal factors, family history, and breast cancer according to the hormonal receptor status.* European journal of cancer prevention, 2014. **23**(5): p. 412-417.

10. Travis, R.C. and T.J. Key, *Oestrogen exposure and breast cancer risk.* Breast Cancer Research, 2003. **5**: p. 1-9.

11. Soroush, A., et al., *The role of oral contraceptive pills on increased risk of breast cancer in Iranian populations: a meta-analysis.* Journal of cancer prevention, 2016. **21**(4): p. 294.

12. Bethea, T.N., et al., *A case–control analysis of oral contraceptive use and breast cancer subtypes in the African American Breast Cancer Epidemiology and Risk Consortium.* Breast Cancer Research, 2015. **17**(1): p. 1-13.

13. McDonald, J.A., A. Goyal, and M.B. Terry, *Alcohol Intake and Breast Cancer Risk: Weighing the Overall Evidence.* Current breast cancer reports, 2013. **5**(3): p. 10.1007/s12609-013-0114-z.

14. Flom, J.D., et al., *Alcohol intake over the life course and mammographic density.* Breast cancer research and treatment, 2009. **117**(3): p. 643-651.

15. Kim, A.S., et al., *Exposure to Secondhand Smoke and Risk of Cancer in Never Smokers: A Meta-Analysis of Epidemiologic Studies.* International journal of environmental research and public health, 2018. **15**(9): p. 1981.

16. Sebastiani, F., et al., *Increased Incidence of Breast Cancer in Postmenopausal Women with High Body Mass Index at the Modena Screening Program.* Journal of breast cancer, 2016. **19**(3): p. 283-291.

17. Srinivasan, M., et al., *A Systematic Review: Does Insulin Resistance Affect the Risk and Survival Outcome of Breast Cancer in Women?* Cureus, 2022. **14**(1): p. e21712-e21712.

18. Dalamaga, M., *Obesity, insulin resistance, adipocytokines and breast cancer: New biomarkers and attractive therapeutic targets.* World journal of experimental medicine, 2013. **3**(3): p. 34-42.

19. Brown, J.C., et al., *Cancer, physical activity, and exercise.* Comprehensive Physiology, 2012. **2**(4): p. 2775-2809.

20. Mehrgou, A. and M. Akouchekian, *The importance of BRCA1 and BRCA2 genes mutations in breast cancer development.* Medical journal of the Islamic Republic of Iran, 2016. **30**: p. 369-369.

21. Kuchenbaecker, K.B., et al., *Risks of Breast, Ovarian, and Contralateral Breast Cancer for BRCA1 and BRCA2 Mutation Carriers.* JAMA, 2017. **317**(23): p. 2402-2416.

22. Bayraktar, S., et al., *Predictive factors for BRCA1/BRCA2 mutations in women with ductal carcinoma in situ.* Cancer, 2012. **118**(6): p. 1515-1522.

23. Goidescu, I.G., et al., *Prevalence of deleterious mutations among patients with breast cancer referred for multigene panel testing in a Romanian population.* Clujul Med, 2018. **91**(2): p. 157-165.

24. Eggertson, L., *Breast density disclosure may do more harm than good.* CMAJ : Canadian Medical Association journal = journal de l'Association medicale canadienne, 2020. **192**(2): p. E48-E49.

25. Kerlikowske, K., et al., *Identifying women with dense breasts at high risk for interval cancer: a cohort study.* Annals of internal medicine, 2015. **162**(10): p. 673-681.

26. Stachs, A., et al., *Benign Breast Disease in Women.* Deutsches Arzteblatt international, 2019. **116**(33-34): p. 565-574.

27. Worsham, M.J., et al., *Risk factors for breast cancer from benign breast disease in a diverse population.* Breast cancer research and treatment, 2009. **118**(1): p. 1-7.

28. Said, S.M., et al., *Flat epithelial atypia and risk of breast cancer: A Mayo cohort study.* Cancer, 2015. **121**(10): p. 1548-1555.

29. Figueroa, J.D., et al., *Risk factors for breast cancer development by tumor characteristics among women with benign breast disease.* Breast Cancer Research, 2021. **23**(1): p. 34.

30. Basu, S.K., et al., *Unilateral and bilateral breast cancer in women surviving pediatric Hodgkin's disease.* International journal of radiation oncology, biology, physics, 2008. **72**(1): p. 34-40.

31. Sun, Y.-S., et al., *Risk Factors and Preventions of Breast Cancer.* International Journal of Biological Sciences, 2017. **13**(11): p. 1387-1397.

32. Feng, Y., et al., *Breast cancer development and progression: Risk factors, cancer stem cells, signaling pathways, genomics, and molecular pathogenesis.* Genes & diseases, 2018. **5**(2): p. 77-106.

33. Sgroi, D.C., *Preinvasive breast cancer.* Annual review of pathology, 2010. **5**: p. 193-221.

34. Van de Vijver, M.J. and H. Peterse, *The diagnosis and management of pre-invasive breast disease: pathological diagnosis--problems with existing classifications.* Breast cancer research : BCR, 2003. **5**(5): p. 269-269.

35. Hanahan, D. and R.A. Weinberg, *Hallmarks of cancer: the next generation.* Cell, 2011. **144**(5): p. 646-74.

36. Lemmon, M.A. and J. Schlessinger, *Cell signaling by receptor tyrosine kinases.* Cell, 2010. **141**(7): p. 1117-34.

37. Zhang, X., K. Powell, and L. Li, *Breast Cancer Stem Cells: Biomarkers, Identification and Isolation Methods, Regulating*

Mechanisms, Cellular Origin, and Beyond. Cancers, 2020. **12**(12): p. 3765.

38. Polyak, K., *Breast cancer: origins and evolution.* The Journal of clinical investigation, 2007. **117**(11): p. 3155-3163.

39. Dai, X., et al., *Breast cancer intrinsic subtype classification, clinical use and future trends.* American journal of cancer research, 2015. **5**(10): p. 2929-2943.

40. Rakha, E.A. and F.G. Pareja. *New advances in molecular breast cancer pathology*. in *Seminars in cancer biology*. 2020. Elsevier.

41. Perou, C.M., et al., *Molecular portraits of human breast tumours.* nature, 2000. **406**(6797): p. 747-752.

42. Sørlie, T., et al., *Gene expression patterns of breast carcinomas distinguish tumor subclasses with clinical implications.* Proceedings of the National Academy of Sciences, 2001. **98**(19): p. 10869-10874.

43. Sorlie, T., et al., *Repeated observation of breast tumor subtypes in independent gene expression data sets.* Proceedings of the National Academy of Sciences of the united States of America, 2003. **100**(14): p. 8418-8423.

44. Vuong, D., et al., *Molecular classification of breast cancer.* Virchows Archiv, 2014. **465**(1): p. 1-14.

45. Tsang, J. and G.M. Tse, *Molecular classification of breast cancer.* Advances in anatomic pathology, 2020. **27**(1): p. 27-35.

46. Vasconcelos, I., et al., *The St. Gallen surrogate classification for breast cancer subtypes successfully predicts tumor presenting features, nodal involvement, recurrence patterns and disease free survival.* The Breast, 2016. **29**: p. 181-185.

47. Gao, J.J. and S.M. Swain, *Luminal a breast cancer and molecular assays: a review.* The oncologist, 2018. **23**(5): p. 556.

48. Hashmi, A.A., et al., *Prognostic parameters of luminal A and luminal B intrinsic breast cancer subtypes of Pakistani patients.* World journal of surgical oncology, 2018. **16**(1): p. 1-6.

49. Rocca, A., et al., *Efficacy of endocrine therapy in relation to progesterone receptor and Ki67 expression in advanced breast cancer.* Breast cancer research and treatment, 2015. **152**(1): p. 57-65.

50. Cheang, M.C., et al., *Ki67 index, HER2 status, and prognosis of patients with luminal B breast cancer.* JNCI: Journal of the National Cancer Institute, 2009. **101**(10): p. 736-750.

51. Goldhirsch, A., et al., *Personalizing the treatment of women with early breast cancer: highlights of the St Gallen International Expert Consensus on the Primary Therapy of Early Breast Cancer 2013.* Annals of oncology, 2013. **24**(9): p. 2206-2223.

52. Tsoutsou, P.G., et al., *How could breast cancer molecular features contribute to locoregional treatment decision making?* Critical reviews in oncology/hematology, 2017. **110**: p. 43-48.

53. Harbeck, N. and M. Gnant, *Interpretation of the evidence for the efficacy and safety of statin therapy.* Lancet, 2017. **389**(10074): p. 1134-1150.

54. Mane, A., et al., *A comparison of clinical features, pathology and outcomes in various subtypes of breast cancer in Indian women.* Journal of clinical and diagnostic research: JCDR, 2015. **9**(9): p. PC01.

55. Pandit, P., et al., *Prevalence of molecular subtypes of breast cancer: a single institutional experience of 2062 patients.* European journal of breast health, 2020. **16**(1): p. 39.

56. Desai, N.V., et al., *Intrinsic molecular subtypes of breast cancers categorized as HER2-positive using an alternative chromosome 17 probe assay.* Breast Cancer Research, 2018. **20**(1): p. 1-6.

57. Llombart-Cussac, A., et al., *HER2-enriched subtype as a predictor of pathological complete response following trastuzumab and lapatinib without chemotherapy in early-stage HER2-positive breast cancer (PAMELA): an open-label, single-group, multicentre, phase 2 trial.* The lancet oncology, 2017. **18**(4): p. 545-554.

58. Tarighati, E., H. Keivan, and H. Mahani, *A review of prognostic and predictive biomarkers in breast cancer.* Clinical and Experimental Medicine, 2023. **23**(1): p. 1-16.

59. Kumar, P. and R. Aggarwal, *An overview of triple-negative breast cancer.* Archives of gynecology and obstetrics, 2016. **293**(2): p. 247-269.

60. Lehmann, B.D., et al., *Refinement of triple-negative breast cancer molecular subtypes: implications for neoadjuvant chemotherapy selection.* PloS one, 2016. **11**(6): p. e0157368.

61. Prat, A., et al., *Phenotypic and molecular characterization of the claudin-low intrinsic subtype of breast cancer.* Breast cancer research, 2010. **12**(5): p. 1-18.

62. Sabatier, R., et al., *Claudin-low breast cancers: clinical, pathological, molecular and prognostic characterization.* Molecular cancer, 2014. **13**(1): p. 1-14.

63. do Nascimento, R.G. and K.M. Otoni, *Histological and molecular classification of breast cancer: what do we know?* Mastology., 2020. **30**: p. 1-8.

64. Makki, J., *Diversity of Breast Carcinoma: Histological Subtypes and Clinical Relevance.* Clinical medicine insights. Pathology, 2015. **8**: p. 23-31.

65. Ciriello, G., et al., *Comprehensive Molecular Portraits of Invasive Lobular Breast Cancer.* Cell, 2015. **163**(2): p. 506-519.

66. McCart Reed, A.E., et al., *Invasive lobular carcinoma of the breast: the increasing importance of this special subtype.* Breast Cancer Research, 2021. **23**(1): p. 6.

67. Edge, S.B. and C.C. Compton, *The American Joint Committee on Cancer: the 7th edition of the AJCC cancer staging manual and the future of TNM.* Ann Surg Oncol, 2010. **17**(6): p. 1471-4.

68. Mittendorf, E.A., et al., *Incorporating Biology Into Breast Cancer Staging: American Joint Committee on Cancer, Eighth Edition, Revisions and Beyond.* American Society of Clinical Oncology Educational Book, 2018(38): p. 38-46.

69. Rakha, E.A., G.M. Tse, and C.M. Quinn, *An update on the pathological classification of breast cancer.* Histopathology, 2023. **82**(1): p. 5-16.

70. Gurcan, M.N., et al., *Histopathological image analysis: a review.* IEEE Rev Biomed Eng, 2009. **2**: p. 147-71.

71. Rakha, E.A., et al., *Breast cancer prognostic classification in the molecular era: the role of histological grade.* Breast cancer research : BCR, 2010. **12**(4): p. 207-207.

72. Ali, A.M.G., et al., *Patient and tumour characteristics, management, and age-specific survival in women with breast cancer in the East of England.* British journal of cancer, 2011. **104**(4): p. 564-570.

73. Tonellotto, F., et al., *Impact of Number of Positive Lymph Nodes and Lymph Node Ratio on Survival of Women with Node-Positive Breast Cancer.* European journal of breast health, 2019. **15**(2): p. 76-84.

74. He, Z., et al., *Identification of Risk Factors Associated with Axillary Lymph Node Metastasis for Sentinel Lymph Node-Positive Breast Cancer Patients.* Journal of Oncology, 2020. **2020**: p. 8884337.

75. Rao, R., et al., *Axillary node interventions in breast cancer: a systematic review.* Jama, 2013. **310**(13): p. 1385-1394.

76. Zhu, H., et al., *Development and validation of prognostic nomograms for patients with metastatic small bowel adenocarcinoma: a retrospective cohort study.* Scientific Reports, 2022. **12**(1): p. 5983.

77. Liao, C.-T., et al., *Influence of Pathological Nodal Status and Maximal Standardized Uptake Value of the Primary Tumor and Regional Lymph Nodes on Treatment Plans in Patients With Advanced Oral Cavity Squamous Cell Carcinoma.* International Journal of Radiation Oncology, Biology, Physics, 2010. **77**(2): p. 421-429.

78. McDonald, J.R., et al., *Lymph node harvest in colon and rectal cancer: Current considerations.* World journal of gastrointestinal surgery, 2012. **4**(1): p. 9-19.

79. Rakha, E.A., et al., *Nottingham Prognostic Index Plus (NPI+): a modern clinical decision making tool in breast cancer.* British journal of cancer, 2014. **110**(7): p. 1688-1697.

80. Green, A.R., et al., *Nottingham prognostic index plus (NPI+) predicts risk of distant metastases in primary breast cancer.* Breast cancer research and treatment, 2016. **157**(1): p. 65-75.

81. Houvenaeghel, G., et al., *Lymphovascular invasion has a significant prognostic impact in patients with early breast cancer, results from a large, national, multicenter, retrospective cohort study.* ESMO open, 2021. **6**(6): p. 100316-100316.

82. Invernizzi, M., et al., *Lymphovascular invasion and extranodal tumour extension are risk indicators of breast cancer related lymphoedema: an observational retrospective study with long-term follow-up.* BMC Cancer, 2018. **18**(1): p. 935.

83. Zhong, Y.-M., F. Tong, and J. Shen, *Lympho-vascular invasion impacts the prognosis in breast-conserving surgery: a systematic review and meta-analysis.* BMC cancer, 2022. **22**(1): p. 102-102.

84. Song, Y.J., et al., *The role of lymphovascular invasion as a prognostic factor in patients with lymph node-positive operable invasive breast cancer.* Journal of breast cancer, 2011. **14**(3): p. 198-203.

85. García-Teijido, P., et al., *Tumor-infiltrating lymphocytes in triple negative breast cancer: the future of immune targeting.* Clinical Medicine Insights: Oncology, 2016. **10**: p. CMO. S34540.

86. Salgado, R., et al., *The evaluation of tumor-infiltrating lymphocytes (TILs) in breast cancer: recommendations by an International TILs Working Group 2014.* Annals of oncology, 2015. **26**(2): p. 259-271.

87. Khan, S., et al., *Role of adipokines and cytokines in obesity-associated breast cancer: therapeutic targets.* Cytokine Growth Factor Rev, 2013. **24**(6): p. 503-13.

88. Sjöberg, E., et al., *Expression of the chemokine CXCL14 in the tumour stroma is an independent marker of survival in breast cancer.* Br J Cancer, 2016. **114**(10): p. 1117-24.

89. Goto, H., et al., *Adipose-derived stem cells enhance human breast cancer growth and cancer stem cell-like properties through adipsin.* Oncogene, 2019. **38**(6): p. 767-779.

90. Beck, A.H., et al., *Systematic analysis of breast cancer morphology uncovers stromal features associated with survival.* Sci Transl Med, 2011. **3**(108): p. 108ra113.

91. Mesker, W.E., et al., *The carcinoma–stromal ratio of colon carcinoma is an independent factor for survival compared to lymph node status and tumor stage.* Analytical Cellular Pathology, 2007. **29**(5): p. 387-398.

92. Huijbers, A., et al., *The proportion of tumor-stroma as a strong prognosticator for stage II and III colon cancer patients: validation in the VICTOR trial.* Ann Oncol, 2013. **24**(1): p. 179-85.

93. Scheer, R., et al., *Tumor-stroma ratio as prognostic factor for survival in rectal adenocarcinoma: A retrospective cohort study.* World J Gastrointest Oncol, 2017. **9**(12): p. 466-474.

94. Lv, Z., et al., *Tumor-stroma ratio is a prognostic factor for survival in hepatocellular carcinoma patients after liver resection or transplantation.* Surgery, 2015. **158**(1): p. 142-50.

95. Xi, K.X., et al., *Tumor-stroma ratio (TSR) in non-small cell lung cancer (NSCLC) patients after lung resection is a prognostic factor for survival.* J Thorac Dis, 2017. **9**(10): p. 4017-4026.

96. de Kruijf, E.M., et al., *Tumor-stroma ratio in the primary tumor is a prognostic factor in early breast cancer patients, especially in triple-negative carcinoma patients.* Breast Cancer Res Treat, 2011. **125**(3): p. 687-96.

97. Kramer, C.J.H., et al., *The prognostic value of tumour–stroma ratio in primary breast cancer with special attention to triple-negative tumours: a review.* Breast Cancer Research and Treatment, 2019. **173**(1): p. 55-64.

98. Mehta, S., et al., *Predictive and prognostic molecular markers for cancer medicine.* Therapeutic advances in medical oncology, 2010. **2**(2): p. 125-148.

99. Hammond, M.E.H., et al., *American Society of Clinical Oncology/College of American Pathologists guideline recommendations for immunohistochemical testing of estrogen and progesterone receptors in breast cancer.* Journal of Clinical Oncology, 2010. **28**(16): p. 2784-2795.

100. Pinhel, I., et al., *ER and HER2 expression are positively correlated in HER2 non-overexpressing breast cancer.* Breast Cancer Research, 2012. **14**(2): p. R46.

101. Oshi, M., et al., *Degree of Early Estrogen Response Predict Survival after Endocrine Therapy in Primary and Metastatic ER-Positive Breast Cancer.* Cancers, 2020. **12**(12): p. 3557.

102. Bracken-Clarke, D.B., M.W. Lucas, and M.J. Higgins, *Extended Adjuvant Endocrine Therapy in Hormone Receptor-Positive Early Breast Cancer.* Breast care (Basel, Switzerland), 2017. **12**(3): p. 138-144.

103. Chen, J.-Q. and J. Russo, *ERalpha-negative and triple negative breast cancer: molecular features and potential therapeutic approaches.* Biochimica et biophysica acta, 2009. **1796**(2): p. 162-175.

104. Nordenskjöld, A., et al., *Progesterone receptor positivity is a predictor of long-term benefit from adjuvant tamoxifen treatment of estrogen receptor positive breast cancer.* Breast cancer research and treatment, 2016. **160**(2): p. 313-322.

105. Wu, V.S., et al., *From bench to bedside: What do we know about hormone receptor-positive and human epidermal growth factor receptor 2-positive breast cancer?* The Journal of Steroid Biochemistry and Molecular Biology, 2015. **153**: p. 45-53.

106. Soliman, N.A. and S.M. Yussif, *Ki-67 as a prognostic marker according to breast cancer molecular subtype.* Cancer Biol Med, 2016. **13**(4): p. 496-504.

107. Feng, X., et al., *Low Ki67/high ATM protein expression in malignant tumors predicts favorable prognosis in a retrospective study of early stage hormone receptor positive breast cancer.* Oncotarget, 2016. **7**(52): p. 85798-85812.

108. Pan, Y., et al., *P53 and Ki-67 as prognostic markers in triple-negative breast cancer patients.* PLoS One, 2017. **12**(2): p. e0172324.

109. Harvey, J.A., et al., *Histologic changes in the breast with menopausal hormone therapy use: correlation with breast density, estrogen receptor, progesterone receptor, and proliferation indices.* Menopause, 2008. **15**(1): p. 67-73.

110. Zhou, C.J., et al., *Expression of ER, Ki-67 and cylinD1 in the pre-cancerous breast of Chinese patients.* Pathol Oncol Res, 2009. **15**(2): p. 153-8.

111. Petrelli, F., et al., *Prognostic value of different cut-off levels of Ki-67 in breast cancer: a systematic review and meta-analysis of 64,196 patients.* Breast Cancer Res Treat, 2015. **153**(3): p. 477-91.

112. Lee, J.S., M.J.M. Magbanua, and J.W. Park, *Circulating tumor cells in breast cancer: applications in personalized medicine.* Breast Cancer Res Treat, 2016. **160**(3): p. 411-424.

113. Smerage, J.B., et al., *Circulating tumor cells and response to chemotherapy in metastatic breast cancer: SWOG S0500.* J Clin Oncol, 2014. **32**(31): p. 3483-9.

114. Fang, C., et al., *Serum CA125 is a predictive marker for breast cancer outcomes and correlates with molecular subtypes.* Oncotarget, 2017. **8**(38): p. 63963.

115. Shao, Y., et al., *Elevated Levels of Serum Tumor Markers CEA and CA15-3 Are Prognostic Parameters for Different Molecular Subtypes of Breast Cancer.* PLoS One, 2015. **10**(7): p. e0133830.

116. Gold, P. and S.O. Freedman, *Specific carcinoembryonic antigens of the human digestive system.* J Exp Med, 1965. **122**(3): p. 467-81.

117. Wu, S.G., et al., *Serum levels of CEA and CA15-3 in different molecular subtypes and prognostic value in Chinese breast cancer.* Breast, 2014. **23**(1): p. 88-93.

118. Duffy, M.J., D. Evoy, and E.W. McDermott, *CA 15-3: uses and limitation as a biomarker for breast cancer.* Clin Chim Acta, 2010. **411**(23-24): p. 1869-74.

119. Li, J., et al., *Tumor markers CA15-3, CA125, CEA and breast cancer survival by molecular subtype: a cohort study.* Breast Cancer, 2020. **27**: p. 621-630.

120. Molina, R., et al., *Tumor markers in breast cancer–European Group on Tumor Markers recommendations.* Tumor Biology, 2005. **26**(6): p. 281-293.

121. Cohen, S., *Isolation of a mouse submaxillary gland protein accelerating incisor eruption and eyelid opening in the new-born animal.* Journal of Biological chemistry, 1962. **237**(5): p. 1555-1562.

122. Cohen, S., *The stimulation of epidermal proliferation by a specific protein (EGF).* Developmental biology, 1965. **12**(3): p. 394-407.

123. Carpenter, G., L. King Jr, and S. Cohen, *Epidermal growth factor stimulates phosphorylation in membrane preparations in vitro.* Nature, 1978. **276**(5686): p. 409-410.

124. Engelbreth-Holm, J. and A.R. Meyer, *Variations in the Percentage of Takes in 3 Strains of Chicken Leukosis.* 1935.

125. Yamamoto, T., et al., *The erbB gene of avian erythroblastosis virus is a member of the src gene family.* Cell, 1983. **35**(1): p. 71-78.

126. Downward, J., et al., *Close similarity of epidermal growth factor receptor and v-erb-B oncogene protein sequences.* Nature, 1984. **307**(5951): p. 521-527.

127. Slamon, D.J., et al., *Human breast cancer: correlation of relapse and survival with amplification of the HER-2/neu oncogene.* science, 1987. **235**(4785): p. 177-182.

128. Slamon, D.J., et al., *Studies of the HER-2/neu proto-oncogene in human breast and ovarian cancer.* Science, 1989. **244**(4905): p. 707-712.

129. Carter, P., et al., *Humanization of an anti-p185HER2 antibody for human cancer therapy.* Proceedings of the National Academy of Sciences, 1992. **89**(10): p. 4285-4289.

130. Fendly, B.M., et al., *Characterization of murine monoclonal antibodies reactive to either the human epidermal growth factor receptor or HER2/neu gene product.* Cancer research, 1990. **50**(5): p. 1550-1558.

131. Kallioniemi, O.P., et al., *ERBB2 amplification in breast cancer analyzed by fluorescence in situ hybridization.* Proc Natl Acad Sci U S A, 1992. **89**(12): p. 5321-5.

132. Appert-Collin, A., et al., *Role of ErbB receptors in cancer cell migration and invasion.* Frontiers in pharmacology, 2015. **6**: p. 283.

133. Ali, R. and M.K. Wendt, *The paradoxical functions of EGFR during breast cancer progression.* Signal transduction and targeted therapy, 2017. **2**(1): p. 1-7.

134. Citri, A. and Y. Yarden, *EGF-ERBB signalling: towards the systems level.* Nat Rev Mol Cell Biol, 2006. **7**(7): p. 505-16.

135. Graus-Porta, D., et al., *ErbB-2, the preferred heterodimerization partner of all ErbB receptors, is a mediator of lateral signaling.* Embo j, 1997. **16**(7): p. 1647-55.

136. Moasser, M.M., *The oncogene HER2: its signaling and transforming functions and its role in human cancer pathogenesis.* Oncogene, 2007. **26**(45): p. 6469-87.

137. Tzahar, E., et al., *A hierarchical network of interreceptor interactions determines signal transduction by Neu differentiation factor/neuregulin and epidermal growth factor.* Mol Cell Biol, 1996. **16**(10): p. 5276-87.

138. Nahta, R., et al., *Insulin-like growth factor-I receptor/human epidermal growth factor receptor 2 heterodimerization contributes to trastuzumab resistance of breast cancer cells.* Cancer Res, 2005. **65**(23): p. 11118-28.

139. Molina, M.A., et al., *NH(2)-terminal truncated HER-2 protein but not full-length receptor is associated with nodal metastasis in human breast cancer.* Clin Cancer Res, 2002. **8**(2): p. 347-53.

140. Scaltriti, M., et al., *Expression of p95HER2, a truncated form of the HER2 receptor, and response to anti-HER2 therapies in breast cancer.* Journal of the National Cancer Institute, 2007. **99**(8): p. 628-638.

141. Wolff, A.C., et al., *Human epidermal growth factor receptor 2 testing in breast cancer: American Society of Clinical Oncology/College of American Pathologists clinical practice guideline focused update.* Archives of pathology & laboratory medicine, 2018. **142**(11): p. 1364-1382.

142. Annaratone, L., I. Sarotto, and C. Marchiò, *HER2 in breast cancer.* 2019.

143. Wolff, A.C., et al., *College of American Pathologists guideline recommendations for human epidermal growth factor receptor 2 testing in breast cancer.* J clin oncol, 2007. **25**(1): p. 118-145.

144. Hauser-Kronberger, C. and N. Dandachi, *Comparison of chromogenic in situ hybridization with other methodologies for HER2 status assesment in breast cancer.* Journal of molecular histology, 2004. **35**: p. 647-653.

145. Hicks, D.G. and R.R. Tubbs, *Assessment of the HER2 status in breast cancer by fluorescence in situ hybridization: a technical review with interpretive guidelines.* Human pathology, 2005. **36**(3): p. 250-261.

146. Larson, J.S., et al., *Analytical validation of a highly quantitative, sensitive, accurate, and reproducible assay (HERmark®) for the measurement of HER2 total protein and HER2 homodimers in FFPE breast cancer tumor specimens.* Pathology research international, 2010. **2010**.

147. Huang, W., et al., *Comparison of Central HER2 Testing With Quantitative Total HER2 Expression and HER2 Homodimer Measurements Using a Novel Proximity-Based Assay.* American Journal of Clinical Pathology, 2010. **134**(2): p. 303-311.

148. Perez, E.A., et al., *HER2 Testing by Local, Central, and Reference Laboratories in Specimens From the North Central Cancer Treatment*

Group N9831 Intergroup Adjuvant Trial. Journal of Clinical Oncology, 2006. **24**(19): p. 3032-3038.

149. Yardley, D.A., et al., *Quantitative measurement of HER2 expression in breast cancers: comparison with 'real-world'routine HER2 testing in a multicenter Collaborative Biomarker Study and correlation with overall survival.* Breast Cancer Research, 2015. **17**: p. 1-13.

150. Benöhr, P., et al., *Her-2/neu expression in breast cancer - A comparison of different diagnostic methods.* Anticancer Research, 2005. **25**(3 B): p. 1895-1900.

151. Baehner, F.L., et al., *Human epidermal growth factor receptor 2 assessment in a case-control study: Comparison of fluorescence in situ hybridization and quantitative reverse transcription polymerase chain reaction performed by central laboratories.* Journal of Clinical Oncology, 2010. **28**(28): p. 4300-4306.

152. Gjerdrum, L.M., et al., *Real-Time Quantitative PCR of Microdissected Paraffin-Embedded Breast Carcinoma: An Alternative Method for HER-2/neu Analysis.* The Journal of Molecular Diagnostics, 2004. **6**(1): p. 42-51.

153. Iverson, A.A., et al., *A Single-Tube Quantitative Assay for mRNA Levels of Hormonal and Growth Factor Receptors in Breast Cancer Specimens.* The Journal of Molecular Diagnostics, 2009. **11**(2): p. 117-130.

154. Vinatzer, U., et al., *Expression of HER2 and the coamplified genes GRB7 and MLN64 in human breast cancer: Quantitative real-time reverse transcription-PCR as a diagnostic alternative to immunohistochemistry and fluorescence in situ hybridization.* Clinical Cancer Research, 2005. **11**(23): p. 8348-8357.

155. Dabbs, D.J., et al., *High false-negative rate of HER2 quantitative reverse transcription polymerase chain reaction of the oncotype DX test: An independent quality assurance study.* Journal of Clinical Oncology, 2011. **29**(32): p. 4279-4285.

156. Jacquemier, J., et al., *SISH/CISH or qPCR as alternative techniques to FISH for determination of HER2 amplification status on breast tumors core needle biopsies: a multicenter experience based on 840 cases.* BMC cancer, 2013. **13**: p. 1-11.

157. Wolff, A.C., et al., *Recommendations for human epidermal growth factor receptor 2 testing in breast cancer: American Society of Clinical Oncology/College of American Pathologists clinical practice guideline update.* Arch Pathol Lab Med, 2014. **138**(2): p. 241-56.

158. Bradley, R., et al., *Trastuzumab for early-stage, HER2-positive breast cancer: a meta-analysis of 13 864 women in seven randomised trials.* The Lancet Oncology, 2021. **22**(8): p. 1139-1150.

159. Slamon, D.J., et al., *Use of chemotherapy plus a monoclonal antibody against HER2 for metastatic breast cancer that overexpresses HER2.* New England journal of medicine, 2001. **344**(11): p. 783-792.

160. Rakha, E.A., et al., *UK recommendations for HER2 assessment in breast cancer: an update.* J Clin Pathol, 2023. **76**(4): p. 217-227.

161. Rakha, E.A., et al., *Updated UK Recommendations for HER2 assessment in breast cancer.* Journal of Clinical Pathology, 2015. **68**(2): p. 93-99.

162. Taucher, S., et al., *Prognostic markers in breast cancer: the reliability of HER2/neu status in core needle biopsy of 325 patients with primary breast cancer.* Wiener klinische Wochenschrift, 2004. **116**.

163. Chen, X., et al., *Accuracy of estrogen receptor, progesterone receptor, and HER2 status between core needle and open excision biopsy in breast cancer: a meta-analysis.* Breast cancer research and treatment, 2012. **134**: p. 957-967.

164. Middleton, L.P., et al., *Implementation of American Society of Clinical Oncology/College of American Pathologists HER2 Guideline Recommendations in a tertiary care facility increases HER2 immunohistochemistry and fluorescence in situ hybridization concordance and decreases the number of inconclusive cases.* Archives of pathology & laboratory medicine, 2009. **133**(5): p. 775-780.

165. Wolff, A., et al., *College of American Pathologists Recommendations for human epidermal growth factor receptor 2 testing in breast cancer: American Society of Clinical Oncology/College of American*

Pathologists clinical practice guideline update. J Clin Oncol, 2013. **31**(31): p. 3997-4013.

166. Venetis, K., et al., *HER2 Low, Ultra-low, and Novel Complementary Biomarkers: Expanding the Spectrum of HER2 Positivity in Breast Cancer.* Frontiers in Molecular Biosciences, 2022. **9**.

167. Sajjadi, E., et al., *Pathological identification of HER2-low breast cancer: Tips, tricks, and troubleshooting for the optimal test.* Frontiers in Molecular Biosciences, 2023. **10**.

168. Rinnerthaler, G., S.P. Gampenrieder, and R. Greil, *HER2 directed antibody-drug-conjugates beyond T-DM1 in breast cancer.* International journal of molecular sciences, 2019. **20**(5): p. 1115.

169. Tarantino, P., et al., *HER2-low breast cancer: pathological and clinical landscape.* Journal of clinical oncology: official journal of the American Society of Clinical Oncology, 2020. **38**(17): p. 1951-1962.

170. Modi, S., et al., *Trastuzumab deruxtecan in previously treated HER2-low advanced breast cancer.* New England Journal of Medicine, 2022. **387**(1): p. 9-20.

171. Bardia, A., et al., *Trastuzumab Deruxtecan after Endocrine Therapy in Metastatic Breast Cancer.* New England Journal of Medicine, 2024.

172. Mosele, F., et al., *Trastuzumab deruxtecan in metastatic breast cancer with variable HER2 expression: the phase 2 DAISY trial.* Nat Med, 2023. **29**(8): p. 2110-2120.

173. Fehrenbacher, L., et al., *Abstract GS1-02: NSABP B-47 (NRG oncology): Phase III randomized trial comparing adjuvant chemotherapy with adriamycin (A) and cyclophosphamide (C)→ weekly paclitaxel (WP), or docetaxel (T) and C with or without a year of trastuzumab (H) in women with node-positive or high-risk node-negative invasive breast cancer (IBC) expressing HER2 staining intensity of IHC 1+ or 2+ with negative FISH (HER2-Low IBC)*. 2018, AACR.

174. Fehrenbacher, L., et al., *NSABP B-47/NRG oncology phase III randomized trial comparing adjuvant chemotherapy with or without trastuzumab in high-risk invasive breast cancer negative for HER2 by FISH and with IHC 1+ or 2+.* Journal of Clinical Oncology, 2020. **38**(5): p. 444.

175. De Cecco, M., D.N. Galbraith, and L.L. McDermott, *What makes a good antibody–drug conjugate?* Expert Opinion on Biological Therapy, 2021. **21**(7): p. 841-847.

176. Marchiò, C., et al. *Evolving concepts in HER2 evaluation in breast cancer: Heterogeneity, HER2-low carcinomas and beyond*. in *Seminars in cancer biology*. 2021. Elsevier.

177. Buckley, N.E., et al., *Quantification of HER2 heterogeneity in breast cancer-implications for identification of sub-dominant clones for personalised treatment.* Sci Rep, 2016. **6**: p. 23383.

178. Agostinetto, E., et al., *HER2-low breast cancer: molecular characteristics and prognosis.* Cancers, 2021. **13**(11): p. 2824.

179. de Moura Leite, L., et al., *HER2-low status and response to neoadjuvant chemotherapy in HER2 negative early breast cancer.* Breast cancer research and treatment, 2021. **190**(1): p. 155-163.

180. Horisawa, N., et al., *The frequency of low HER2 expression in breast cancer and a comparison of prognosis between patients with HER2-low and HER2-negative breast cancer by HR status.* Breast Cancer, 2022: p. 1-8.

181. Jacot, W., et al., *Prognostic value of HER2-low expression in non-metastatic triple-negative breast cancer and correlation with other biomarkers.* Cancers, 2021. **13**(23): p. 6059.

182. Schettini, F., et al., *Clinical, pathological, and PAM50 gene expression features of HER2-low breast cancer.* NPJ breast cancer, 2021. **7**(1): p. 1.

183. Miglietta, F., et al., *Evolution of HER2-low expression from primary to recurrent breast cancer.* NPJ Breast Cancer, 2021. **7**(1): p. 137.

184. Zhang, H., et al., *HER2-low breast cancers: incidence, HER2 staining patterns, clinicopathologic features, MammaPrint and BluePrint genomic profiles.* Mod Pathol, 2022. **35**(8): p. 1075-1082.

185. van den Ende, N.S., et al., *HER2-low breast cancer shows a lower immune response compared to HER2-negative cases.* Sci Rep, 2022. **12**(1): p. 12974.

186. Denkert, C., et al., *Clinical and molecular characteristics of HER2-low-positive breast cancer: pooled analysis of individual patient data from four prospective, neoadjuvant clinical trials.* The Lancet Oncology, 2021. **22**(8): p. 1151-1161.

187. Molinelli, C., et al., *Prognostic value of HER2-low status in breast cancer: a systematic review and meta-analysis.* ESMO Open, 2023. **8**(4): p. 101592.

188. Lai, H.-Z., et al., *Targeted approaches to HER2-low breast cancer: current practice and future directions.* Cancers, 2022. **14**(15): p. 3774.

189. Molinelli, C., et al., *HER2-low breast cancer: where are we?* Breast Care, 2022. **17**(6): p. 533-545.

190. Nicolò, E., P. Tarantino, and G. Curigliano, *Biology and treatment of HER2-low breast cancer.* Hematology/Oncology Clinics, 2023. **37**(1): p. 117-132.

191. Atallah, N.M., et al., *Characterisation of luminal and triple-negative breast cancer with HER2 Low protein expression.* European Journal of Cancer, 2023. **195**: p. 113371.

192. Fernandez, A.I., et al., *Examination of low ERBB2 protein expression in breast cancer tissue.* JAMA oncology, 2022. **8**(4): p. 607-610.

193. Tarantino, P., G. Curigliano, and S.M. Tolaney, *Navigating the HER2-low paradigm in breast oncology: new standards, future horizons.* Cancer Discovery, 2022. **12**(9): p. 2026-2030.

194. Harigopal, M., et al., *Multiplexed assessment of the Southwest Oncology Group-directed Intergroup Breast Cancer Trial S9313 by AQUA shows that both high and low levels of HER2 are associated with poor outcome.* The American journal of pathology, 2010. **176**(4): p. 1639-1647.

195. Moutafi, M., et al., *Quantitative measurement of HER2 expression to subclassify ERBB2 unamplified breast cancer.* Laboratory Investigation, 2022. **102**(10): p. 1101-1108.

196. Jensen, K., et al., *A novel quantitative immunohistochemistry method for precise protein measurements directly in formalin-fixed, paraffin-embedded specimens: analytical performance measuring HER2.* Modern Pathology, 2017. **30**(2): p. 180-193.

197. Griguolo, G., et al., *ERBB2 mRNA expression and response to ado-trastuzumab emtansine (T-DM1) in HER2-positive breast cancer.* Cancers, 2020. **12**(7): p. 1902.

198. Navin, N., et al., *Inferring tumor progression from genomic heterogeneity.* Genome research, 2010. **20**(1): p. 68-80.

199. Hanna, W.M., et al., *HER2 in situ hybridization in breast cancer: clinical implications of polysomy 17 and genetic heterogeneity.* Modern Pathology, 2014. **27**(1): p. 4-18.

200. Bartlett, A.I., et al., *Heterogeneous HER2 gene amplification: Impact on patient outcome and a clinically relevant definition.* American Journal of Clinical Pathology, 2011. **136**(2): p. 266-274.

201. Chang, M.C., et al., *'Genetic heterogeneity' in HER2/neu testing by fluorescence in situ hybridization: a study of 2522 cases.* Modern Pathology, 2012. **25**(5): p. 683-688.

202. Hou, Y., et al., *HER2 intratumoral heterogeneity is independently associated with incomplete response to anti-HER2 neoadjuvant chemotherapy in HER2-positive breast carcinoma.* Breast Cancer Research and Treatment, 2017. **166**(2): p. 447-457.

203. Lee, H.J., et al., *Clinicopathologic significance of the intratumoral heterogeneity of HER2 gene amplification in HER2-positive breast cancer patients treated with adjuvant trastuzumab.* American Journal of Clinical Pathology, 2015. **144**(4): p. 570-578.

204. Lee, H.J., et al., *HER2 heterogeneity affects trastuzumab responses and survival in patients with HER2-positive metastatic breast cancer.* American journal of clinical pathology, 2014. **142**(6): p. 755-766.

205. Yang, Y.-l., et al., *Genetic heterogeneity of HER2 in breast cancer: impact on HER2 testing and its clinicopathologic significance.* Breast Cancer Research and Treatment, 2012. **134**(3): p. 1095-1102.

206. Allison, K.H., S.M. Dintzis, and R.A. Schmidt, *Frequency of HER2 heterogeneity by fluorescence in situ hybridization according to CAP Expert Panel Recommendations: Time for a new look at how to report*

heterogeneity. American Journal of Clinical Pathology, 2011. **136**(6): p. 864-871.

207. Seol, H., et al., *Intratumoral heterogeneity of HER2 gene amplification in breast cancer: its clinicopathological significance.* Modern pathology, 2012. **25**(7): p. 938-948.

208. Shafi, H., et al., *Clinicopathological significance of HER2/neu genetic heterogeneity in HER2/neu non-amplified invasive breast carcinomas and its concurrent axillary metastasis.* Journal of Clinical Pathology, 2013. **66**(8): p. 649-654.

209. Lee, S., et al., *Evaluation of Intratumoral HER-2 Heterogeneity by Fluorescence In Situ Hybridization in Invasive Breast Cancer: A Single Institution Study.* J Korean Med Sci, 2011. **26**(8): p. 1001-1006.

210. Marchiò, C., et al., *The Dilemma of HER2 Double-equivocal Breast Carcinomas: Genomic Profiling and Implications for Treatment.* Am J Surg Pathol, 2018. **42**(9): p. 1190-1200.

211. Moelans, C.B., R.A. de Weger, and P.J. van Diest, *Absence of chromosome 17 polysomy in breast cancer: analysis by CEP17 chromogenic in situ hybridization and multiplex ligation-dependent probe amplification.* Breast Cancer Research and Treatment, 2010. **120**(1): p. 1-7.

212. Varga, Z., et al., *Co-amplification of the HER2 gene and chromosome 17 centromere: a potential diagnostic pitfall in HER2 testing in breast*

cancer. Breast Cancer Research and Treatment, 2012. **132**(3): p. 925-935.

213. Yeh, I.T., et al., *Clinical validation of an array CGH test for HER2 status in breast cancer reveals that polysomy 17 is a rare event.* Modern Pathology, 2009. **22**(9): p. 1169-1175.

214. Kurozumi, S., et al., *HER2 intratumoral heterogeneity analyses by concurrent HER2 gene and protein assessment for the prognosis of HER2 negative invasive breast cancer patients.* Breast Cancer Research and Treatment, 2016. **158**(1): p. 99-111.

215. Perez, E.A., et al., *Relationship between tumor biomarkers and efficacy in MARIANNE, a phase III study of trastuzumab emtansine ± pertuzumab versus trastuzumab plus taxane in HER2-positive advanced breast cancer.* BMC Cancer, 2019. **19**(1).

216. Rye, I.H., et al., *Intratumor heterogeneity defines treatment-resistant HER2+ breast tumors.* Molecular Oncology, 2018. **12**(11): p. 1838-1855.

217. Song, H., et al., *Intratumoral heterogeneity impacts the response to anti-neu antibody therapy.* BMC Cancer, 2014. **14**(1).

218. Metzger Filho, O., et al., *HER2 heterogeneity as a predictor of response to neoadjuvant T-DM1 plus pertuzumab: Results from a prospective clinical trial*. 2019, American Society of Clinical Oncology.

219. Vance, G.H., et al., *Genetic Heterogeneity in HER2 Testing in Breast Cancer: Panel Summary and Guidelines.* Archives of Pathology & Laboratory Medicine, 2009. **133**(4): p. 611-612.

220. Cameron, D., et al., *11 years' follow-up of trastuzumab after adjuvant chemotherapy in HER2-positive early breast cancer: final analysis of the HERceptin Adjuvant (HERA) trial.* The Lancet, 2017. **389**(10075): p. 1195-1205.

221. Perez, E.A., et al., *Trastuzumab plus adjuvant chemotherapy for human epidermal growth factor receptor 2–positive breast cancer: planned joint analysis of overall survival from NSABP B-31 and NCCTG N9831.* Journal of clinical oncology, 2014. **32**(33): p. 3744.

222. Slamon, D., et al., *Adjuvant Trastuzumab in HER2-Positive Breast Cancer.* New England Journal of Medicine, 2011. **365**(14): p. 1273-1283.

223. Swain, S.M., et al., *Pertuzumab, trastuzumab, and docetaxel for HER2-positive metastatic breast cancer (CLEOPATRA study): overall survival results from a randomised, double-blind, placebo-controlled, phase 3 study.* The Lancet Oncology, 2013. **14**(6): p. 461-471.

224. Atallah, N., et al., *Differential response of HER2-positive breast cancer to anti-HER2 therapy based on HER2 protein expression level.* British Journal of Cancer, 2023. **129**(10): p. 1692-1705.

225. Chen, W., et al., *Differences between the efficacy of HER2 (2+)/FISH-positive and HER2 (3+) in breast cancer during dual-target neoadjuvant therapy.* The Breast, 2023. **71**: p. 69-73.

226. Jiao, D., et al., *Comparison of the Response to Neoadjuvant Therapy Between Immunohistochemistry HER2 (3+) and HER2 (2+)/ISH+ Early-Stage Breast Cancer: A Retrospective Multicenter Cohort Study.* The Oncologist, 2024.

227. Katayama, A., et al., *Predictors of pathological complete response to neoadjuvant treatment and changes to post-neoadjuvant HER2 status in HER2-positive invasive breast cancer.* Modern Pathology, 2021. **34**(7): p. 1271-1281.

228. Krystel-Whittemore, M., et al., *Pathologic complete response rate according to HER2 detection methods in HER2-positive breast cancer treated with neoadjuvant systemic therapy.* Breast cancer research and treatment, 2019. **177**(1): p. 61-66.

229. Chen, J., M. Colosimo, and E. Lim, *The management of HER2-positive early breast cancer: Current and future therapies.* Asia-Pacific Journal of Clinical Oncology, 2021. **17**: p. 3-12.

230. Piccart-Gebhart, M.J., et al., *Trastuzumab after adjuvant chemotherapy in HER2-positive breast cancer.* New England Journal of Medicine, 2005. **353**(16): p. 1659-1672.

231. Von Minckwitz, G., et al., *Adjuvant pertuzumab and trastuzumab in early HER2-positive breast cancer.* New England Journal of Medicine, 2017. **377**(2): p. 122-131.

232. Gianni, L., et al., *5-year analysis of neoadjuvant pertuzumab and trastuzumab in patients with locally advanced, inflammatory, or early-stage HER2-positive breast cancer (NeoSphere): a multicentre, open-label, phase 2 randomised trial.* The lancet oncology, 2016. **17**(6): p. 791-800.

233. Baselga, J., et al., *Pertuzumab plus trastuzumab plus docetaxel for metastatic breast cancer.* New England Journal of Medicine, 2012. **366**(2): p. 109-119.

234. Martin, M., et al., *Neratinib after trastuzumab-based adjuvant therapy in HER2-positive breast cancer (ExteNET): 5-year analysis of a randomised, double-blind, placebo-controlled, phase 3 trial.* The lancet oncology, 2017. **18**(12): p. 1688-1700.

235. Saura, C., et al., *Neratinib plus capecitabine versus lapatinib plus capecitabine in HER2-positive metastatic breast cancer previously treated with≥ 2 HER2-directed regimens: phase III NALA trial.* Journal of Clinical Oncology, 2020. **38**(27): p. 3138.

236. Geyer, C.E., et al., *Lapatinib plus capecitabine for HER2-positive advanced breast cancer.* New England journal of medicine, 2006. **355**(26): p. 2733-2743.

237. Murthy, R.K., et al., *Tucatinib, trastuzumab, and capecitabine for HER2-positive metastatic breast cancer.* New England Journal of Medicine, 2020. **382**(7): p. 597-609.

238. Xu, B., et al., *Pyrotinib plus capecitabine versus lapatinib plus capecitabine for the treatment of HER2-positive metastatic breast cancer (PHOEBE): a multicentre, open-label, randomised, controlled, phase 3 trial.* The Lancet Oncology, 2021. **22**(3): p. 351-360.

239. Krop, I.E., et al., *Trastuzumab emtansine versus treatment of physician's choice for pretreated HER2-positive advanced breast cancer (TH3RESA): a randomised, open-label, phase 3 trial.* The Lancet Oncology, 2014. **15**(7): p. 689-699.

240. Von Minckwitz, G., et al., *Trastuzumab emtansine for residual invasive HER2-positive breast cancer.* New England Journal of Medicine, 2019. **380**(7): p. 617-628.

241. Modi, S., et al., *Trastuzumab deruxtecan in previously treated HER2-positive breast cancer.* New England Journal of Medicine, 2020. **382**(7): p. 610-621.

242. Yan, H., et al., *Association between the HER2 protein expression level and the efficacy of neoadjuvant chemotherapy in HER2-positive breast cancer.* Cancer Management and Research, 2020. **12**: p. 12715.

243. Rakha, E.A., et al., *Retrospective observational study of HER2 immunohistochemistry in borderline breast cancer patients undergoing neoadjuvant therapy, with an emphasis on Group 2 (HER2/CEP17*

ratio≥ 2.0, HER2 copy number< 4.0 signals/cell) cases. British journal of cancer, 2021. **124**(11): p. 1836-1842.

244. Xu, B., et al., *HER2 protein expression level is positively associated with the efficacy of neoadjuvant systemic therapy in HER2-positive breast cancer.* Pathology-Research and Practice, 2022. **234**: p. 153900.

245. Zhao, J., et al., *HER2 immunohistochemistry staining positivity is strongly predictive of tumor response to neoadjuvant chemotherapy in HER2 positive breast cancer.* Pathology-Research and Practice, 2020. **216**(11): p. 153155.

246. Chen, H.-l., Q. Chen, and Y.-c. Deng, *Pathologic complete response to neoadjuvant anti-HER2 therapy is associated with HER2 immunohistochemistry score in HER2-positive early breast cancer.* Medicine, 2021. **100**(44).

247. Capelan, M., et al., *Pertuzumab: new hope for patients with HER2-positive breast cancer.* Annals of oncology, 2013. **24**(2): p. 273-282.

248. Junttila, T.T., et al., *Ligand-independent HER2/HER3/PI3K complex is disrupted by trastuzumab and is effectively inhibited by the PI3K inhibitor GDC-0941.* Cancer cell, 2009. **15**(5): p. 429-440.

249. Molina, M.A., et al., *Trastuzumab (herceptin), a humanized anti-Her2 receptor monoclonal antibody, inhibits basal and activated Her2 ectodomain cleavage in breast cancer cells.* Cancer research, 2001. **61**(12): p. 4744-4749.

250. Collins, D.M., et al., *Preclinical characteristics of the irreversible pan-HER kinase inhibitor neratinib compared with lapatinib: implications for the treatment of HER2-positive and HER2-mutated breast cancer.* Cancers, 2019. **11**(6): p. 737.

251. Swain, S.M., M. Shastry, and E. Hamilton, *Targeting HER2-positive breast cancer: Advances and future directions.* Nature Reviews Drug Discovery, 2023. **22**(2): p. 101-126.

252. Montemurro, F., G. Valabrega, and M. Aglietta, *Lapatinib: a dual inhibitor of EGFR and HER2 tyrosine kinase activity.* Expert opinion on biological therapy, 2007. **7**(2): p. 257-268.

253. Rabindran, S.K., et al., *Antitumor activity of HKI-272, an orally active, irreversible inhibitor of the HER-2 tyrosine kinase.* Cancer research, 2004. **64**(11): p. 3958-3965.

254. LoRusso, P.M., et al., *Trastuzumab emtansine: a unique antibody-drug conjugate in development for human epidermal growth factor receptor 2–positive cancer.* Clinical Cancer Research, 2011. **17**(20): p. 6437-6447.

255. Cardoso, F., et al., *Early breast cancer: ESMO Clinical Practice Guidelines for diagnosis, treatment and follow-up.* Annals of oncology, 2019. **30**(8): p. 1194-1220.

256. Curigliano, G., et al., *De-escalating and escalating treatments for early-stage breast cancer: the St. Gallen International Expert*

Consensus Conference on the Primary Therapy of Early Breast Cancer 2017. Annals of Oncology, 2017. **28**(8): p. 1700-1712.

257. Buzdar, A.U., et al., *Fluorouracil, epirubicin, and cyclophosphamide (FEC-75) followed by paclitaxel plus trastuzumab versus paclitaxel plus trastuzumab followed by FEC-75 plus trastuzumab as neoadjuvant treatment for patients with HER2-positive breast cancer (Z1041): a randomised, controlled, phase 3 trial.* The Lancet Oncology, 2013. **14**(13): p. 1317-1325.

258. Buzdar, A.U., et al., *Neoadjuvant therapy with paclitaxel followed by 5-fluorouracil, epirubicin, and cyclophosphamide chemotherapy and concurrent trastuzumab in human epidermal growth factor receptor 2–positive operable breast cancer: an update of the initial randomized study population and data of additional patients treated with the same regimen.* Clinical Cancer Research, 2007. **13**(1): p. 228-233.

259. Gianni, L., et al., *Neoadjuvant chemotherapy with trastuzumab followed by adjuvant trastuzumab versus neoadjuvant chemotherapy alone, in patients with HER2-positive locally advanced breast cancer (the NOAH trial): a randomised controlled superiority trial with a parallel HER2-negative cohort.* The Lancet, 2010. **375**(9712): p. 377-384.

260. Untch, M., et al., *Neoadjuvant treatment with trastuzumab in HER2-positive breast cancer: results from the GeparQuattro study.* Journal of Clinical Oncology, 2010. **28**(12): p. 2024-2031.

261. Cortazar, P., et al., *Pathological complete response and long-term clinical benefit in breast cancer: the CTNeoBC pooled analysis.* The Lancet, 2014. **384**(9938): p. 164-172.

262. Untch, M., et al., *Pathologic complete response after neoadjuvant chemotherapy plus trastuzumab predicts favorable survival in human epidermal growth factor receptor 2–overexpressing breast cancer: results from the TECHNO trial of the AGO and GBG study groups.* Journal of Clinical Oncology, 2011. **29**(25): p. 3351-3357.

263. Baselga, J., et al., *Lapatinib with trastuzumab for HER2-positive early breast cancer (NeoALTTO): a randomised, open-label, multicentre, phase 3 trial.* The Lancet, 2012. **379**(9816): p. 633-640.

264. Carey, L.A., et al., *Molecular heterogeneity and response to neoadjuvant human epidermal growth factor receptor 2 targeting in CALGB 40601, a randomized phase III trial of paclitaxel plus trastuzumab with or without lapatinib.* Journal of Clinical Oncology, 2016. **34**(6): p. 542.

265. Robidoux, A., et al., *Lapatinib as a component of neoadjuvant therapy for HER2-positive operable breast cancer (NSABP protocol B-41): an open-label, randomised phase 3 trial.* The lancet oncology, 2013. **14**(12): p. 1183-1192.

266. Gianni, L., et al., *Efficacy and safety of neoadjuvant pertuzumab and trastuzumab in women with locally advanced, inflammatory, or early*

HER2-positive breast cancer (NeoSphere): a randomised multicentre, open-label, phase 2 trial. The lancet oncology, 2012. **13**(1): p. 25-32.

267. Moja, L., et al., *Trastuzumab containing regimens for early breast cancer.* Cochrane database of systematic reviews, 2012(4).

268. Romond, E.H., et al., *Trastuzumab plus adjuvant chemotherapy for operable HER2-positive breast cancer.* New England journal of medicine, 2005. **353**(16): p. 1673-1684.

269. Earl, H.M., et al., *6 versus 12 months of adjuvant trastuzumab for HER2-positive early breast cancer (PERSEPHONE): 4-year disease-free survival results of a randomised phase 3 non-inferiority trial.* The Lancet, 2019. **393**(10191): p. 2599-2612.

270. von Minckwitz, G., et al., *Trastuzumab Emtansine for Residual Invasive HER2-Positive Breast Cancer.* New England Journal of Medicine, 2018. **380**(7): p. 617-628.

271. Ogitani, Y., et al., *Bystander killing effect of DS-8201a, a novel anti-human epidermal growth factor receptor 2 antibody–drug conjugate, in tumors with human epidermal growth factor receptor 2 heterogeneity.* Cancer science, 2016. **107**(7): p. 1039-1046.

272. Modi, S., *Trastuzumab deruxtecan in previously treated HER2-positive metastatic breast cancer: plain language summary of the DESTINY-Breast01 study.* Future oncology, 2021. **17**(26): p. 3415-3424.

273. André, F., et al., *Trastuzumab deruxtecan versus treatment of physician's choice in patients with HER2-positive metastatic breast cancer (DESTINY-Breast02): a randomised, open-label, multicentre, phase 3 trial.* The Lancet, 2023. **401**(10390): p. 1773-1785.

274. Cortés, J., et al., *Trastuzumab deruxtecan versus trastuzumab emtansine for breast cancer.* New England Journal of Medicine, 2022. **386**(12): p. 1143-1154.

275. Hurvitz, S.A., et al., *Trastuzumab deruxtecan versus trastuzumab emtansine in patients with HER2-positive metastatic breast cancer: updated results from DESTINY-Breast03, a randomised, open-label, phase 3 trial.* The Lancet, 2023. **401**(10371): p. 105-117.

276. Antonarelli, G., et al., *Management of patients with HER2-positive metastatic breast cancer after trastuzumab deruxtecan failure.* ESMO open, 2023. **8**(4): p. 101608.

277. Sánchez-Lorenzo, L., et al. *Current management and future perspectives in metastatic HER2-positive breast cancer*. in *Seminars in Oncology Nursing*. 2024. Elsevier.

278. Miles, D., et al., *Final results from the PERUSE study of first-line pertuzumab plus trastuzumab plus a taxane for HER2-positive locally recurrent or metastatic breast cancer, with a multivariable approach to guide prognostication.* Annals of Oncology, 2021. **32**(10): p. 1245-1255.

279. Arpino, G., et al., *Pertuzumab, Trastuzumab, and an Aromatase Inhibitor for HER2-Positive and Hormone Receptor–Positive Metastatic or Locally Advanced Breast Cancer: PERTAIN Final Analysis.* Clinical Cancer Research, 2023. **29**(8): p. 1468-1476.

280. Verma, S., et al., *Trastuzumab Emtansine for HER2-Positive Advanced Breast Cancer.* New England Journal of Medicine, 2012. **367**(19): p. 1783-1791.

281. Krop, I.E., et al., *Trastuzumab emtansine versus treatment of physician's choice in patients with previously treated HER2-positive metastatic breast cancer (TH3RESA): final overall survival results from a randomised open-label phase 3 trial.* The Lancet Oncology, 2017. **18**(6): p. 743-754.

282. Curigliano, G., et al., *Tucatinib versus placebo added to trastuzumab and capecitabine for patients with pretreated HER2+ metastatic breast cancer with and without brain metastases (HER2CLIMB): final overall survival analysis.* Annals of Oncology, 2022. **33**(3): p. 321-329.

283. Rugo, H.S., et al., *Margetuximab Versus Trastuzumab in Patients With Previously Treated HER2-Positive Advanced Breast Cancer (SOPHIA): Final Overall Survival Results From a Randomized Phase 3 Trial.* Journal of Clinical Oncology, 2023. **41**(2): p. 198-205.

284. Vernieri, C., et al., *Resistance mechanisms to anti-HER2 therapies in HER2-positive breast cancer: Current knowledge, new research*

directions and therapeutic perspectives. Critical reviews in oncology/hematology, 2019. **139**: p. 53-66.

285. Giugliano, F., et al., *Unlocking the Resistance to Anti-HER2 Treatments in Breast Cancer: The Issue of HER2 Spatial Distribution.* Cancers, 2023. **15**(5): p. 1385.

286. Sperinde, J., et al., *Quantitation of p95HER2 in paraffin sections by using a p95-specific antibody and correlation with outcome in a cohort of trastuzumab-treated breast cancer patients.* Clinical Cancer Research, 2010. **16**(16): p. 4226-4235.

287. Loibl, S., et al., *Validation of p95 as a predictive marker for trastuzumab-based therapy in primary HER2-positive breast cancer: a translational investigation from the neoadjuvant GeparQuattro study.* Journal of Clinical Oncology, 2011. **29**(15_suppl): p. 530-530.

288. Castiglioni, F., et al., *Role of exon-16-deleted HER2 in breast carcinomas.* Endocrine-related cancer, 2006. **13**(1): p. 221-232.

289. Castagnoli, L., et al., *Activated d16HER2 homodimers and SRC kinase mediate optimal efficacy for trastuzumab.* Cancer research, 2014. **74**(21): p. 6248-6259.

290. Palladini, A., et al., *HER2 isoforms co-expression differently tunes mammary tumor phenotypes affecting onset, vasculature and therapeutic response.* Oncotarget, 2017. **8**(33): p. 54444.

291. Nagy, P., et al., *Decreased accessibility and lack of activation of ErbB2 in JIMT-1, a herceptin-resistant, MUC4-expressing breast cancer cell line.* Cancer research, 2005. **65**(2): p. 473-482.

292. Zhang, S., et al., *Combating trastuzumab resistance by targeting SRC, a common node downstream of multiple resistance pathways.* Nature medicine, 2011. **17**(4): p. 461-469.

293. Scaltriti, M., et al., *Cyclin E amplification/overexpression is a mechanism of trastuzumab resistance in HER2+ breast cancer patients.* Proceedings of the National Academy of Sciences, 2011. **108**(9): p. 3761-3766.

294. Berns, K., et al., *A functional genetic approach identifies the PI3K pathway as a major determinant of trastuzumab resistance in breast cancer.* Cancer cell, 2007. **12**(4): p. 395-402.

295. Kataoka, Y., et al., *Association between gain-of-function mutations in PIK3CA and resistance to HER2-targeted agents in HER2-amplified breast cancer cell lines.* Annals of Oncology, 2010. **21**(2): p. 255-262.

296. Chandarlapaty, S., et al., *Frequent mutational activation of the PI3K-AKT pathway in trastuzumab-resistant breast cancer.* Clinical Cancer Research, 2012. **18**(24): p. 6784-6791.

297. Nagata, Y., et al., *PTEN activation contributes to tumor inhibition by trastuzumab, and loss of PTEN predicts trastuzumab resistance in patients.* Cancer cell, 2004. **6**(2): p. 117-127.

298. Dave, B., et al., *Loss of phosphatase and tensin homolog or phosphoinositol-3 kinase activation and response to trastuzumab or lapatinib in human epidermal growth factor receptor 2–overexpressing locally advanced breast cancers.* Journal of clinical oncology, 2011. **29**(2): p. 166.

299. Elster, N., et al., *A preclinical evaluation of the PI3K alpha/delta dominant inhibitor BAY 80-6946 in HER2-positive breast cancer models with acquired resistance to the HER2-targeted therapies trastuzumab and lapatinib.* Breast cancer research and treatment, 2015. **149**: p. 373-383.

300. Lu, C.-H., et al., *Preclinical testing of clinically applicable strategies for overcoming trastuzumab resistance caused by PTEN deficiency.* Clinical Cancer Research, 2007. **13**(19): p. 5883-5888.

301. O'Brien, N.A., et al., *Targeting PI3K/mTOR overcomes resistance to HER2-targeted therapy independent of feedback activation of AKT.* Clinical Cancer Research, 2014. **20**(13): p. 3507-3520.

302. Loibl, S., et al., *PIK3CA mutations are associated with reduced pathological complete response rates in primary HER2-positive breast cancer: pooled analysis of 967 patients from five prospective trials investigating lapatinib and trastuzumab.* Annals of Oncology, 2016. **27**(8): p. 1519-1525.

303. Hellyer, N.J., M.-S. Kim, and J.G. Koland, *Heregulin-dependent activation of phosphoinositide 3-kinase and Akt via the ErbB2/ErbB3*

co-receptor. Journal of Biological Chemistry, 2001. **276**(45): p. 42153-42161.

304. Ritter, C.A., et al., *Human breast cancer cells selected for resistance to trastuzumab in vivo overexpress epidermal growth factor receptor and ErbB ligands and remain dependent on the ErbB receptor network.* Clinical Cancer Research, 2007. **13**(16): p. 4909-4919.

305. Sergina, N.V., et al., *Escape from HER-family tyrosine kinase inhibitor therapy by the kinase-inactive HER3.* Nature, 2007. **445**(7126): p. 437-441.

306. Lu, Y., et al., *Insulin-like growth factor-I receptor signaling and resistance to trastuzumab (Herceptin).* Journal of the National Cancer Institute, 2001. **93**(24): p. 1852-1857.

307. Shattuck, D.L., et al., *Met receptor contributes to trastuzumab resistance of Her2-overexpressing breast cancer cells.* Cancer research, 2008. **68**(5): p. 1471-1477.

308. Wang, Y.-C., et al., *Different mechanisms for resistance to trastuzumab versus lapatinib in HER2-positive breast cancers-role of estrogen receptor and HER2 reactivation.* Breast Cancer Research, 2011. **13**: p. 1-19.

309. Zhuang, G., et al., *Elevation of receptor tyrosine kinase EphA2 mediates resistance to trastuzumab therapy.* Cancer research, 2010. **70**(1): p. 299-308.

310. Landis, M.W., et al., *Cyclin D1-dependent kinase activity in murine development and mammary tumorigenesis.* Cancer cell, 2006. **9**(1): p. 13-22.

311. Finn, R.S., et al., *PD 0332991, a selective cyclin D kinase 4/6 inhibitor, preferentially inhibits proliferation of luminal estrogen receptor-positive human breast cancer cell lines in vitro.* Breast Cancer Research, 2009. **11**(5): p. 1-13.

312. Gianni, L., et al., *Neoadjuvant treatment with trastuzumab and pertuzumab plus palbociclib and fulvestrant in HER2-positive, ER-positive breast cancer (NA-PHER2): an exploratory, open-label, phase 2 study.* The Lancet Oncology, 2018. **19**(2): p. 249-256.

313. Goel, S., et al., *Overcoming therapeutic resistance in HER2-positive breast cancers with CDK4/6 inhibitors.* Cancer cell, 2016. **29**(3): p. 255-269.

314. Clynes, R.A., et al., *Inhibitory Fc receptors modulate in vivo cytoxicity against tumor targets.* Nature medicine, 2000. **6**(4): p. 443-446.

315. Martinez, V.G., et al., *Resistance to HER2-targeted anti-cancer drugs is associated with immune evasion in cancer cells and their derived extracellular vesicles.* Oncoimmunology, 2017. **6**(12): p. e1362530.

316. Loi, S., et al. *Phase Ib/II study evaluating safety and efficacy of pembrolizumab and trastuzumab in patients with trastuzumab-resistant HER2-positive advanced breast cancer: results from the*

PANACEA study (IBCSG 45-13/BIG 4-13/KEYNOTE-014). in *SABCS*. 2017.

317. Rexer, B.N., et al., *Human breast cancer cells harboring a gatekeeper T798M mutation in HER2 overexpress EGFR ligands and are sensitive to dual inhibition of EGFR and HER2.* Clinical Cancer Research, 2013. **19**(19): p. 5390-5401.

318. Hyman, D.M., et al., *HER kinase inhibition in patients with HER2-and HER3-mutant cancers.* Nature, 2018. **554**(7691): p. 189-194.

319. Beitsch, P., et al., *Pertuzumab/trastuzumab/CT versus trastuzumab/CT therapy for HER2+ breast cancer: results from the prospective neoadjuvant breast registry symphony trial (NBRST).* Annals of Surgical Oncology, 2017. **24**(9): p. 2539-2546.

320. Schneeweiss, A., et al., *Pertuzumab plus trastuzumab in combination with standard neoadjuvant anthracycline-containing and anthracycline-free chemotherapy regimens in patients with HER2-positive early breast cancer: a randomized phase II cardiac safety study (TRYPHAENA).* Annals of oncology, 2013. **24**(9): p. 2278-2284.

321. Swain, S., et al., *Pertuzumab, trastuzumab, and standard anthracycline-and taxane-based chemotherapy for the neoadjuvant treatment of patients with HER2-positive localized breast cancer (BERENICE): a phase II, open-label, multicenter, multinational cardiac safety study.* Annals of oncology, 2018. **29**(3): p. 646-653.

322. Giuliano, M., M.V. Trivedi, and R. Schiff, *Bidirectional Crosstalk between the Estrogen Receptor and Human Epidermal Growth Factor Receptor 2 Signaling Pathways in Breast Cancer: Molecular Basis and Clinical Implications.* Breast Care (Basel), 2013. **8**(4): p. 256-62.

323. Houssami, N., et al., *Meta-analysis of the association of breast cancer subtype and pathologic complete response to neoadjuvant chemotherapy.* European journal of cancer, 2012. **48**(18): p. 3342-3354.

324. Harbeck, N., et al., *De-Escalation Strategies in Human Epidermal Growth Factor Receptor 2 (HER2)–Positive Early Breast Cancer (BC): Final Analysis of the West German Study Group Adjuvant Dynamic Marker-Adjusted Personalized Therapy Trial Optimizing Risk Assessment and Therapy Response Prediction in Early BC HER2- and Hormone Receptor–Positive Phase II Randomized Trial—Efficacy, Safety, and Predictive Markers for 12 Weeks of Neoadjuvant Trastuzumab Emtansine With or Without Endocrine Therapy (ET) Versus Trastuzumab Plus ET.* Journal of Clinical Oncology, 2017. **35**(26): p. 3046-3054.

325. Cejalvo, J.M., et al., *Intrinsic subtypes and gene expression profiles in primary and metastatic breast cancer.* Cancer research, 2017. **77**(9): p. 2213-2221.

326. Prat, A., et al., *Research-based PAM50 subtype predictor identifies higher responses and improved survival outcomes in HER2-positive*

breast cancer in the NOAH study. Clin Cancer Res, 2014. **20**(2): p. 511-21.

327. Brandão, M., et al., *What Is the Real Impact of Estrogen Receptor Status on the Prognosis and Treatment of HER2-Positive Early Breast Cancer?* Clin Cancer Res, 2020. **26**(12): p. 2783-2788.

328. Pernas, S. and S.M. Tolaney, *Targeting HER2 heterogeneity in early-stage breast cancer.* Current Opinion in Oncology, 2020. **32**(6): p. 545-554.

329. von Minckwitz, G., et al., *Survival after adding capecitabine and trastuzumab to neoadjuvant anthracycline-taxane-based chemotherapy for primary breast cancer (GBG 40--GeparQuattro).* Ann Oncol, 2014. **25**(1): p. 81-9.

330. Rakha, E.A., K. Vougas, and P.H. Tan, *Digital technology in diagnostic breast pathology and immunohistochemistry.* Pathobiology, 2022. **89**(5): p. 334-342.

331. Williams, B., et al., *Digital pathology for primary diagnosis of screen-detected breast lesions–experimental data, validation and experience from 4 centres.* Histopathology, 2020.

332. Williams, B.J., et al., *Digital pathology for the primary diagnosis of breast histopathological specimens: an innovative validation and concordance study on digital pathology validation and training.* Histopathology, 2018. **72**(4): p. 662-671.

333. Al-Janabi, S., et al., *Whole slide images as a platform for initial diagnostics in histopathology in a medium-sized routine laboratory.* Journal of clinical pathology, 2012. **65**(12): p. 1107-1111.

334. Abels, E., et al., *Computational pathology definitions, best practices, and recommendations for regulatory guidance: a white paper from the Digital Pathology Association.* J Pathol, 2019. **249**(3): p. 286-294.

335. Al-Janabi, S., A. Huisman, and P.J. Van Diest, *Digital pathology: current status and future perspectives.* Histopathology, 2012. **61**(1): p. 1-9.

336. Rocha, R., et al., *Digital slides: present status of a tool for consultation, teaching, and quality control in pathology.* Pathology-Research and Practice, 2009. **205**(11): p. 735-741.

337. Dee, F.R., *Virtual microscopy in pathology education.* Human pathology, 2009. **40**(8): p. 1112-1121.

338. Nielsen, P.S., et al., *Virtual microscopy: an evaluation of its validity and diagnostic performance in routine histologic diagnosis of skin tumors.* Human pathology, 2010. **41**(12): p. 1770-1776.

339. Li, X., et al., *A feasibility study of virtual slides in surgical pathology in China.* Human pathology, 2007. **38**(12): p. 1842-1848.

340. Amin, M., et al., *Integration of digital gross pathology images for enterprise-wide access.* Journal of Pathology Informatics, 2012. **3**(1): p. 10.

341. Evans, A.J., et al., *US Food and Drug Administration approval of whole slide imaging for primary diagnosis: a key milestone is reached and new questions are raised.* Archives of pathology & laboratory medicine, 2018. **142**(11): p. 1383-1387.

342. Menter, T., et al., *Intraoperative frozen section consultation by remote whole-slide imaging analysis–validation and comparison to robotic remote microscopy.* Journal of clinical pathology, 2020. **73**(6): p. 350-352.

343. Robertson, S., et al., *Digital image analysis in breast pathology—from image processing techniques to artificial intelligence.* Translational Research, 2018. **194**: p. 19-35.

344. Jackson, S.L., et al., *Diagnostic Reproducibility: What Happens When the Same Pathologist Interprets the Same Breast Biopsy Specimen at Two Points in Time?* Ann Surg Oncol, 2017. **24**(5): p. 1234-1241.

345. Ram, S., et al., *Pixelwise H-score: A novel digital image analysis-based metric to quantify membrane biomarker expression from immunohistochemistry images.* PLoS One, 2021. **16**(9): p. e0245638.

346. Bankhead, P., et al., *QuPath: Open source software for digital pathology image analysis.* Scientific Reports, 2017. **7**(1): p. 16878.

347. Ibrahim, A., et al., *Artificial intelligence in digital breast pathology: techniques and applications.* The Breast, 2020. **49**: p. 267-273.

348. Pallua, J.D., et al., *The future of pathology is digital.* Pathology - Research and Practice, 2020. **216**(9): p. 153040.

349. Jahn, S.W., M. Plass, and F. Moinfar, *Digital Pathology: Advantages, Limitations and Emerging Perspectives.* J Clin Med, 2020. **9**(11).

350. Bishop, C.M., *Pattern recognition and machine learning*. 2006: springer.

351. Haykin, S., *Neural networks: a comprehensive foundation*. 2007: Prentice-Hall, Inc.

352. Ehteshami Bejnordi, B., et al., *Diagnostic Assessment of Deep Learning Algorithms for Detection of Lymph Node Metastases in Women With Breast Cancer.* JAMA, 2017. **318**(22): p. 2199-2210.

353. Harmon, S.A., et al., *Multiresolution application of artificial intelligence in digital pathology for prediction of positive lymph nodes from primary tumors in bladder cancer.* JCO clinical cancer informatics, 2020. **4**: p. 367-382.

354. Colling, R., et al., *Artificial intelligence in digital pathology: a roadmap to routine use in clinical practice.* The Journal of pathology, 2019. **249**(2): p. 143-150.

355. Couture, H.D., et al., *Image analysis with deep learning to predict breast cancer grade, ER status, histologic subtype, and intrinsic subtype.* NPJ breast cancer, 2018. **4**(1): p. 1-8.

356. Andre, F., N. Ismaila, and V. Stearns, *Use of Biomarkers to Guide Decisions on Adjuvant Systemic Therapy for Women With Early-Stage Invasive Breast Cancer: ASCO Clinical Practice Guideline Update Summary.* Journal of Oncology Practice, 2019. **15**(9): p. 495-497.

357. Thomson, T.A., et al., *HER-2/neu in breast cancer: Interobserver variability and performance of immunohistochemistry with 4 antibodies compared with fluorescent in situ hybridization.* Modern Pathology, 2001. **14**(11): p. 1079-1086.

358. Mengel, M., et al., *Inter-laboratory and inter-observer reproducibility of immunohistochemical assessment of the Ki-67 labelling index in a large multi-centre trial.* The Journal of Pathology, 2002. **198**(3): p. 292-299.

359. Shamai, G., et al., *Artificial Intelligence Algorithms to Assess Hormonal Status From Tissue Microarrays in Patients With Breast Cancer.* JAMA Network Open, 2019. **2**(7): p. e197700-e197700.

360. Senaras, C., et al. *Creating synthetic digital slides using conditional generative adversarial networks: application to Ki67 staining*. in *Medical Imaging 2018: Digital Pathology*. 2018. International Society for Optics and Photonics.

361. Osareh, A. and B. Shadgar. *Machine learning techniques to diagnose breast cancer*. in *2010 5th International Symposium on Health Informatics and Bioinformatics*. 2010.

362. Ferroni, P., et al., *Breast cancer prognosis using a machine learning approach.* Cancers, 2019. **11**(3): p. 328.

363. Wulczyn, E., et al., *Deep learning-based survival prediction for multiple cancer types using histopathology images.* PLoS One, 2020. **15**(6): p. e0233678.

364. Wahab, N., et al., *AI-enabled routine H&E image based prognostic marker for early-stage luminal breast cancer.* npj Precision Oncology, 2023. **7**(1): p. 122.

365. Colotta, F., et al., *Cancer-related inflammation, the seventh hallmark of cancer: links to genetic instability.* Carcinogenesis, 2009. **30**(7): p. 1073-1081.

366. Sun, P., et al., *A computational tumor-infiltrating lymphocyte assessment method comparable with visual reporting guidelines for triple-negative breast cancer.* EBioMedicine, 2021. **70**.

367. Brügmann, A., et al., *Digital image analysis of membrane connectivity is a robust measure of HER2 immunostains.* Breast cancer research and treatment, 2012. **132**: p. 41-49.

368. Hartage, R., et al., *A validation study of human epidermal growth factor receptor 2 immunohistochemistry digital imaging analysis and its correlation with human epidermal growth factor receptor 2 fluorescence in situ hybridization results in breast carcinoma.* Journal of pathology informatics, 2020. **11**(1): p. 2.

369. Koopman, T., et al., *What is the added value of digital image analysis of HER 2 immunohistochemistry in breast cancer in clinical practice? A study with multiple platforms.* Histopathology, 2019. **74**(6): p. 917-924.

370. Wang, S., et al., *Assessment of HER-2/neu Status in Breast Cancer: Automated Cellular Imaging System (ACIS)-Assisted Quantitation of Immunohistochemical Assay Achieves High Accuracy in Comparison With Fluorescence In Situ Hybridization Assay as the Standard.* American Journal of Clinical Pathology, 2001. **116**(4): p. 495-503.

371. Rexhepaj, E., et al., *Novel image analysis approach for quantifying expression of nuclear proteins assessed by immunohistochemistry: application to measurement of oestrogen and progesterone receptor levels in breast cancer.* Breast Cancer Research, 2008. **10**(5): p. R89.

372. Skaland, I., et al., *Comparing subjective and digital image analysis HER2/neu expression scores with conventional and modified FISH scores in breast cancer.* Journal of Clinical Pathology, 2008. **61**(1): p. 68.

373. Oliveira, S.P., et al., *Weakly-supervised classification of HER2 expression in breast cancer haematoxylin and eosin stained slides.* Applied Sciences, 2020. **10**(14): p. 4728.

374. Lu, W., et al., *SlideGraph+: Whole slide image level graphs to predict HER2 status in breast cancer.* Medical Image Analysis, 2022. **80**: p. 102486.

375. Bui, M.M., et al., *Quantitative image analysis of human epidermal growth factor receptor 2 immunohistochemistry for breast cancer: Guideline from the College of American Pathologists.* Archives of pathology & laboratory medicine, 2019. **143**(10): p. 1180-1195.

376. Furrer, D., et al., *Validation of a new classifier for the automated analysis of the human epidermal growth factor receptor 2 (HER2) gene amplification in breast cancer specimens.* Diagnostic pathology, 2013. **8**: p. 1-10.

377. Nitta, H., et al., *The assessment of HER2 status in breast cancer: the past, the present, and the future.* Pathology international, 2016. **66**(6): p. 313-324.

378. Prins, M.J., et al., *Evaluation of the HER2 amplification status in oesophageal adenocarcinoma by conventional and automated FISH: a tissue microarray study.* Journal of clinical pathology, 2014. **67**(1): p. 26-32.

379. Reljin, B., et al., *Breast cancer evaluation by fluorescent dot detection using combined mathematical morphology and multifractal techniques.* Diagnostic Pathology, 2011. **6**(1): p. S21.

380. Tafe, L.J., et al., *Automated processing of fluorescence in-situ hybridization slides for HER2 testing in breast and gastro-esophageal carcinomas.* Experimental and Molecular Pathology, 2014. **97**(1): p. 116-119.

381. Theodosiou, Z., et al., *Evaluation of FISH image analysis system on assessing HER2 amplification in breast carcinoma cases.* The Breast, 2008. **17**(1): p. 80-84.

382. Kohlberger, T., et al., *Whole-slide image focus quality: Automatic assessment and impact on ai cancer detection.* Journal of pathology informatics, 2019. **10**.

383. Cruz-Roa, A., et al., *Accurate and reproducible invasive breast cancer detection in whole-slide images: A Deep Learning approach for quantifying tumor extent.* Scientific reports, 2017. **7**(1): p. 1-14.

384. Doyle, S., et al., *A boosted Bayesian multiresolution classifier for prostate cancer detection from digitized needle biopsies.* IEEE transactions on biomedical engineering, 2010. **59**(5): p. 1205-1218.

385. Rakha, E.A., et al., *The prognostic significance of lymphovascular invasion in invasive breast carcinoma.* Cancer, 2012. **118**(15): p. 3670-3680.

386. Aleskandarany, M.A., et al., *Prognostic significance of androgen receptor expression in invasive breast cancer: transcriptomic and protein expression analysis.* Breast Cancer Res Treat, 2016. **159**(2): p. 215-27.

387. Rakha, E.A., et al., *Prognostic stratification of oestrogen receptor-positive HER2-negative lymph node-negative class of breast cancer.* Histopathology, 2017. **70**(4): p. 622-631.

388. Rakha, E.A., et al., *Triple-negative breast cancer: distinguishing between basal and nonbasal subtypes.* Clin Cancer Res, 2009. **15**(7): p. 2302-10.

389. Muftah, A.A., et al., *Ki67 expression in invasive breast cancer: the use of tissue microarrays compared with whole tissue sections.* Breast Cancer Res Treat, 2017. **164**(2): p. 341-348.

390. Urruticoechea, A., I.E. Smith, and M. Dowsett, *Proliferation marker Ki-67 in early breast cancer.* Journal of clinical oncology, 2005. **23**(28): p. 7212-7220.

391. Goldhirsch, A., et al., *Strategies for subtypes--dealing with the diversity of breast cancer: highlights of the St. Gallen International Expert Consensus on the Primary Therapy of Early Breast Cancer 2011.* Ann Oncol, 2011. **22**(8): p. 1736-47.

392. Rakha, E.A., et al., *Prognostic significance of Nottingham histologic grade in invasive breast carcinoma.* J Clin Oncol, 2008. **26**(19): p. 3153-8.

393. Health, N.I.f. and C. Excellence, *Gene expression profiling and expanded immunohistochemistry tests to guide the use of adjuvant chemotherapy in breast cancer management: MammaPrint, Oncotype DX, IHC4 and Mammostrat*. 2012, National Institute for Health and Clinical Excellence London.

394. Bear, H.D., et al., *Using the 21-gene assay from core needle biopsies to choose neoadjuvant therapy for breast cancer: a multicenter trial.* Journal of surgical oncology, 2017. **115**(8): p. 917-923.

395. Baehner, F.L., *The analytical validation of the Oncotype DX Recurrence Score assay.* ecancermedicalscience, 2016. **10**.

396. Curtis, C., et al., *The genomic and transcriptomic architecture of 2,000 breast tumours reveals novel subgroups.* Nature, 2012. **486**(7403): p. 346-352.

397. Wang, Z., M.A. Jensen, and J.C. Zenklusen, *A Practical Guide to The Cancer Genome Atlas (TCGA).* Methods Mol Biol, 2016. **1418**: p. 111-41.

398. Gutman, D.A., et al., *Cancer Digital Slide Archive: an informatics resource to support integrated in silico analysis of TCGA pathology data.* J Am Med Inform Assoc, 2013. **20**(6): p. 1091-8.

399. Koboldt, D., et al., *Comprehensive molecular portraits of human breast tumours.* Nature, 2012. **490**(7418): p. 61-70.

400. Fekete, J.T. and B. Győrffy, *ROCplot.org: Validating predictive biomarkers of chemotherapy/hormonal therapy/anti-HER2 therapy using transcriptomic data of 3,104 breast cancer patients.* International Journal of Cancer, 2019. **145**(11): p. 3140-3151.

401. Ilyas, M., et al., *Guidelines and considerations for conducting experiments using tissue microarrays.* Histopathology, 2013. **62**(6): p. 827-839.

402. Gustavson, M.D., D.L. Rimm, and M. Dolled-Filhart, *Tissue microarrays: leaping the gap between research and clinical adoption.* Personalized Medicine, 2013. **10**(5): p. 441-451.

403. Shergill, I.S., et al., *Tissue microarrays: a current medical research tool.* Current medical research and opinion, 2004. **20**(5): p. 707-712.

404. Dancau, A.-M., et al., *Tissue microarrays.* Cancer Gene Profiling: Methods and Protocols, 2016: p. 53-65.

405. Lacombe, A., et al., *Re-punching tissue microarrays is possible: why can this be useful and how to do it.* Microarrays, 2015. **4**(2): p. 245-254.

406. Allison, K.H., et al., *Estrogen and Progesterone Receptor Testing in Breast Cancer: ASCO/CAP Guideline Update.* J Clin Oncol, 2020. **38**(12): p. 1346-1366.

407. Cheang, M.C.U., et al., *Basal-Like Breast Cancer Defined by Five Biomarkers Has Superior Prognostic Value than Triple-Negative Phenotype.* Clinical Cancer Research, 2008. **14**(5): p. 1368-1376.

408. Zhen, H., et al., *Correlation analysis between molecular subtypes and Nottingham Prognostic Index in breast cancer.* Oncotarget, 2017. **8**(43): p. 74096-74105.

409. Yersal, O. and S. Barutca, *Biological subtypes of breast cancer: Prognostic and therapeutic implications.* World J Clin Oncol, 2014. **5**(3): p. 412-24.

410. McCarty, K.S., Jr. and K.S. McCarty, Sr., *Histochemical approaches to steroid receptor analyses.* Semin Diagn Pathol, 1984. **1**(4): p. 297-308.

411. Camp, R.L., M. Dolled-Filhart, and D.L. Rimm, *X-tile: a new bio-informatics tool for biomarker assessment and outcome-based cut-point optimization.* Clinical cancer research, 2004. **10**(21): p. 7252-7259.

412. Chaw, Y.F., et al., *Isolation and identification of cross-links from formaldehyde-treated nucleic acids.* Biochemistry, 1980. **19**(24): p. 5525-31.

413. Lin, Y., et al., *Optimization of FFPE preparation and identification of gene attributes associated with RNA degradation.* NAR Genom Bioinform, 2024. **6**(1): p. lqae008.

414. Zhao, J., et al., *Determination of HER2 gene amplification by chromogenic in situ hybridization (CISH) in archival breast carcinoma.* Modern Pathology, 2002. **15**(6): p. 657-665.

415. Jahanifar, M., et al. *Robust interactive semantic segmentation of pathology images with minimal user input*. in *Proceedings of the IEEE/CVF International Conference on Computer Vision*. 2021.

416. Graham, S., et al., *Hover-net: Simultaneous segmentation and classification of nuclei in multi-tissue histology images.* Medical Image Analysis, 2019. **58**: p. 101563.

417. Ronneberger, O., P. Fischer, and T. Brox. *U-net: Convolutional networks for biomedical image segmentation*. in *Medical Image Computing and Computer-Assisted Intervention–MICCAI 2015: 18th International Conference, Munich, Germany, October 5-9, 2015, Proceedings, Part III 18*. 2015. Springer.

418. Gamper, J., et al. *PanNuke: an open pan-cancer histology dataset for nuclei instance segmentation and classification*. in *Digital Pathology: 15th European Congress, ECDP 2019, Warwick, UK, April 10–13, 2019, Proceedings 15*. 2019. Springer.

419. Macenko, M., et al. *A method for normalizing histology slides for quantitative analysis*. in *2009 IEEE International Symposium on Biomedical Imaging: From Nano to Macro*. 2009.

420. Ruifrok, A.C. and D.A. Johnston, *Quantification of histochemical staining by color deconvolution.* Anal Quant Cytol Histol, 2001. **23**(4): p. 291-9.

421. Schmidt, U., et al. *Cell detection with star-convex polygons*. in *Medical Image Computing and Computer Assisted Intervention–MICCAI 2018: 21st International Conference, Granada, Spain, September 16-20, 2018, Proceedings, Part II 11*. 2018. Springer.

422. Stringer, C., et al., *Cellpose: a generalist algorithm for cellular segmentation.* Nature methods, 2021. **18**(1): p. 100-106.

423. Couetil, J., et al., *Predicting melanoma survival and metastasis with interpretable histopathological features and machine learning models.* Front Med (Lausanne), 2022. **9**: p. 1029227.

424. Bayat, A., *Science, medicine, and the future: Bioinformatics.* Bmj, 2002. **324**(7344): p. 1018-22.

425. Sun, K., *Ktrim: an extra-fast and accurate adapter- and quality-trimmer for sequencing data.* Bioinformatics, 2020. **36**(11): p. 3561-3562.

426. Dobin, A., et al., *STAR: ultrafast universal RNA-seq aligner.* Bioinformatics, 2013. **29**(1): p. 15-21.

427. Metsalu, T. and J. Vilo, *ClustVis: a web tool for visualizing clustering of multivariate data using Principal Component Analysis and heatmap.* Nucleic Acids Res, 2015. **43**(W1): p. W566-70.

428. Liao, Y., et al., *WebGestalt 2019: gene set analysis toolkit with revamped UIs and APIs.* Nucleic acids research, 2019. **47**(W1): p. W199-W205.

429. Shannon, P., et al., *Cytoscape: a software environment for integrated models of biomolecular interaction networks.* Genome research, 2003. **13**(11): p. 2498-2504.

430. Chin, C.-H., et al., *cytoHubba: identifying hub objects and sub-networks from complex interactome.* BMC Systems Biology, 2014. **8**(4): p. S11.

431. Chen, T. and C. Guestrin, *XGBoost: A Scalable Tree Boosting System*, in *Proceedings of the 22nd ACM SIGKDD International Conference on Knowledge Discovery and Data Mining*. 2016, Association for Computing Machinery: San Francisco, California, USA. p. 785–794.

432. Tarwidi, D., et al., *An optimized XGBoost-based machine learning method for predicting wave run-up on a sloping beach.* MethodsX, 2023. **10**: p. 102119.

433. Fawcett, T., *An introduction to ROC analysis.* Pattern recognition letters, 2006. **27**(8): p. 861-874.

434. Hanley, J.A. and B.J. McNeil, *The meaning and use of the area under a receiver operating characteristic (ROC) curve.* Radiology, 1982. **143**(1): p. 29-36.

435. Zweig, M.H. and G. Campbell, *Receiver-operating characteristic (ROC) plots: a fundamental evaluation tool in clinical medicine.* Clinical chemistry, 1993. **39**(4): p. 561-577.

436. Garcia Rojo, M., et al., *Digital pathology in Europe: coordinating patient care and research efforts.* Stud Health Technol Inform, 2009. **150**: p. 997-1001.

437. Al-Janabi, S., A. Huisman, and P.J. Van Diest, *Digital pathology: current status and future perspectives.* Histopathology, 2012. **61**(1): p. 1-9.

438. Caccomo, S. and F. Administration, *FDA allows marketing of first whole slide imaging system for digital pathology.* Administration FaD, editor.: US Department of Health and Human Services, 2017.

439. Mukhopadhyay, S., et al., *Whole slide imaging versus microscopy for primary diagnosis in surgical pathology: a multicenter blinded randomized noninferiority study of 1992 cases (pivotal study).* The American journal of surgical pathology, 2018. **42**(1): p. 39-52.

440. Fraggetta, F., et al., *The importance of eSlide macro images for primary diagnosis with whole slide imaging.* Journal of Pathology Informatics, 2018. **9**.

441. Williams, B.J. and D. Treanor, *Practical guide to training and validation for primary diagnosis with digital pathology.* Journal of Clinical Pathology, 2020. **73**(7): p. 418-422.

442. Hanna, M.G., et al., *Implementation of digital pathology offers clinical and operational increase in efficiency and cost savings.* Archives of pathology & laboratory medicine, 2019. **143**(12): p. 1545-1555.

443. Wright, A.M., et al., *Digital slide imaging in cervicovaginal cytology: a pilot study.* Archives of pathology and laboratory medicine, 2013. **137**(5): p. 618-624.

444. Williams, B.J., et al., *A systematic analysis of discordant diagnoses in digital pathology compared with light microscopy.* Archives of pathology & laboratory medicine, 2017. **141**(12): p. 1712-1718.

445. Pilewskie, M. and M. Morrow, *Margins in breast cancer: How much is enough?* Cancer, 2018. **124**(7): p. 1335-1341.

446. Rakha, E.A., et al., *Breast cancer histologic grading using digital microscopy: concordance and outcome association.* Journal of clinical pathology, 2018. **71**(8): p. 680-686.

447. Cross, S., et al., *Best practice recommendations for implementing digital pathology January 2018.* The Royal College of Pathologists, 2018.

448. Wright, A.I., et al., *The effect of quality control on accuracy of digital pathology image analysis.* IEEE Journal of Biomedical and Health Informatics, 2020.

449. Rakha, E.A., et al., *Current and future applications of artificial intelligence in pathology: a clinical perspective.* Journal of clinical pathology, 2021. **74**(7): p. 409-414.

450. Quail, D.F. and J.A. Joyce, *Microenvironmental regulation of tumor progression and metastasis.* Nat Med, 2013. **19**(11): p. 1423-37.

451. Dekker, T., et al., *Prognostic significance of the tumor-stroma ratio: validation study in node-negative premenopausal breast cancer patients from the EORTC perioperative chemotherapy (POP) trial*

(10854). Breast cancer research and treatment, 2013. **139**(2): p. 371-379.

452. Gujam, F., et al., *The relationship between the tumour stroma percentage, clinicopathological characteristics and outcome in patients with operable ductal breast cancer.* British journal of cancer, 2014. **111**(1): p. 157-165.

453. Micke, P., et al., *The prognostic impact of the tumour stroma fraction: A machine learning-based analysis in 16 human solid tumour types.* EBioMedicine, 2021. **65**: p. 103269.

454. Millar, E.K., et al., *Tumour stroma ratio assessment using digital image analysis predicts survival in triple negative and luminal breast cancer.* Cancers, 2020. **12**(12): p. 3749.

455. Moorman, A., et al., *The prognostic value of tumour-stroma ratio in triple-negative breast cancer.* European Journal of Surgical Oncology (EJSO), 2012. **38**(4): p. 307-313.

456. Roeke, T., et al., *The prognostic value of the tumour-stroma ratio in primary operable invasive cancer of the breast: a validation study.* Breast Cancer Research and Treatment, 2017. **166**(2): p. 435-445.

457. Staal, E.F.C., et al., *Reproducibility and validation of tumour stroma ratio scoring on oesophageal adenocarcinoma biopsies.* European Journal of Cancer, 2011. **47**(3): p. 375-382.

458. West, N., et al., *The proportion of tumour cells is an independent predictor for survival in colorectal cancer patients.* British journal of cancer, 2010. **102**(10): p. 1519-1523.

459. Lahrmann, B., et al., *Automatic tumor-stroma separation in fluorescence TMAs enables the quantitative high-throughput analysis of multiple cancer biomarkers.* PLoS One, 2011. **6**(12): p. e28048.

460. Sprenger, J., et al., *Toward a quantitative method for estimating tumour-stroma ratio in breast cancer using polarized light microscopy.* Biomedical Optics Express, 2021. **12**(6): p. 3241-3252.

461. Courrech Staal, E.F.W., et al., *Reproducibility and validation of tumour stroma ratio scoring on oesophageal adenocarcinoma biopsies.* European Journal of Cancer, 2011. **47**(3): p. 375-382.

462. Zhao, K., et al., *Artificial intelligence quantified tumour-stroma ratio is an independent predictor for overall survival in resectable colorectal cancer.* EBioMedicine, 2020. **61**: p. 103054.

463. van Pelt, G.W., et al., *The tumour–stroma ratio in colon cancer: the biological role and its prognostic impact.* Histopathology, 2018. **73**(2): p. 197-206.

464. Yu, K.-H., et al., *Predicting non-small cell lung cancer prognosis by fully automated microscopic pathology image features.* Nature communications, 2016. **7**(1): p. 1-10.

465. Yu, K.-H., A.L. Beam, and I.S. Kohane, *Artificial intelligence in healthcare.* Nature Biomedical Engineering, 2018. **2**(10): p. 719-731.

466. Bianconi, F., A. Álvarez-Larrán, and A. Fernández, *Discrimination between tumour epithelium and stroma via perception-based features.* Neurocomputing, 2015. **154**: p. 119-126.

467. Werb, Z. and P. Lu, *The Role of Stroma in Tumor Development.* Cancer J, 2015. **21**(4): p. 250-3.

468. Micke, P. and A. Ostman, *Tumour-stroma interaction: cancer-associated fibroblasts as novel targets in anti-cancer therapy?* Lung Cancer, 2004. **45 Suppl 2**: p. S163-75.

469. Egeblad, M. and Z. Werb, *New functions for the matrix metalloproteinases in cancer progression.* Nature Reviews Cancer, 2002. **2**(3): p. 161-174.

470. Kessenbrock, K., V. Plaks, and Z. Werb, *Matrix metalloproteinases: regulators of the tumor microenvironment.* Cell, 2010. **141**(1): p. 52-67.

471. Nguyen-Ngoc, K.-V., et al., *ECM microenvironment regulates collective migration and local dissemination in normal and malignant mammary epithelium.* Proceedings of the National Academy of Sciences, 2012. **109**(39): p. E2595-E2604.

472. Dotto, G.P., *Multifocal epithelial tumors and field cancerization: stroma as a primary determinant.* J Clin Invest, 2014. **124**(4): p. 1446-53.

473. Brennen, W.N., et al., *Targeting carcinoma-associated fibroblasts within the tumor stroma with a fibroblast activation protein-activated prodrug.* J Natl Cancer Inst, 2012. **104**(17): p. 1320-34.

474. Dauer, P., et al., *Inactivation of Cancer-Associated-Fibroblasts Disrupts Oncogenic Signaling in Pancreatic Cancer Cells and Promotes Its Regression.* Cancer Res, 2018. **78**(5): p. 1321-1333.

475. Gagliano, T., et al., *PIK3Cδ expression by fibroblasts promotes triple-negative breast cancer progression.* J Clin Invest, 2020. **130**(6): p. 3188-3204.

476. Leca, J., et al., *Cancer-associated fibroblast-derived annexin A6+ extracellular vesicles support pancreatic cancer aggressiveness.* J Clin Invest, 2016. **126**(11): p. 4140-4156.

477. Paulsson, J. and P. Micke, *Prognostic relevance of cancer-associated fibroblasts in human cancer.* Semin Cancer Biol, 2014. **25**: p. 61-8.

478. Strell, C., et al., *Impact of Epithelial-Stromal Interactions on Peritumoral Fibroblasts in Ductal Carcinoma in Situ.* J Natl Cancer Inst, 2019. **111**(9): p. 983-995.

479. Clocchiatti, A., et al., *Androgen receptor functions as transcriptional repressor of cancer-associated fibroblast activation.* J Clin Invest, 2018. **128**(12): p. 5531-5548.

480. Robin, F., et al., *Molecular profiling of stroma highlights stratifin as a novel biomarker of poor prognosis in pancreatic ductal adenocarcinoma.* Br J Cancer, 2020. **123**(1): p. 72-80.

481. Takahashi, Y., et al., *Fibrous stroma is associated with poorer prognosis in lung squamous cell carcinoma patients.* J Thorac Oncol, 2011. **6**(9): p. 1460-7.

482. Downey, C., et al., *The prognostic significance of tumour–stroma ratio in oestrogen receptor-positive breast cancer.* British journal of cancer, 2014. **110**(7): p. 1744-1747.

483. Downey, C.L., et al., *Prognostic significance of tumour stroma ratio in inflammatory breast cancer.* Springerplus, 2015. **4**: p. 68.

484. Yu, K.-H., et al., *Association of omics features with histopathology patterns in lung adenocarcinoma.* Cell systems, 2017. **5**(6): p. 620-627. e3.

485. Elston, C.W. and I.O. Ellis, *Pathological prognostic factors in breast cancer. I. The value of histological grade in breast cancer: experience from a large study with long-term follow-up.* Histopathology, 1991. **19**(5): p. 403-10.

486. Gieniec, K.A., et al., *Cancer-associated fibroblasts-heroes or villains?* Br J Cancer, 2019. **121**(4): p. 293-302.

487. Wahab, N., et al., *Semantic annotation for computational pathology: Multidisciplinary experience and best practice recommendations.* The Journal of Pathology: Clinical Research, 2022. **8**(2): p. 116-128.

488. Hagenaars, S.C., et al., *Standardization of the tumor-stroma ratio scoring method for breast cancer research.* Breast Cancer Res Treat, 2022. **193**(3): p. 545-553.

489. Heindl, A., S. Nawaz, and Y. Yuan, *Mapping spatial heterogeneity in the tumor microenvironment: a new era for digital pathology.* Laboratory Investigation, 2015. **95**(4): p. 377-384.

490. Fu, T., et al., *Spatial architecture of the immune microenvironment orchestrates tumor immunity and therapeutic response.* Journal of Hematology & Oncology, 2021. **14**(1): p. 98.

491. Vangangelt, K.M.H., et al., *The prognostic value of the tumor-stroma ratio is most discriminative in patients with grade III or triple-negative breast cancer.* Int J Cancer, 2020. **146**(8): p. 2296-2304.

492. Geessink, O.G.F., et al., *Computer aided quantification of intratumoral stroma yields an independent prognosticator in rectal cancer.* Cellular Oncology, 2019. **42**(3): p. 331-341.

493. Bartoschek, M., et al., *Spatially and functionally distinct subclasses of breast cancer-associated fibroblasts revealed by single cell RNA sequencing.* Nat Commun, 2018. **9**(1): p. 5150.

494. Wu, S.Z., et al., *Single-cell analysis reveals diverse stromal subsets associated with immune evasion in triple-negative breast cancer.* Biorxiv, 2020.

495. Maley, C.C., et al., *An ecological measure of immune-cancer colocalization as a prognostic factor for breast cancer.* Breast Cancer Research, 2015. **17**(1): p. 1-13.

496. Galon, J., et al., *Type, density, and location of immune cells within human colorectal tumors predict clinical outcome.* Science, 2006. **313**(5795): p. 1960-1964.

497. Brechbuhl, H.M., et al., *Fibroblast Subtypes Regulate Responsiveness of Luminal Breast Cancer to Estrogen.* Clin Cancer Res, 2017. **23**(7): p. 1710-1721.